NASA CONTRACTOR REPORT

NASA CR-1620

NASA CR-1620

LUNAR ESCAPE SYSTEMS (LESS) FEASIBILITY STUDY

Volume II - Final Technical Report

by J. O. Matzenauer

Prepared by
NORTH AMERICAN ROCKWELL CORPORATION
Downey, Calif.
for Langley Research Center

NATIONAL AERONAUTICS AND SPACE ADMINISTRATION • WASHINGTON, D. C. • SEPTEMBER 1970

NASA CR-1620

LUNAR ESCAPE SYSTEMS (LESS)

FEASIBILITY STUDY

Volume II - Final Technical Report

By J. O. Matzenauer

Issued by Originator as SD 69-598

Prepared under Contract No. NAS 1-8923 by
SPACE DIVISION, NORTH AMERICAN ROCKWELL CORPORATION
Downey, Calif.

for Langley Research Center

NATIONAL AERONAUTICS AND SPACE ADMINISTRATION

For sale by the Clearinghouse for Federal Scientific and Technical Information
Springfield, Virginia 22151 – CFSTI price $10.00

FOREWORD

This report was prepared by the Space Division of North American Rockwell Corporation under Contract NAS1-8923 for NASA-Langley Research Center (LRC). A summary volume, SD 69-598-1, was also prepared. Both reports were prepared in the style required by NASA Publication Manual SP-7013, 1964.

The primary study team consisted of the following persons:

J.O. Matzenauer	- Program Manager
D.H. Hengeveld	- Project Engineer, Parametric Operational Information
D.A. Engels and G.C. McGee	- Project Engineers, Stability and Control
R.E. Oglevie	- Project Engineer, Guidance and Navigation
V.V. VanCamp	- Project Engineer, Design Integration
A.D. Kazanowski	- Consultant for Lunar Science and Visibility
D.F. Bender and M.R. Helton	- CSM Rendezvous Analysis
D.W. Peebles	- Design Supervisor

ABSTRACT

The contractor has conducted a Phase A lunar emergency escape-to-orbit systems (LESS) feasibility study for NASA-Langley Research Center (LRC) under Contract NAS1-8923. The concept calls for a relatively simple system to carry two astronauts to a safe orbit for rendezvous with the Apollo CSM in the event that the LM cannot take off safely. The objectives of the study were to determine technically feasible and simple escape system concepts, to provide parametric operational data and conceptual design data on these concepts for use in future NASA planning, and to support the fixed-base simulation testing being conducted at NASA-LRC by D. Middleton.

The basic LESS concept of a relatively simple system for carrying two astronauts to a safe orbit was found to be feasible technically and operationally.

Trajectory data and boost profile characteristics have been developed for a variety of possible ascent profiles and conditions. Sensitivity of these trajectories to controllable and uncontrollable variables has been evaluated. An interesting variant of the conventional ascent trajectory profiles has been posed as the bent two-step profile combining good performance with simplicity. Rendezvous requirements for simple LESS concepts have been evaluated and found to be compatible with existing CSM capabilities.

Visibility problems and sun-angle phenomena have been examined for missions of 3, 7, and 14-day stay-times. The resulting wide range of possible sun angles has been analyzed to identify problems with guidance elements and vehicle rendezvous operations.

Guidance sensors of the visual and instrument classes have been examined. Although visual systems promise simplicity, they may require stable vehicle platforms with low piloting workload and are prone to have visibility, glare, and cross-coupling difficulties. Consequently, the manual stability and control modes do not integrate readily with visual displays. All things considered, the gyro-horizon all-attitude display appears to minimize problems under diverse mission and system conditions.

Extensive manual stability and control analyses have been conducted, and the hardwire (direct engine vectoring) control mode was found to be slightly superior to kinesthetic control in terms of anticipated handling qualities. A relationship between control torque available and vehicle

inertias was postulated and may be important in predicting design features that will maximize favorable handling qualities. Additional simulation test data for verification were found to be needed. Special configurations designed to improve stability/control have been evaluated against the complexity involved. Reduced-thrust operation at later stages of boost flight and other concepts were found attractive to match more efficiently the ratio of control torque available to the inertias as reduced with fuel burnout.

Guidance elements have been evaluated in concert with stability modes and vehicle configuration design. Special hardwire mode variations, usually involving engine translation rather than gimbaling, were examined with a view to uncoupling rotational and translational axis dynamics as well as elimination of a guidance error source. Pulsed multiple engines of Apollo RCS type also provide this feature as well as configuration packaging advantages and early engine availability.

Estimated errors in final vehicle orbits have been developed statistically from available error source data including a sampling of runs conducted in NASA-LRC simulations of the kinesthetic control mode. The analyses, which are believed to be slightly conservative, indicate that the resulting LESS orbits will be marginally acceptable for kinesthetic and hardwire control modes and that they may be improved with further studies and testing.

Typical configuration designs suitable for kinesthetic and hardwire control were generated. The hardwire concept provides somewhat greater configuration freedom, which is important for optimizing handling qualities and for packaging. Stowage on the side of the LM was found to be possible, but difficult, because of space limitations and possible interaction with LM RCS jets. Several alternative approaches for LM stowage that were identified may require LM interface analysis beyond the scope of this study. A concept of initially collapsed tanks, expanded upon fueling, was generated and appears to have promise for relieving the stowage problem. Initial deployment from the LM was found to take 45 minutes; preparations for launch will require two hours.

When adapted as a long-range lunar flyer, the LESS vehicle requires landing gear, communications, throttleable engine, and stability augmentation. In one configuration, utilizing 1200 pounds of propellant (sized for a practical escape profile), the long-range flyer version provided a 40 nm mission radius with a horizontal-translation "cruise" altitude of 1000 feet. With 1600 pounds of propellants, appropriate for a LESS vehicle sized for a coarse ascent profile, the radius would be 60 nm. Ranges of these magnitudes should be attractive to mission planners concerned with safety/rescue and with extending lunar surface site reconnaissance and exploration. The changes for the flyer mission were found to have a small effect on the escape mission configuration. These changes would, incidentally, tend to provide increased guidance accuracy and improved capability for escape and other missions.

CONTENTS

ILLUSTRATIONS

*Large-scale, integrated working drawings are available upon request from:
NASA Langley Research Center
Att: Photographic Branch, Mail Stop 171
Hampton, Virginia 23365

*Large-scale, integrated working drawings are available upon request from:
NASA Langley Research Center
Att: Photographic Branch, Mail Stop 171
Hampton, Virginia 23365

TABLES

LUNAR ESCAPE SYSTEMS (LESS) FEASIBILITY STUDY, FINAL TECHNICAL REPORT

By J. O. Matzenauer
Space Division, North American Rockwell Corporation

INTRODUCTION

This report presents results of the Phase A feasibility study of emergency vehicle concepts for escape of two men from the lunar surface to the orbiting CSM. The study, conducted by North American Rockwell Space Division for the NASA, Langley Research Center, is identified as Contract NAS1-8923. Mr. A. W. Vogeley was Technical Manager for the study at NASA-LRC.

Objective

The purpose of the study has been to determine the technical and operational feasibility of simple escape-system concepts and to provide parametric operational and design data that can be utilized in a related NASA-LRC simulation test program and that, together with the simulation results, will provide a basis for NASA decisions on escape-system development.

Approach

The approach taken has been to utilize the data and material from particularly pertinent NASA and contractor studies in generating parametric performance and systems data. Stability and control analyses and simulations experience on the recent Phase B Lunar Flying Vehicle (LFV) Study (Contract NAS9-9045) were particularly applicable. This parametric information was utilized in system and concept synthesis and integration effort, particularly for the key guidance and control techniques. Extensive propulsion studies conducted in the LFV study provided strong inputs for

propulsion-performance-design trades. Conceptual development layout effort provided practical constraints and included iterations back through the parametric data possibilities. Design experience with control mechanization for the NASA-LRC flying lunar excursion experimental platform (FLEEP) proposal effort was helpful. Contractor knowledge of Apollo interfaces and advanced mission planning studies were most useful in analyzing CSM capabilities for rendezvous and for studying visibility problems. Again, in the surface operations and the surface flyer applications of LESS, the immediate background of the LFV study was of substantial benefit.

The outputs of the study include a spectrum of parametric performance and operational data that can be utilized in future studies under varying ground rules and conditions. The conceptual configurations effectively highlighted practical constraints and problem areas, and made possible realistic weight and balance data needed in guidance and control analyses. In keeping with the exploratory nature of a Phase A study, key systems, such as guidance and control, structure, and propulsion tradeoff data were generated and parametric characteristics developed. Where clear choice of a subsystems technique could not be made, the tradeoff considerations were specified.

Support was provided to the important and concurrent fixed-base simulation test program at NASA-LRC. Information on trajectories, guidance mechanization, propulsion, and system design was furnished. Specific trajectory data of interest were informally transmitted. Some simulation results were made available to the contractor during the study and were extremely useful in evaluating the contribution of steering errors to potential guidance accuracy obtainable.

Recommendations for further effort are provided.

Ground Rules and Guiding Considerations

A minimum number of basic ground rules were applied to this study. The principal ones were:

1. Emphasis on simplicity rather than system redundancy
2. Propellants up to 5000 pounds are available from LM/ELM ascent stage
3. Astronaut backpacks to provide ECS/LSS and telecommunications

4. Missions up to 14 days stay-time

5. Single-pilot control

6. Safe orbit with single burn desirable

7. Conditions leading to use of the escape system not specified in detail

8. Compatibility with Apollo CSM and LM

For some time into the future, the lunar module (LM) and its direct derivatives, such as extended LM (ELM), will be used as the means of crew transport to and from the lunar surface and orbit. A serious failure in the descent stage could be accommodated during most of the descent phase by in-flight separation (abort) of the ascent stage. Provisions are also made for LM rescue in the event the LM can take off but cannot ascend beyond minimum altitude (50, 000 feet); the CSM can descend to conduct the rendezvous operation without help from the LM. In the ascent stage, dependence is placed entirely upon extensive built-in system redundancies and reserves to provide the necessary assurance of mission safety. Provision of additional emergency equipment or systems such as LESS might make it possible to extend the conservative operating envelope or capability limits of LM/ELM such that increased mission capability could result. Even slight improvements in mission accomplishment and capability may become quite important in carrying out lunar exploration with minimum cost yet acceptable safety.

A logical question on first consideration of an alternative or emergency backup surface escape scheme is, "how simple can such a system concept be?" Its corollary question is, "how complex does it need to be?" These and many other operational and technical feasibility questions about the system must be considered, along with serious reflection on the system's potential for multiple-mission use.

Reliability of an emergency system can be approached through simplicity rather than redundancy. Another consideration involves the Apollo CSM, which is known to be a versatile and sophisticated spacecraft. Exploiting these CSM inherent capabilities for supporting and complementing the escape mission vehicle permits the escape system to be simple in concept and in equipment mechanization. Simplicity of function in the LESS may also aid in terms of minimum escape vehicle mass and size. Reduced size reduces the critical problems of stowage and transport aboard the LM/ELM. Although ample propellants for the escape vehicle can be obtained from the 5000-pound capacity of the LM ascent tankage, the size of the vehicle should be minimized from several standpoints in addition to that of restricted LM/ELM

stowage. Some of the other reasons are difficulty of unloading and deploying the LESS, time required to refuel, and LM/ELM payload weight limitations.

Escape-system development could evolve in either of two basic ways. One could be an administrative decision to reduce further the risk factors inherent in the LM ascent phase of the present lunar mission concept. This decision could come very soon in the lunar program and would require a highly accelerated escape system development program, perhaps in less than half the normal development cycle. In this event, the system concept (not necessarily the simplest) could well be biased in the direction of the one promising the highest probability of successful development. The second basic approach to system procurement would be a more normal development cycle with greater attention to optimizing system performance. It is likely, however, that overall space program economics will require consideration of the alternative applications or missions to which the LESS could also be applied or adapted. Preliminary studies by this Contractor have identified many such possibilities for LESS alternative uses. Of particular appeal are adaptation of the LESS to perform long-range surface flying vehicle missions, conversion to a supplementary lunar sample return-to-orbit vehicle, and orbit-to-surface shuttle, experiment lander, or rescue vehicle. The long-range flyer adaptation of the LESS is the subject of a task in this study. The possible escape mission application of the lunar flying vehicle was also a task under that study (NAS9-9045).

ABBREVIATIONS AND NOMENCLATURE

LESS	Lunar (emergency) escape system, also Lunar Excape Systems Study
LM	Lunar module
ELM	Extended lunar module (three-day stay)
COV	Calculus of variation (optimum trajectory)
RCS	Reaction control system (attitude jets)
CSM	Apollo command and service module
CMC	Command module guidance computer
SOR	Stable-orbit rendezvous (technique for LM rescue - Program 38)
COR	Concentric-orbit rendezvous (technique for LM rendezvous)
LMRR	LM rendezvous radar
ARS	Attitude reference system
G&C	Guidance and control
G&N	Guidance and navigation
SCS	Stabilization and control system
AGS	Abort Guidance System in LM
LRV	Lunar roving vehicle
PLSS	Portable life support system (backpack)
LFV	Lunar flying vehicle under study by NASA-MSC

OPS	Oxygen purge subsystem of backpack (PLSS)
SLSS	Secondary life support system (part of advanced backpack)
PECS	Portable environmental control system (an advanced backpack concept)
NM	Nautical miles
LOS	Line-of-sight
T/W	Thrust-to-weight

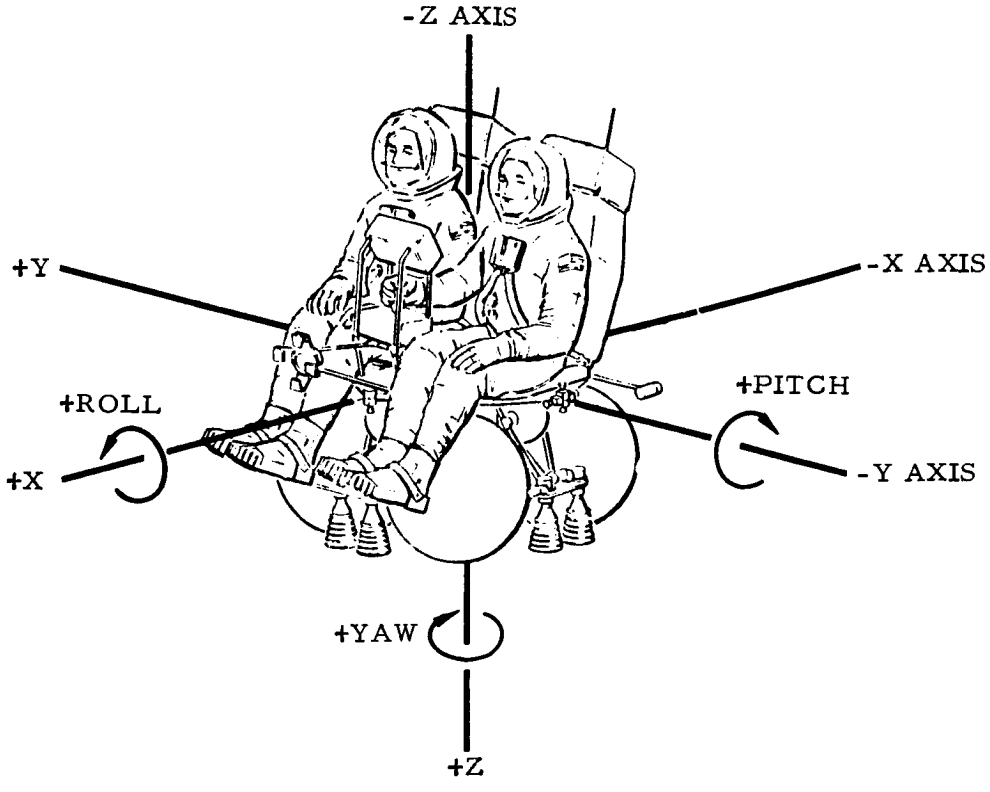

VEHICLE AXIS AND ROTATION
DIRECTION DEFINITION

NOTE — AXES INTERSECT AT VEHICLE C.G., EXCEPT FOR SECTION 3.0 WHERE Z MEASUREMENTS ARE FROM BOTTOM OF PLATFORM

1.0 STUDY RESULTS - PARAMETRIC OPERATIONAL DATA

This section presents results of parametric trajectory and performance analyses of the boost and rendezvous phases of the LESS mission. The purpose of the LESS is to provide capability for an emergency launch from the surface of the moon to the orbiting Apollo CSM in the event that the lunar module should become unsafe for ascent from the lunar surface. The basic requirement to be satisfied by the LESS then is to safely reach a condition where the crew can transfer into the CSM, employing such assistance for rendezvous as can be provided by the CSM itself. Figure 1-1 illustrates the basic phases of the mission treated in this section: (1) boost and (2) rendezvous, including docking and crew transfer. Boost is treated parametrically. Rendezvous is treated parametrically as regards energy requirements since they are dependent on the properties of the LESS. CSM capabilities, constraints, and limitations are identified, and requirements are placed on the LESS consistent with the desire to minimize modifications to the CSM and to keep the LESS simple, light, and safe.

The issue of visibility permeates the entire study. It is discussed in individual sections of the report where appropriate, and it is discussed at some length in this section as a special subject.

A symbol list is provided at the end of this section (page 1-199).

Boost Ascent Trajectories

Objectives. - This section presents results of the parametric launch performance analysis for which the main objective was to identify LESS performance requirements and sensitivities. Another objective was to provide information in support of the NASA-LRC flight vehicle simulation test program, which has been exploring system performance characteristics, and to support the concept design integration effort. Since the objective was to create parametric information, no conclusions or recommendations are drawn in this section.

Approach. - The basic tradeoff for the LESS is system simplicity versus vehicle weight. The simplest systems tend to result in large errors, thus necessitating high-energy orbits and large propellant requirements both in the LESS for boost and, for the case of CSM-active rendezvous, in the CSM. The more complex systems tend to be more accurate and so can be used to reduce

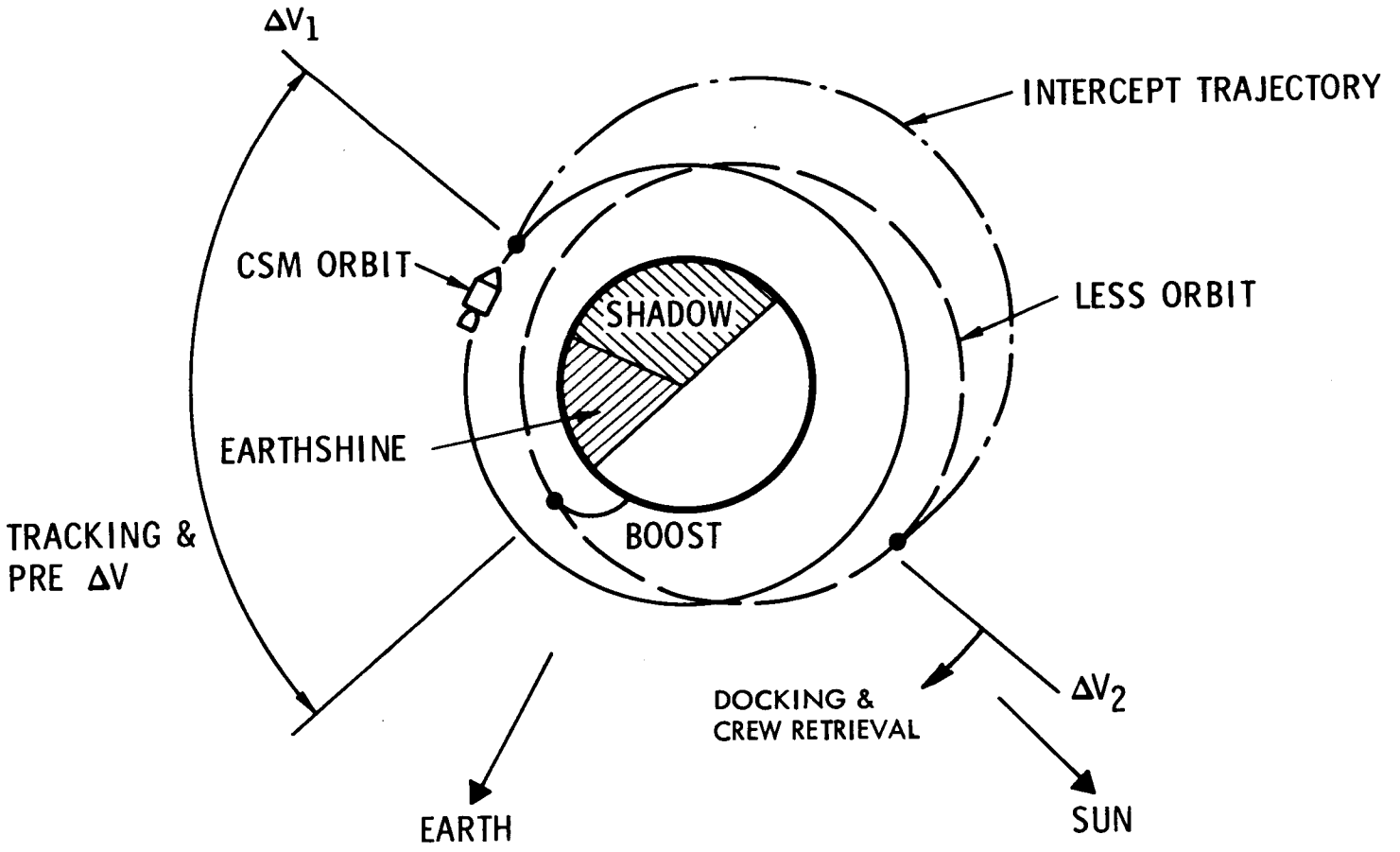

Figure 1-1. - Gross Mission Profile

energy requirements. With regard to LESS propellant requirements, it is noted that while there is an ample supply of propellant available from the lunar module ascent stage tanks, larger propellant expenditures imply larger LESS propellant tanks in terms of both weight and volume. This impacts the overall vehicle design and the means of deployment. This section of the report gives the results of the parametric analysis of the boost phase of the LESS mission and illustrates energy requirements, trajectory characteristics and steering angles, and error sensitivities.

As specified by the NASA-LRC, study emphasis was placed on simple systems and concepts. In the area of guidance, this is manifested in concepts employing constant thrust-attitude segments, the minimum being two segments. As these concepts tend to result in large energy expenditures, optimal solutions were also derived to form the basis for systems trades, such as guidance simplicity versus propulsion system requirements.

Taking the concept of simplicity further, some ground rules were established that reflect simplicity and that limit the range of parametric analyses conducted. Multiple-burn ascent trajectories were not considered desirable. They obviously require at least two burns of the propulsion system and thus imply a more complicated system. For the same reason, throttling was not considered initially. However, as the study progressed, it was found that the throttling could be used to improve vehicle handling qualities (see the Stability and Control section). Consequently, the performance effects of employing a two-step thrust schedule were also investigated.

From the foregoing, it is clear that substantial tradeoff studies will be necessary to define the optimum vehicle for the mission. To support these studies, the parametric results of the ascent-to-orbit phase are herewith submitted.

The results shown were obtained by numerically integrating the equations of motion of a particle subjected to the lunar gravitational potential (neglecting anomalies) and to a directed thrust force.

Energy requirements were developed to reflect simple two- and three-step thrust attitude profiles for liftoff thrust-to-weight ratios of 0.2, 0.3, 0.4 and 0.5 pounds per pound, constant thrust, and orbit altitudes (circular) of 20, 40, 60, and 80 nautical miles. Also shown are equivalent solutions derived by the classical calculus-of-variations (COV) method. When these results were compared with the three-step results, it was seen that very little improvement in energy requirements could be realized by employing more steps than three. Therefore, no four- or five-step trajectories were considered. A complete set of error sensitivities was derived for the three-step profile. Error sensitivities of a typical calculus-of-variations trajectory and a typical two-step trajectory were found to agree substantially with those of the comparable

three-step trajectory. Thus, a complete set of error sensitivities is shown only for the three-step profile. The desirable aspects of the two-step profile (only two attitude segments) and the three-step profile (low energy penalty) were combined to form what NR has dubbed the "bent two-step" profile. Some of the properties of this profile are identified.

Most of the analyses are based on nominal circular target orbits. However, a short analysis of effects of employing elliptical target orbits is presented. The performance tradeoffs associated with a two-step thrust schedule for boost to a 60-nm orbit are also presented.

Calculus-of-variations trajectories. - In most studies of this type, boost energy requirements are based on optimized trajectories derived by calculus-of-variations (COV) steering techniques. Guidance mechanizations are then developed that usually match the COV solution closely and that can be programmed into on-board computer systems. In this study, the approach is to employ guidance concepts so simple that they may not be able to even approximate the steering profiles derived by the COV formulation. However, to perform the optimization trade studies for this vehicle, it is necessary to know what the optimum solutions are, what their energy requirements are, and what form their steering profiles take.

Figure 1-2 depicts the variation in boost energy requirements with liftoff thrust-to-weight ratio and with orbit altitude (circular). The vertical boost parameter depicted is relevant to the LESS problem by virtue of some of the visual sighting schemes being postulated. They may be mechanized to sight on a landmark to obtain azimuth information. To assure that the pitchover maneuver occurs at the proper yaw attitude, it may be necessary to boost vertically in order to sight an appropriate landmark and to provide time for the pilot to take action based on the sighting. This would be particularly true if the landing site were the floor of a crater, such as Copernicus. For a 20-nm orbit, the energy variation is approximately 400 feet per second for the range of vertical boost altitudes from 2000 to 20 000 feet. As would be expected, the variation diminishes for higher altitudes and is approximately 80 feet per second for an 80-nm orbit. Figure 1-3 depicts the variation of vertical boost time with altitude for the liftoff thrust-to-weight ratios considered in the previous figure. From these data, a vertical boost altitude of 10 000 feet was selected as the basis for subsequent analyses. Figure 1-4 depicts the variation in thrust attitude angle immediately following the vertical boost (to 10 000 feet) and at burnout. The time histories are roughly linear between the two end points (see fig. 1-7 for a typical case). For higher orbit altitudes, it is seen that initial thrust attitude is quite close to vertical and that at burnout it is quite negative. This can be explained by considering the large displacement (altitude) changes that must be made during a relatively short burning time (especially for cases having high liftoff acceleration). During the early part of the trajectory, as much altitude as possible must be gained, necessitating a near-vertical flight

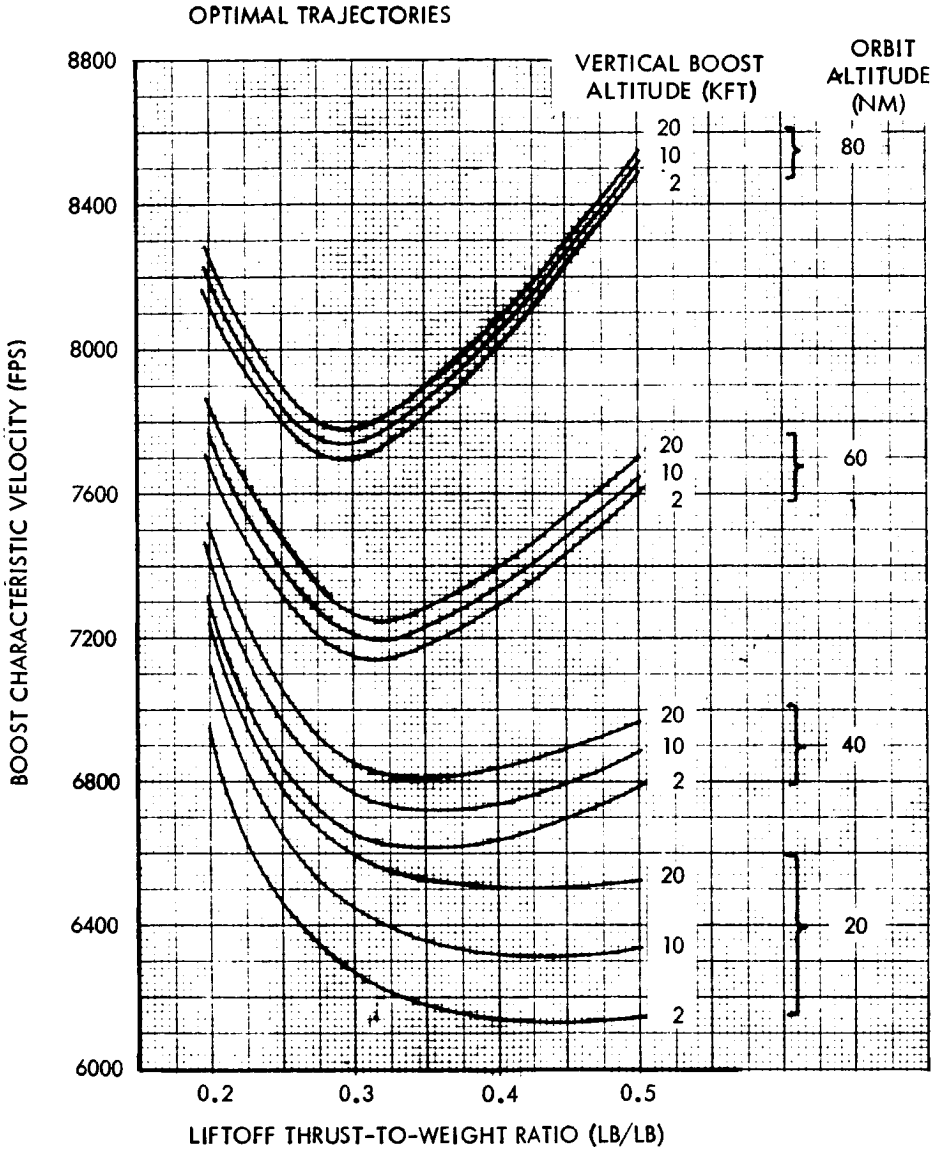

Figure 1-2. - Variation of Boost Energy Requirements With Liftoff Thrust-to-Weight Ratio Vertical Boost Altitude, and Orbit Altitude for Optimally Steered Trajectories

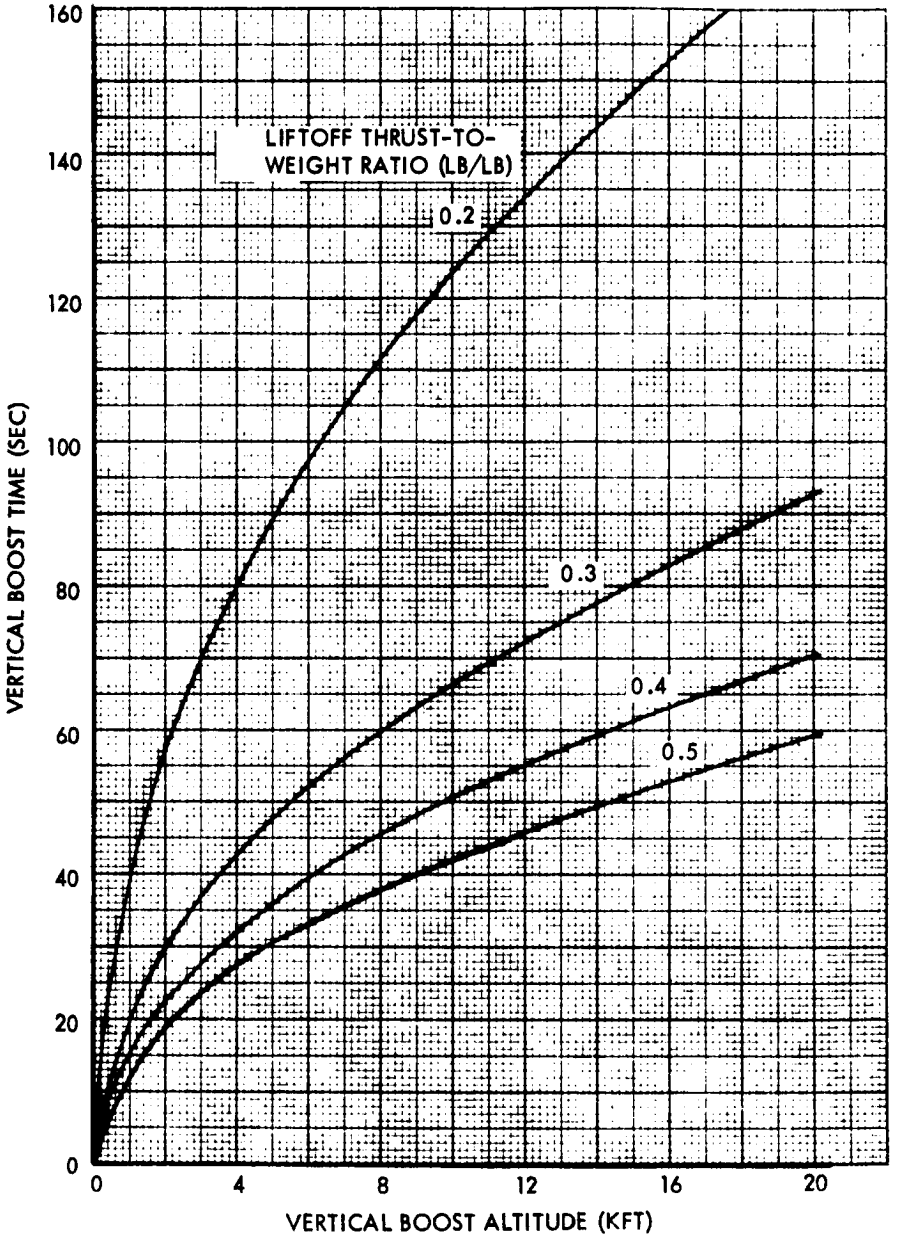

Figure 1-3. - Variation of Vertical Boost Time With Altitude

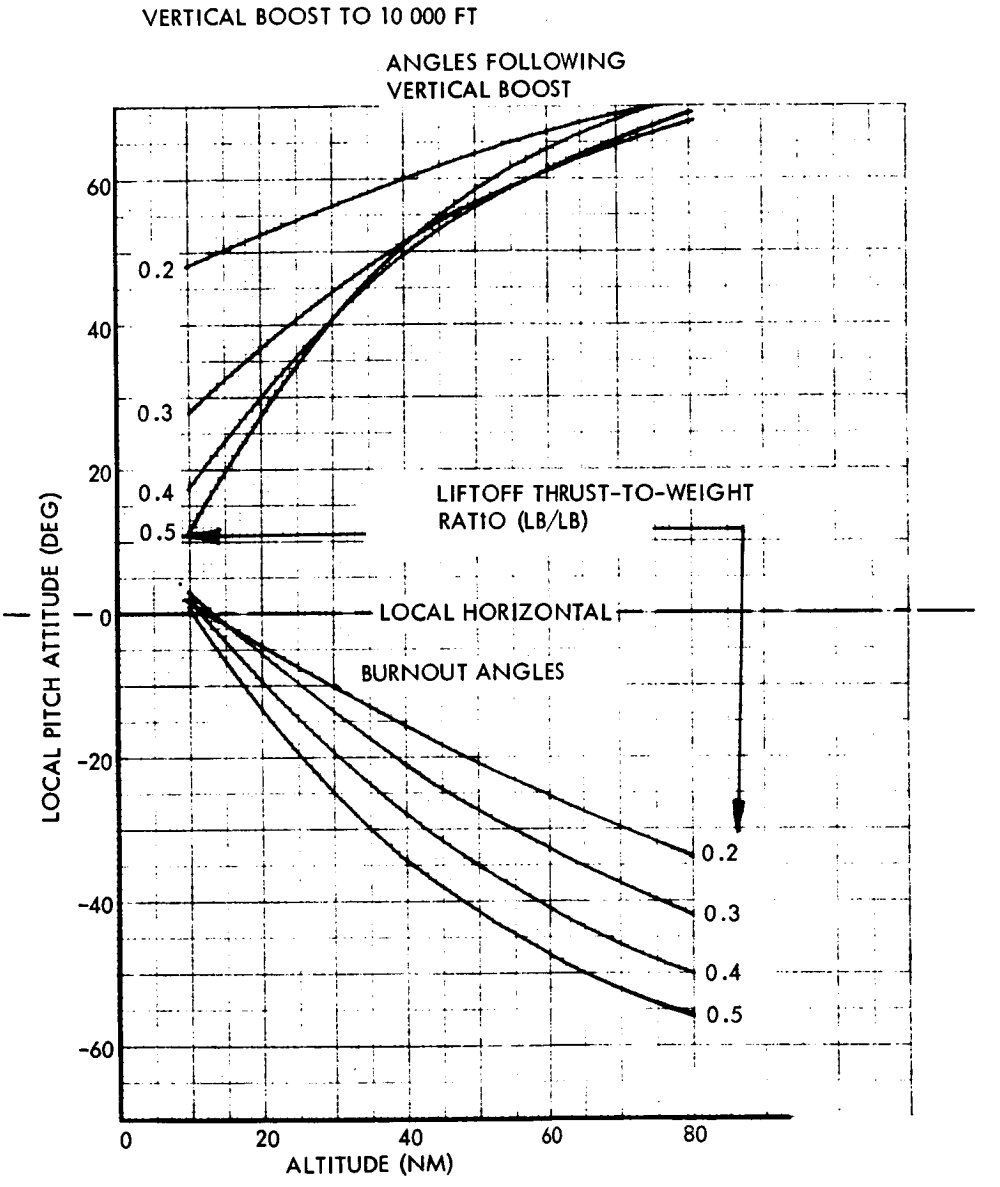

Figure 1-4. - Variation of Initial and Final Steering Angles for Optimally Steered Trajectories

path. Toward the end of the trajectory, large negative angles-of-attack must be applied to bring the flight path angle to zero. Figures 1-5 and 1-6 depict a typical trajectory reflecting boost to 60 nm, assuming a liftoff thrust-to-weight ratio of 0.3 pound per pound. Figure 1-7 depicts the steering angle history. It is plotted against time, ΔV, and altitude and is seen to be nearly linear with altitude. In this regard, it was found that the linear solution with respect to time noted could be obtained for an energy penalty of only 24 feet per second.

Figures 1-8 and 1-9 illustrate the effects of pitch attitude and thrust-to-weight ratio errors respectively on perilune and apolune altitudes of the orbits that are produced. A target orbit of 60 nm and a liftoff thrust-to-weight ratio of 0.3 pound per pound are reflected. An error in pitch attitude (fig. 1-8) of, for example, plus two degrees is here taken to mean that a constant bias of two degrees in thrust application angle is applied from liftoff to cutoff. Cutoff occurs at the nominal time, and open-loop steering is implied. These assumptions are representative of the concepts being postulated for this vehicle. The data of figure 1-9 reveal a dramatic reduction in error sensitivities if control according to ΔV produced can be employed instead of time. Cutoff according to time produces significant variations in ΔV produced in the event that the acceleration history is not nominal. Therefore, perilune and apolune altitudes are more strongly affected by errors in thrust-to-weight ratio. The error effects for this typical case were found to be within five percent of those of the three-step profile, for which a full treatment of error effects was accomplished. Consequently, a complete treatment of error effects for this steering profile was not attempted.

Two-step trajectories. - The simplest guidance scheme that can be postulated appears to be one in which the thrust attitude is allowed to have only two values. If the angles and the time increments during which they are applied are chosen correctly, a trajectory to a desired set of ending conditions can be produced.

If the ground rules are chosen that the first segment must be a vertical boost and that full thrust is to be used to orbit insertion, then the control variables become vertical boost time, the steering angle during the second segment, and burn time. Burn time has the strongest control on burnout velocity. Values of vertical boost time and steering angle can be found that produce the desired flight path angle and altitude.

Figure 1-10 depicts the variation in conditions at termination of the vertical boost as a function of target orbit altitude and liftoff thrust-to-weight ratio.

Figure 1-11 depicts the total boost energy requirements and the corresponding pitch angles during the second segment. The second segment is seen to be nearly horizontal; indeed, if the liftoff thrust-to-weight ratio is chosen

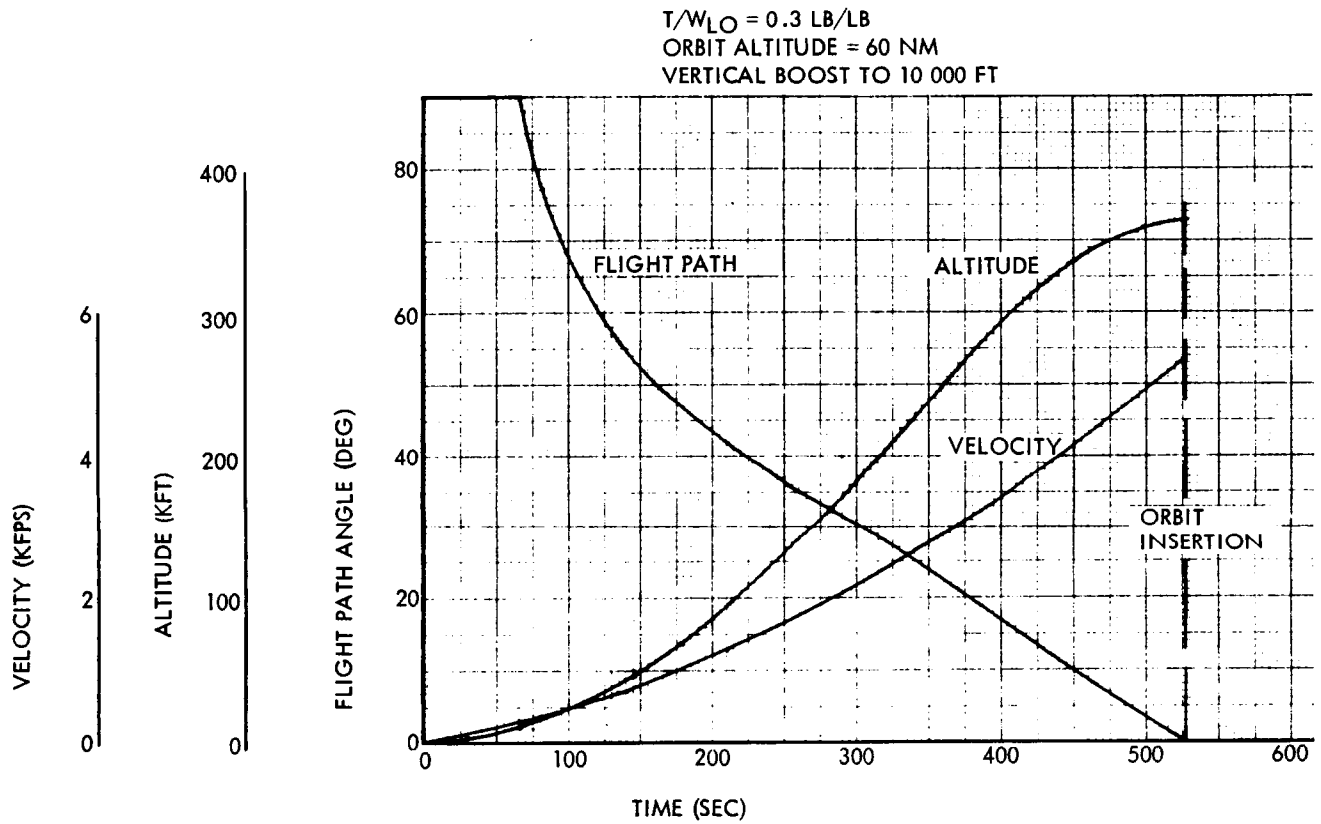

Figure 1-5. - Flight Parameters for Typical COV-Steered LESS Boost

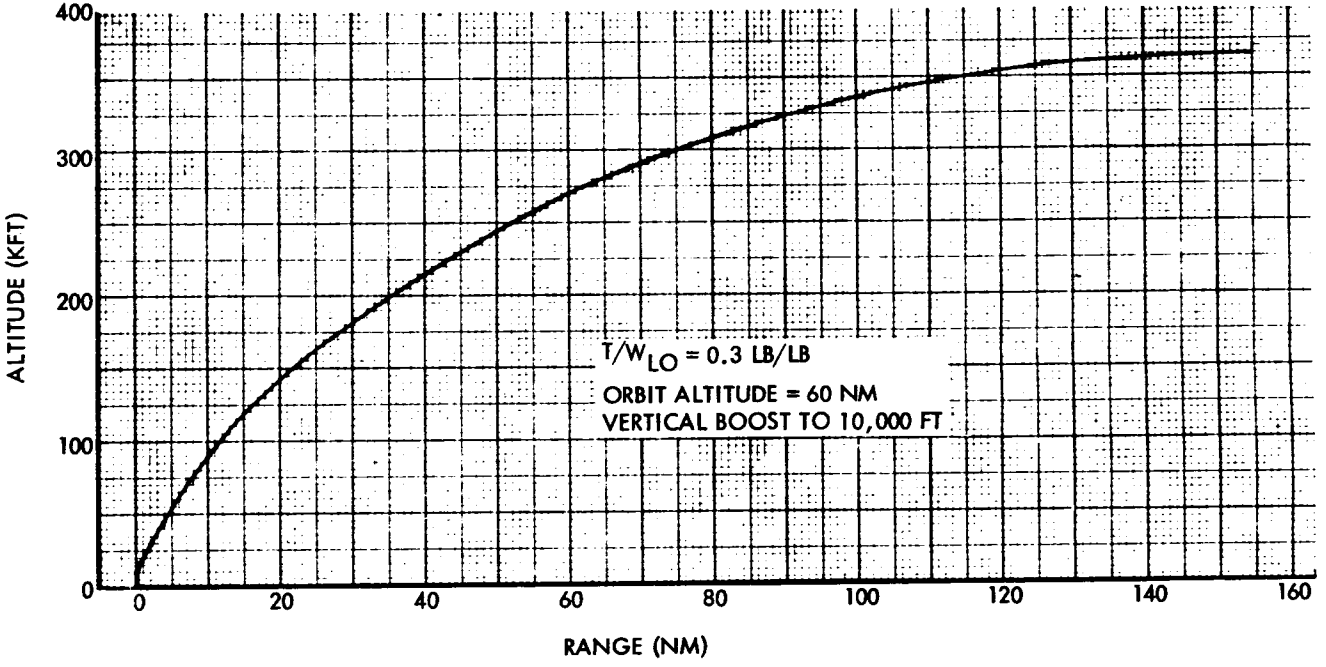

Figure 1-6. - Altitude/Range Profile for Typical COV-Steered LESS Boost

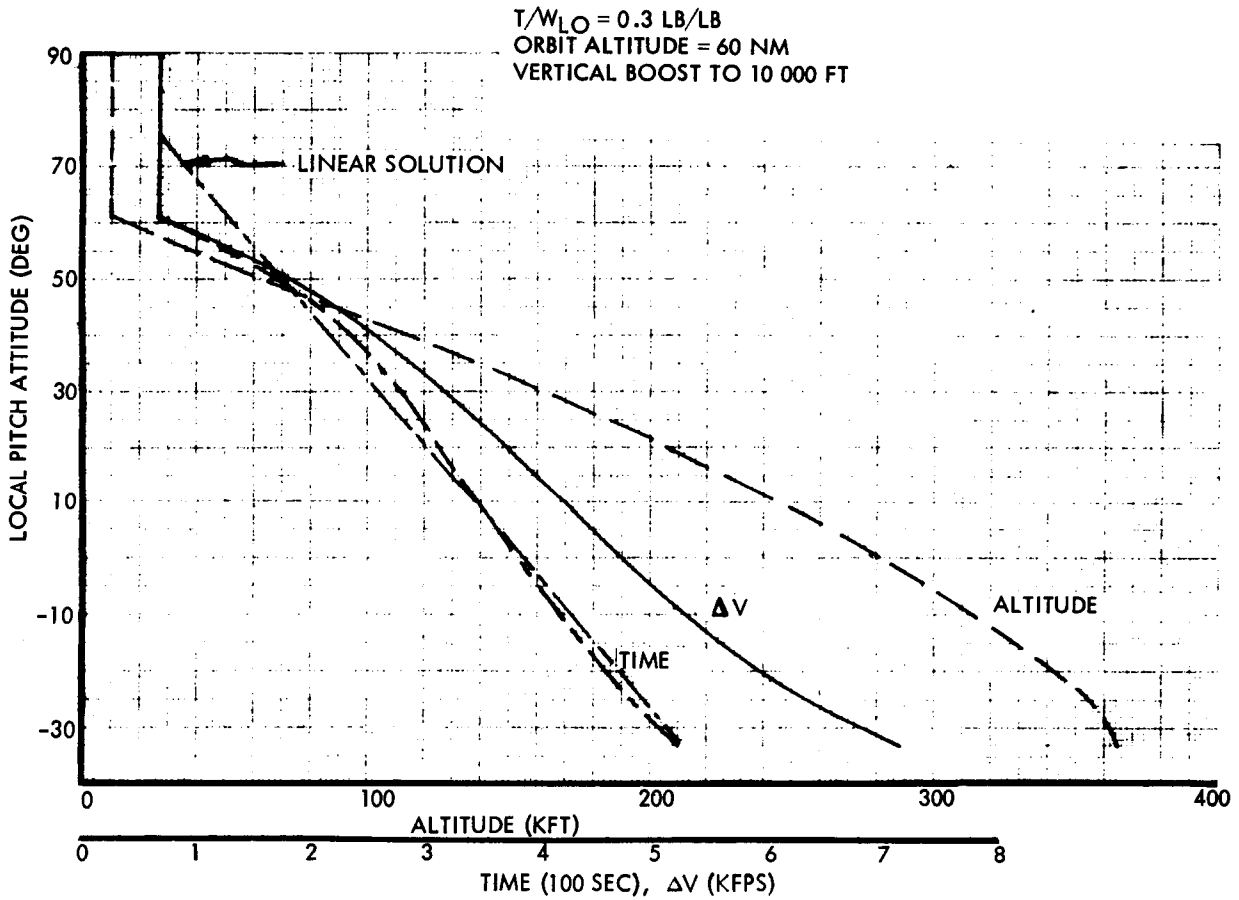

Figure 1-7.- Pitch Attitude as a Function of Altitude, Time, and ΔV for a Typical COV-Steered LESS Boost

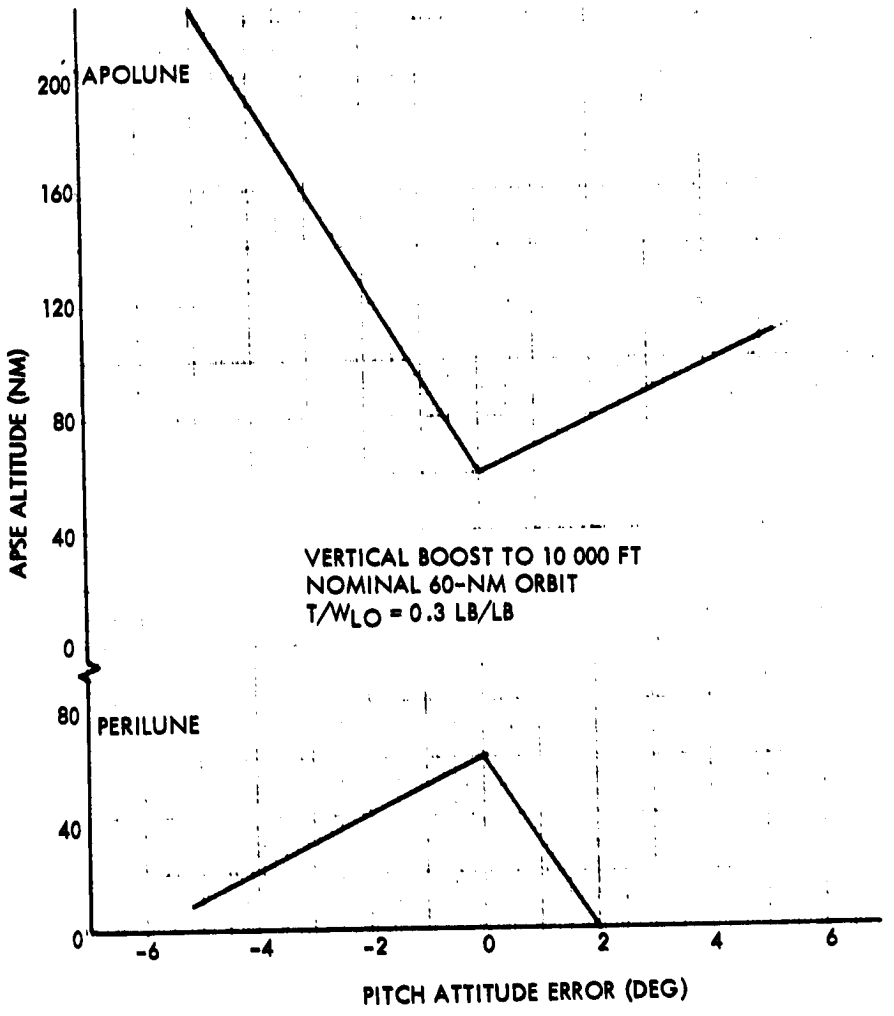

Figure 1-8. - Variation of Apse Altitude With Pitch Attitude Error for Typical COV-Steered LESS Boost

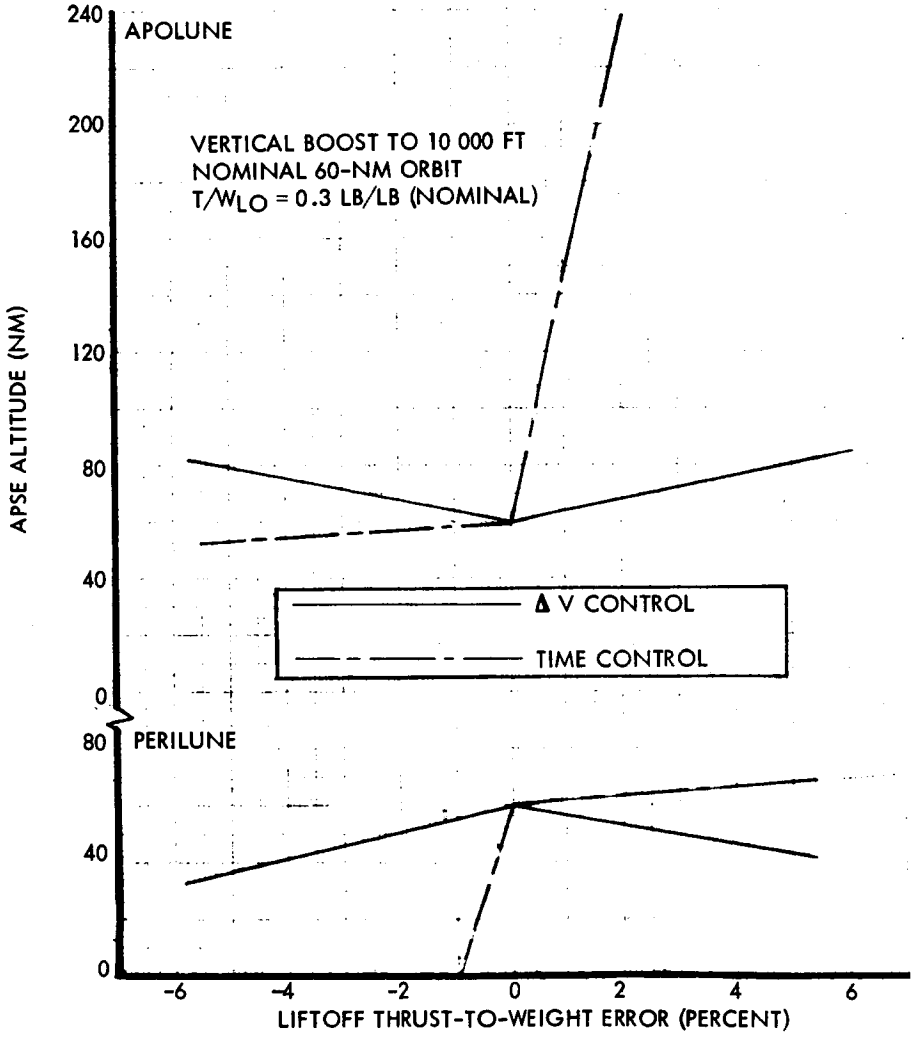

Figure 1-9. - Variation of Apse Altitude With Liftoff Thrust-to-Weight Error for Typical COV-Steered LESS Boost

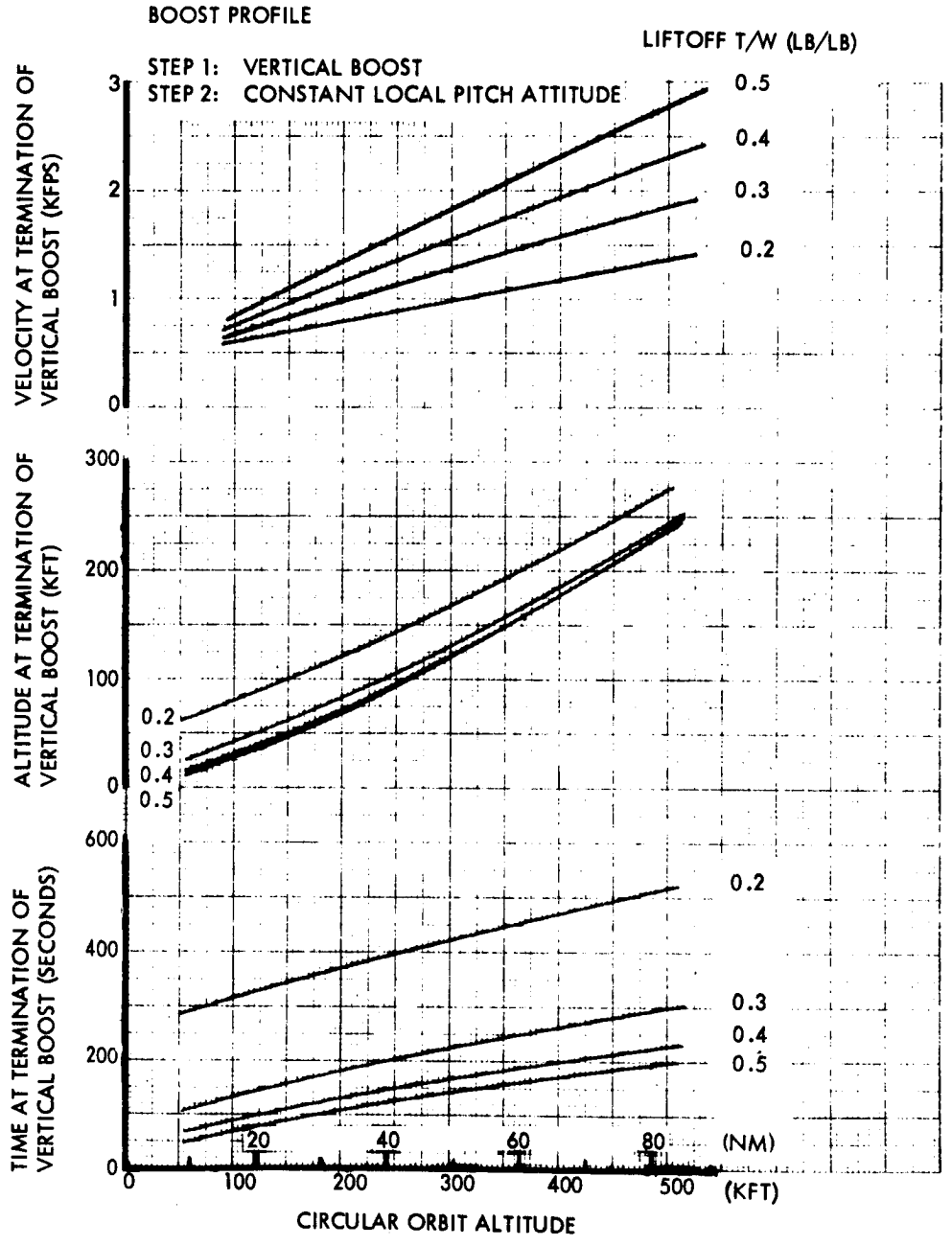

Figure 1-10. - Conditions at Termination of Vertical Boost for Boost to Circular Lunar Orbits With Two-Step LESS Steering Profiles

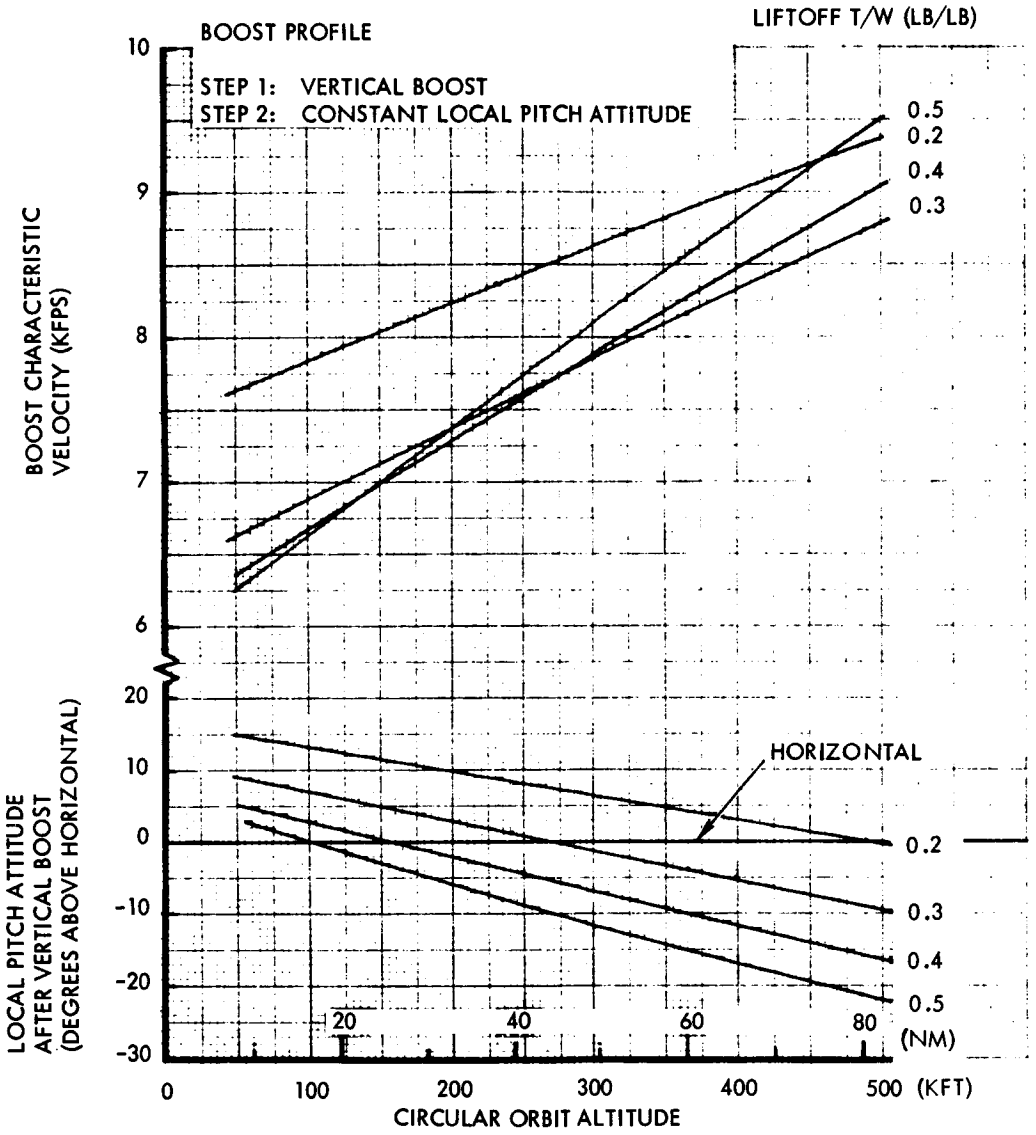

Figure 1-11.- Energy Requirements and Second-Step Steering Angle for Boost to Circular Lunar Orbits With Two-Step LESS Steering Profiles

correctly, any orbit altitude in the range of interest can be reached while making attitude horizontal. Figure 1-12 depicts the energy data of figure 1-11 plotted as a function of liftoff thrust-to-weight ratio. The requirements for the COV solutions are shown for comparison. It is seen that the penalty for the two-step steering profile is on the order of 1000 feet per second for the higher orbits. For orbits above 40 nm, the optimum liftoff thrust-to-weight ratio (for minimum energy) is seen to be approximately 0.3 pound per pound both for the COV and the two-step trajectories.

Figure 1-13 depicts the total burn time and boost range (measured along the lunar surface) as a function of orbit altitude. Figure 1-14 depicts a typical trajectory reflecting boost to an orbit slightly above 60 nm (366 380 feet), assuming a liftoff thrust-to-weight ratio of 0.3 pound per pound. Immediately after termination of the vertical boost, the thrust attitude is changed to four degrees below the local horizontal (fig. 1-11). This, in combination with the gravitational force, causes a negative velocity rate for approximately 50 seconds, as indicated by the velocity plot.

Figure 1-15 illustrates the variation in the two-step control parameters with the average rate employed during the pitch-over maneuver. The preceding parametric data were based on discontinuous attitude segments. A closer approximation to the real situation is to join the two segments by a ramp, as illustrated in figure 1-16. It is seen that the pitch maneuver timing data change significantly, while the variation in the constant attitude segment is on the order of two degrees. A modest reduction in boost energy results if a slow pitch rate can be employed.

Figure 1-17 and 1-18 illustrate the effects of pitch attitude and thrust-to-weight ratio errors, respectively, on apse altitudes. A target orbit of near 60 nm and a liftoff thrust-to-weight ratio of 0.3 pound per pound are reflected. Figure 1-17 shows the attitude error effects. Cutoff occurs at the nominal time, and open-loop steering is implied. These assumptions are representative of the concepts being postulated for this vehicle. As with COV trajectories, the data of figure 1-18 reveal a significant reduction in error sensitivities if cutoff according to ΔV produced can be employed instead of time. Cutoff according to time produces significant variations in ΔV produced in the event that the acceleration history is not nominal. Therefore, perilune and apolune altitudes are more strongly affected by errors in thrust-to-weight ratio. Further reductions in error sensitivities occur if the pitch step can be scheduled on the basis of ΔV.

The error effects for this typical case were found to match closely (within 10 percent for pitch errors and T/W errors controlled by ΔV) those of the three-step profile, for which a full treatment of error effects can be found in the following section. Consequently, a complete treatment of error effects for this steering profile was not attempted.

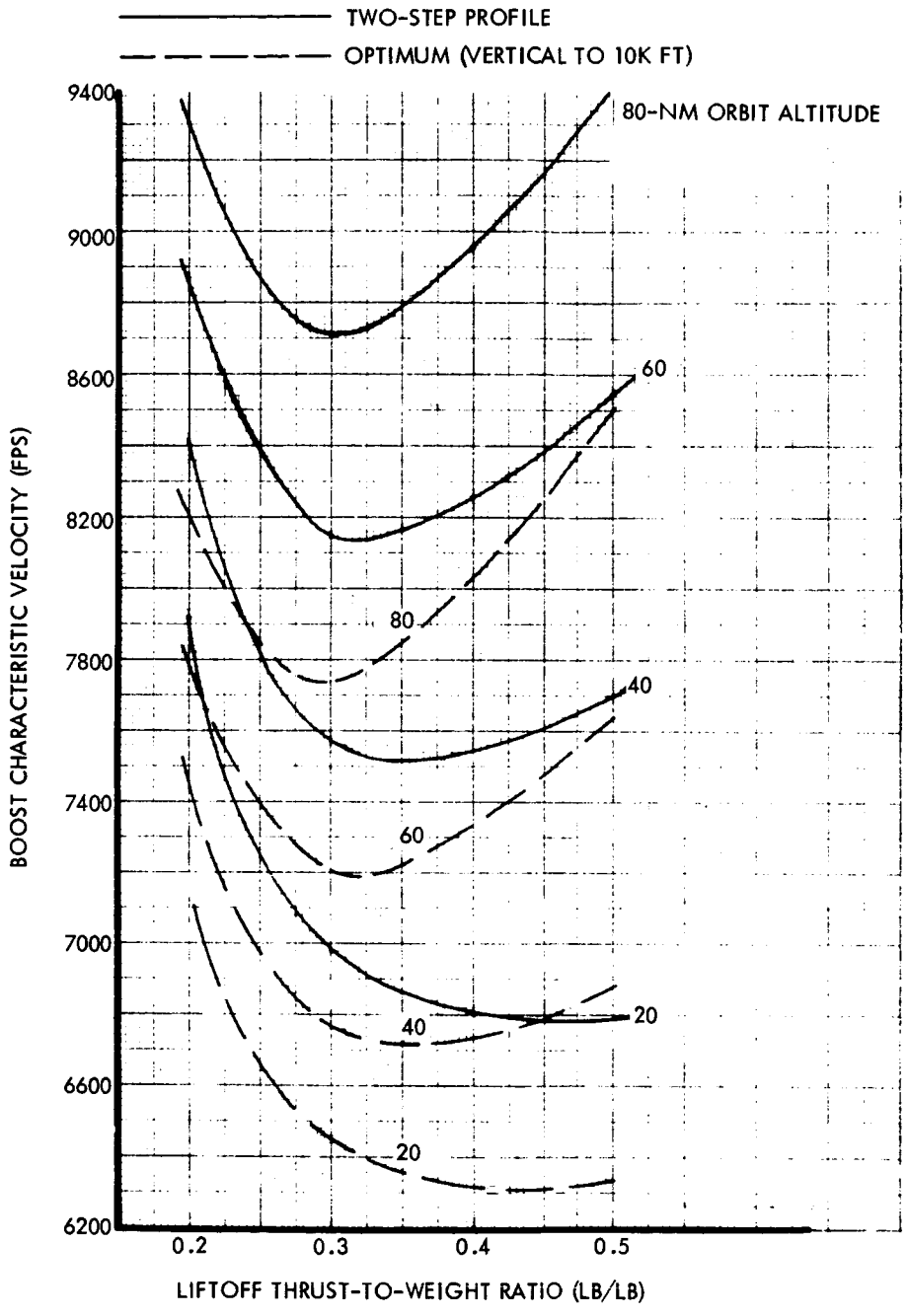

Figure 1-12. - Comparison of Energy Requirements for Two-Step LESS Steering Profile With Requirements for Optimum

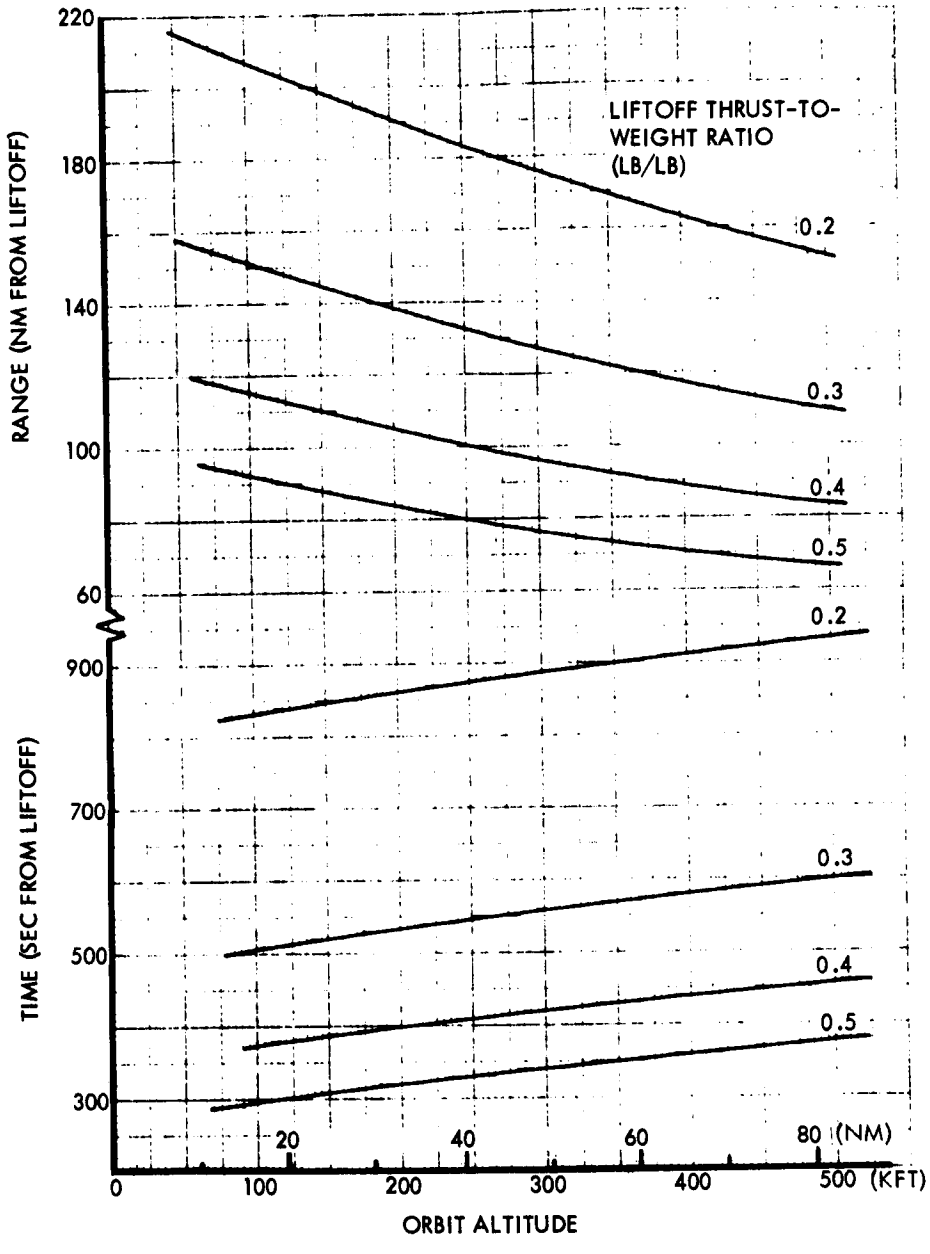

Figure 1-13. - Range and Time at Termination of Two-Step LESS Boost

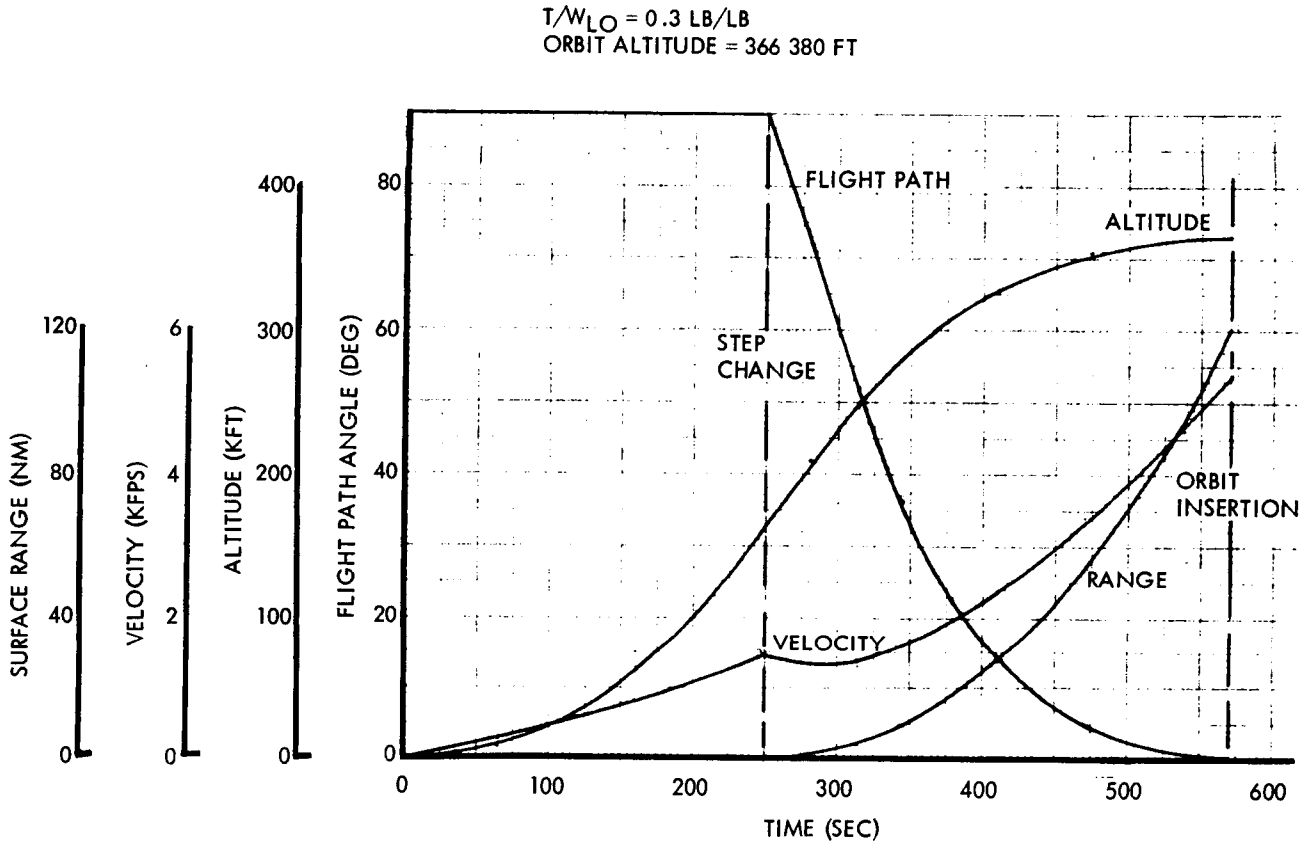

Figure 1-14. - Flight Parameters for Typical Two-Step LESS Boost

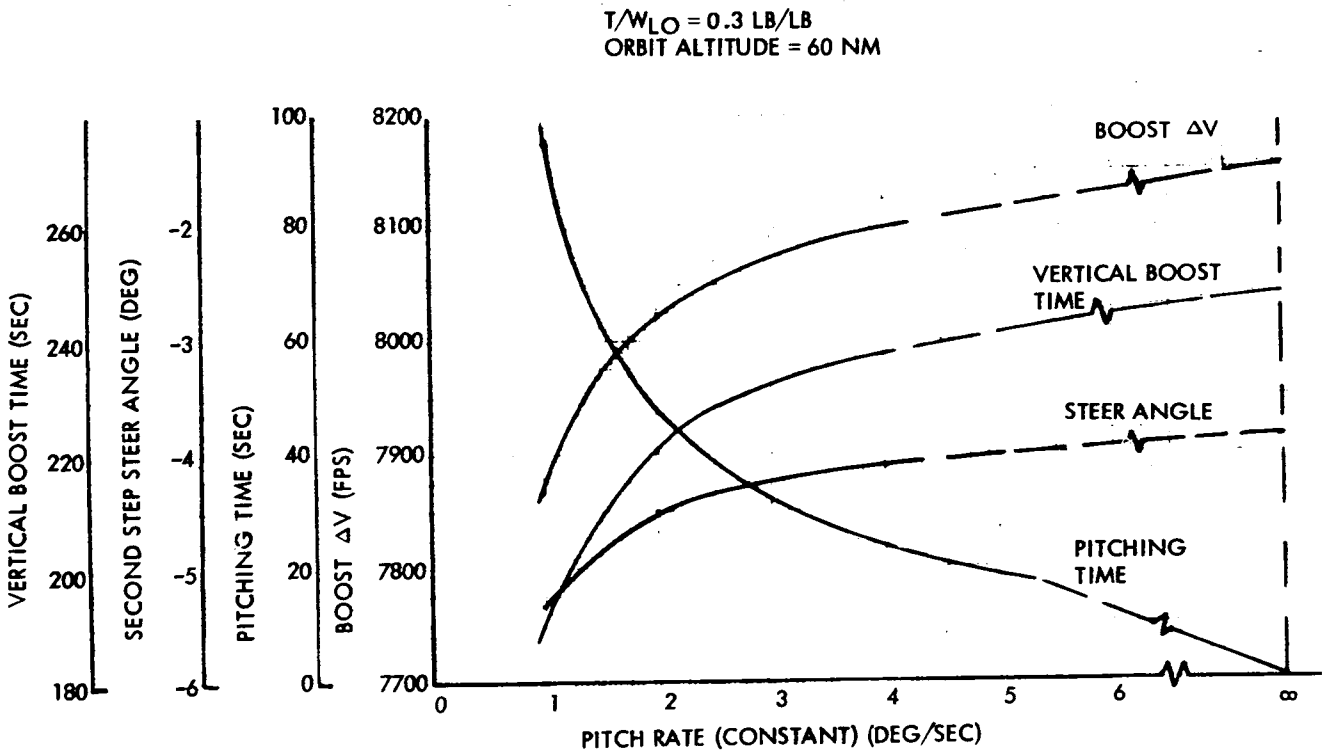

Figure 1-15. - Variation of Two-Step LESS Boost Parameters With Pitch Rate Used During Pitch Maneuver

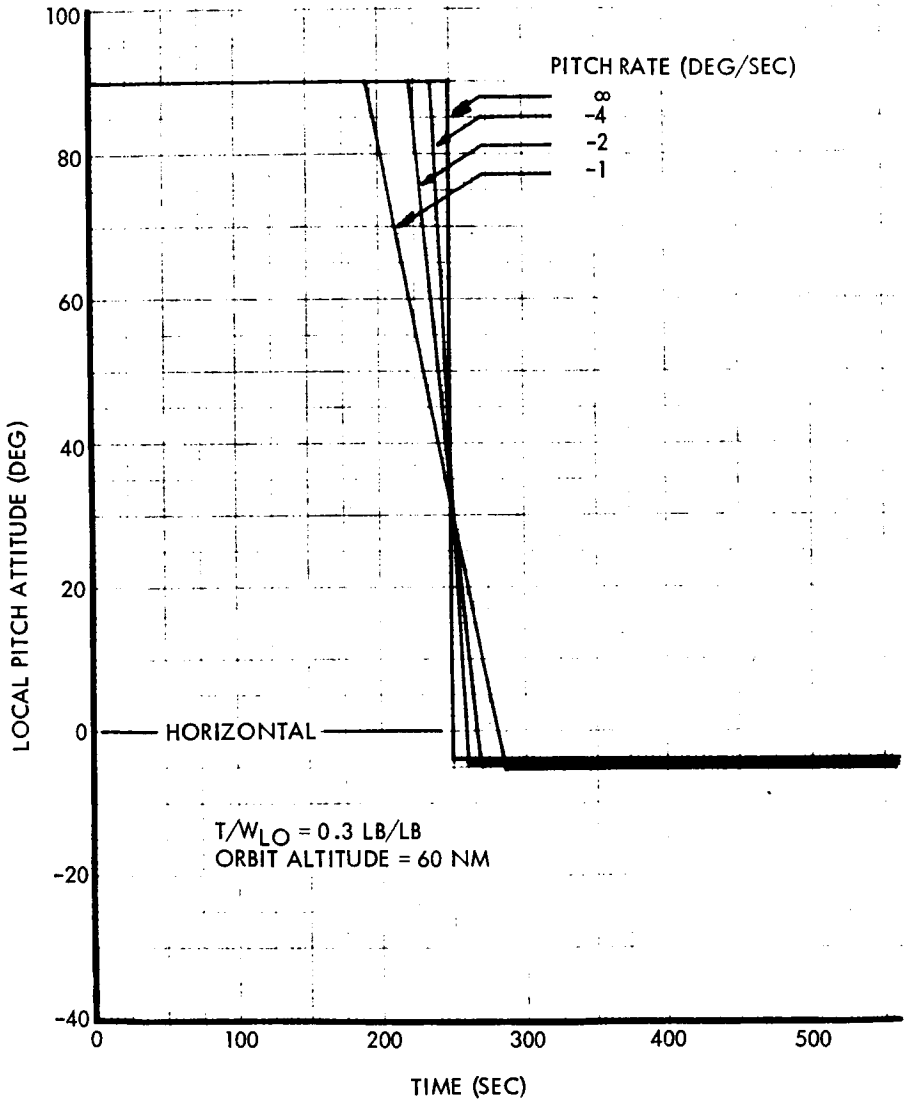

Figure 1-16. - Variation of Two-Step Attitude Profile With Pitch Rate

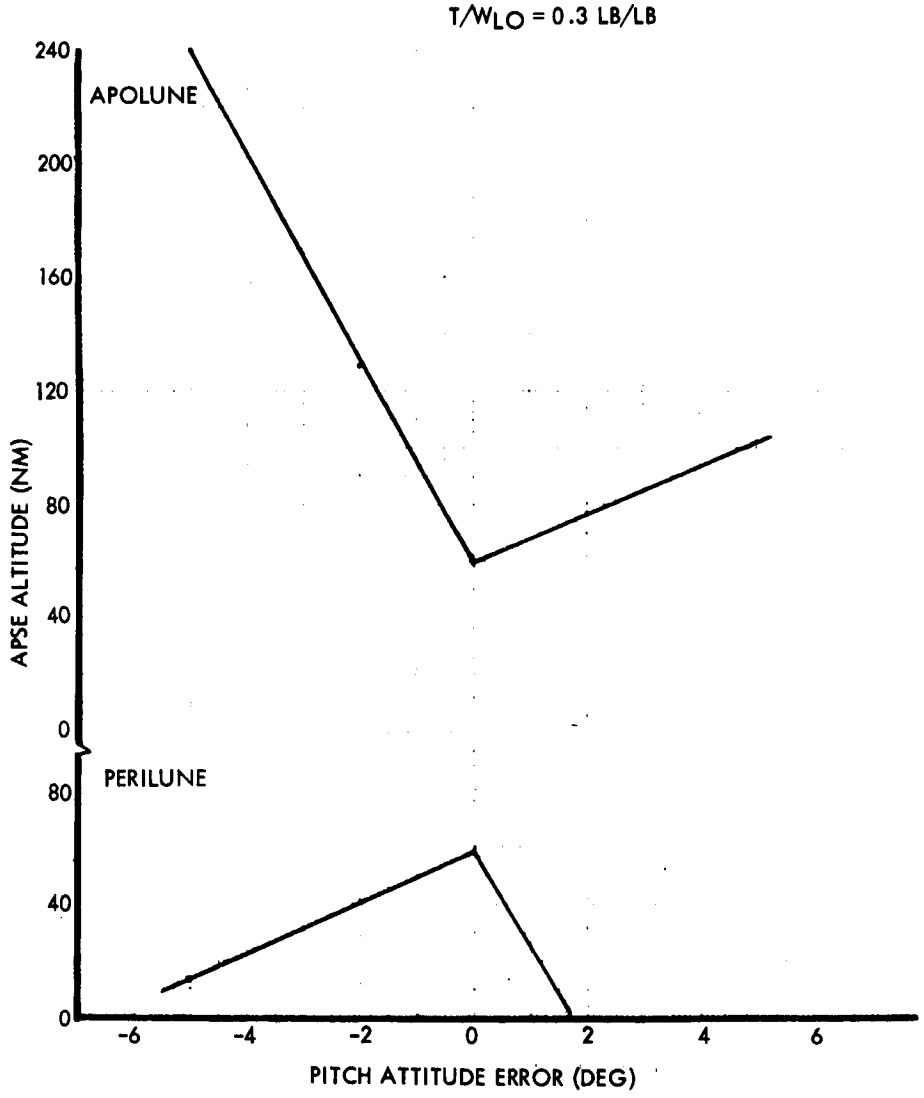

Figure 1-17. - Variation of Apse Altitude With Pitch Attitude Errors for Two-Step Boost to Near 60-Nautical-Mile Orbit

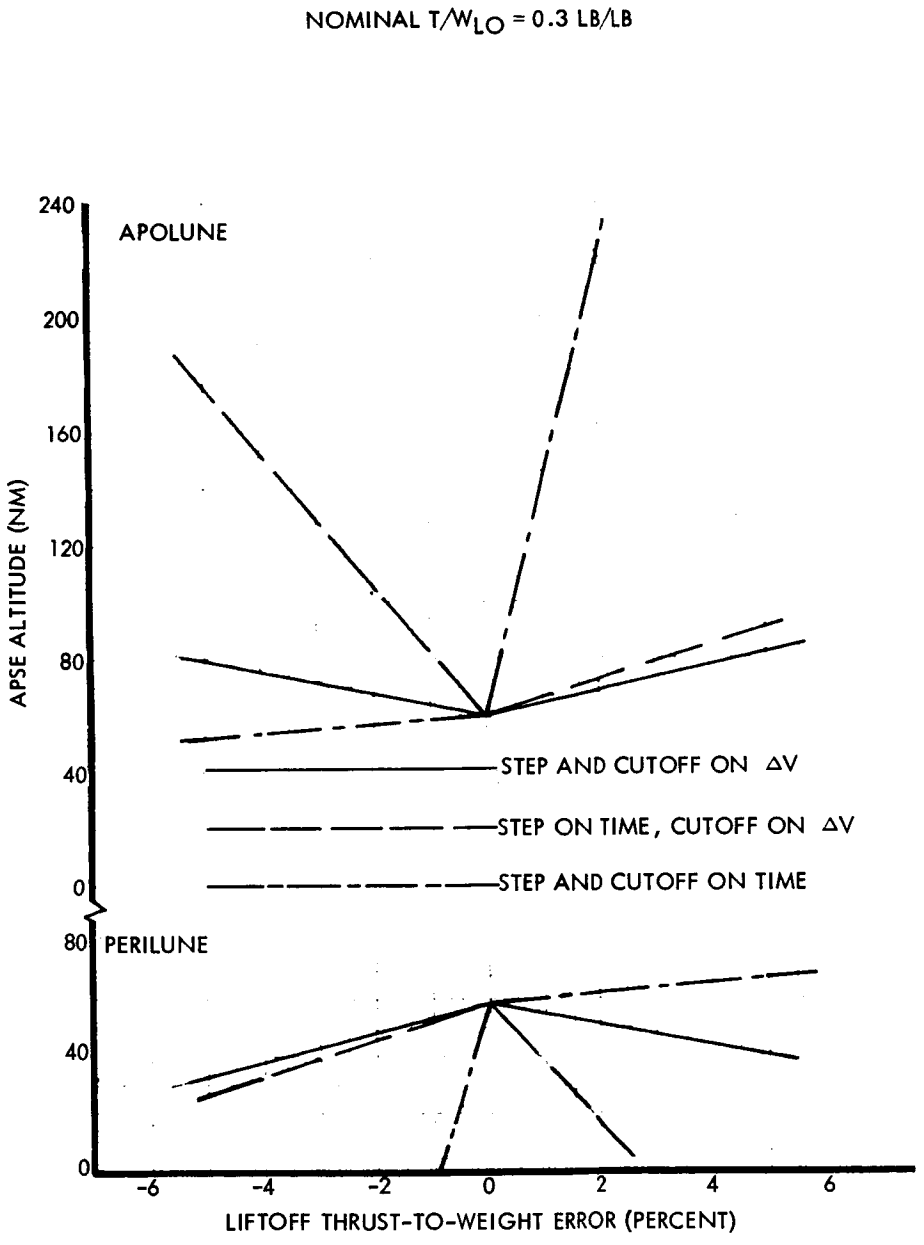

Figure 1-18. - Variation of Apse Altitude With Errors in Liftoff Thrust-to-Weight Ratio for Two-Step Boost to Near 60-Nautical-Mile Orbit

Three-step trajectories. - If a third constant-attitude step can be introduced into the steering profile, a significant performance advantage results, compared to the two-step profile just discussed. However, it complicates analysis of the problem somewhat as there are now more degrees of freedom than there are end conditions to satisfy. For boost energy requirements to be minimized, vertical boost time should be short, as indicated in the section discussing COV trajectories. A 10 000-foot vertical rise appears to be a reasonable (but somewhat arbitrary) choice, considering lurain clearance and landmark sighting requirements. To eliminate one more degree of freedom, the criteria for switching from the second attitude step to the third were considered. One reasonable criterion is to select the step-change time such that total boost energy is minimized. With this thought in mind, a series of trajectories to 60-nm orbit was computed. Results are shown in figure 1-19. It is seen that the minima of the curves occur approximately along the line that represents an equal ΔV split between the second and third steps. For a liftoff thrust-to-weight ratio of 0.3, figure 1-20 depicts steering profiles representing an equal time split, an equal ΔV split and a case where $\Delta V_2 \approx \Delta V_3 + 1100$ fps (1100 is a representative value). Along with these three-step profiles, other typical profiles are shown, including the COV solution, a linearized solution, and a two-step profile employing a vertical boost as the first segment. The inset shows the variation in total boost energy with the number of attitude segments. A vertical boost segment is assumed for all cases. Criteria of a vertical boost of 10,000 feet and a step change such that $\Delta V_2 \approx \Delta V_3$ were used in computing trajectories for liftoff thrust-to-weight ratios ranging from 0.2 through 0.5 pound per pound and orbit altitudes ranging from 20 through 80 nm. The boost energy requirements are shown in figure 1-21 compared with those of the equivalent COV solutions. The energy penalty relative to an optimum trajectory for the higher altitude orbits is seen to be reduced from approximately 1000 feet per second for the two-step trajectories discussed previously to approximately 200 feet per second. Trajectory attitude, timing of steps, and ranges are shown in figures 1-22, 1-23, and 1-24. Figure 1-25 depicts the variation in burnout thrust-to-weight ratio (acceleration). As stated, the step change time was selected such that $\Delta V_2 \approx \Delta V_3$. The parametric results presented here could change slightly since an iteration to make $\Delta V_2 \approx \Delta V_3$ was not done. The variations, however, would be small. These data reflect a nominal specific impulse of 300 seconds. Since the boost ΔV is not strongly affected by specific impulse (fig. 1-26) the effect of, for example, a lower specific impulse would be to make boost time and range slightly shorter and burnout thrust-to-weight ratio slightly higher.

A typical ascent trajectory is depicted in figure 1-27. The trajectory is initiated with a liftoff thrust-to-weight ratio of 0.3 pound per pound and results in a 60-nm circular orbit. The trajectory tends to be smoother than the two-step trajectory. The slope of the velocity curve changes at the step change point, but it does not go negative, as occurs in the simple two-step profile.

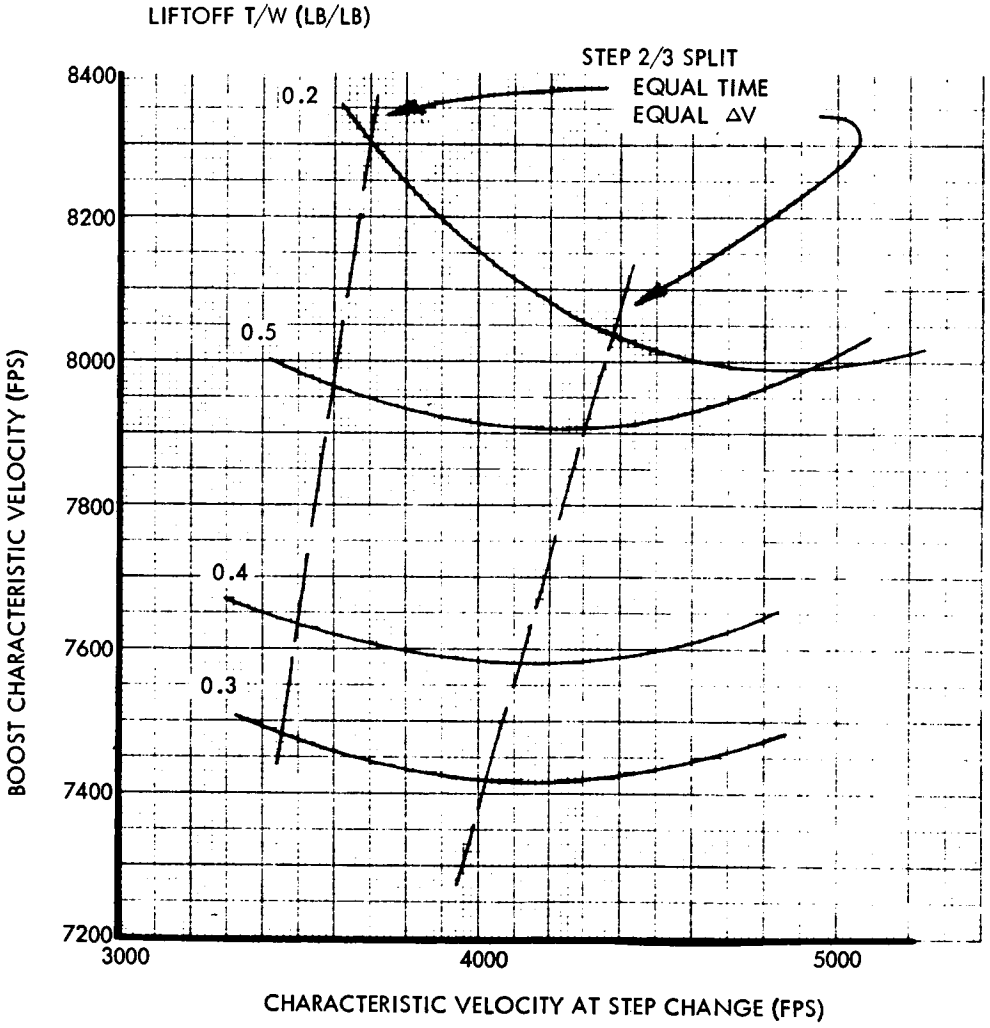

Figure 1-19. - Effect of Step Time Selection on Energy Requirements for Three-Step LESS Steering Profiles

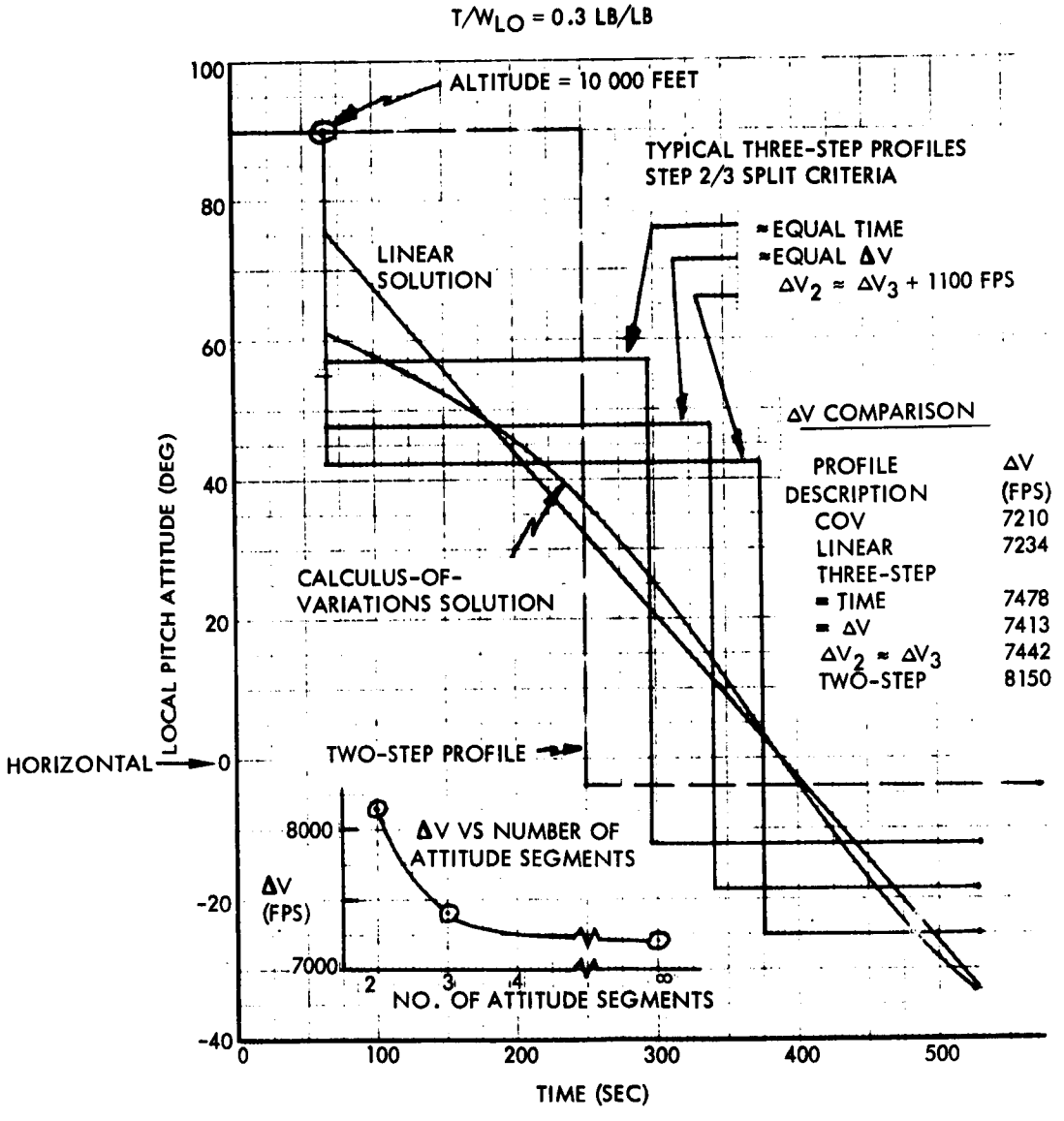

Figure 1-20. - Comparison of Steering Histories for LESS Boost to 60-Nautical-Mile Orbit

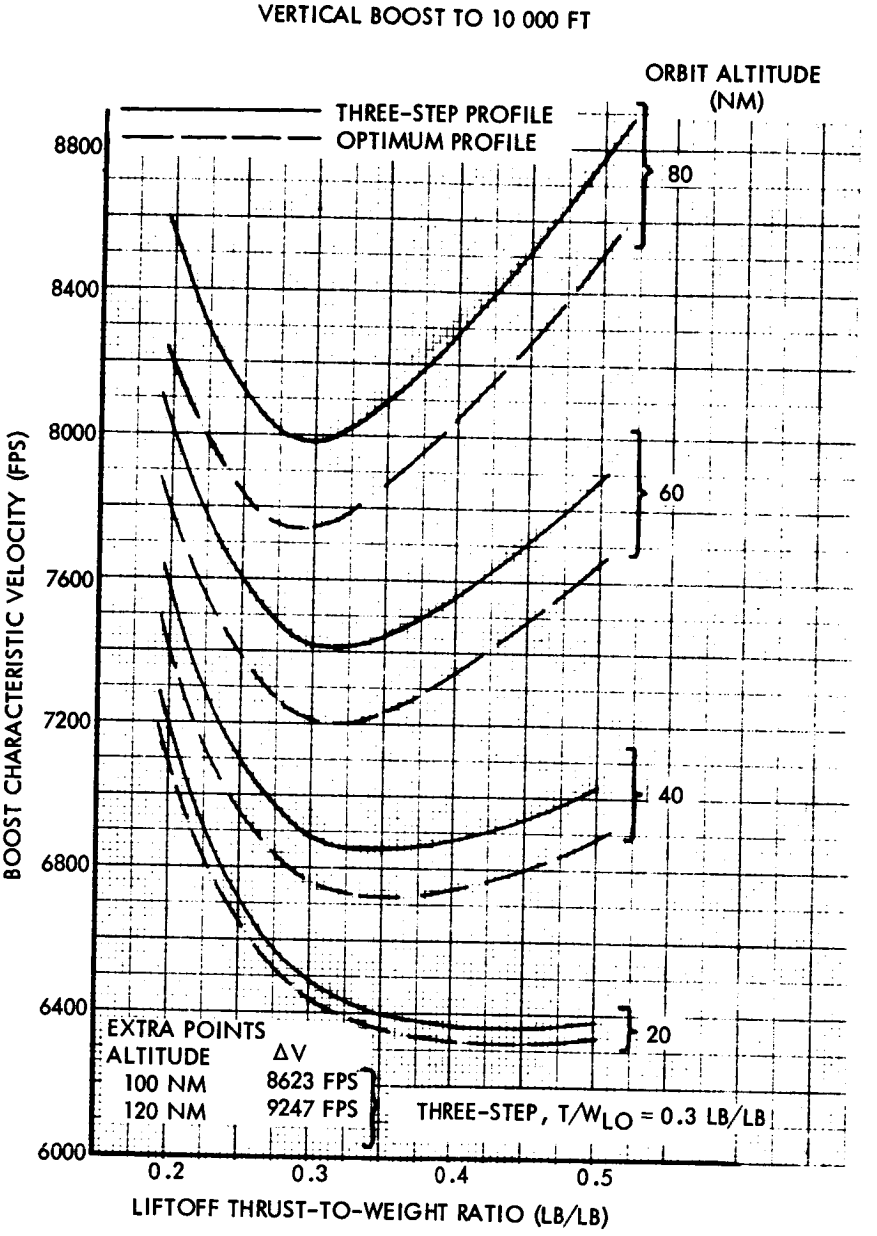

Figure 1-21.- Comparison of Energy Requirements for Three-Step LESS Steering Profile With Requirements for Optimum

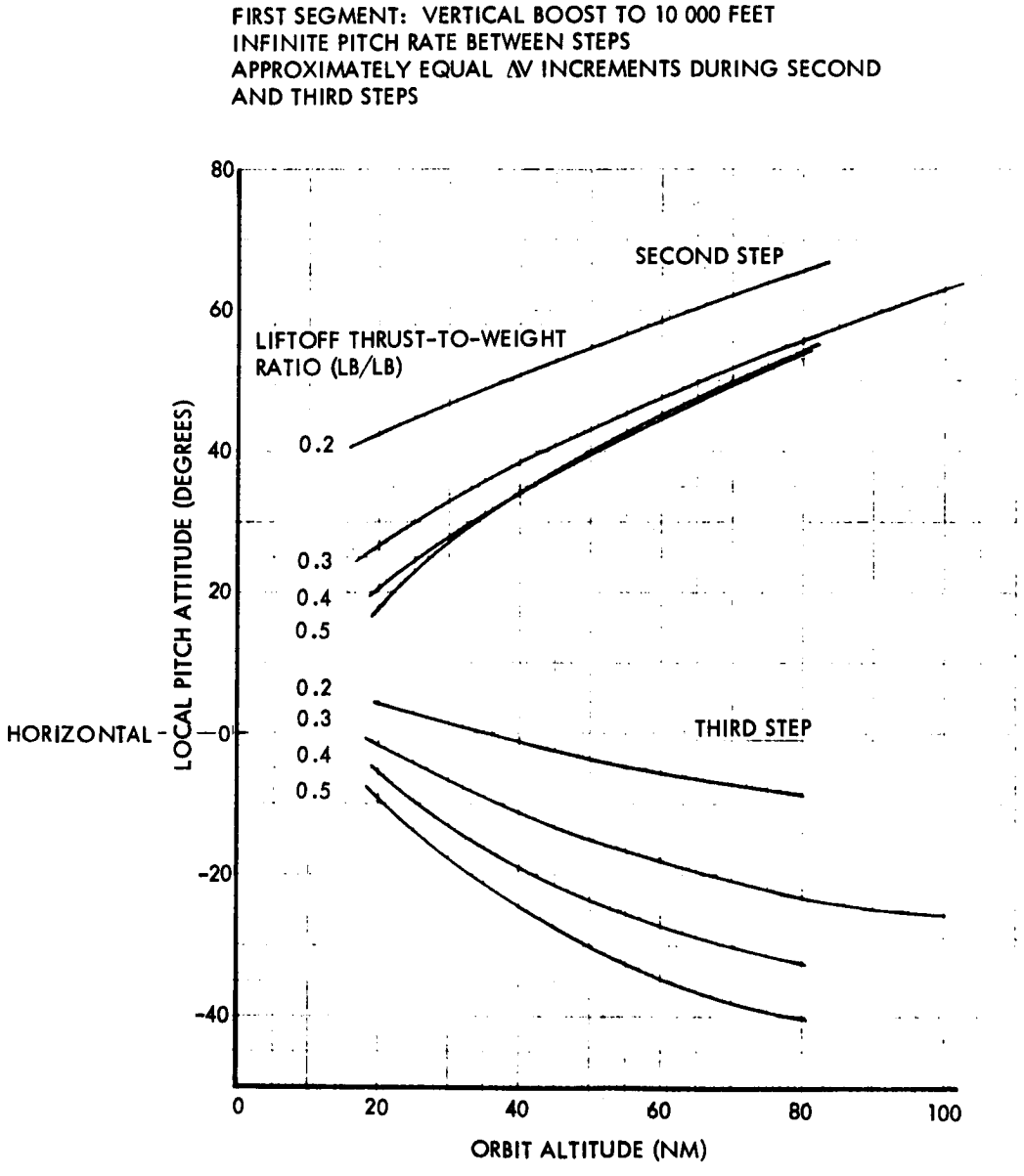

Figure 1-22. - Variation of Constant Pitch Attitude Segments for Three-Step LESS Steering Profile

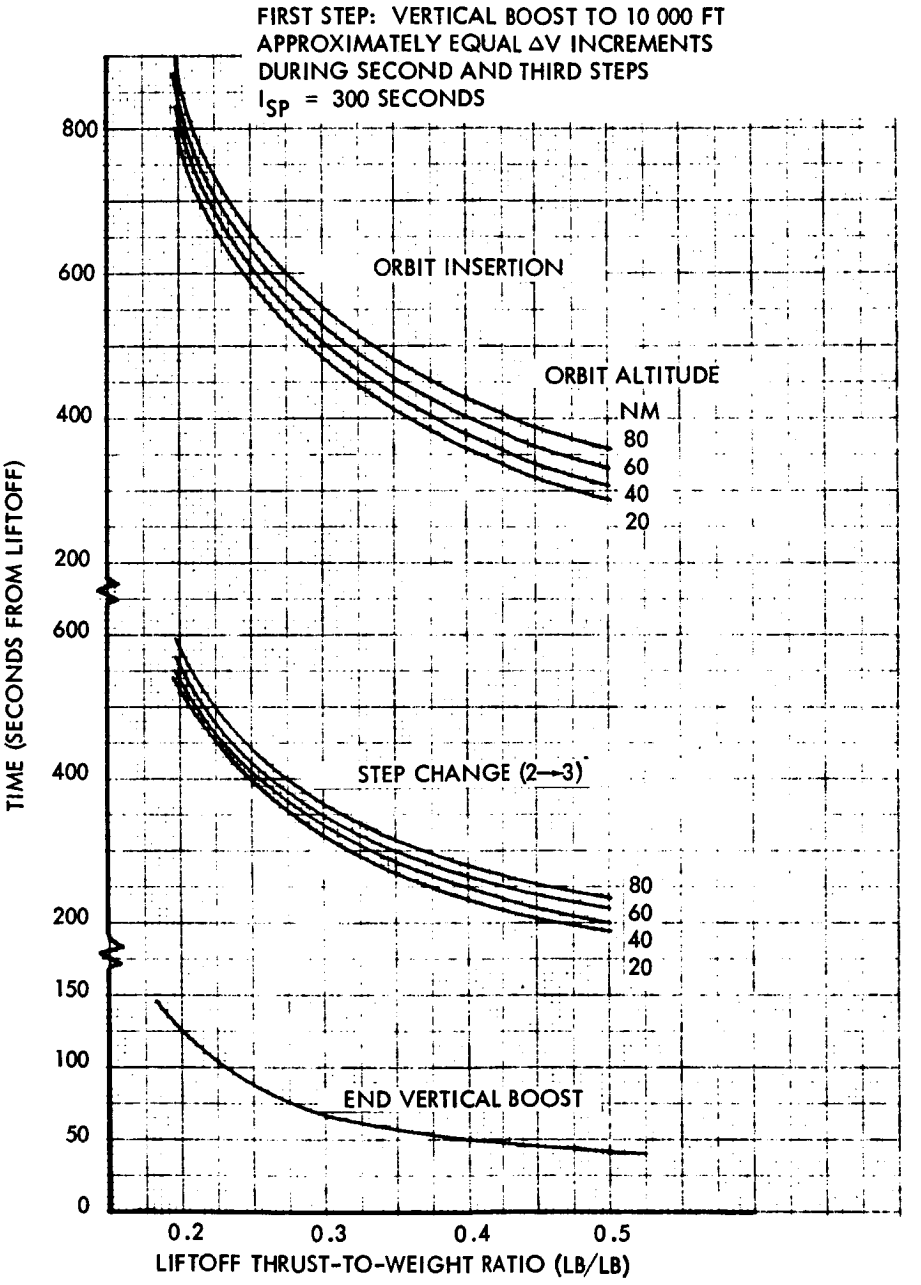

Figure 1-23. - Timing of Key Events During Three-Step LESS Boost Profile

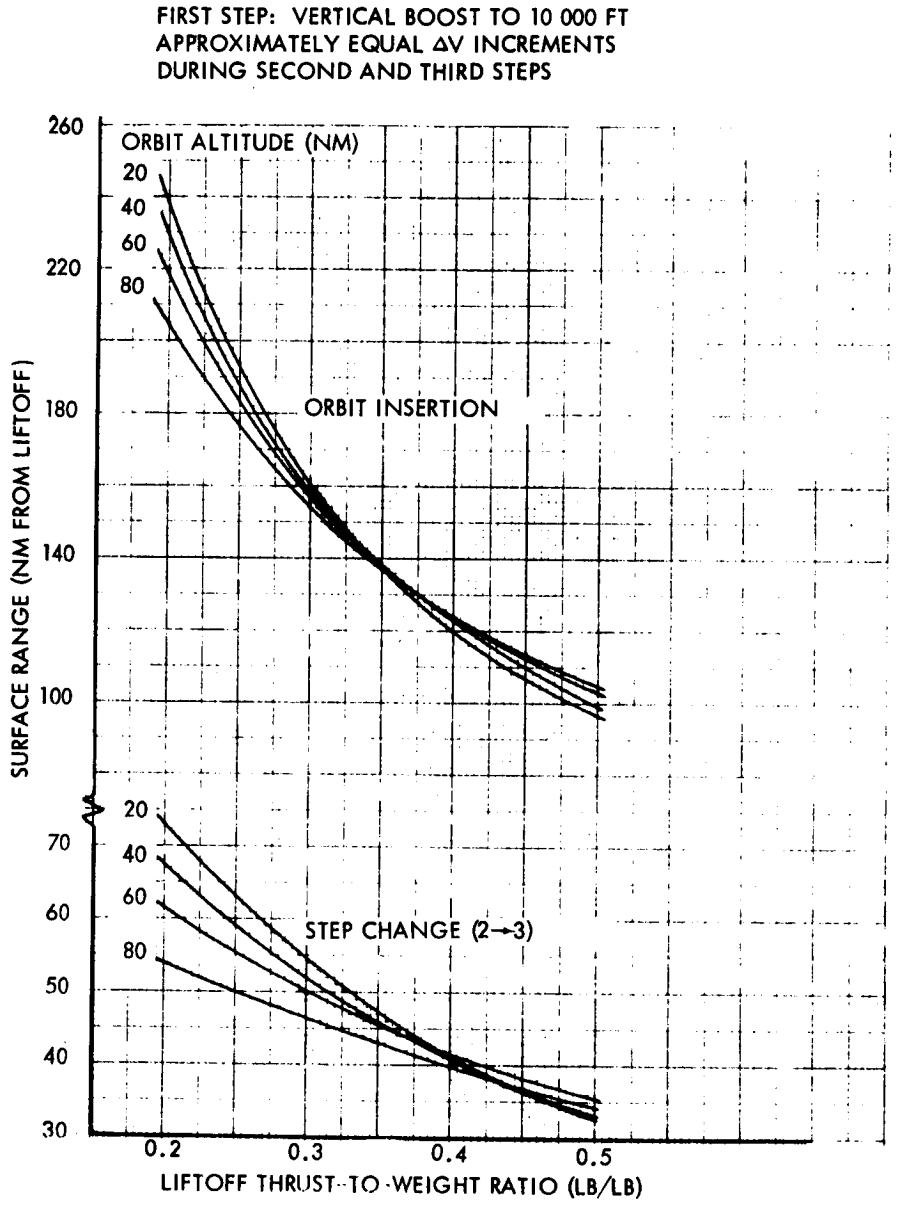

Figure 1-24. - Range at Key Events During Three-Step LESS Boost

I_{SP} = 300 SEC
FIRST STEP: VERTICAL BOOST TO 10 000 FT
APPROXIMATELY EQUAL ΔV INCREMENTS
DURING SECOND AND THIRD STEPS

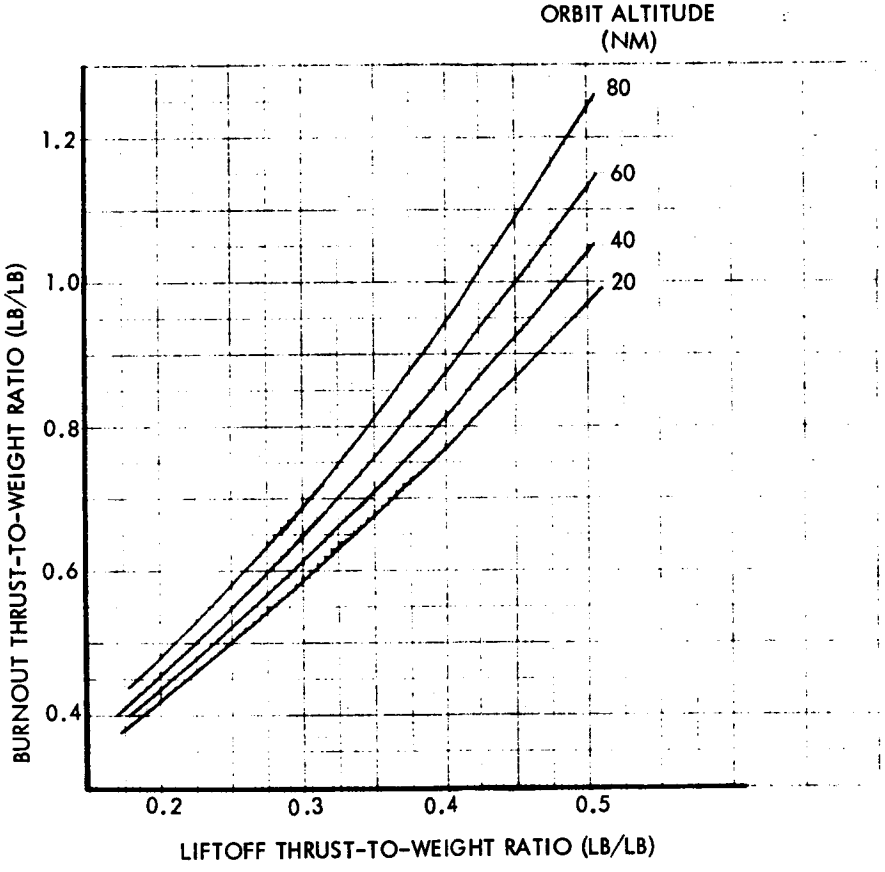

Figure 1-25. - Variation of Burnout Acceleration for Three-Step LESS Boost

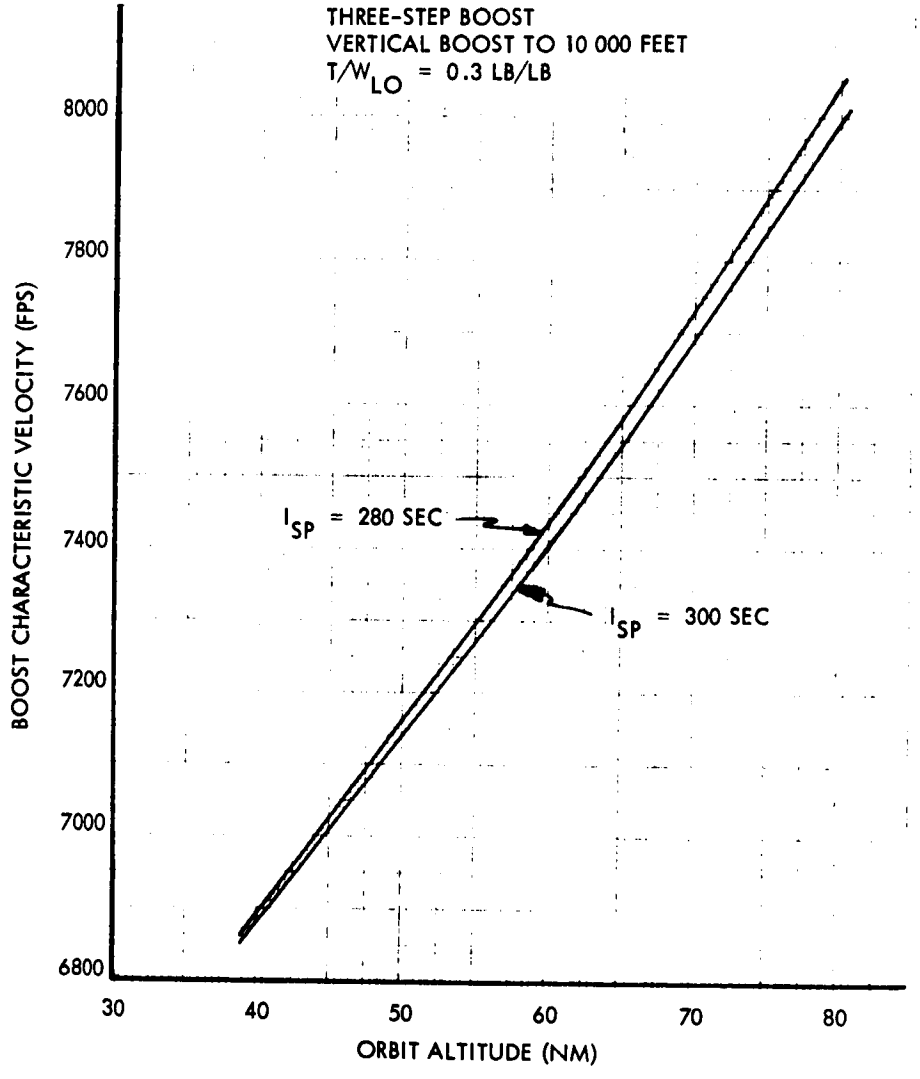

Figure 1-26. - Effect of Specific Impulse on LESS Boost Energy Requirements

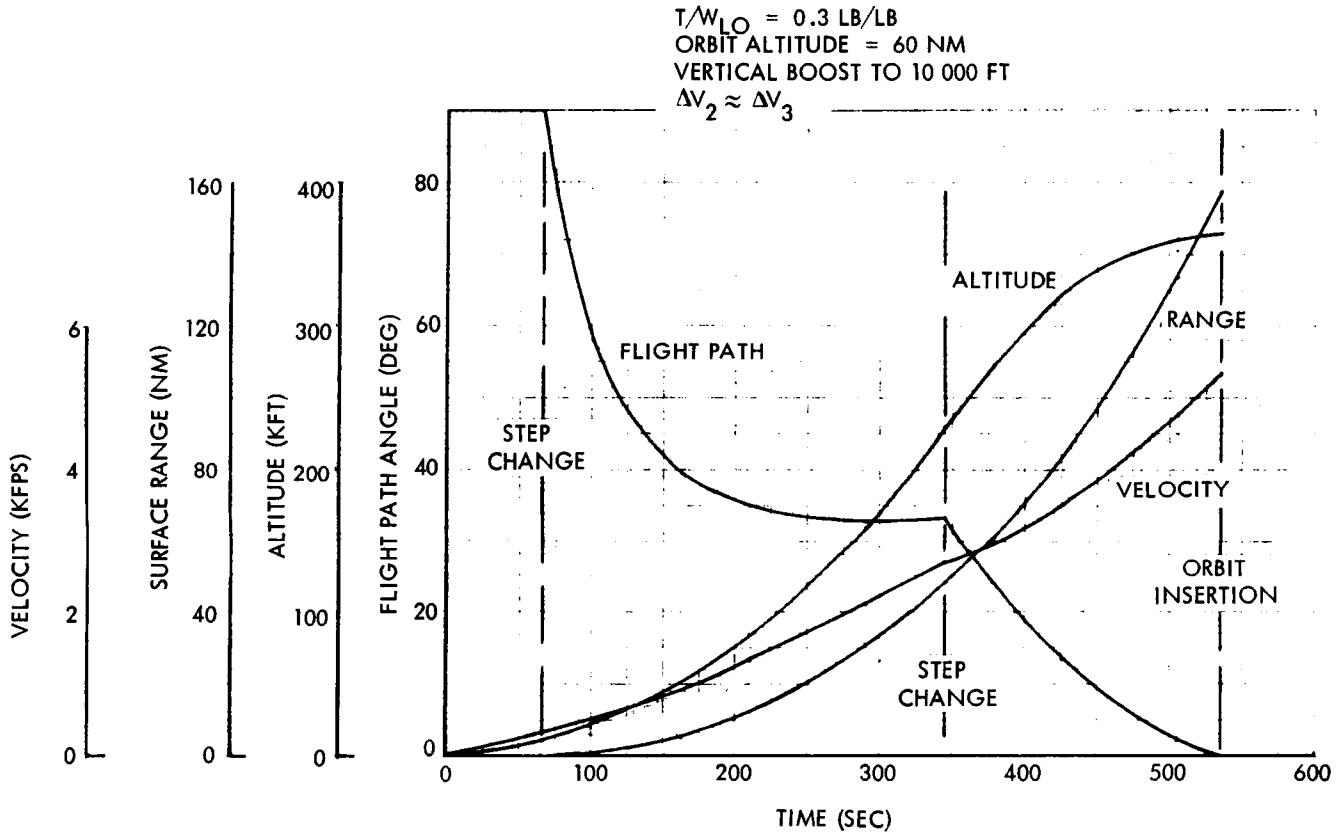

Figure 1-27. - Flight Parameters for Typical Three-Step LESS Boost

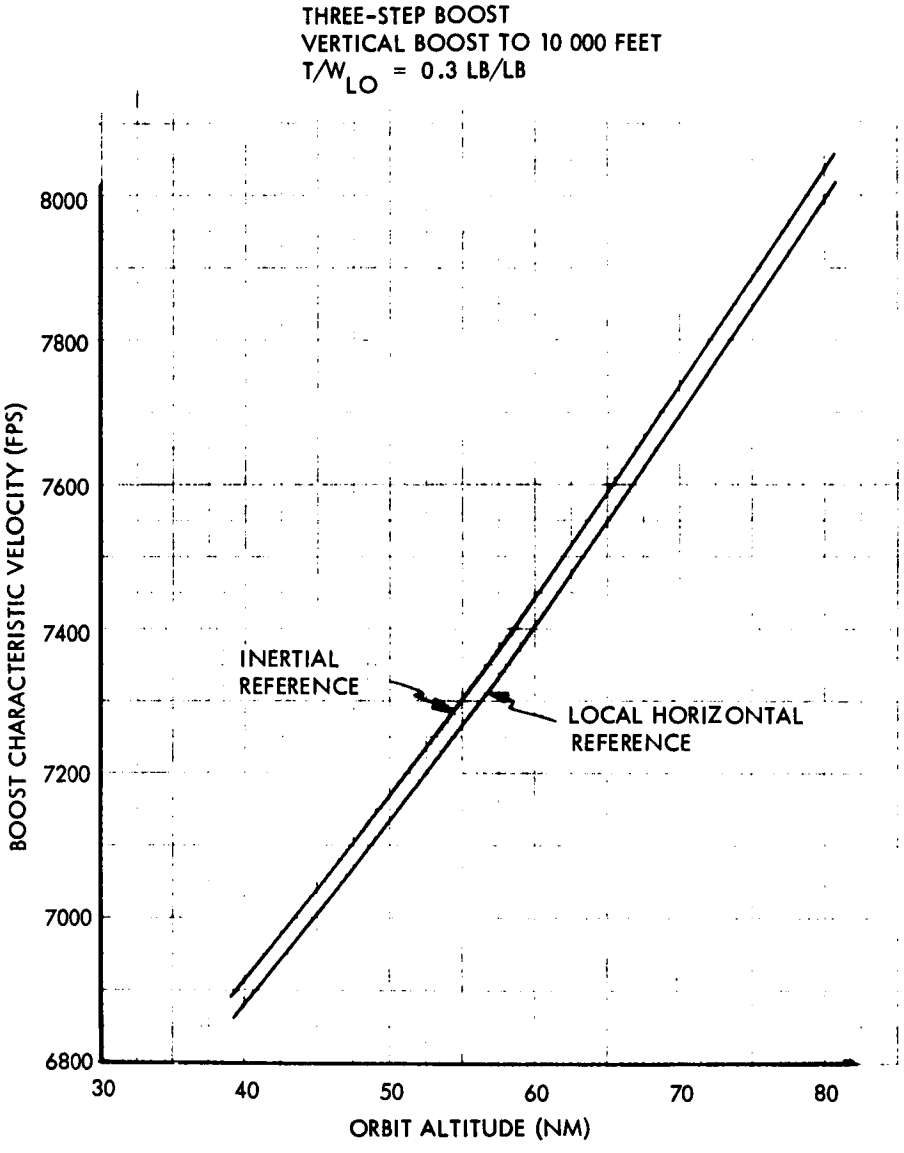

Figure 1-28. - Comparison of Boost Energy Requirements for Steering Three-Step LESS Profile to Inertial Reference With Those for Steering to Local Horizontal Reference

Some variation in boost energy requirements with specific impulse is indicated in figure 1-26. The variation is seen to be quite small. Note that it is the variation in ΔV that is illustrated and that the propellant requirements will vary more strongly with specific impulse. Figure 1-28 indicates little variation in boost energy requirements if an inertial attitude reference is used. The reference frame on which all data in this report are based is the local horizontal (the normal to the radius to the center of the Moon).

The preceding data are based on infinite pitch rates at the junctions of the attitude segments. A closer approximation to the real situation is to join the attitude segments by "ramps." Figure 1-29 depicts the variations in control parameters, with the pitch rate used to simulate the pitchovers for boost to 60-nm orbit with a liftoff thrust-to-weight ratio of 0.3 pound per pound. As with the two-step profile, there is a modest saving in energy if slow pitch rates can be used.

Figures 1-30 through 1-54 involve the variation in burnout conditions with errors in some of the salient LESS parameters for three-step boost profiles. The family of nominal boost trajectories includes ascent to orbits of 20, 40, 60, and 80 nm initiated by liftoff thrust-to-weight ratios of 0.2, 0.3, 0.4 and 0.5 pound per pound. The data are all based on open-loop trajectory simulations; that is, there is no updating of steering information based on knowledge of the actual trajectory being produced. The target orbits are circular.

Figures 1-30 through 1-32 depict the variation in apse altitudes with pitch attitude error. An error of, for example, plus two degrees is here taken to mean that a constant bias of two degrees in thrust application angle is applied from liftoff to cutoff. Cutoff occurs at the nominal ΔV, which, since all other parameters are nominal, is the same as saying cutoff occurs at the nominal time. The data indicate a stronger variation in perilune altitude with positive errors than with equivalent negative errors. The tendency with a positive error is for the trajectory to follow a steeper path than nominal, thereby incurring larger energy losses and resulting in a lower energy orbit. Since the burnout point is higher than nominal and has a positive flight path angle (all because the total trajectory was steeper), apolune will be somewhat higher than the target orbit, and perilune will be significantly lower as indicated. This situation could be relieved somewhat by employing a slight overburn to raise perilune. Abiding by our assumption of no feedback information, this does not appear feasible. However, if the target orbit were to be elliptical, with burnout at the nominal perilune, there would automatically be an overburn with respect to circular conditions. It will be seen in a following section that this technique does offer some advantages. Figure 1-33 illustrates the variation in the in-plane burnout parameters for a typical case.

Figures 1-34 through 1-42 depict the variation in apse altitudes with liftoff thrust-to-weight ratio errors. Figures 1-34, 1-35, and 1-36 show their

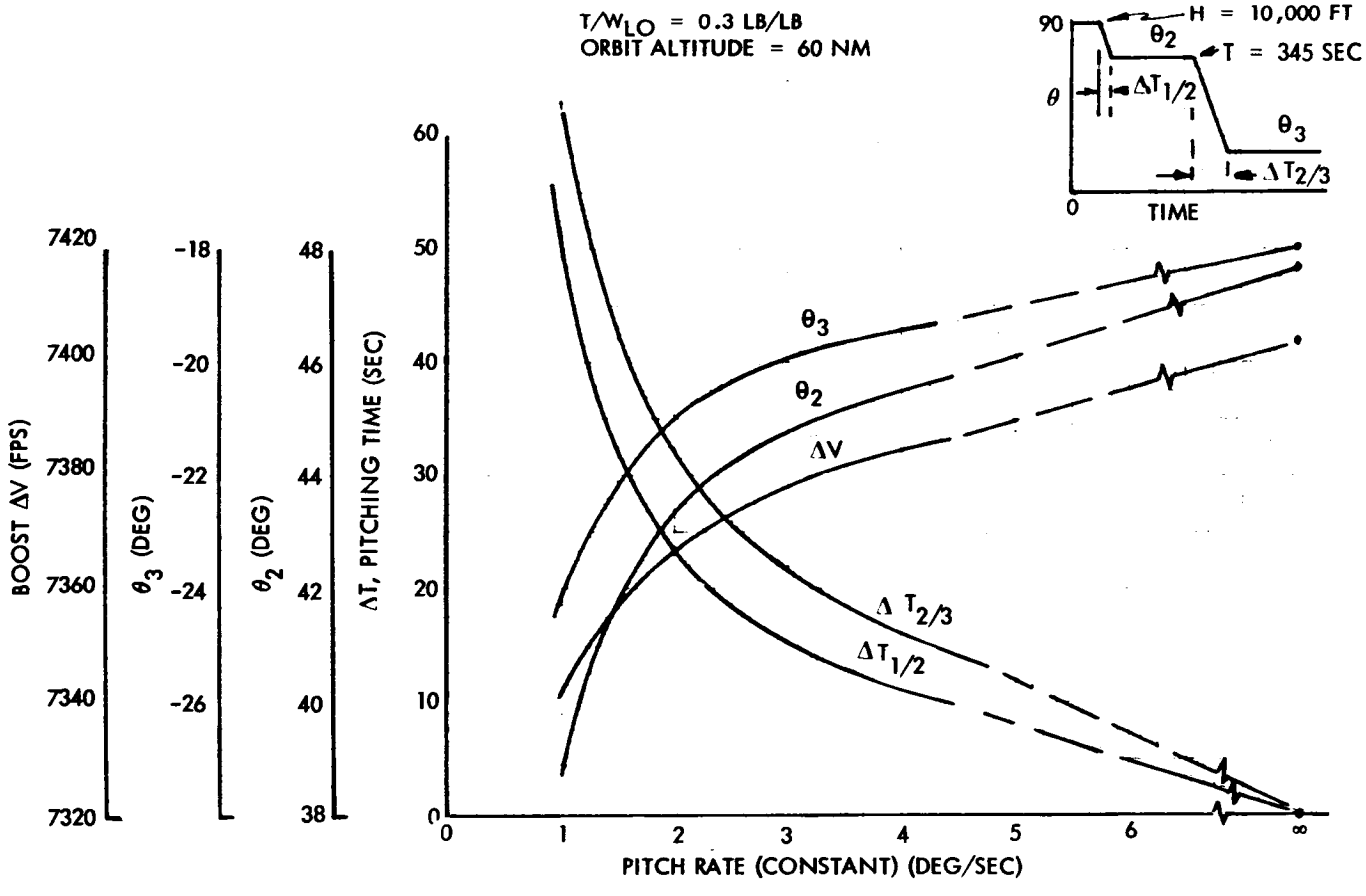

Figure 1-29. - Variation of Three-Step LESS Boost Parameters With Pitch Rate Used During Pitch Maneuvers

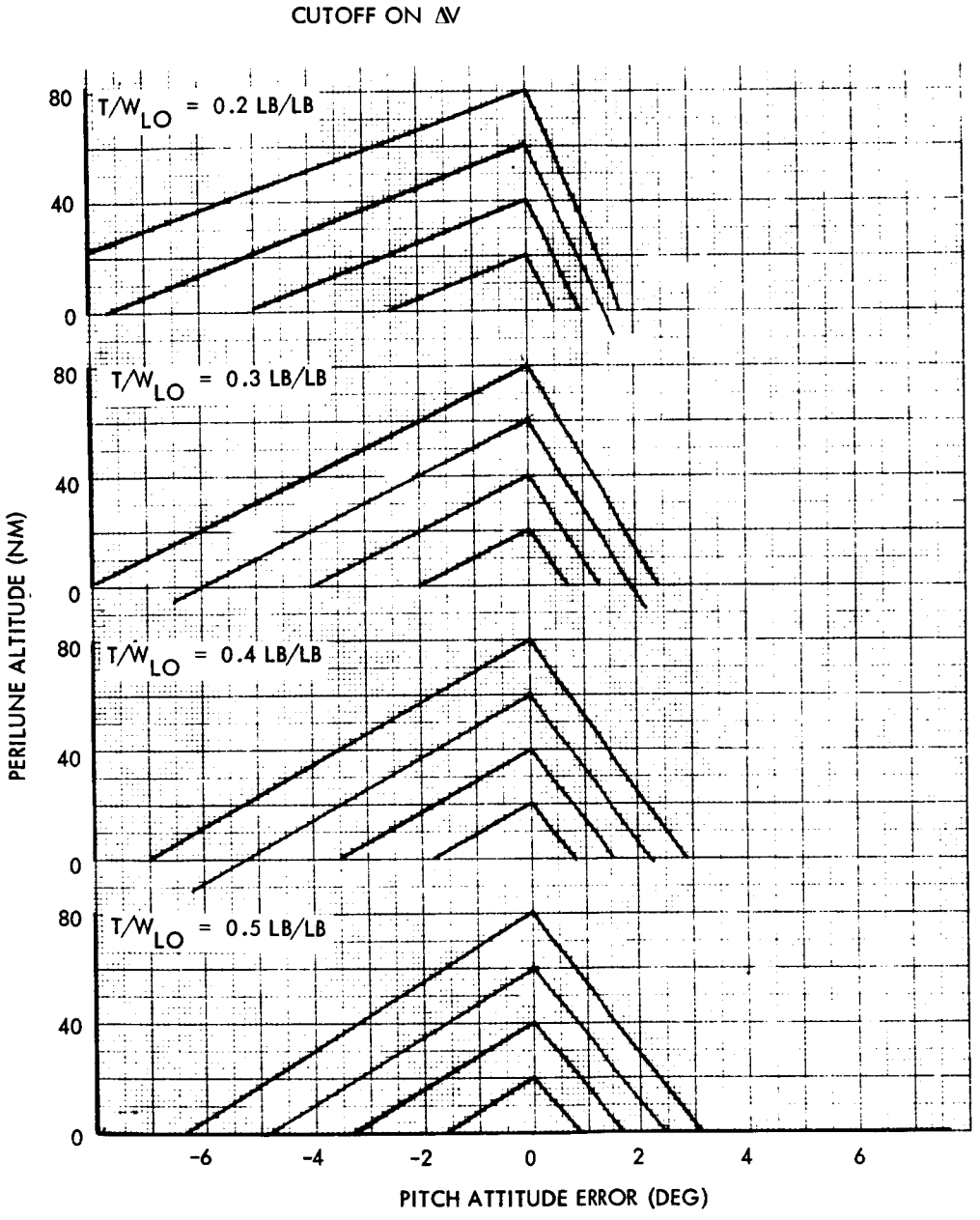

Figure 1-30. - Variation of Perilune Altitude With Pitch Attitude Error

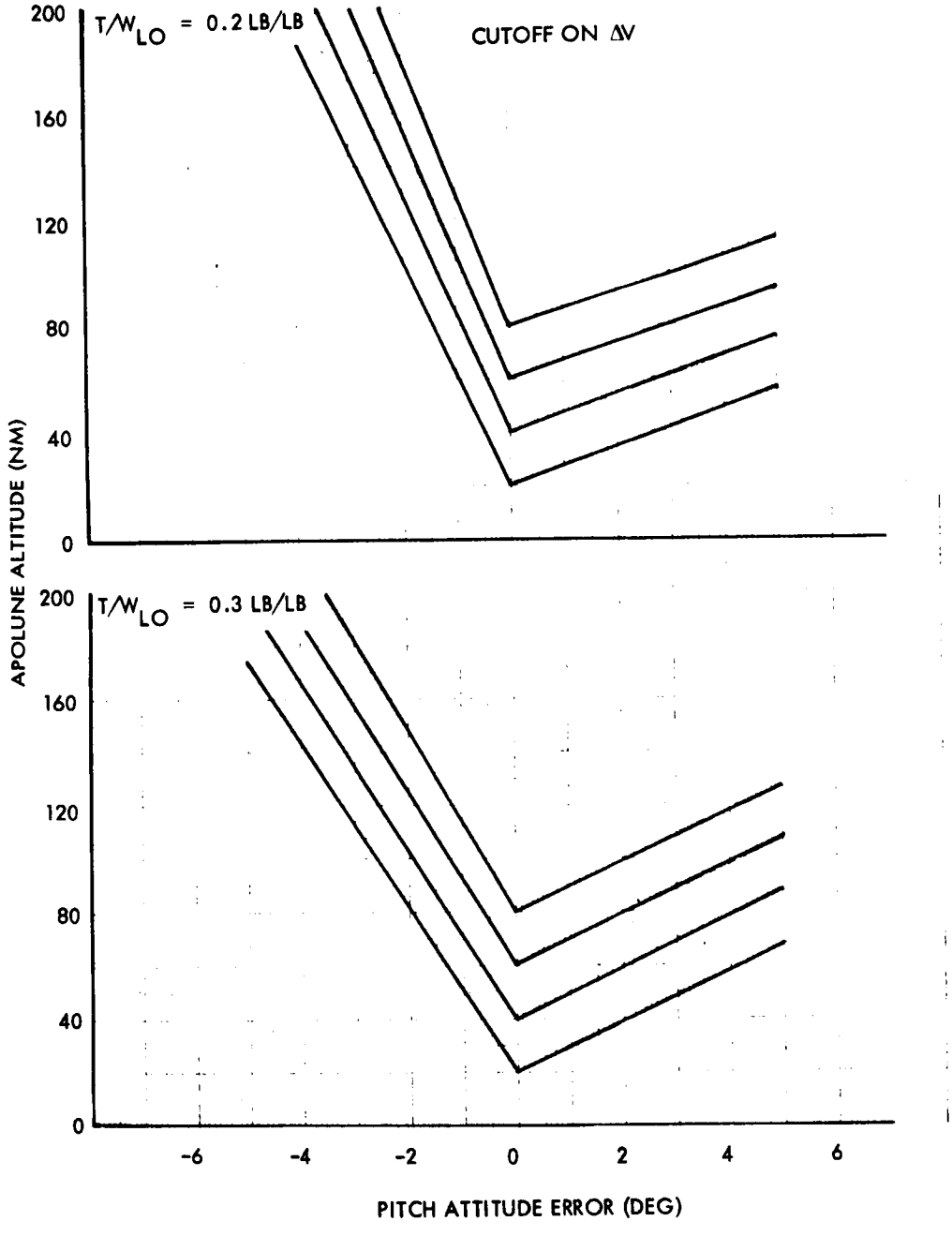

Figure 1-31. - Variation of Apolune Altitude With Pitch Attitude Error (T/W_{LO} = 0.2 and 0.3 lb/lb)

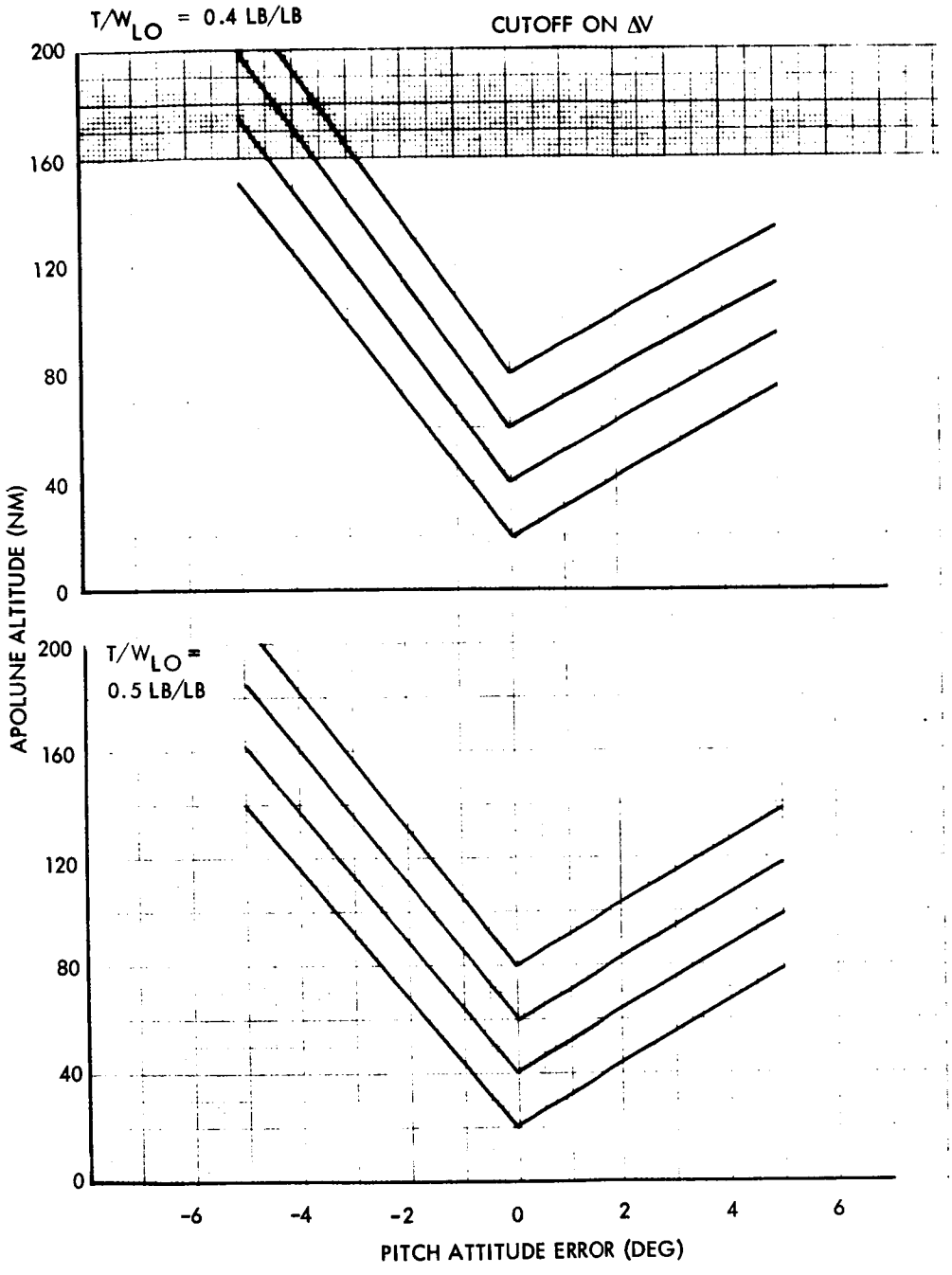

Figure 1-32. - Variation of Apolune Altitude With Pitch Attitude Error (T/W_{LO} = 0.4 and 0.5 lb/lb)

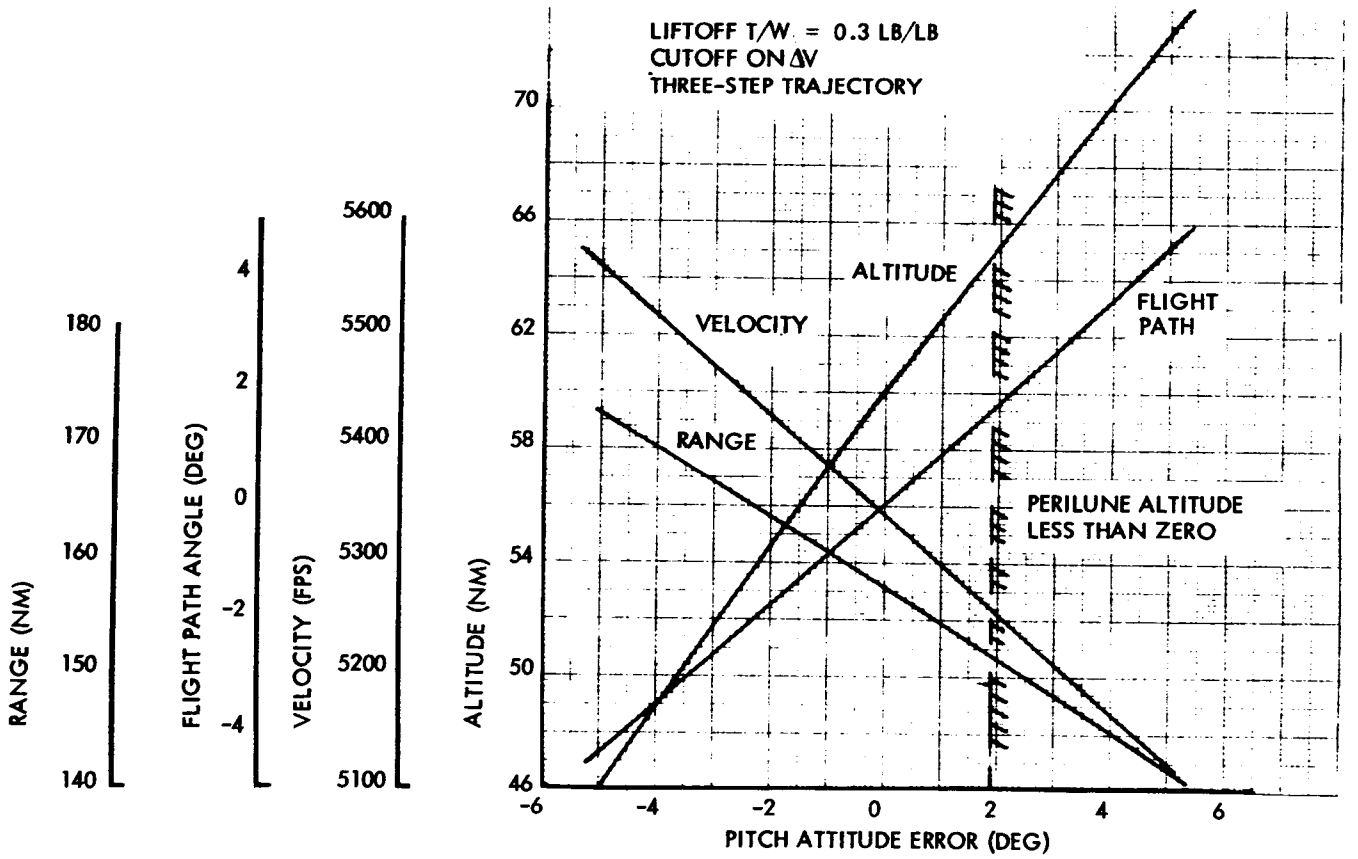

Figure 1-33.- Typical Variation of In-Plane LESS Burnout Conditions With Pitch Attitude Error (60 Nautical-Mile Orbit)

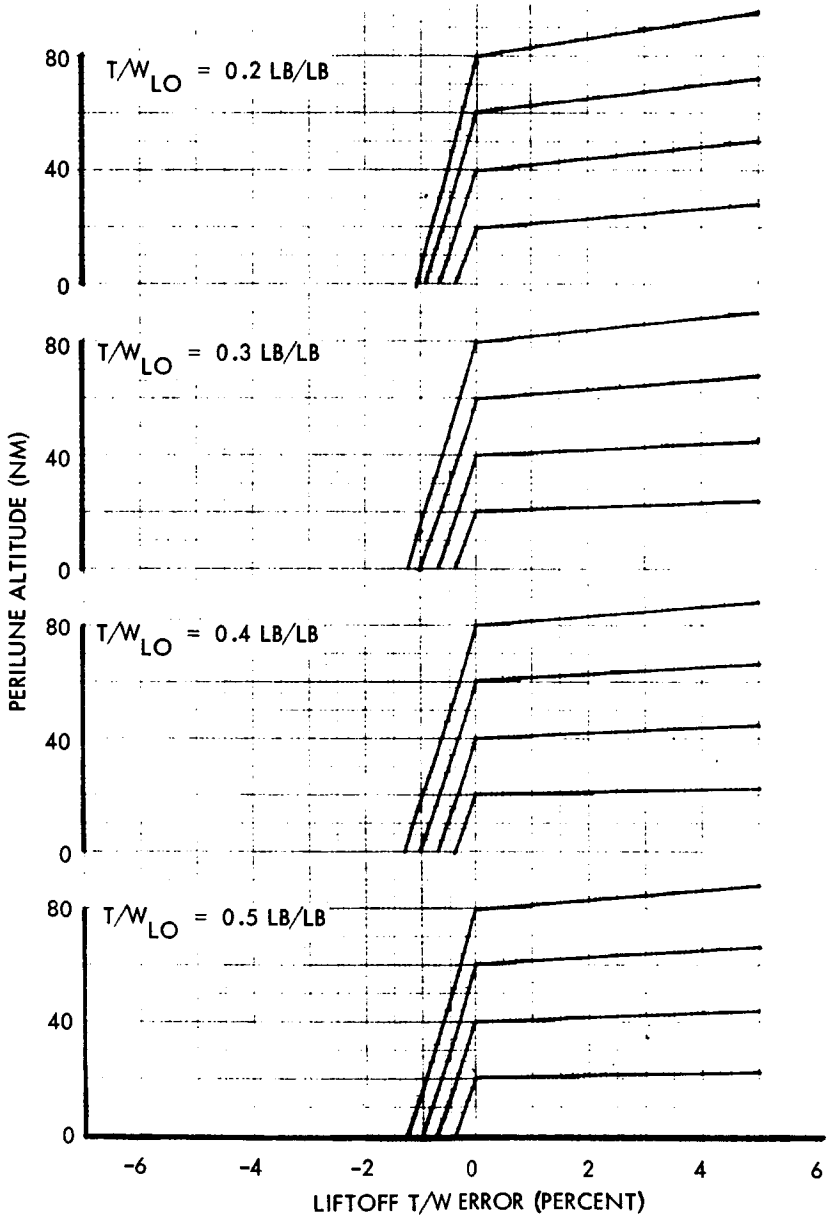

Figure 1-34. - Variation of Perilune Altitude With Liftoff Thrust-to-Weight Error, Cutoff on Time, Steps on Time

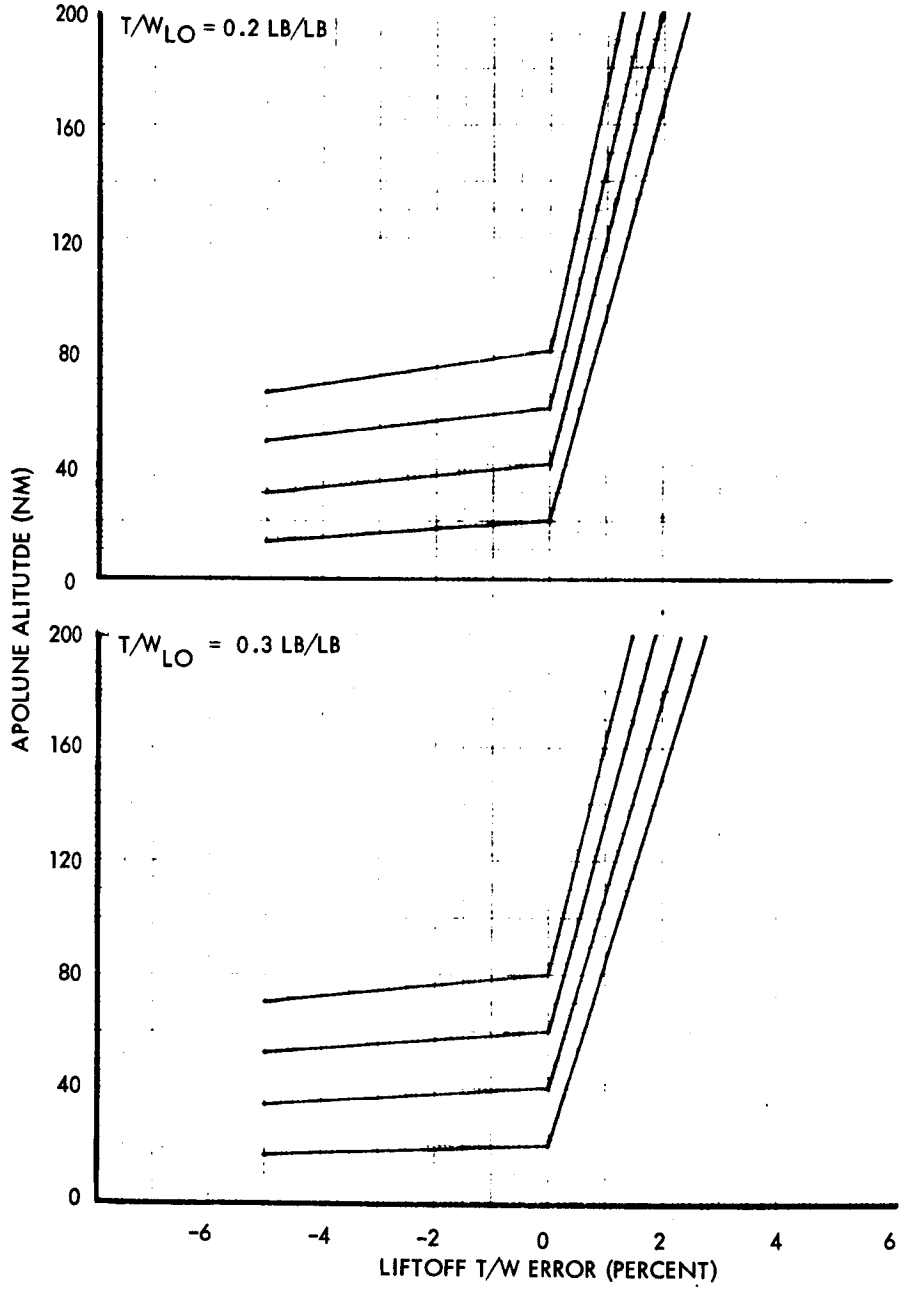

Figure 1-35. - Variation of Apolune Altitude With Liftoff Thrust-to-Weight Error (T/W_{LO} = 0.2 and 0.3 lb/lb), Cutoff on Time, Steps on Time

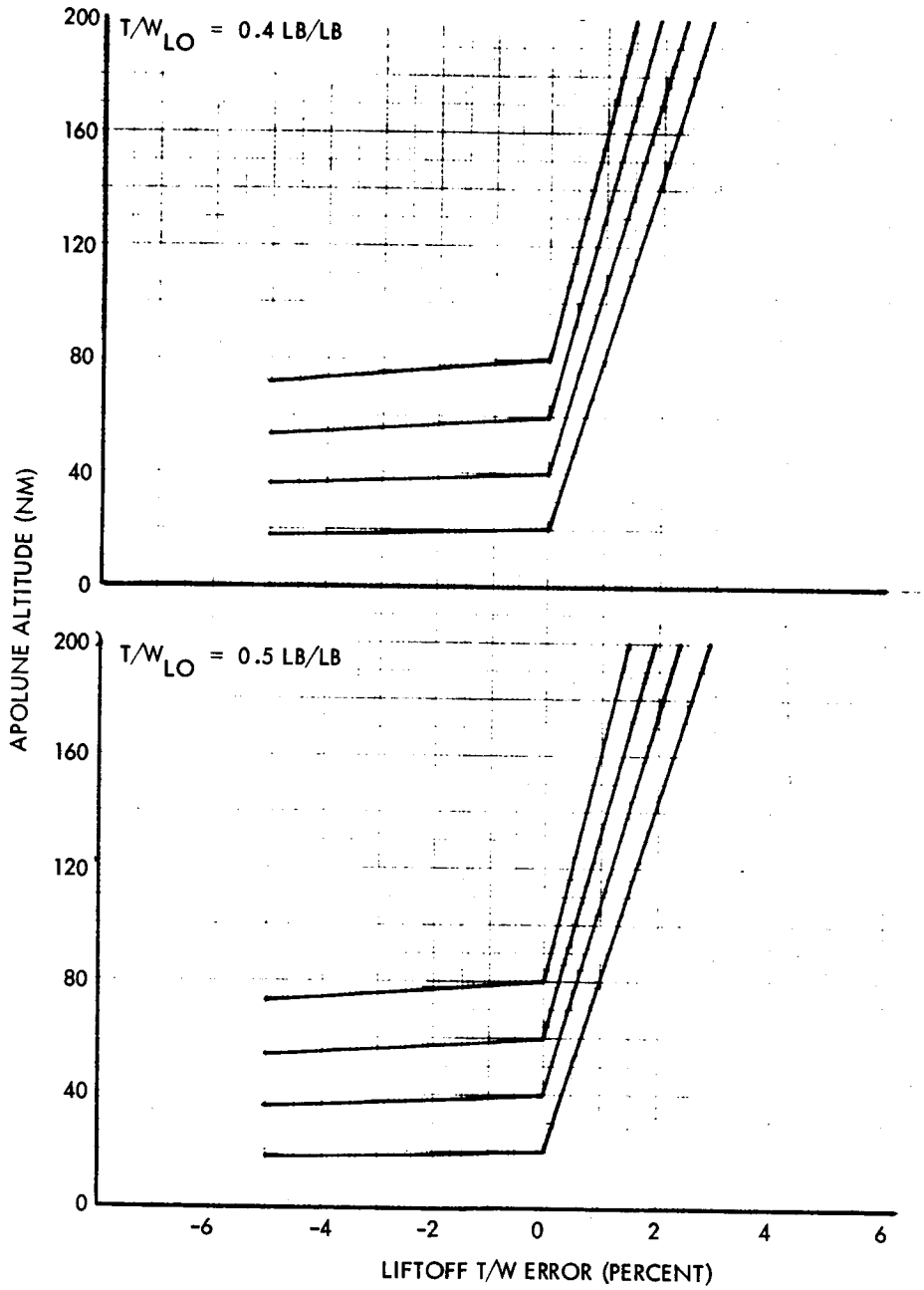

Figure 1-36. - Variation of Apolune Altitude With Liftoff Thrust-to-Weight Error (T/W_{LO} = 0.4 and 0.5 lb/lb), Cutoff on Time, Steps on Time

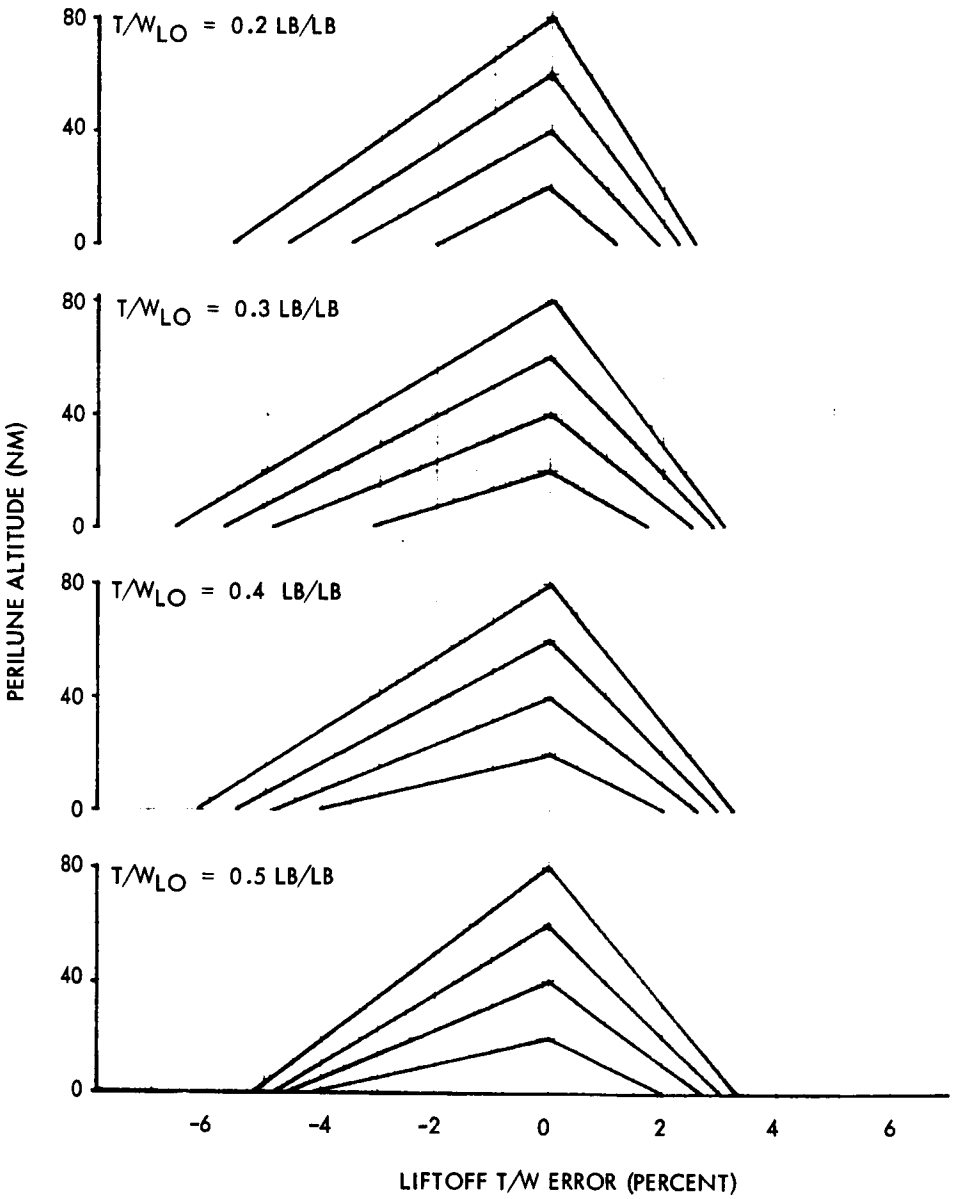

Figure 1-37. - Variation of Perilune Altitude With Liftoff Thrust-to-Weight Error, Cutoff on ΔV, Steps on Time

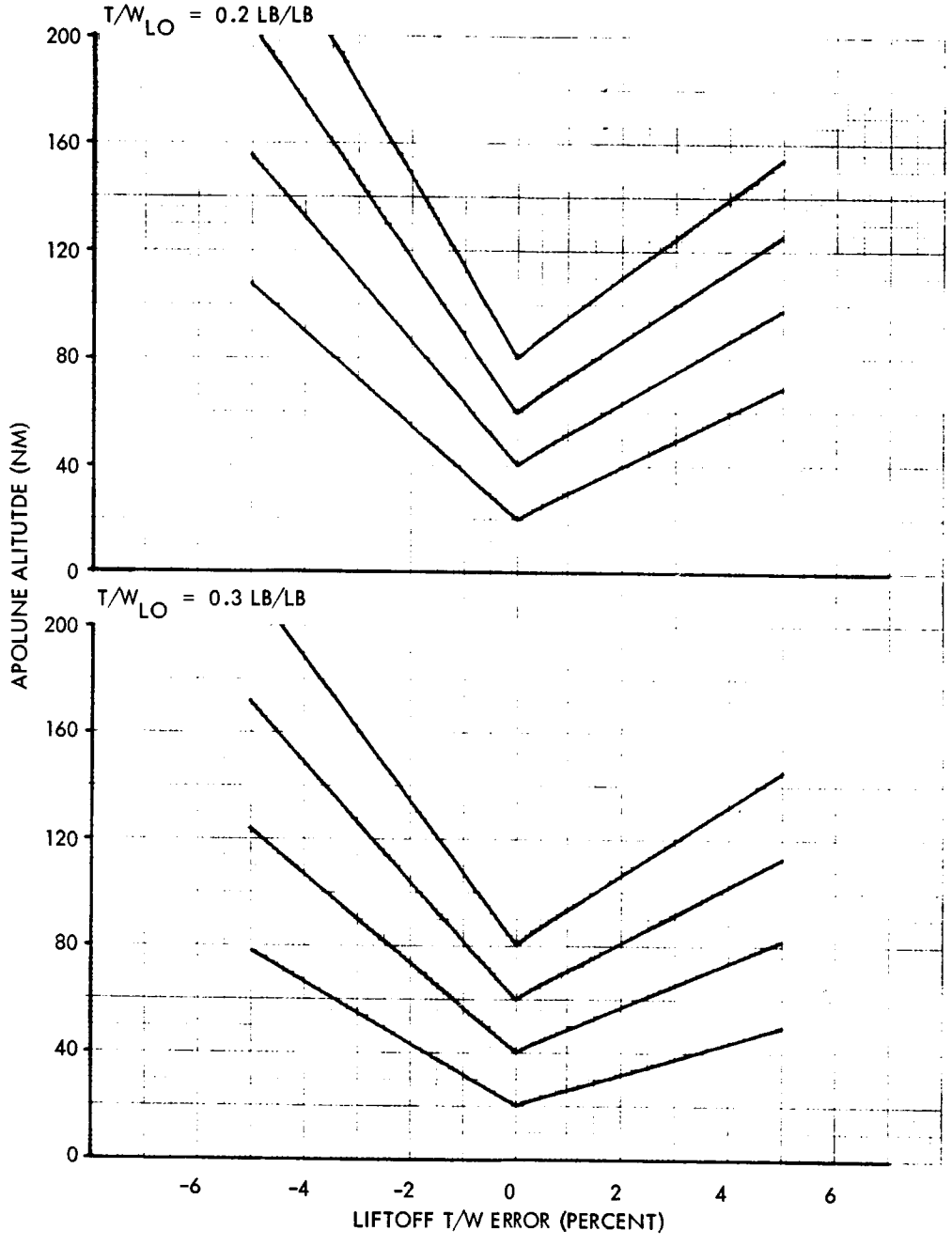

Figure 1-38. - Variation of Apolune Altitude With Liftoff Thrust-to-Weight Error (T/W_{LO} = 0.2 and 0.3 lb/lb), Cutoff on ΔV, Steps on Time

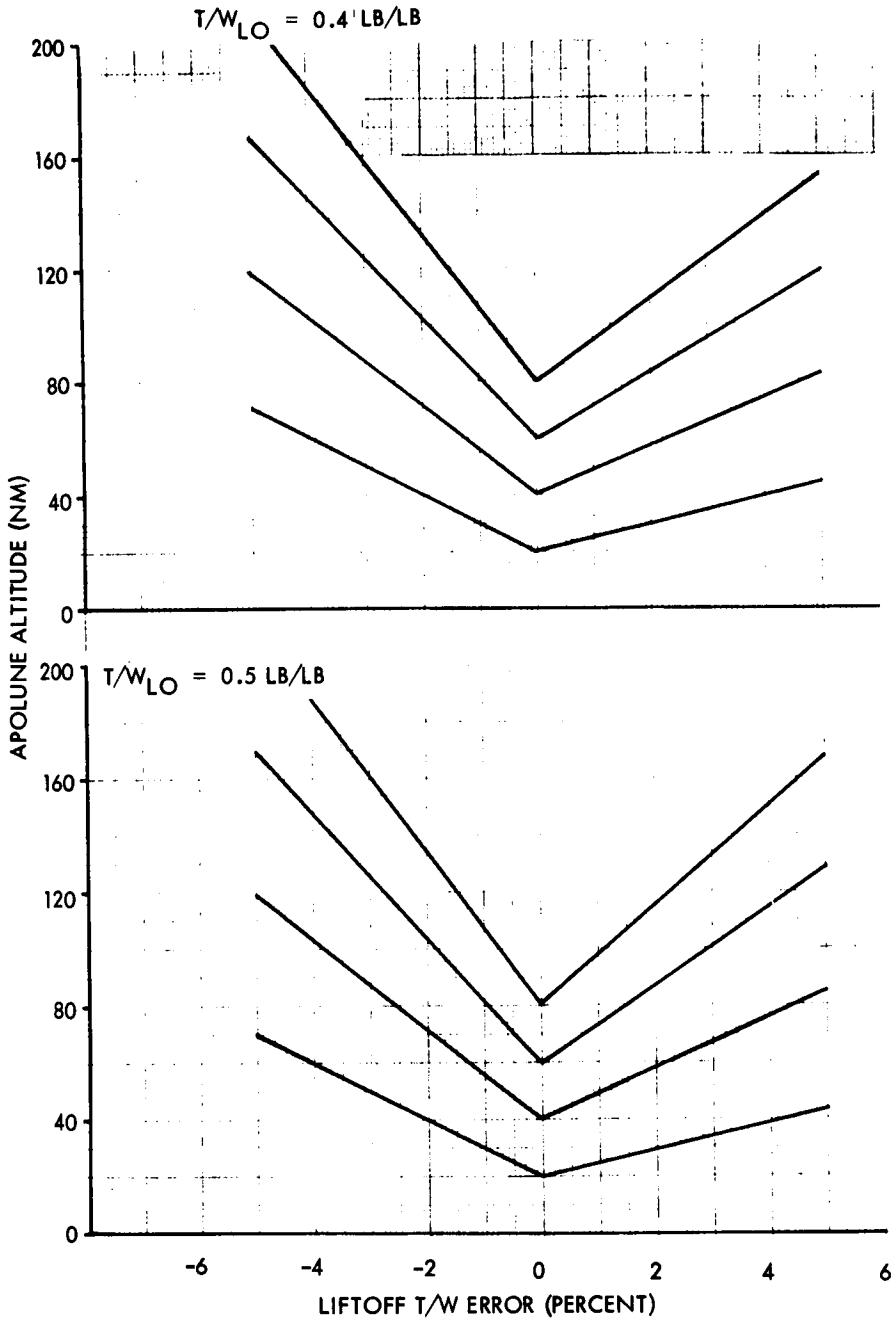

Figure 1-39. - Variation of Apolune Altitude With Liftoff Thrust-to-Weight Error (T/W_{LO} = 0.4 and 0.5 lb/lb), Cutoff on ΔV, Steps on Time

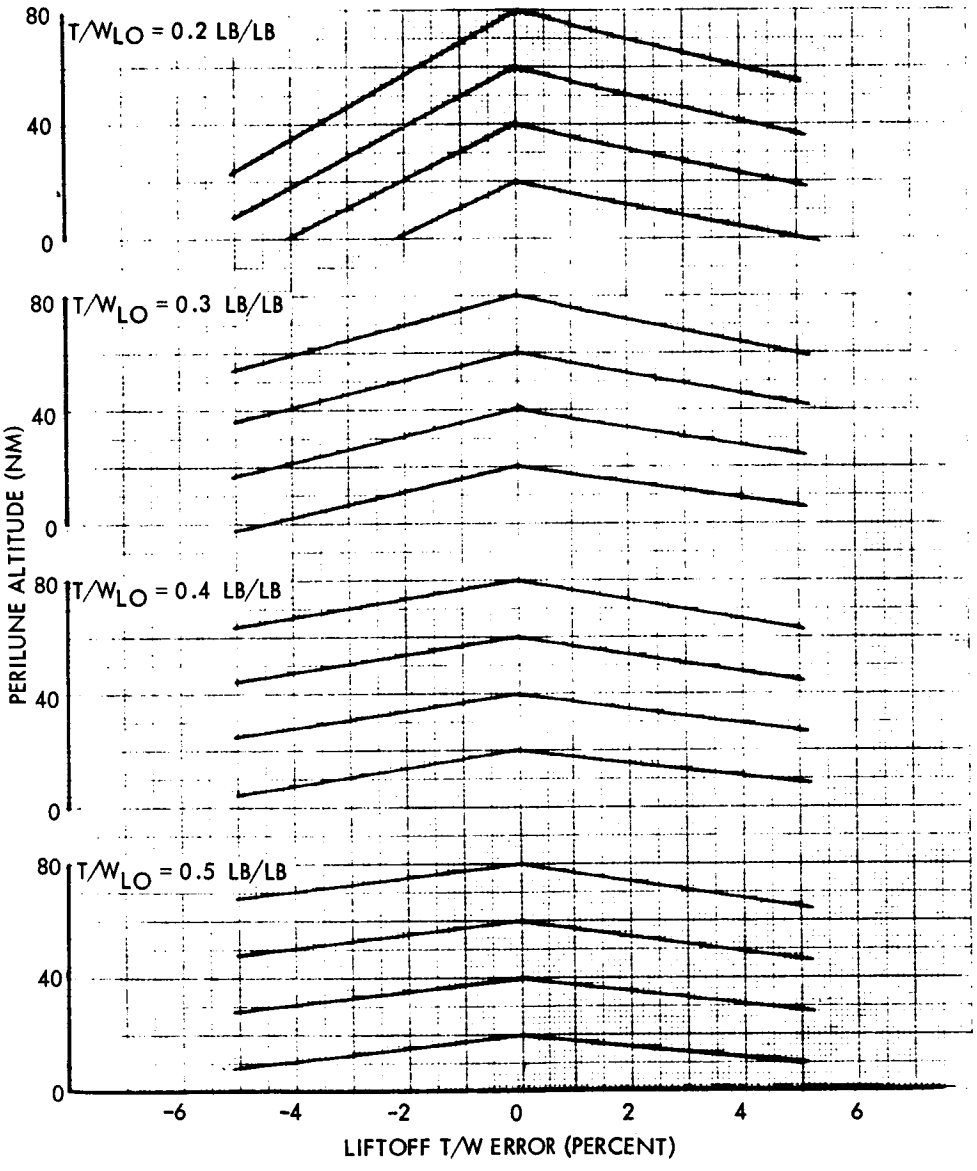

Figure 1-40. - Variation of Perilune Altitude With Liftoff Thrust-to-Weight Error, Cutoff on ΔV, Steps on ΔV

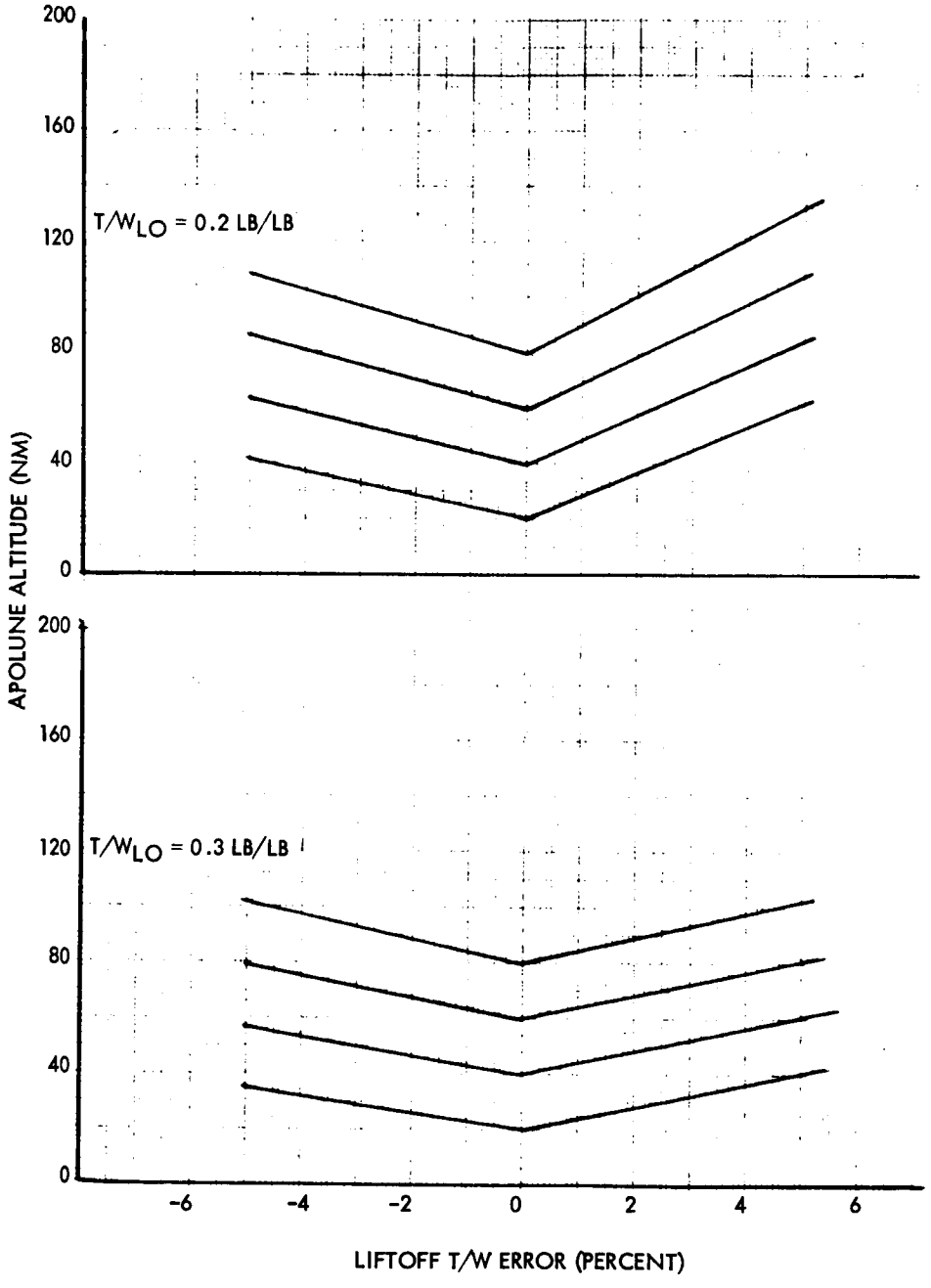

Figure 1-41. - Variation of Apolune Altitude With Liftoff Thrust-to-Weight Error (T/W_{LO} = 0.2 and 0.3 lb/lb), Cutoff on ΔV, Steps on ΔV

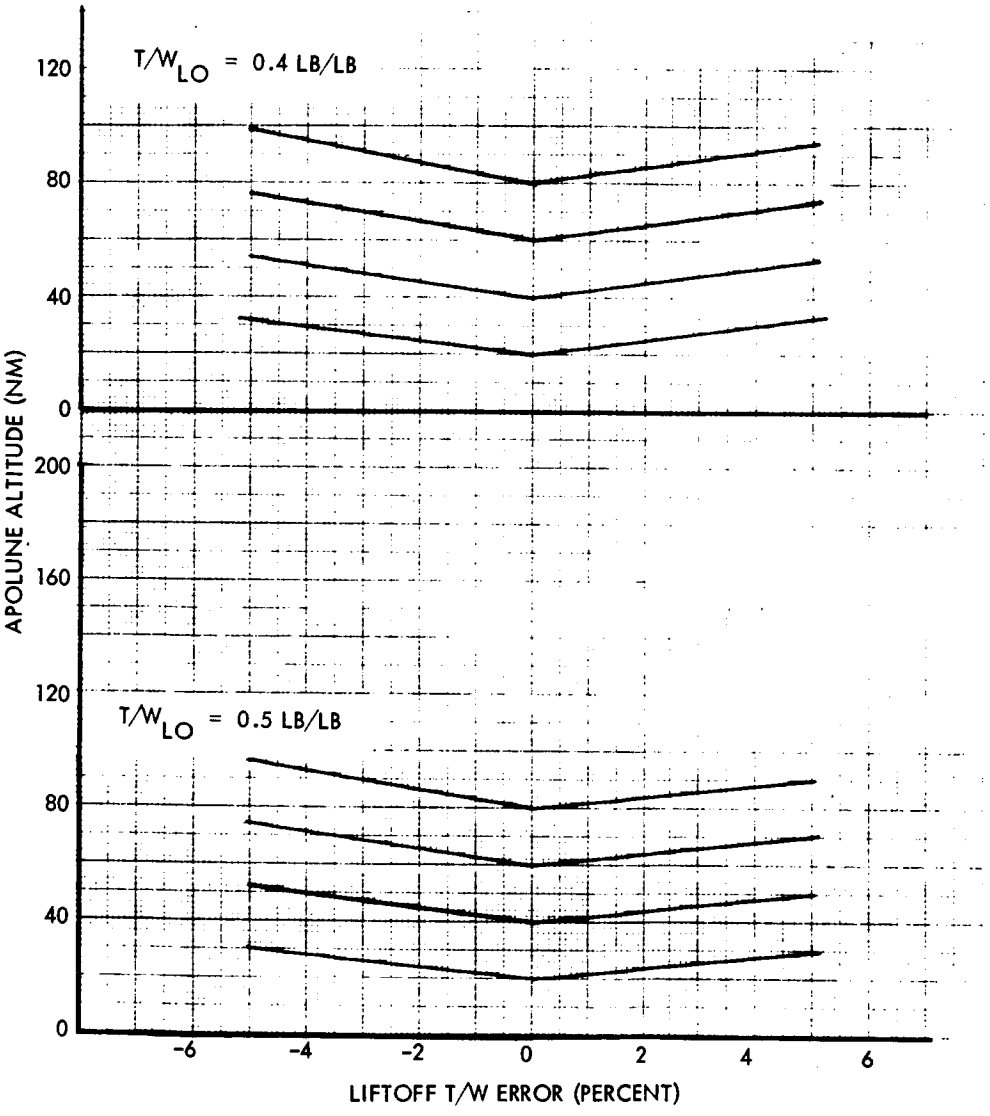

Figure 1-42. - Variation of Apolune Altitude With Liftoff Thrust-to-Weight Error (T/W_{LO} = 0.4 and 0.5 lb/lb), Cutoff on ΔV, Steps on Δ V

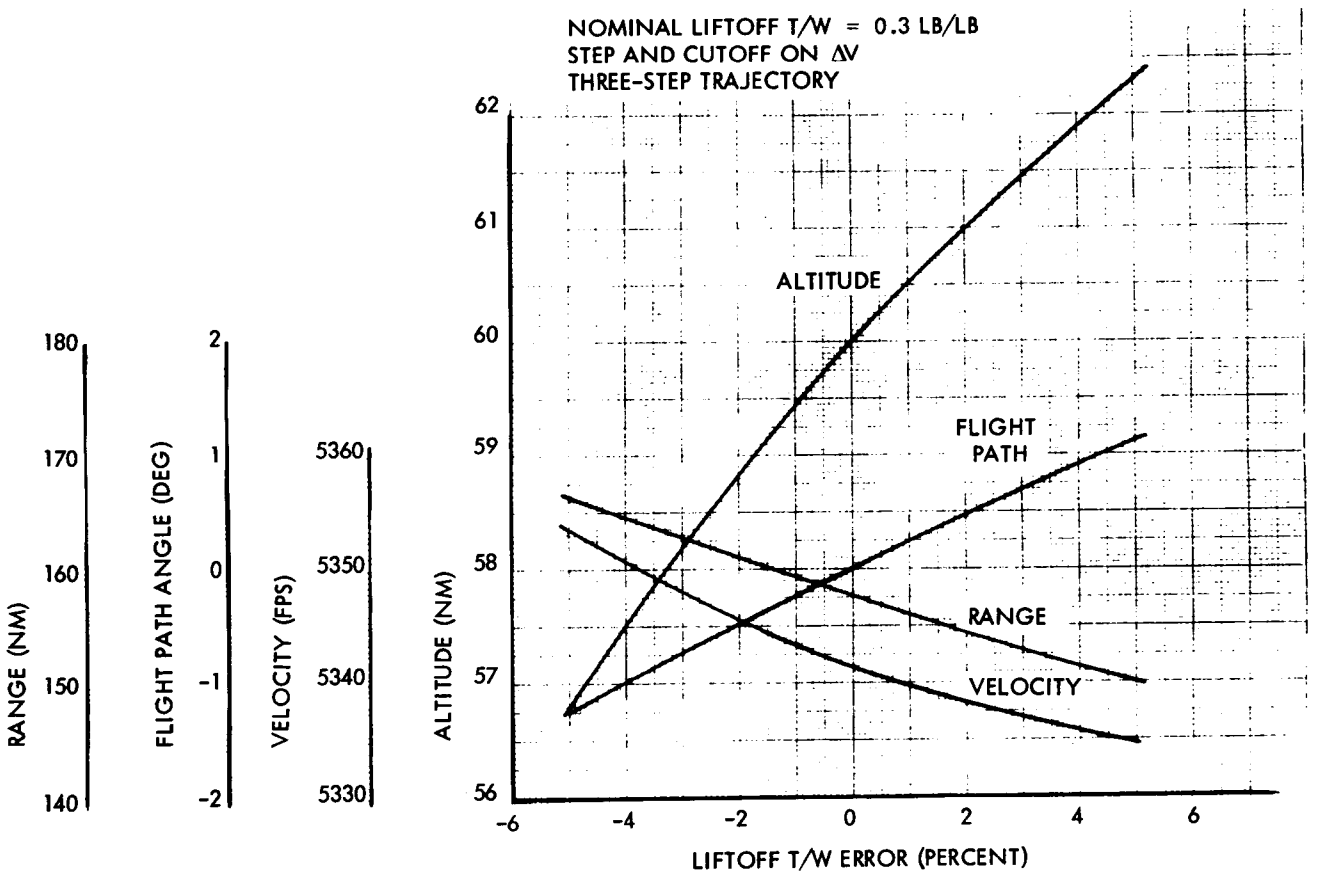

Figure 1-43. - Typical Variation of In-Plane LESS Burnout Conditions With Liftoff Thrust-to-Weight Error, 60-Nautical-Mile Orbit

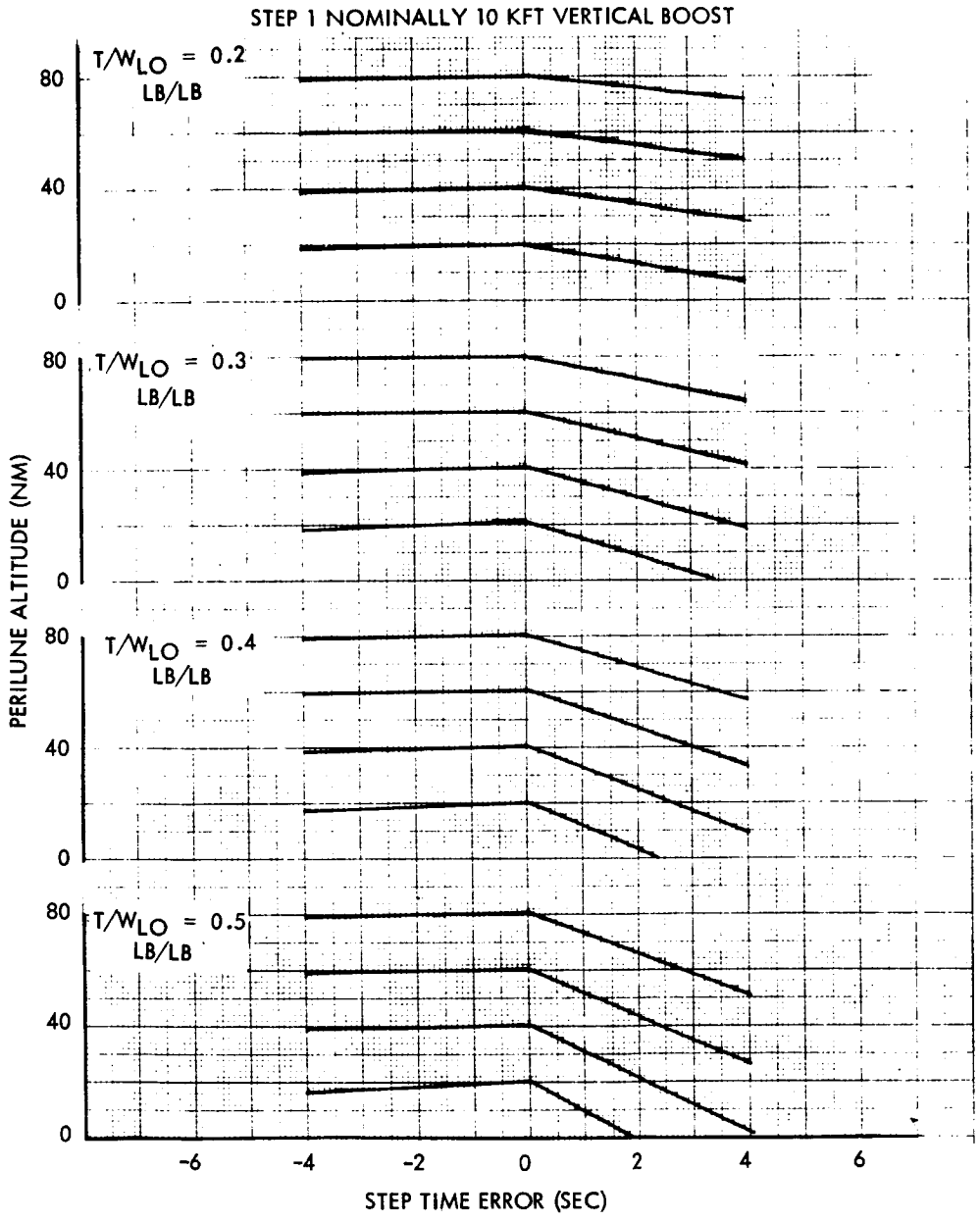

Figure 1-44. - Variation of Perilune Altitude With Error in Time Change From Step 1 to Step 2

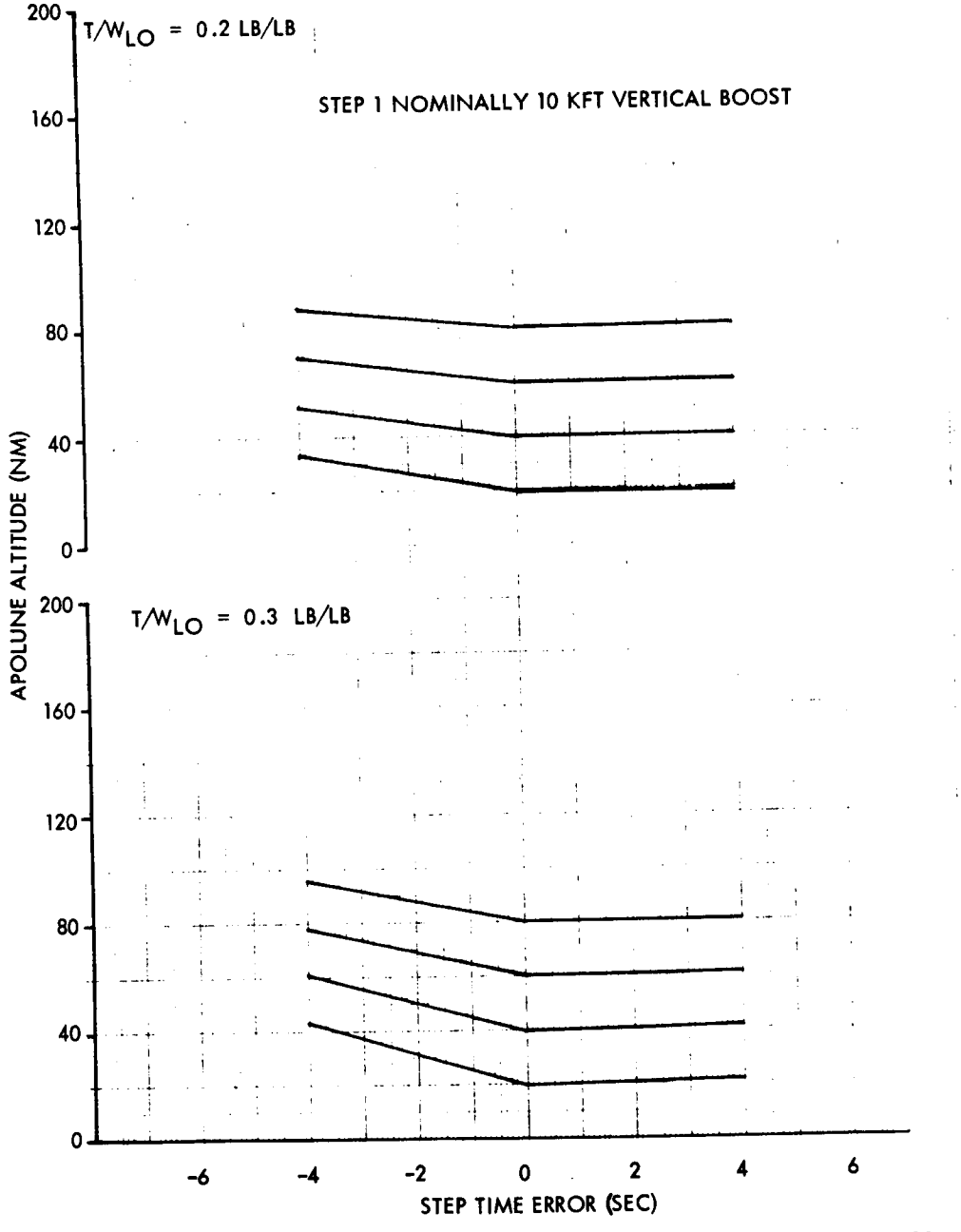

Figure 1-45. - Variation of Apolune Altitude With Error in Time Change From Step 1 to Step 2 (T/W_{LO} = 0.2 and 0.3 lb/lb)

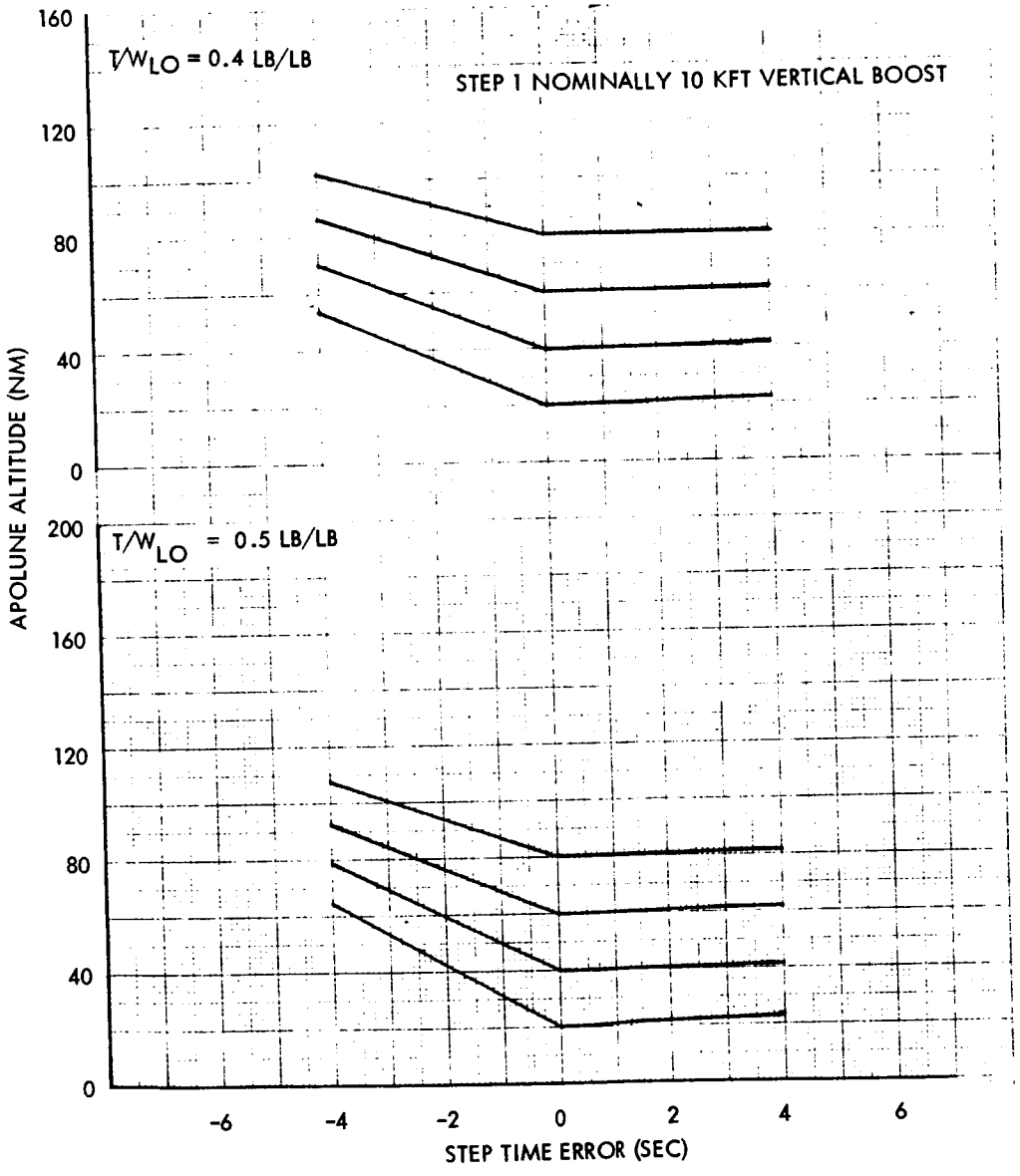

Figure 1-46. - Variation of Apolune Altitude With Error in Time Change From Step 1 to Step 2 (T/W_{LO} = 0.4 and 0.5 lb/lb)

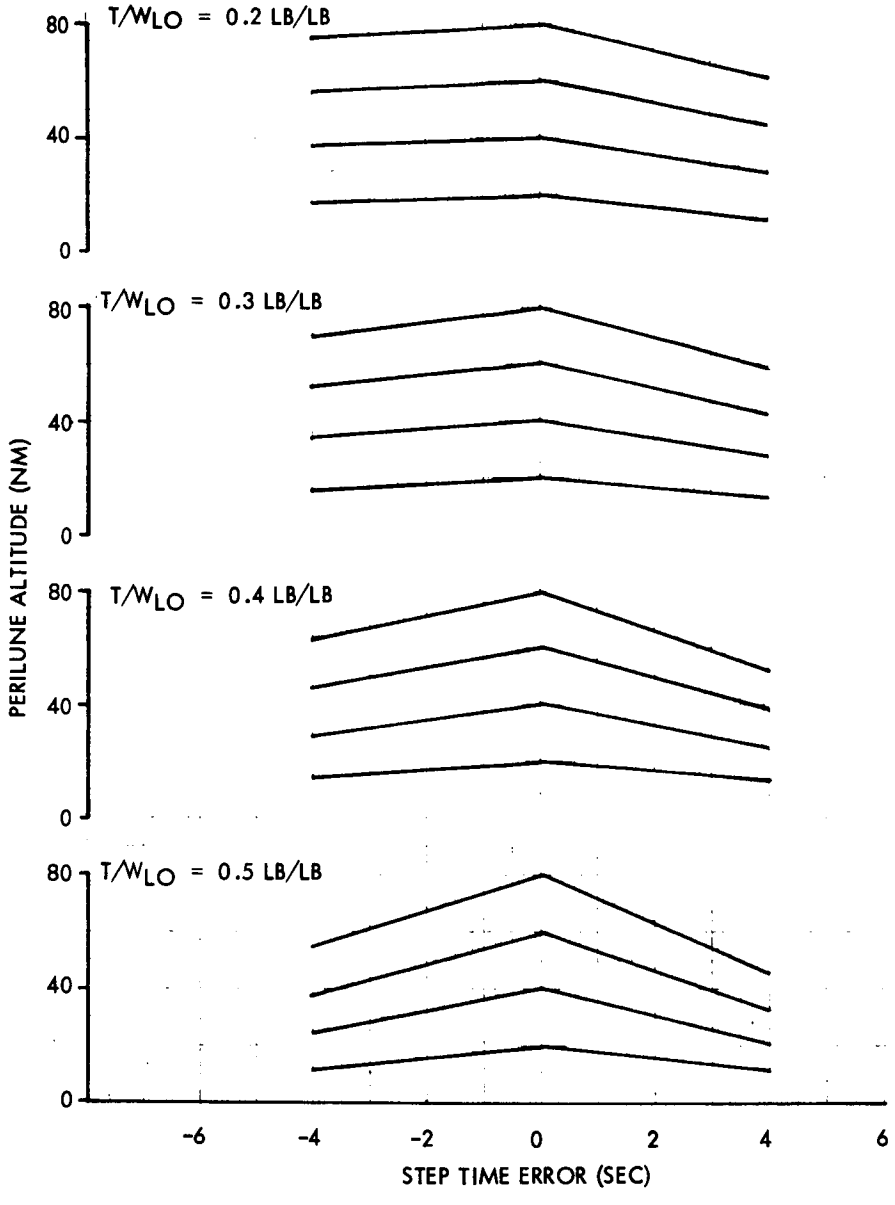

Figure 1-47. - Variation of Perilune Altitude With Error in Time Change From Step 2 to Step 3

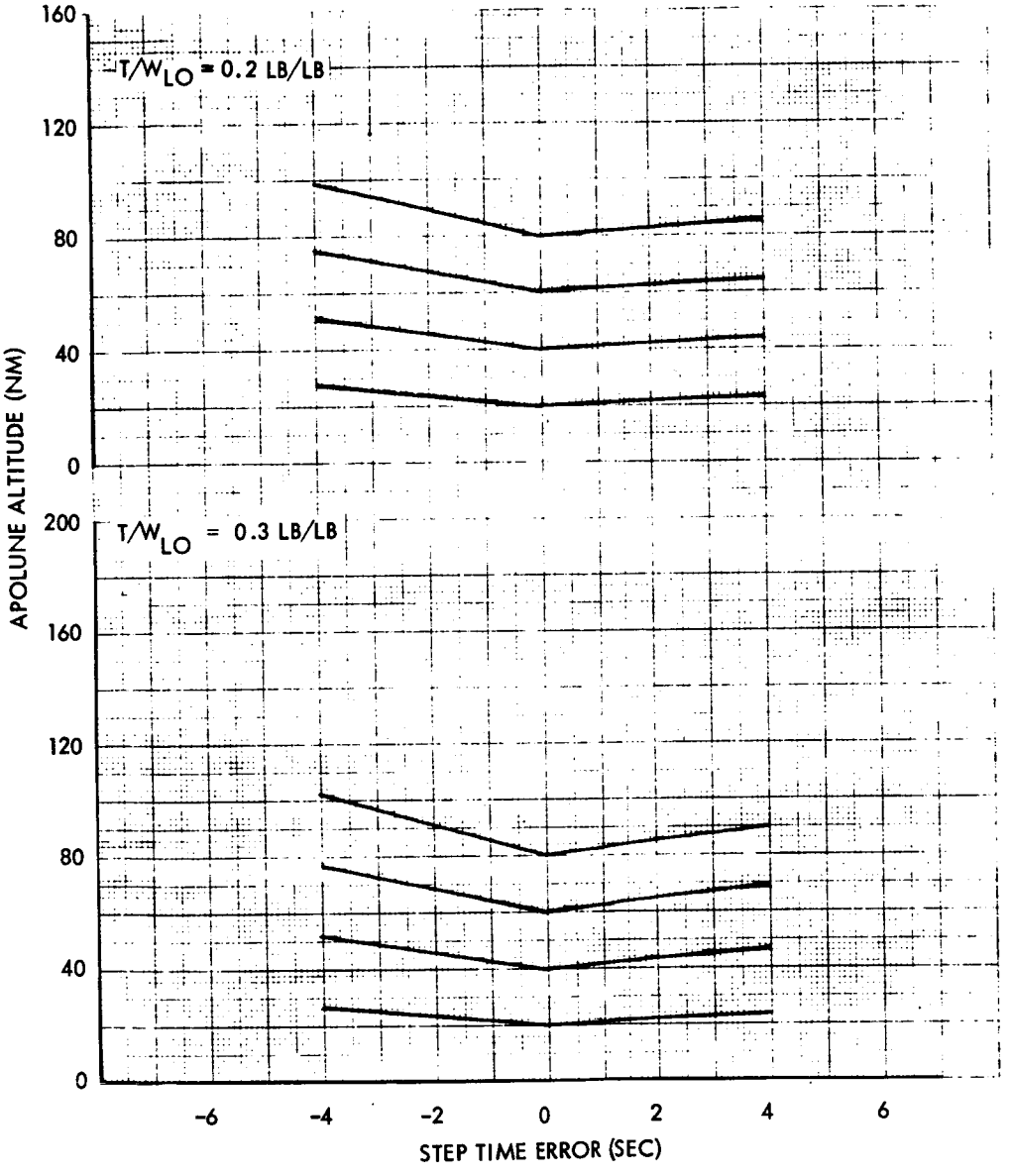

Figure 1-48. - Variation of Apolune Altitude With Error in Time Change From Step 2 to Step 3 (T/W_{LO} = 0.2 and 0.3 lb/lb)

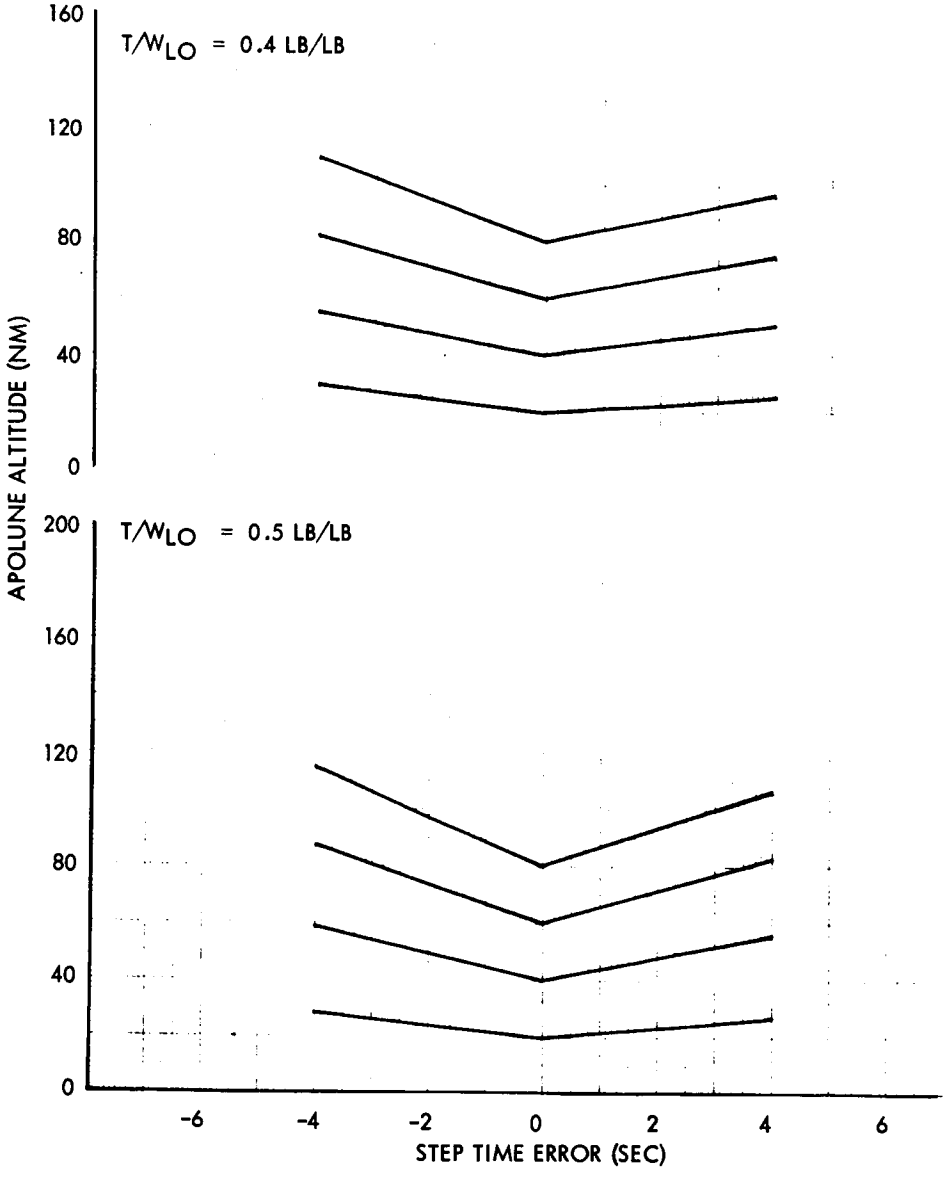

Figure 1-49. - Variation of Apolune Altitude With Error in Time Change From Step 2 to Step 3 (T/W_{LO} = 0.4 and 0.5 lb/lb)

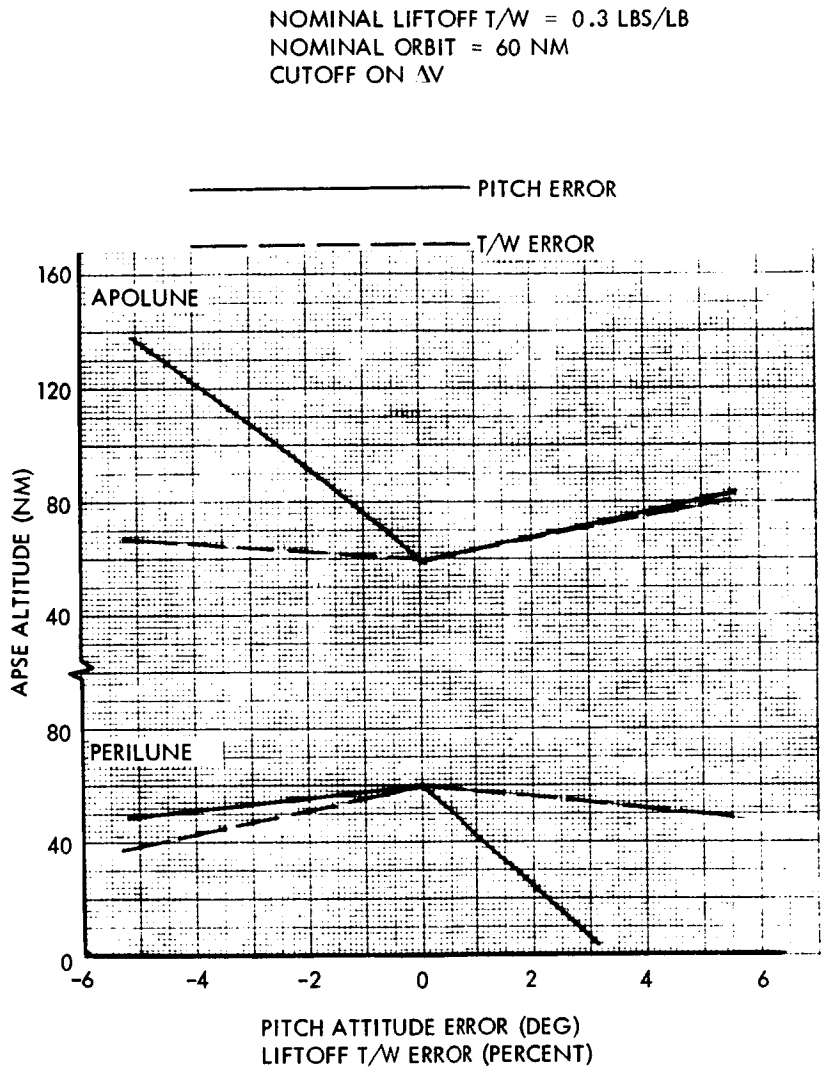

Figure 1-50. - Variation of Apse Altitude With Liftoff Thrust-to-Weight and Pitch Attitude Errors When Step Changes of Three-Step Trajectory are Made on the Basis of Altitude

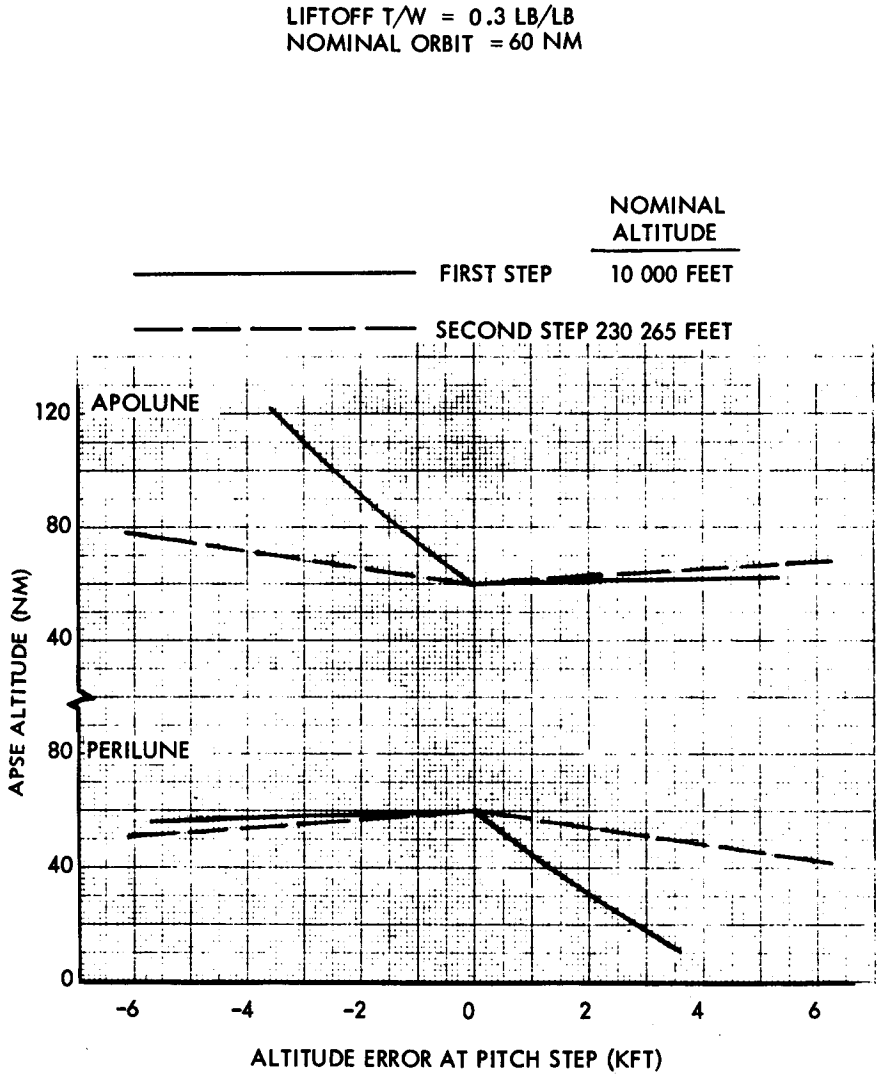

Figure 1-51. - Variation of Apse Altitude With Error in Altitude at Step Change for Three-Step Trajectory

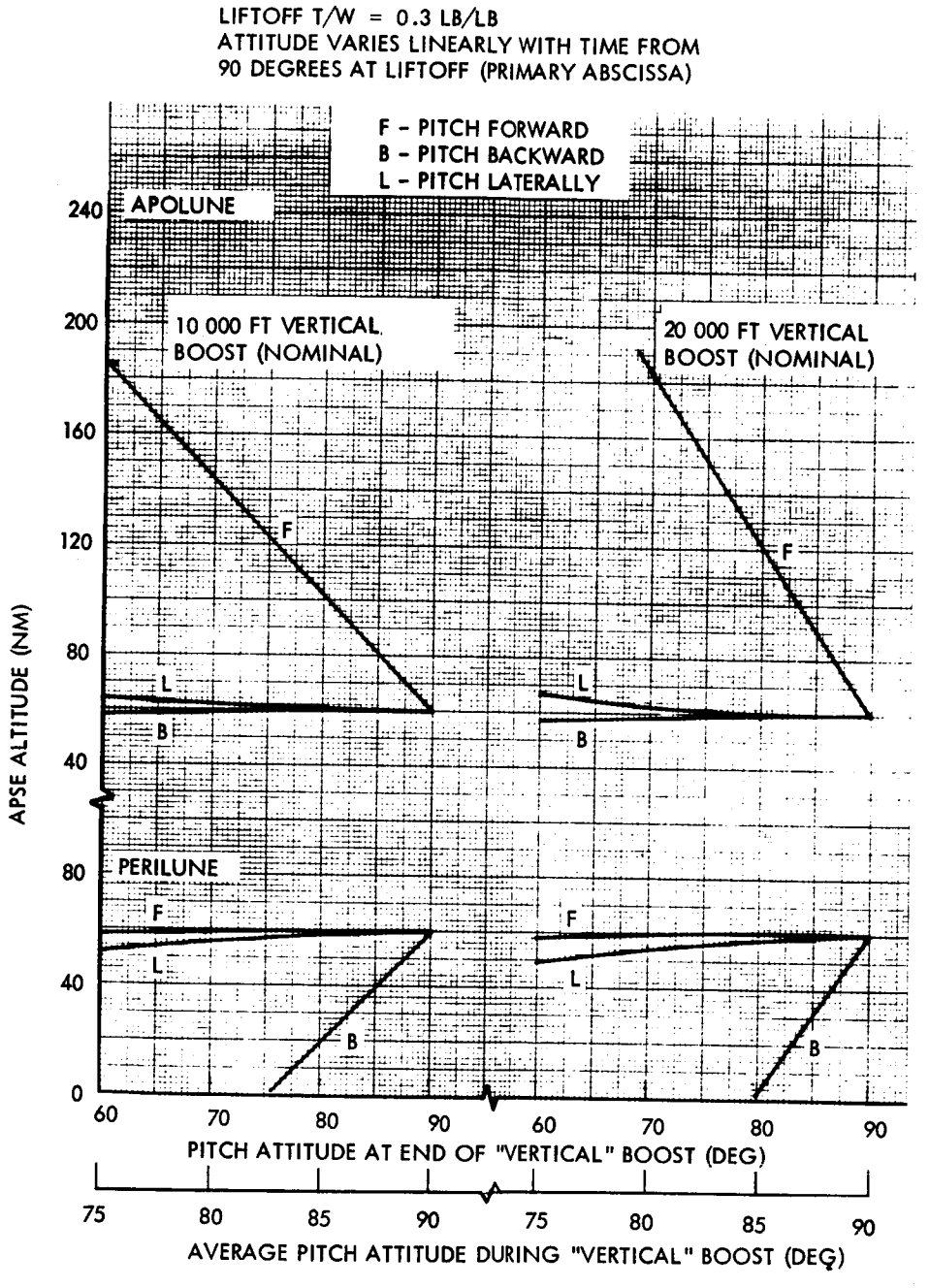

Figure 1-52. - Variation of Apse Altitude With Pitch Error During Vertical Boost Phase for Three-Step Trajectory to 60-Nautical-Mile Orbit

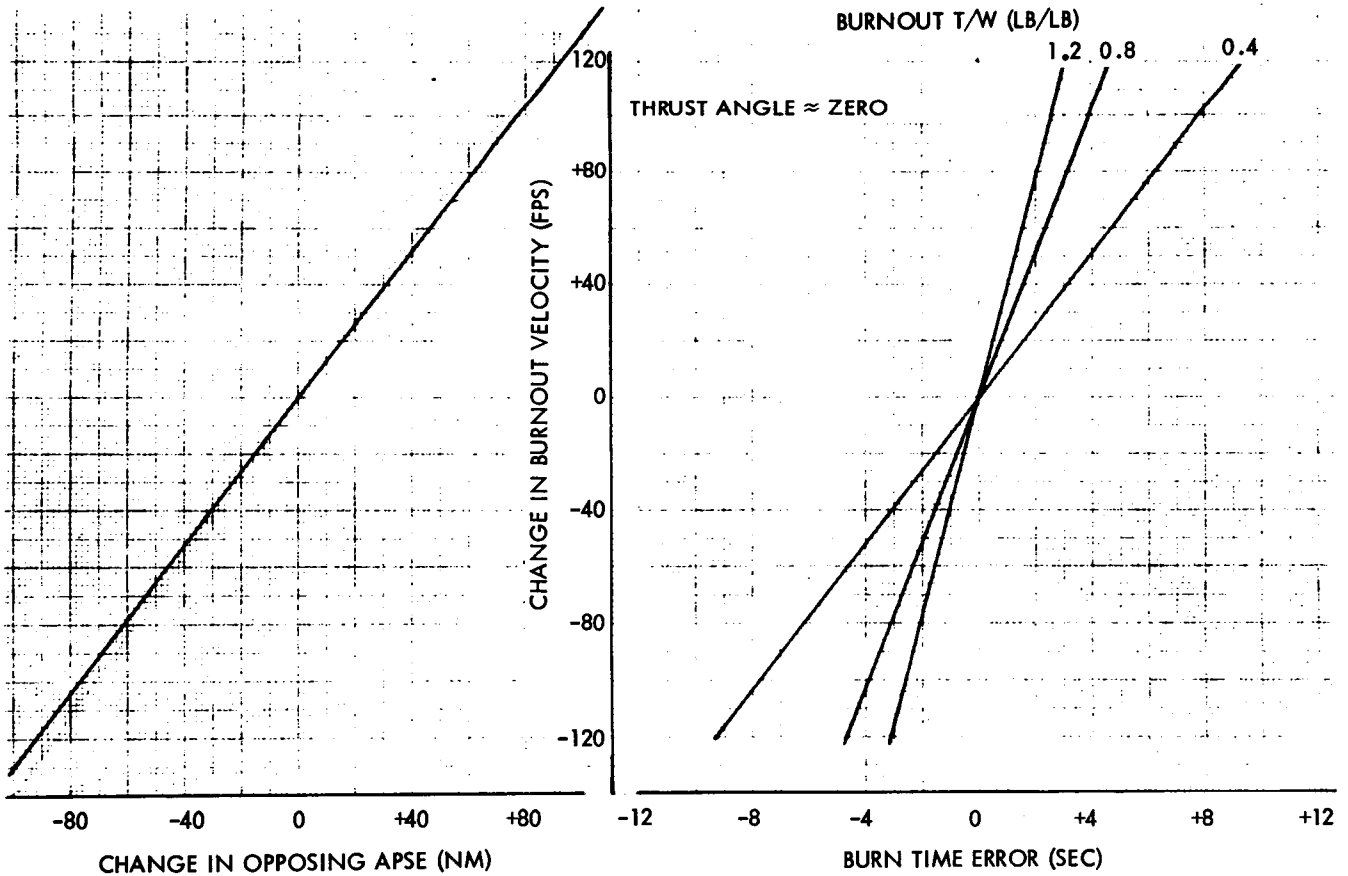

Figure 1-53. - Variation in Opposing Apse With Burn Time Error for Near-Circular, Low-Altitude Lunar Orbits

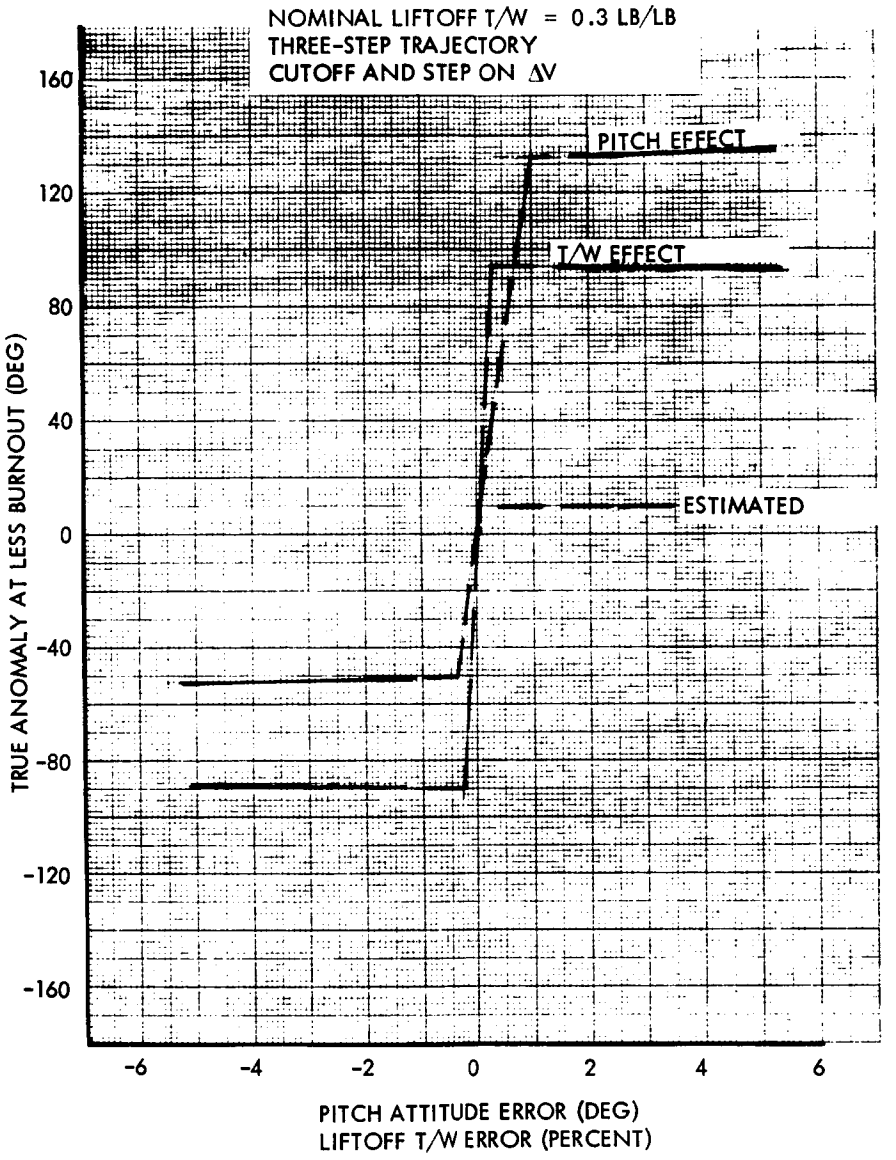

Figure 1-54. - Variation of True Anomaly at LESS Burnout With Pitch Attitude and Liftoff Thrust-to-Weight Errors for Boost to 60-Nautical-Mile Orbit

variation if all control is according to time; that is, the pitch steps and engine shutdown are all scheduled on the basis of nominal time. For systems of the type being considered for the LESS, thrust-to-weight ratio errors of the order of plus or minus five percent may be encountered. It is clear that errors of this magnitude cannot be accommodated by a timer mechanization. The basic problem with timer control is that the ΔV produced by the propulsion system in the nominal time is in error by roughly the same percentage as the error in initial thrust-to-weight ratio.

A significant improvement results if the cutoff command can be given on the basis of ΔV. Figures 1-37, 1-38, and 1-39 give the results if this technique is used. It is still assumed that the pitch maneuvers are scheduled on the basis of nominal time.

The benefits of cutoff by ΔV command having been indicated, it is interesting to note the benefits gained if the pitch maneuvers are also scheduled on the basis of ΔV. The results are depicted in figures 1-40, 1-41, and 1-42. It is seen that the variations in apse conditions are now quite small when compared with those resulting from timer control.

From the foregoing results it appears that a ΔV meter is necessary, at least to generate the cutoff signal. The ΔV meter having been justified, it then appears that the pitch steps should be scheduled according to output from it to achieve an additional gain.

Figure 1-43 illustrates the variations in the in-plane burnout conditions for a typical case employing steering control and cutoff according to ΔV.

Figures 1-44 through 1-49 depict the variation in apse altitudes with errors in pitch maneuver times. As would be expected, the effects grow stronger with increased liftoff acceleration as there is a larger energy increment produced during the specified error interval.

It may be possible to display altitude information to the pilot and have him perform the attitude steps on that basis. Figure 1-50 depicts the variation in apse altitude with pitch attitude error and liftoff thrust-to-weight ratio for this mechanization. Cutoff is assumed on the basis of ΔV. Since altitude converges to the desired value exponentially, it is not suitable for cutoff control. The apse altitude variations are smaller than the comparable ones where the steps are scheduled on the basis of ΔV. However, if the mechanization and displays are simple, there may be a substantial error in evaluating altitude. The effects of errors in sensing altitude are illustrated in figure 1-51.

If a guidance scheme requiring sighting on the horizon (either lateral or downrange) is employed, the pilot may have difficulty ascertaining the vertical if he must launch from the floor of a deep crater or if the site is near some

particularly rough ground. The variation of perilune and apolune altitude with pitch attitude errors during the initial vertical rise is shown in figure 1-52. The two cases illustrated have vertical rises (nominal) of 10 000 and 20 000 feet followed by two nominal constant-attitude steps. Perilune altitude is not sensitive to forward or lateral errors, but is seen to be very sensitive to backward-leaning errors.

Figure 1-53 depicts an approximation to the variation in the opposing apse with variations in cutoff conditions. It is assumed that the burnout conditions are at one apse and that the error in the cutoff conditions causes a pure underburn or overburn condition. It is expected that ΔV sensing accuracy for cutoff will be approximately ±0.1 percent, or typically on the order of seven feet per second, corresponding to variations in the opposing apse of ±6 nm.

Depending on system accuracy and astronaut performance capability, variations in apse dimensions due to pitch and thrust-to-weight errors will be substantially greater. If these errors are such that the burnout conditions are low and shallow,* then perilune will be "ahead of" the burnout point. If the boost errors cause a steeper trajectory than nominal, perilune will be "behind" the burnout point. The variation of burnout true anomaly is shown in figure 1-54 as a function of pitch and thrust-to-weight ratio errors for a typical boost to 60-nm orbit. Thus, even though for a circular target orbit, the perilune location of the actual orbit could theoretically be anywhere; the variation in its dimensions will be much more extreme if perilune is in the neighborhood of ±90 degrees from burnout.

"Bent two-step" trajectories. - The desirable aspects of the two-step profile (simplicity of only two attitude segments) and the three-step profile (low energy penalty) can be combined to form what NR has dubbed the "bent two-step" profile. If burn time and the two constant-attitude steps are considered, there are enough degrees of freedom to control burnout conditions of velocity, altitude, and flight path angle. There is still one redundant degree of freedom in the problem, namely the time to switch from the first attitude step to the second. As in the three-step profile (which this profile closely resembles, except that the 10 000 foot vertical boost has been reduced to zero), a reasonable criterion is to select the step-change time such that total boost energy is minimized. Results of optimizing that profile indicated that the two steps should be divided approximately equally according to ΔV. These criteria and a liftoff thrust-to-weight ratio of 0.3 pound per pound were used to initiate a series of trajectories to circular orbits. Their energy requirements are shown in figure 1-55 compared with those of some other salient profiles. It is seen that the energy penalties associated with the bent two-step trajectories are quite low compared to the COV trajectories.

*below target altitude and negative on nose-down flight path angle

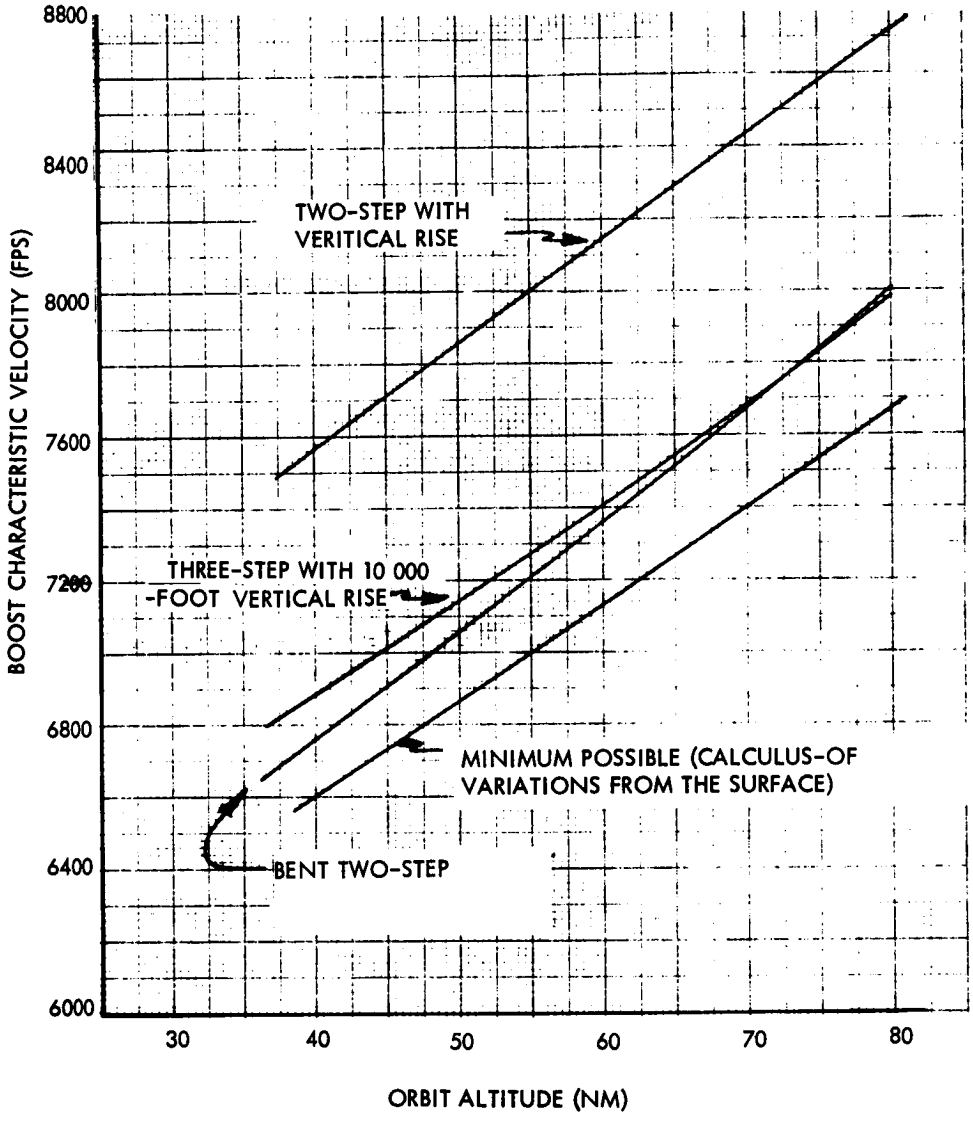

Figure 1-55.- Comparison of Energy Requirements for Various LESS Boost Profiles Having Liftoff Thrust-to-Weight Ratios of 0.3 lb/lb

Figure 1-56 depicts the steering angles required for this flight mode. The inset illustrates the time history for boost to a 60-nm orbit, while figure 1-57 shows the trajectory. Figure 1-58 depicts altitude/range profiles for target orbits of 40, 60, and 80 nm. It is seen that the trajectories tend to be quite low in the vicinity of the launch site. This could present a problem, depending on the site and its surroundings. Because of the strong similarity between this profile and the three-step profile, the error sensitivities were considered similar and were not computed separately.

Out-of-plane errors. - The gross effects of out-of-plane launch errors are shown in figure 1-59. If there is an initial out-of-plane angle between the site and the CSM orbit, the plane change angle is minimized if the LESS is targeted to intersect the CSM orbit 90 degrees from launch. Errors in launch azimuth followed by a planar launch cause variations in relative inclination and in location of the node, as illustrated in figure 1-59.

For small errors in azimuth and small initial out-of-plane angles, the locations of the node will tend to be quite random. This is because of random oscillations of thrust heading about the nominal. It follows that the inclination errors will also be small so that subsequent CSM energy requirements for rendezvous plane change will be small. It is seen that for larger initial out-of-plane angles, (1) inclination and nodal location are both less sensitive to azimuth errors and (2) that for large azimuth errors, there is an appreciable performance advantage gained by delaying plane change until after LESS launch.

It is noted that present Apollo mission plans (through Apollo 20) call for the CSM to have plane change capability sufficient to allow a planar lunar module launch at any time during the surface stay. Mission plans and criteria are presently not well defined for the missions. Thus, it is not clear whether the additional ΔV for anytime abort, compared to that required for LM launch at the end of its nominal stay, is charged against the LM-rescue allocation. This difference is a function of very complex interrelationships among launch date, site location, and stay time and is strongly affected by the flight mode employed. Presently, multi-impulse maneuvers for lunar orbit insertion and transearth injection are being considered by NASA at MSC. This technique allows sites to be reached that can not be reached with single-impulse maneuvers. (This mode has the disadvantage that mission time is increased and thus consumable requirements are increased.) However, regarding out-of-plane requirements for anytime LM launch, they can be reduced by approximately 15 degrees for a typical 3-day mission to Marius Hills by utilizing 3-impulse techniques.

Thus it is not now possible to identify initial out-of-plane angle requirements for any but the first few missions. As the mission definitions and rationale become more clear, it will be possible to evaluate them exactly.

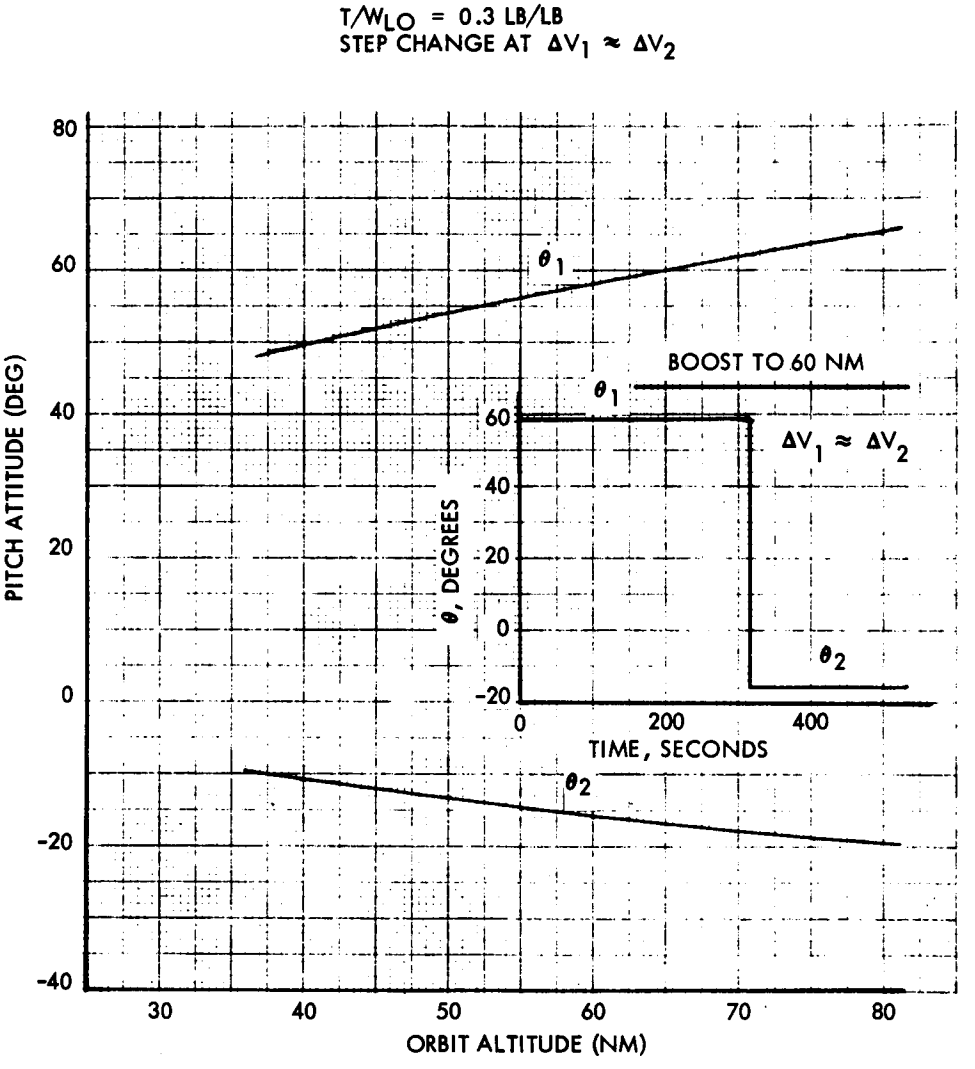

Figure 1-56. - Variation of Steering Angles With Orbit Altitude for Bent Two-Step LESS Boost Profile

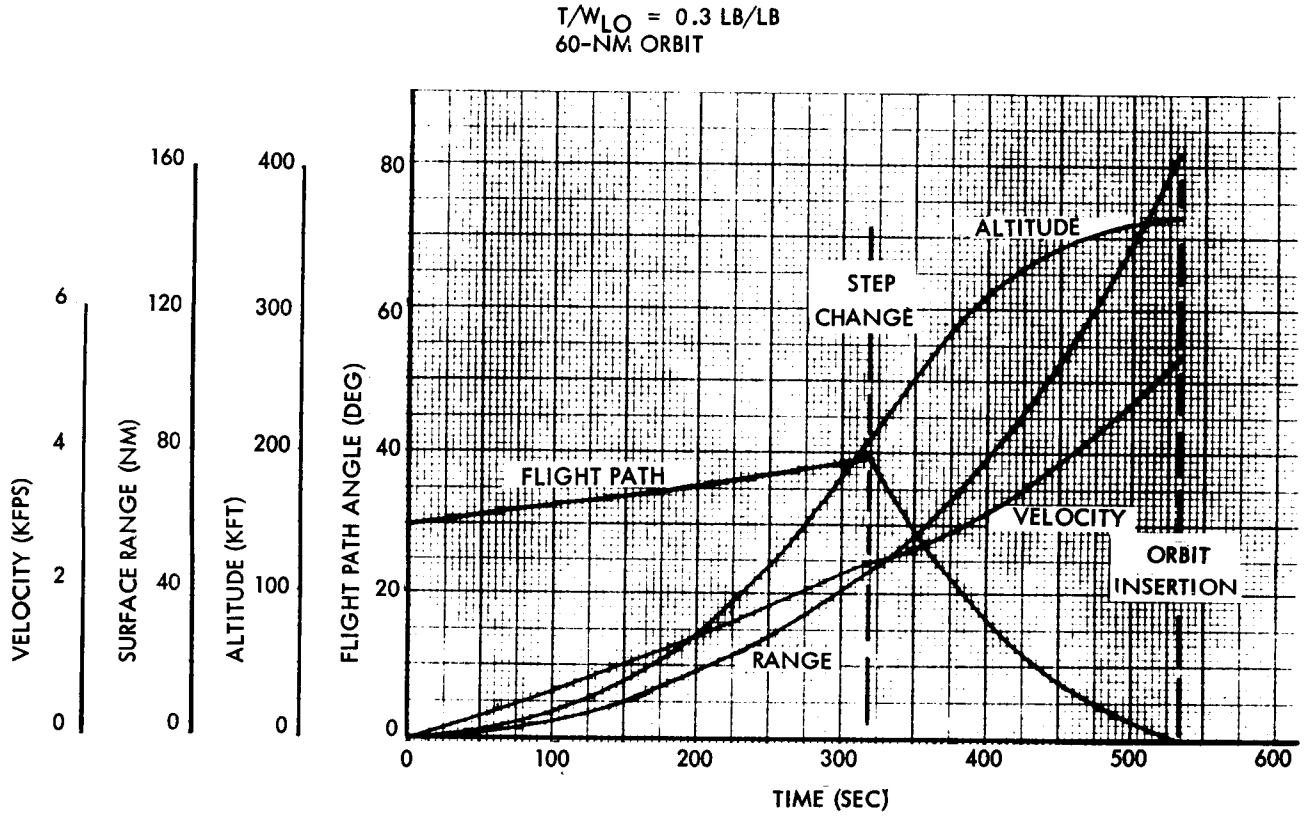

Figure 1-57.- Flight Parameters for Typical Bent Two-Step LESS Boost

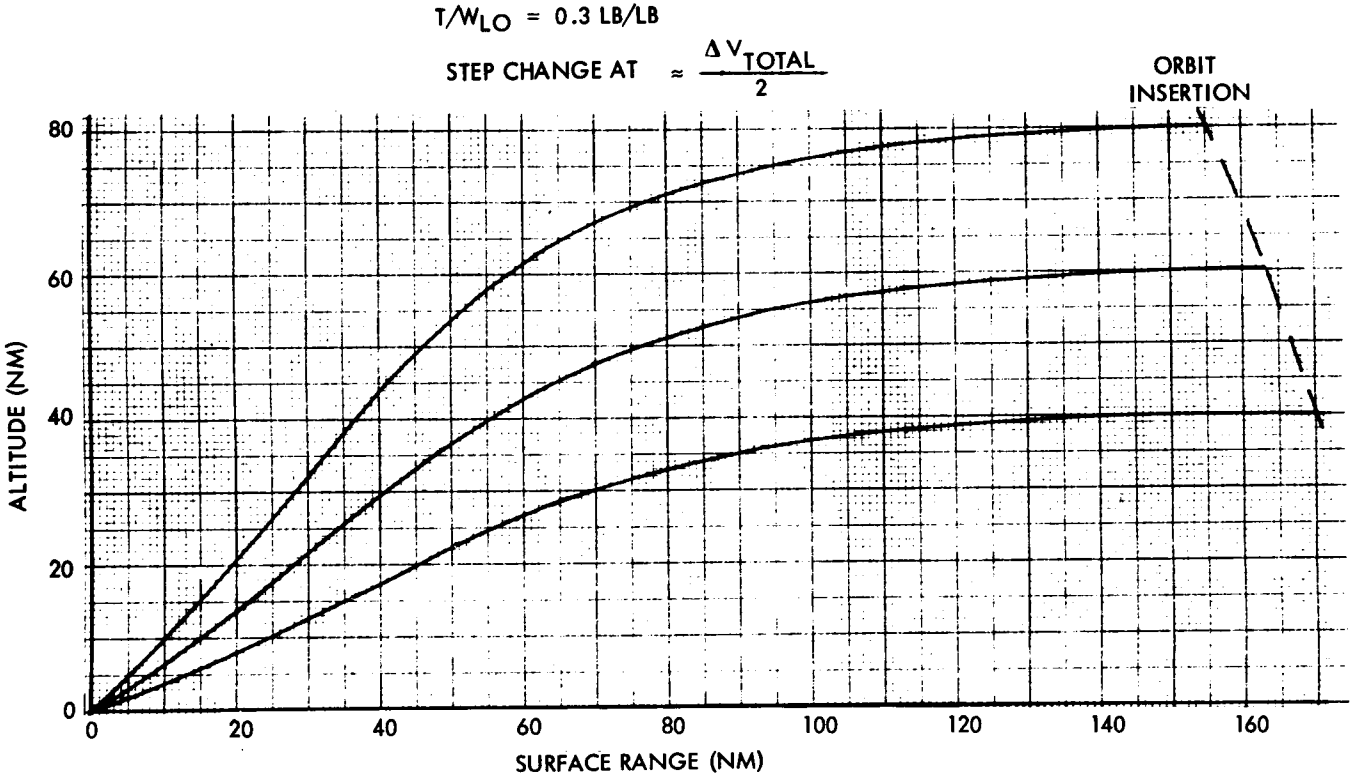

Figure 1-58.- Altitude/Range Profiles for Typical Bent Two-Step LESS Boost Trajectories

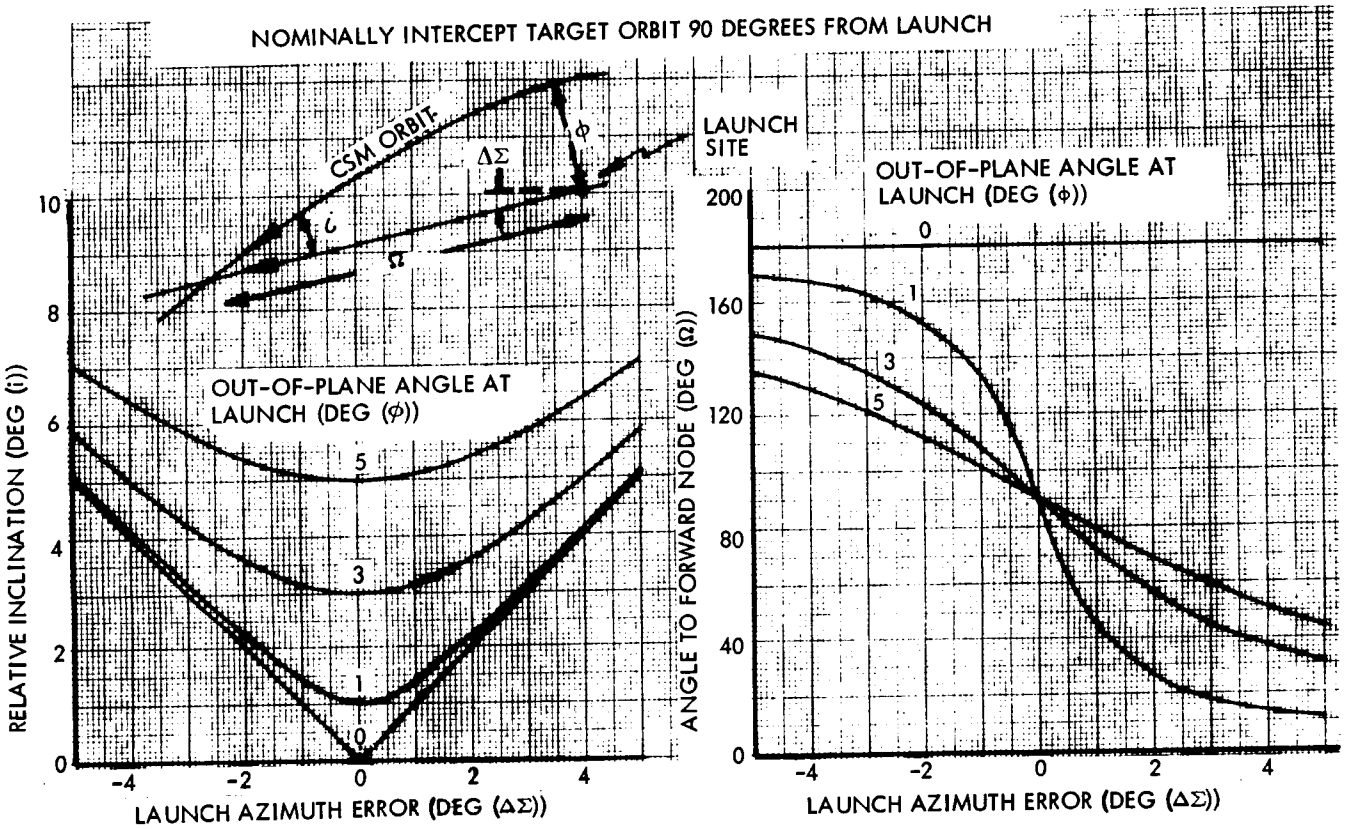

Figure 1-59. - Effect of Launch Azimuth Errors on Inclination and Angle to the Forward Node

Following current philosophy, however, it seems safe to assume that the overall mission plan in each case will have a proper energy provision in the CSM budget to accomplish whatever aborts are considered necessary at the time, and this energy can alternately be utilized with a LESS under similar mission circumstances.

Elliptical orbits. - A brief look was taken at elliptical target orbits. Figure 1-60 depicts the variation in pitch angles and total boost ΔV for boost to elliptical orbits with 60-nm perilune altitudes, assuming a liftoff thrust-to-weight ratio of 0.3 pound per pound, a three-step steering profile, and orbit insertion at perilune. The data are seen to be not strongly dependent on apolune altitude.

Figure 1-61 depicts the variation of apse altitude with pitch attitude errors. When these variations are compared with the corresponding data for circular orbits, it is seen that the perilune sensitivity has been reduced somewhat, while the apolune sensitivity is roughly the same except that the origin has shifted. Figure 1-62 illustrates the variation of in-plane burnout conditions as a function of pitch errors.

Figures 1-63 and 1-64 depict the variation in apse altitude with liftoff thrust-to-weight ratio errors for two elliptical orbits (60-by-120 and 60-by-180 nm). As in the treatment of circular orbits, three control methods are indicated. And as concluded before, it appears that a ΔV meter is necessary to provide the cutoff command. Also as before, since the ΔV meter is necessary, it should be used as the reference for the steering angles. Figure 1-65 illustrates the variation of the in-plane burnout parameters with thrust-to-weight ratio errors employing ΔV for steering control and cutoff. As with the pitch error results, the data are very similar to the comparable circular orbit data.

Using elliptical target orbits reduces the variation in perilune locations, as is evident when figures 1-66 and 1-67 are compared with the data for circular orbits (fig. 1-54). As the target orbit ellipticity increases, the variation in perilune location decreases. It will be seen in the following Rendezvous section that substantially more energy from the CSM is required for rendezvous if CSM-active rendezvous is employed. Thus the apparent advantage gained by reducing perilune sensitivity is largely negated.

Two-step thrust schedules. - A two-step thrusting schedule has potential for enhancing the controllability of the LESS by reducing thrust (control torques) when the vehicle's mass and inertia are low (see the Stability and Control section). The performance effects are shown here. Figures 1-68 and 1-69 illustrate the variation in total boost energy with ΔV at thrust reduction for a range of second-step thrust levels from 80 percent to 10 percent of nominal for liftoff thrust-to-weight ratios of 0.3 and 0.5 pound per pound, respectively. The steering profile employs a vertical boost to 10 000 feet,

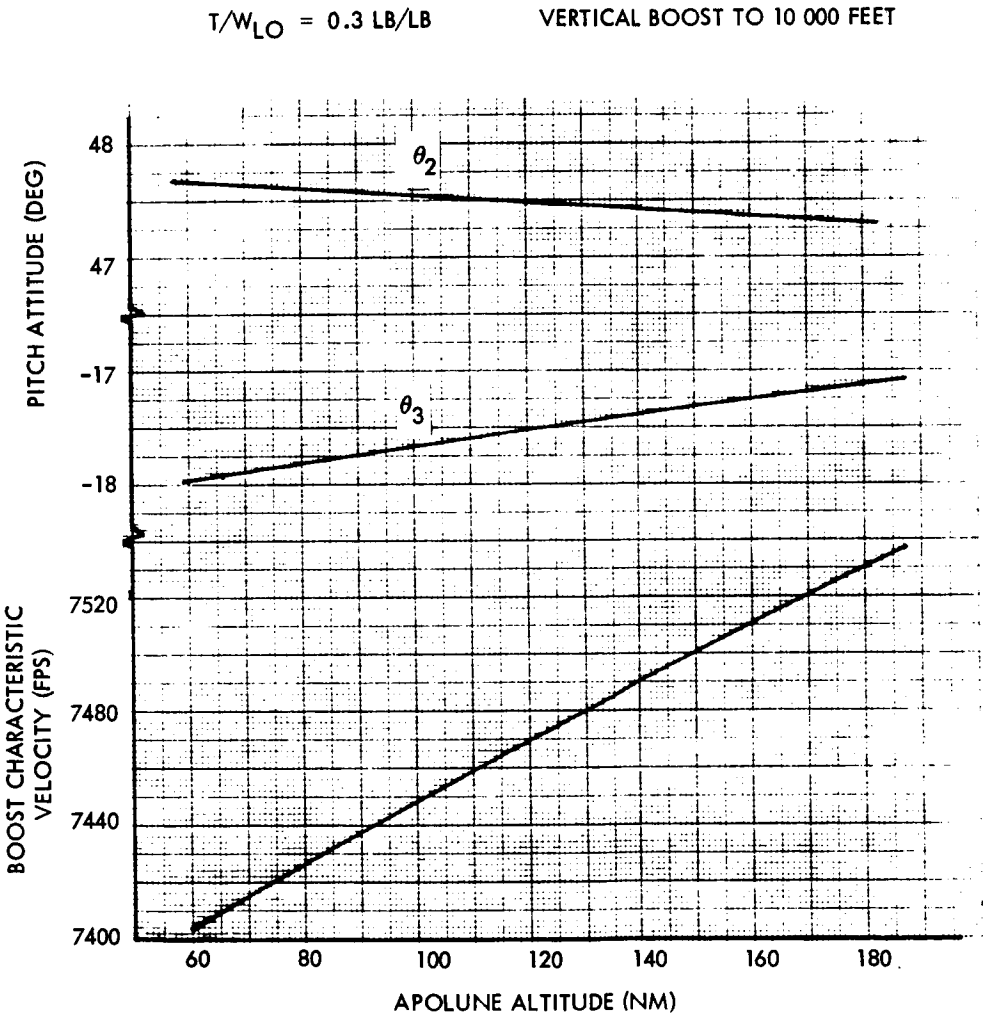

Figure 1-60. - Variation of Pitch Angles and Boost Energy With Apolune Altitude for Three-Step LESS Boost to 60-Nautical-Mile Perilune

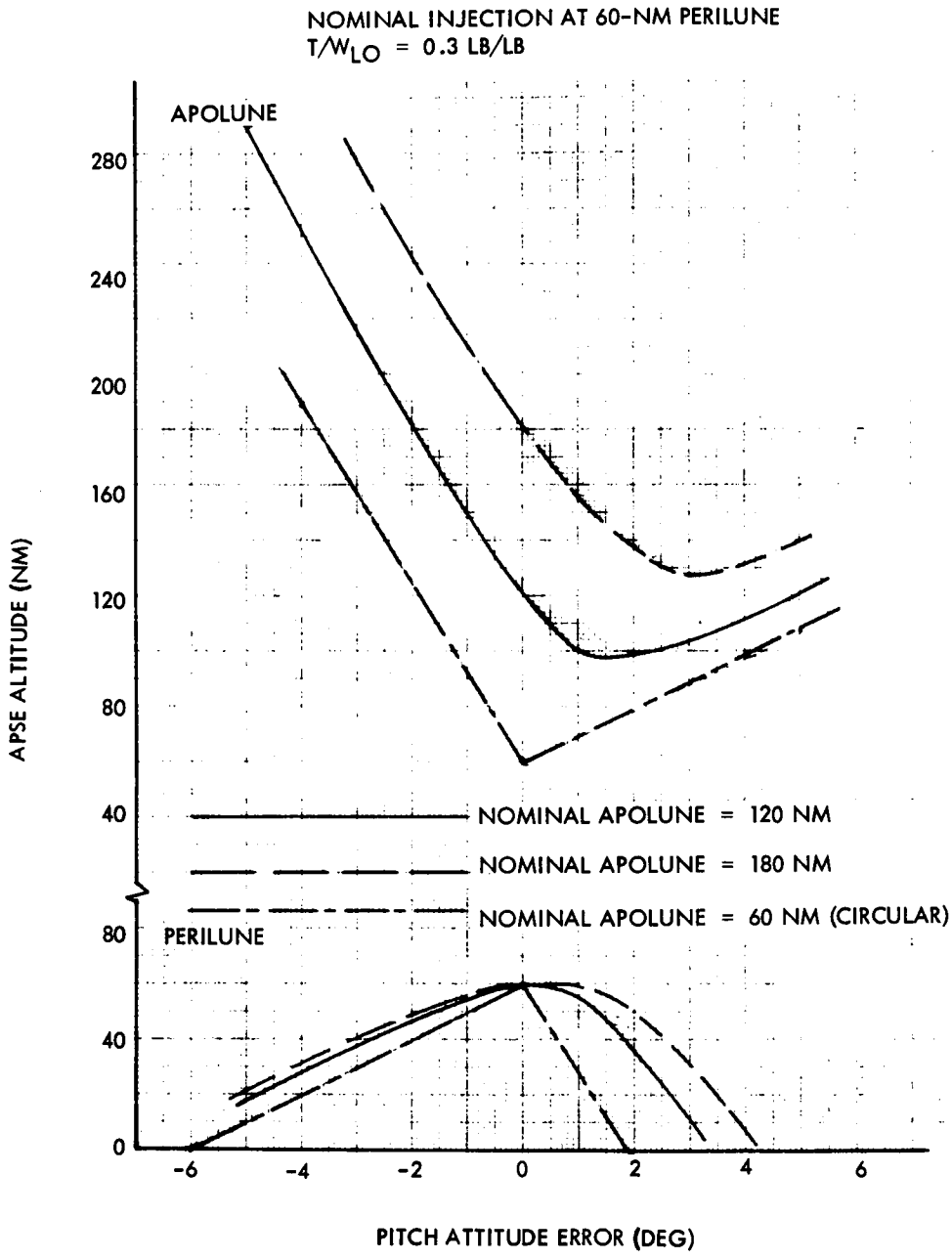

Figure 1-61.- Variation of Apse Altitude With Pitch Attitude Error for Three-Step LESS Boost to Elliptical Orbits

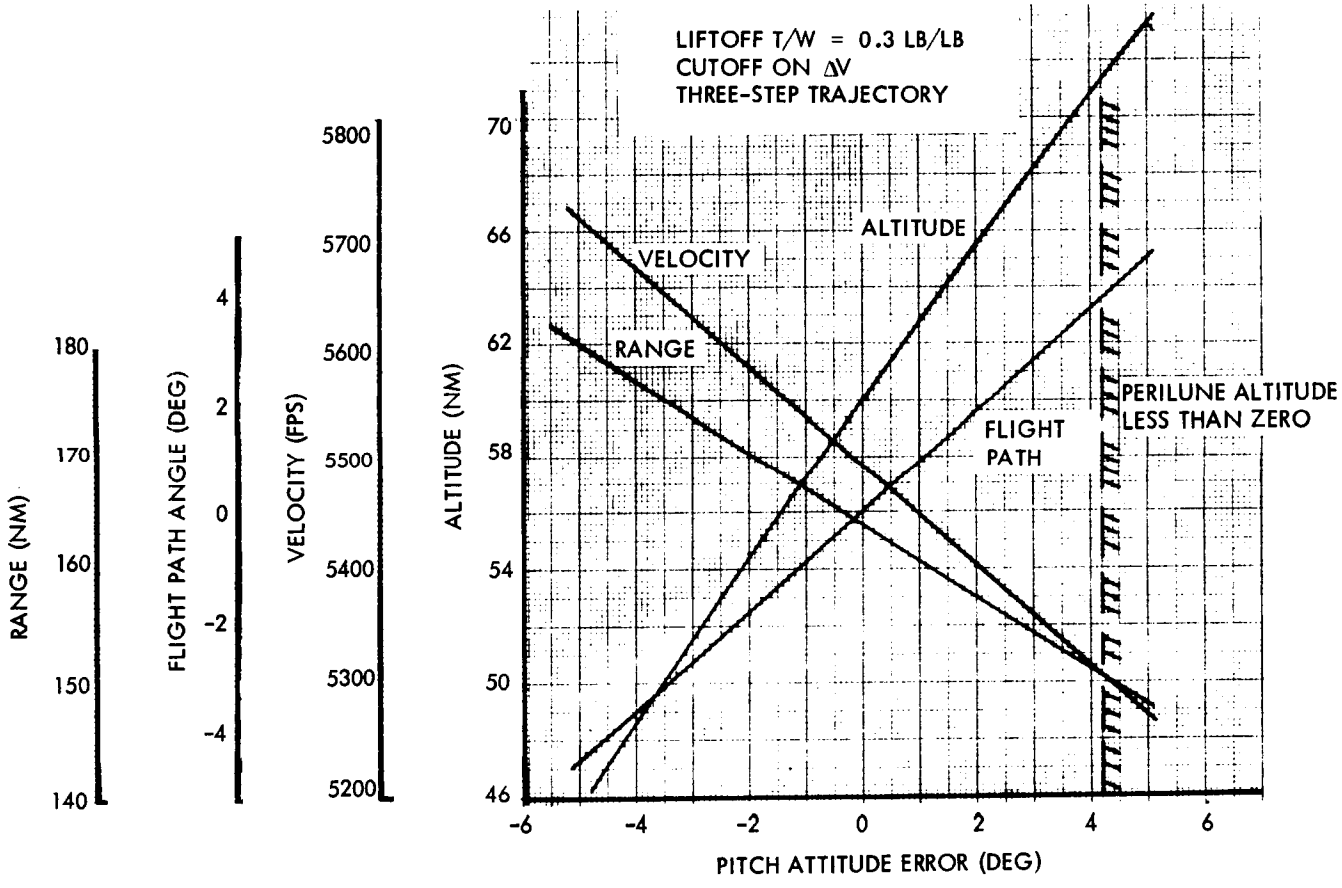

Figure 1-62.- Variation of In-Plane LESS Burnout Conditions With Pitch Attitude Error for Nominal 60- by 180-Nautical-Mile Orbit

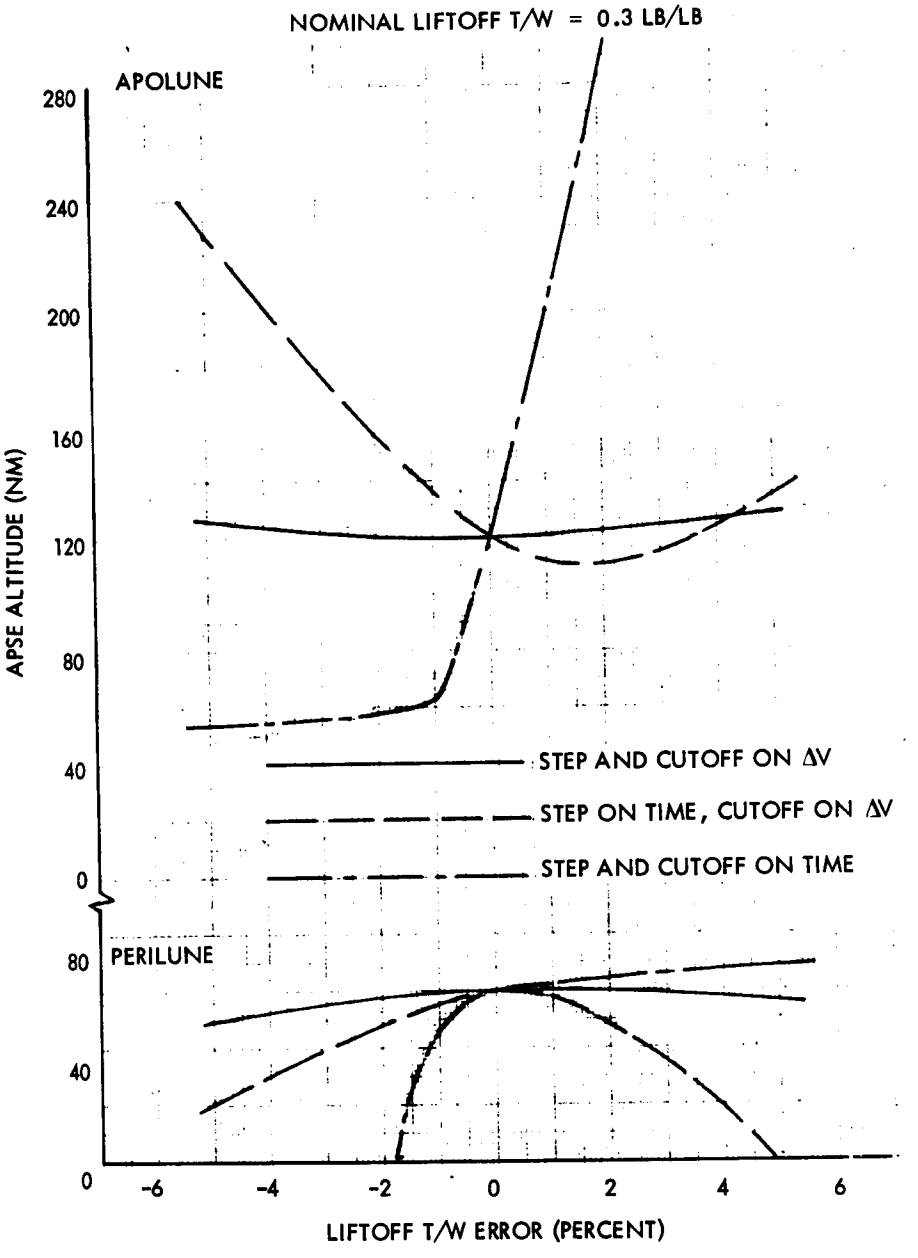

Figure 1-63. - Variation of Apse Altitude With Liftoff Thrust-to-Weight Error for Three-Step LESS Boost to 60- by 120-Nautical-Mile Orbit

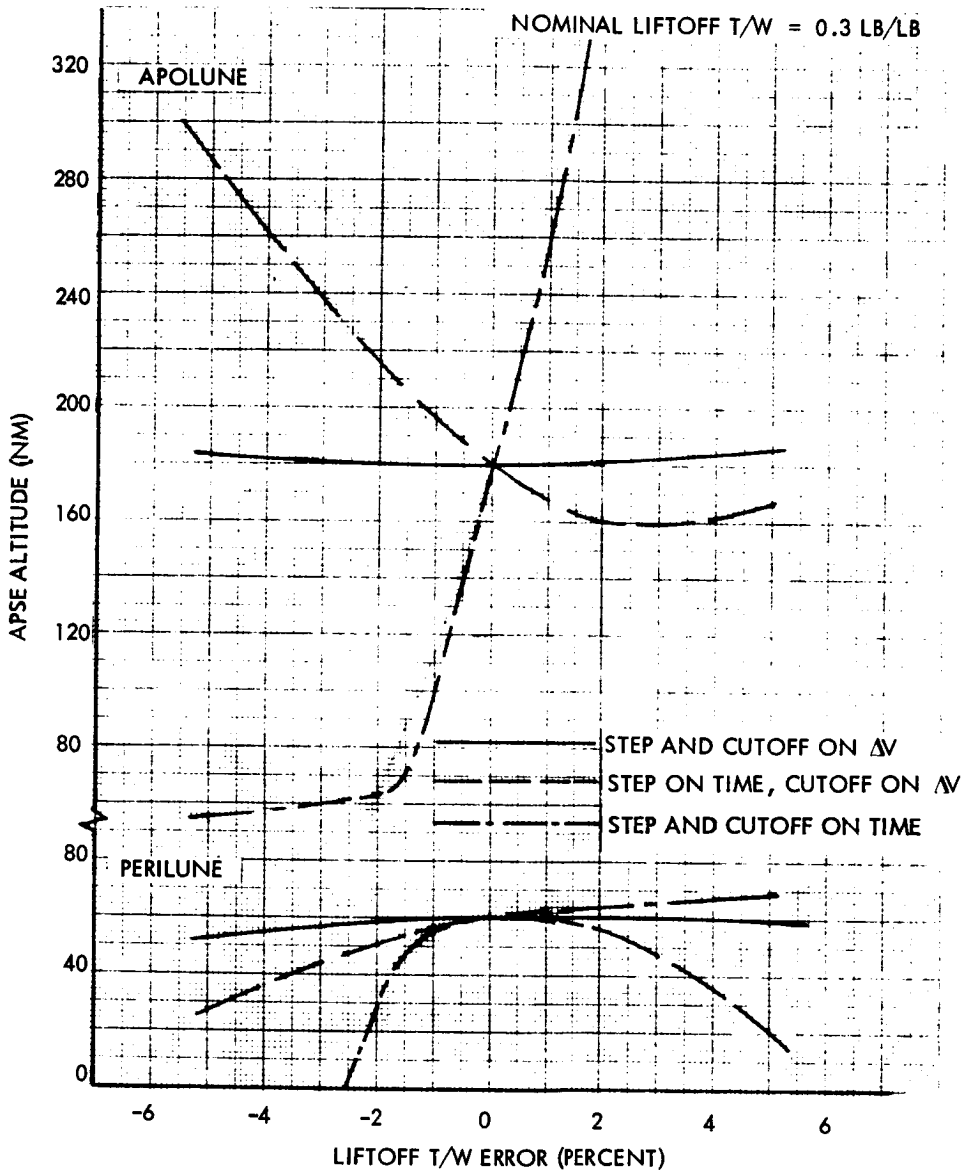

Figure 1-64. - Variation of Apse Altitude With Liftoff Thrust-to-Weight Error for Three-Step LESS Boost to 60- by 180-Nautical-Mile Orbit

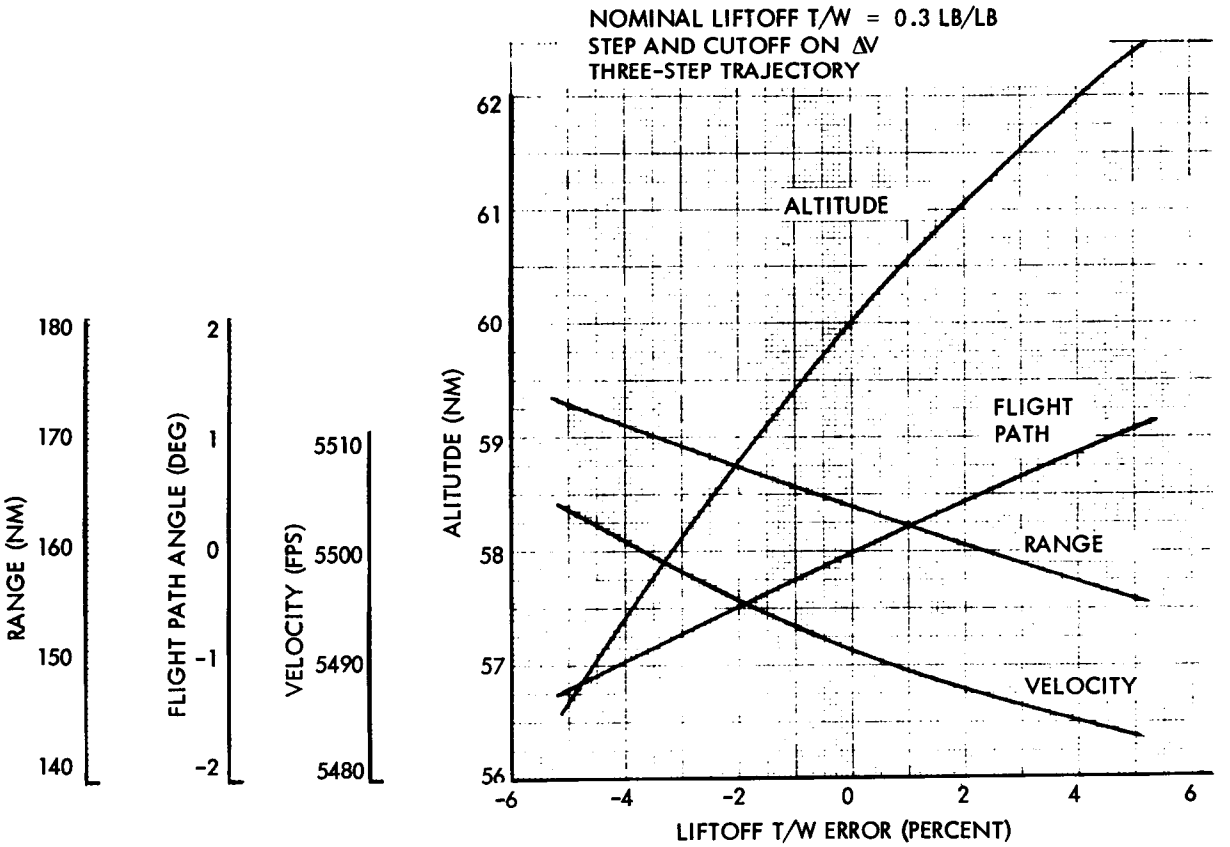

Figure 1-65. - Variation of In-Plane LESS Burnout Conditions With Liftoff Thrust-to-Weight Error for Nominal 60- by 180-Nautical-Mile Orbit

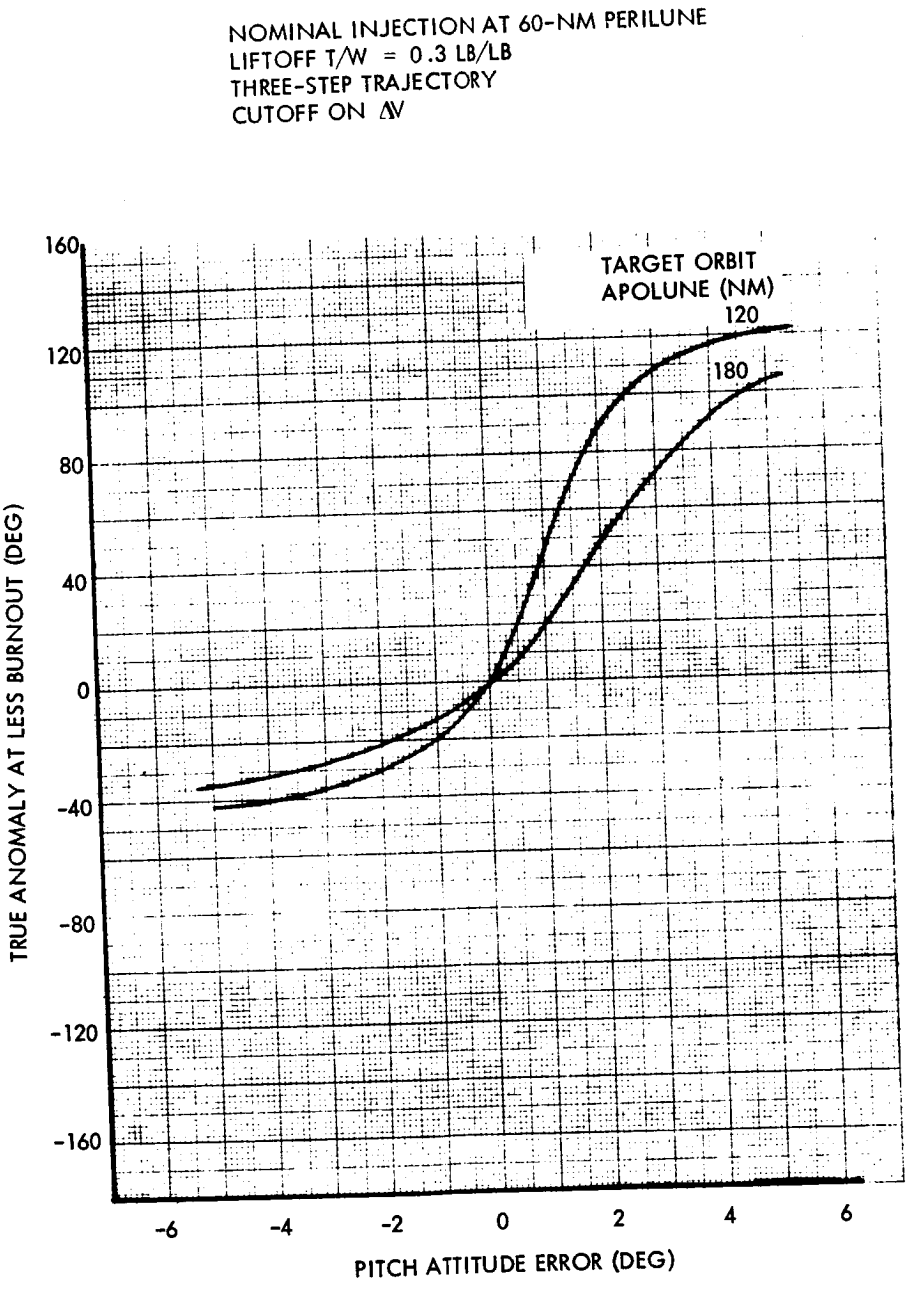

Figure 1-66. - Variation of True Anomaly at LESS Burnout With Pitch Attitude Error for Boost to Perilune of Elliptical Orbits

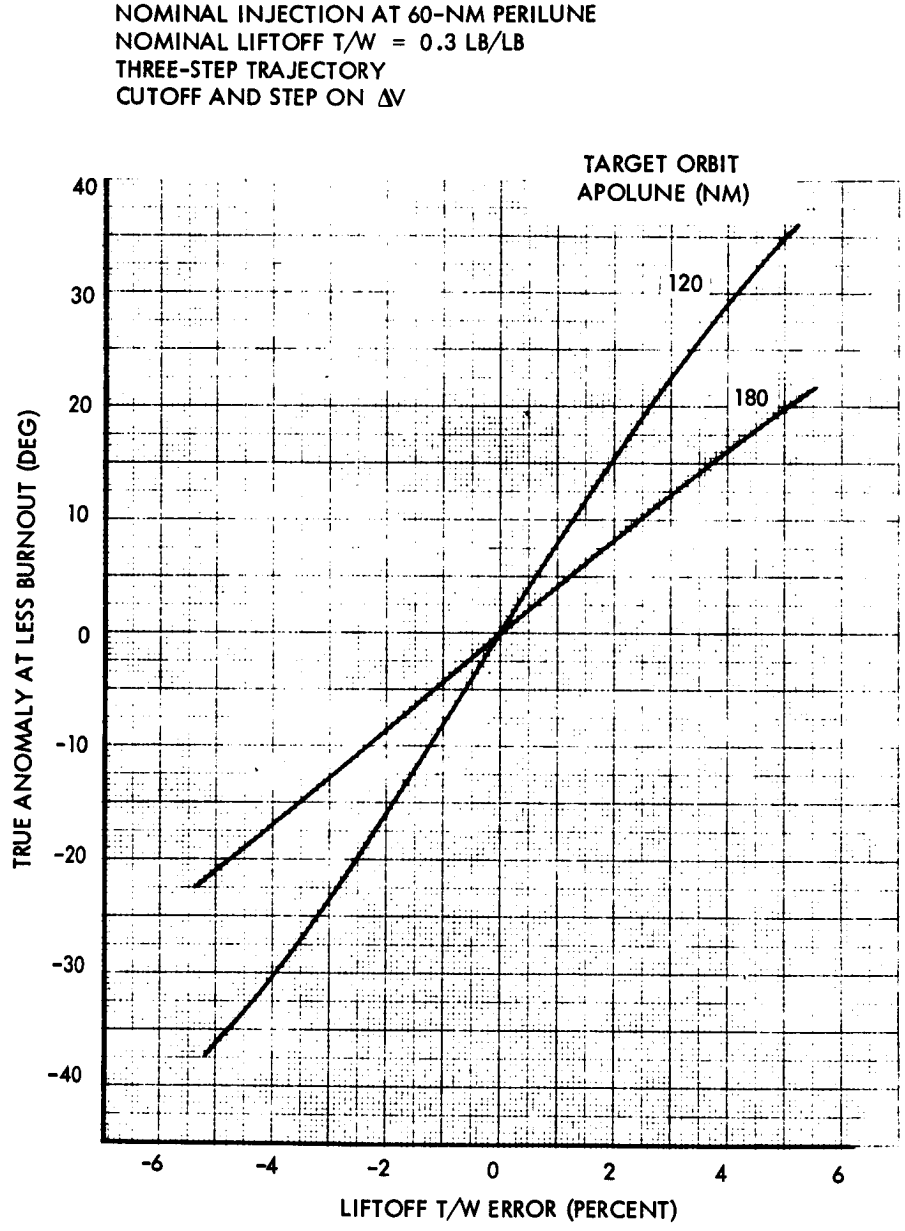

Figure 1-67. - Variation of True Anomaly at LESS Burnout With Liftoff Thrust-to-Weight Error for Boost to Perilune of Elliptical Orbits

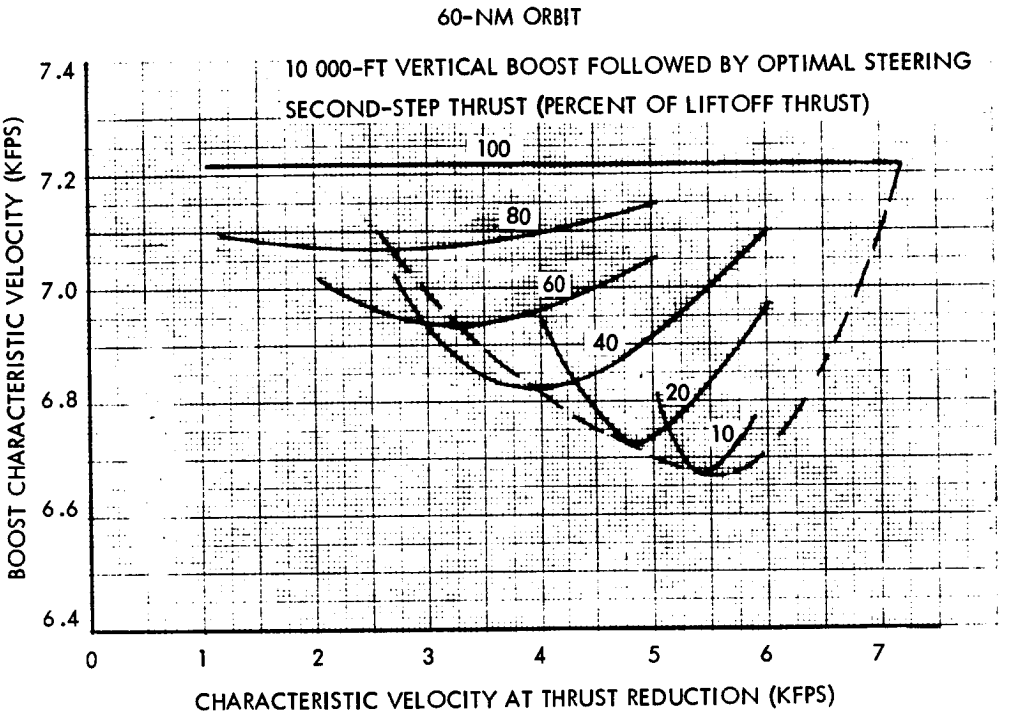

Figure 1-68.- Variation of Boost Energy With Two-Step Thrusting Parameters for Liftoff Thrust-to-Weight of 0.3 lb/lb

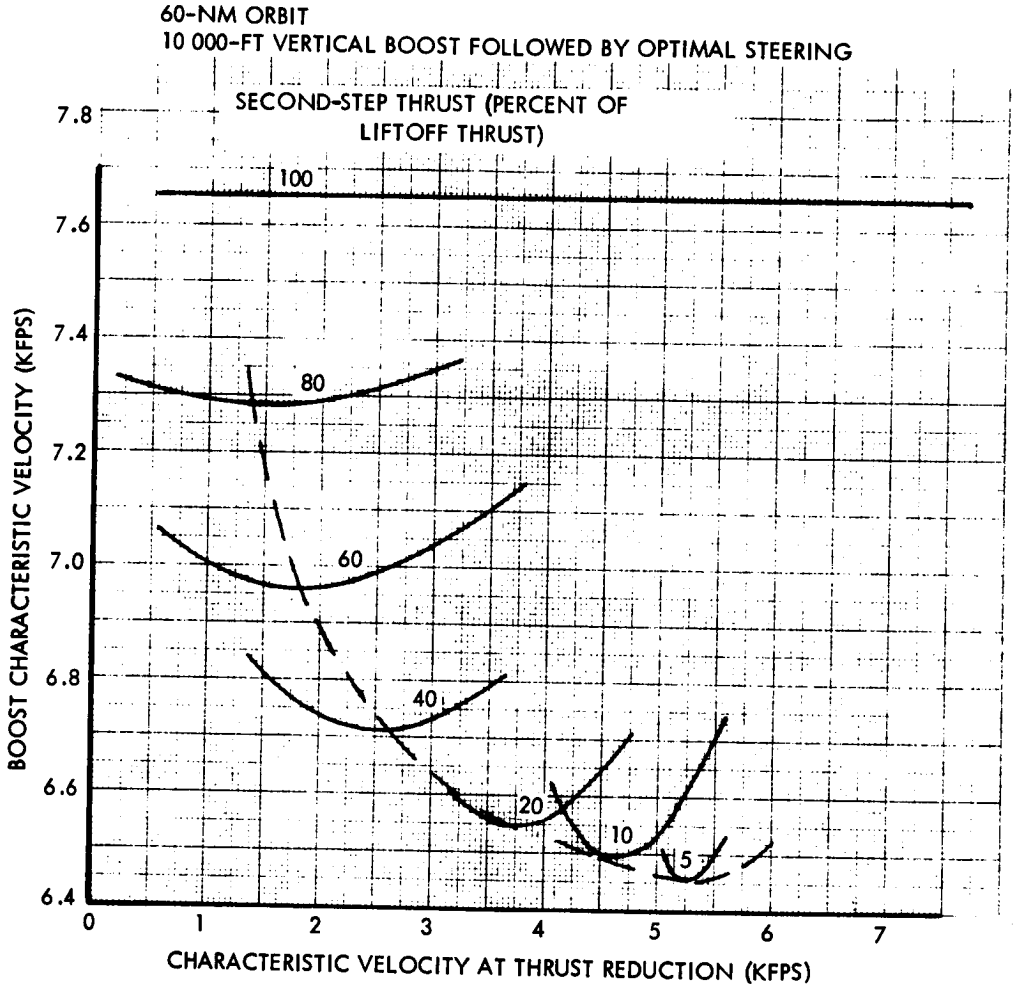

Figure 1-69.- Variation of Boost Energy With Two-Step Thrusting Parameters for Liftoff Thrust-to-Weight of 0.5 lb/lb

followed by optimal steering to orbit insertion and should be typical for most profiles. The locus of minimum energy solutions is shown in figure 1-70 together with those resulting from liftoff thrust-to-weight ratios of 0.4 and 0.7 pound per pound. Figure 1-71 shows the same data as a function of thrust-to-weight ratio prior to the thrust reduction point. It is seen that energy minimums occur for high initial thrust followed by low second-step thrust and that substantial energy reductions can be achieved compared to assuming a single thrust value.

Based on these results, two configurations were selected for more detailed analysis. They employ a liftoff thrust-to-weight ratio of 0.4 pound per pound with the second-step thrust level being 30 and 10 percent, respectively, of nominal. The bent 2-step steering profile was used. Figures 1-72 and 1-73 show the results of optimizing the point for switching to the second steering step. The total energy expenditures are seen to be less than those shown in figure 1-70 for optimum steering. Because the bent 2-step profiles (by definition) do not employ a vertical boost, their energy expenditures are lower than the optimums for which 10 000-foot vertical boosts were assumed.

Altitude/range and acceleration profiles for the two selected trajectories are shown in figures 1-74 and 1-75. These trajectories were used as the basis for determining effects of pitch attitude and thrust errors. The results are shown in figures 1-76 and 1-77. When compared with comparable data for single-valued thrust (the three-step data shown in figures 1-30, 1-32, 1-40, and 1-42), the apse variations are seen to be a maximum of 20 percent more severe with stepped thrust. Thus, while energy gains and stability/control gains are to be realized with stepped thrust, a penalty is paid in terms of error sensitivities.

Appendix E contains a computer printout of a trajectory to 60-nm orbit used as the basis for some simulation studies at NASA-LRC. It reflects a two-step thrust schedule with the first step characterized by a liftoff thrust-to-weight ratio of 0.3 pound per pound and the second step representing a reduction in thrust to one-third the liftoff value. The parameters for thrust reduction are based on LESS handling quality considerations (see the Guidance and Control section). A modified bent two-step steering profile is employed. It is initiated by a 10-second vertical boost followed by two constant attitude steps corresponding to the thrust level steps.

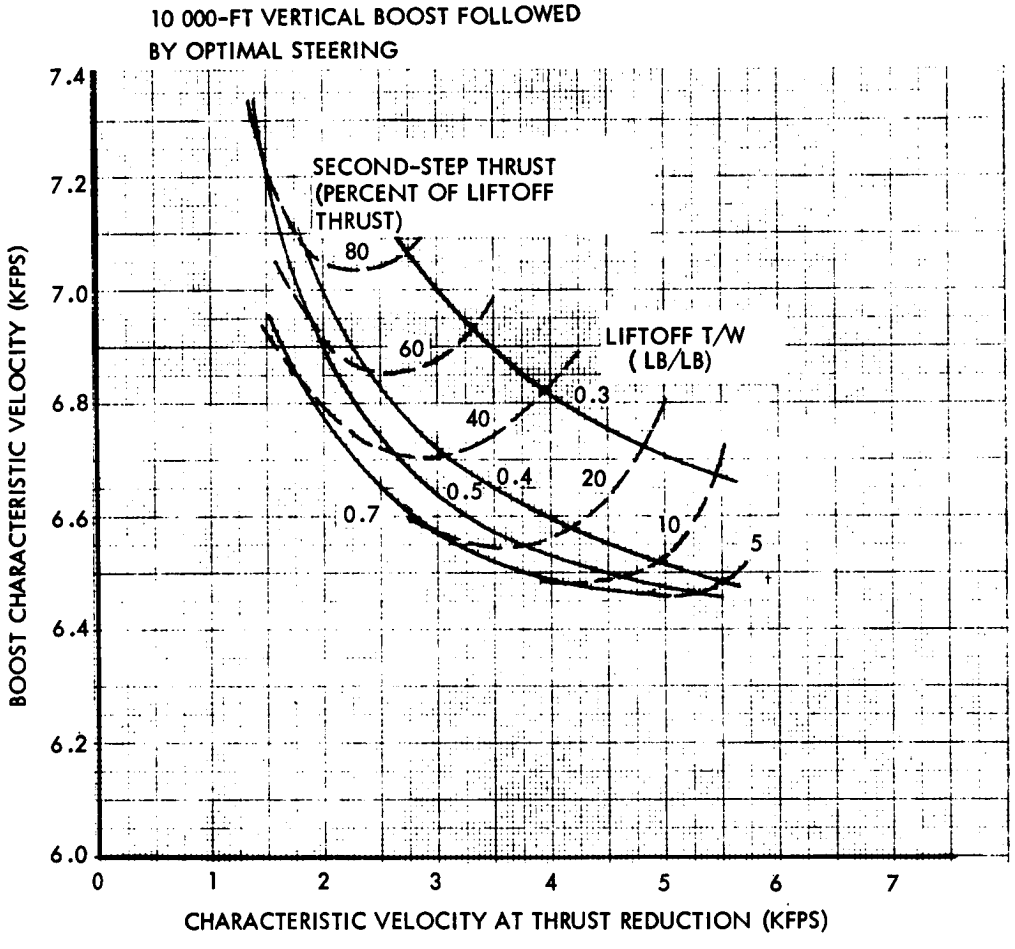

Figure 1-70. - Optimum Two-Step Thrust Schedules for Boost to 60-Nautical-Mile Orbit in Terms of Characteristic Velocity at Thrust Reduction

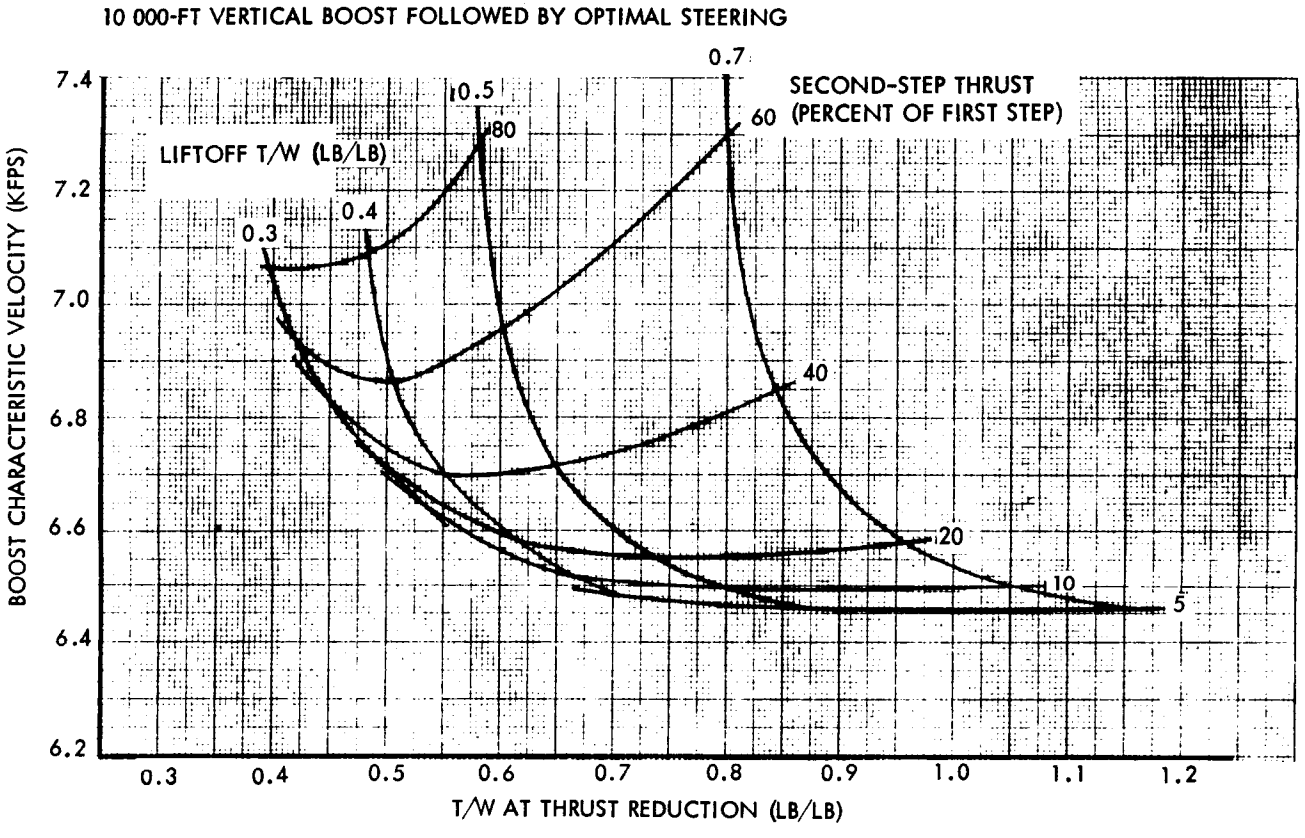

Figure 1-71. - Optimum Two-Step Thrust Schedules for Boost to **60-Nautical**-Mile Orbit in Terms of Thrust-to-Weight at Thrust Reduction

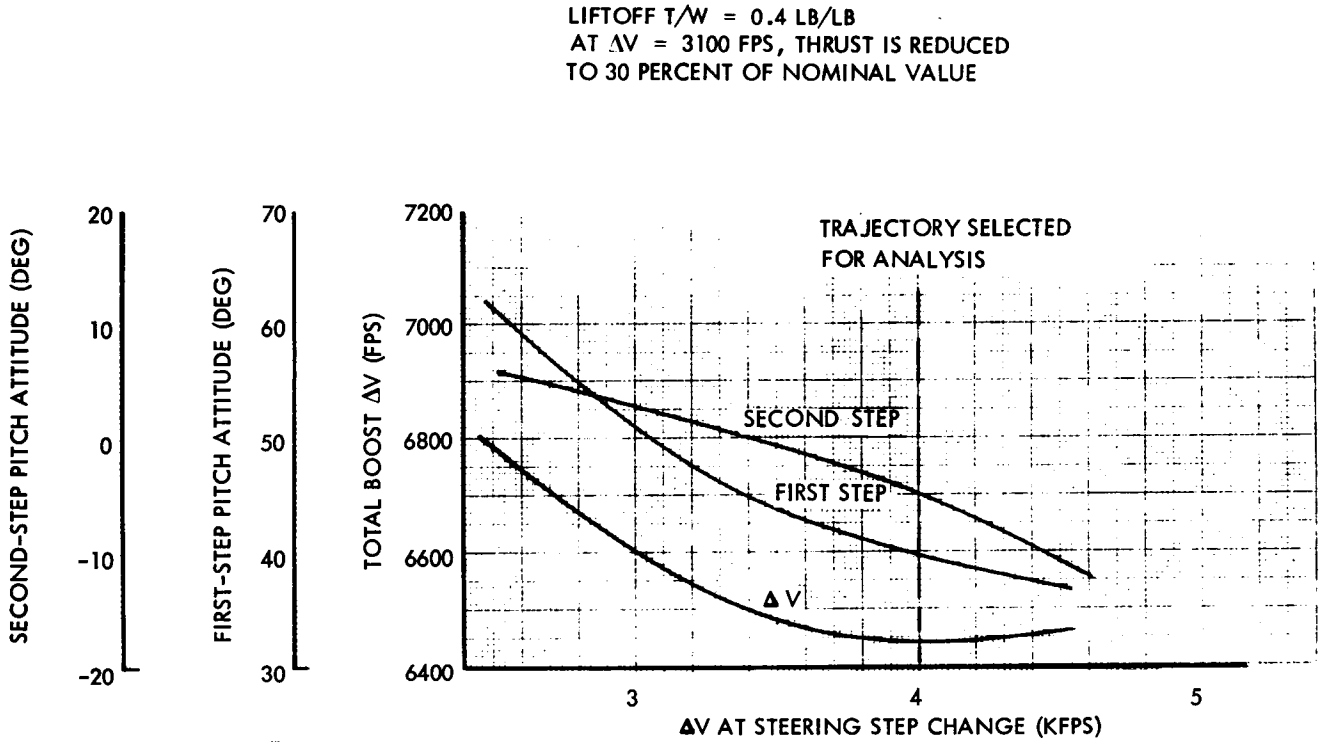

Figure 1-72. - Variation of Bent Two-Step Steering Parameters for Boost to 60-Nautical-Mile Orbit With Two-Step Thrust Schedule

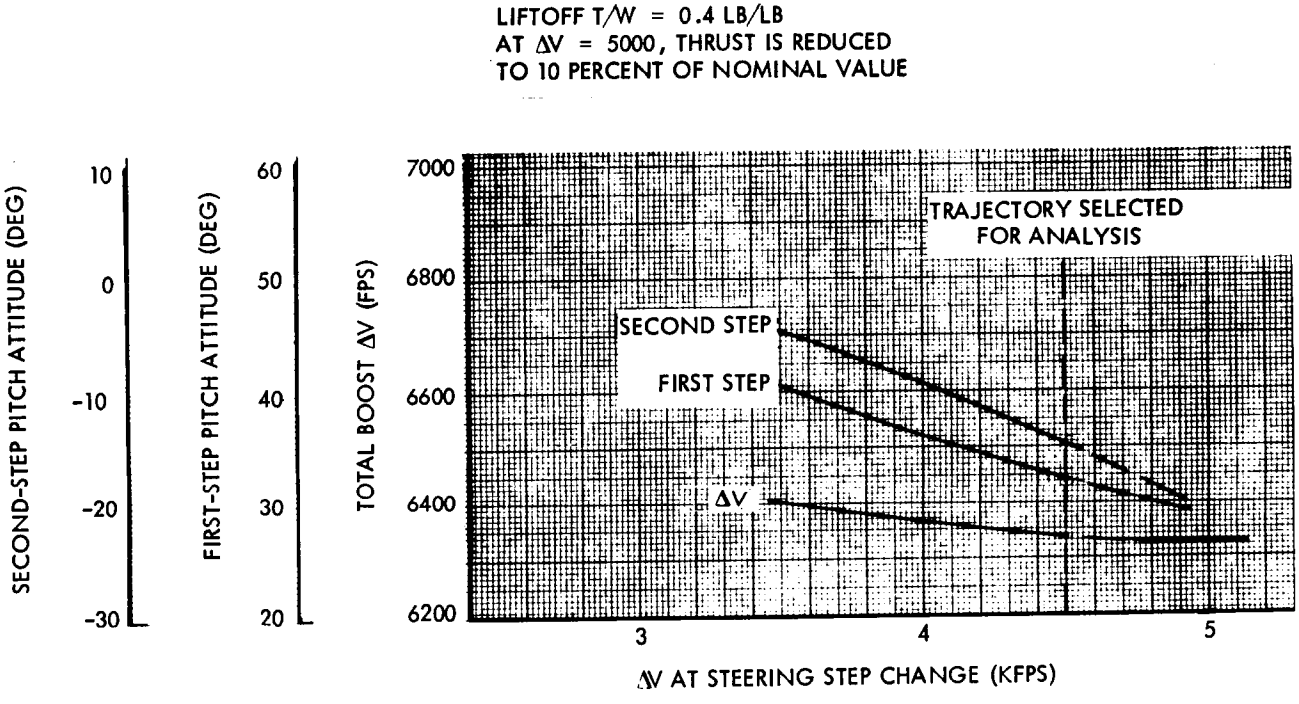

Figure 1-73. - Variation of Bent Two-Step Steering Parameters for Boost to 60-Nautical-Mile Orbit With Two-Step Thrust Schedule

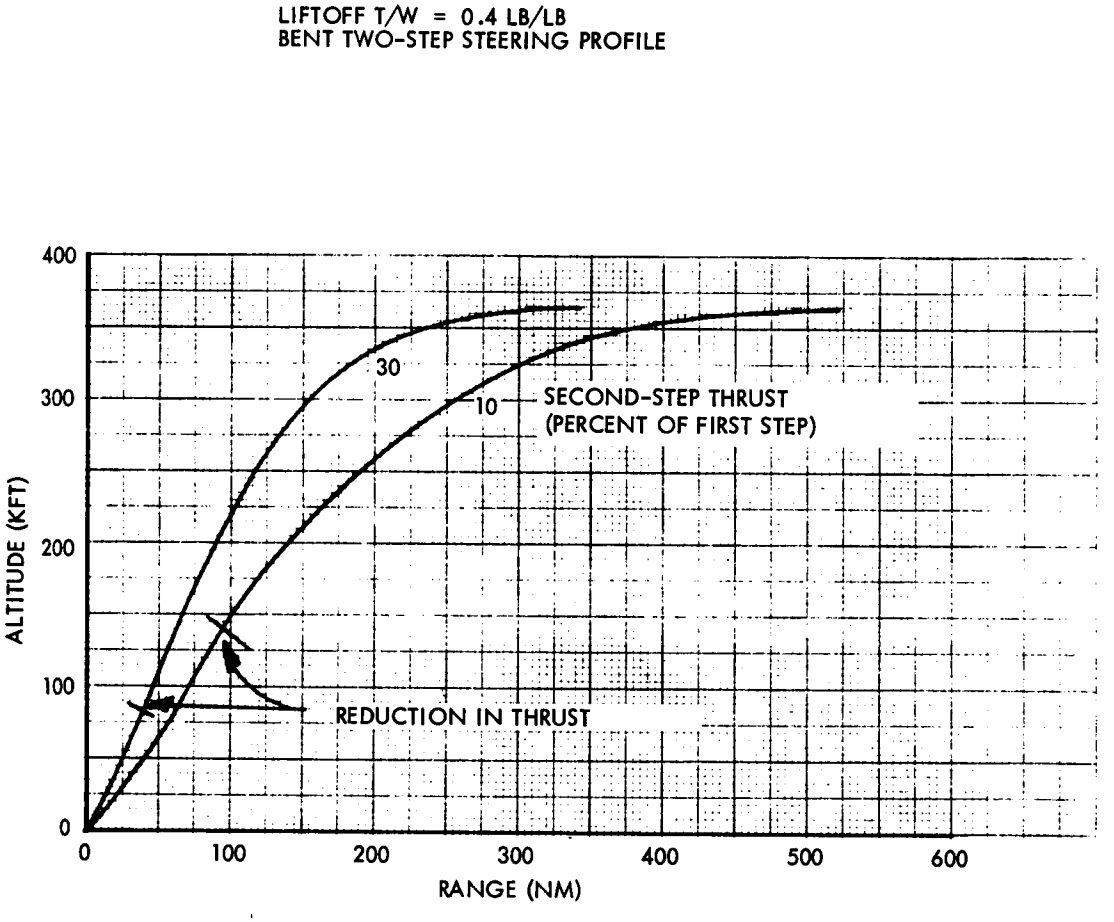

Figure 1-74. - Altitude/Range Profiles for Two Typical Two-Step Thrust Schedules Boosting to 60-Nautical-Mile Orbit

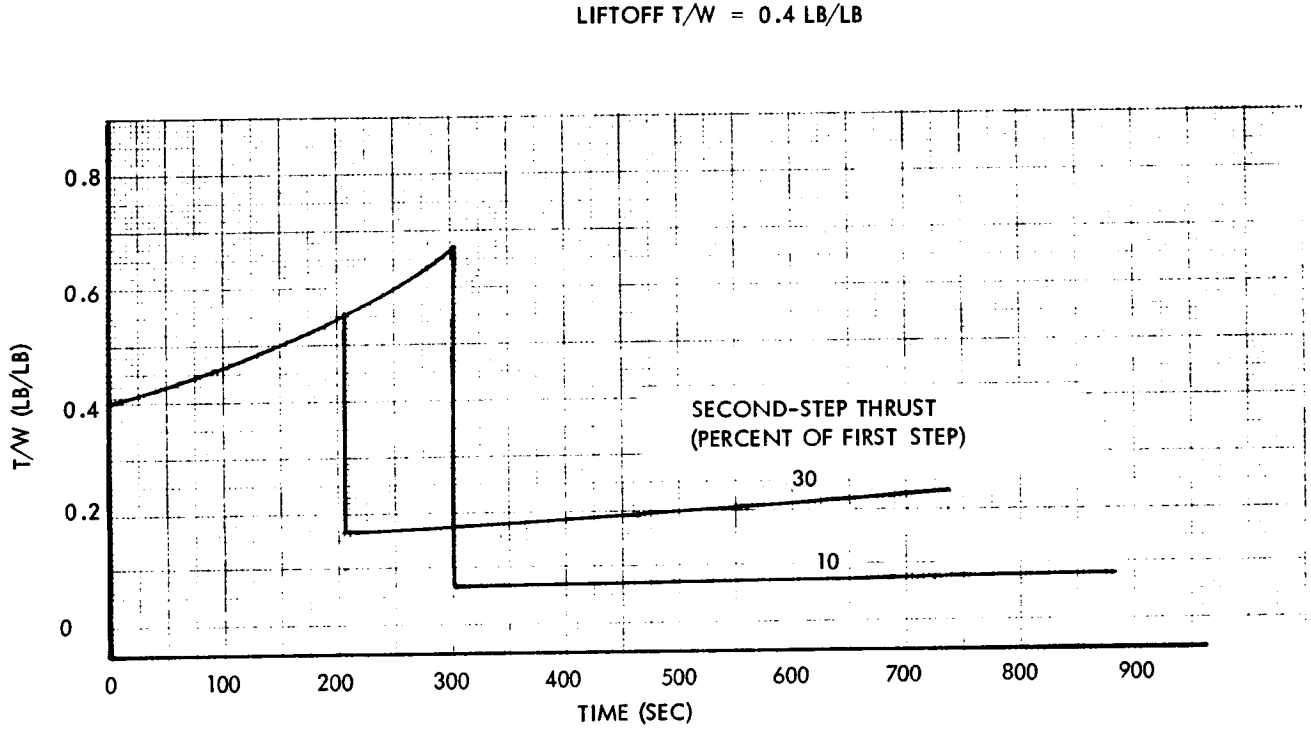

Figure 1-75. - Acceleration Profiles for Two Typical Two-Step Thrust Schedules Boosting to 60-Nautical-Mile Orbit

BENT TWO-STEP STEERING PROFILE
STEP AND CUTOFF ON ΔV

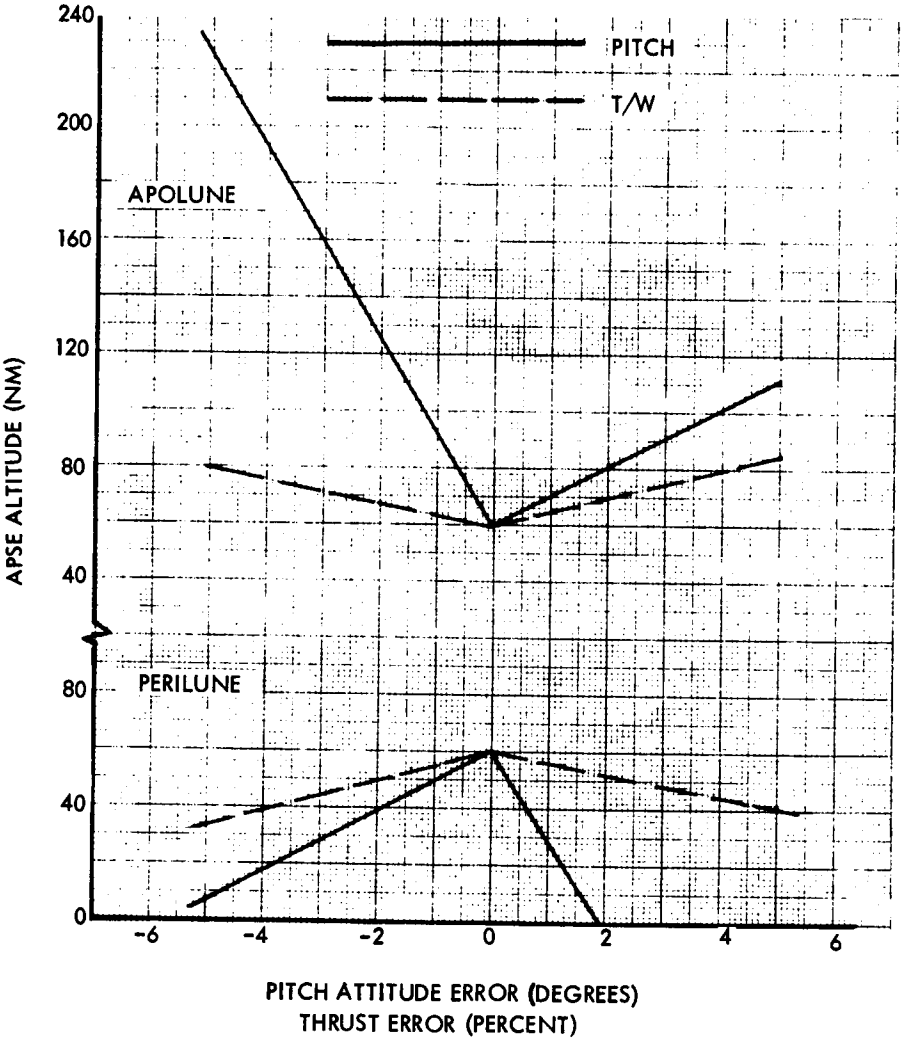

Figure 1-76. - Variation of Apse Altitude With Pitch Attitude and Thrust Errors for Two-Step Thrust Schedule Having Nominal Liftoff Thrust-to-Weight of 0.4 lb/lb and Second Step Thrust of 30 Percent of First Step

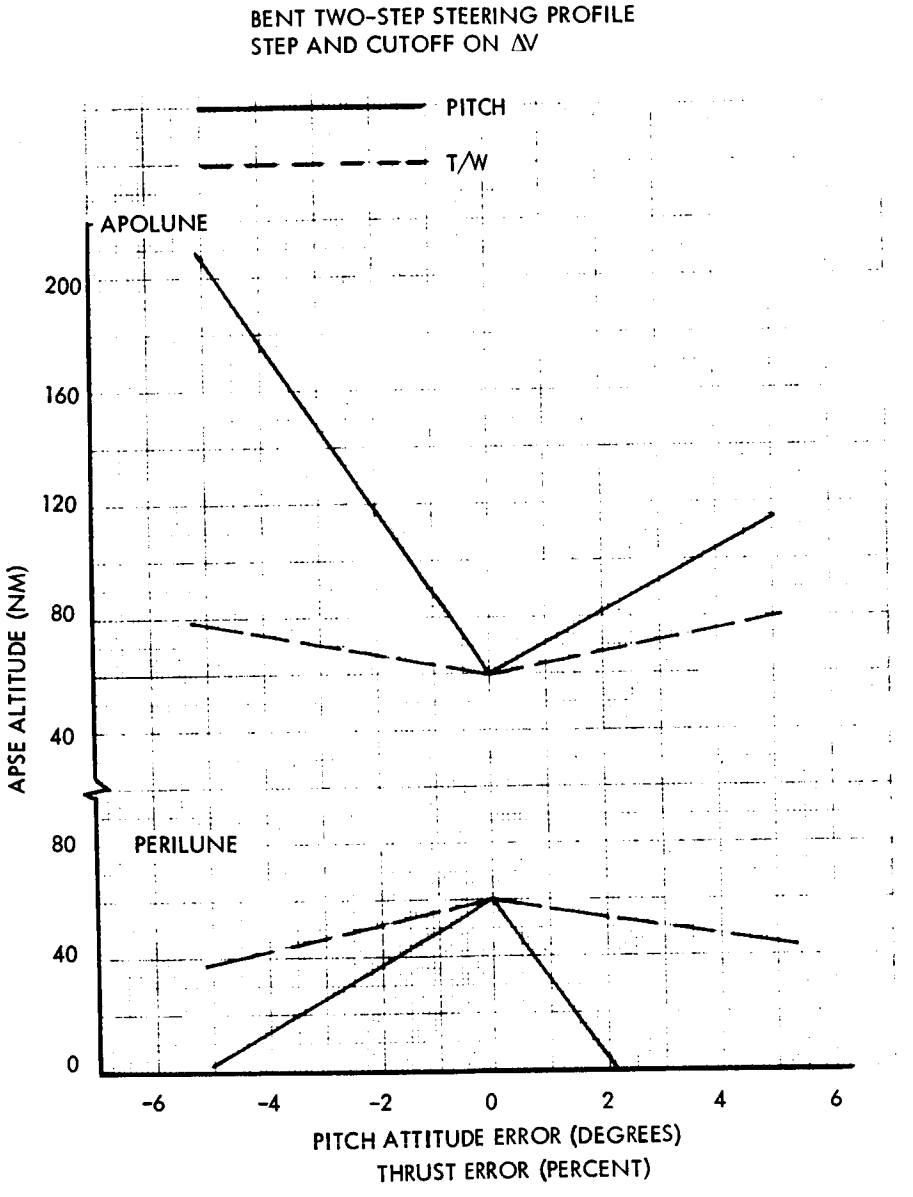

Figure 1-77. - Variation of Apse Altitude With Pitch Attitude and Thrust Errors for Two-Step Thrust Schedule Having Nominal Liftoff Thrust-to-Weight of 0.4 lb/lb and Second Step Thrust of 10 Percent of First Step

Visibility

Objectives and scope of effort. - The primary purpose in examining the visibility conditions prevailing during lunar missions was to establish the feasibility and the limitations of using visual cues for LESS guidance and navigation. The purpose of examining sun angles was to determine their effects on guidance and navigation sensors and other equipment for the duration of expected missions.

Method of approach. - The approach used in investigating the visibility considerations entailed analyzing the proposed missions and thus determining the range of prevailing lighting conditions to be encountered. Next, the effect of the lighting conditions, and hence visibility on sources of visual cues (i.e., down-range horizon, lunar surface, sun, stars, etc.), was determined.

Three discrete mission categories were considered: 3 days, 7 days, and 14 days. Since landings must be made at sun angles between 6 degrees and 20 degrees to permit good visual inspection of the landing area prior to commitment, primary emphasis was placed on the examination of daytime sunlight conditions. Secondary emphasis was placed on examination of visibility under possible earthshine conditions.

Lighting conditions prevailing during lunar missions. - LM landing requirements currently specify sun angles varying between 6 degrees and 20 degrees at the landing site. It is assumed for this study that these requirements will prevail during the post-Apollo missions, although some possibility exists that the higher number may be raised for later missions. The currently planned landing missions are up to 3-day-staytime, dawn missions. A sunset mission may be made to investigate lunar sunset and earthshine conditions. Figure 1-78 depicts illumination conditions during typical 3-day-staytime, dawn and sunset missions, as well as the lighting conditions for a 7-day-staytime, dawn mission (to Copernicus). The dawn landing (Censorinus: 0 degrees 23 S, 32 degrees 32 E) is assumed to be made at a near-minimum 10-degree sun angle. During the 3-day stay mission, the sun angle would increase by 36.6 degrees to an inclination of 47 degrees at launch. At landing, the earth appears as slightly more than one-half illuminated (third quarter).

For near-maximum earthshine to be experienced while a 3-day staytime limit and a 6-degree to 20-degree sun angle upon landing were adhered to, the sunset mission was assumed to visit the Marius Hills (14 degrees N,

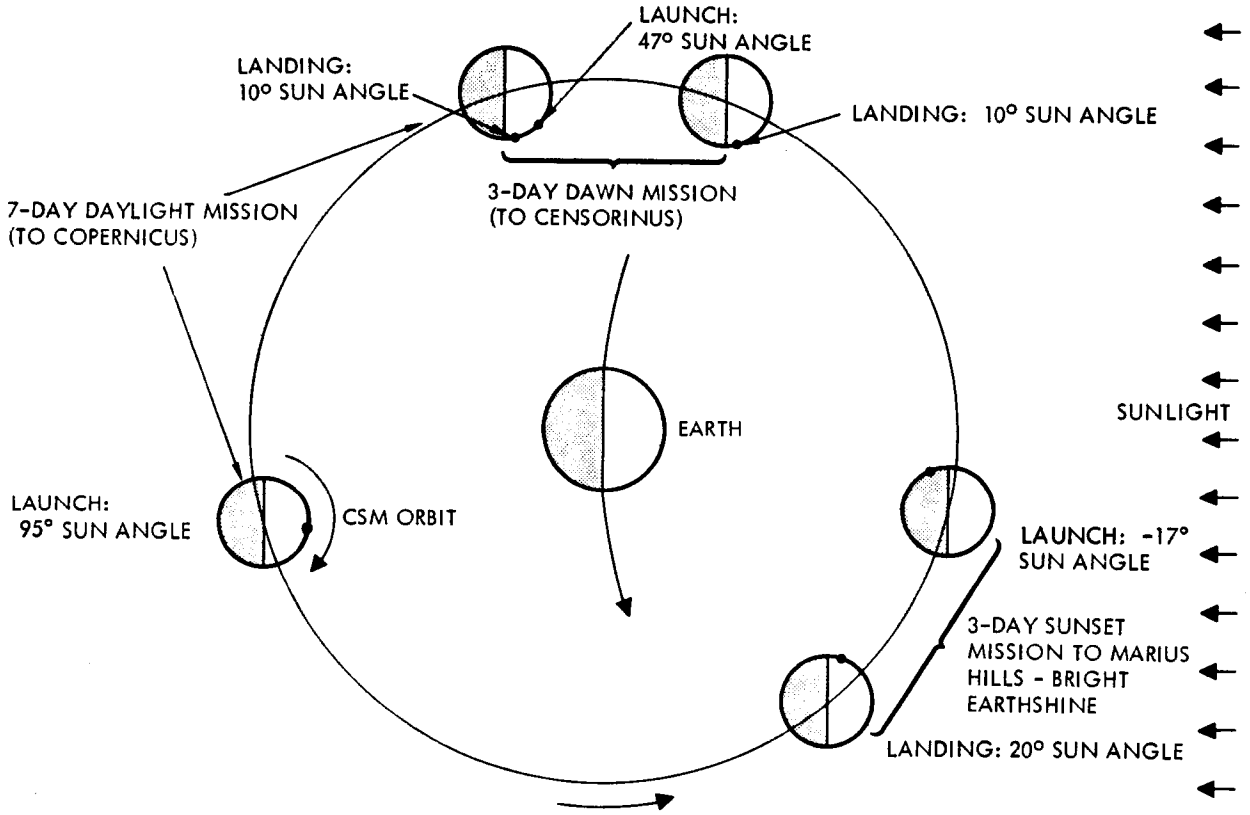

Figure 1-78. - Illumination Conditions During Typical Lunar Missions

56 degrees E). If landing was at the maximum allowable sun angle (20 degrees), sunset would occur late on the second day.* By launch time, there would be almost full earthshine. Figure 1-78 can be used to determine lighting conditions at any (near-equatorial) location during any phase of the moon.

Illumination conditions during a typical lunar mission. - Visibility during LESS ascent bears directly on guidance system selection, design, and evaluation. Guidance cues can be obtained from internal or external systems, as discussed in the Guidance and Control section of this report. In the internal category are such systems as gyro-controlled horizon, gyro compass, inertial reference, etc. External systems are those that make use of either lunar or celestial references. The ability to detect and use the references depends to a large extent on the prevailing lighting conditions and on system designs that permit compensation for adverse lighting conditions. The visibility of the cues depends largely upon lighting conditions, which also change during the lunar staytime. Figure 1-79 shows the sun incidence as a function of that staytime. It is assumed that touchdown occurs at a nominal sun angle of 10 degrees (in a near-equatorial region). The figure shows the sun angle at 24-hour intervals after touchdown for 3-day (FLM), 7-day, and 14-day missions. Mission conditions estimated to be encountered are summarized in table 1-1.

During 3-day ELM missions, sun angles can vary from a minimum of 9 degrees for early abort to a maximum of 60 degrees for late abort with a high landing sun angle. Visibility during this 3-day period is the area of major study emphasis because all currently planned missions fall into this period. (Mission plans beyond this are extremely speculative, although the subject of many studies.) During LESS vertical ascent, the sun will be essentially over the shoulder and from behind and below the pilot during the horizontal thrust step portion of ascent to orbit.

Sun angles for 7-day extended ELM missions are shown for staytimes of up to seven days or sun angles of 9 degrees to about 95 degrees. For these missions, a dual launch mode (such as dual Saturn V) was assumed to provide the necessary staytime extension logistics support. This implies a very substantial step increase in mission capability. Similarly, it is reasonable to assume that the LESS could also have a step change for increased capability.

For staytimes of up to 14 days, sun angles could vary from the nominal 9 degrees to 180 degrees (on the downrange horizon). This represents another large step in mission capability, so a step change in LESS capability could also be appropriate.

* Landing occurs against the sun unless a posigrade lunar orbit is employed.

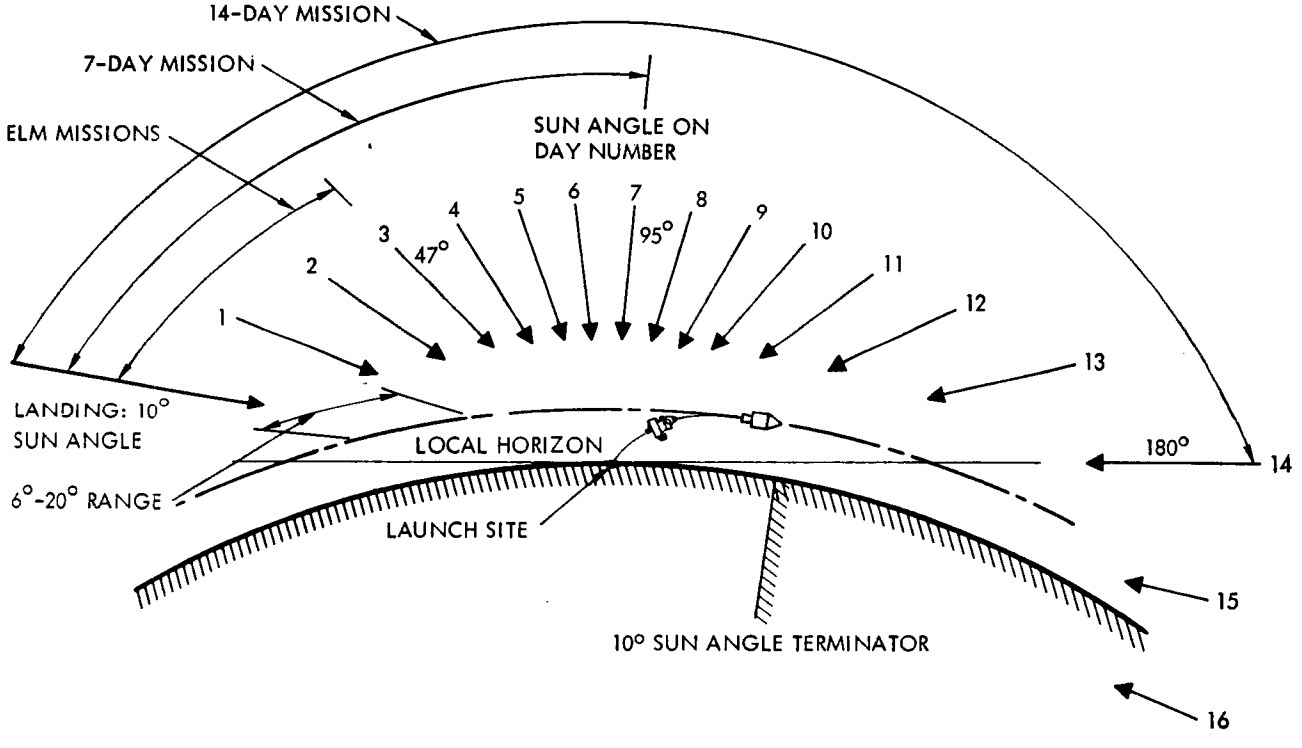

Figure 1-79. - Sun Incidence as a Function of Staytime

TABLE 1-1. - ASSUMED CATEGORIES OF LUNAR MISSIONS

	Apollo - LM	ELM	Advanced Apollo Dual Launch	Orbital-Surface Bases
Time period	1969-1971	1972-1973	1974-1976	1977-
Transportation	Basic Apollo systems	Extended Apollo systems	Saturn V/LM plus logistics	Orbit-to-surface shuttle
Staytime	1 day	1-3 days	7+ days	>14 days
Sun angles Landing range Maximum	 6°-20° 32°	 6°-20° 60°	 6°-20°+ 108°	 6°-20°+ 194° (below horizon)
Mobility system	Walk	LRV/LESS/LFV	LRV, LESS/flyer	LRV, LESS/flyer
Backpack life	PLSS 3-1/2 - 4 hr	PLSS + OPS or PECS 5.5-6 hr	PECS 6-8 hr	PECS 8+ hr

An ascent trajectory to a nominal 60-nm orbit is also shown, so that the effect of the sun angle on visibility (lunar, stellar, or instrument) can be investigated. An adverse sun angle can produce glare off instruments, reduce contrast definition, obliterate the downrange horizon by obscuring it in the lunar shadow or by having the horizon so close to the sun so that it cannot be visually observed because of the blinding intensity of the sunlight, and can obscure the CSM during ascent and rendezvous because of the proximity to the solar disk.

Time lines. - A nominal 3-day, dawn mission time line (table 1-2) was constructed to place in perspective the lunar activities associated with the use of the LESS for abort. A brief analysis of circumstances necessitating abort indicated that the realization for the need to abort via the LESS would most likely occur shortly after touchdown or prior to launch.

A LESS abort time line was also prepared and is included in the Surface Operations section of this report. An analysis of this time line showed that if the acceptable sun angle at touchdown ranged from 6 degrees to 20 degrees, then the minimum sun angle at LESS abort during a nominal 3-day mission could be as low as 9 degrees or as high as 60 degrees.

Range of lighting conditions during typical abort ascent. - The maximum staytime during the currently planned lunar program (1969-73, 10 missions) is 3 days. Hence, the nominal ELM mission was assumed to be a 3-day dawn mission, and visibility conditions that would prevail during LESS ascent to orbit during this period were emphasized. Figure 1-80 shows LESS-CSM-sun angle orientation during a nominal abort. The LESS trajectory was based on calculus of variations equations. The lines connecting the CSM orbit and the ascent trajectory show the relative positions of the CSM and LESS at various times after lift-off. To ascend close to the CSM in a 60-nm orbit, the LESS must lift off when the CSM is 9 degrees above the horizon. A preliminary analysis of lunar operations shows that between four and six hours could be required after touchdown to prepare for LESS abort. During four hours, the sun angle changes by 2 degrees. Thus, if a 7-degree sun angle prevailed at touchdown, and LESS abort was immediately required, the sun angle at lift-off would be 9 degrees. If the cause for abort were discovered toward the end of the 3-day stay, then the sun angle could be as high as (20° +37° +3°=) 60 degrees. As the two spacecraft drew close, the CSM would be coming out of that portion of the sky containing the sun and would be virtually impossible to observe. Indeed, the CSM could be crossing the solar disk as viewed from the LESS.

The results indicate that the line of sight to the CSM during most of the abort trajectory would be so close to the sun that visual observation of the

TABLE 1-2. - NOMINAL THREE-DAY DAWN MISSION TIMELINE

Assumptions/constraints:

- Lunar dawn landing with 10° sun angle at landing (-50 F) and 47° sun angle at lift-off (180 F)
- Lunar equatorial region mission (±15° lat)
- 3-day lunar surface staytime
- 2-man ELM with 1 LFV and 1 LESS
- 11 hours of personal maintenance/rest per day
- 1000 lb of propellant for LFV excursions

Event Start Time	Lunar Staytime Events		Event Duration Time
:00	ELM touchdown on lunar surface, surface temp -50 F		
:00	Checkout and activation of ELM for lunar stay		2:00
	Post-landing checkout	:30	
	Launch simulation	1:30	
2:00	Science conference with earth		:30
2:30	Personal maintenance (lunch)		1:00
3:30	Preparation for EVA		:30
	Don and check out PLSS	:25	
	Dump cabin pressure and egress	:05	
4:00	EVA (1 and 2), surface temp -20 F		3:00
	ELM inspection	:15	
	Erection of solar array	:20	
	Erection of radiator	:30	
	Erection of antenna	:20	
	Dismount LESS sections	:15	

TABLE 1-2. - NOMINAL THREE-DAY DAWN MISSION TIMELINE - Continued

Event Start Time	Lunar Staytime Events		Event Duration Time
	Assemble LESS and prepare servicing lines	:15	
	Check out LESS mechanical systems	:05	
	Transport LESS to launch area (50 ft)	:05	
	Shroud LESS	:05	
	Dismount LFV	:10	
	Assemble LFV, mount scientific equipment	:05	
	Set up LFV landing mats and aids 50 ft from ELM	:10	
	Move LFV to landing mat	:05	
	Check out LFV 1 (electronics/controls)	:10	
	Deploy fuel and oxidizer hoses	:10	
7:00	Ingress to ELM and hook up ELM-ECS		:10
7:10	Repressurize ELM and doff pressure suits		:20
7:30	Personal maintenance (supper)		1:00
8:30	Housekeeping and maintenance check		1:00
9:30	Sleep/rest		7:00
16:30	Personal maintenance (breakfast)		1:00
17:30	Preparation for EVA		1:00
	Don and check out pressure suits	:30	
	Don and check out PLSS	:25	
	Dump cabin pressure and egress	:05	
18:30	EVA (3 and 4), surface temp 45 F		3:00
	Scientist-astronaut 1		
	Fuel LFV on mat and mount helium tank	:25	
	Check out LFV	:10	
	Flight out -0.5 nm qualification flight	:03	
	Post-landing checkout	:05	
	Deploy launching mat	:10	
	Local exploration	:30	
	Preflight checkout	:05	

TABLE 1-2. - NOMINAL THREE-DAY DAWN MISSION TIMELINE - Continued

Event Start Time	Lunar Staytime Events		Event Duration Time
	Flight back - 0.5 nm	:02	
	Post-landing checkout	:05	
	Monitor S/A 2 flight	:30	
	Complete setting up advanced ALSEP	:55	
	Scientist-astronaut 2		
	Start setting up advanced ALSEP	:60	
	Monitor S/A 1 flight	:30	
	LFV qualification flight same as above	:60	
	Refuel LFV - deploy thermal blanket	:30	
21:30	Ingress to ELM and hook up ELM-ECS		:10
21:40	Repressurize ELM and doff pressure suits		:20
22:00	Personal maintenance (lunch)		1:00
23:00	Science conference with earth		1:00
24:00	Preparation for EVA (same as hour 17:30)		1:00
25:00	EVA (5), Scientist-astronaut 1, surface temp 85 F		3:00
	Replace helium tanks and batteries	:10	
	Check out LFV	:10	
	Flight out - 7 nm	:04	
	Post-landing checkout	:05	
	Deploy launching mat	:10	
	Local exploration	1:37	
	Preflight checkout	:05	
	Flight back - 7 nm	:04	
	Post-landing checkout	:05	
	Refuel LFV - deploy thermal blanket	:30	
	Scientist-astronaut 2 monitors	3:00	
28:00	Ingress to ELM and hook up ELM-ECS		:10
28:10	Repressurize ELM and doff pressure suits		:20

TABLE 1-2. - NOMINAL THREE-DAY DAWN MISSION

TIMELINE - Continued

Event Start Time	Lunar Staytime Events	Event Duration Time
28:30	Personal maintenance (supper)	1:00
29:30	Review results of flight with earth scientists	1:00
30:30	Housekeeping and maintenance check	1:00
31:30	Sleep/rest	8:00
39:30	Personal maintenance (breakfast)	1:00
40:30	Preparation for EVA (same as hour 17:30)	1:00
41:30	EVA (6), Scientist-astronaut 2, surface temp 130 F Same as EVA (5) Scientist-astronaut 1 monitors	3:00
44:30	Ingress to ELM and hook up ELM-RCS	:10
44:40	Repressurize ELM and doff pressure suits	:20
45:00	Personal maintenance (lunch)	1:00
46:00	Science conference with earth	1:00
47:00	Preparation for EVA (same as hour 17:30)	1:00
48:00	EVA (7), Scientist-astronaut 1, surface temp 150 F Same as EVA (5) Scientist-astronaut 2 monitors	3:00
51:00	Ingress to ELM and hook up ELM-ECS	:10
51:10	Repressurize ELM and doff pressure suits	:20
51:30	Personal maintenance (supper)	1:00

TABLE 1-2. - NOMINAL THREE-DAY DAWN MISSION TIMELINE - Concluded

Event Start Time	Lunar Staytime Events	Event Duration Time
52:30	Housekeeping and maintenance check	1:00
53:30	Sleep/rest	8:00
61:30	Personal maintenance (breakfast)	1:00
62:30	Preparation for final EVA's (same as hour 17:30)	1:00
63:30	EVA (8 and 9), surface temp 165 F Sample selection Sample storage Check ALSEP Check out ELM ascent stage	3:00
66:30	Ingress to ELM and hook up ELM-ECS	:10
66:40	Repressurize ELM	:05
66:45	Personal maintenance (lunch)	1:00
67:45	Prelaunch countdown and checkout	3:00
70:45	Liftoff, surface temp 175 F	-

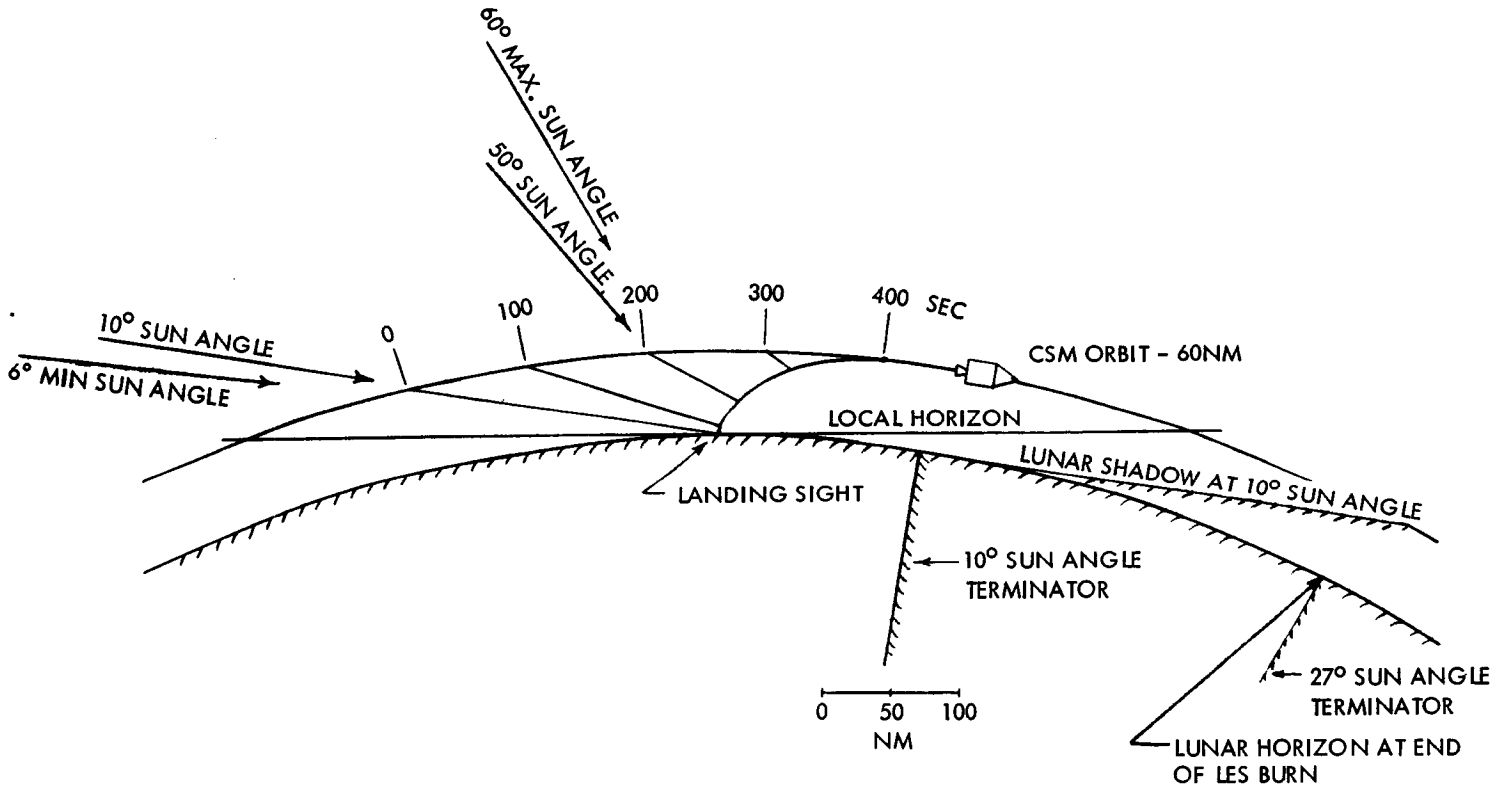

Figure 1-80. - Range of Lighting Conditions During Typical Abort Ascent

CSM for guidance information would not be possible unless the CSM significantly leads the LESS. The figure reveals that the powered phase would be concluded before passage over the terminator in the event of early abort.

Figure 1-80 also shows that in the event of a liftoff of the LESS at a 10-degree sun angle, the CSM and LESS would be in sunlight for approximately 7.5 minutes before they both entered the lunar shadow. A T/W of 0.3 was used for the ascent. If a trajectory T/W of 0.4 were used, the ascent would be accomplished within three-fourths of the distance shown. Analysis of lighting conditions over a variety of situations is possible with this to-scale diagram.

During almost all lunar missions on the earth side, some earthshine will be visible. The extent of earthshine, assuming dawn (or sunset) landings, depends on the landing location. The phase (fraction illuminated) of the earth as viewed from the moon, plus the phase of the moon as viewed from the earth, always equals unity. An examination of figure 1-78 reveals that maximum earthshine, during the 3-day staytime, dawn (or sunset) missions considered here, would occur if the landings were made on either the extreme western (leading) or eastern (trailing) edges of the lunar disk. Analyses of 30 condidate landing sites of greatest scientific interest reveals that the average site is approximately 11 degrees W longitude. Figure 1-81 shows the total brightness of the moon as a function of the phase angle. A similar relationship is believed to exist for the brightness of earthshine, although earthshine would probably be more variable since it would depend on the percent, composition, and location of cloud cover and on the earth surface displayed. A dawn landing at 11 degrees W longitude would encounter (at earliest possible abort-terminator at 20° W) approximately 5 percent of the total possible brightness of earthshine. If abort is assumed after 3 days of staytime (terminator at 71 degrees W), approximately 1 percent of the total possible brightness of earthshine would be experienced. Even if surface features could be discerned under full earthshine, beyond the terminator the low probability of encountering this condition tends to preclude dependence on earthshine illumination for discerning lunar surface features for guidance and navigation.

Use of visual cues during abort ascent. - The visual cues available for reference during LESS abort may be categorized as lunar or nonlunar (i.e., sun, earth, stars). Use could be made of the earth or sun for reference, but other references would be needed (see Guidance and Control section). Since all of the currently planned lunar missions are sunlight missions and since, based on astronaut observations, stars were not normally visible when in sunlight, the use of stars for reference during abort was considered highly questionable.

Effect of horizon roughness on visibility. - An analysis was made of the horizon roughness during typical abort ascent from seven typical landing sites of scientific interest. The seven for which topographic maps were available were:

1. Copernicus Center (9° 43'N, 20°0'W)
2. Copernicus Wall (10° 51'N, 20° 9'W)
3. Censorinus (0° 23'S, 32° 32'E)
4. Marius Hills (14° 35'N, 56° 37'W)
5. Abulfeda (14° 57'S, 14° 18'E)
6. Schroters Valley (24° 20'N, 49° 29'W)
7. Hadley Rille (24° 42'N, 2° 57'E)

Figure 1-82 shows the results of the analysis. Roughness was defined as the angular projection of proximate surface features above the line of sight to the lunar horizon or point of tangency. Horizon roughness could present a moderate problem in orientation only during the initial portion of the ascent trajectory, and that only in rough terrain. At an altitude of 5 nautical miles, the maximum roughness that would be encountered at these 7 sites was found to be less than 0.4 degree. Since this value was obtained for isolated peaks or rilles, the error due to horizon roughness should be substantially less than 0.4 degree because an optically averaged horizon profile would be used as reference rather than the anomalous peaks.

An analysis of the curvature of the lunar horizon when viewed from an altitude of 60 nautical miles revealed that, with a field of view of 17 degrees, the curvature of the horizon drops less than 30 seconds of arc from the horizontal and so appears almost as a straight line. Figure 1-83 shows the curvature with respect to a straight line. Consequently, it should be possible to use the lunar horizon as an accurate reference.

Down-range horizon visibility. - A basic concept of LESS guidance and navigation would make use of the downrange horizon as a reference for pitch attitude. If LESS abort were required at a near minimum sun angle (7 degrees + 2 degrees = 9 degrees), the downrange horizon would be visible for approximately two minutes of a nominal 7-minute powered ascent. The terminator would intervene, and the horizon would not be visible as it would be beyond the terminator. This condition, during which the lunar downrange horizon would be beyond the terminator and hence not discernible, would

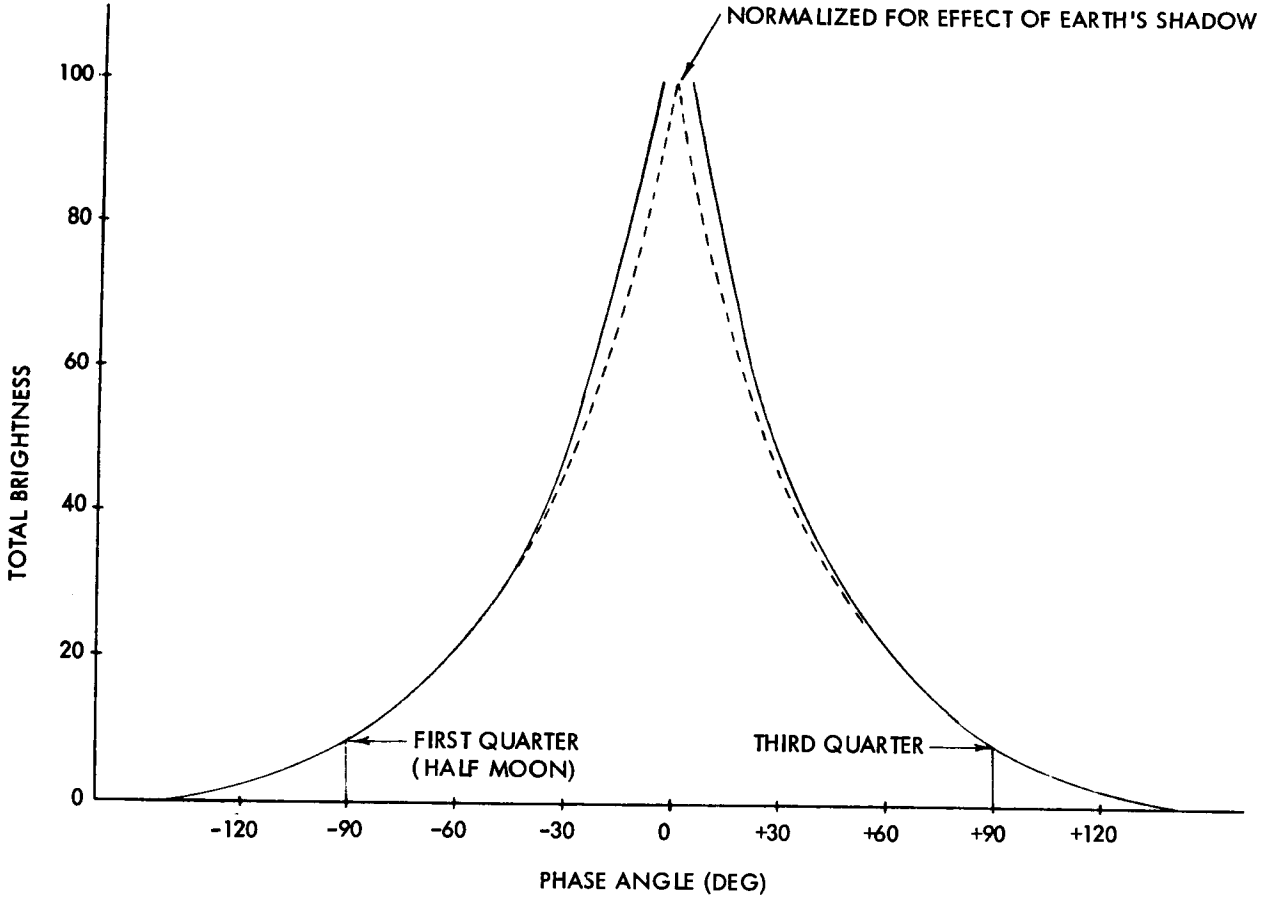

FROM Z. KOPAL, PHYSICS AND ASTRONOMY OF THE MOON, ACADEMIC PRESS, PP. 102 - 104 (1962).

Figure 1-81. - Total Brightness of the Moon as a Function of Phase Angle

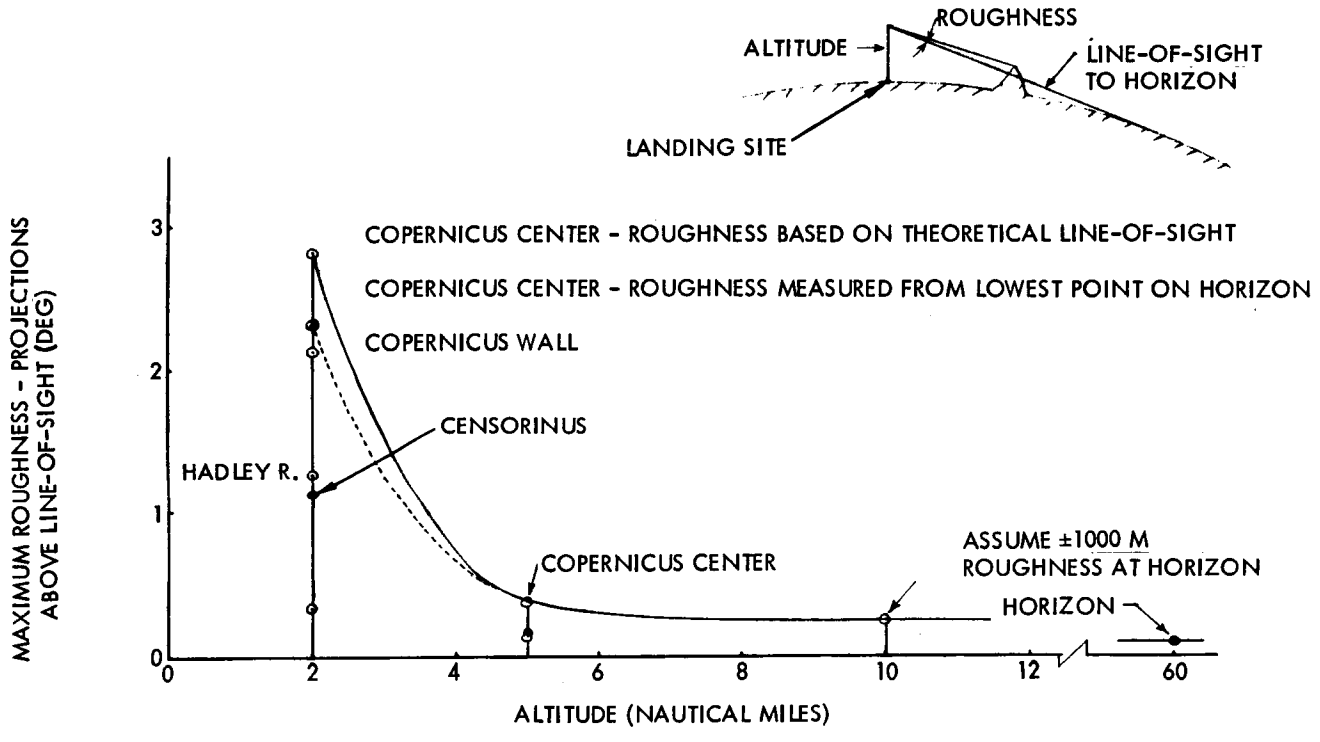

Figure 1-82. - Typical Lunar Horizon Roughness as a Function of Altitude

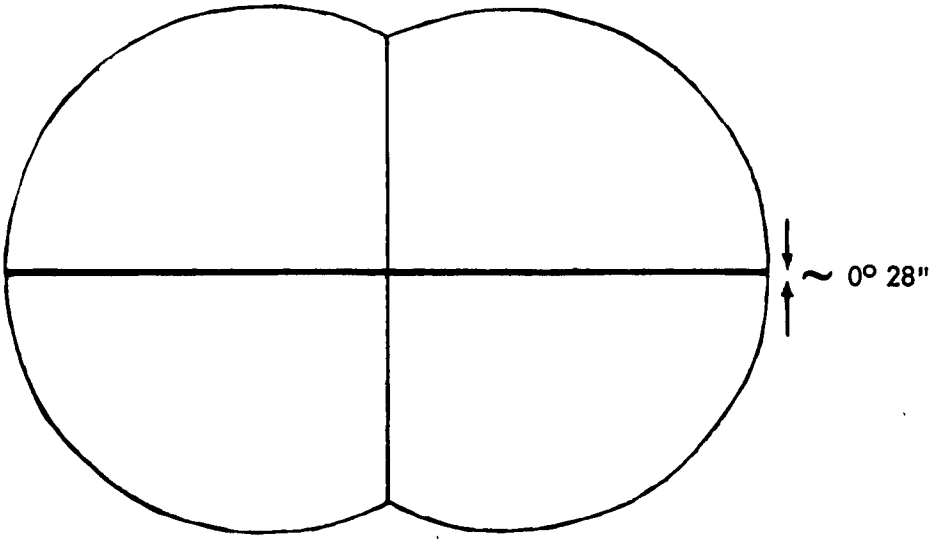

Figure 1-83. -Full-Scale View of Lunar Horizon Through T-Sight at 60-Nautical-Mile Altitude

prevail until approximately 40 hours after a 7-degree sun-angle touchdown. Touchdown at maximum sun angle (20 degrees) would reduce the period during which the horizon would not be discernible to approximately 14 hours. Once the sun angle has increased to 27 degrees, the downrange horizon could be used for reference until about the 14th day. Then the sun would be on the horizon (or possible even just below it) upon launch. If a calculus-of-variations trajectory were assumed for ascent on the 14th day, then once an altitude of 12 nautical miles were attained (8 nautical miles downrange), the angle between the horizon and the sun would be greater than 10 degrees. It was assumed that a sun elevation of 10 degrees above the horizon would not appreciably interfere with use of the horizon for reference. Figure 1-79 shows that between the 14th and 16th days, the launch would occur under night conditions. However, as the LESS ascended it would rise into sunlight, at which point the sun would be on the downrange horizon, thus precluding its use. The luminance of the sun is 7×10^8 millilamberts (mL) (Ref. 1-3) as viewed from outside the earth's atmosphere. Filters could be used to reduce the intensity to a maximum comfortable value of approximately 7×10^3 mL or by 10^5 mL. The luminance of the lunar surface, however, is on the order of 10^3 mL so that the sun filter would reduce this intensity to approximately 10^{-2} mL. This would require general dark adaptation for the lunar surface to be visible. But more than just general visibility is required. Features may be visible and yet not identifiable because several levels of contrast are usually necessary for feature recognition. Furthermore, it is doubtful whether adequate adaptation could be achieved rapidly enough because of the intensity of the filtered sunlight.

The inability to discern the downrange horizon in the event of a launch before 40 hours after touchdown cannot be appreciably circumvented by going to a lower orbital altitude. If an altitude lower than 60 nautical miles is specified, say 40 nautical miles, the horizon is approximately 35 miles, or 2 degrees, closer. However, the downrange distance required for reaching orbital velocity is increased. Consequently, in the event of LESS launch about 36 hours after landing, the downrange horizon would be obscured by the terminator when viewed at the end of burn at 60 nautical miles, whereas with a 40-nm orbit, the downrange horizon would be visible throughout the entire powered phase. The advantage of a 40-nm orbit over a 60-nm orbit with respect to visibility conditions may be overcome by an additional 4-hour wait. During the 4 hours (two lunar orbits of the CSM), the terminator would advance the 2 degrees that constitute the visibility difference between 60 and 40 nautical miles.

If escape is necessary shortly after touchdown, when the terminator would obscure the downrange horizon during some portion of the ascent trajectory, then the terminator itself could possibly be used to obtain a pitch angle. The basic problem with the use of the terminator is that it is generally a wide, irregular band that depends on local topography for its contour. An examination of many photographs of the terminator (Ref. 1-4) indicated that its width is on the order of 4 degrees (65 nautical miles when measured from solid black (except for occasional, isolated mountain peaks) to solid white (except for crater floors, etc.). This width, however, is foreshortened when viewed at shallow angles. If viewed vertically downward from an altitude of 60 nautical miles, the terminator would span approximately 57 degrees. However, as figure 1-84 indicates, the LESS would be in a 60-nm orbit before overflying the terminator even if launch occurred simultaneously with touchdown. Actually, approximately a six-hour period would probably be necessary to dismount, assemble, fuel, and check out the LESS and to obtain trajectory and guidance data (azimuth, etc.). Also, time would be required to recharge the backpacks. Figure 1-84 shows the apparent width of the terminator as seen at the end of powered flight if launch occured 10 hours after touchdown. To use the terminator for pitch reference, its center would need to be determined within approximately 1 degree. If its apparent width is on the order of 10 degrees to 20 degrees, it is doubtful whether its center could be determined with sufficient accuracy (possibly an expandable scale or grid could be used to increase the accuracy of the center determination). If launch could be delayed until approximately ten hours after touchdown, the maximum apparent width (at the end of ascent) of the terminator would be approximately nine degrees, as shown in figure 1-84. For three-fourths of the ascent time, the terminator would appear to be less than 3 degrees wide. Additional postponement of the launch would further reduce the apparent width of the terminator. Figure 1-85 shows the relationship between staytime and the maximum apparent width of the terminator for a 60-nm orbit.

Effect of glare and contrast on visibility. - Contrast: During nominal 3-day daylight missions, visibility would be adequate for identification of lunar landmarks at the nadir during the entire ascent phase. Downrange visibility would be limited during the terminal phase of ascent in the event of abort shortly after touchdown. In the event of a LESS abort during a 7-day mission, such as that shown in figure 1-86, the high sun angles could create visibility problems by reducing the contrast necessary for discernment and recognition of surface features. The human eye can discern contrasts as low as 1 percent (Ref. 1-3)(i.e., one surface reflecting 50.0 percent of the light striking it while a superimposed object reflects 50.5 percent). Differences in color, texture, etc., all enhance the contrast. Figure 1-86 relates the distance between well illuminated contrasting surfaces with the

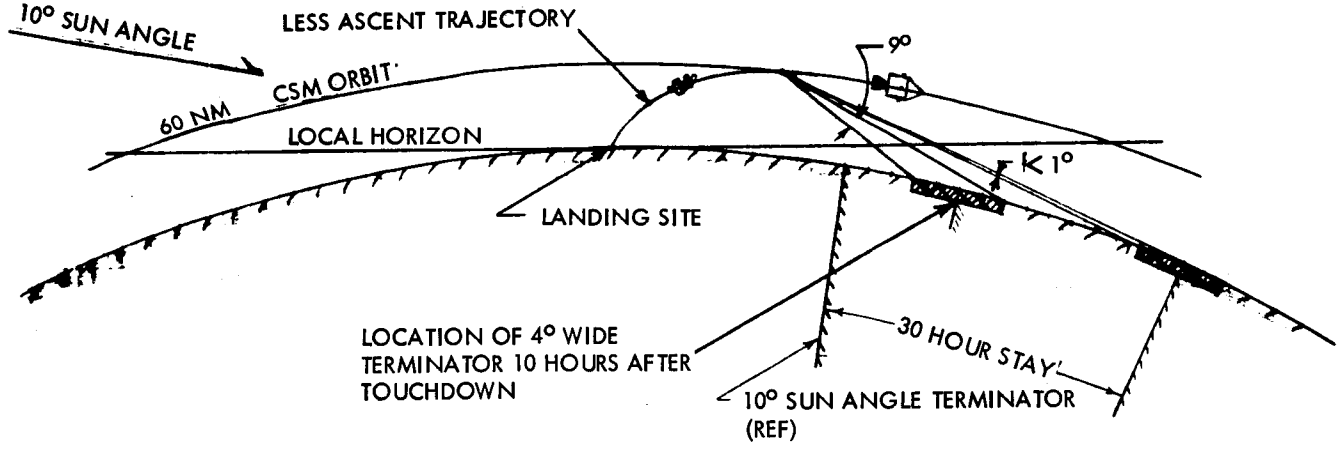

Figure 1-84. - Terminator Visibility Downrange

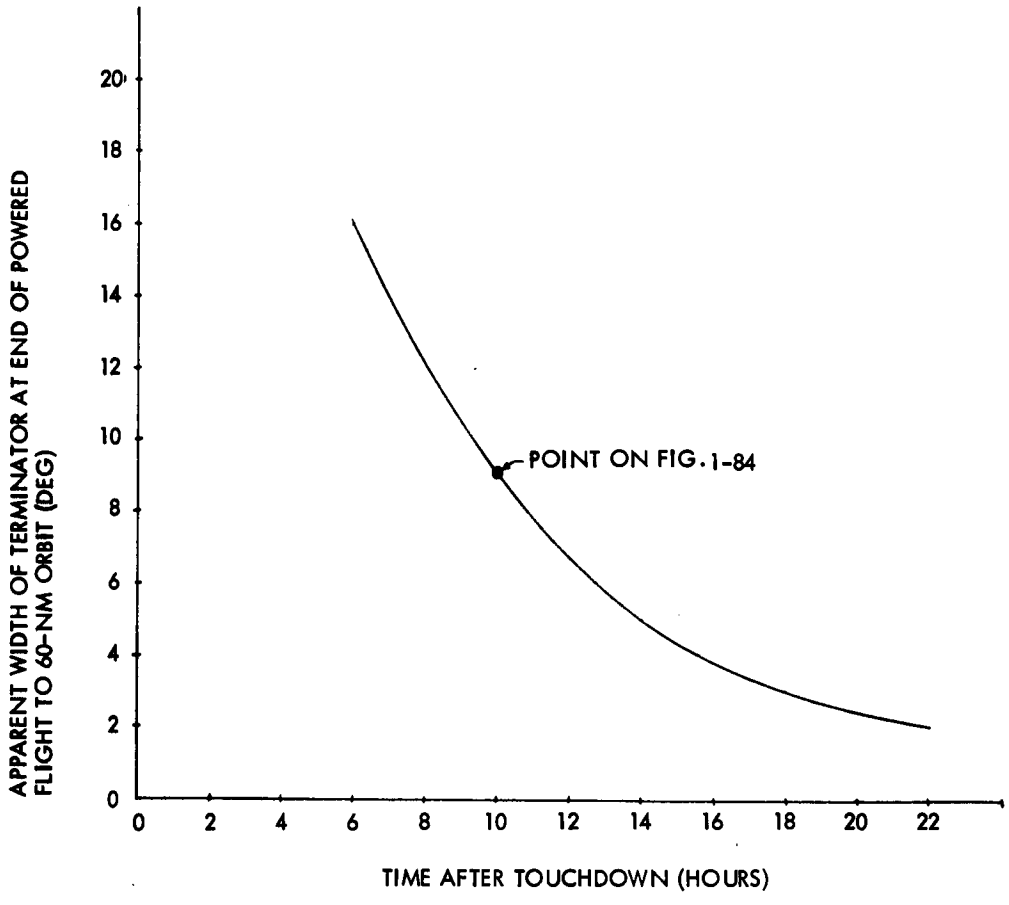

Figure 1-85. - Maximum Apparent Terminator Width Versus Staytime

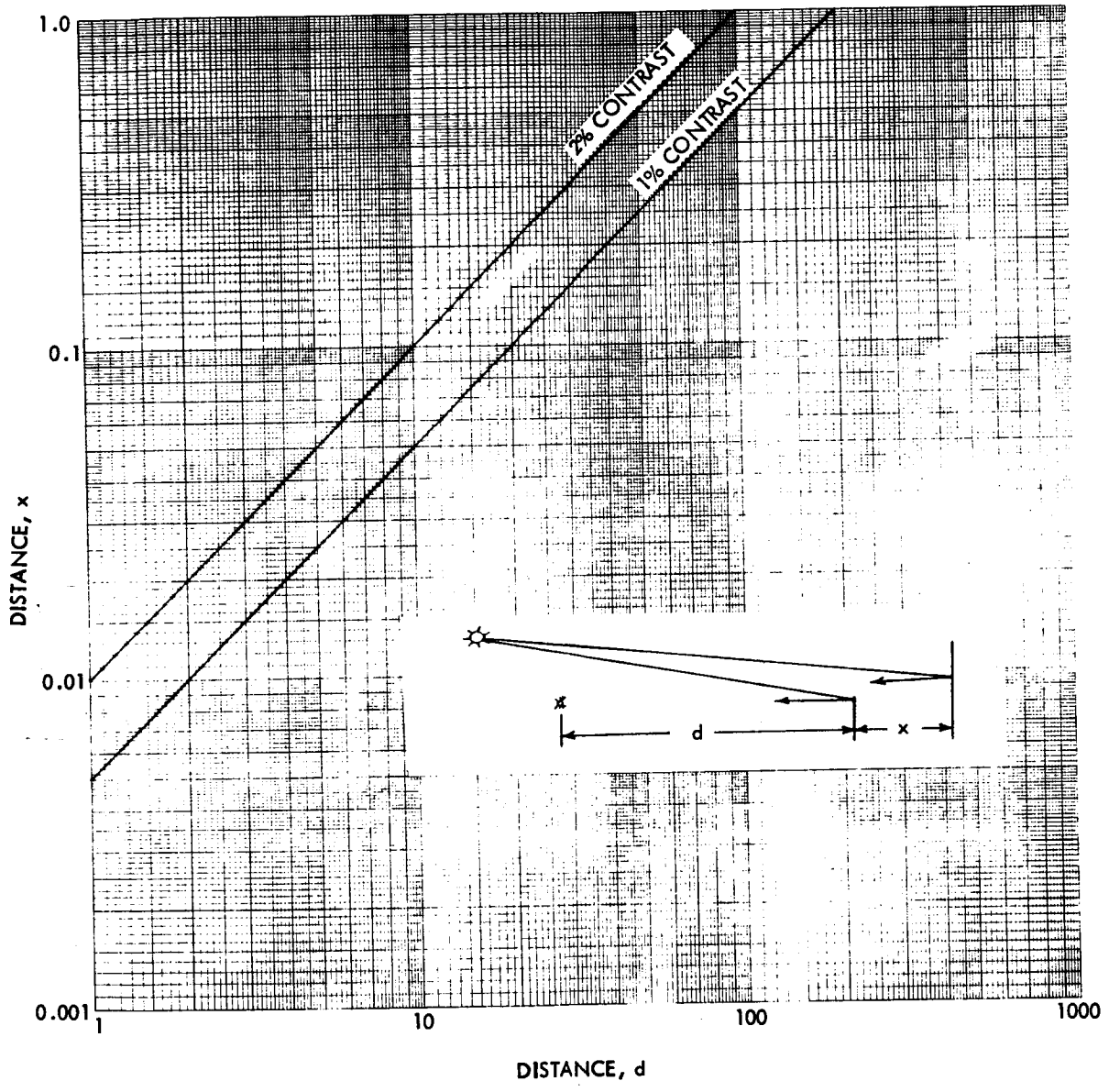

Figure 1-86. - Inverse Square Relationship Between Contrast and Distance

distance of the observer from them. It is assumed in figure 1-86 that the sole source of the contrast arises from diminution of the light from the two surfaces in accordance with the inverse square law. Figure 1-86 shows the distance (x) by which two surfaces can be separated for various ranges (d) and still yield 1-percent or 2-percent contrast. If the reflecting surfaces are separated by less than the distance shown for 1-percent contrast, then they blend together so that no visible demarcation exists that would permit visual distinction of the two surfaces. Neither the ordinate or abscissa shows units because the relationships shown hold as long as both the abscissa and ordinate have the same units, i.e., feet, yards, etc.

Surface visibility during abort at the end of a 7-day mission, as shown in figure 1-86, could present washout problems if local surface albedo and texture are such that they inhibit feature discernment and identification. In the case of high sun angles such as those encountered during abort from the sub-solar point, reference objects would need to be selected whose walls or surfaces are separated in the line-of-sight direction by distances greater than that required for 2-percent contrast.

The incidence of direct sunlight on guidance instruments may reduce contrast between the optically projected image of the object being used for guidance and the screen. The intensity of the sunlight would require that hoods and/or light shields be provided if star references are used. For example, a star image projected onto a plate exposed to direct sunlight would not be sufficiently discernible without (complex) electronic enhancement. The projection of the lunar horizon onto a frosted screen would probably be washed out by impinging sunlight and by the attenuation of the intensity of the light by the opaqueness of the frosted glass. The direct observation of the lunar horizon (via T-tube optical sight) could be accomplished in full sunlight. By way of analogy, a flashlight beam (lunar horizon) shining on the backside of a frosted plate would be barely discernible in full sunlight, whereas the flashlight beam reflected by a mirror also in sunlight would be discernible.

Glare: During a nominal ascent trajectory, the pitch angle will change by approximately 110 degrees (from a vertical thrust of +90 degrees to a below-horizontal thrust of -20 degrees). Consequently, sunlight will be normal to the instruments during at least some portion of the trajectory if the ascent is made between LM touchdown (at a 7-degree sun angle) and the eighth day (sun angle approximately 110 degrees). The nominal ascent is down-sun, which may result in the sun's shining directly on the face of the instruments located in front of the astronaut during a portion of the ascent during this 8-day period.

Artifical horizon devices and gyro compasses with transparent windows could probably function satisfactorily in full sunlight if the lenses were coated with a non-glare finish (e.g., magnesium flouride). The use of high-contrast paints on the instrument dials (possible fluorescent) could assure good instrument visibility and readability even in full sunlight. A dark, non-reflecting honeycomb grid over the face of the instruments could be used in place of a hood to reduce solar glare from illuminated instruments.

Visibility of LESS from the CSM: During daylight ascents, the LESS would be difficult to observe from the CSM because of the bright lunar landscape that would form the background for observations from the CSM. An appreciation of the LESS visibility problem may be gained from a simple analogy. The LESS would be smaller than an automobile. Automobiles are discernible from an aircraft flying at 30 000 feet only by sighting along a road. If the automobile were in a field, it would probably escape detection at that distance (5 nautical miles). Paradoxically, the Sputniks, which were smaller than an automobile, were visible at a distance of approximately 125 nautical miles (perigee) when illuminated by the sun against a night sky. A similar condition will prevail in viewing the LESS. It may not be discernible against the illuminated lunar surface until it is within several miles of the CSM (without augmentation). It is significant that, during the Apollo 11 mission, astronaut Collins could not locate the LM on the lunar surface during repeated passes over the landing site. A flashing beacon on board the LESS would help assure its visibility from the CSM. The LESS should be readily visible in sunlight against the dark lunar surface or night sky.

The visibility of the CSM from the LESS also presents problems. If the LESS ascent took place during the first 7 days after touchdown, and the trajectory and timing was such as to yield a minimum miss distance for rendezvous, then the CSM could be in the sun as seen from the LESS during at least some part of the ascent. The position of the CSM close to the sun would preclude the visual use of the CSM for guidance during the ascent trajectory. Even if the CSM were 30 degrees or 40 degrees away from the sun, it would probably not be visible if it were more than several miles away because of the incident sunlight and because the illumination would be in the form of a thin, outline glint on the sunward side of the CSM.

Dark adaptation characteristics. - Statements made by Apollo astronauts indicate that, by orienting their spacecraft so that a minimal amount of sunlight entered the CM and by reducing the illumination level within the CM, they could dark-adapt their eyes so that stars were visible. Figure 1-87 (Ref. 1-4) shows the rate at which human eyes become dark-adapted after exposure to white light of various brightness. Depending on the astronaut's activities, he could be exposed to brightness on the order of several thousand mL, which could impair stellar vision on the order of a minute or more, depending on the magnitude of the star, its location, and the astronaut's

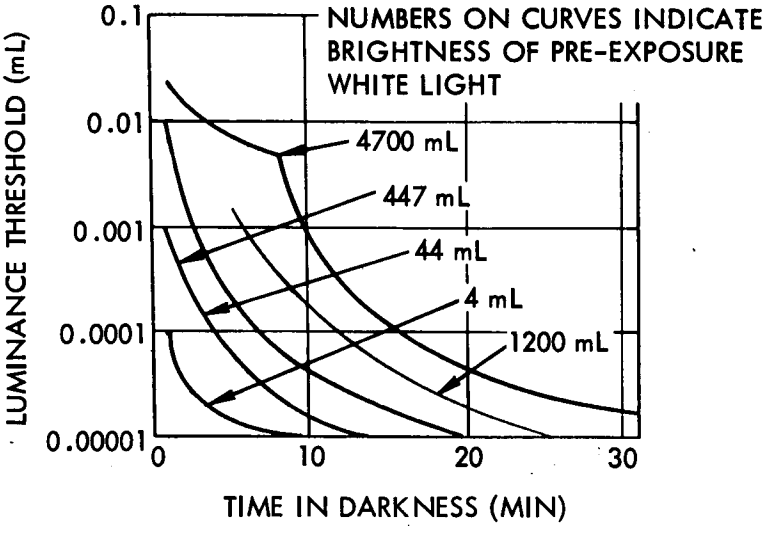

Figure 1-87. Rate of Dark Adaptation

physiological state. During an abort, cues other than stars would likely need to be used (i. e., lunar horizon angle used to verify pitch angle). A look at the sunlit lunar surface or the sunlit LESS itself could impair his ability to quickly reacquire the stellar reference even if displayed in a light-proof hooded device. This presents what is believed to be an unacceptable and unsafe operational procedure (hazard). Consequently, it is believed that practical safety considerations tend to preclude the use of theoretically feasible dark-adaptation for stellar observation for guidance and navigation.

Summary and Conclusions. - Table 1-3 summarizes the conclusions reached during the investigation of lunar visibility conditions. It is significant that under appropriate conditions any one of the cues or features is visible and could possibly serve as a reference for abort guidance and navigation. However, except for the sun, no single cue or feature is consistently clearly visible over the full range of staytimes indicated. Since the conditions (times) when LESS abort would be needed is unknown, the lack of consistency in the manifestation of good visual cues strongly indicates that an internal reference system such as gyros is highly desirable. Likewise, the problems of glare and constrast on or from instruments is certain to be a problem at some sun angles with simple visual aids. Again, this favors use of a gyro display. Visibility of one vehicle from the other is likely to be a problem against a low contrast background such as bright moon or when looking close to the sun.

An extensive effort to survey the astronauts was accomplished to ascertain if they could contribute to the knowledge of visibility limitations. In particular, they were asked their opinions about the possible viewing of the dark horizon for use as a pitch reference and relative visibility from one spacecraft to another under various sun lighting conditions. Their comments were not particularly conclusive on these matters because of the lack of such observations as a specific task objective or limited experience under controlled conditions of sun orientations relative to backgrounds.

TABLE 1-3. - SUMMARY OF LUNAR VISIBILITY CONDITIONS

Cues/Feature	Minimum Staytime Abort 9° Sun Angle	Abort After Stay of		
		3 Days	7 Days	14 Days
Non-Lunar Sun	Visible	Visible	Visible	Visible
Earth	Undependable, may be thin crescent	Undependable, may be thin crescent	May not be visible or else too close to sun	May not be visible or else too close to sun
Stellar	Visible after dark-adaptation	Visible after dark-adaptation	Visible after dark-adaptation	Visible after dark-adaptation
Lunar Downrange horizon	Not visible during major portion of ascent	Not visible during end of ascent until after approx 36 hours of staytime	Visible	Not visible—too close to sun
Lateral horizon	Partially visible (segment)	Visible	Visible	Partially visible (segment)
Rear horizon	Not visible—too close to sun	Visible	Visible	Not visible—lunar night
Nadir surface	Good relief	Fair relief	Poor relief-washout	Poor relief—too much shadow
45° Downrange	Poor relief—too much shadow	Good	Fair	Poor—too much shadow

CSM-LESS Rendezvous and Docking

Objectives. - The primary purpose of the effort reflected in this section was to identify requirements, capabilities, and constraints of the CSM and the LESS for accomplishing CSM-active rendezvous. The goal was to devise a rendezvous mode that could be accomplished with minimum changes (preferably none) to the CSM and with a relatively simple LESS. A brief analysis was also conducted of the feasibility and implications of LESS-active rendezvous. Potential modes of docking and crew transfer to the CSM were to be identified.

Approach. - It was assumed at the outset that the CSM could probably perform the necessary tracking calculations and maneuvers for LESS rendezvous, utilizing existing LM-rescue provisions. This, if proved correct, would make maximum use of the extensive capabilities of the CSM and would tend to keep the LESS simple. Requirements for performing orbit transfers, plane changes, and phasing maneuvers necessary in rendezvous operations were first parametrically examined. Then they were iterated with LESS boost trajectory error relationships to provide practical approaches and possible operating parameters for the rendezvous phase. Close iterations with CSM crew/equipment capabilities were conducted during this analysis. LESS-active rendezvous was also considered in view of the efficiency achieved by maneuvering with the smaller vehicle and to account for the possibility that the CSM energy budget for rescue could be reduced at some future time. Also, the visibility problems in tracking the LESS under a variety of solar illumination conditions were studied to determine what effects they might have on the operations of equipment.

To complete the LESS mission successfully, it is necessary to rendezvous and transfer the crew into the CSM while the crew is still depending upon the backpack for life support. These maneuvers must be accomplished quickly. Each astronaut's portable life support system (PLSS) must sustain him until he can draw on the CSM life support equipment. Since a charged PLSS lasts a maximum of four hours, the LESS crewmen must reach the CSM well within four hours of the time they leave the lunar module. Thus, rendezvous must be accomplished with essentially no aid from earth controllers. There is not time for the Manned Space Flight Network (MSFN) to determine the LESS orbit and for ground controllers to direct the rendezvous maneuvers. Improvements to the PLSS such as adding SLSS (secondary life support system) can be expected to increase total allowable time by 50 percent (to 6 hours) in the early 1970's.

1-117

Astronaut/system capabilities and limitations for CSM-active rendezvous. - The Apollo CSM is designed to perform lunar orbital rendezvous with an incapacitated LM. This same rendezvous capability may be employed for CSM-active rendezvous with the LESS.

Within the Apollo CM guidance computer (CMC), programs have been mechanized to provide the necessary guidance for alternative rendezvous modes. The concentric orbit rendezvous mode is the technique normally employed. It typically requires 3 hours and 50 minutes from liftoff to the completion of the docking maneuver. The stable orbit rendezvous (SOR) mode (Program 38) has been incorporated to permit the more rapid achievement of rendezvous when circumstances are time-critical. This mode typically requires 2 hours and 20 minutes from liftoff to the completion of the docking. The SOR mode is, therefore, more appropriate for the LESS rendezvous, considering the time limitations imposed by the PLSS.

The fundamental elements of the CSM rendezvous guidance system are the VHF range measurement, the sextant measurement of line-of-sight angles, and the guidance computer and its programs. A typical mission profile for CSM-active rendezvous with the LESS, using the SOR program, is given in figure 1-88.

To permit the CSM-active rendezvous with the LESS, it is necessary to add a flashing beacon and a VHF ranging transponder to the LESS. The flashing beacon is necessary for sextant tracking when the LESS is not illuminated by the sun. The VHF transponder is required for VHF range measurement.

Characteristics of the LM and CSM flashing beacons are given in table 1-4. LM beacon performance exceeds LESS requirements for beacon tracking at 200 nautical miles and would require up to 40 pounds of batteries to power it during the LESS mission. The CSM beacon may not provide sufficient range capability for some LESS missions. The Gemini beacon has even less range capability than the CSM beacon. The ranges shown are the best estimates based upon all available test data obtained from literature and conversations with cognizant NASA and subcontractor personnel.

For the above reasons, the LESS will probably require a new beacon. The assumed performance requirements and estimated performance properties of such a beacon are also given in table 1-4. The requirements and performance of this LESS beacon have not been optimized. They do, however, indicate that a beacon can be constructed that promises to satisfy the performance requirements without requiring an unduly large battery power system.

The VHF ranging transponder is estimated to weight 20 pounds and requires 40 watts of power. This gear includes receiver and transmitter telecommunication elements that can also be used to provide a voice communication link between the LESS and CSM.

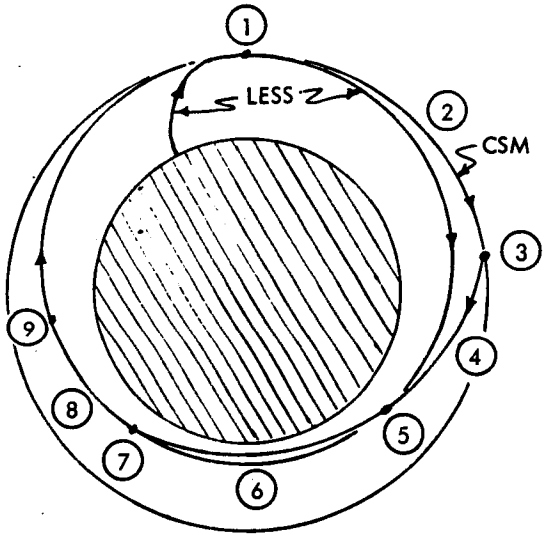

1. LESS ASCENT - INJECTS INTO NEAR VICINITY OF CSM (≈10 NM)
2. CSM TRACKS LESS- SEXTANT SIGHTINGS AND VHF RANGING, SOLVE FOR STABLE ORBIT INSERTION (SOI) - PREPARES TO EXECUTE SOI BURN
3. SOI - SPS BURN
4. CSM TRACKS LESS AND CALCULATES MIDCOURSE CORRECTION (IF REQUIRED)
5. RCS MIDCOURSE CORRECTION (IF REQUIRED)
6. CSM TRACKS LESS - SOLVES FOR STABLE ORBIT RENDEZVOUS (SOR) BURN - PREPARES TO EXECUTE SOR BURN
7. SOR - SPS BURN - RANGE ≈ 3000 FT
8. NULL DRIFTS AND SET UP 10 FPS CLOSURE - RCS
9. STATION KEEPING

Figure 1-88. - CSM-Active Rendezvous With LESS Using Stable-Orbit Rendezvous Guidance Mode

TABLE 1-4. - FLASHING BEACONS FOR RENDEZVOUS TRACKING

Beacon Data	Application		
	CSM	LM	New LESS Beacon
Manufacturer	E.G.&G. Incorp. Bedford, Mass.	Reeves Instrument Co.	?
Weight (lb)	10	25	10
Power (watts)	30	200 (max)	21
Volume (cubic feet)	0.4	<1	0.4
Flash frequency (PPM)	55 ±5	60	60
Flashing intensity (BCPS)	120 (min)	2000	141
Directional properties, cone angle (deg)	120	60	90
Max visible range			
Bare eye (nm)	60	130	65
With sextant (nm)	160	400	200
Battery weight for LESS use, redundant batteries (lb)	6	40	4.2

The stable orbit rendezvous mode mechanized in CMC program P-38 provides the capability for two-impulse rendezvous between two non-coplanar elliptical orbits. All maneuvers are based on precision trajectory computations considering, for instance, the effects of lunar gravitational anomalies. To operate P-38, the astronaut inserts the time of the first burn and the central range angle to be traversed between the two burns. The program then computes the ΔV's and the perilune altitude of the transfer orbit. The astronaut may then readjust the two input parameters to search iteratively for an acceptable ΔV magnitude and transfer orbit perilune altitude. Having thus selected the conditions for the SOR maneuvers, the astronaut operates the pre-ΔV programs similarly to any other powered maneuver. Reference 1-5 contains a more detailed description of the system operation.

No actual flight experience with the SOR mode has as yet been obtained. However, rendezvous navigation utilizing sextant and VHF range observations has been confirmed in the Apollo 9, 10 and 11 missions. The only remaining portion of the system not exercised in flight is P-38. It has been confirmed on several simulators across the country, including the NR Mission Evaluator Simulator.

It has been observed in the NR simulator that the workload on the CM pilot is extremely high during rendezvous. This gives rise to the possibility of procedural errors. The problem is amplified because Mission Control in Houston cannot monitor the operation when the CSM is behind the moon. Use of the SOR mode will require the astronaut to be trained to a high level of proficiency to assure reliable performance.*

The following hardware system limitations affecting the success of the CSM/LESS rendezvous have been identified.

1. VHF Range - This sytem is capable of providing unambiguous range measurements to within ±250 feet to a maximum range of 200 nautical miles. This accuracy has been demonstrated to be more than adequate in the NR Mission Evaluation Simulator. Also, the CSM/LESS rendezvous is typically performed within a range of less than 125 nautical miles, which is well within the range limitations of this sensor.

*It is noteworthy that a recent mission planning decision has been made to eliminate the requirement for the SOR mode. This is because of the absence of requirements that necessitate a time-critical rendezvous in the Apollo lunar landing program. At this time, no official change notices have been received for the removal of the program from the guidance computer. If it is removed, it is thought that it could be reinserted if a requirement for it could be established. If the LESS becomes an integral part of the lunar mission system, the SOR mode would need to be reinstated.

2. Sextant Measurements - This instrument has an angular measurement accuracy of approximately 20 arc seconds. Simulator experience with the CSM/LM rendezvous has shown this to be more than adequate. In fact, it is shown later in this section (fig. 1-89) that the combination of VHF range and sextant observations produces more accurate navigation than can be achieved with the LM rendezvous radar.

As shown in table 1-5, the sextant is capable of tracking the sunlit LM and LM flashing beacon at ranges in excess of 270 nautical miles (Apollo 10 and 11 flight experience). The maximum visible ranges of the sun-illuminated LM indicated in table 1-5 are based on flight-test experience (sextant) and study estimates (telescope and bare eye). The maximum visible range of the LESS has been extrapolated from these data based on characteristic dimensions of the two vehicles. Additional reflective areas can be added to the LESS if test data indicate that the estimated range capability cannot be achieved.

It is noteworthy that the maximum visible range in sun illumination is a strong function of background illumination and eye adaptation. The data given for sun-illuminated conditions are probably representative of close to ideal conditions. It is understood that the visibility of the sun-illuminated LM has recently been the subject of considerable attention at the NASA Manned Spacecraft Center. When the studies are complete, they should provide considerable information on the subject.

3. Scanning Telescope - Use of the sextant at great ranges is contingent upon the target having been acquired in the field of view. This requires the auto-optics mode to point the sextant automatically at the target. The LESS orbit injection position dispersions have been estimated to be as large as ±5 nautical miles. This readily removes it from the sextant field of view (1.8 degrees) for reasonable ranges. Therefore, it may be necessary to acquire the LESS manually, using the scanning telescope with its 60-degree field of view. It is estimated that the scanning telescope is capable of tracking the LESS in sunlight and the LESS flashing beacon in the dark at a range of approximately 50 nautical miles (table 1-5). It is concluded that the LESS should be injected with a maximum range to the CSM of less than 50 nautical miles to assure that acquisition with the scanning telescope can be performed.

To assure that the LESS will be easily acquired within the field of view of the telescope, it is desirable that the minimum range

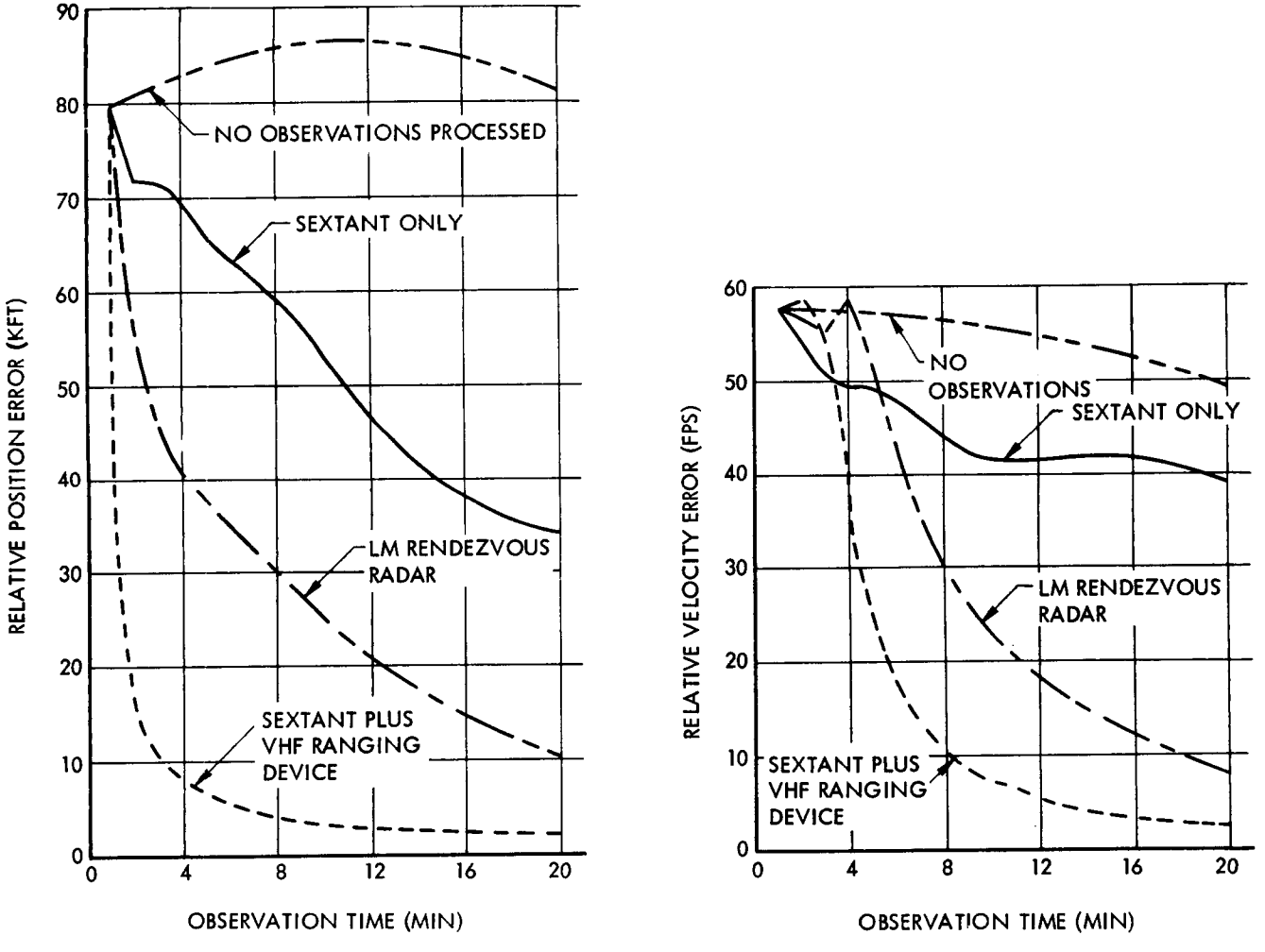

Figure 1-89. - Rendezvous Navigation Errors Versus Tracking Time

TABLE 1-5. - RANGE CAPABILITY OF SEXTANT AND TELESCOPE
(~NAUTICAL MILES)

	Sextant	Telescope	Bare Eye
LM beacon tracking	400 (design goal) 410* >385 (Apollo 009) >360 (Apollo 010)	77 (study estimate)	130 (design goal) 137*
CSM beacon tracking	160 (specification requirement) 150*		60 (specification requirement) 50*
LESS beacon tracking	200 (design requirement)	50	65
Sun-illuminated LM	>270 (Apollo 011)	>57	>90
Sun-illuminated LESS	>150	50	>50

*Conservative performance estimate based on test results obtained at NASA-MSC.

to the CSM be 10 nautical miles at injection. This will eliminate the time-consuming reorientation to search for the LESS. Injection should be planned so that neither the moon's lighted disk nor the sun is in background when the LESS is viewed from the CSM.

4. Voice Communication Range Limits - The LESS-to-CSM maximum communication range is approximately 40 nautical miles. This range is adequate for the terminal phase of rendezvous, docking, and crew transfer but will not permit continuous communications during ascent.

The following time constraints on critical CSM functions reflect system dynamics and crew operational procedures:

1. Tracking Time Required to Update the Navigation - Navigation accuracy achievable as a function of CSM sextant and VHF tracking time is given in figure 1-89. It may be observed that reasonably good convergence of the position and velocity errors can be achieved in 15 to 20 minutes. It is also noteworthy that the navigation accuracy achievable with the sextant and VHF range observation combination is superior to that obtainable with the LM rendezvous radar.

2. Operation of Pre-ΔV Guidance Programs - CSM simulation experience and flight test experience have indicated that 8 to 15 minutes should be allowed to operate the pre-ΔV guidance programs and configure the propulsion system and flight control systems for thrusting maneuvers.

3. Post-ΔV Housekeeping - CSM simulation and flight-test experience have shown that approximately 5 minutes should be allowed to reconfigure the propulsion and flight control systems from the thrusting maneuver settings to coasting flight configuration.

The above time constraints have been incorporated into the rendezvous operational time line shown at the end of this section. It indicates that these time constraints are not unduly severe and that rendezvous can be achieved within the lifetime restrictions of the PLSS.

Results of the investigation of CSM-active rendezvous system and astronaut limitations can be summarized as follows:

1. Use of the existing SOR mode appears to satisfy all the presently defined requirements for the CSM/LESS rendezvous. Rendezvous can be achieved safely within the system and astronaut limitations.

2. CSM active rendezvous imposes a severe workload on the astronaut remaining in the CSM. By its nature the SOR mode is less forgiving than the concentric-orbit-rendezvous mission profile and thus requires flawless system operation. Considerable training and experience is, therefore, required to minimize the possibility of crew procedural error.

3. To assure simple and rapid visual acquisition of the LESS by the CSM, using the G&N optics, it is desirable to complete the ascent orbit injection at a relative range between 10 and 50 nautical miles and at such a condition that neither the moon's lighted disk nor the sun will be in the background when the LESS is viewed from the CSM. This would be a factor in mission planning and would be one of the elements affecting launch timing.

4. A VHF ranging transponder and a flashing beacon having modest weight and power requirements must be added to the LESS to permit the CSM to track it. No modifications to the CSM are required to perform the rendezvous with the LESS.

Rendezvous energy requirements and trajectories. -

Approach: The number of variables upon which rendezvous energy requirements depend is so great that it is essential to restrict the analysis as much as possible and yet consider the most meaningful parameters. This is especially true of the LESS in view of the boost dispersions expected. The simple systems being postulated tend to produce wide dispersions in apse dimensions and locations and in relative inclination and nodal orientation.

Because of the time limitations imposed by the PLSS and the time increments needed to accomplish prelaunch, launch, orbit determination, and final docking and crew transfer, the gross rendezvous itself must be accomplished in something on the order of 1 to 1.5 hours. This means that it is not possible to employ multiple phasing orbits and that rendezvous must be accomplished with essentially a two-impulse transfer, with the transfer angle being on the order of 180 to 270 degrees.

The problem was approached by first considering orbit transfer and rendezvous in general. Various parameters affecting performance requirements were tested to find their relative effect in the expected operating regime of the LESS. After this analysis was completed, the problem was narrowed to conditions that could arise due to the LESS and its general properties.

Because the CSM ΔV allocation that would be available for the LESS mission could be changed at some future time, the parametric results are generally presented for rendezvous ΔV requirements of 400, 600, and 800 feet per second. The present allocation for LM rescue is 790 feet per second.

It is noted that if LM rescue is not required, this ΔV can be used to shorten the transearth transit time. Likewise, some additional rescue ΔV could be traded for an unusually long transit time (requiring another set of complex mission calculations involving life support margins, trajectories, reentry, recovery timing, etc.).

Parametric results: The relative importance of various LESS orbit parameters was first determined by considering transfer from the CSM orbit (60 nautical miles and circular) to a wide range of LESS orbits without regard to phasing problems. Figure 1-90 gives a summary of the results. The target orbit was assumed to have a 15-nm perilune with varying apolunes, relative inclinations, and perilune orientations. A perilune of 15 nautical miles was chosen as a reasonable minimum value to assure a safe orbit. Relative inclination is seen to have a strong effect on energy requirements. Perilune orientation (ω) has a varying effect, depending on the ellipticity of the orbit.

Figure 1-91 is a machine-made contour map typical of many from which the foregoing data were developed. It represents an elliptical LESS orbit of 15 by 120 nautical miles with a relative inclination of 5 degrees and perilune at a relative node. The ΔV contours identified represent departure angles (ϕ_1) of the CSM in its orbit and arrival angles (ϕ_2) in the LESS orbit that can be accommodated with that energy expenditure. The regions containing asterisks require transfers with perilunes lower than the lunar surface.

Some inferences can be drawn from this plot. As would be expected, transfers of approximately 180 degrees beginning and ending near relative nodes require minimum energy expenditures. Table 1-6 summarizes those points. If the transfer must be initiated at a relative antinode ($\phi_1 = 90$ degrees), then a 180-degree transfer cannot be made ($\phi_2 = 270$ degrees) as that energy requirement is seen to exceed the highest contour value by a substantial amount. However, 90- or 270-degree transfers can be made for 650 feet per second as compared to 476 feet per second as the absolute minimum. The arrival points are relative nodes ($\phi_2 \approx 180$ or 360 degrees).

TABLE 1-6. - SUMMARY OF OPTIMUM IMPULSIVE TRANSFERS FROM 60-NAUTICAL-MILE ORBIT TO 15- BY 120-NAUTICAL-MILE ORBIT INCLINED AT 5 DEGREES HAVING PERILUNE AT THE NODE

Optimum No.	ϕ_1 (deg)	ϕ_2 (deg)	ΔV (fps)
1	0.907	179.427	476.066
2	358.806	180.757	476.251
3	180.608	359.111	494.544
4	179.242	1.102	494.566

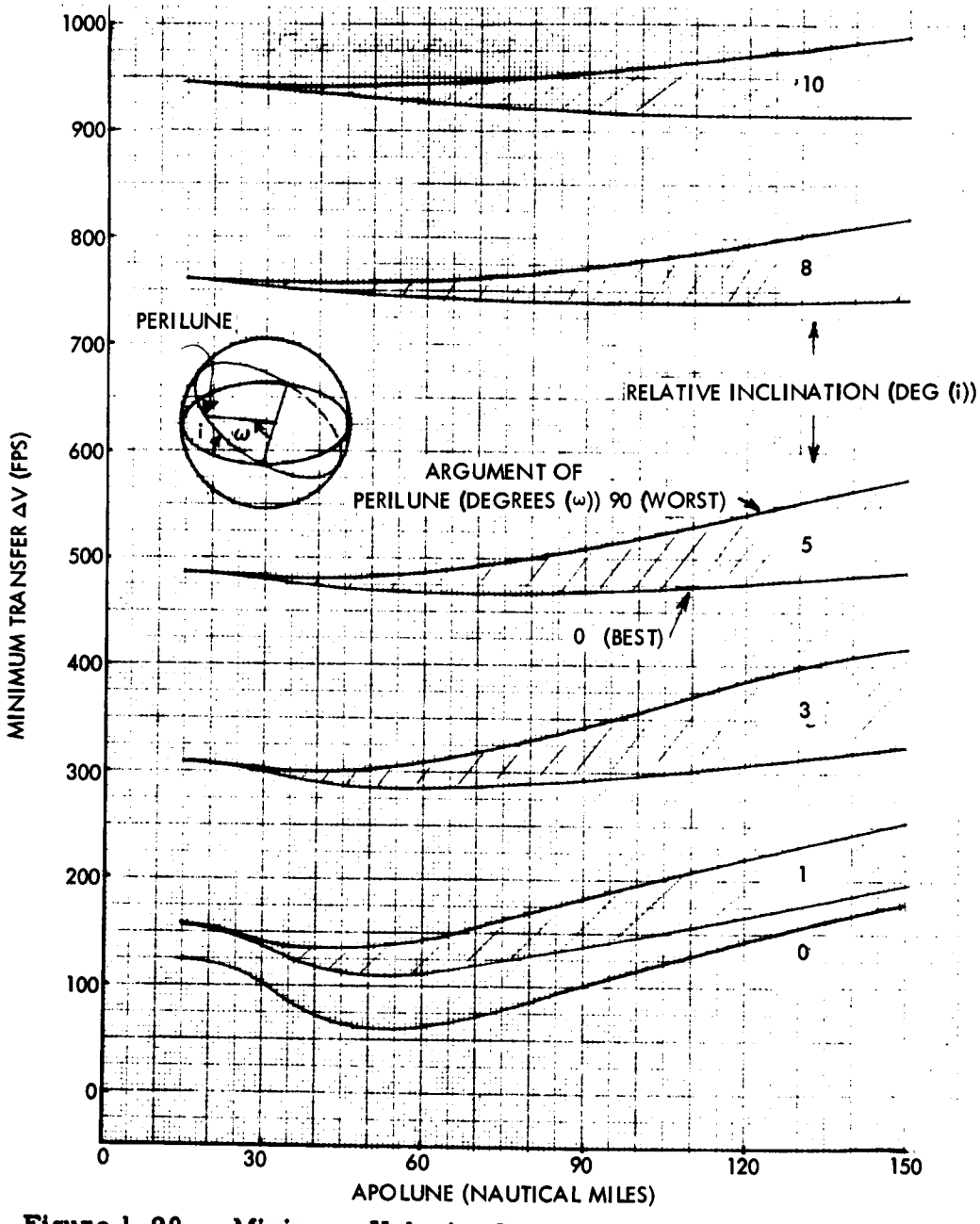

Figure 1-90. - Minimum Velocity Requirements for Transfer from 60-Nautical-Mile Circular Orbit to Elliptical Orbits Having Perilune Altitudes of 15 Nautical Miles

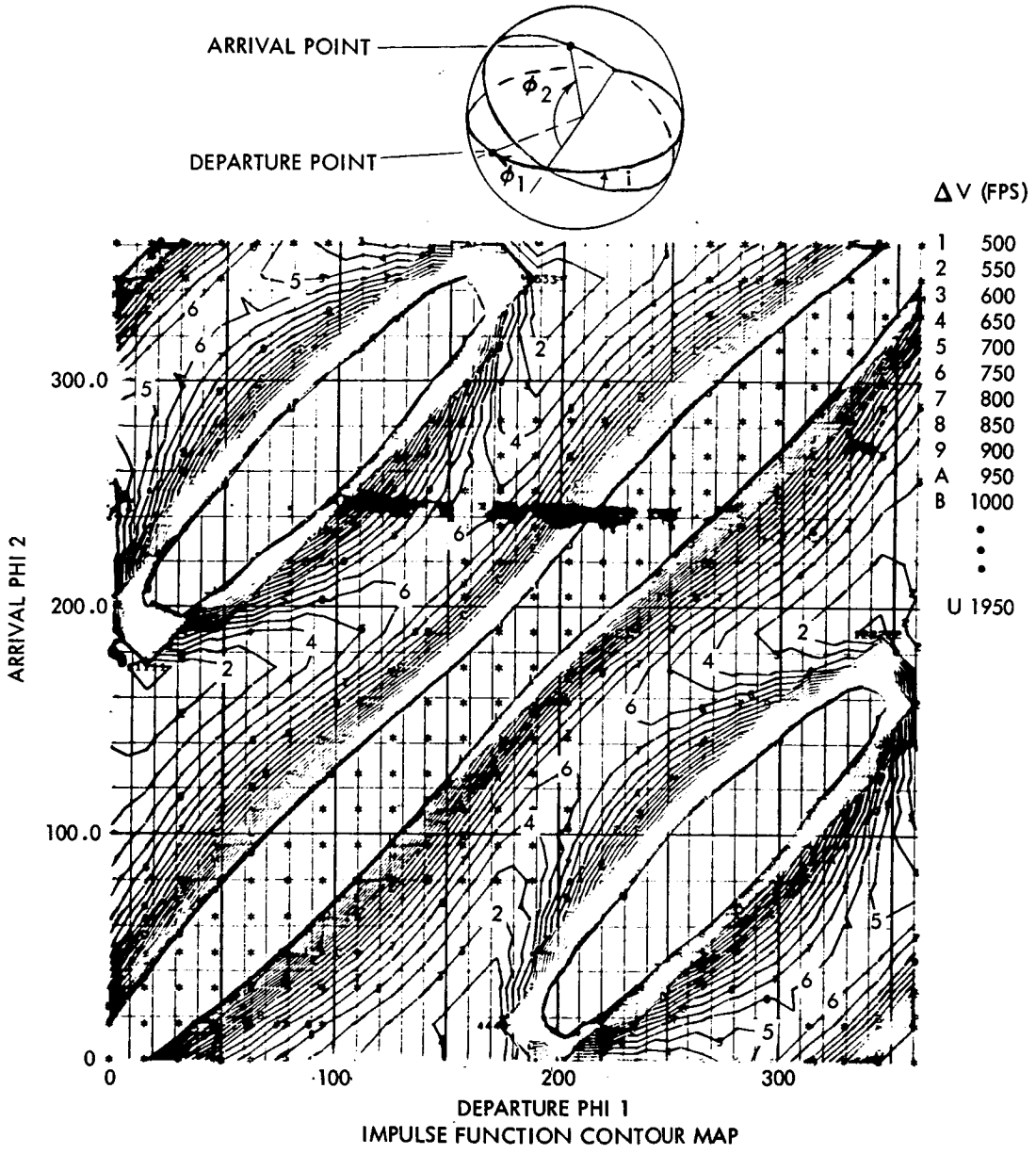

Figure 1-91. - Velocity Requirements for Transfer from 60-Nautical-Mile Circular Orbit to 15- by 120-Nautical-Mile Elliptical Orbit, Perilune at the Node, Relative Inclination of Five Degrees

Requirements for rendezvous depend strongly on the initial phase relationship between the two vehicles, generally illustrated in figure 1-92. Figures 1-93 through 1-100 are machine-made plots showing parametrically the effects of phase angle and departure angle on energy requirements. Because there were not resources to examine all parameters exhaustively, some typical but illustrative LESS orbits were selected for intensive examination.

Figures 1-93 and 1-94 illustrate the CSM requirements for rendezvous from a 60-nm orbit to a 15- by-120-nm LESS orbit inclined at 5 degrees. The LESS perilune is 90 degrees past the node in figure 1-93 and at the node in figure 1-94.

The abscissas of the graphs represent departure point (ϕ_1) in the first orbit; they span the full range, from -180 degrees to +180 degrees. A time scale in units of kiloseconds corresponding to ϕ_1 is also shown. It is linear since the initial orbit is circular. The ordinate represents the relative phase of the two spacecraft ($\delta = \phi_2 - \phi_1$). As distinguished from the ϕ_2 notation in the previous discussion of pure orbit transfer, ϕ_2 is here defined as the angle of the target vehicle from the node measured in its orbit at rendezvous initiation (fig. 1-92). The angle δ is the angular separation of the two spacecraft if the two orbits are coplanar; however, this is generally not the case since ϕ_2 and ϕ_1 are measured along their respective orbits. The smooth sinusoidal curves represent the changes that will occur in relative phase if both vehicles are allowed to coast in their respective orbits for some arbitrary time. Discrete energy levels for rendezvous are indicated by the numbered contours. Solutions in the regions marked by "X" have perilune altitudes of less than 10 nautical miles. The ΔV to rendezvous directly from some initial vehicle position (ϕ_1) and some relative target position ($\delta = \phi_2 - \phi_1$) may be found by interpolating between the energy contours. If it is desirable or necessary to wait before making the first ΔV maneuver, the energy requirement for rendezvous can be inferred by moving the initial point parallel to the nearby sinusoidal curves, thereby propagating the initial conditions to an appropriate position to initiate the transfer. Depending on the initial conditions, the total energy may increase or decrease.

As an example of the application of these plots to the LESS problem, see figure 1-93 and consider the following: The LESS launch time is selected so that at burnout the relative phase angle δ is zero, the LESS reaches a 15- by-120-nm orbit inclined at 5 degrees to the 60-nm CSM orbit, and the LESS argument of perilune (ω) is 90 degrees. The foregoing is sufficient to say that the initial conditions lie somewhere along the abscissa and that the LESS perilune is at the point marked B. Consider four special points (A, B, C, and D) for analysis of their significance.

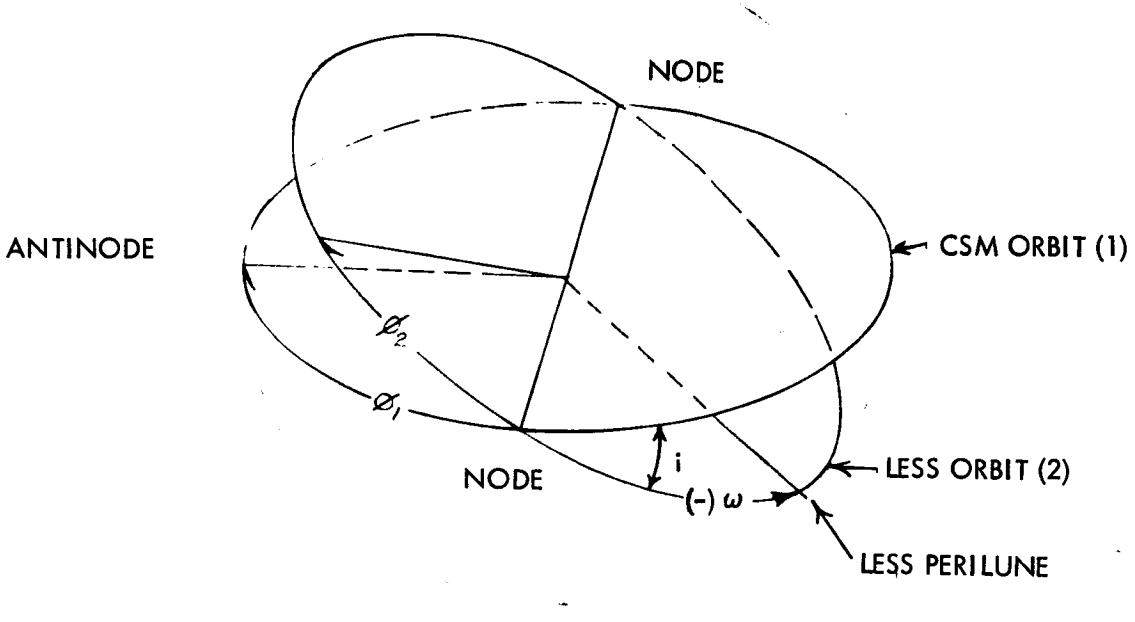

RELATIVE PHASE ANGLE, $\delta = \phi_2 - \phi_1$

Figure 1-92. - Angular Definitions of Conditions at Initiation of CSM-LESS Rendezvous

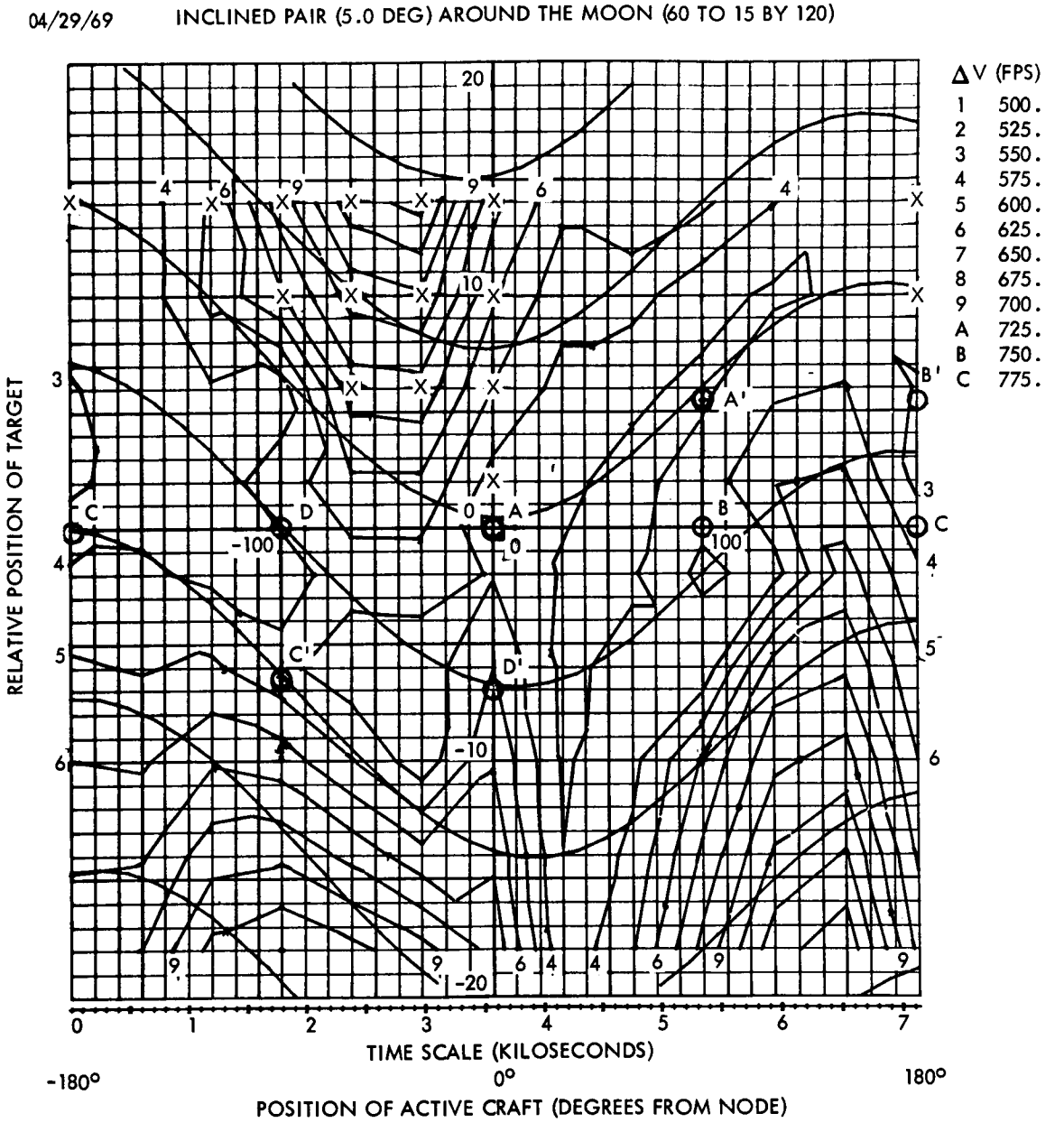

Figure 1-93. - Rendezvous Contour Map for Rendezvous From 60-Nautical-Mile Circular Orbit to 15- by 120-Nautical-Mile Elliptical Orbit Inclined at Five Degrees With Argument of Perilune of 90 Degrees

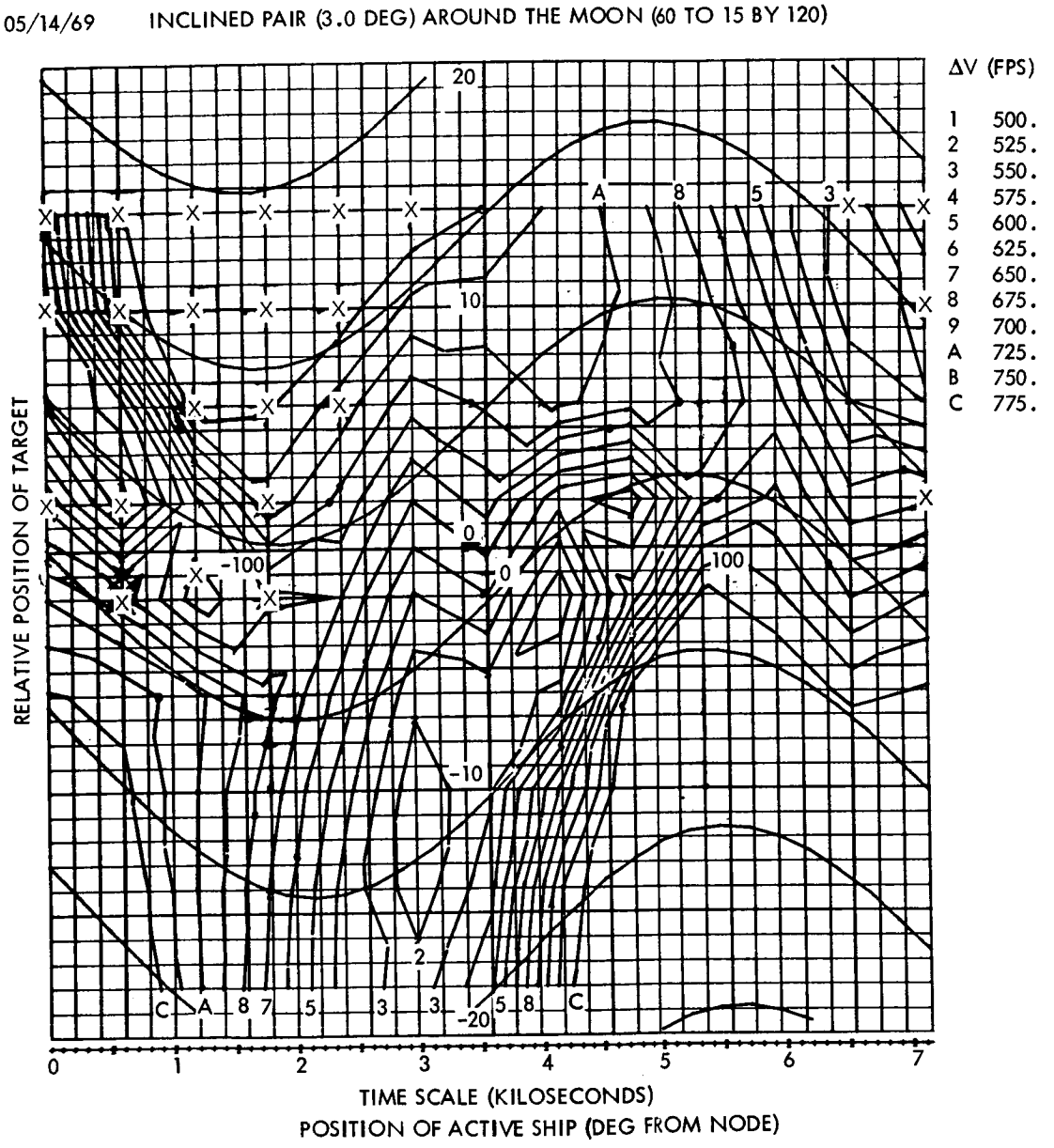

Figure 1-94. - Rendezvous Contour Map for Rendezvous From 60-Nautical-Mile Circular Orbit to 15- by 120-Nautical-Mile Elliptical Orbit Inclined at Five Degrees With Argument of Perilune of Zero Degrees

Point A represents the situation where the CSM is at the node at LESS burnout and the LESS perilune is 90 degrees ahead. It was shown in the preceding section that a 30-minute interval is required by the CSM to perform orbit determination and to prepare to execute the first rendezvous ΔV maneuver. If the initial conditions, A, are propagated through a 90-degree ($\approx$ 30 minutes) interval in $\emptyset_1$, the conditions A' are found for initiation of the transfer. As would be expected from the description of the initial conditions, the LESS has traveled faster through its orbit segment, producing a positive relative phase angle at A'. A' is a relative antinode. The rendezvous ΔV is seen to be slightly below 550 feet per second.

Point B represents the case where the CSM is 90 degrees past the node (i.e. at the antinode) and the LESS is at perilune in its orbit. In the initial conditions, B, are propagated through 90 degrees, the nodal conditions B' are found for initiation of the transfer. Again, the rendezvous ΔV is slightly less than 550 feet per second.

Point C represents the case where the CSM is at a node and the LESS is 90 degrees past perilune in its orbit. Point C propagates to C', at which time the CSM is at a relative antinode and the LESS is at apolune in its orbit. The LESS trails the CSM at this point. The ΔV requirement is approximately 585 feet per second.

Point D represents the case where the LESS is at apolune and the CSM is at an antinode. Because the LESS is traveling through the slow part of its orbit as the point D propagates to D', it has a negative relative phase at D'. The ΔV requirement for rendezvous is the highest of the cases examined, being approximately 605 feet per second.

Except for the D, D' case, it is desirable from an energy point of view to initiate the rendezvous maneuver as soon after the 90-degree tracking and pre-ΔV segment as possible. In the case of D, D', on the order of 60 feet per second can be saved if the transfer initiation is delayed another 35 degrees (or approximately 12 minutes).

As shown, the mission analyst may use these plots to investigate the gross effects of various parameters. For instance, the effect of launch timing can be found by locating the initial points at some value off the abscissa (plus for early launches or minus for late launches). The effect of the tracking and pre-ΔV phase can be evaluated by simply propagating the initial conditions through some different interval of CSM coasting orbit ($\emptyset_1$).

Figures 1-94 through 1-100 illustrate the same type of data for various orbit pairs. The same type of analysis technique can be used with them.

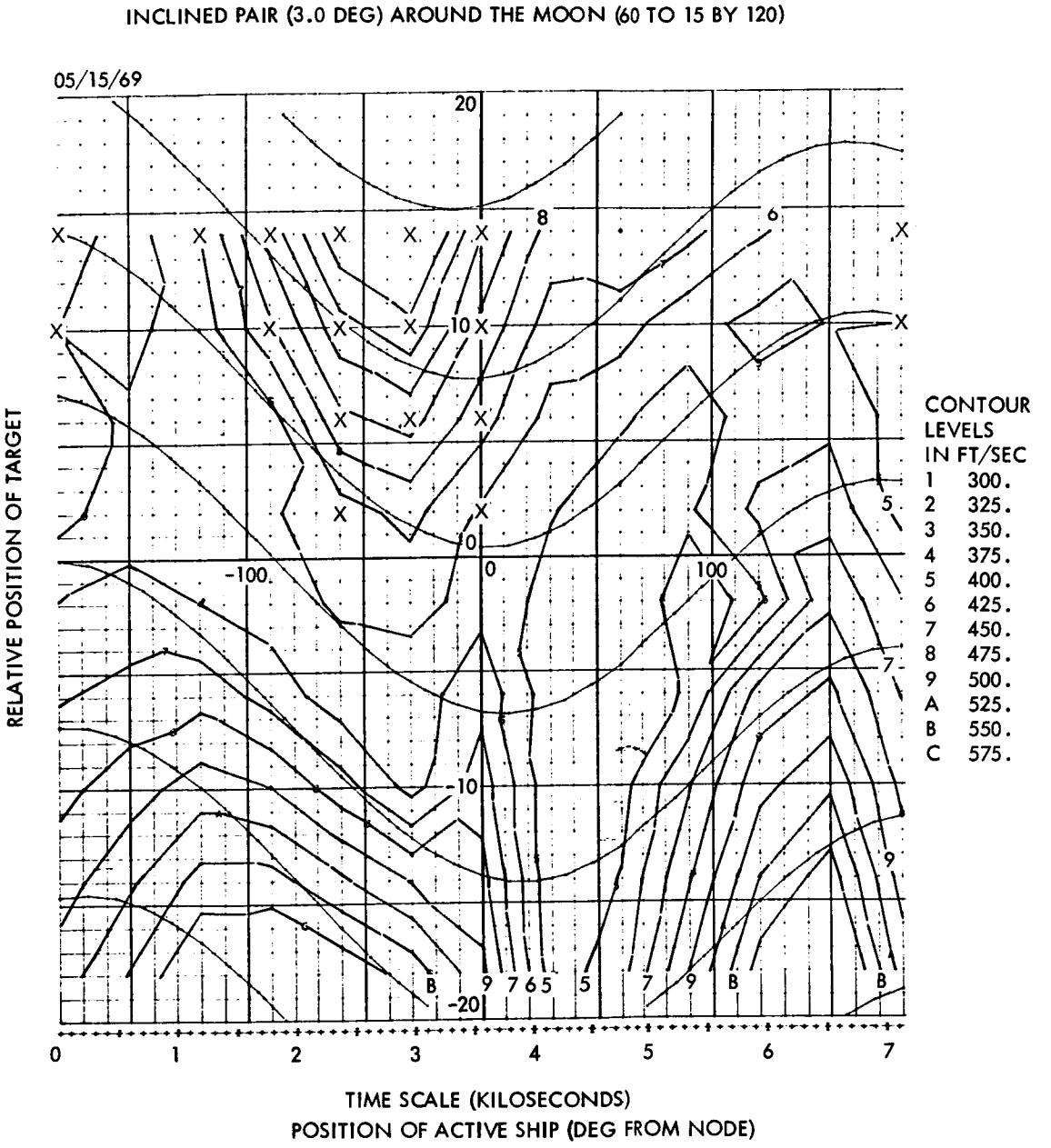

Figure 1-95. - Rendezvous Contour Map for Rendezvous From 60-Nautical-Mile Circular Orbit to 15- by 120-Nautical-Mile Elliptical Orbit Inclined at Three Degrees With Argument of Perilune of 90 Degrees

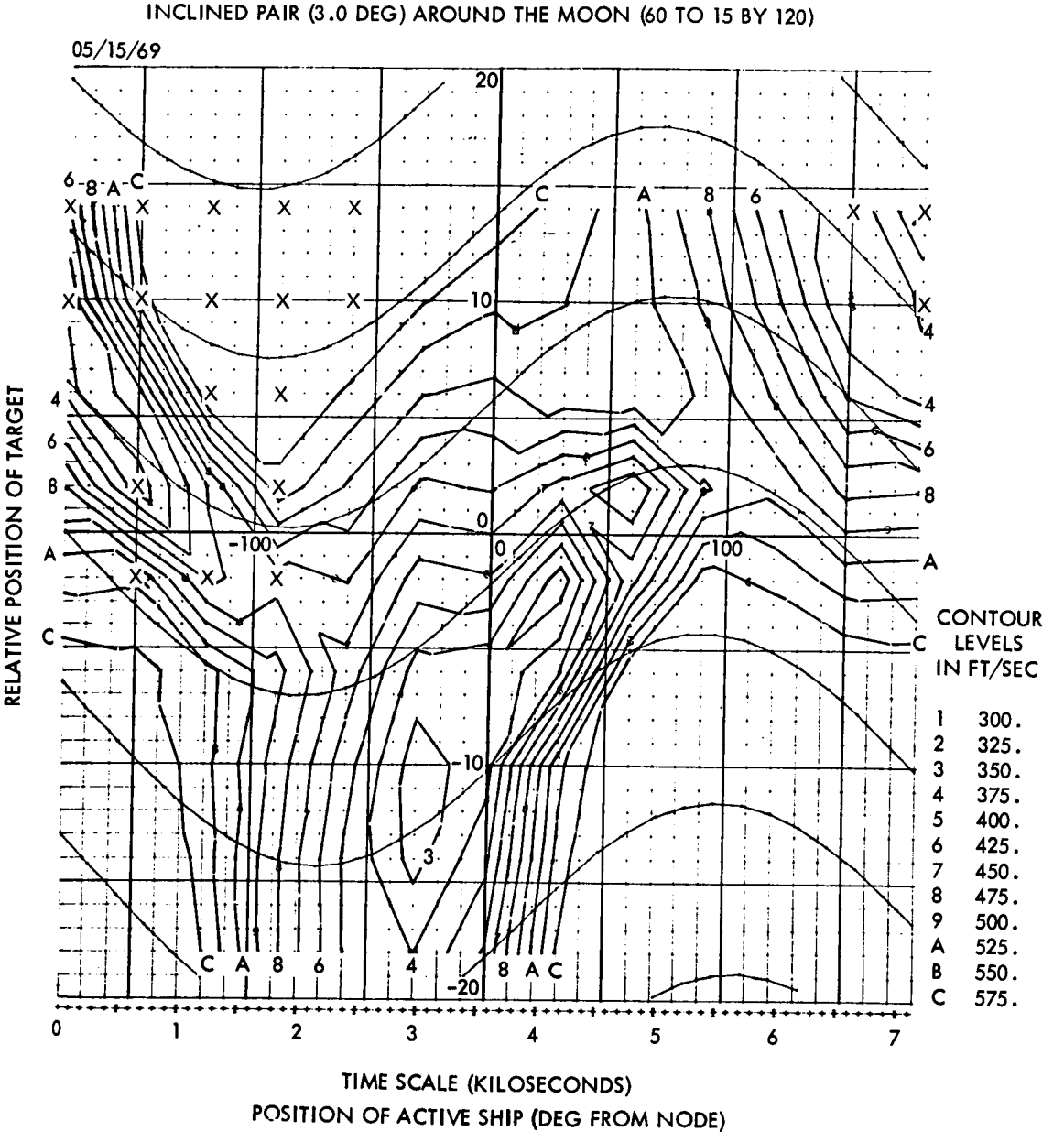

Figure 1-96. - Rendezvous Contour Map for Rendezvous From 60-Nautical-Mile Circular Orbit to 15- by 120-Nautical-Mile Elliptical Orbit Inclined at Three Degrees With Argument of Perilune of Zero Degrees

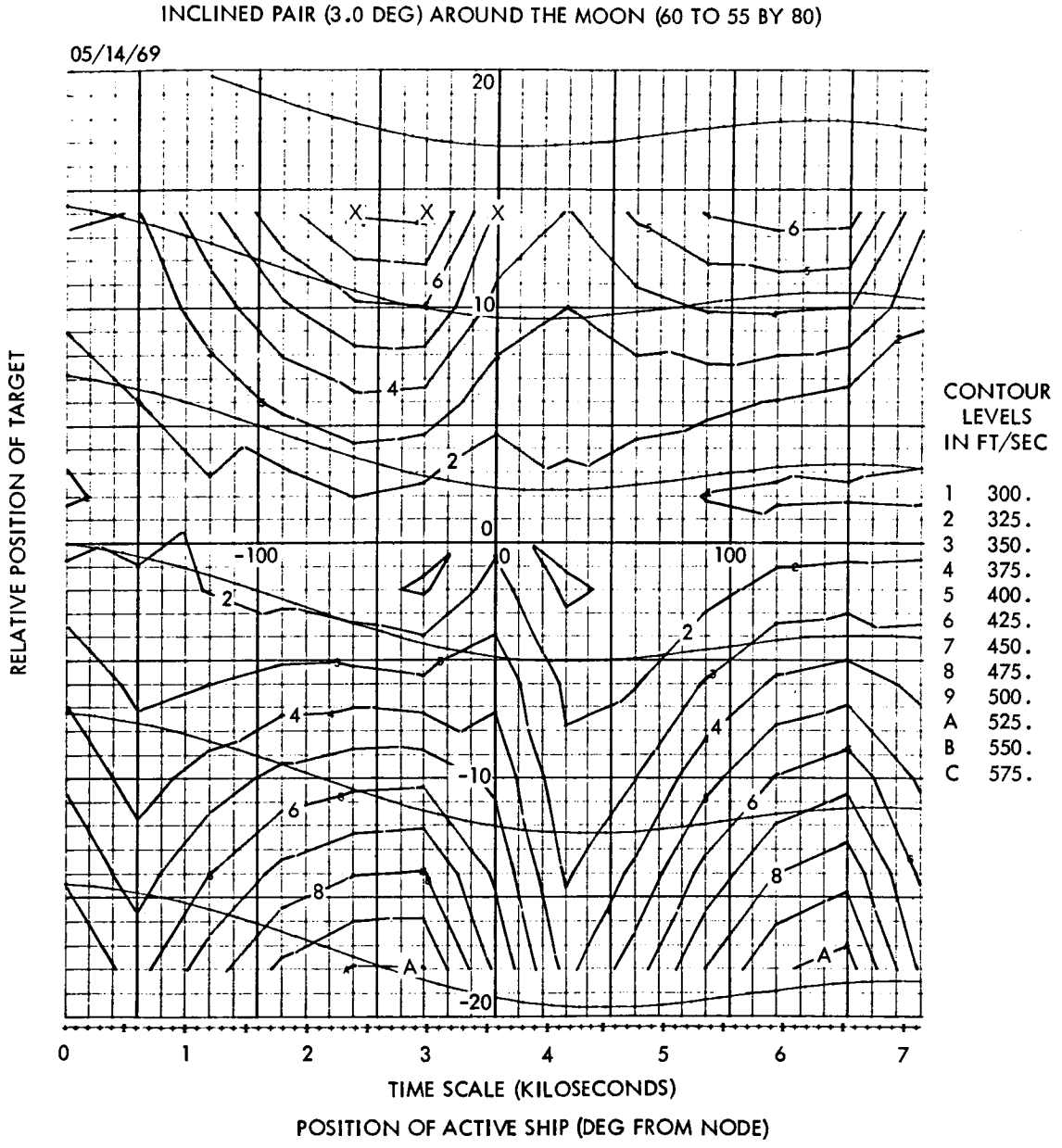

Figure 1-97. - Rendezvous Contour Map for Rendezvous From 60-Nautical-Mile Circular Orbit to 55- by 80-Nautical-Mile Elliptical Orbit Inclined at Three Degrees With Argument of Perilune of 90 Degrees

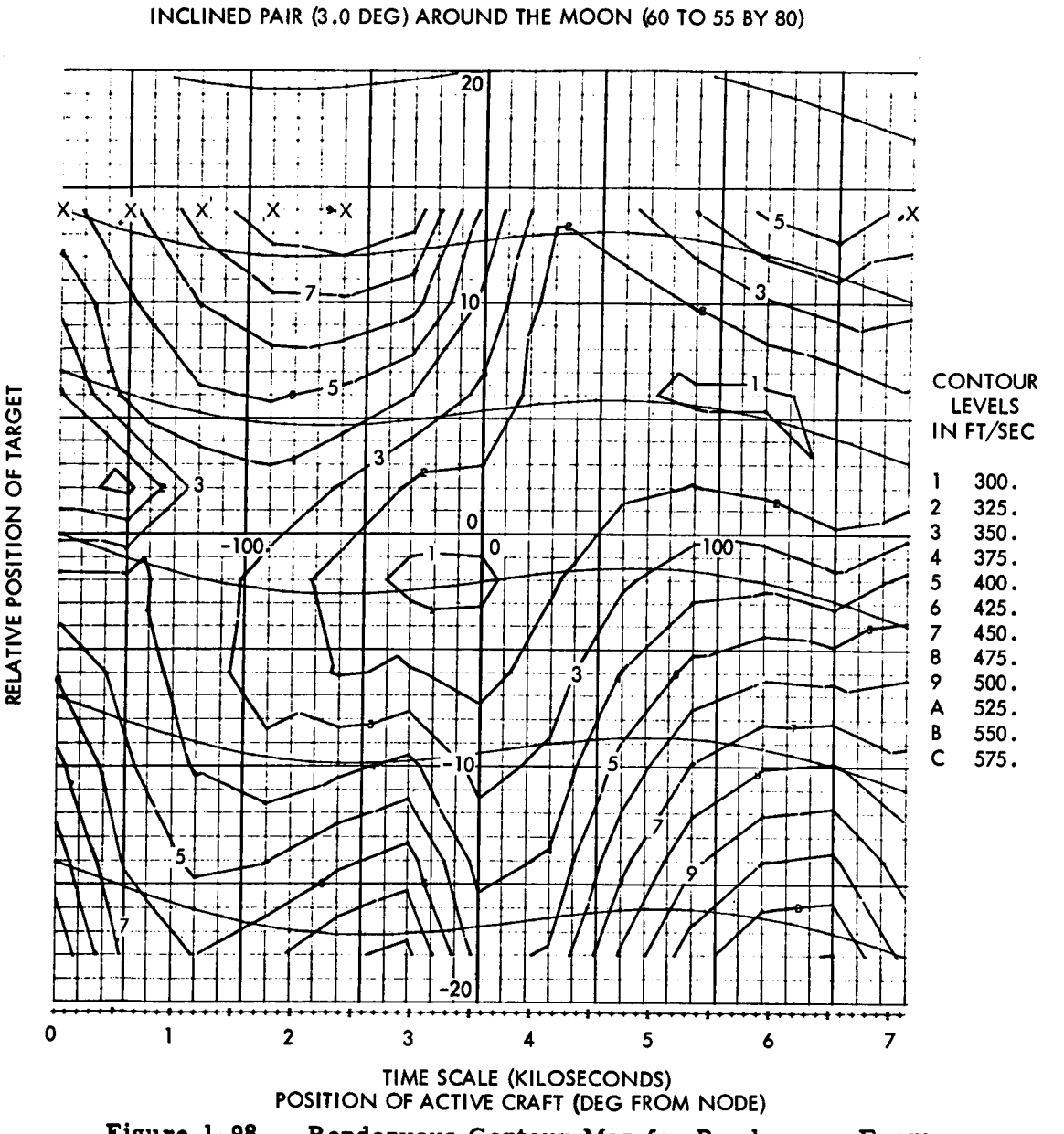

Figure 1-98. - Rendezvous Contour Map for Rendezvous From 60-Nautical-Mile Circular Orbit to 55- by 80-Nautical-Mile Elliptical Orbit Inclined at Three Degrees With Argument of Perilune of Zero Degrees

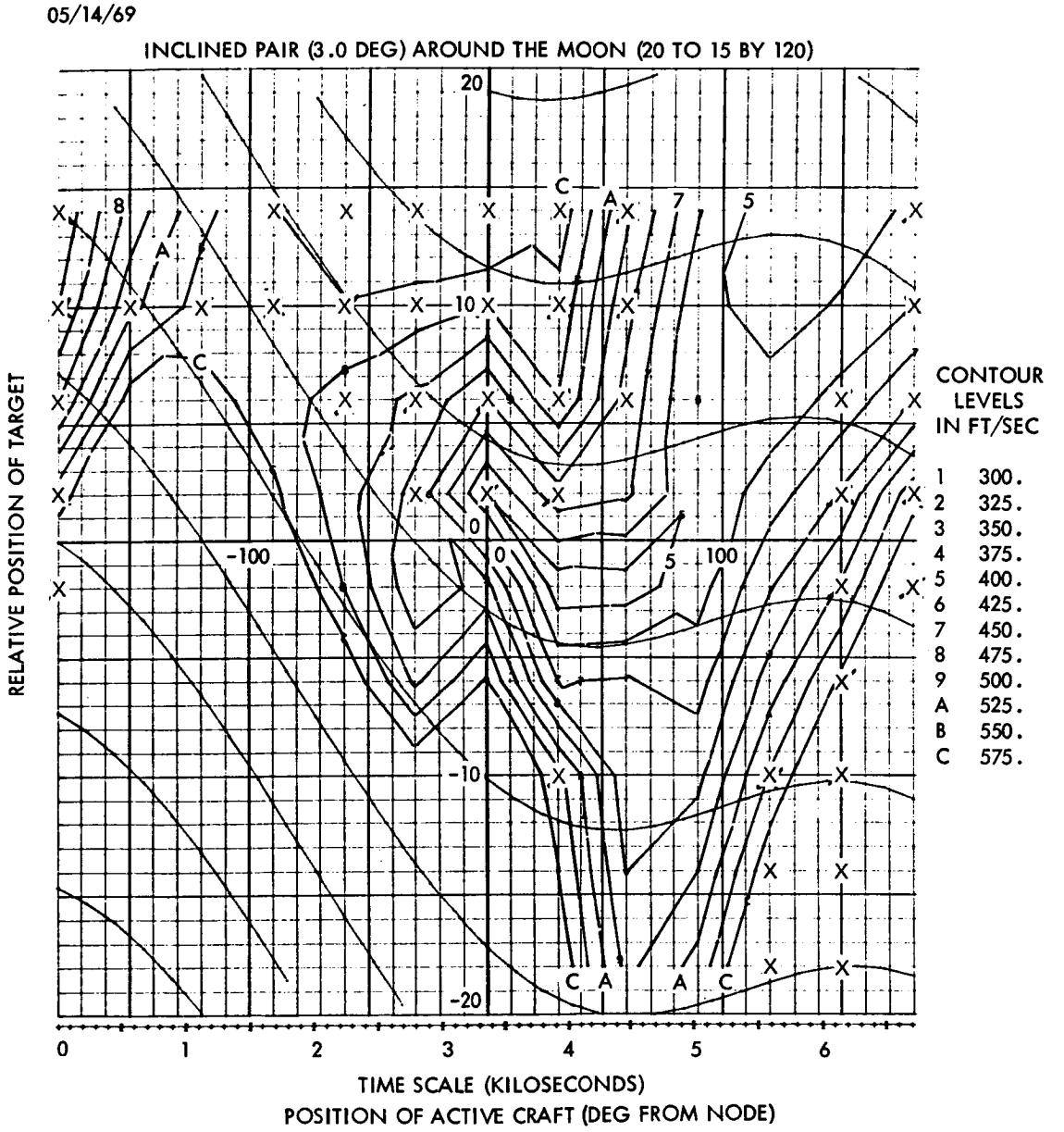

Figure 1-99. - Rendezvous Contour Map for Rendezvous From 20-Nautical-Mile Circular Orbit to 15- by 120-Nautical-Mile Elliptical Orbit Inclined at Three Degrees With Argument of Perilune of 90 Degrees

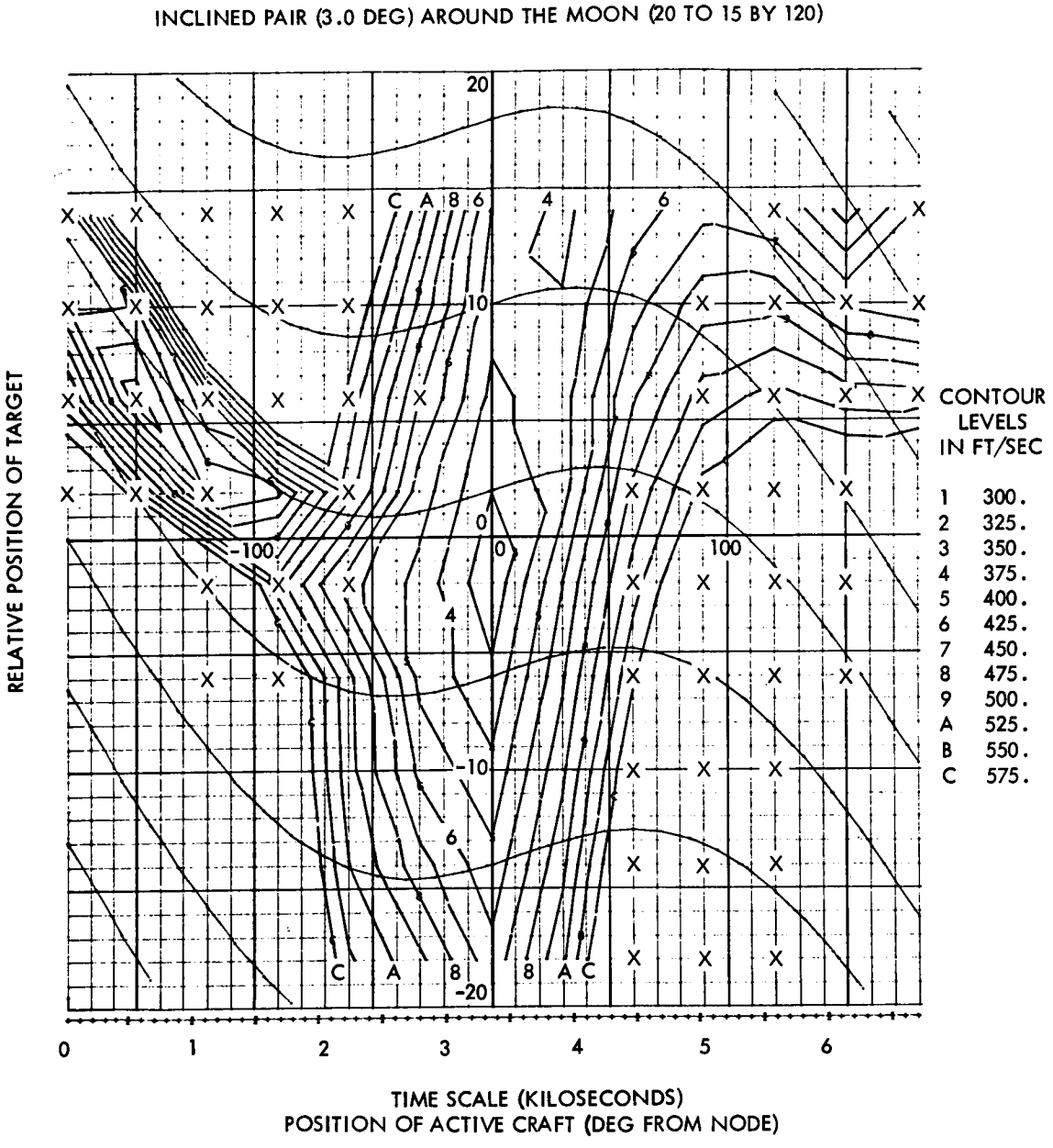

Figure 1-100. - Rendezvous Contour Map for Rendezvous From 20-Nautical-Mile Circular Orbit to 15- by 120-Nautical-Mile Elliptical Orbit Inclined at Three Degrees With Argument of Perilune of Zero Degrees

The following analysis illustrates in more detail the problem of rendezvous from a 60-nm circular orbit to a 15- by 120-nm orbit. It shows the effects of perilune orientation, departure point, relative inclination, phase angle, and transfer angle.

Figures 1-101 through 1-104 show the maximum relative inclination that can be tolerated as a function of relative phase angle for specific ΔV allocations. Figures 1-101 and 1-102 illustrate 270-degree transfer capabilities (originating at a relative antinode) for ΔV allocations of 600 feet per second and for 400 and 800 feet per second, respectively. LESS perilune locations, defined as the in-plane angle from rendezvous initiation to perilune positions of 0, 90, 180, and 270 degrees, are noted.

Similar data are shown in figures 1-103 and 1-104 for 180-degree transfers originating at a relative node. It is seen that these results are more sensitive to initial relative phase angle than were results for 270-degree transfers. Some long transfers are noted in these figures where short transfers cannot be made because of the minimum perilune altitude constraint.

Correlation With LESS Boost: The following analysis considers the energy requirements and transfer orbit characteristics specifically associated with a three-step LESS boost trajectory initiated with a liftoff thrust-to-weight ratio of 0.3 pounds per pound. Parametric data were developed to reflect rendezvous requirements as a function of pitch attitude error during boost.

Figures 1-105 and 1-108 illustrate the in-plane conditions at rendezvous initiation for cases of a LESS 60-nm circular target orbit and for a 60- by 180-nm elliptical target orbit respectively, as a function of the average pitch attitude error incurred during boost. In each case, the CSM is assumed to be in the target orbit prior to launch (to minimize line-of-sight range) and the LESS is targeted to intercept it at termination of boost. A 30-minute (1/4 orbit) coast phase is assumed from LESS orbit injection to CSM ΔV_1 for tracking and ΔV preparation. Figures 1-106 and 1-109 depict the corresponding energy requirements for rendezvous parametrically as a function of maximum permissible relative inclination. For reasonable CSM ΔV budgets (as noted earlier, 790 fps is presently available) plane changes on the order of several degrees can be accommodated in conjunction with pitch errors of 1 or 2 degrees.

Whether the transfer initiation point is a relative node or an antinode is seen to have little effect on the energy requirements for the circular case if 270-degree transfers can be employed. The variation is somewhat higher for the elliptical case. The data reflect exactly 180- or 270-degree transfers; in some cases these transfers are not exactly optimum, and a slight energy savings (10 to 20 fps) could be realized if the transfer angle could be a bit different.

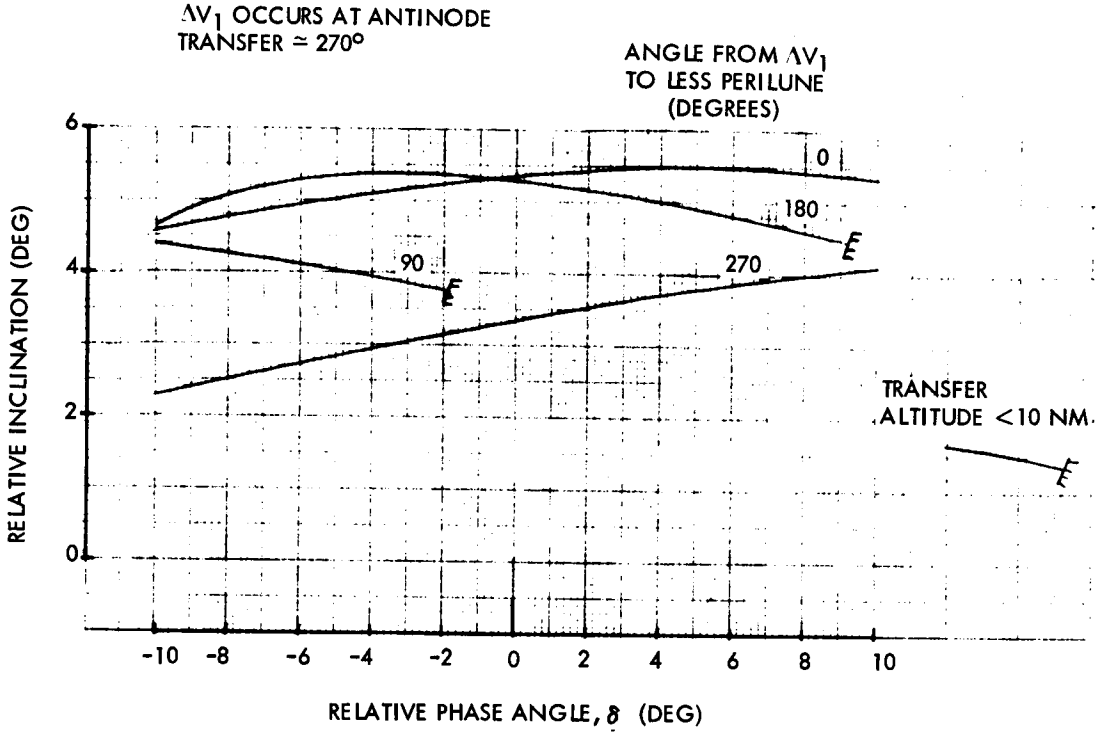

Figure 1-101. - Rendezvous Capability for ΔV of 600 Feet per Second Employing Long Transfers From 60-Nautical-Mile CSM Orbit to 15- by 120-Nautical-Mile LESS Orbit

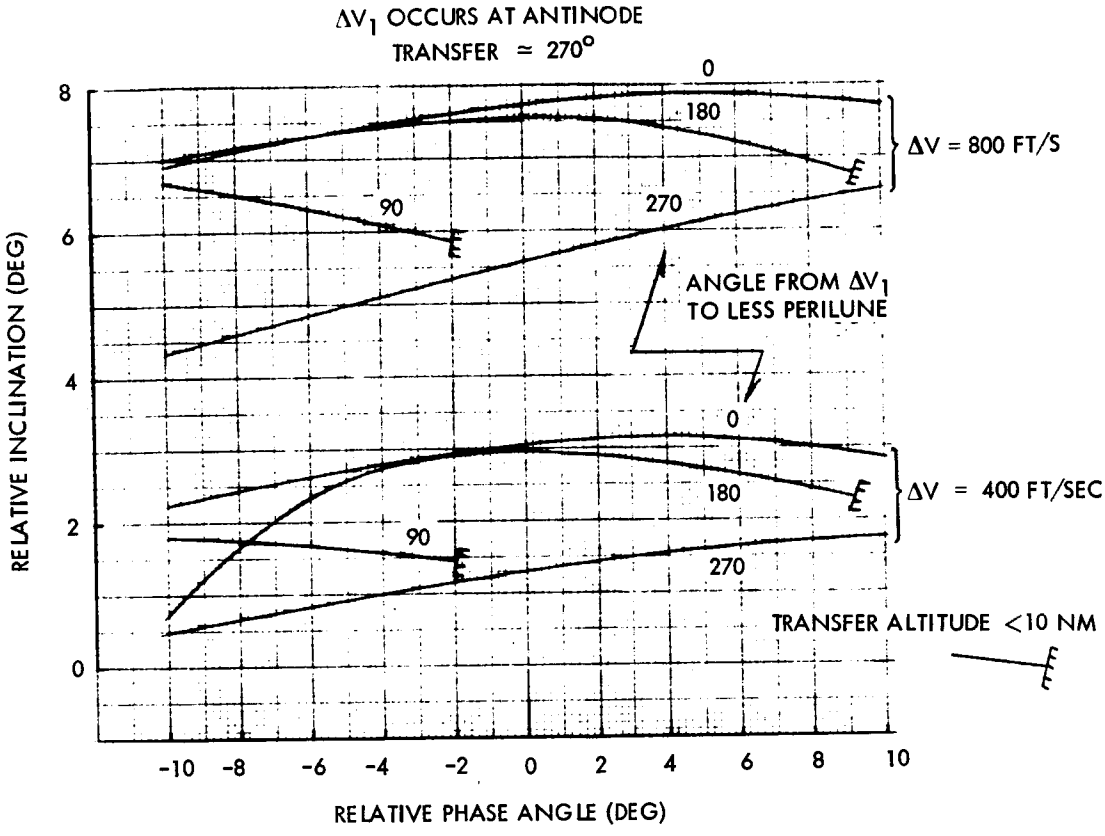

Figure 1-102. - Rendezvous Capability for ΔV of 400 and 800 Feet per Second Employing Long Transfers From 60-Nautical-Mile CSM Orbit to 15- by 120-Nautical-Mile LESS Orbit

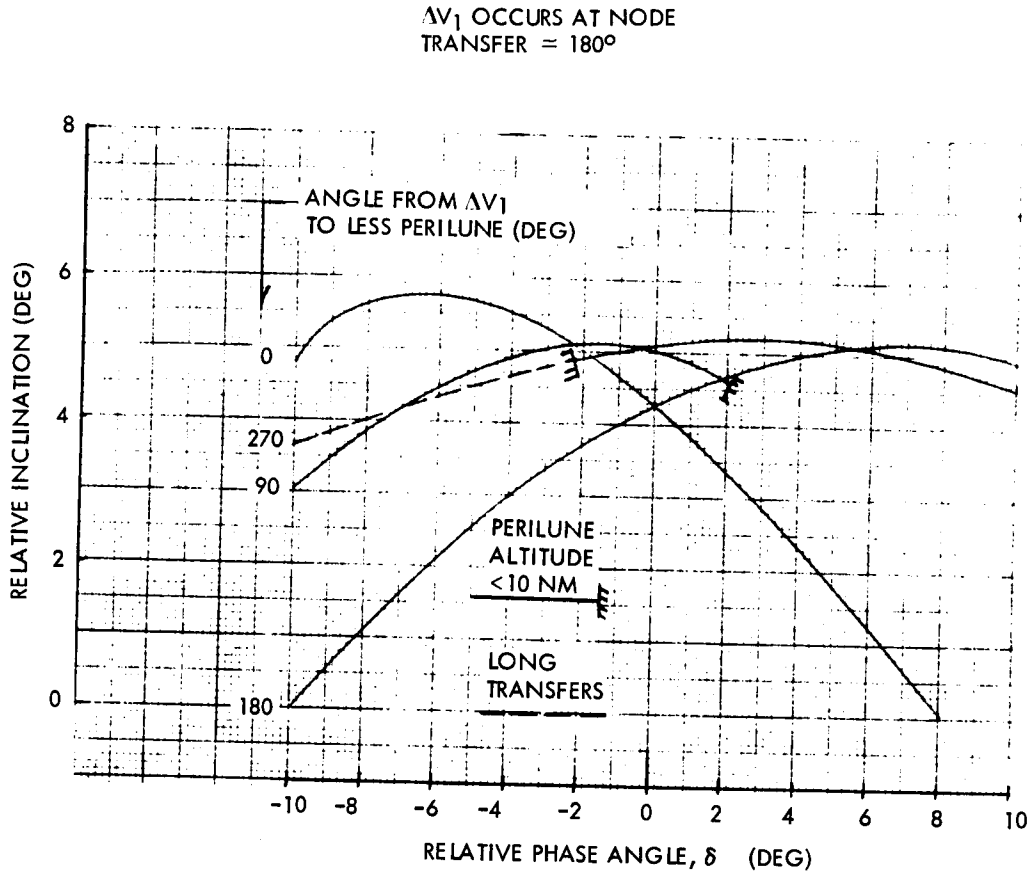

Figure 1-103. - Rendezvous Capability for ΔV of 600 Feet per Second Employing Short Transfers From 60-Nautical-Mile CSM Orbit to 15- by 120-Nautical-Mile LESS Orbit

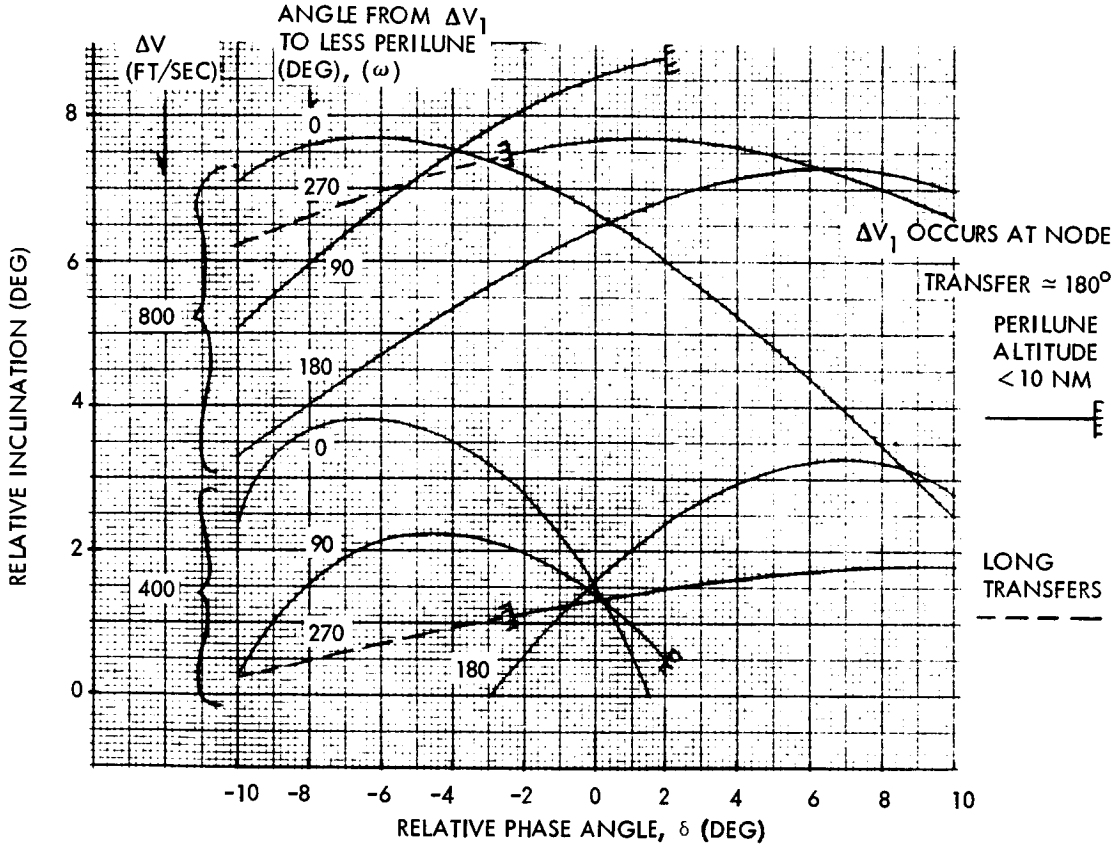

Figure 1-104. - Rendezvous Capability for ΔV of 400 and 800 Feet per Second Employing Short Transfers From 60-Nautical-Mile CSM Orbit to 15- by 120-Nautical-Mile LESS Orbit

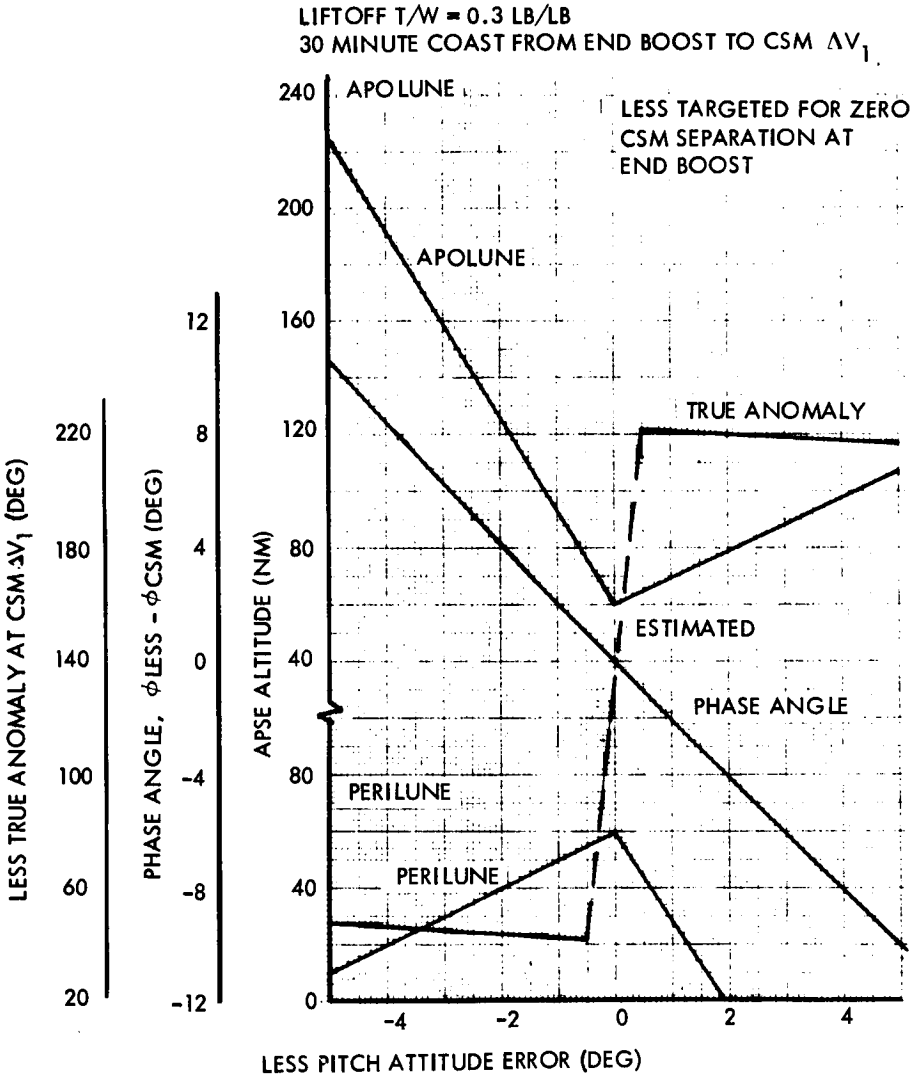

Figure 1-105. - Variation of In-Plane LESS Parameters at CSM ΔV_1 With Pitch Attitude Errors for Boost to 60-Nautical-Mile Target Orbit

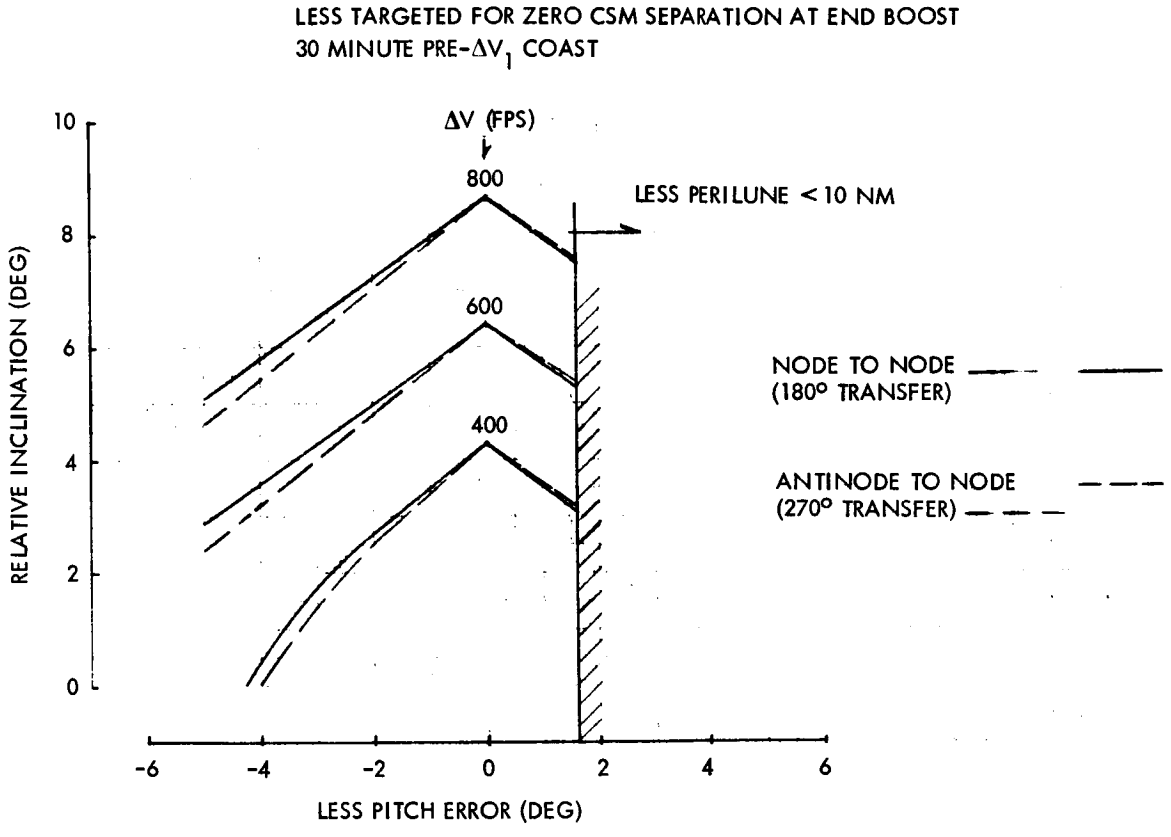

Figure 1-106. - Variation of Rendezvous Capability With Pitch Attitude Error Incurred During LESS Boost to 60-Nautical-Mile Target Orbit

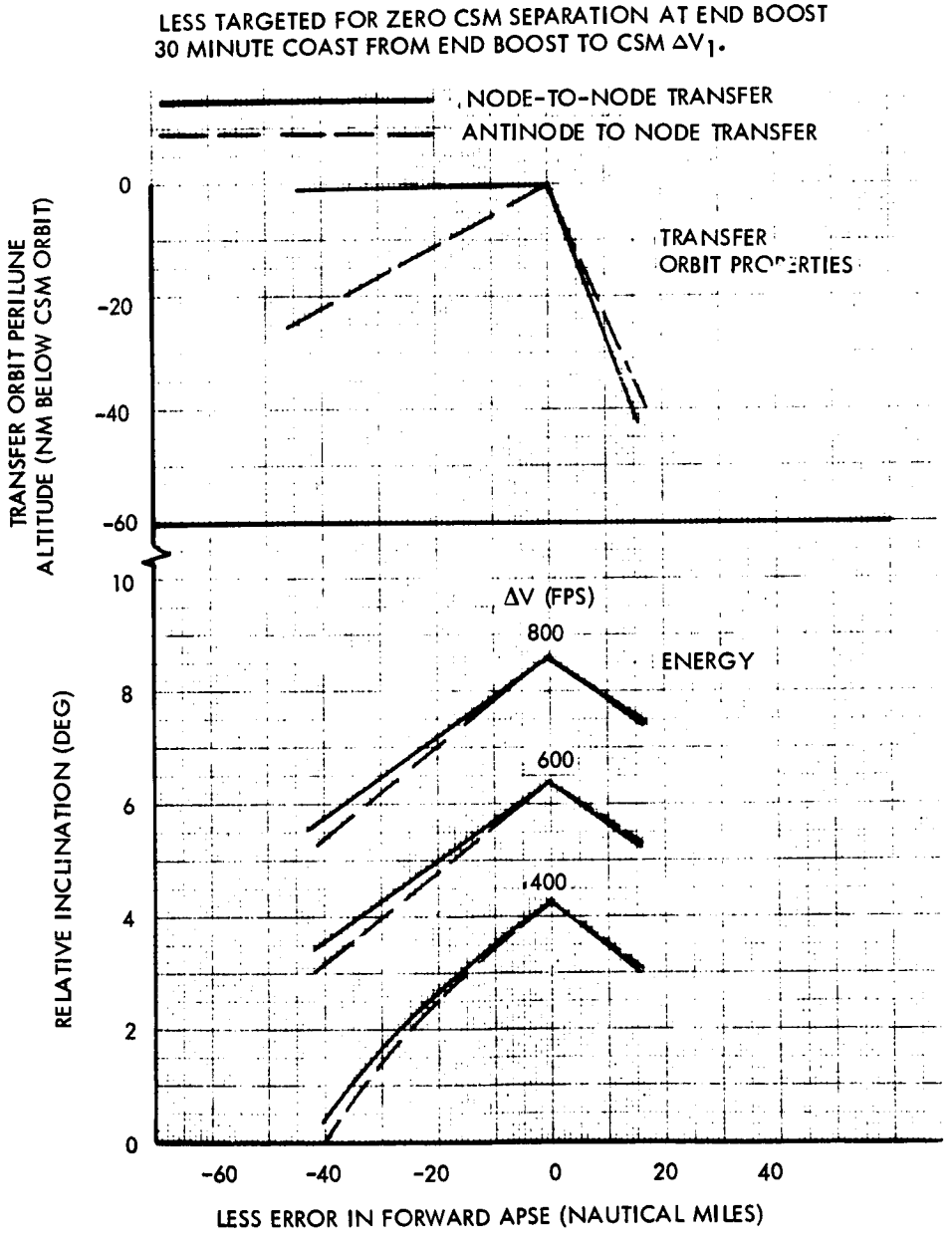

Figure 1-107. - Approximate Generalized Rendezvous Capability Based on Error in Forward Apse

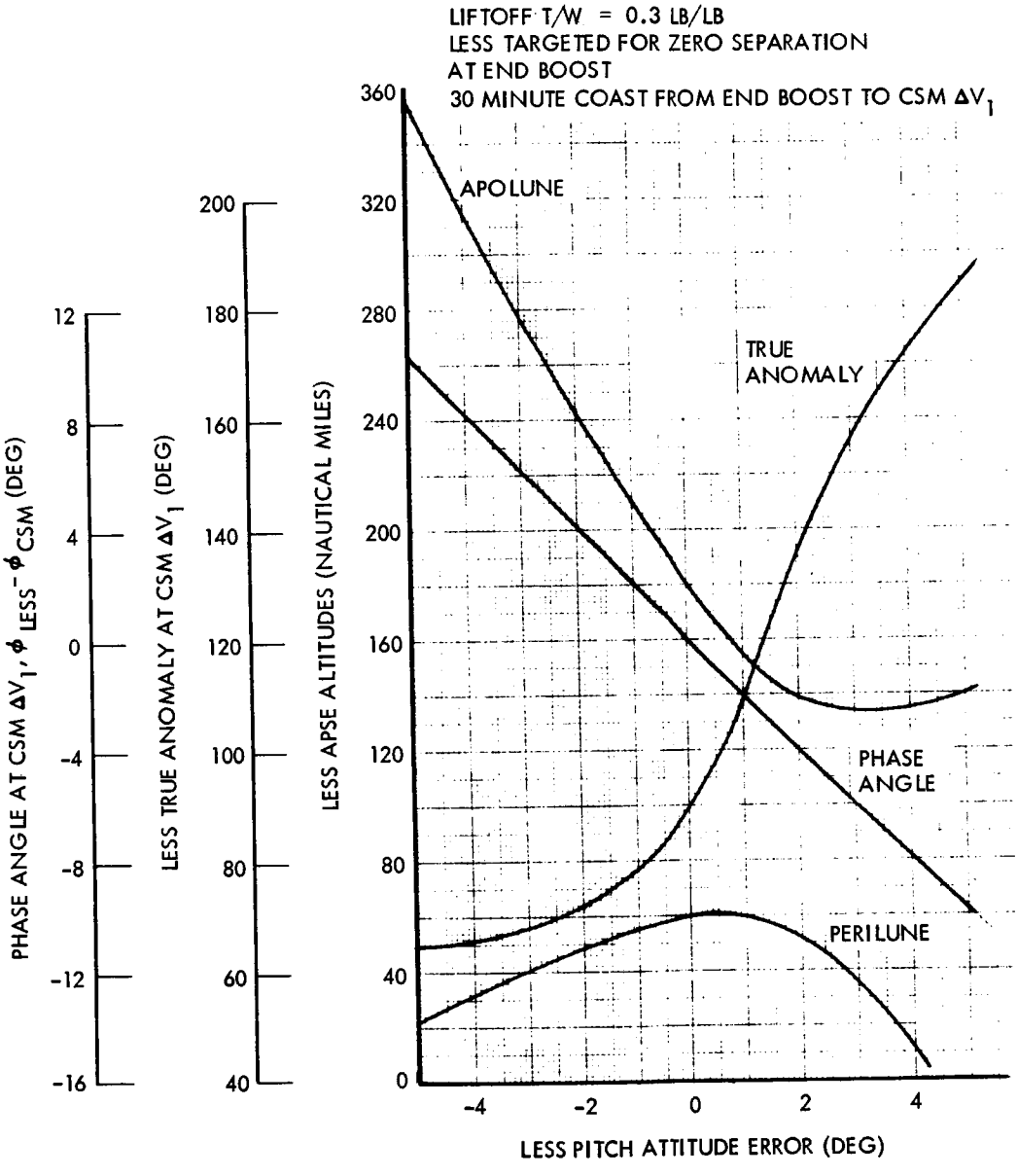

Figure 1-108. - Variation of In-Plane LESS Parameters at CSM ΔV_1, With Pitch Attitude Errors for Boost to 60- by 180-Nautical-Mile Target Orbit

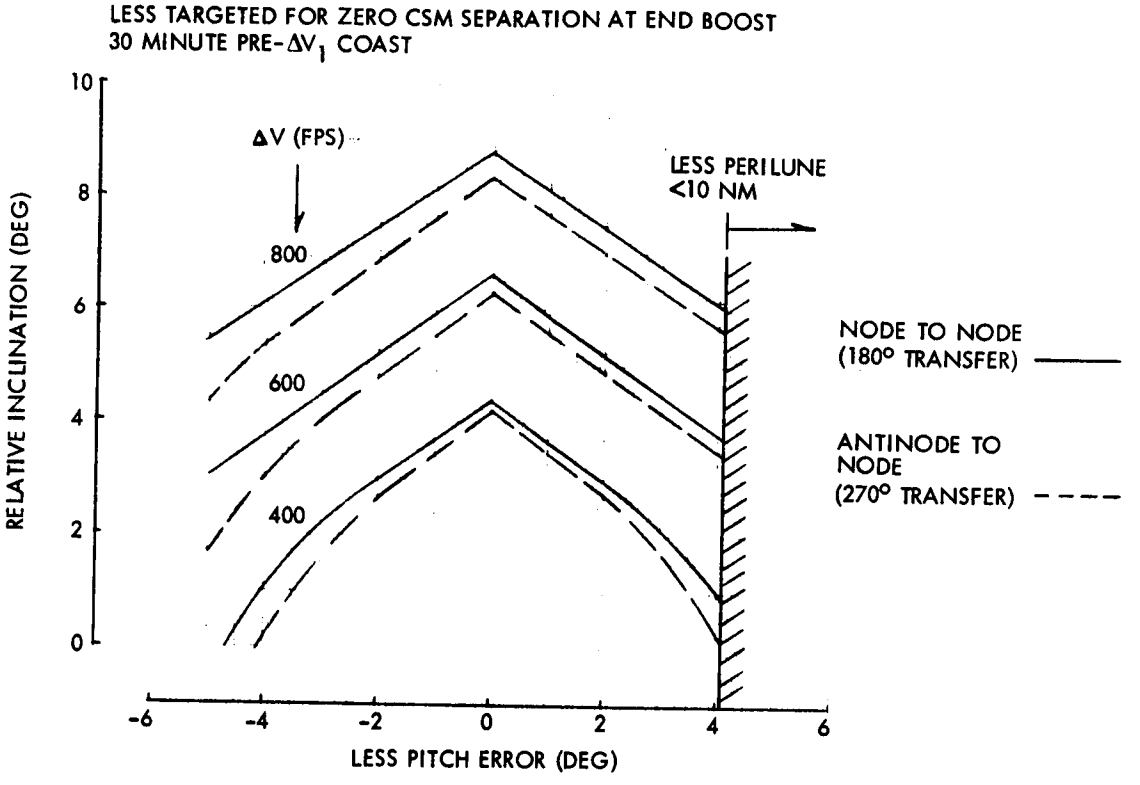

Figure 1-109. - Variation of Rendezvous Capability With Pitch Attitude Error Incurred During LESS Boost to 60- by 180-Nautical-Mile Target Orbit

The data of figure 1-106 are shown in figure 1-107 as a function of the error in the forward apse. Results correspond specifically only to the actual cases they represent. However, the mission analyst can use the generalized data of figure 1-107 to take a first look at the rendezvous requirements resulting from other kinds of errors and from combinations of errors. He could, for example, choose a number of error sources and find their individual effects on apse altitudes (from the Boost section). These could be root-sum-squared to get a reasonable statistical variation due to the combined effects. If the perilune altitude obtained by this process is safe, he can enter figure 1-107 with the error in the forward apse. He is able thereby to get a first estimate of rendezvous requirements.

The energy requirements for rendezvous presented are noted to represent CSM requirements to compensate only for LESS boost errors and are seen to be substantially the same whether circular or elliptical target orbits are used. However, in the elliptical case, it is necessary for the CSM to perform a ΔV maneuver prior to LESS launch of 149 feet per second to transfer from a 60-nm orbit into the 60- by 180-nm LESS target orbit. Transearth injection must subsequently be made from the neighborhood of apolune. This costs on the order of 70 feet per second more than for departure from a circular orbit. Thus the total CSM penalty for the elliptical case is on the order of 219 feet per second. From these data, it appears that the rendezvous energy requirements themselves are relatively insensitive to orbit ellipticity. A first estimate of the energy penalty for elliptical orbits can be taken simply as the difference between the energy required to do transearth injection from a 60-nm orbit and the energy required to transfer to some higher altitude and leave from there. These requirements are shown in figure 1-110 for a typical transearth injection energy level.

Figure 1-111 shows a comparison of circular and elliptical target orbits considering the penalty for transearth injection from apolune. While it is not always necessary to leave from apolune, the variation in apse orientation (figures 1-54 and 1-66) requires that it be considered. It appears that the circular target orbit allows larger errors if the pitch angle is biased.

Figure 1-112 depicts parametrically the maximum line-of-sight range experienced during the transfer trajectories for circular target orbits. As noted, these results are based on zero targeted separation between the CSM and the LESS at termination of boost. To assure acquisition of the LESS with the CSM optics, it is required that there be an initial stand-off range of at least 10 nautical miles. (See previous discussion.) The maximum dimension of the LESS burnout ellipsoid is on the order of 10 nautical miles (for ± one degree pitch error). Therefore, assuring that the CSM is at least 10 nautical miles from LESS burnout requires a stand-off distance on the order of

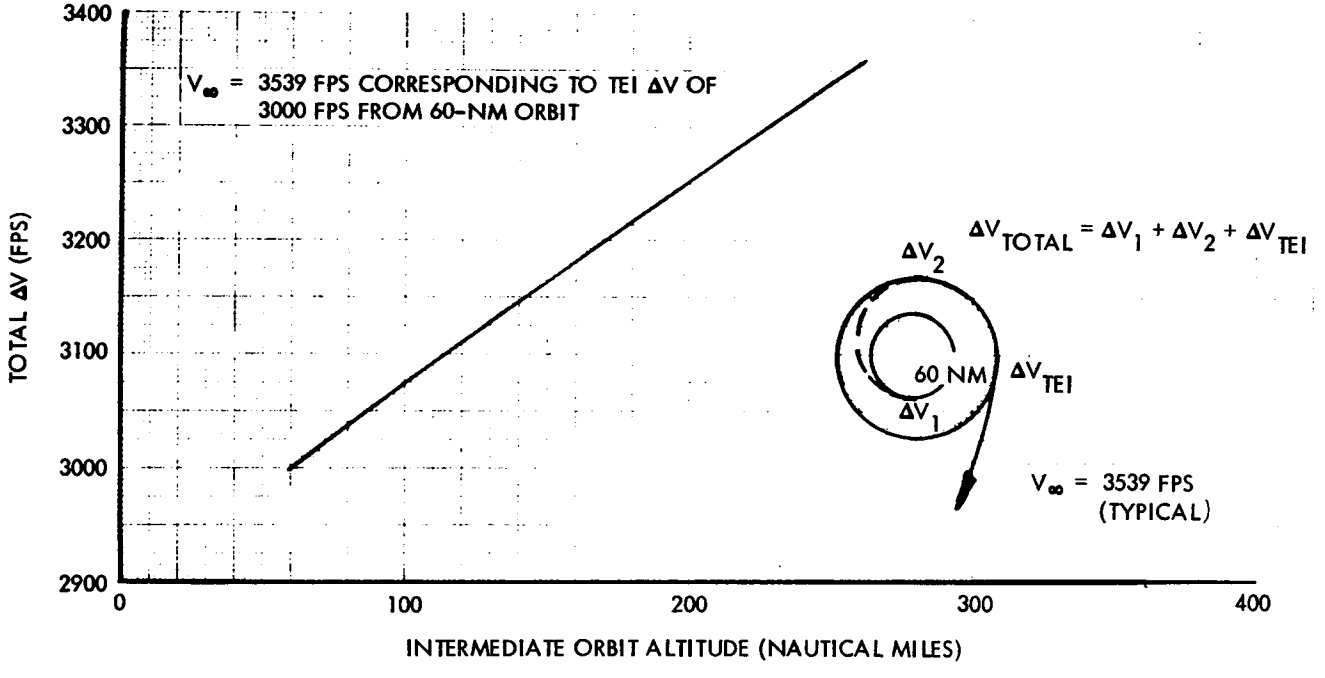

Figure 1-110. - Transearth Injection Energy Requirements for Leaving 60-Nautical-Mile Lunar Orbit via a Higher Circular Orbit

CSM ΔV ALLOCATION OF 800 FPS ACCOMPLISHES RENDEZVOUS AND INCLUDES ENERGY PENALTY FOR PERFORMING TEI AT APOLUNE OF LESS ORBIT

LESS TARGETED FOR ZERO CSM SEPARATION AT END BOOST
30 MINUTE PRE-ΔV_1 COAST

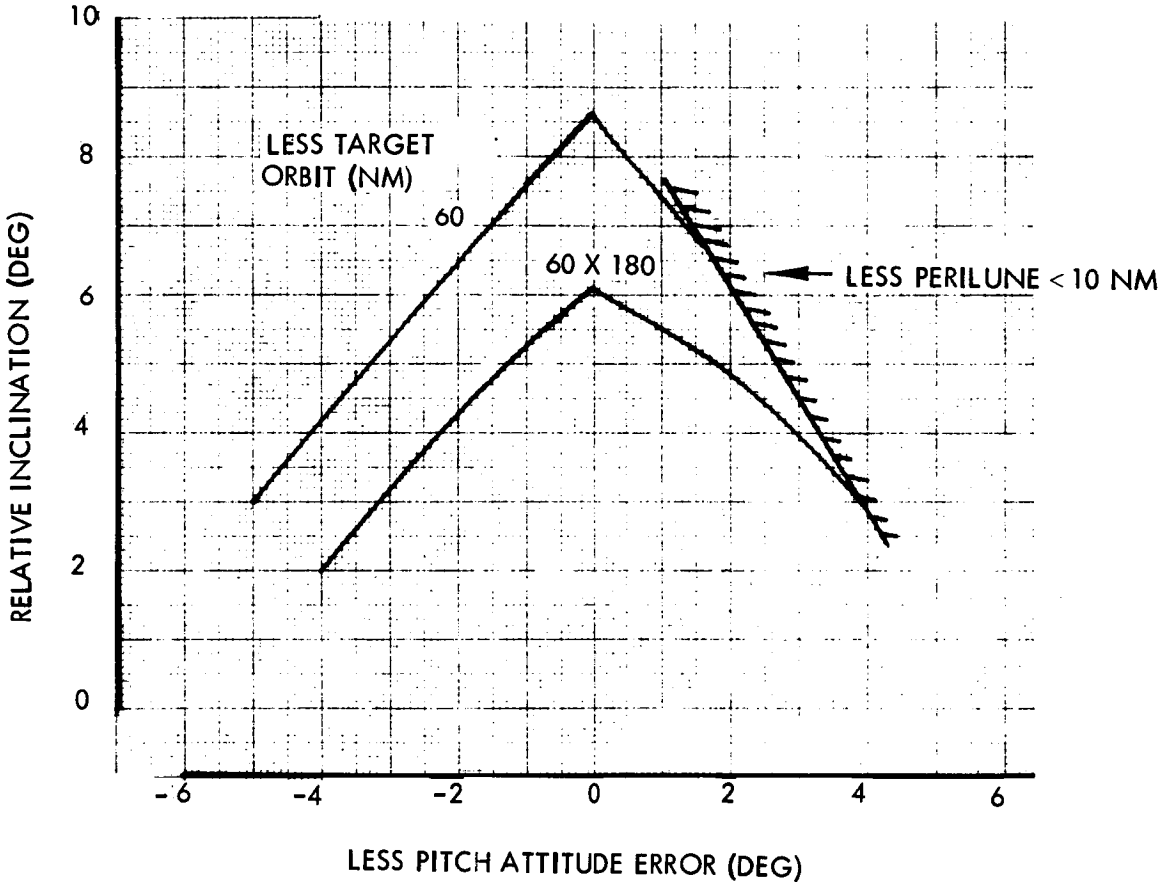

Figure 1-111. - Comparison of Circular and Elliptical LESS Target Orbits Including Effects of Transearth Injection

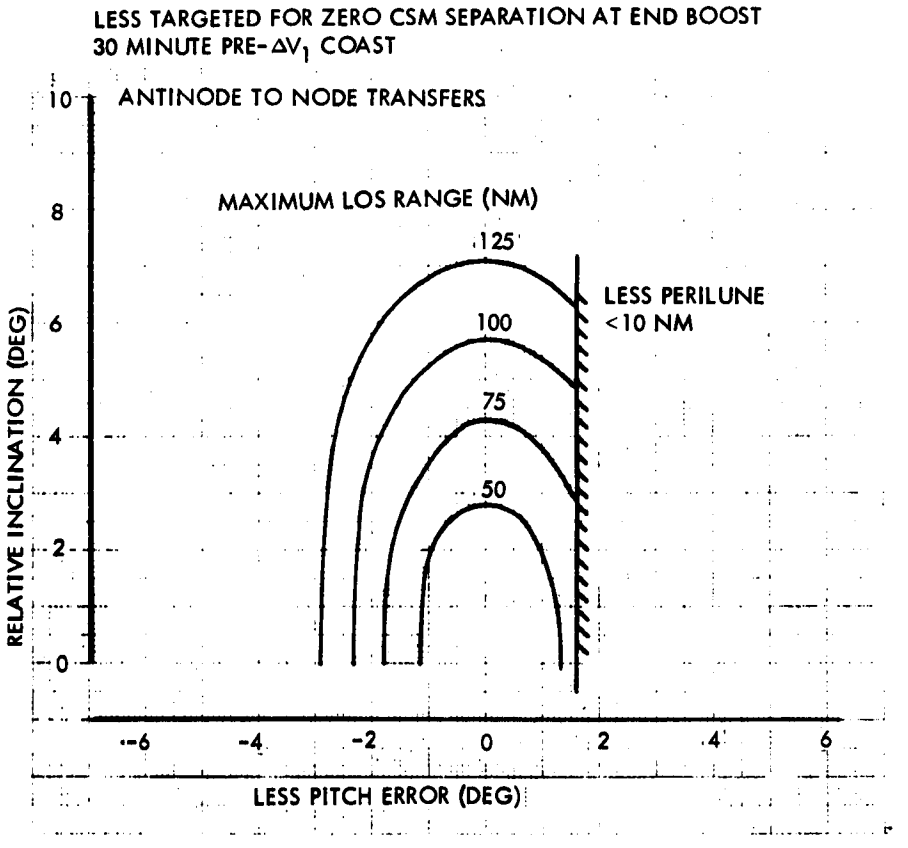

Figure 1-112. - Variation of Maximum LOS Range During Rendezvous With Error Incurred During LESS Boost to 60- by 180-Nautical- Mile Target Orbit

15 nautical miles from the nominal LESS burnout point. In most cases, satisfying this requirement will somewhat increase the maximum range incurred during transfer. Results for the elliptical target orbits are similar.

Typical Rendezvous Trajectories: Figures 1-114 through 1-140 illustrate some properties of typical off-nominal transfer trajectories. They show the time histories of line-of-sight (LOS) range and its direction and viewing conditions of the LESS as seen from the CSM. LOS direction is described by the angles of yaw (Y) and pitch (P). Yaw is measured in the local horizontal plane from the forward motion of the CSM. Pitch is measured in the vertical plane positive above the local horizontal (slightly different from the more general, LESS-centered, axis definitions, page xxviii).

The following angles are shown as viewing conditions (see fig. 1-113):

S: LESS - CSM - sun
H: LESS - CSM - horizon
R: (CSM - LESS) - surface - sun (when surface is illuminated)
1: 180 - (sun - horizon - CSM)
2: 180 - (sun - horizon - LESS)

The sun angle, S, indicates the nearness of the LESS to the sun when viewed from the CSM. It does not exist when the CSM is in shadow. (Although the automatic plotter has connected the last point prior to passing into shadow with the first illuminated point, this line segment should be ignored.)

The horizon angle, H, indicates the nearness of the LESS to the horizon and is negative if the moon's disk is in the background. If the moon's disk is illuminated, the reflection angle, R, is shown to describe the viewing conditions more completely. Angles marked 1 and 2 are shown to describe the lighting of the CSM and LESS, respectively. (Angle 2 is not shown in figure 1-113.) When these angles are negative, the vehicles are in shadow. Nine typical off-nominal cases were picked to illustrate the characteristics of the rendezvous trajectories. Common properties of the cases are:

1. Launch was made near the terminator so that the vehicles pass into shadow approximately 400 seconds after LESS orbit insertion.

2. Nominal separation at termination of LESS boost is zero.

3. The target orbit is 60 nautical miles.

4. A 30-minute coasting orbit segment precedes the ΔV maneuver to initiate the transfer.

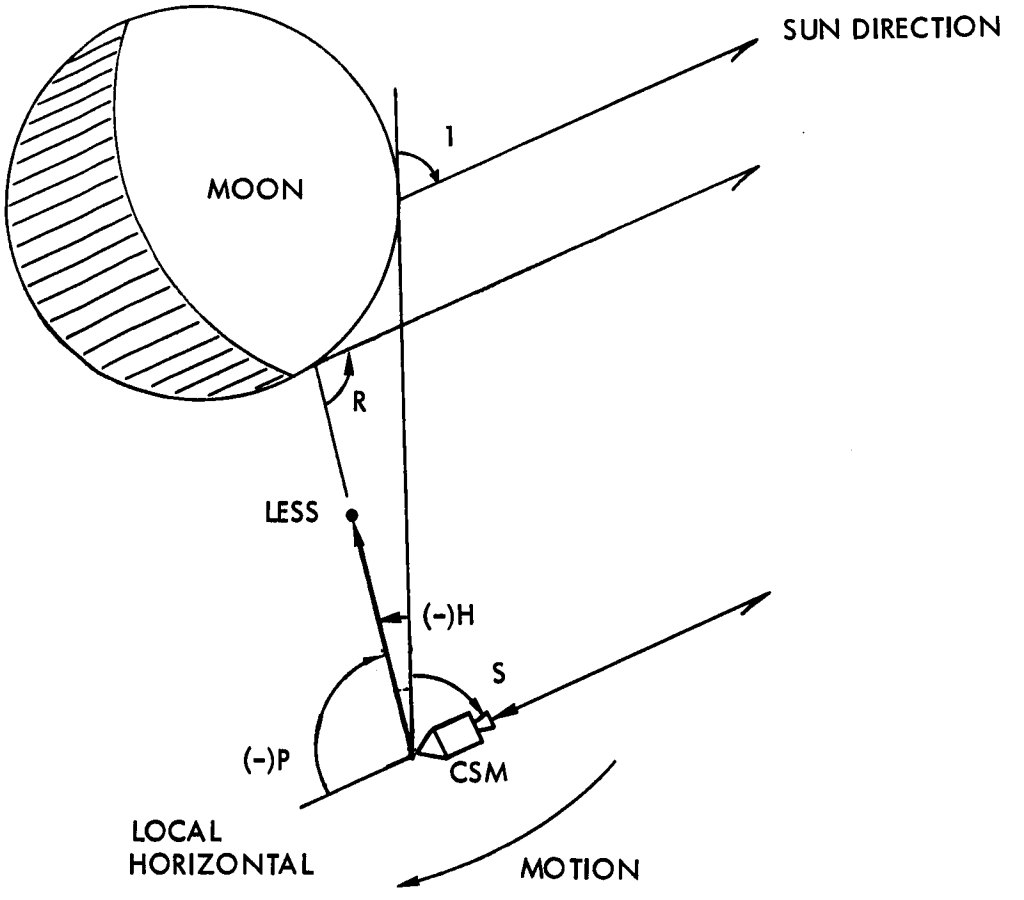

Figure 1-113. -Definition of Viewing Angles for Rendezvous Conditions (CSM-centered)

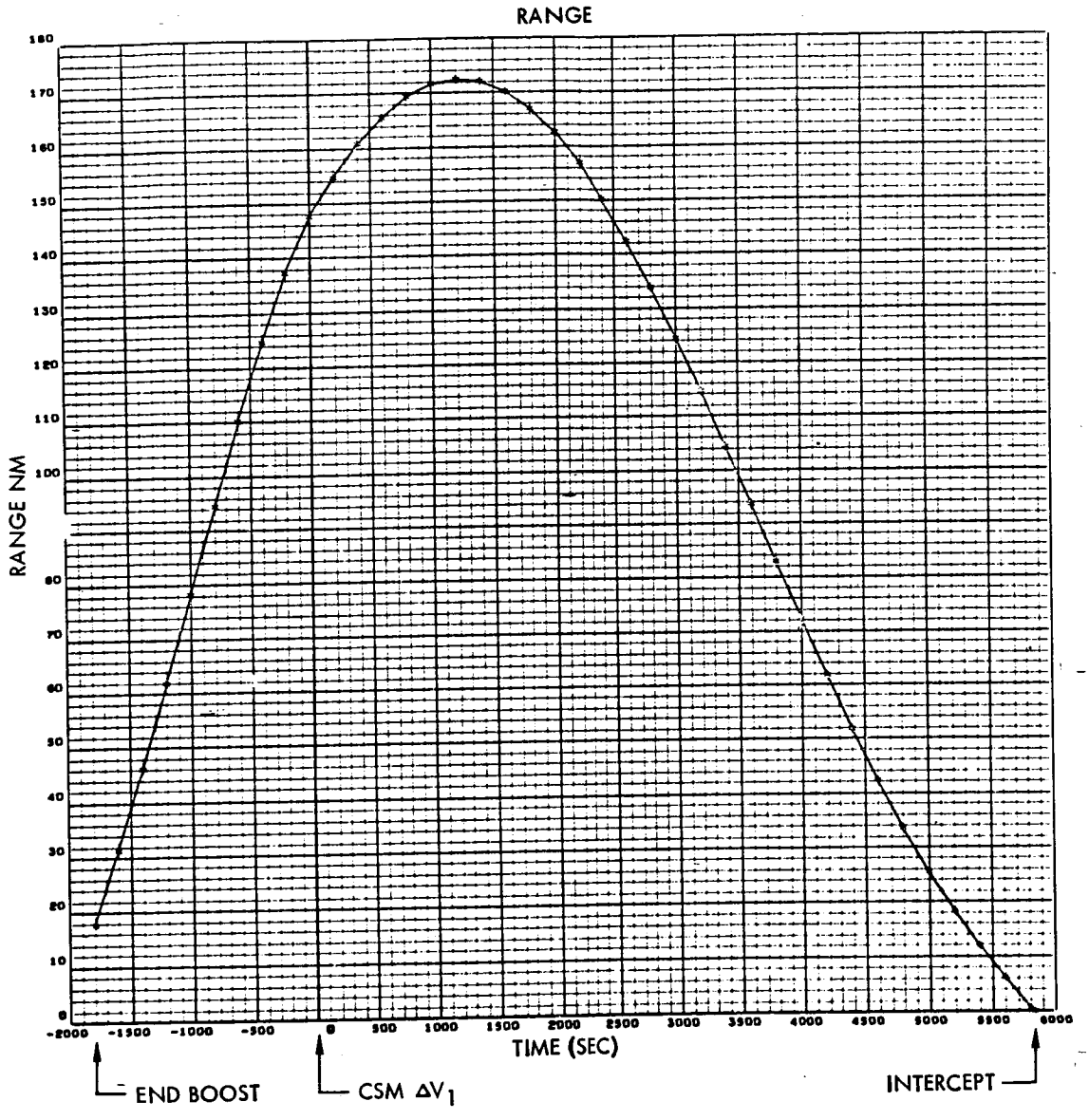

Figure 1-114. - LOS Range: LESS Orbit = 20 by 190 Nautical Miles (Due to Pitch Error of -4°), Inclination = 0°

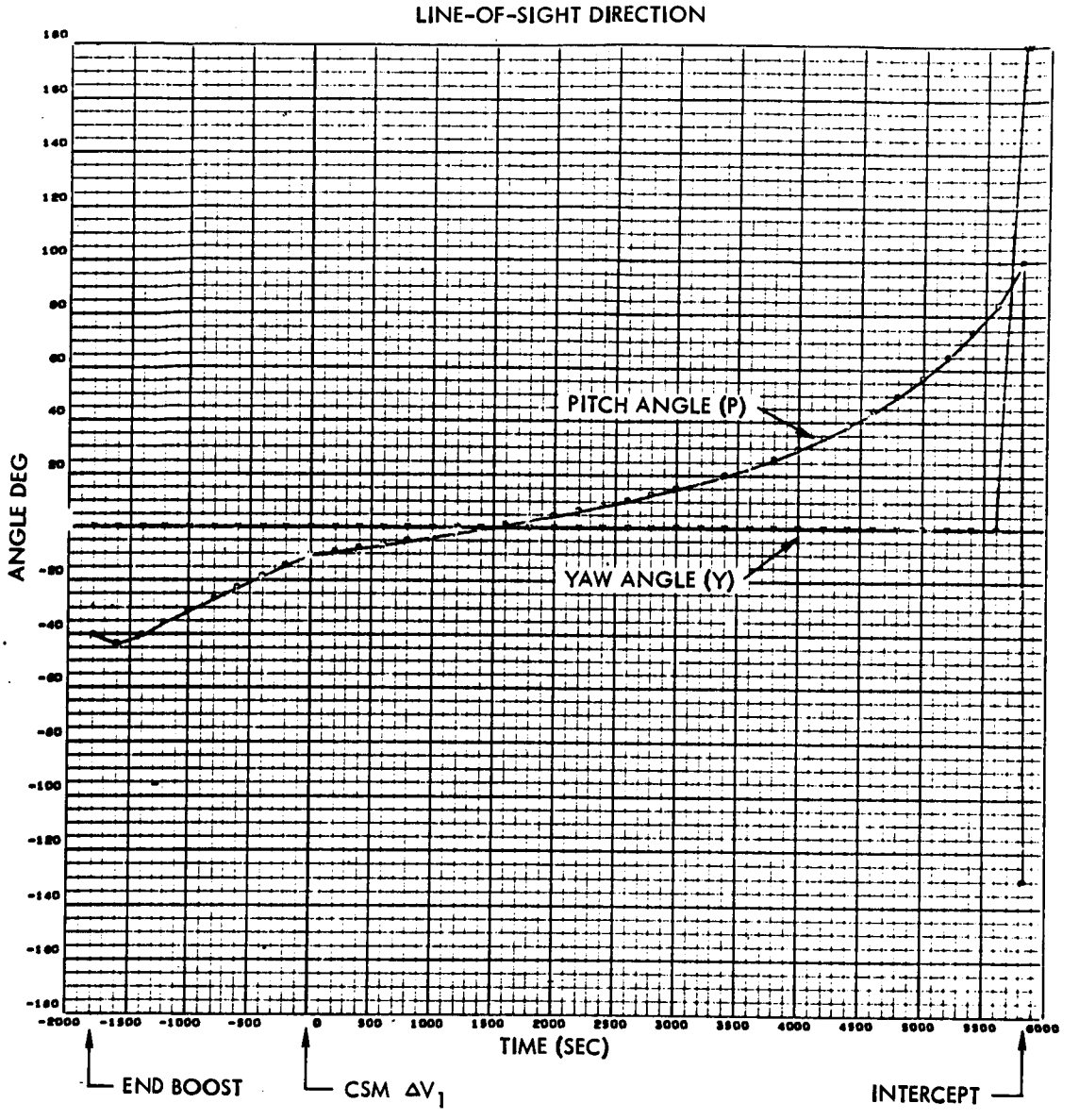

Figure 1-115. - LOS Direction: LESS Orbit = 20 by 190 Nautical Miles (Due to Pitch Error of -4°), Inclination = 0°

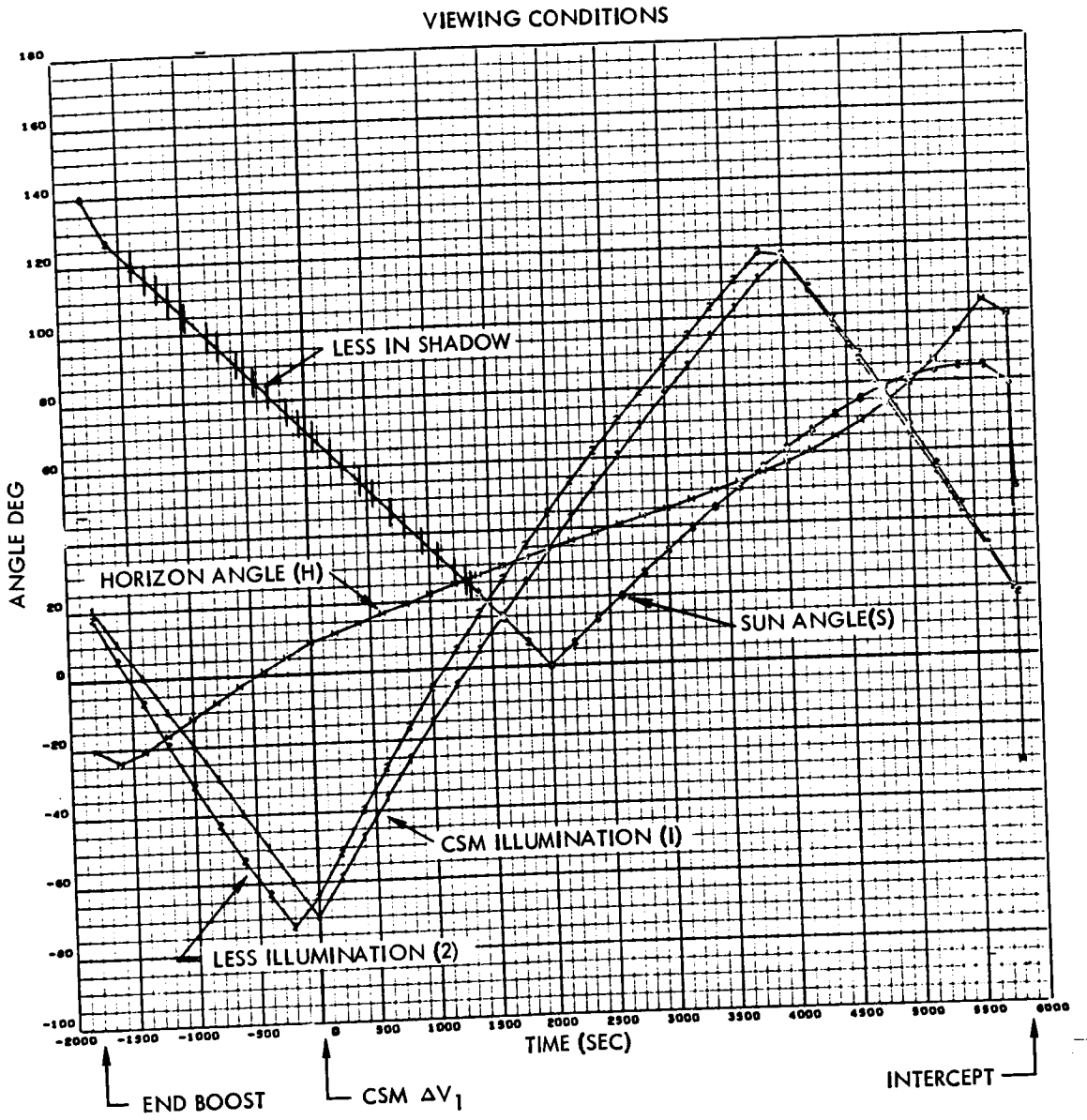

Figure 1-116. Viewing Conditions: LESS Orbit = 20 by 190 Nautical Miles (Due to Pitch Error of -4°), Inclination = 0°

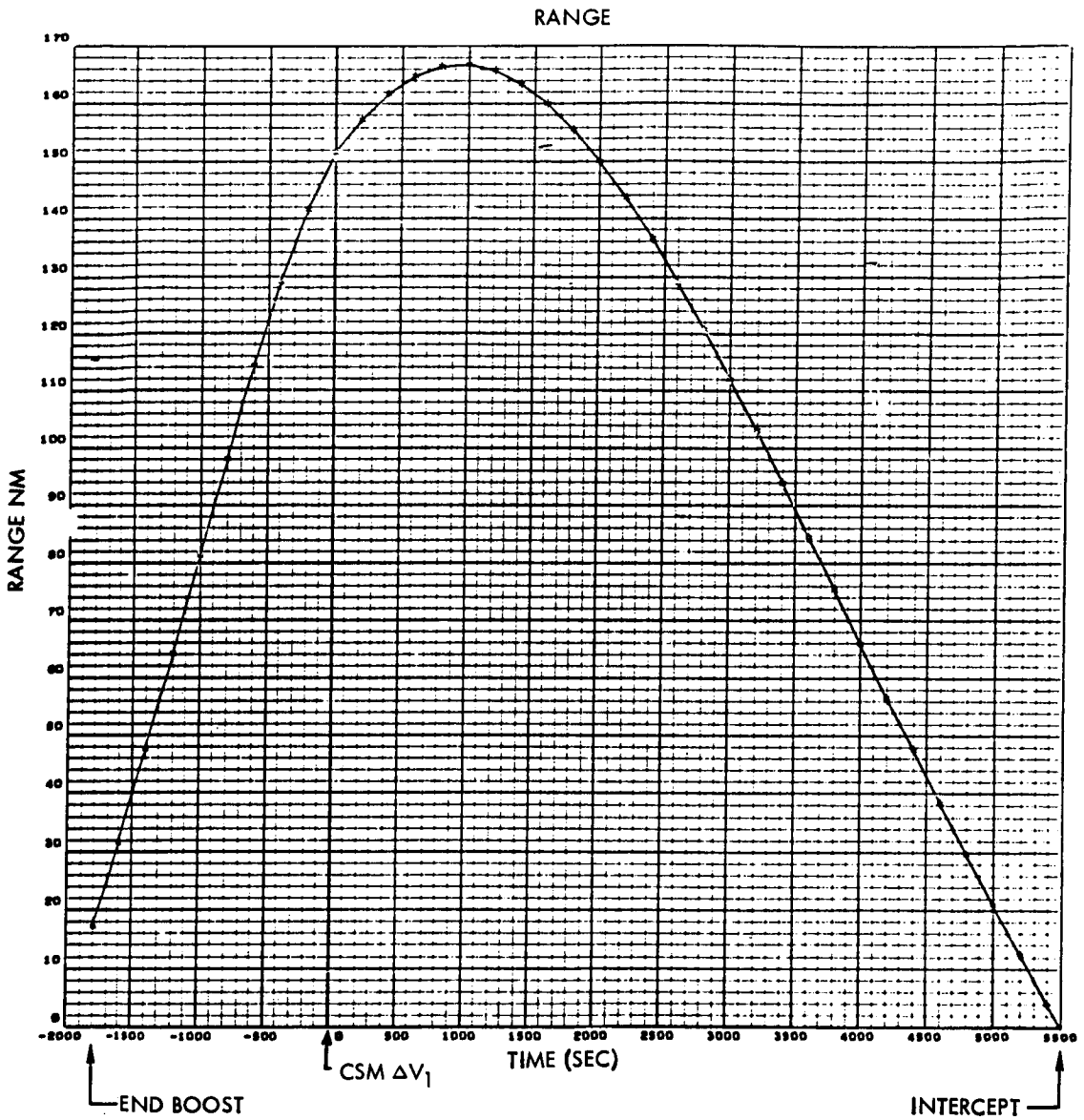

Figure 1-117. - LOS Range: LESS Orbit = 20 by 190 Nautical Miles (Due to Pitch Error of -4°), Inclination = 2°

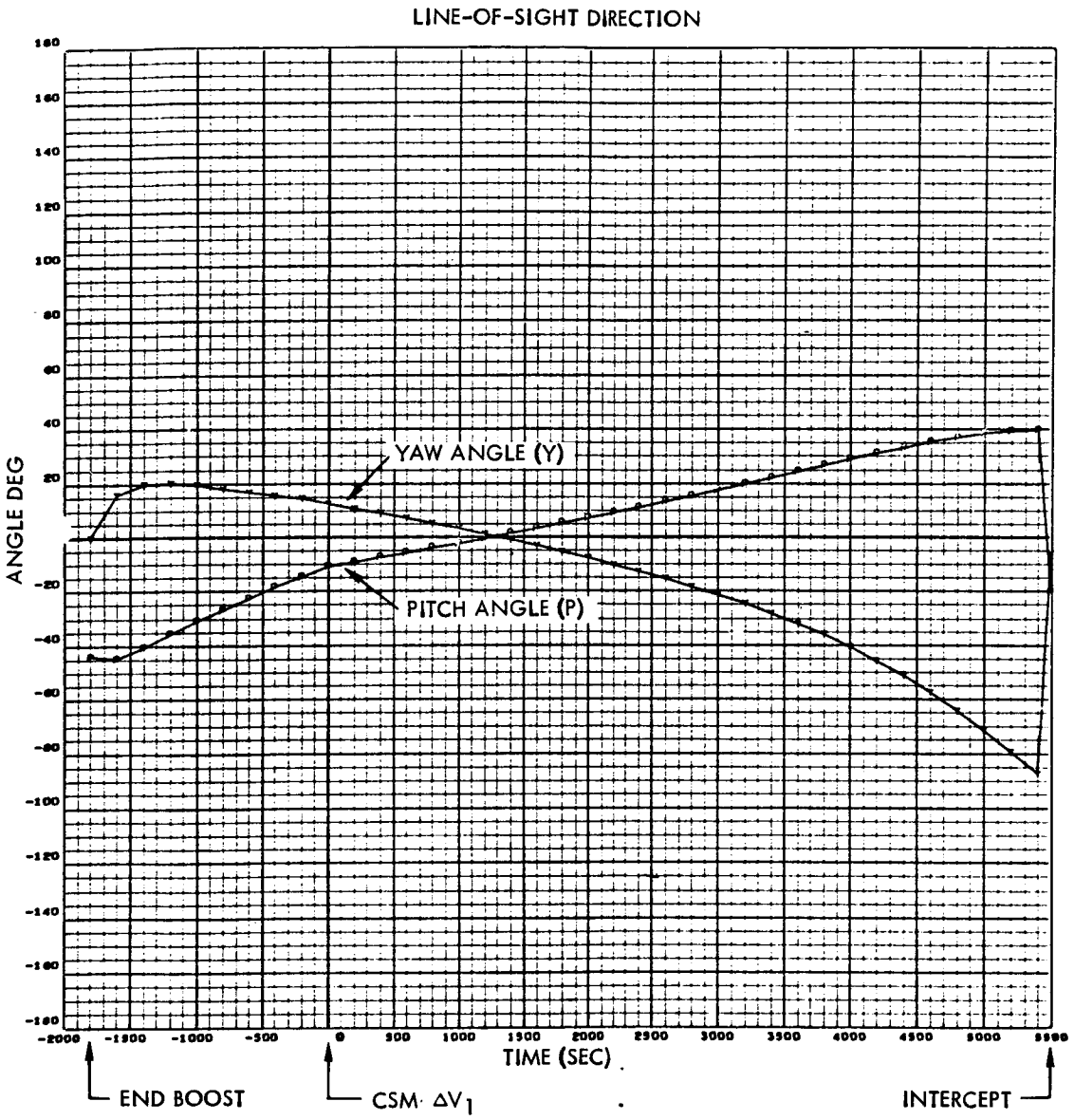

Figure 1-118. LOS Direction: LESS Orbit = 20 by 190 Nautical Miles (Due to Pitch Error of -4°), Inclination = 2°

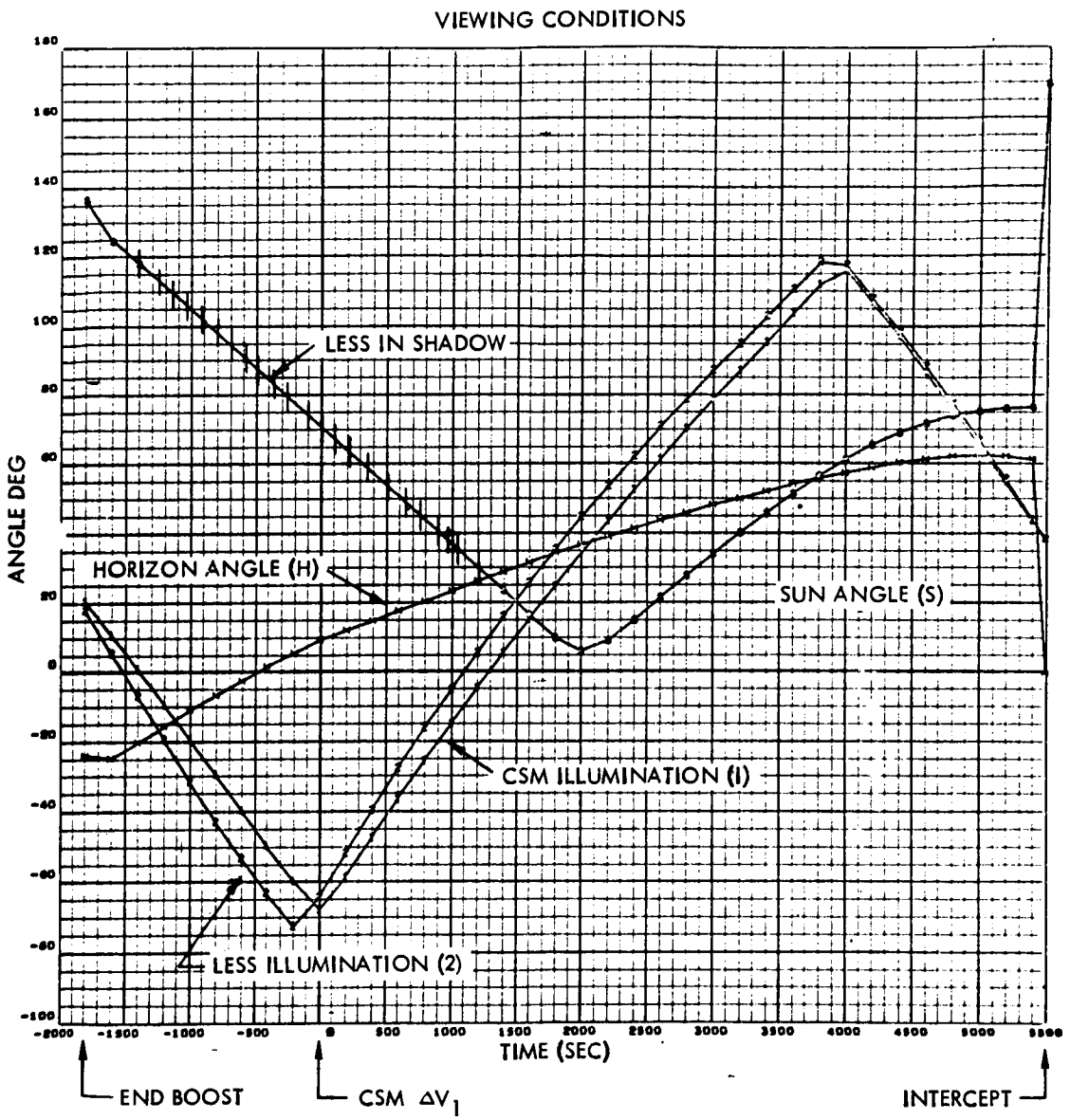

Figure 1-119. - Viewing Conditions: LESS Orbit = 20 by 190 Nautical Miles (Due to Pitch error of -4°), Inclination = 2°

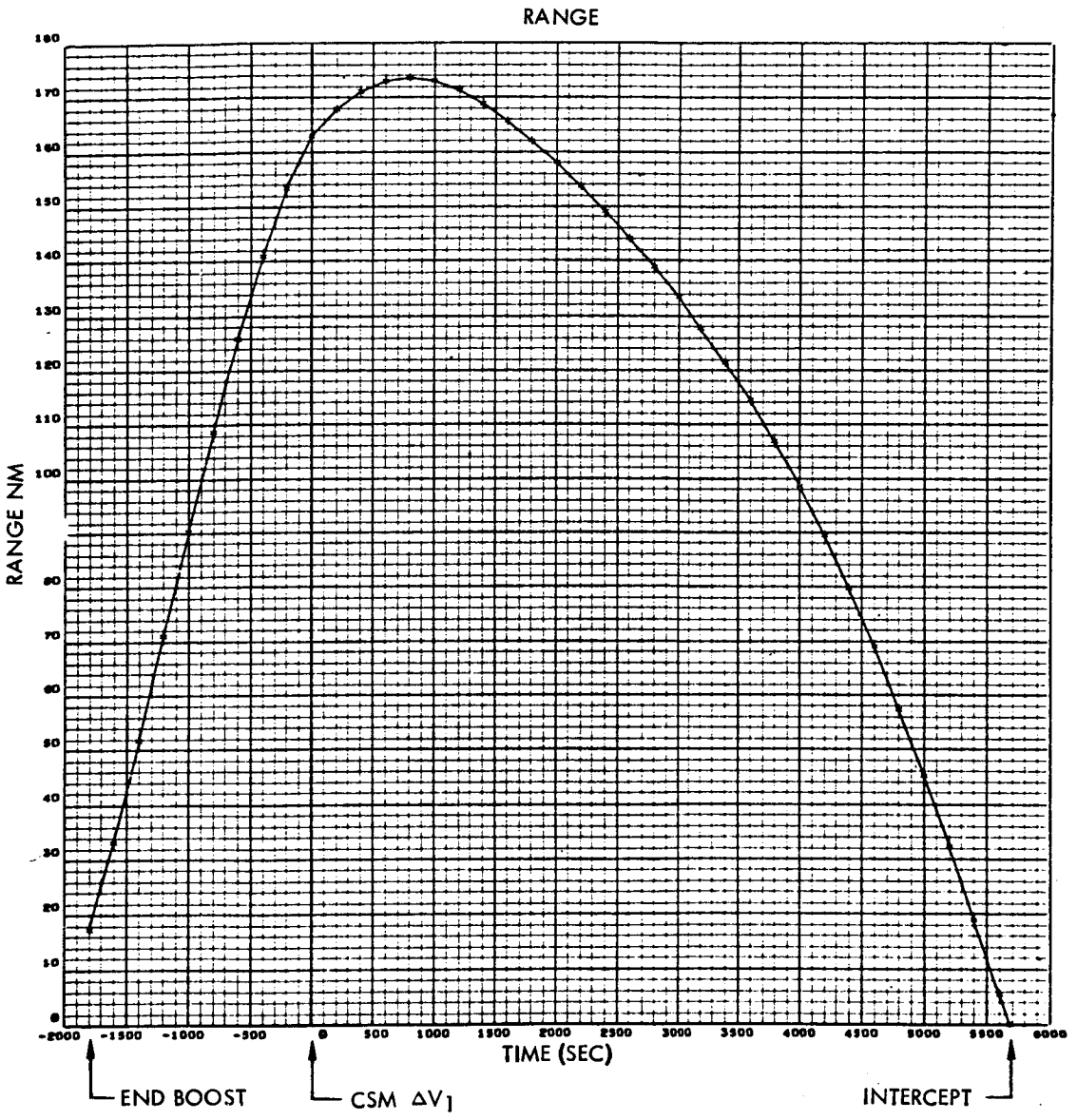

Figure 1-120. - LOS Range: LESS Orbit = 20 by 190 Nautical Miles (Due to Pitch Error of -4°), Inclination = 4°

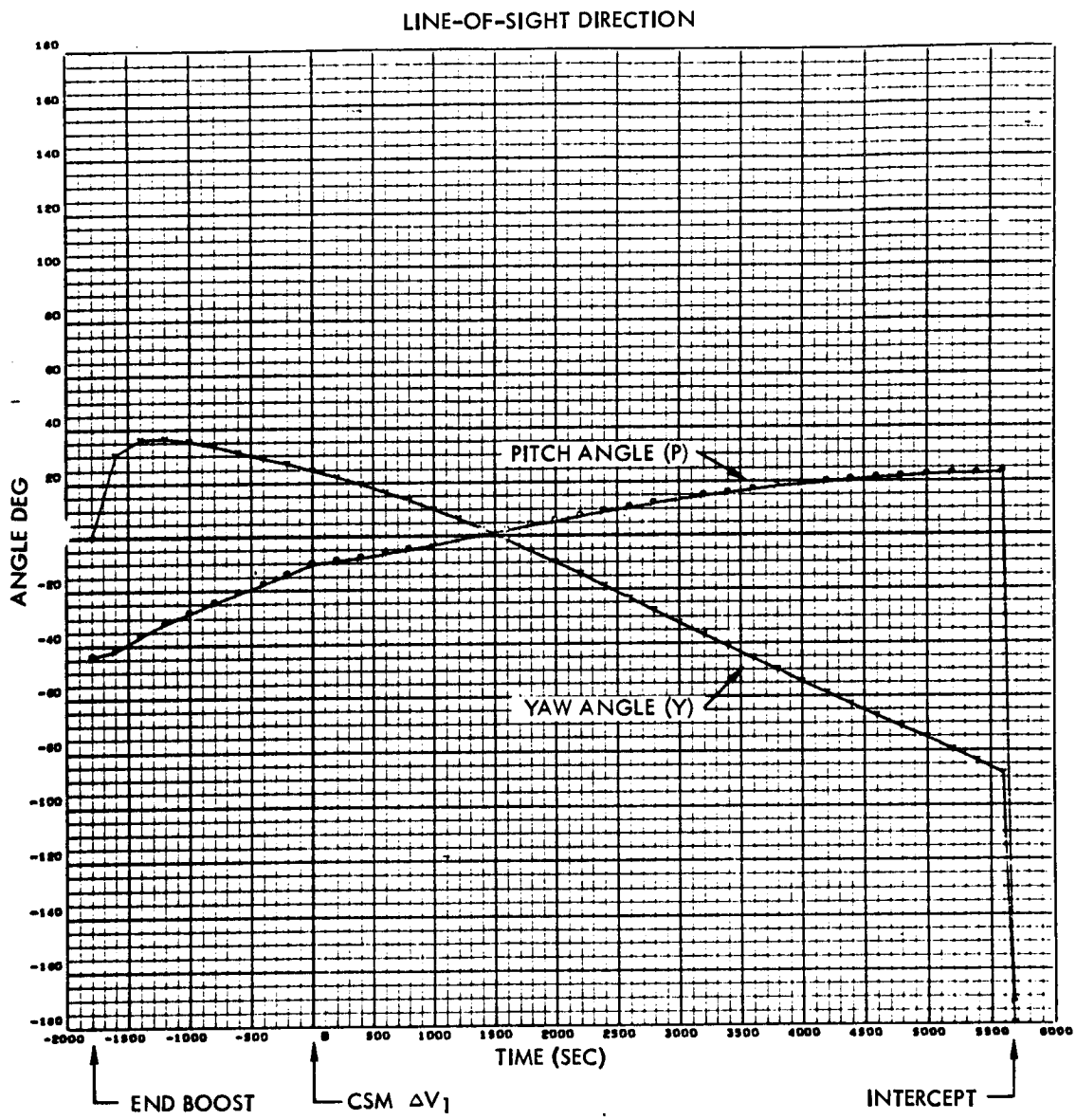

Figure 1-121. - LOS Direction: LESS Orbit = 20 by 190 Nautical Miles (Due to Pitch Error of -4°), Inclination = 4°

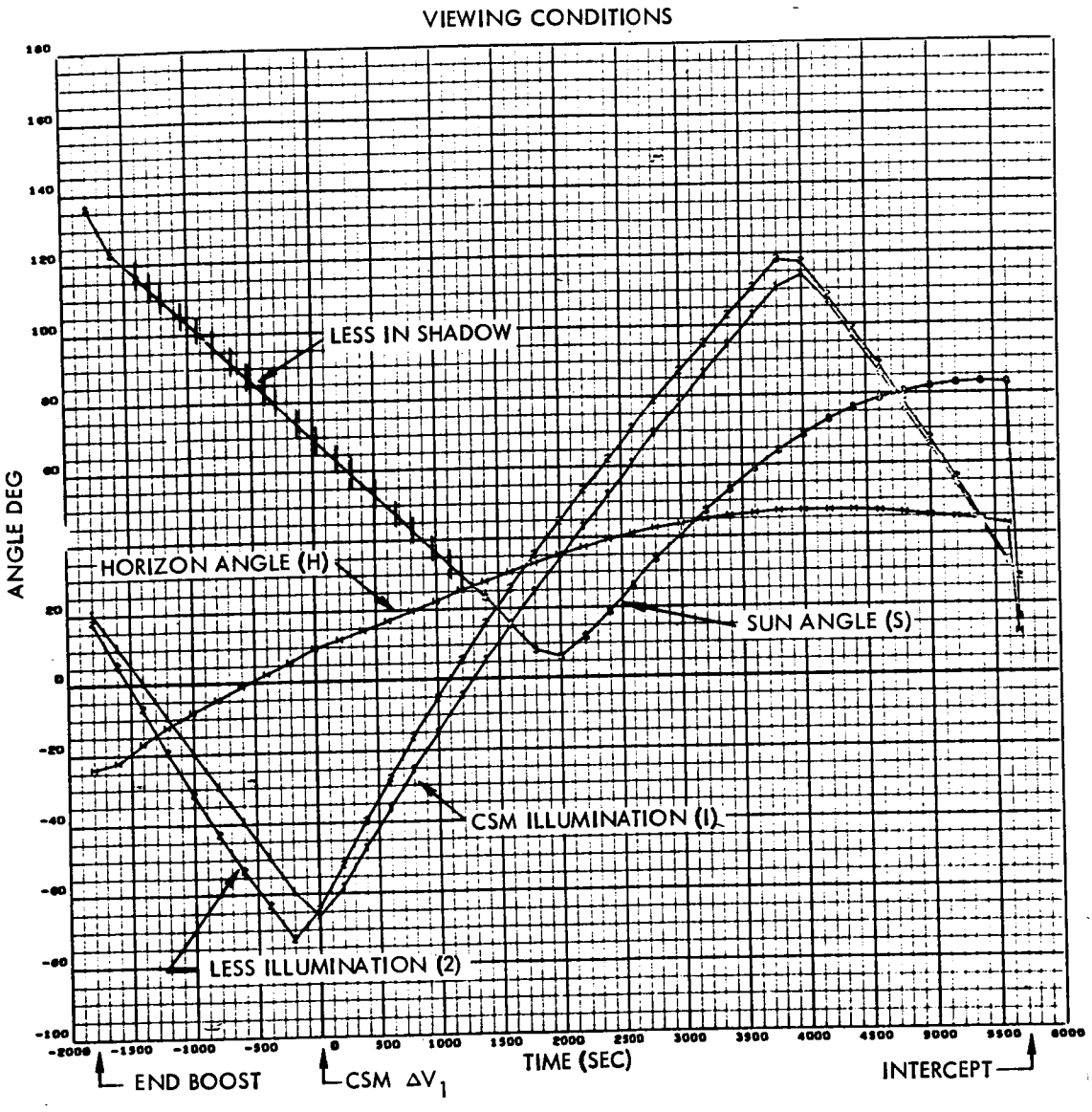

Figure 1-122. - Viewing Conditions: LESS Orbit = 20 by 190 Nautical Miles (Due to Pitch Error of -4°), Inclination = 4°

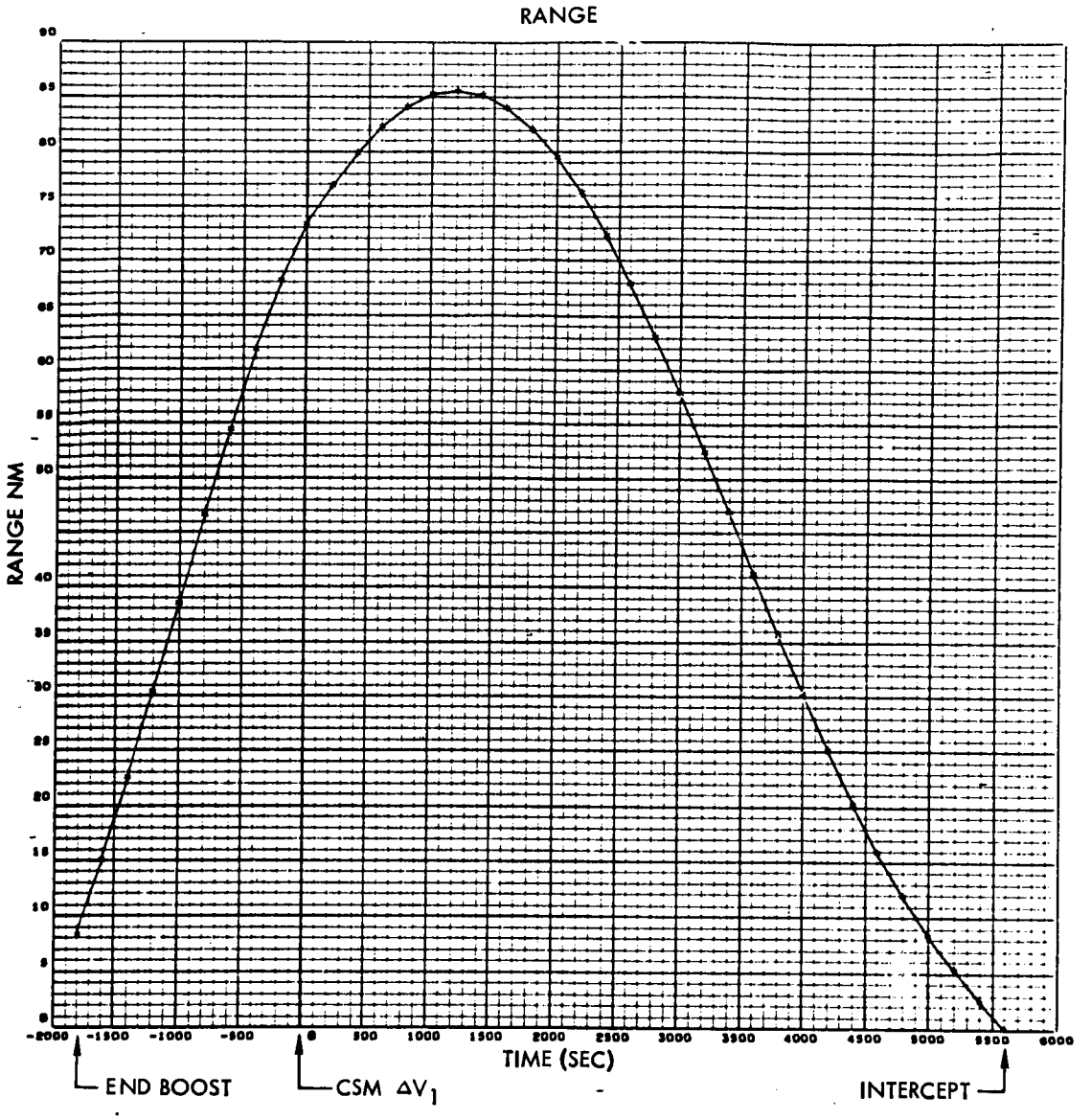

Figure 1-123. - LOS Range: LESS Orbit = 40 by 125 Nautical Miles (Due to Pitch Error of -2°), Inclination = 0°

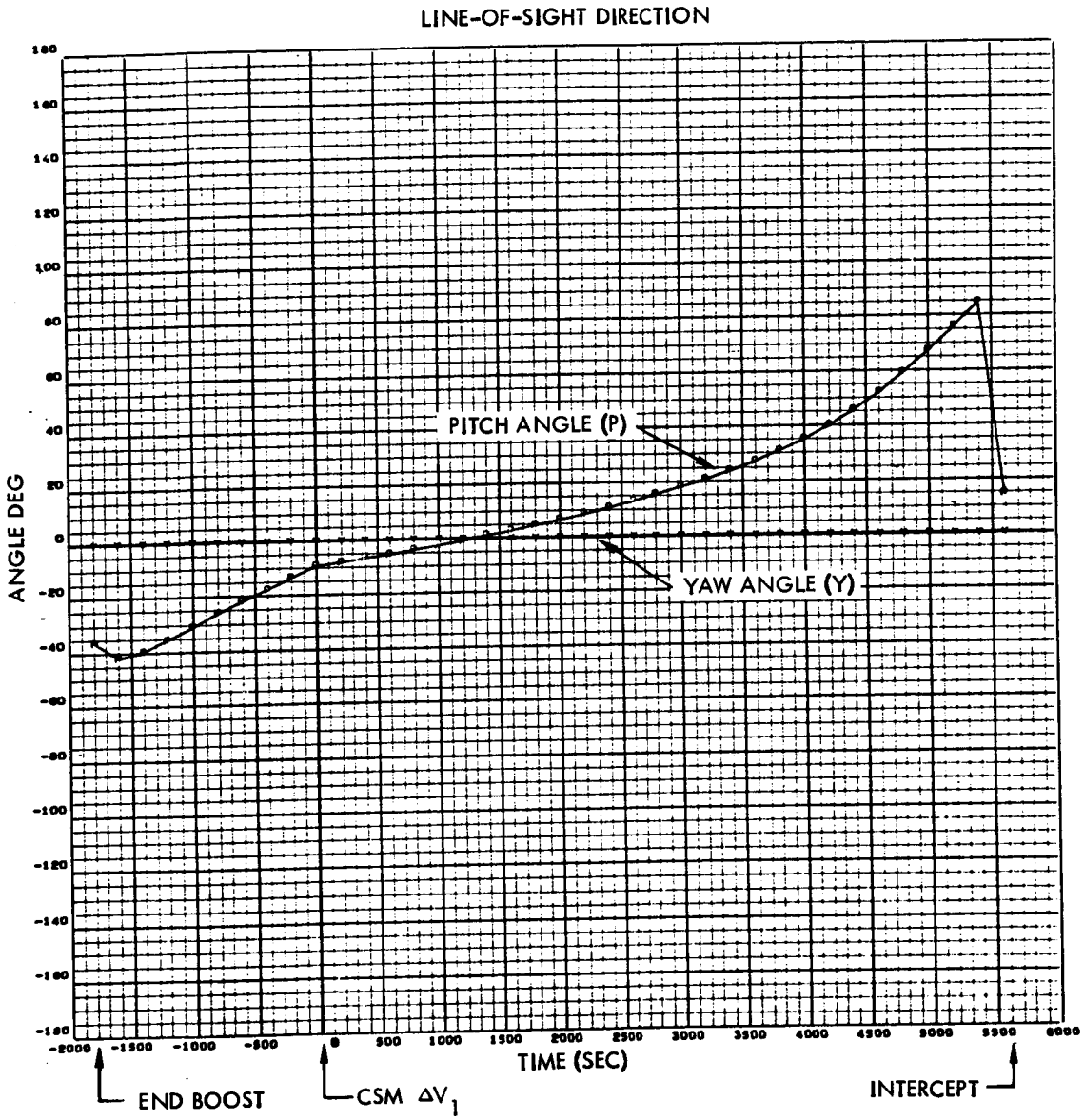

Figure 1-124. - LOS Direction: LESS Orbit = 40 by 125 Nautical Miles (Due to Pitch Error of -2°), Inclination = 0°

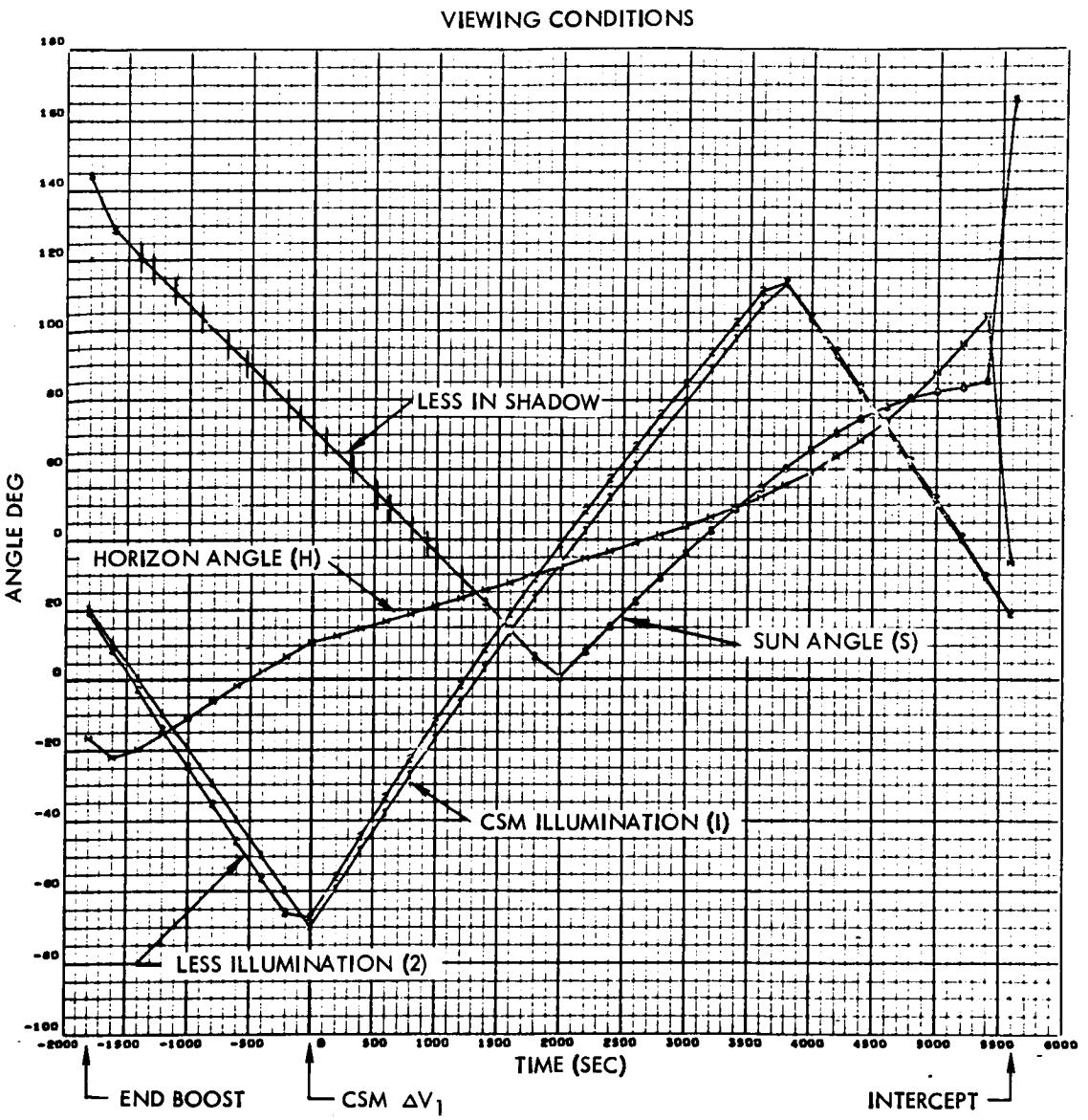

Figure 1-125. - Viewing Conditions: LESS Orbit = 40 by 125 Nautical Miles (Due to Pitch Error of -2°), Inclination = 0°

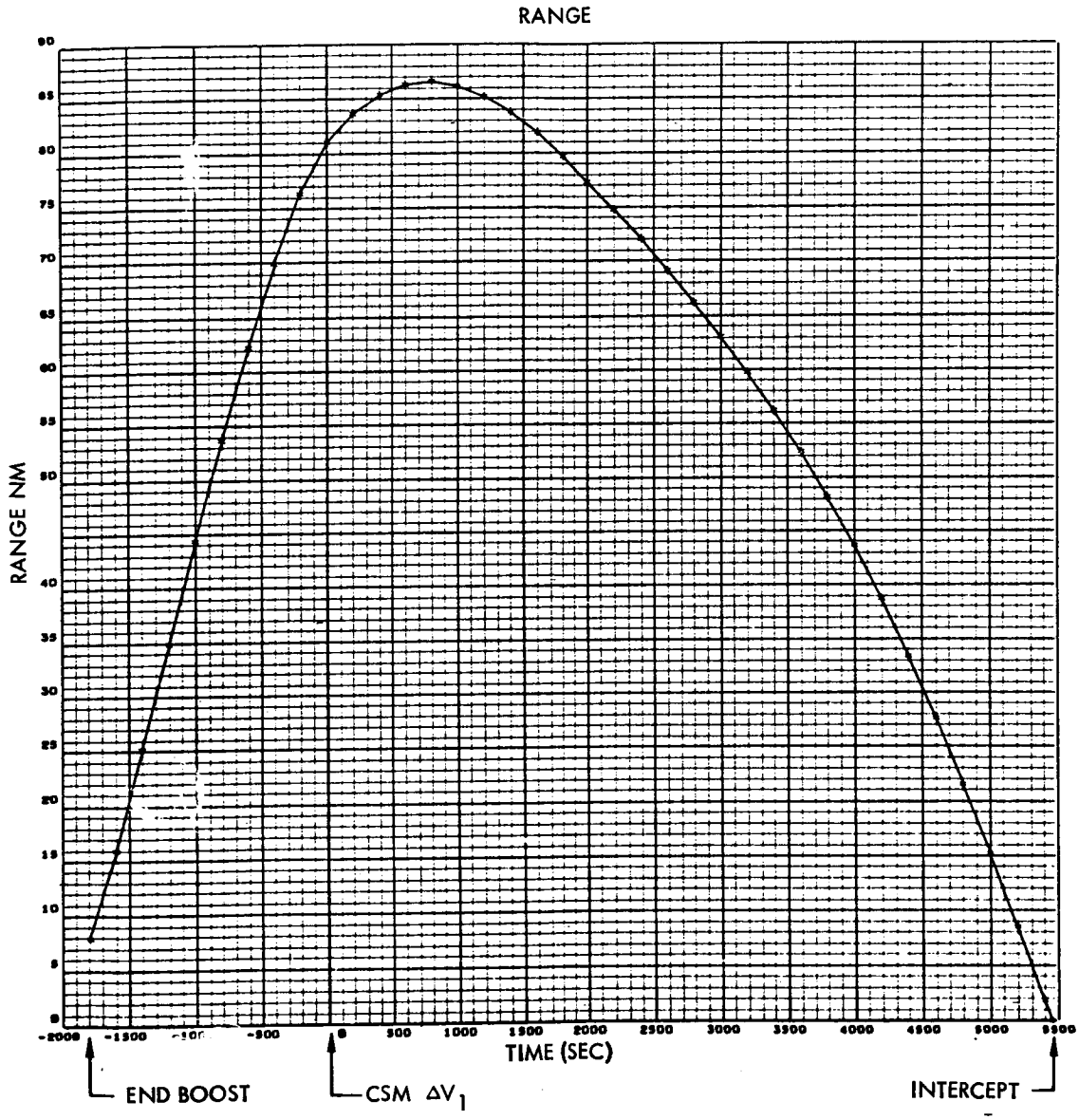

Figure 1-126. - LOS Range: LESS Orbit = 40 by 125 Nautical Miles (Due to Pitch Error of -2°), Inclination = 2°

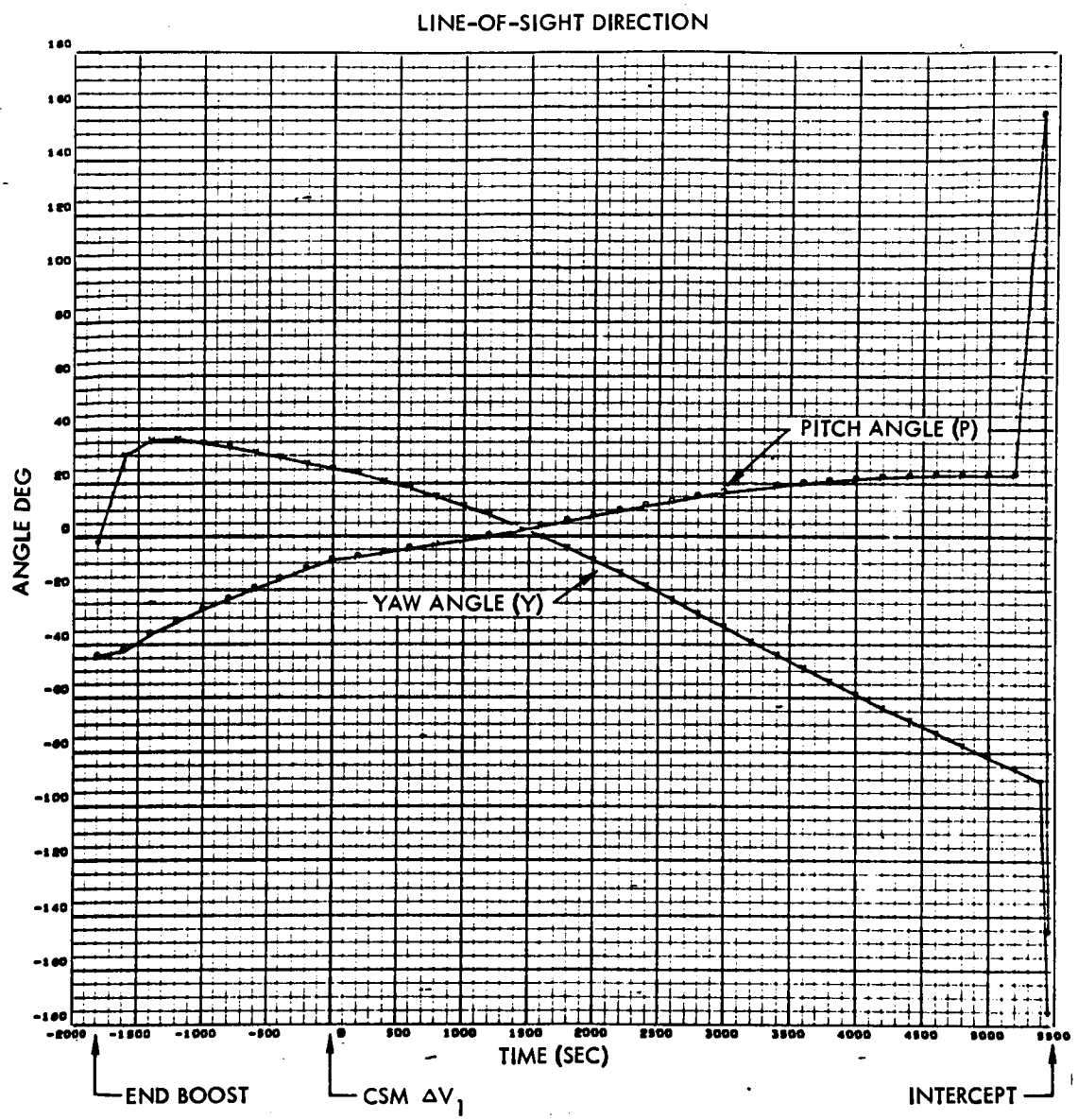

Figure 1-127. - LOS Direction: LESS Orbit = 40 by 125 Nautical Miles (Due to Pitch Error of -2°), Inclination = 2°

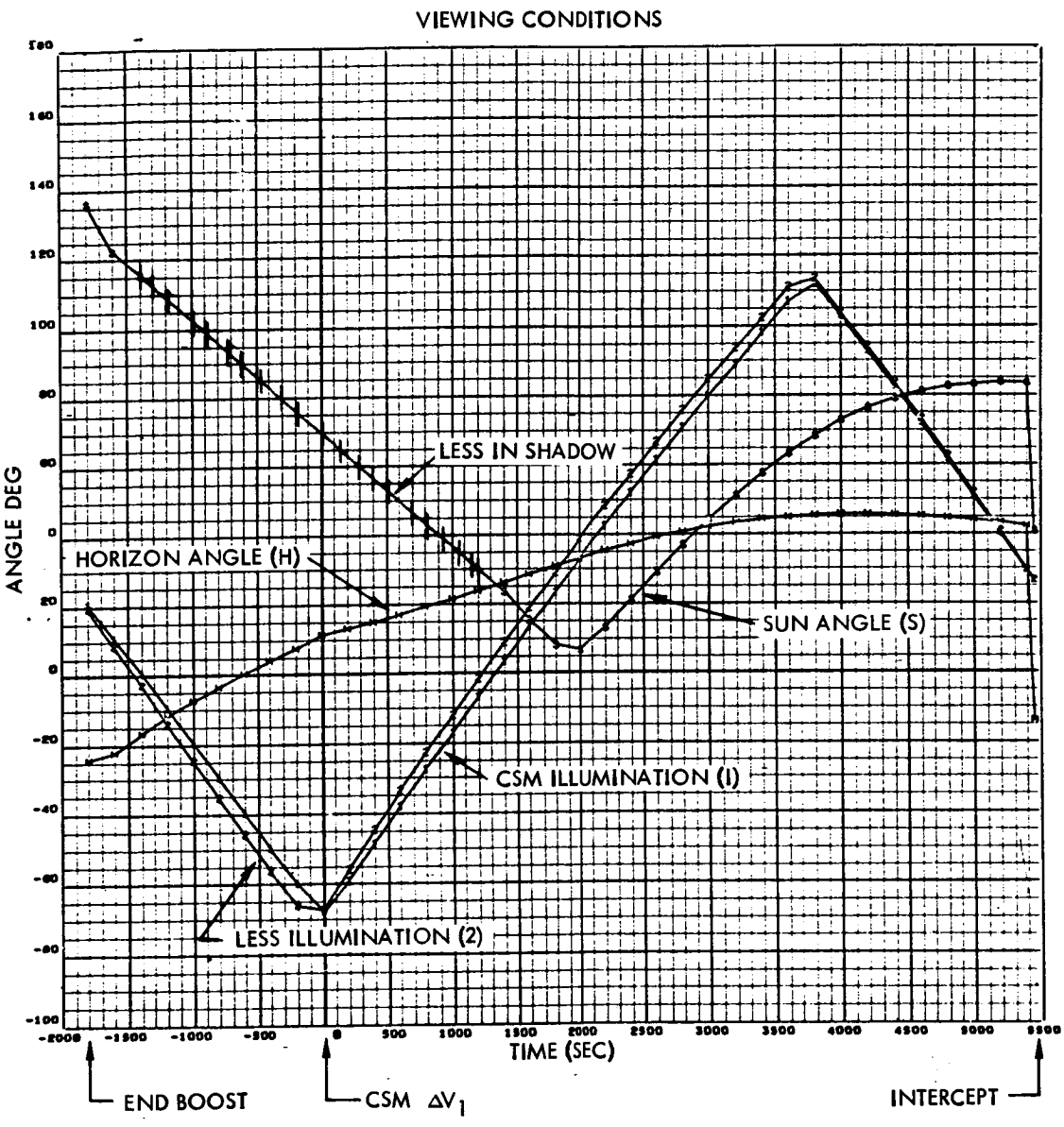

Figure 1-128. - Viewing Conditions: LESS Orbit = 40 by 125 Nautical Miles (Due to Pitch Error of -2°), Inclination = 4°

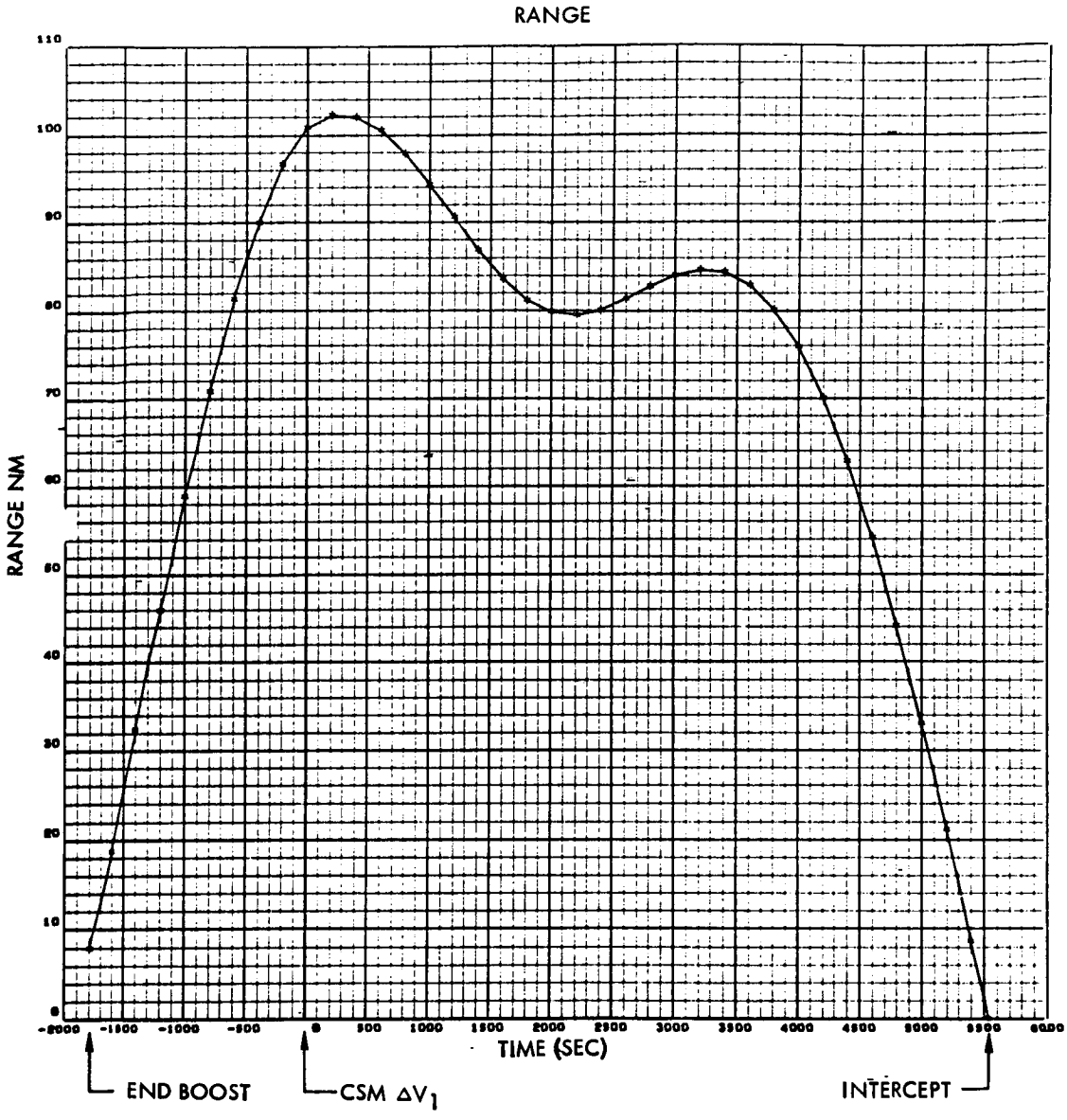

Figure 1-129. - LOS Range: LESS Orbit = 40 by 125 Nautical Miles (Due to Pitch Error of -2°), Inclination = 4°

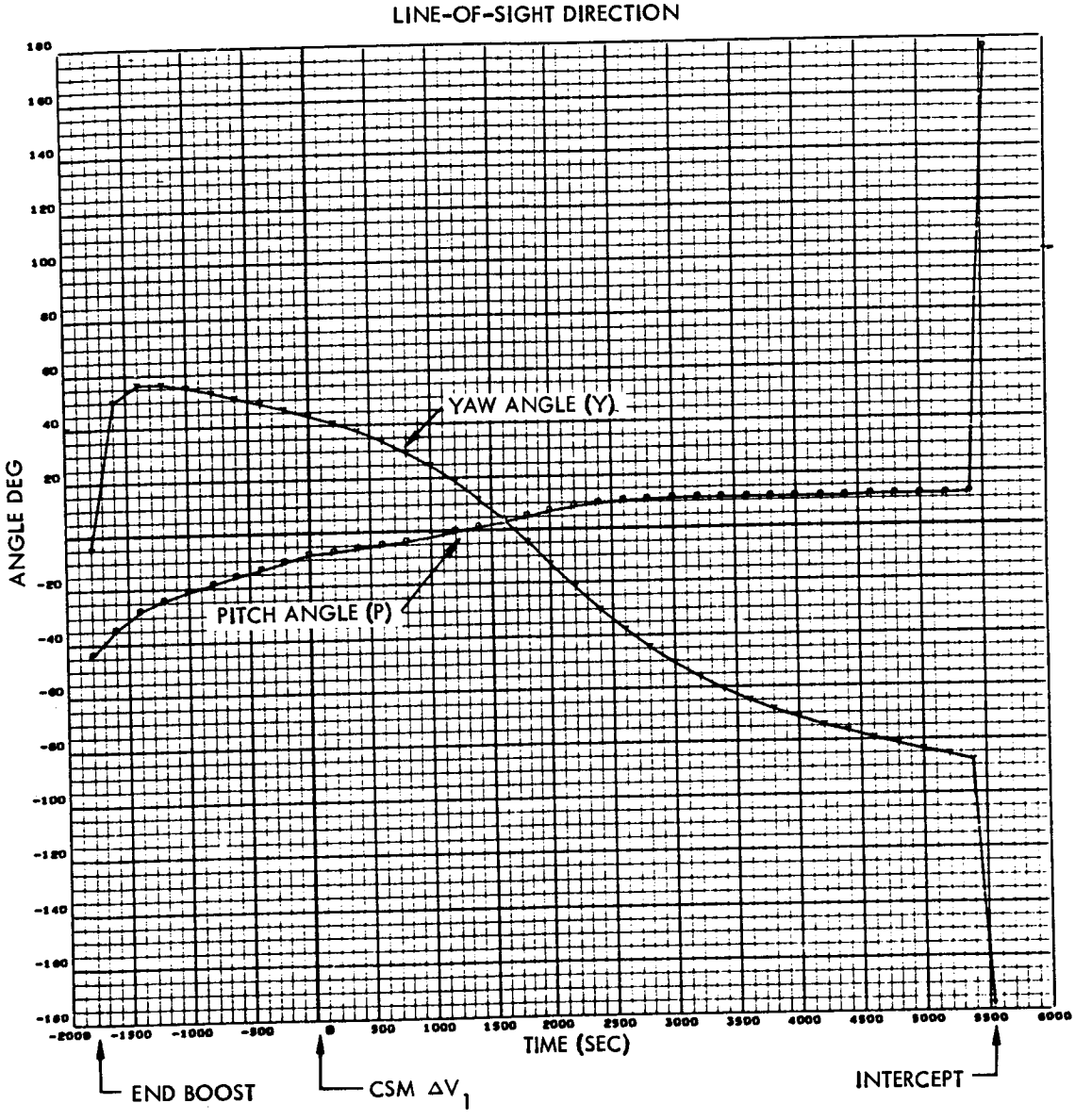

Figure 1-130. - LOS Direction: LESS Orbit = 40 by 125 Nautical Miles (Due to Pitch Error of -2°), Inclination = 4°

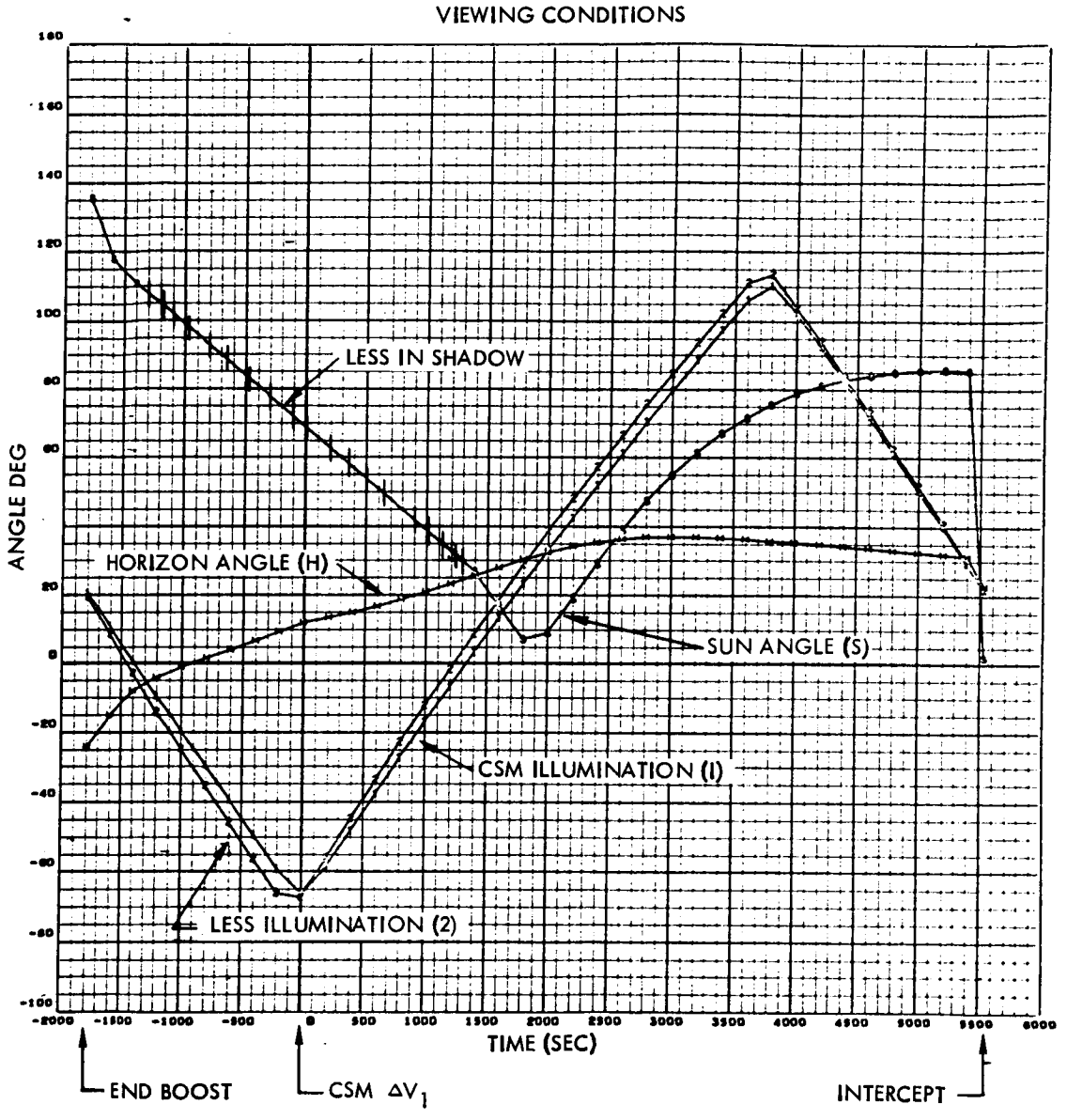

Figure 1-131. - Viewing Conditions: LESS Orbit = 40 by 125 Nautical Miles (Due to Pitch Error of -2°), Inclination = 4°

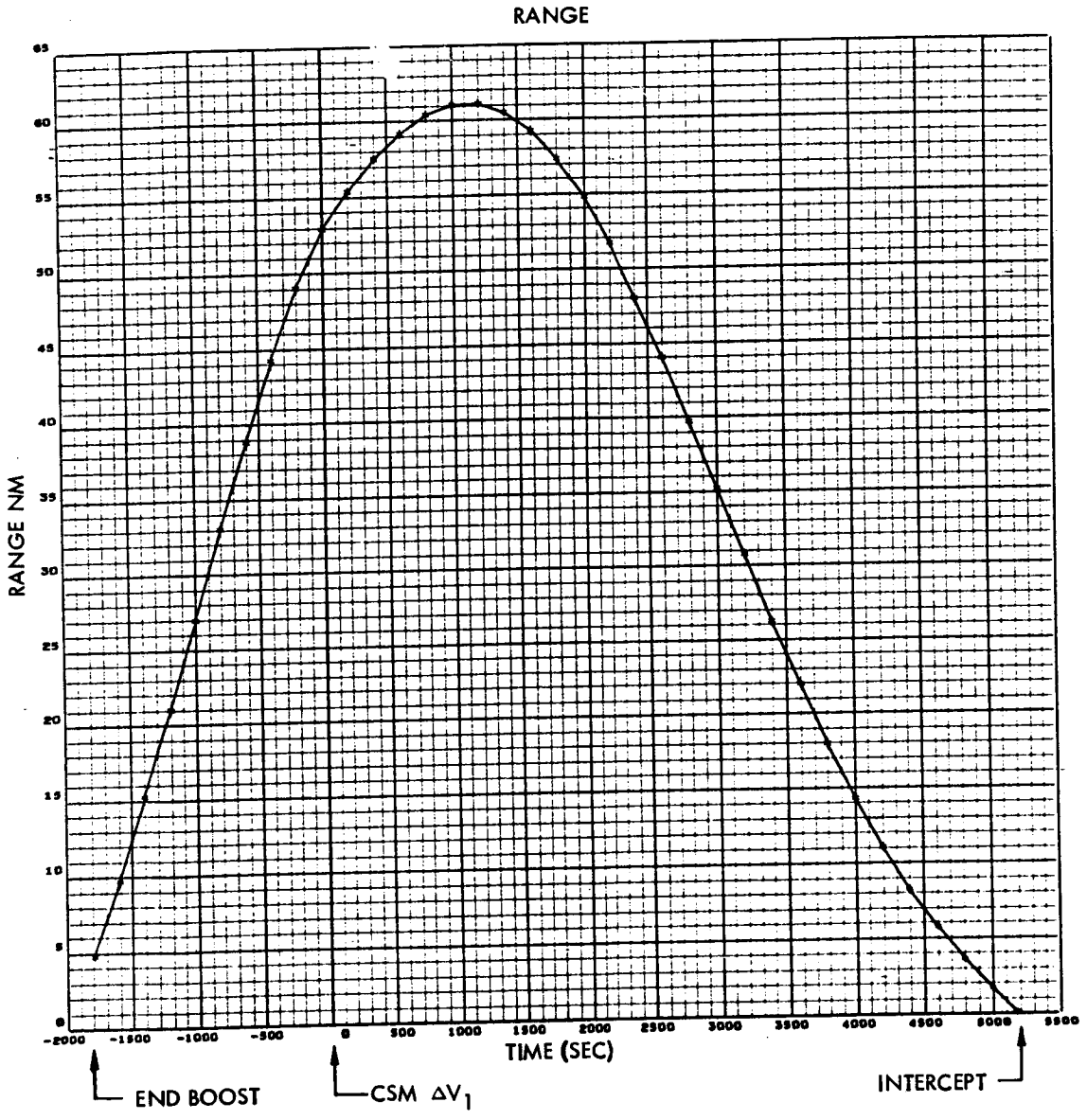

Figure 1-132. - LOS Range: LESS Orbit = 75 by 10 Nautical Miles (Due to Pitch Error of +1.6°), Inclination = 0°

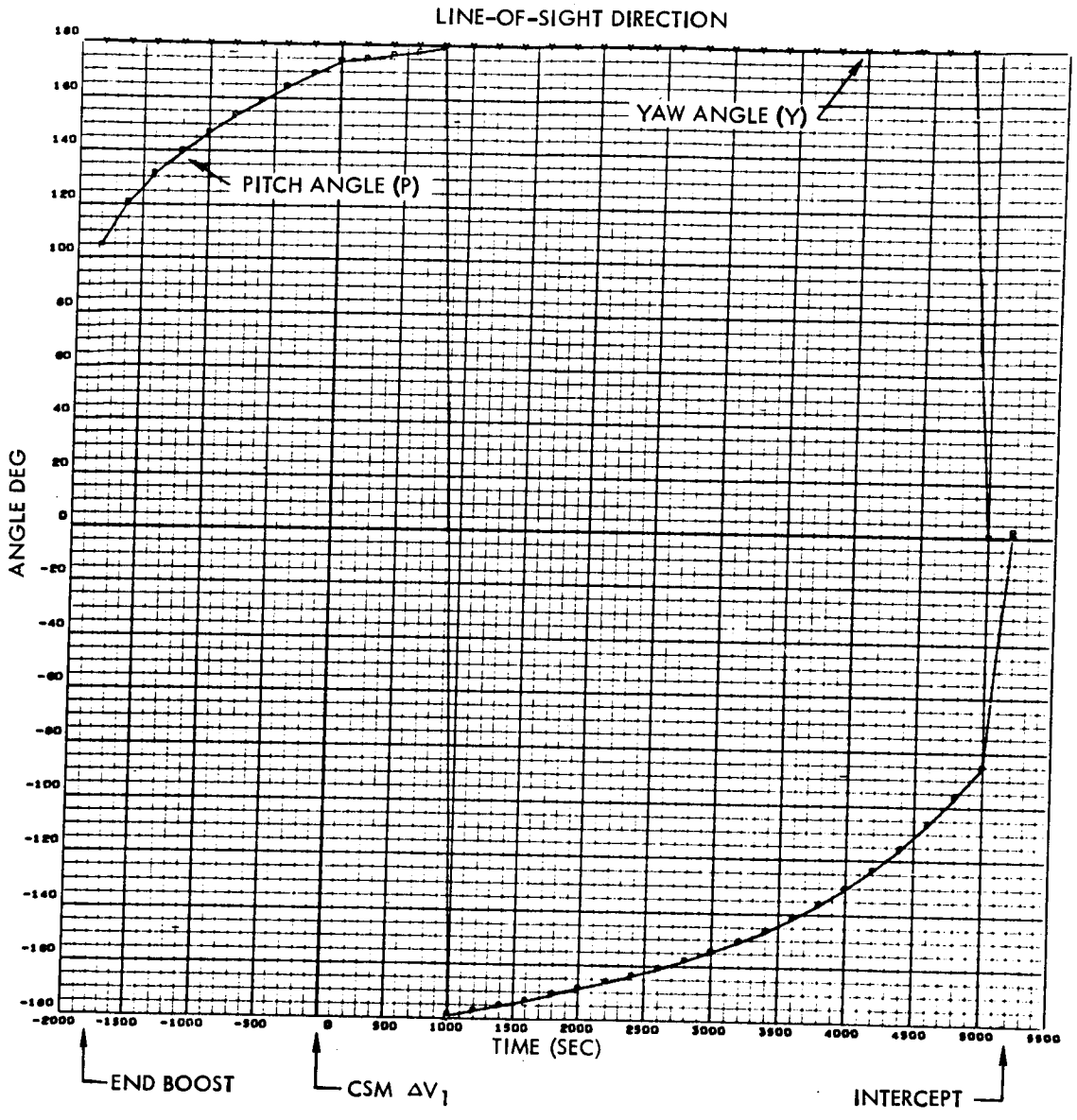

Figure 1-133. - LOS Direction: LESS Orbit = 75 by 10 Nautical Miles (Due to Pitch Error of +1.6°), Inclination = 0°

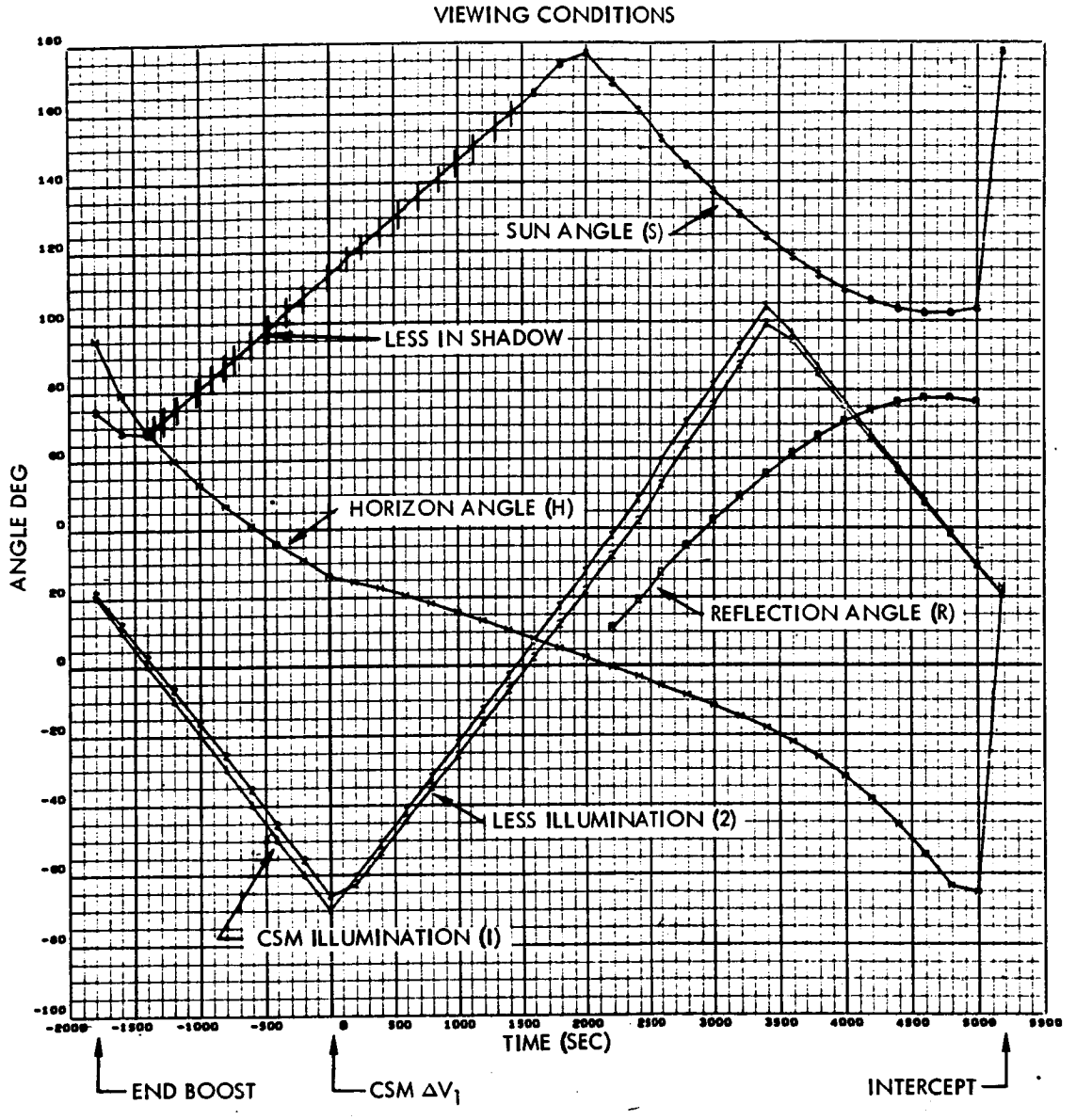

Figure 1-134. - Viewing Conditions: LESS Orbit = 75 by 10 Nautical Miles (Due to Pitch Error of +1.6°), Inclination = 0°

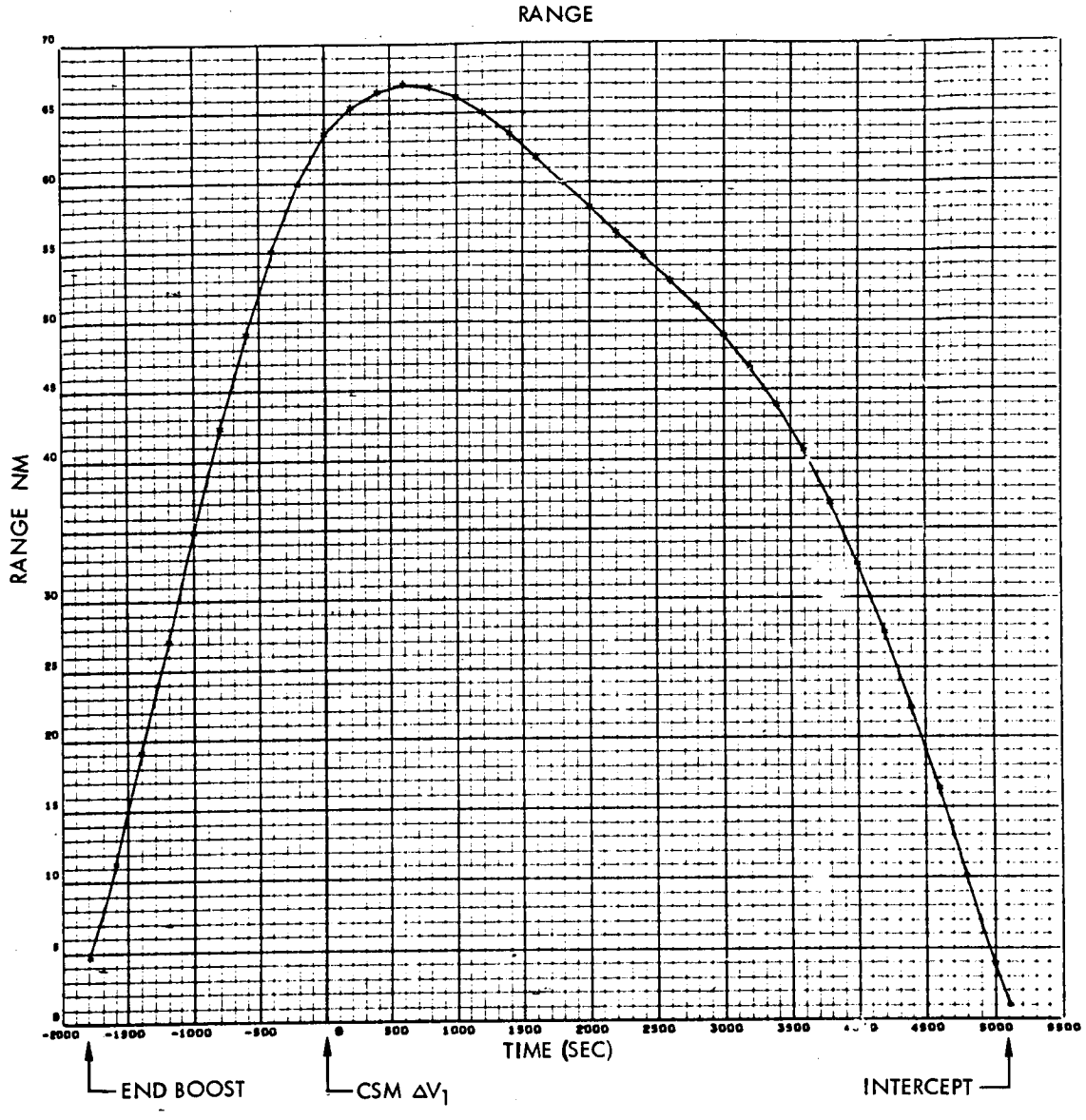

Figure 1-135. LOS Range: LESS Orbit = 75 by 10 Nautical Miles (Due to Pitch Error of +1.6°), Inclination = 2°

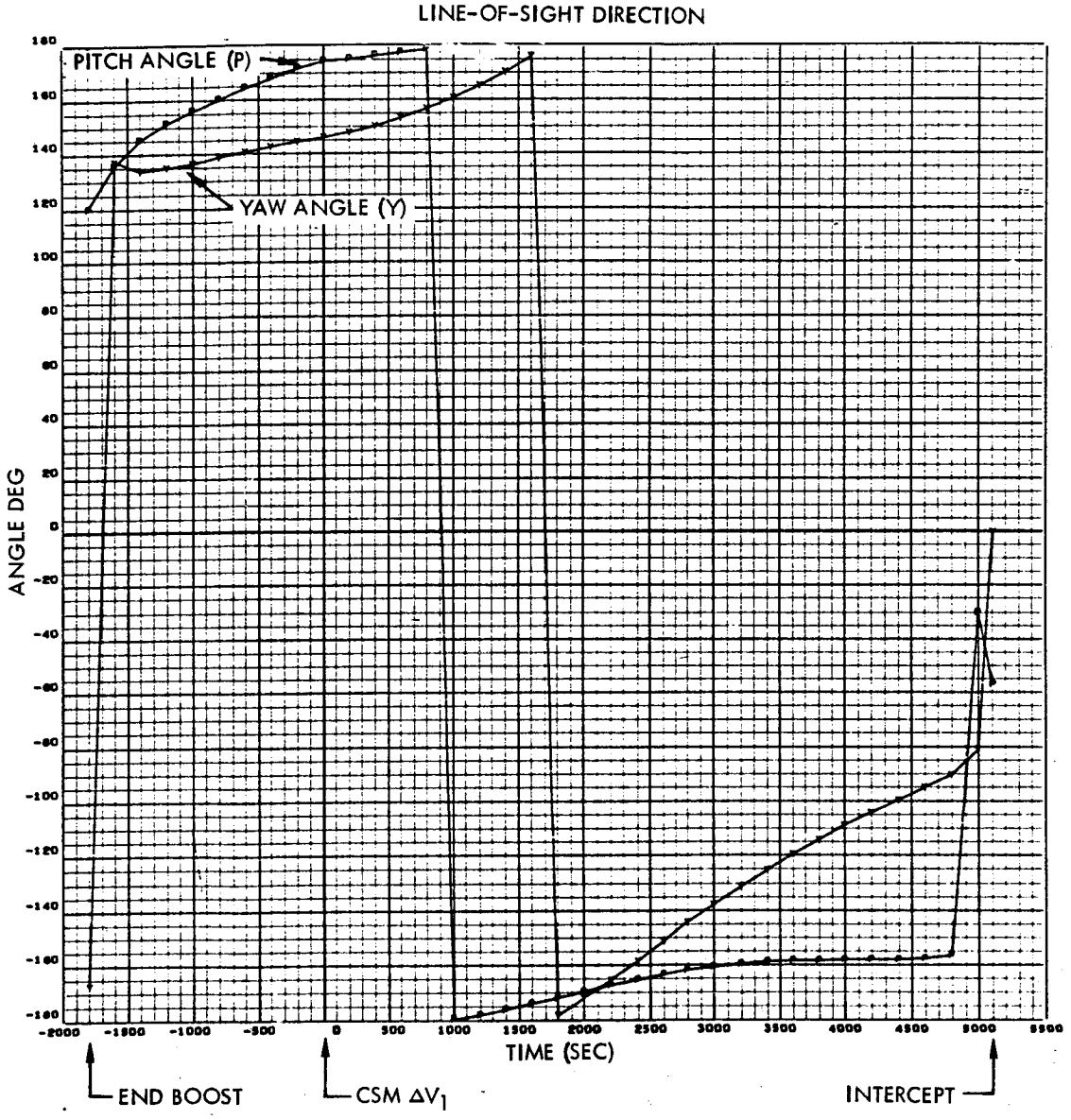

Figure 1-136. LOS Direction: LESS Orbit = 75 by 10 Nautical Miles (Due to Pitch Error of+1.6°), Inclination = 2°

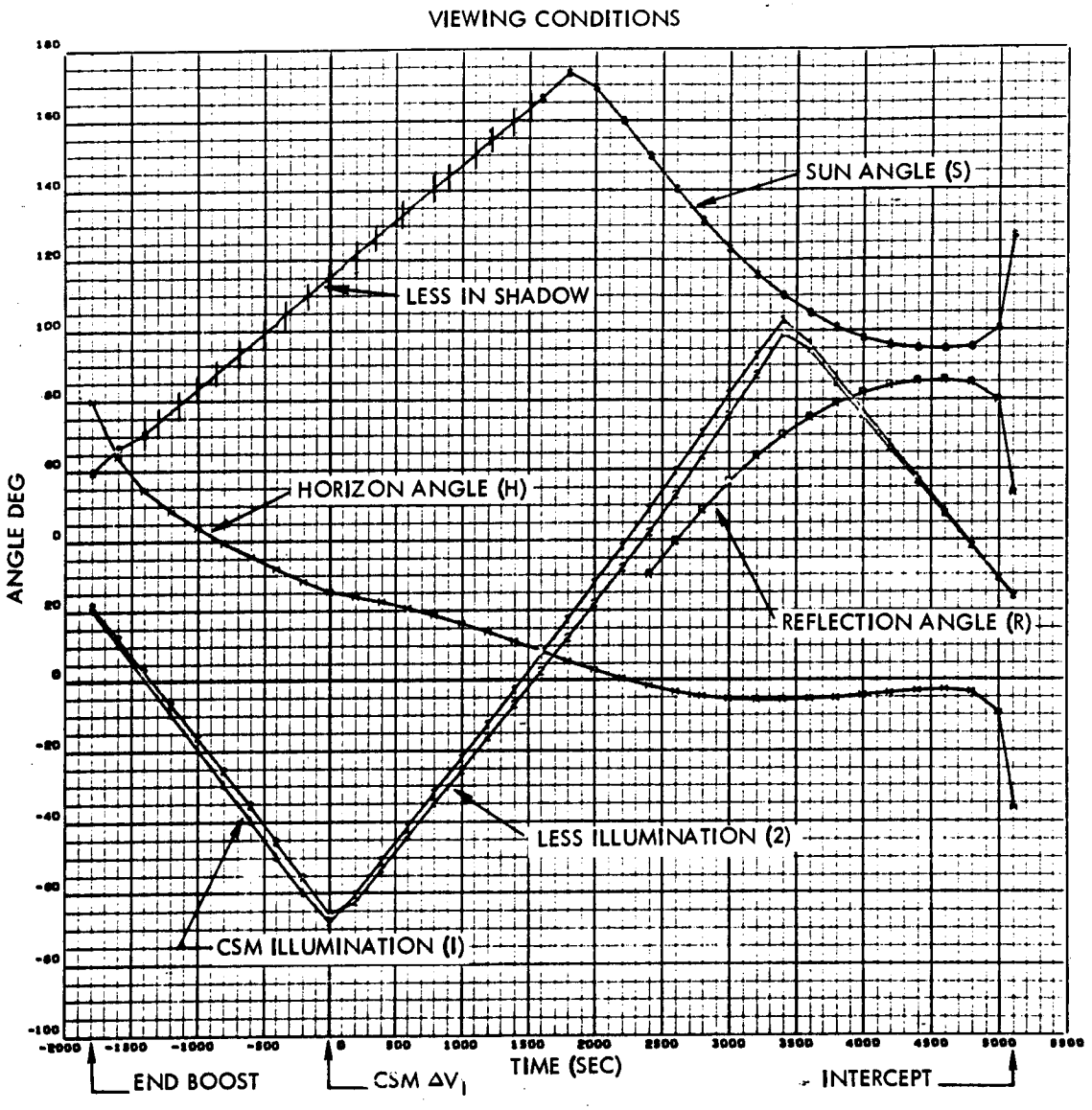

Figure 1-137. - Viewing Conditions: LESS Orbit = 75 by 10 Nautical Miles (Due to Pitch Error of +1.6°), Inclination = 2°

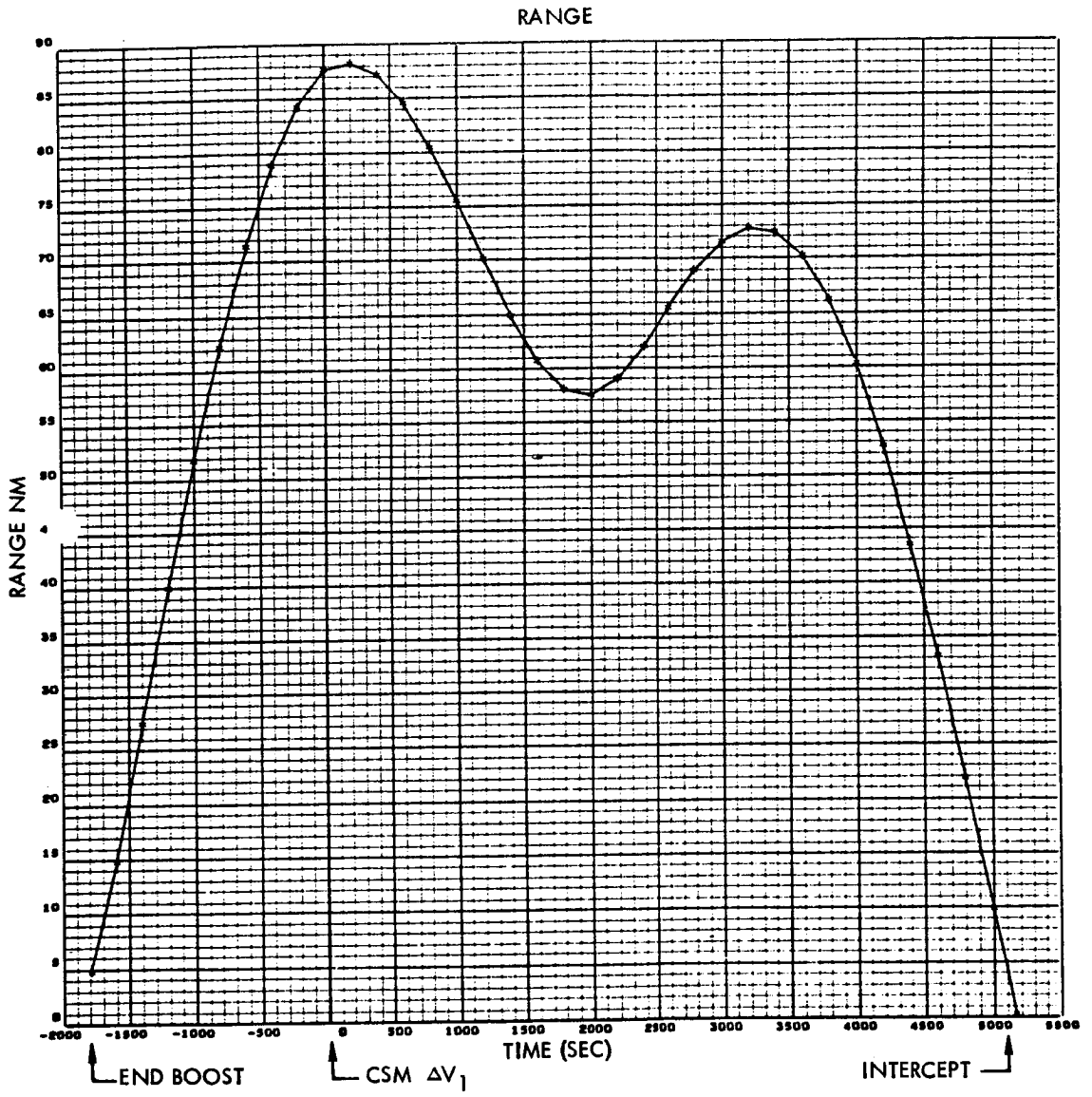

Figure 1-138. - LOS Range: LESS Orbit = 75 by 10 Nautical Miles (Due to Pitch Error of +1.6°), Inclination = 4°

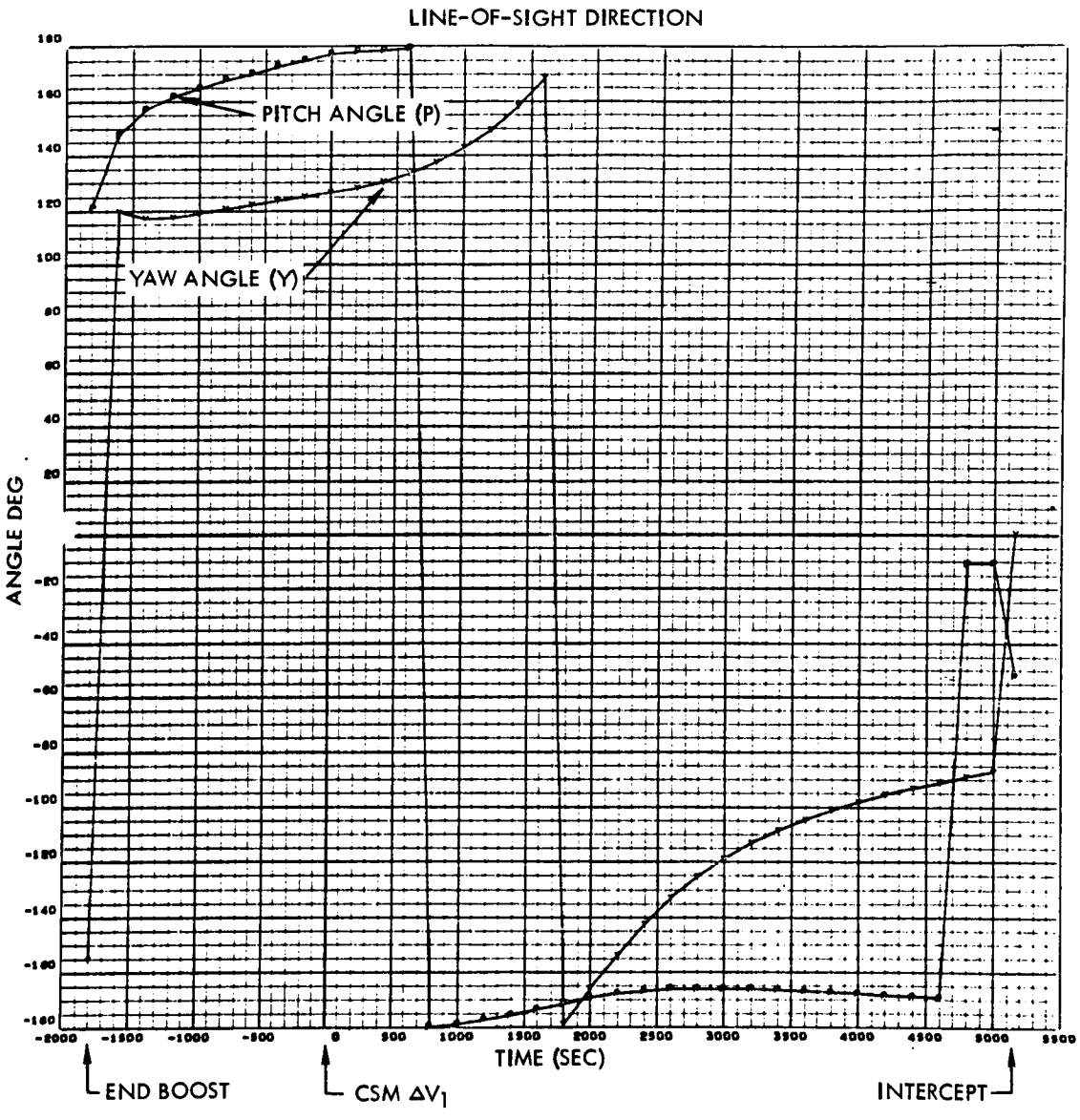

Figure 1-139. - LOS Direction: LESS Orbit = 75 by 10 Nautical Miles (Due to Pitch Error of +1.6°), Inclination = 4°

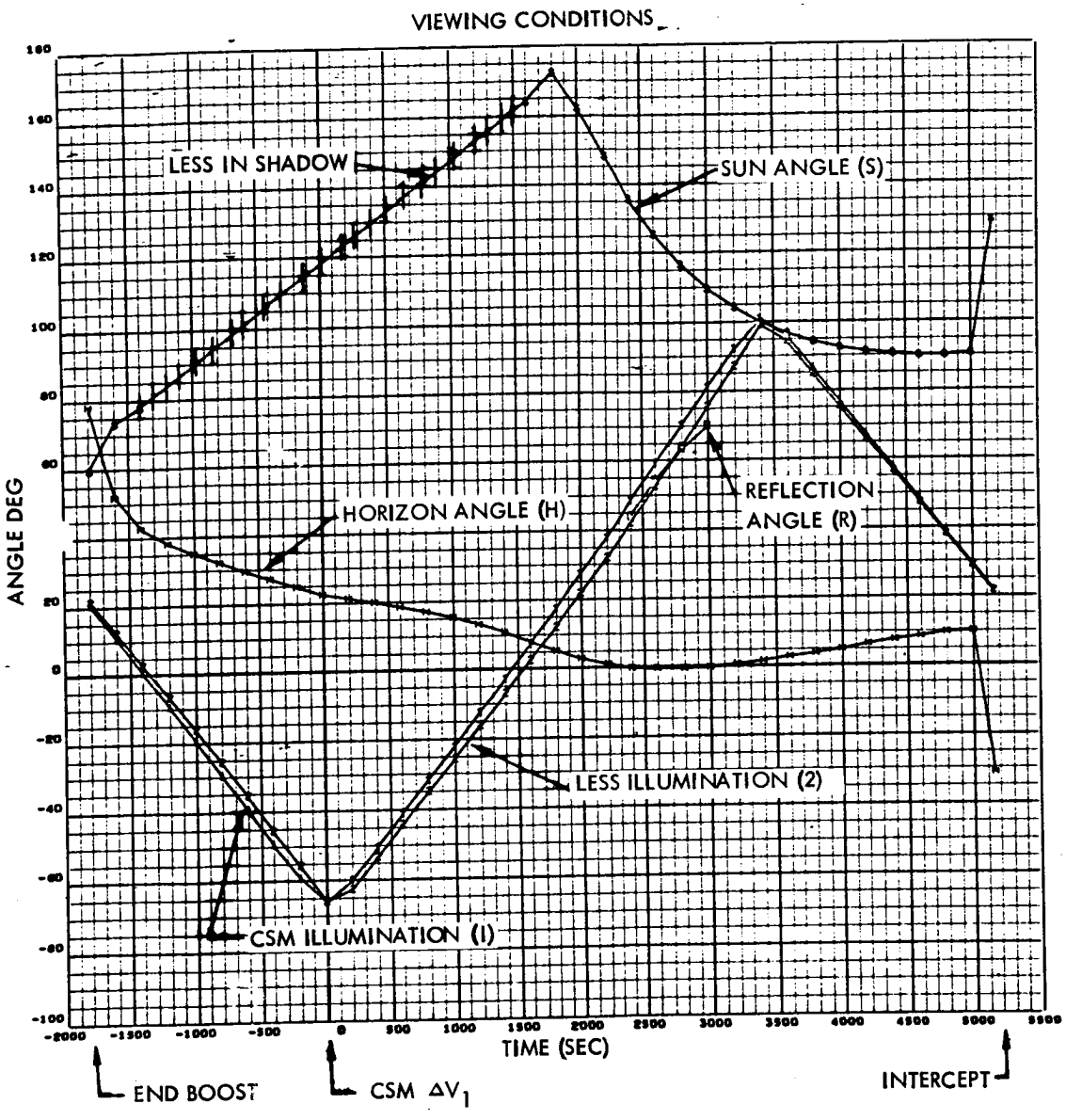

Figure 1-140. - Viewing Conditions: LESS Orbit = 75 by 10 Nautical Miles (Due to Pitch Error of +1.6°), Inclination = 4°

5. The transfer is initiated at an antinode and traverses nearly a 270-degree central angle to intercept.

The cases illustrate the effects of low, fast boosts (the results of -4 and -2 degree pitch angle errors during boost) and of high, slow boosts (the result of a + 1.6 degree pitch error). Planar results are shown for each case; also for each case, the effects of 2-degree and 4-degree relative inclinations are shown.

The time scale originates at initiation of the intercept trajectory; the negative portion represents the 30-minute coasting phase with boost burnout conditions located at the extreme left of the plots.

Examination of these cases reveals some difficult viewing conditions. The cases representing low, fast burnout have the sun in the background ($S \approx 0$) shortly after the vehicles pass out of the shadow. The angle from the LESS to the sun is less than 20 degrees for typically 15 minutes. The high, slow cases have the moon's lighted surface in the background for 45 minutes, ending at intercept. After the ΔV_1 execution, there is a period of approximately twenty minutes spent in shadow and visibility conditions for operating the sextant will then be excellent; i. e. the beacon-marked LESS will be readily observable. Thus, trajectory information should be quite accurate prior to the spacecraft's passing into the sunlit region.

It was assumed in developing these data that the sun is contained in the plane of the CSM; thus out-of-plane effects associated with particular mission opportunities are neglected.

Conclusions. - The results of this parametric analysis indicate:

1. Launch timing must be accurate to reduce phase errors at initiation of rendezvous.

2. Mission planning must be based on 270-degree transfer trajectories, although in some cases shorter transfers can be employed.

3. Visibility is a potential problem during rendezvous. Conditions at initial acquisition can be controlled by planning boost properly. However, visibility after the craft pass from shadow is not easily controllable and depends largely on the errors incurred during boost, which cause large variations in the LESS trajectory with respect to the CSM trajectory.

4. Elliptical target orbits for the LESS require higher CSM energy expenditures when subsequent transearth injection is considered.

LESS-active rendezvous. -

Introduction: LESS-active rendezvous is an attractive concept from a performance viewpoint. It allows the major ΔV requirements for rendezvous to be satisfied by the LESS propulsion system rather than by the CSM. In addition, there may be some future missions where the CSM (or some other target vehicle) does not have the capability to perform active rendezvous. Thus it is important to have some knowledge of requirements for LESS-active rendezvous.

Approach: A survey and analysis were conducted of guidance and navigation techniques appropriate for LESS-active rendezvous. A brief study was conducted to identify requirements for other systems, especially the propulsion system. A performance analysis was not undertaken since the energy requirements and key variables for rendezvous will be substantially the same as for CSM active rendezvous.

LESS-active rendezvous guidance and navigation: During the past 10 years, considerable research has been conducted at NASA-LRC and elsewhere into rendezvous trajectories, guidance, and performance optimization. The success of the Gemini and Apollo rendezvous programs has demonstrated successful implementation of some of this work. For the present study it is more appropriate to deal with the penalties incurred to implement an LESS-active rendezvous system than to rediscuss the application of various rendezvous guidance theories. The approach utilized will be to adopt a qualified guidance scheme and assess the relative penalties of mechanizing such a system.

Some early rendezvous guidance techniques proposed for spacecraft utilized modified forms of "proportional navigation" originally developed for missile guidance. These techniques utilized relative motion variables which were sensed by instruments and/or visually. Proportional navigation does not correct the gravitational gradient existing in the inverse square force field and results in less efficient use of thrusting maneuvers than can be obtained from guidance techniques that utilize more exact modeling of the gravitational field. An example of a simplified technique of this type is given in Reference 1-10. The technique utilizes a hand-held sextant of the type tested in the Gemini program and a portable, self-powered, digital computer described Reference 1-11. Unfortunately, the concept is inappropriate for LESS application. Two reasons are:

1. The bright sunlight environment will not permit the necessary dark adaptation of the eye when a simple sextant is used in conjunction with the present space suit faceplate configuration.

2. The convergence of the orbit determination solutions is very slow when only sextant observations are used. This slow rate of convergence is inconsistent with the time constraints placed on the rendezvous because of PLSS limitations. A measure of the convergence rate may be seen in figure 1-89. It is seen that the addition of range information to the sextant observations produces a much more suitable rate of convergence.

The guidance technique selected for the present analysis is patterned after Apollo LM/CSM rendezvous guidance techniques. The SOR mode provides the targeting for the sequence of thrusting maneuvers required for the time-critical rendezvous. A more detailed description of the SOR mode, with a representative mission profile, is given in the CSM-active rendezvous section of this report. The computational complexity of the Kalman filtering of observational data and the faster-than-real-time integrated trajectory solutions used for navigation and targeting are admittedly complex. However, guidance computer technology is now sufficiently advanced to permit the mechanization of these equations with a computer having only a fraction of the weight and power requirements of the CSM and LM guidance computers. The hand-held, self-powered computer described in reference 1-8 weighs only five pound and is typical of this technology.

Rendezvous course corrections can require a vehicle orientation in virtually any direction, which necessitates an all-attitude-reference. A gyro-driven, 8-ball, attitude display provides this capability, whereas the attitude limitations inherent in visual attitude reference concepts do not. Gyro drift rate requirements for the LESS are then slightly more severe than with CSM-active rendezvous. This is because the required operating period for the gyros extends considerably past the ascent phase. Gyros with drift rates on the order of a few tenths of a degree per hour are easily within current state of the art, and their use would preclude the necessity of a gyro realignment after orbit insertion.

A stability-augmented SCS (rate command) or autopilot SCS is selected to accommodate the larger number of powered maneuvers and coasting flight attitude maneuvers imposed by the rendezvous. This mode will reduce pilot workload and provide him the time to make sightings and/or operate a guidance computer.

The choice of a guidance method utilizing state estimation techniques somewhat reduces requirements on rendezvous sensors in that it is not necessary to sense higher derivative information than position. In some cases, not even all components of position are required. Table 1-7 presents some properties of relative motion sensing equipment that has been used or proposed

TABLE 1-7. - RENDEZVOUS SENSOR DATA

System	Maximum Range (~nm)	Weight (~lb)	Power (~watts)
Lunar Module rendezvous radar (LMRR)	405	72	160
Advanced LMRR proposed by Raytheon (ALMRR)	400	35	140
Gemini rendezvous radar (GRR)	250	68	78
Command Module sextant and VHF ranging system	200	Not Applicable	
Laser rendezvous radar (currently being developed by ITT Federal under contract to NASA MSFC)	75	26	32

for spacecraft rendezvous. It is noteworthy that the power requirements of the longer-range radars could be appreciably reduced if the maximum range capability could be reduced to the LESS requirement of less than 150 nautical miles.

For assessment of the impact of several possible system mechanizations, the systems described in table 1-8 have been identified. Estimates of the weight and power requirements of these systems are tabulated in table 1-9 and are compared with a hard-wire-controlled vehicle considered appropriate if LESS-active capability is not required. The G&C systems noted are described fully in the Guidance and Control section of this report. The battery weight required to operate the systems is estimated on the basis of 40 watt-hours of energy per pound of battery weight. The LESS-active systems are assumed to use the stability-augmented or auto-pilot SCS modes just discussed. The laser rendezvous radar is excluded because of its requirement for additional development.

Concept No. 1 employs the advanced LM rendezvous radar (ALMRR) and is functionally similar to the LM rendezvous system. A strap-down inertial navigator is employed to provide LESS navigation data more quickly than if landmark observations were used for this purpose. System operation can be initiated during the ascent phase, permitting a more accurate injection and reduction in the time to rendezvous, as well as reduced energy requirements both for boost and rendezvous.

TABLE 1-8. - LESS-ACTIVE RENDEZVOUS CONCEPTS

Concept	Description	Comment
1	Add rendezvous radar and guidance computer to LESS. Radar transponder exists on CSM.	Most complex system, automated tracking relieves crew workload. Still plenty of work operating computer and flight control system.
2	Add telescope, VHF ranging and guidance computer to LESS. Flashing beacon and VHF range transponder exist on CSM.	Low-power telescope for manual angle measurement. Potential visibility problems because of glare and reflections in faceplate of space-suit. Highest crew workload.
3	CSM performs SOR guidance computations but solves for "mirror image" burns to be performed by LESS. ΔV parameters are voice-linked to LESS.	Minimum complexity system and practically no changes to CSM. Reliability is strongly affected by voice link reliability. Crew can perform burns with simple LESS system more quickly and easily than CSM can perform them with primary G&N.

Concept No. 2 utilizes optical sightings of the CSM (angle information) and VHF range data in the same fashion as does the CSM in the CSM-active rendezvous mode.

Concept No. 3 is a hybrid. It is unique in that the rendezvous sensing and navigation and guidance computations are performed in the CSM with existing equipment. The powered-maneuver requirements are then relayed by voice link to the LESS, which carries only the SCS gear necessary to execute these ΔV maneuvers. This concept eliminates the need for carrying heavy G&N gear to the lunar surface and reduces the crew's workload since all guidance and navigation functions are accomplished in the CSM. The principal disadvantage of the concept is that a communication failure results in the failure of the complete system. The communication system, however, requires only a small portion of the weight and power of the Concept No. 1 rendezvous guidance gear. Therefore, considerable refinement and redundancy could be added to the communication link before the weight and power requirements tradeoff associated with locating the rendezvous gear on the LESS is exceeded.

TABLE 1-9. - GUIDANCE AND CONTROL SYSTEM RELATED WEIGHT PENALTIES FOR LESS-ACTIVE RENDEZVOUS

Concept	Description	System Elements	Power (watts)	Weight (lbs)	Weight Penalty (lbs)
Reference	Hard-wire control (appropriate for CSM-active mode)	G&C system No. 3	108	77	
		Batteries	-	8	
		Totals	(108)	(85)	-
1	Radar system	Advanced LM rendezvous radar	140	35	
		G&C system No. 8	336	124	
		Hand controller	5	5	
		Additional guidance computer capacity	60	20	
		Batteries	-	51	
		Totals	(541)	(235)	150
2	Visual and VHF ranging	Telescope	-	10	
		VHF ranging electronics	26	6	
		G&C system No. 8	336	124	
		Hand controller	5	5	
		Additional computer capacity	60	20	
		Batteries	-	40	
		Totals	(427)	(205)	120
3	Hybrid, G&N functions in CSM, voice link to LESS	G&C system No. 6	223	98	
		Batteries	-	17	
		Totals	(223)	(115)	30

Other systems changes to provide Concept (3) LESS-active capability: While the major problem associated with LESS-active rendezvous is the guidance and navigation concept, there are other ramifications. For instance, this operational mode will require multiple engine starts. They somewhat complicate the engine and propellant feed systems. With current technology for design of retention screens, reliable feed under zero-g starts is feasible, with propellant settling provided by the cold-gas RCS jets, if needed. Assuming three restarts, on the order of 10 pounds more nitrogen gas may be required. The additional functional requirements reflect also upon RCS requirements by virtue of more stable orientation requirements and larger mass.

For the preferred hybrid G&N concept identified above, a reliable VHF relay is required to assure communication of guidance data from CSM to LESS. The same VHF ranging transponder used for CSM tracking of LESS could be used for this purpose. An alternative concept would be a small relay package working through the backpack communicator. Thus no special effort by the pilot would be required. These equipment items and provisions would add on the order of 25 pounds to the vehicle burnout weight.

Conclusions: Results of this study indicate that:

1. LESS-active rendezvous capability can be implemented with a minimum of weight and complex mechanization, by using guidance and navigation data derived by present CSM equipment and voice-linked to the LESS. This constitutes a realistic hybrid mode wherein the CSM furnishes the complex brains (tracking and computing capability already aboard) and the small LESS provides the efficient muscles to execute the ΔV's. The dry weight of the LESS is estimated to be about 62 pounds heavier than the comparable vehicle designed for passive rendezvous. This increase, while noticeable, is probably not severe enough to alter stowage or deployment concepts materially.

2. True or independent LESS-active rendezvous capability using contemporary G&N equipment (Concept No. 1, identified in table 1-9) and locating the equipment in the LESS imposes a severe weight and complexity penalty on the LESS. This equipment must be carried to the lunar surface and deployed and operated under less than ideal conditions. Dry LESS weight is estimated to be 192 pounds more than the comparable vehicle designed for passive rendezvous. This increase constitutes a severe penalty being approximately 53 percent of the dry weight of the reference vehicle. It is noted that this concept does operate independently of the CSM and thus could be used to rendezvous with passive targets such as

a quiescent CSM or a lunar orbital space station. The system could also be readily adapted for unmanned remote operation such as for a sample return (to CSM) system.

3. Selection of the LESS-active or the hybrid LESS-active concept in lieu of the CSM-active mode will probably depend on such criteria as the procurement schedule and alternative mission applications, if any. The basic LESS mission, as studied herein, can be satisfied by the CSM-active mode. It allows the simplest, lightest LESS and requires no modifications to the present CSM.

Docking and crew transfer. -

Introduction: This portion of the report discusses techniques for performing short-range closure, docking, and crew transfer. Various issues affecting selection of a preferred concept are analyzed. CSM-active and LESS-active docking are both considered.

Ground rules: The LESS study ground rules affecting the docking and crew transfer are:

1. The system must be capable of accommodating one incapacitated crewman.

2. It must be safe.

3. Damage to the CSM must be prevented

4. LESS complexity and CSM changes must be minimized.

Active vehicle: The CSM currently has the capability to dock actively with the LESS. The LESS need, therefore, only maintain attitude control such that the CSM can dock with it. A docking target on the LESS may be required to facilitate this operation. The minimum number of control jets required by the LESS is six. They will provide plus and minus torques about all three vehicle axes (see fig. 1-141). To obtain redundancy for attitude control, it is necessary to add six jets for a total of 12. These 12 jets will also provide torque couples, which may make the docking somewhat easier. The addition of four jets, for a total of 16, provides capability for translation along all three axes of the vehicle, enabling active docking control. Thus the LESS could become the active vehicle in the docking with only a moderate increase in the number of reaction jets and gas supply required to perform this function.

Control method: Manually controlled free-flight docking techniques have been employed and proved in the Gemini and Apollo spacecraft programs.

NUMBER OF JETS	COMMENT	SCHEMATIC
6	MINIMUM NUMBER OF JETS FOR ± TORQUES ABOUT 3 AXES	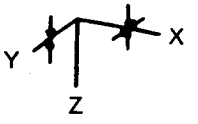
8	SAME AS ABOVE BUT TORQUE IS DOUBLED IN YAW, REDUNDANT JETS IN YAW, TORQUE COUPLES IN YAW	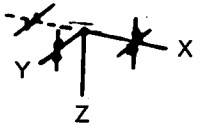
12	± TORQUE COUPLES ABOUT 3 AXES, 100% JET REDUNDANCY	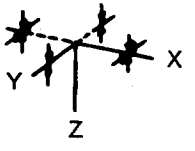
16	± TORQUE COUPLES ABOUT ALL 3 AXES, DOUBLE CONTROL POWER AVAILABLE IN YAW, AT LEAST 100% JET REDUNDANCY AS TORQUE PRODUCERS, ± TRANSLATION FORCES AVAILABLE ALONG 3 VEHICLE AXES SUITABLE FOR LESS ACTIVE DOCKING.	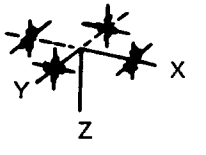

Figure 1-141. - Reaction Jet Configurations for LESS

These manual techniques result in extremely simple system mechanizations. For this reason the manually controlled free-flight docking method is preferred for the LESS application.

Docking mechanisms: Existing docking system technology has provided numerous rigid and semi-rigid docking mechanism concepts (for instance, see refs. 1-9 and 1-10. Also the post-contact dynamics associated with several docking mechanisms have been thoroughly treated (Refs. 1-13 through 1-16). In the case of the LESS, the long docking probe is desirable to minimize such problems as RCS impingement on crew and spacecraft. However, short docking probes are preferable from the standpoint of flexible dynamics, attitude control, and crew retrieval. The automatic latching of docking probes is preferable to a hand-actuated latching or a manual tie-down of the two spacecraft. This minimizes the LESS crew workload and metabolic rates. Use of a rigid or semi-rigid docking mechanism is preferable to free-flying crew transfer techniques because of possible complications in transferring the incapacitated crewman. Also, the use of long tethers for crew retrieval is objectionable because of the possible dynamics problems associated with the conservation of angular momentum (Ref. 1-17).

PLSS limitations: The present PLSS has, in addition to its 4-hour operating lifetime, a requirement that the crew be in the pressurized cabin before disconnecting the PLSS and connecting space suits to a life-support umbilical. If it were possible for the crewmen to connect the life-support umbilical to their space suits before entering the command module, the time required for PLSS operation could be reduced. An extra dumping of CSM pressure and atmosphere could be eliminated and safety would thus be improved. The current PLSS does not have the valving to accommodate the connection of the umbilical in a hard vacuum. It is understood that adding this valving does not severely complicate the space suit. However, to achieve the crew transfer with a minimum of design changes, it is assumed that the space suit will not be modified.

Command module ingress: The docking tunnel and the side hatch both provide openings into the command module. Since it is not possible for a crewman to enter the docking tunnel with the backpack PLSS attached to the space suit, the side hatch is the only opening through which the LESS crewmen can enter the command module. Hand holds between the command module docking tunnel and the side hatch are currently provided for crew transfer between the lunar module and the command module in the event that the command module docking probe becomes jammed in the tunnel and crew ingress through the tunnel becomes impossible.

Crew retrieval methods: The crew can transfer from the LESS through the command module hatch by using such devices as boat hooks, tethers, clothesline/pulley arrangements, portable railings, etc. For LESS application, the existing hand holds on the command module are sufficient for the

able crewmen to make the transfer. A short tether and assist from the able crewmen is the simplest method of transferring an incapacitated crewman and is recommended. It is emphasized that tethers be as short as possible. This will minimize the dynamics problems associated with them.

Potential problems: The lack of mobility of pressurized space suits can constitute a severe problem during crew transfer. For example, if a crewman should lose his grip on a hand hold and float freely off into space, considerable maneuvering of the CSM might be required to retrieve him. This additional maneuvering time could exceed the remaining PLSS life time. A short tether is recommended to prevent this contingency.

CSM RCS exhaust and/or propellant impingement on the space suit constitutes an unknown hazard and potential problem. The toxic effect of the propellants on the space suits could be a hazard when the crewmen have returned to the pressurized space cabin (Ref. 1-18). Also, there is the possibility of high-speed particles from the RCS exhaust penetrating the suits. These RCS impingement problems can be minimized if one or more of the most offensive jets are disabled during docking and by disabling all jets during crew transfer. This would complicate the maneuvering procedures. Alternatively, the LESS could be made the active docking vehicle at the expense of complicating the RCS system, as already discussed.

Geometric arrangements for the docking: Figure 1-142 presents four possible geometric arrangements for docking. Configuration No. 1 utilizes the existing CSM probe. Mouse-trap-type latches are provided in the 1-ft.-radius drogue. The crew is retrieved by using existing hand holds on the command module and short rope tethers are added. The principal problem with this concept is the possibility of CSM RCS plume impingement effects, as discussed. However, this problem does not exist if the LESS becomes the active docking vehicle.

Configuration No. 2 utilizes a retractable probe attached to the outer mold line of the service module. The initial docking can be accomplished at a reasonably large distance, thereby minimizing effects of CSM RCS plume impingement. The probe could be retracted to a position near the command module hatch door, facilitating crew transfer. The principal problem with this concept is that a fairly complex, retractable docking probe must be developed.

Docking concept No. 3 provides a rectangular docking adapter on the LESS that mates directly to the command module side hatch. Crew transfer would be through the center of the fitting. The CSM crewman could assist in the mating and latching operation. The concept has one undesirable feature. It would probably require hatch redesign to assure that docking could be accomplished with no damage to the command module. Also, the CSM flight path in performing the docking closure is not orthogonal with the CSM

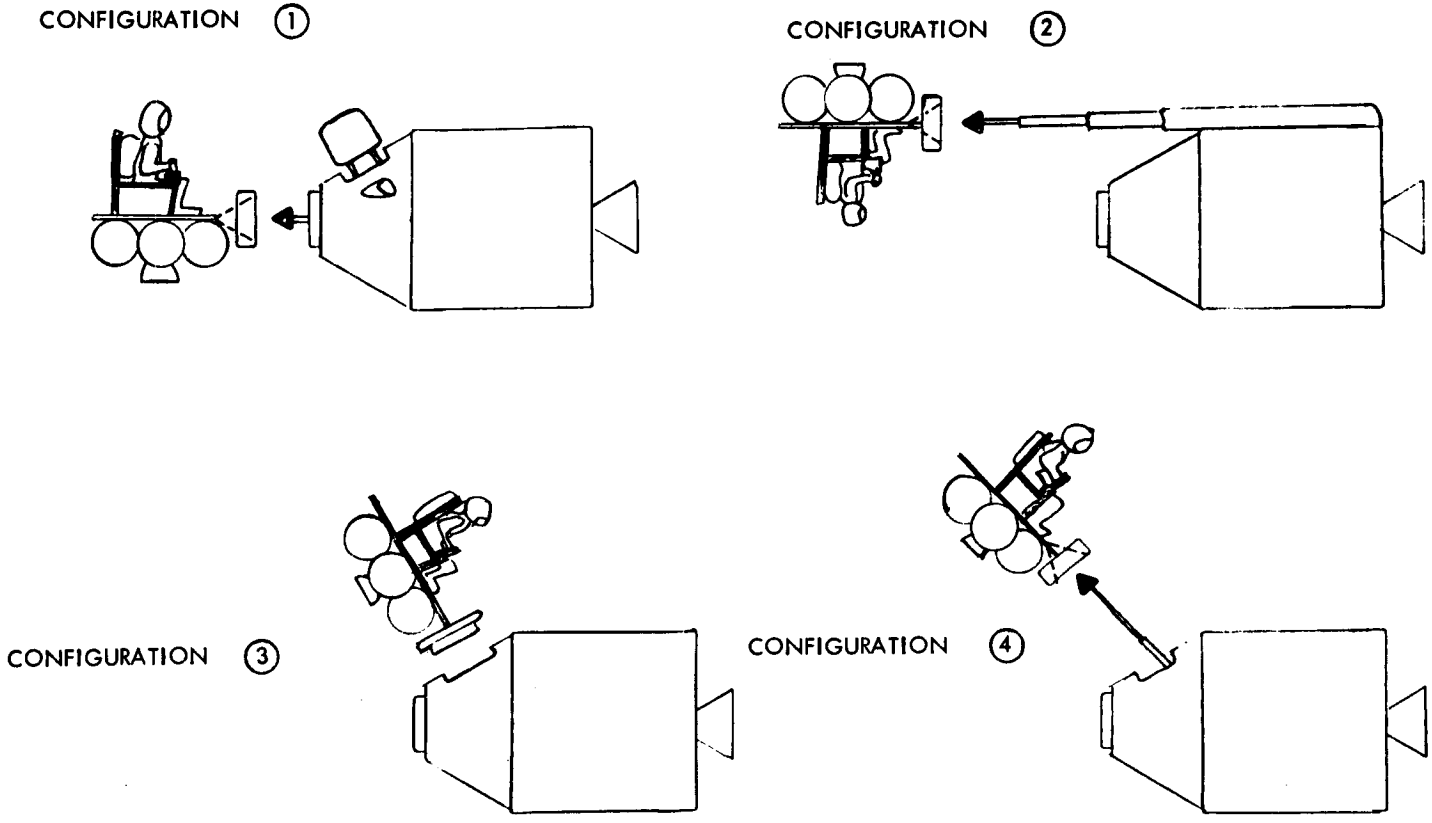

Figure 1-142. - Docking Configurations

control axes and could present a more difficult control task for the CSM astronaut. This problem is eliminated if the LESS performs the active docking maneuver.

Docking concept No. 4 is functionally similar to concept No. 2 except that the extendible probe protrudes from the command module hatch. The principal disadvantages of this concept are a requirement for a complex extendible docking probe and the nonorthogonality of the closure maneuver with respect to CSM control axes.

Based on the above discussion, concept No. 1 with the CSM as the active vehicle is the preferred for docking and crew transfer for the LESS. It has virtually no requirements for new hardware or changes in the CSM. It is anticipated that the plume impingement problem conjectured herein will be thoroughly evaluated within the present Apollo space program and that any potential hazard from this source will be identified.

Docking time requirements: Estimates of the time increments required for this phase of the mission have been made based on Apollo operational time lines and on work done in the NR Mission Evaluation Simulator. These estimates are:

Operation	Minimum	Maximum
Closure and docking	15 min	30 min
Crew transfer	10 min	20 min
Cabin repressurization	5 min	10 min

These data have been factored into the overall mission time line.

Conclusions: Results of this study of docking and transfer indicate that:

1. CSM/LESS docking and crew transfer can be accomplished quite simply and efficiently with virtually no changes to the present CSM.

2. A rigid or semi-rigid docking fixture is preferable to free-flight docking concepts or other concepts requiring greater crew participation.

3. CSM-active docking is recommended with the comment that, if future studies show CSM RCS plume effects to be a hazard, the LESS-active mode is an alternative.

Summary conclusions—rendezvous and docking. - Based on the preceding analyses, the following conclusions are reached:

1. The LESS mission can be accomplished employing CSM-active rendezvous and docking modes with no changes to the CSM and with a relatively simple LESS within the constraints of the PLSS. Table 1-10 lists the preliminary mission time line considering both the maximum and minimum predicted times for the key mission events.

2. LESS-active rendezvous capability can be implemented by having guidance and navigation functions performed in the CSM and transmitting the maneuver information by voice link to the LESS. The LESS then executes the required maneuver. This technique requires an improved voice link but still allows a relatively simple LESS.

3. The CSM RCS plume is potentially hazardous to the crew. Its severity must be assessed in order that the feasibility of CSM-active docking can be confirmed. An alternative is to employ LESS-active docking, which requires a more complex LESS.

4. Visibility during rendezvous is a potential problem, especially immediately after the spacecraft has passed from shadow.

TABLE 1-10. - PRELIMINARY MISSION TIMELINE

Mission Events	Phase Time (minutes)		Cumulative Time (hours:minutes)	
	Min	Max	Min	Max
Charge PLSS			0:00	0:00
Prelaunch	10	25		
Liftoff			0:10	0:25
Boost	5	10		
Begin rendezvous phase			0:15	0:35
Tracking	15	20		
Pre-ΔV_1	8	15		
ΔV_1 (Establish intercept trajectory)			0:38	1:10
Post-ΔV_1	2	5		
*Tracking (45 - 100 min)	35	80		
Pre-ΔV_2	8	15		
ΔV_2 (Gross rendezvous)			1:23	2:50
Post-ΔV_2	2	5		
Closure and docking	15	30		
First contact			1:40	3:25
Crew transfer	10	20		
Repressurize cabin	5	10		
Mission completed			1:55	3:55

*If required, RCS course correction could be inserted.

SECTION 1 SYMBOLS

COV	Calculus-of-variation method of optimum boost energy/ trajectory calculation
KFT	Thousands of feet
KFPS	Thousands of feet per second
T/W_{LO}	Lift-off thrust-to-weight ratio
T/W	Thrust-to-weight ratio
ΔV	Change in vehicle velocity
Sec	Seconds
Deg	Degrees
fps	Feet per second
I_{sp}	Engine specific impulse $\frac{\text{lb. thrust}}{\text{lb. propellant/sec}}$
ϕ	Out of plane angle at launch
$\Delta\Sigma$	Launch azimuth error (degrees)
θ_1	Boost trajectory angle with respect to surface, first step
θ_2	Boost trajectory angle with respect to surface, second step
θ_3	Boost trajectory angle with respect to surface, third step
mL	Millilamberts luminance of the sun
VHF	Very high frequency
ω	Perilune orientation of LESS orbit
ϕ_1	Departure angle of CSM for start of transfer to LESS orbit
ϕ_2	Arrival angle for CSM at LESS orbit intercept, also LESS angle at CSM departure
δ	$\phi_2 - \phi_1$
SOI	Stable orbit insertion
i	Relative phase angle, inclination of orbit plane
ΔV_{TEI}	Trans-Earth injection velocity increase requirement
LOS	Line-of-sight, one vehicle to another

Y	Angle of yaw
P	Angle of pitch
S	Angle between LESS and sun, viewed from CSM
H	Angle between LESS and lunar horizon, viewed from CSM
R	Angle between CSM-LESS line to lunar surface and sun (lunar background reflection angle)
1	Complement angle between line from CSM to horizon and sun (CSM illumination)
2	Complement angle between line from LESS to horizon and sun (LESS illumination)

2.0 STUDY RESULTS - GUIDANCE AND CONTROL TECHNIQUES

This section identifies, analyzes, and compares guidance and control concepts appropriate to a LESS vehicle; a broad variety of concepts are identified. The approach emphasizes the achievement of adequate safety and reliability through the employment of simple techniques. The relative performance capability and the operational limitations of these concepts are defined. Gross comparisons and tradeoffs are made to establish a relatively small family of preferred concepts. The resulting concepts and data are thus appropriate for the more intensive evaluation that may be the subject of a Phase B treatment.

Figure 2-1 is a functional flow diagram of the guidance and control system and introduces the terminology used. The stabilization and control system controls attitude dynamics of the vehicle and includes any additional stability augmentation devices necessary to achieve adequate stability. Guidance refers to controlling the path or trajectory of the center of mass of the spacecraft. For LESS this consists of propulsion ignition timing, thrust vector steering, and propulsion cutoff control. The steering requires an attitude reference sensing system and may employ additional trajectory measurements or navigation data to achieve the desired trajectory.

The relatively small size of a LESS vehicle offers an attractive possibility for the use of extremely simple manually operated stabilization and control concepts. The following Manual Stabilization and Control System Analysis section identifies the handling qualities and relative merits of these control methods. The approach is analytically oriented and has been designed to complement the research and simulation efforts being conducted at the Langley Research Center.

The Guidance and Navigation Concept Synthesis section identifies and contrasts visual and instrument techniques for attitude and trajectory sensing. The section results in a family of integrated guidance and control concepts, which are then considered from a mechanization and guidance accuracy standpoint in the Guidance and Control Systems Considerations section. The detailed Guidance and Control Techniques Conclusions are then summarized as the last part of section 2.0. The guidance and control considerations for the rendezvous and docking phase or lunar flying vehicle applications are included in the other report sections with those titles.

Pertinent symbols and definitions are provided at the end of this section (page 2-144).

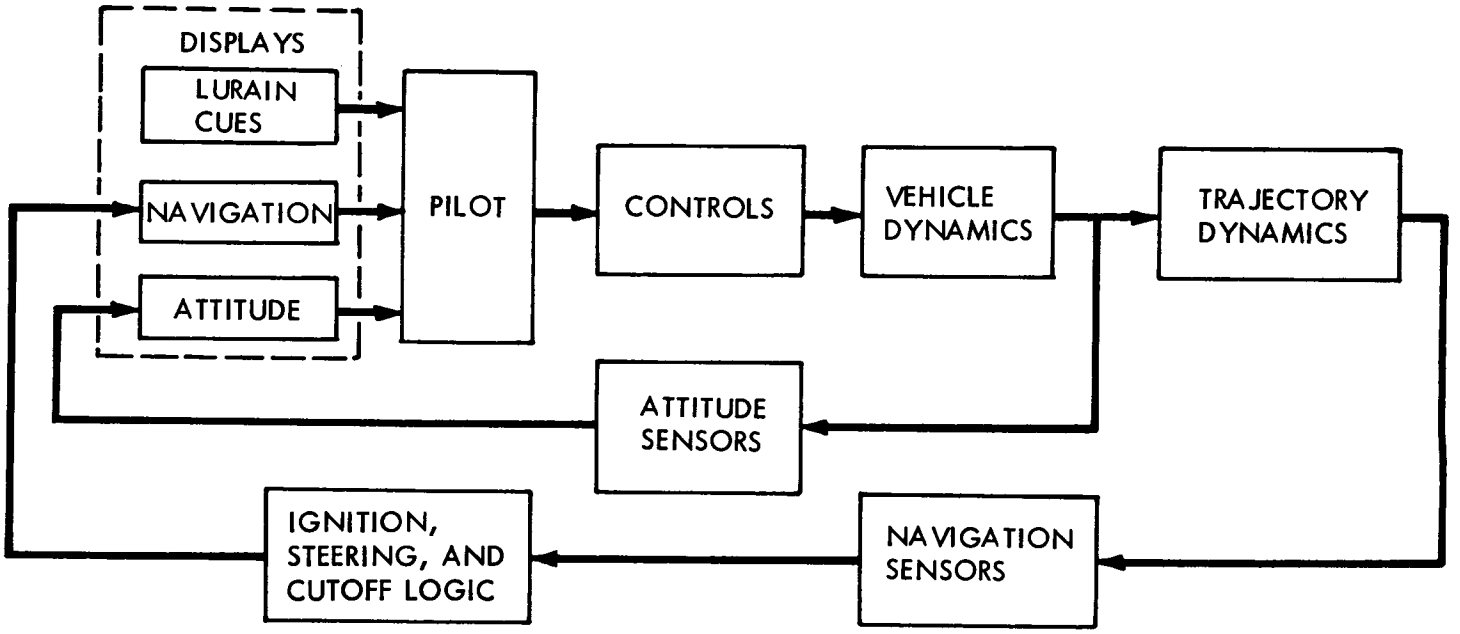

Figure 2-1. - LESS Ascent Guidance and Control Functional Block Diagram

Manual Stabilization and Control Techniques

All of the candidate stability and control methods for the LESS are discussed in this section. These systems fall into the general categories of stabilization types: kinesthetic (balance reflex control torque generation), hardwire (control torque generation by use of a rotation hand controller), and stability augmentation (angular velocity command by use of a rotation hand controller). Each type has two or more variations. To avoid unnecessarily strict design constraints on the entire vehicle simply to provide comfortable flying qualities for the pilot, the variations of each stabilization type are aimed at decoupling the vehicle design constraints from pilot requirements. In nearly all cases, the efforts to accomplish this decoupling result in either a more complex, heavy, or costly system. Many of the approaches are conceptual and are not well founded in simulation or historical proof of their effectiveness.

During the development of the lunar flying vehicle (Ref. 2-15), it was found that a pilot could not effectively cope with the eighteen variables simultaneously that were required for mission performance using either the kinesthetic or hardwire control methods. These variables were three axis attitude and translation, and their first and second derivatives. He had under his direct control only the three angular accelerations and thrust level. The result was that a stability augmentation system was recommended which effectively reduced the number of controllable variables to twelve for maneuvers and nine for attitude hold conditions. The lunar flying vehicle mission, that of transportation to a predetermined point and landing, required tight limits on attitude and translational position, which are the variables furthest removed from the pilot's direct control. Since the mission of the LESS requires only the continuous control of three attitudes and their two derivatives (nine variables), the recommendations for the lunar flying vehicle need not be imposed. The kinesthetic and hardwire control methods for the LESS may be feasible and appropriate.

All of the available data describing the handling qualities of various stabilization methods for the LESS are used in this section, but are not sufficient for showing clear-cut superiority of one system over another. The pilot will be capable, if he is in prime condition, of handling a well designed acceleration control system, provided his guidance and navigation task is not overly demanding. The combination of the stabilization, maneuvering, guidance, navigation, and event timing tasks must be fully and simultaneously simulated under realistic conditions to confidently recommend a system.

Objectives. - The stability and control study effort was accomplished to evaluate the feasibility of various stabilization techniques for possible use with LESS concepts. Manual modes were to be emphasized for encouraging system simplicity. Another objective was to evaluated available data from various simulation programs to improve their correlation with theory.

Approach. - Apart from using available man-in-the-loop simulation data to assess the handling qualities of LESS configurations, the mathematical modeling technique was employed. This method consists of constructing a set of simultaneous differential equations of motion for the pilot and vehicle. The pilot's response and the form of the human equation has been the subject of study and is well founded. The total set of equations is used in evaluation by the root locus method which involves the Laplace transform to the complex frequency plane. Correlations between pilot opinion and the parameters involving operating frequency bandwidth and damping ratio then provide the handling qualities assessment of each configuration.

Comparison of the Cornell and Cooper pilot opinion rating systems. - It was discovered late in this study that NR and LRC have been using different rating systems to judge the handling qualities of simulated lunar flight vehicles. To define common denominators between the two systems, a short study has been conducted. The study results show that a comparison between the systems tends to be somewhat subjective, and depends on each individual's personal interpretation of the verbal rating defintions.

Tables 2-1 and 2-2 present the two rating systems. Table 2-3 compares the two systems from a verbal standpoint. While they appear to agree on the overall objective, the approaches differ in that the Cooper system separates flight and landing phases while the Cornell system evaluates the overall mission. Since the primary mission of LESS does not include landing, the difference in approaches is negligible. There is almost no common wording between the systems below the number 3 rating; thus major differences appear in the region which usually causes critical design change decisions.

Table 2-4 is a preliminary attempt to match the numerical ratings. It indicates that a rating of 5 on a vehicle by an LRC pilot using the Cornell scale might be interpreted by NR personnel using the Cooper scale (at number 5) as having marginal and doubtful handling equalities, although the pilot actually only experienced "moderately objectionable deficiencies," according to the Cornell scale.

Since much effort and material have been produced using both scales, the recommendation for the immediate future is to correlate data based on Table 2-4. These data are duplicated in figure 2-2 using a graphical presentation and the general verbal categories of each system.

TABLE 2-1. - COOPER PILOT OPINION RATING SYSTEM FOR UNIVERSAL USE

	Adjective Rating	Numerical Rating	Description	Primary Mission Accomplished?	Can be Landed
Normal Operation	Satisfactory	1	Excellent, includes optimum	Yes	Yes
		2	Good, pleasant to fly	Yes	Yes
		3	Satisfactory, but with some mildly unpleasant characteristics	Yes	Yes
Emergency Operation	Unsatisfactory	4	Acceptable, but with unpleasant characteristics	Yes	Yes
		5	Unacceptable for normal operation	Doubtful	Yes
		6	Acceptable for emergency condition only*	Doubtful	Yes
No Operation	Unacceptable	7	Unacceptable even for emergency condition*	No	Doubtful
		8	Unacceptable - dangerous	No	No
		9	Unacceptable - uncontrollable	No	No
	Catastrophic	10	Motions possibly violent enough to prevent pilot escape	-	-

*Failure of a Stability Augmenter

TABLE 2-2. CORNELL SYSTEM

Controllable Capable of being controlled or managed in context of mission with available pilot attention.	Acceptable May have deficiencies which warrant improvement, but adequate for mission. Pilot compensation if required to achieve acceptable performance is feasible.	Satisfactory Meets all requirements and expectations. Good enough without improvement. Clearly adequate for mission.	Excellent, highly desirable	A_1
			Good, pleasant, well behaved	A_2
			Fair. Some mildly unpleasant characteristics. Good enough for mission without improvement.	A_3
		Unsatisfactory Reluctantly acceptable. Deficiencies which warrant improvement. Performance adequate for mission with feasible pilot compensation.	Some minor but annoying deficiencies. Improvement is requested. Effect on performance is easily compensated for by pilot.	A_4
			Moderately objectionable deficiencies. Improvement is needed. Reasonable performance requires considerable pilot compensation.	A_5
			Very objectionable deficiencies. Major improvements are needed. Requires best available pilot compensation to achieve acceptable performance.	A_6
	Unacceptable Deficiencies which require mandatory improvement. Inadequate performance for mission even with maximum feasible pilot compensation.		Major deficiencies which require mandatory improvement for acceptance. Controllable performance inadequate for mission, or pilot compensation required. For minimum acceptable performance in mission is too high.	U_7
			Controllable with difficulty. Requires substantial pilot skill and attention to retain control and continue mission.	U_8
			Marginally controllable in mission. Requires maximum available pilot skill to retain control.	U_9
Uncontrollable Control will be lost during some portion of mission.			Uncontrollable in mission.	10

TABLE 2-3. - PILOT OPINION RATING SYSTEM COMPARISON BASED ON VERBAL DESCRIPTIONS OF CATEGORIES

	Cornell System	Cooper System
Major Objective	To rate vehicle handling qualities	
Major Approach	Rates entire mission, independent of phases	Separates mission into flight and landing phases
Major Differences	Acceptable region includes both satisfactory and unsatisfactory flight conditions	Acceptable region includes satisfactory and 1/3 of unsatisfactory flight conditions
	Makes no distinction between normal and emergency operation	2/3 of unsatisfactory region is acceptable for emergencies only
	Unacceptable region is controllable; mission may still be accomplished	Unacceptable region is uncontrollable; mission cannot be accomplished

TABLE 2-4. - PRELIMINARY PILOT OPINION RATING SYSTEM COMPARISON BASED ON NUMERICAL RATINGS

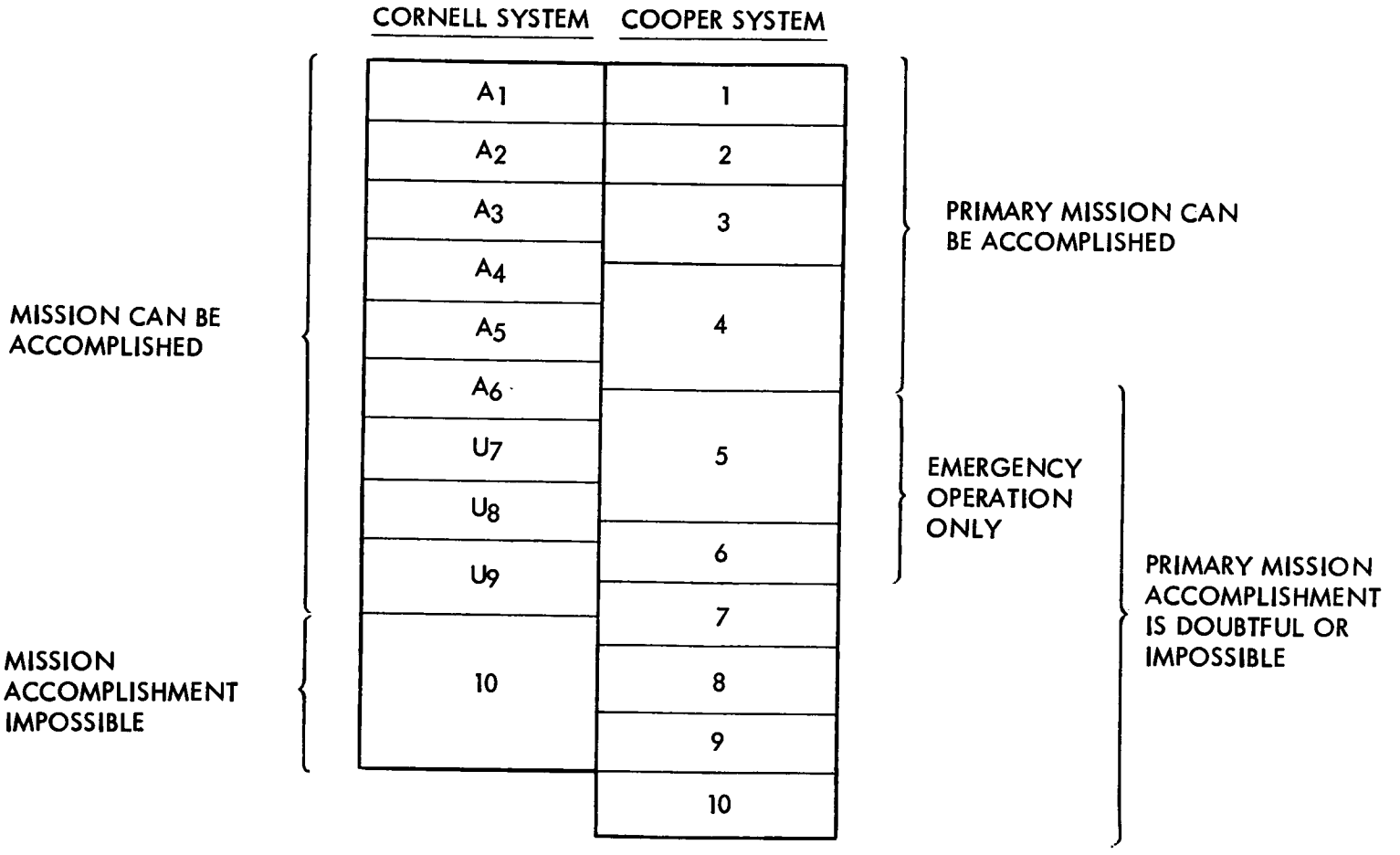

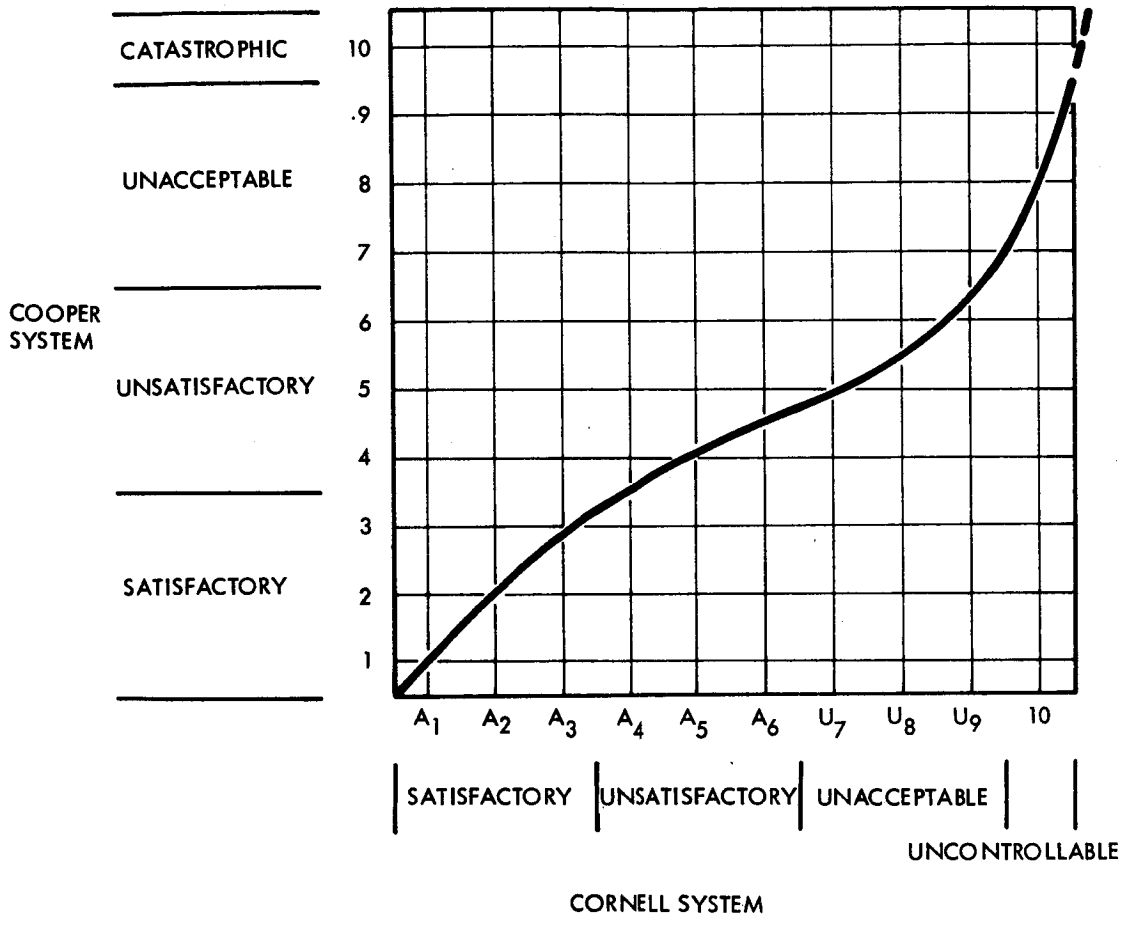

Figure 2-2. - Preliminary Graphical Comparison of Pilot Opinion Rating Systems

Stabilization systems analysis. - The step-by-step method of analysis by which the candidate stabilization systems are compared are discussed in this section. It begins with a discussion and evaluation of appropriate simulations. Equations of motion for both the pilot and vehicle are described. The resulting mathematical models are used, one by one, in evaluating the various configurations of kinesthetic and hardwire control. Stability augmentation as an alternative control method is discussed. Methods of improving hardwire control by compensation networks are analyzed in detail. Tradeoffs between rotation controller sensitivity gear ratio and boost propulsion throttling are investigated for potential improvements in handling qualities.

Comments on manned lunar propulsion system simulations. - A number of simulations recently have been or are being conducted at NASA, NR, and other companies to study the handling qualities and performance of small, manned propulsion devices. Although most of the studies deal primarily with lunar flying vehicle designs, some, such as the current LRC fixed base visual simulation program, are applicable to the lunar escape system. This report summarizes and discusses the available data. A similar survey (with a wider scope) is given in Reference 2-1.

All of the simulations discussed appear to have many outstanding qualities and accomplish the design task. Since their results do not agree, however, it is necessary to examine reasons for the differences. This section points out potential reasons for the differences, based on system descriptions appearing in the simulator reports.

Although the simulation studies vary in scope and size, they all have objectives of measuring the handling qualities and/or performance of various control methods and vehicle configurations. They also use mission-oriented tasks as a common basis for run comparisons.

To complete the mission, the man in the loop must be given a quantity of information during flight, part of which depends on the control mode. The mission description involves navigation procedures. Depending on the flight mode, there are system stabilization tasks for normal and emergency operation. The stabilization task is reduced to a command task if the pilot is not actually part of the stability loop. This differentiates between the stability augmentation system, and kinesthetic and hardwire control methods. All of the information, navigation and stabilization requirements are definable. The concept is described in figure 2-3.

The quantity of information the pilot receives from visual and proprioceptive cues, and the maximum workload he is able to accept in performing his navigation and stabilization tasks are not directly definable. Simulation

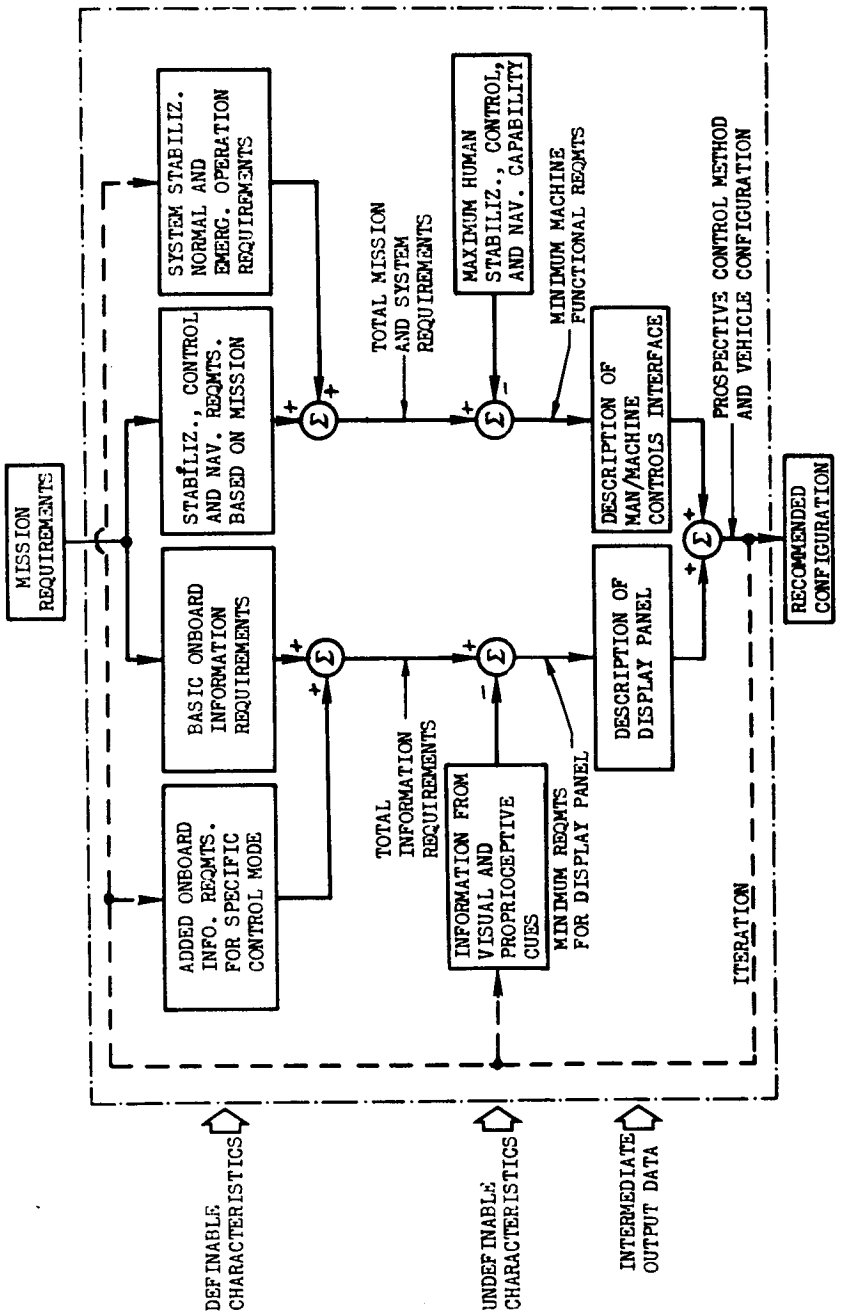

Figure 2-3. - Generalized Small, Manned Propulsion Device Study Objectives

studies therefore attempt to measure a pilot's ability to operate a simulator based on a specific set of requirements which includes both the mission and the control mode. A small manned propulsion device inherently pushes the pilot to his maximum capability to minimize hardware weight and complexity. As yet, there is little assurance that the maximum capability will be recognized if observed. The Cooper Pilot Opinion Rating system is an attempt to measure the capability. Further attempts have resulted in comparisons of the rating system with performance. Both techniques are only as accurate as the simulation itself.

The typical study incorporates an iteration process to arrive at a recommended vehicle description (figure 2-3). Displayed information is used in conjunction with pilot controls to produce trial configurations of the vehicle.

The major objective of a small manned propulsion device study is to provide data showing measures of pilot workload and performance for various vehicle configurations. Because the measurement techniques are subjective, the data vary between studies. The 1969 visual simulation at NR/SD sought to overcome subjectivism by mission requirement uniformity and statistical smoothing of the data. More rigorous methodology exists, but is usually beyond the time and funding scope of the study.

Because disagreements between study results occur when the studies are conducted by different groups, detailed comparisons of technical simulation are necessary to judge their validity. Several typical types of limitations to be used as comparison points are discussed below. A summary of the characteristics of the simulators is presented in table 2-5. Photographs of several simulators appear in figures 2-4 through 2-9.

Studies 1, 2, and 9 of table 2-5 were conducted using tethered flight vehicles; and study 8 is scheduled to begin in 1970. The two SD flight vehicles were constrained to a horizontal area by ground tethers, as well as top and bottom vertical tethers, and nitrogen inlet lines from the stationary source. Both the FLEEP and Bell vehicles use a single overhead tether or a 1/6-g suspension device.

The most prominent disturbing influences on tethered vehicles are the tethers themselves. The SD tethered flight vehicles also had nitrogen supply hoses which produced disturbances. Both the hoses and tethers, while slack, produce a very small amount of damping which is a stabilizing effect. They also produce destabilizing torques when whipping back and forth in the thrust plume. The net effect of the tethers and hoses in pitch and roll while the vehicle is flying is not measurable. In yaw, all rotational rate is highly damped; the hoses also produce a restoring moment. Ground tethers and hoses change the vehicle center of gravity slightly as altitude changes.

TABLE 2-5. SUMMARY OF SIMULATION PROGRAMS

Configuration	NP/SD				MSC	LRC			Bell
	- 1 - 1968 One-Man Propulsion Device	- 2 - 1969 Tethered Flight Vehicle	- 3 - 1968 Visual Simulator	- 4 - 1969 Visual Simulator	- 5 - 1968 Inclined Plane Simulator	- 6 - 1969 Lunar Flying Platform Simulator	- 7 - 1969 Fixed Base Kinesthetic Simulator	- 8 - 1970 FLEEP (Flying Lunar Excursion Experimental Platform)	- 9 - 1968 Bell Flying Vehicle
Principal Investigator	G. M. Hanley	G. M. Hanley	G. M. Hanley	G. M. Hanley	R. L. Barton H. A. Pope	P. R. Hill D. F. Thomas	D. Middleton	D. E. Hewes M. Long	C. E. Satterlee
Type of Simulation	Tethered Flight, N_2	Tethered Flight, N_2	Fixed Base	Rotating Base (Pitch & Roll)	Tethered, Air Bearing, N_2	Air Bearing	Fixed Base	Tethered Flight, H_2O_2	Tethered Flight, H_2O_2
Degrees of Freedom	5	5	6	6	3	5	6	6	6
Environmental Conditions Studied	Earth	Earth	Earth (1) Moon	Moon	Moon	Moon	Moon	Moon	Earth Moon
Pitch and/or Roll Control Type	Kinesthetic	Kinesthetic, Hardwire TVC	Kinesthetic, Hardwire TVC, Stab. Aug.	Kinesthetic, Hardwire TVC, Stab. Aug.	Kinesthetic	Kinesthetic	Kinesthetic Hardwire - TVC Hardwire - RCS	Kinesthetic Hardwire	Kinesthetic Hardwire
Yaw Control Type	-	-	Hardwire TVC, Stab. Aug.	Hardwire TVC, Stab. Aug.	-	Hardwire RCS	Hardwire RCS	Hardwire RCS	Hardwire Jetavators
Pitch or Roll Total Moment of Inertia Range, Slug-Ft^2	33 - 141	105 - 600	1-G: 33-1000 1/6-G: 126-182	112 - 195	84 - 94	300 - 900	200 - 12,000	317 - 338	1-G Kin: 62-168 1-G Hardwire: 168 1/6-G Kin: 57-175 1/6-G Hardwire: 175
Total Weight, lb	244 - 363	339 - 453	678 - 978	598 - 908	436 - 476	395 - 475 (Neglects Pilot?)	2600	892 - 1281	1-G: 505-599 1/6-G: 626-673
Pilot Weight (lb)	190	190	1-G: 190 1/6-G: 380	380	165	-	380	190 - 375	1-G: 180 1/6-G: 190
Total CG Relative to Pilot	2.6 - 1.6 Ft Above Pilot Feet	2.1 - 2.2 Ft Above Pilot Feet	2.1 - 1.3 Ft Above Pilot Feet	2.1 - 1.3 Ft Above Pilot Feet	8.5 - 9.7 Inches Above Ankles	At Pilot CG	0 - 1.8 Above Pilot Feet	10.7 - 2.9 Inches Above Pilot Feet	29-30 Inches Above Pilot Feet
Thrust to Weight Range	0.9 - 1.1	.9 - 1.1	0.30 - 1.5	0.38 - 2.	No Data	No Data	0.28 - 1.0	0.24 - 2.4	0.28 - 1.2
Flight Task	Hovering and Short Transport	Hovering and Short Translation	Hovering and Complete LFV Flights	Hovering and Complete LFV Flights	Hovering and Short Flights	Hovering and Short Flights	Lunar Escape	Hovering and Short Flights	Hovering and Short Flights
Pilot Opinion Rating Range	5-7 (2)	Kin: 5-9 (2) Hrdwr: 7-9	Kin: 9-10 (2) Hrdwr: 6-9 Stab. Aug: 3	Kin: 9-10 (2) Hrdwr: 6-9 Stab. Aug: 3	4-6 (2)	3.5 - 5 (2)	3-7	-	1-G Kinesthetic: 8 1-G Hardwire: 4 1/6-G Kinesthetic: 7 1/6-G Hardwire: 7
Reference and Figure No.	2-2 2	2-2 3	2-2 4	2-2 5	2-2 6	2-2 7	- -	- -	2-3 -

Notes: All simulators used standing pilots
(1) Earth tests to verify similarity between studies (1) and (3); no Cooper ratings given
(2) Cooper scale ratings based on flight tests by NR/SD pilots

Figure 2-4. - Lunar Flying Unit and Pressure Garment Assembly

Figure 2-5. - Tethered Flight Vehicle

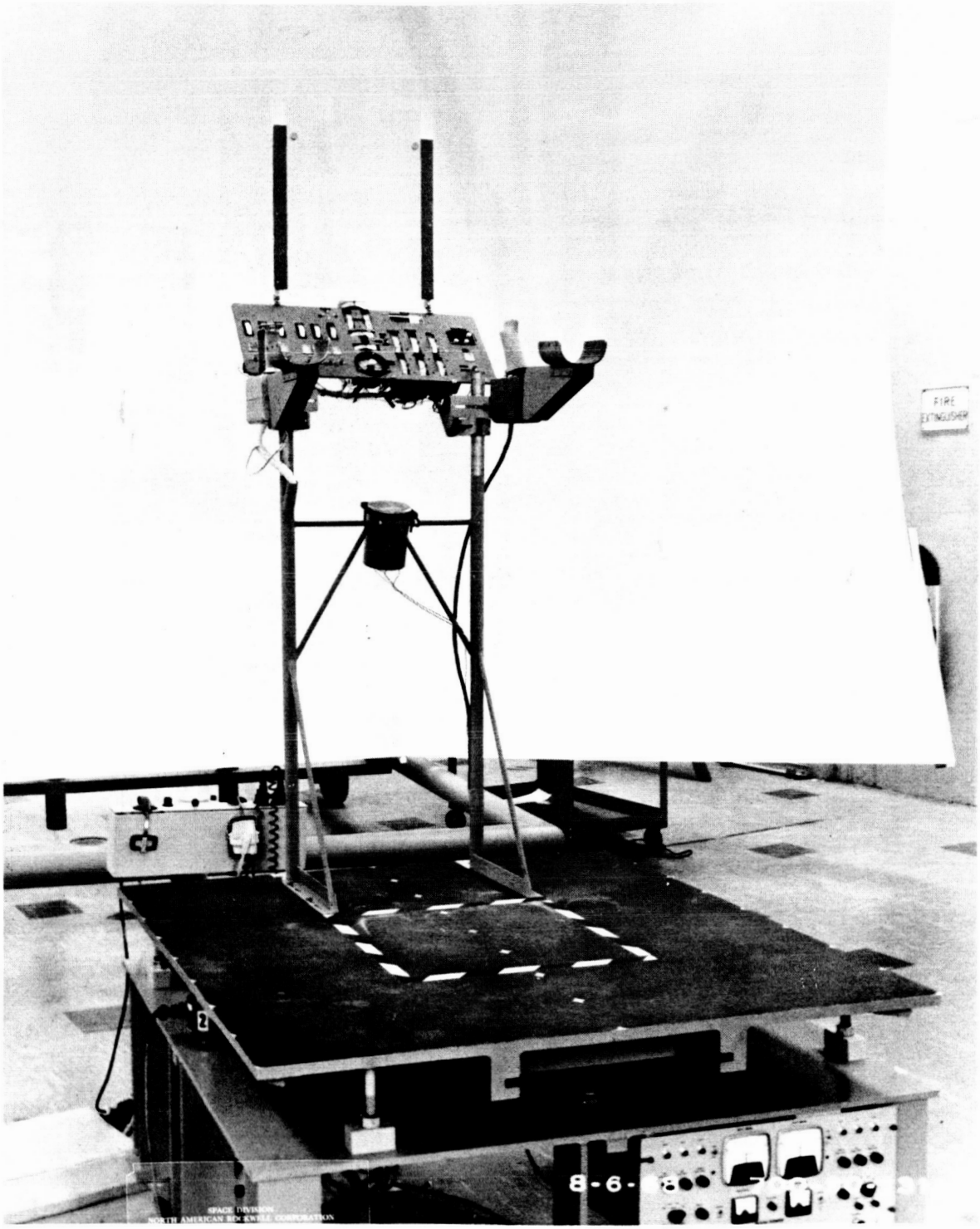

Figure 2-6. - Lunar Flying Vehicle Visual Simulation Platform

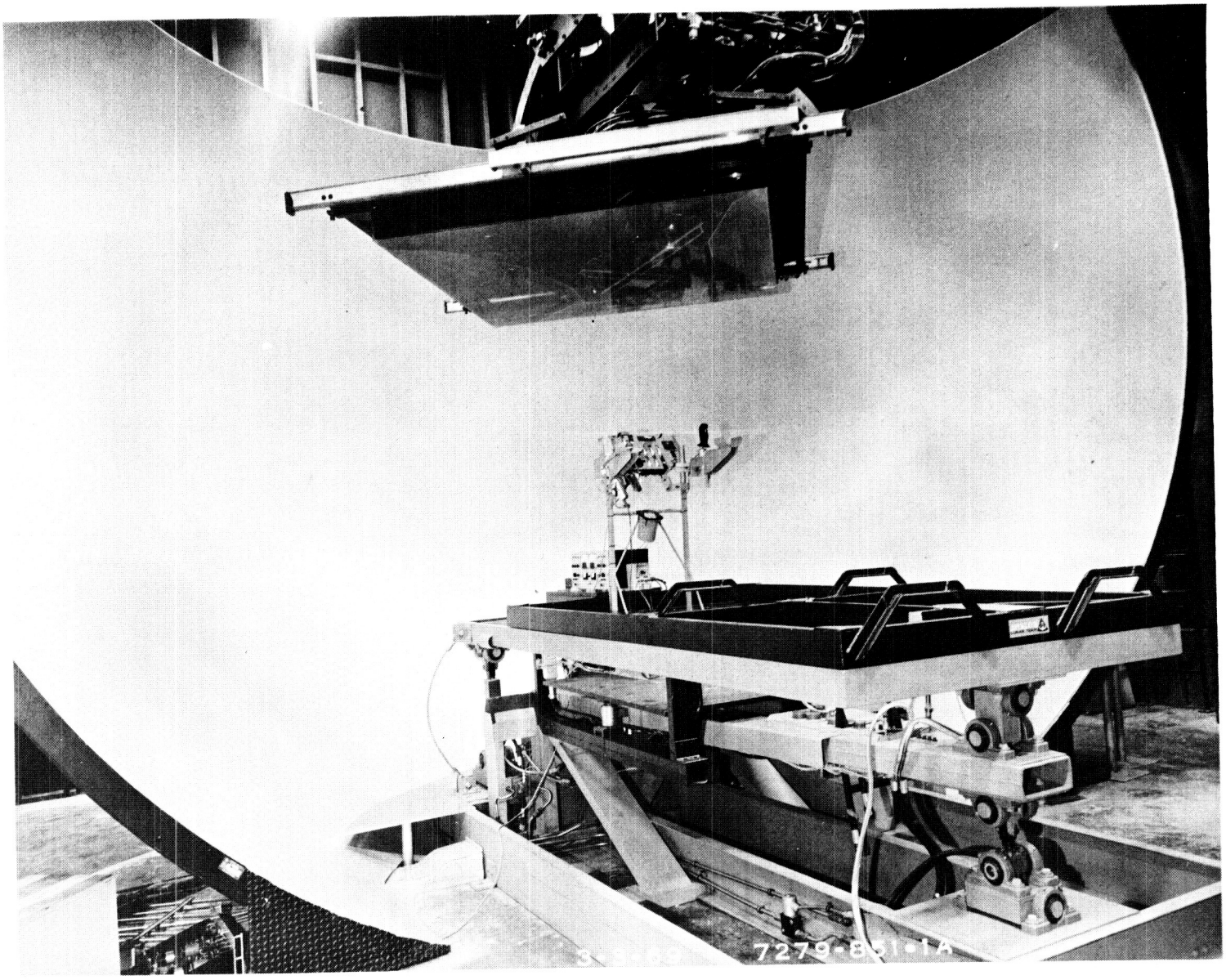

Figure 2-7. - Hotran Simulator Facility

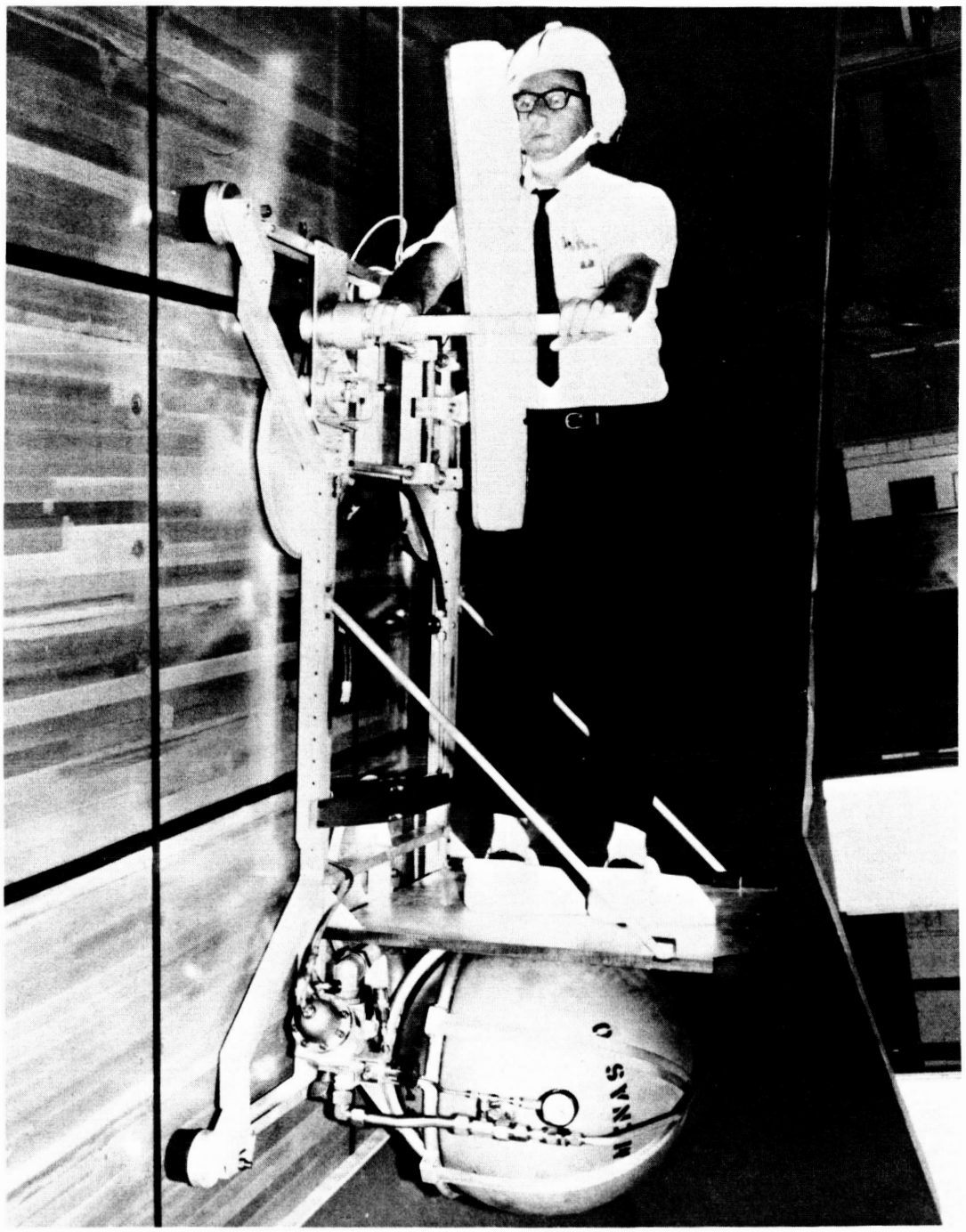

Figure 2-8. - NASA/MSC Inclined Plane Simulator

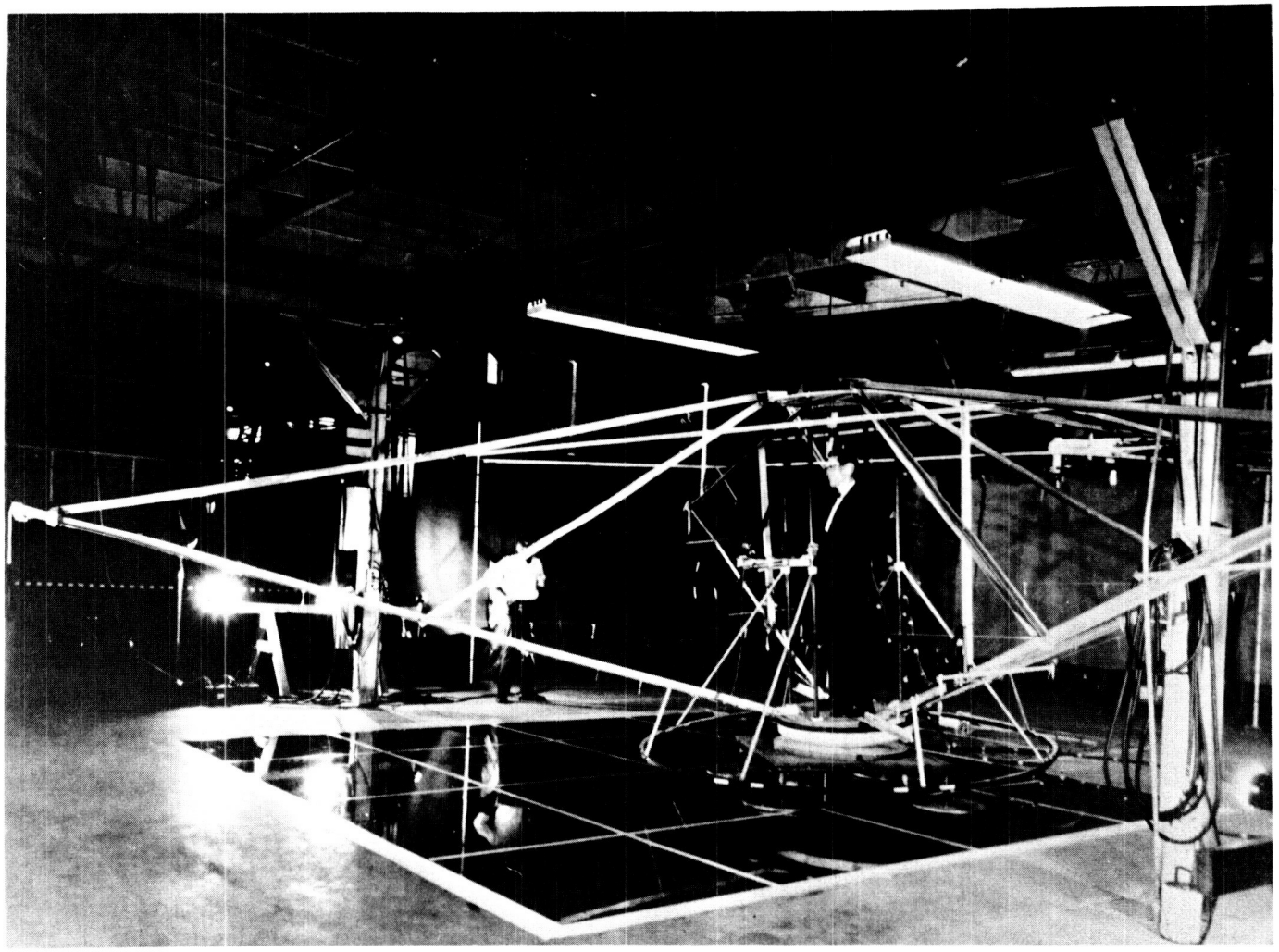

Figure 2-9. - NASA Lunar Flying Platform Simulator

With the tethered flight vehicles pilots were often forced to resort to drastic control inputs to avoid tether limits, increasing the danger of over-controlling. Sluggish vehicle response at high inertias required the pilot to maintain command inputs for longer time durations, resulting in large phase errors and pilot-induced oscillations. If the tethers and all obstructions were absent, the vehicle might have been easier to fly, but safety regulations precluded this.

The Bell study (9) utilized relief of 5/6 of the total weight to produce accurate lunar thrust effects. The vehicle and pilot were suspended from a constant force vacuum cylinder by means of two-axis gimbals attached to their respective centers of gravity. The cylinder is supported by a low friction trolley on an overhead rail that permits horizontal travel. Adding both damping and hysteresis to the vertical dimension of flight, the suspension system effectively made the vehicle response to throttle changes unrealistic.

When oscillograph recordings of visual simulation flights are compared with those of tethered flight vehicles, it appears that both the tethers and the suspension systems tend to stabilize altitude. Visual simulator recordings display a nearly sinusoidal altitude time history, with a frequency of one-half of the pilot's instrument scan frequency (approximately 0.1 cps). The pilot would manipulate the hardwire throttle to check an ascending rate and then return his attention to other aspects of flight. Later he would again adjust the throttle to check the descending rate resulting from the previous correction.

The independent pilot suspension system relies on the pilot attachment being at his center of gravity. Any motion, other than pivoting about the ankles, may upset the balance of the system. Bending of the body at the hips or movement of the head and limbs will tend to move the center of gravity away from the suspension gimbal axes and create disturbance moments on the vehicle.

Translational motion of the vehicle relative to the overhead trolley and motion of the pilot relative to the vehicle create restoring moments. These tend to add stability and upgrade handling qualities assessments of the vehicle.

Any change in the total weight due to propellant usage changes the suspension system response. This effect is probably not a significant influence on stability, but may appreciably change performance characteristics, such as propellant usage and flight time, over a complete flight.

All of these influences are carefully minimized, but cannot be completely eliminated. They therefore become factors which degrade the system fidelity.

While probably negligible at the low horizontal velocities experienced at NR/SD, if an appreciable velocity is attained, air resistance is a factor. Unless the frontal area centroid lies at the total center of gravity, the moment arm between the two will produce a disturbing moment that should be considered.

Studies 5 and 6 utilized air bearing pads to provide nearly frictionless horizontal motion. Study 5 used an inclined plane to produce 1/6 the total weight along the vehicle vertical axis. The other 5/6 of the weight was supported by the air bearing pads. The pilot essentially laid on his side during a flight. A spherical segment resting on an air pad dolly gave three rotational and two translational degrees of freedom to the simulator in study 6. The pilot stood atop the spherical segment.

Does the air escaping from the pad clearances produce perfectly balanced forces, or does the air damp horizontal motion? Do unbalanced loads on the pads generate horizontal forces? These questions may be unanswerable without conducting elaborate tests.

When a pilot kinesthetically controls in study 6, part of the rotary reaction of the vehicle to his motions is simulated by translation of the air pad dolly. The substitution of translational for rotational effects does not appear to be precise, based on a preliminary study of the equations of motion. The mathematical models of a flying vehicle and the simulator were derived separately. Both models assume the pilot and rotational vehicle centers of gravity coincide. The flying version did not contain the air pad dolly mass. Both derivations are shown in Appendix B. Also shown are transfer functions of pilot attitude per degree of his deflection from the thrust vector (eqs. (38) and (67)). No attempt was made to determine whether the simulator differences stabilized or destabilized the vehicle.

Simulations which do not utilize six degrees of freedom do not directly measure the total pilot workload and may lead to optimistic conclusions. As an example, a pilot may easily control a single degree of freedom which is four integrals removed. If, however, a disturbance or an erroneous input by the pilot happens, his entire concentration is required for a period of time to regain control. When other degrees of freedom are added, these periods of intense concentration on one variable permit the others to diverge. In this case whether the pilot can regain control in all variables depends on how rapidly he corrects each in turn. Because the recommended system must be one which allows the pilot time to make sequential corrections, a simulation which does not assess this feature is not reflecting the true navigation and control task. Typically, such a simulation results in higher pilot opinion ratings for each control method.

Optimistic flight performance answers may also be obtained from a limited degree of freedom simulator. Each time a small error occurs in a variable, a small increase in flight time accumulates. Frequently these errors, although corrected at once, result in additional maneuvering to reach the desired landing point and further contribute to flight time. Vacuum flights with human control elements consist of a steady influx of these errors in all axes, hence the flight time from one point to another is appreciably longer than limited degree of freedom simulations would predict. Disturbances which may be omitted when less than six degrees of freedom are simulated arise from the following sources:

1. Interaxis coupling due to cross products of inertia
2. Interaxis coupling due to cg misalignment with the neutral thrust vector
3. Euler angle coupling
4. Multiengine static and dynamic mismatches
5. Failure modes

Probably the most versatile simulation technique is the visual method. All of the dynamics of flight are calculated by an analog computer, while all of the man/machine interfaces are hardware. The analog mechanization may be easily and quickly modified to produce any desired variation in vehicle parameters. Much of the man/machine interface dynamics may be altered by changing the analog side. It is difficult, however, to give the pilot the feel of a real vehicle in all of his senses using a visual simulator. A wide screen on which a moving scene is projected may be used for visual cues, but other sensory cues must be obtained without large pilot motions since the screen cannot be moved with the pilot. This inherent lack of motion cues in visual simulators is one of its major deficiencies, and is especially important when simulating a rapidly responding vehicle. A study of this effect was conducted during 1968 using the NR/SD one-man propulsion device and the lunar flying vehicle visual simulation. Average frequencies were compared for various pitch and roll moments of inertia. Both the propulsion device and the visual simulation reflected earth conditions and kinesthetic control. The results of the study are shown in figure 2-10. They indicate that the visual simulation did not provide a good man/machine interface at very low values of moment of inertia but improved as moment of inertia was increased. It is believed that the two frequencies converge at increased moment of inertia because the pilot depends more on his vision for cues at higher inertias. Similar circumstances exist in everyday experiences. For example, on a flat surface with no obstructions present, a bicycle is easily stabilized by a blindfolded rider; his visual cues are not as rapidly interpreted as are his proprioceptive cues

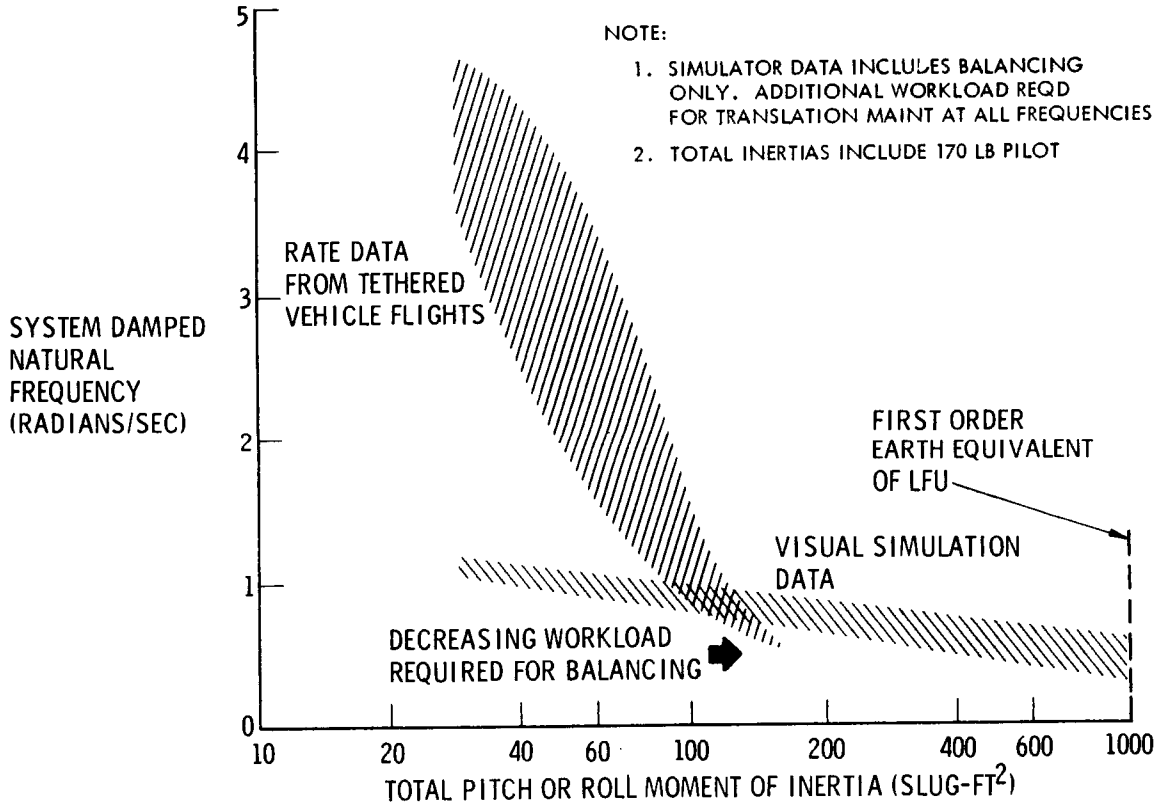

Figure 2-10. - Comparison of Flight and Visual Simulation Kinesthetic Data at 1 G

and serve better as a navigational information source. If the stability response frequency of the bicycle were decreased significantly, the rider's balance cues would become redundant with his visual cues and would no longer be necessary. The predominance of visual cues over proprioceptive cues at high moment of inertia seems to be true with a visual simulator also. Other visual simulator limitations include shortcomings of the scene and unrealistic controls and displays. All of these may be improved by using more elaborate equipment.

Probably the truest evaluation of a small, manned propulsion device in lunar conditions is obtained by combining the data from a tethered device with one-sixth gravity suspension and a visual simulation. Tasks could be divided between the two. The tethered device better evaluates short period influences such as stability, time critical emergency operation, and landing conditions; but cannot be used for navigational performance evaluations without exorbitant costs. Visual simulations lose short-period cues but provide the best source of complete flight data.

Nearly all of the limitations discussed have effects on handling qualities and performance which cannot be precisely measured. Their importance can only be discussed intuitively at this time. The relative merits and demerits of each study therefore become an issue subjective to argumentative skills. Since handling qualities are ultimately to be measured by pilot opinion, a better method of comparing studies is by using the opinion ratings. To assure that each pilot gains the perspective necessary to judge the studies, he must fly all of the simulators. Further qualifications are that a sufficient number of pilots fly the simulators and that they fly them in different orders to eliminate learning trends. The judgements given by the pilots would be relative and not absolute unless real vehicles in lunar environment were included. Thus astronauts with lunar landing experience should be a part of the pilot team. All of the simulated ratings would then be analyzed for consistency and the data would be used for voting on the ratings for each control mode, each mission phase, and each simulator. Incremental ratings would be established for limited degrees of freedom, differences between visual and flight vehicle simulators, and between simulations and real conditions based on lunar landings. To assure the validity of each rating a set of tests could be devised which would measure the moment of inertia of the vehicle and pilot, the vehicle sensitivity to command, and as much of the damping and disturbance moment influence as possible. These factors would comprise supplemental data to aid in establishing the simulator ratings.

To pursue the objective of gaining relative pilot opinion ratings between various studies, NR/SD has sent one pilot to fly several current simulators at NASA-MSC and NASA-Langley. The pilot reports are presented in reference 2-2 and his ratings are given in table 2-5.

In conclusion, it is felt that the required simulation effort for LESS has only begun. No simulation to date has adequately studied all of the candidate control methods. None has provided realistic environment for all aspects of LESS flight. During boost, high frequency effects involving stability should be simulated using six degree-of-freedom flight vehicles. The FLEEP promises to supply the required realism. Long term guidance and navigation aspects of the mission should be simulated using fixed base visual simulators as at NASA-LRC, with sufficient high frequency response included in the computer to produce the proper pilot workload. Orbital operations, from boost thrust termination through Apollo CSM docking, could also be simulated using techniques and equipment developed for the Apollo program.

For maximum effectiveness of simulations, a data recording format should be established. The resulting data are of vital importance in future LESS vehicle design. If a select group of pilots fly all the simulators, and use a common rating scale, the fidelity of the resulting data is assured.

Mathematical models used in the analyses. -

Mathematical modeling of the human pilot: If kinesthetic control is to be satisfactorily achieved, the LESS must be dynamically "matched" to the pilot's sensing and control force capabilities in much the same way an actuator/gyro package are "matched" to an airframe flight control system. Extensive tests with human subjects (see ref. 2-4 through 2-7) have revealed that pilots performing tracking tasks will assume transfer functions of the form:

$$\frac{\delta}{\theta_\epsilon} = K_{\rho\theta} e^{-\tau S}\left[\frac{(S + 1/T_L)}{(S + 1/T_N)}\right] = \frac{\text{Pilot Lean Angle}}{\text{Attitude Error}} \qquad (2\text{-}1)$$

where S is the Laplace transform variable. The transport delay, τ, represents two components: an inherent neuromuscular system delay which is relatively fixed and a mental computation time delay that depends on pilot workload. The time constant $1/T_N$ represents neuromuscular dynamics and is relatively fixed. He will adjust his gain $K_{\rho\theta}$, and his lead time constant, $1/T_L$, as necessary to obtain satisfactory kinesthetic control. That is, he will adjust $K_{\rho\theta}$ and $1/T_L$ such that the system is suitably stable and well damped, with sufficient bandwidth to meet performance requirements. His pilot opinion is closely related to the values of T_L and $K_{\rho\theta}$ and to the resulting vehicle closed loop performance. A vehicle requiring a T_L of zero for satisfactory stabilization would be rated "good" if the gain were not required to be too low ("touchy vehicle") or too high ("not enough control authority"). A T_L of 2 is difficult to generate and difficult to maintain and would earn the vehicle a "poor" rating. Similarly, very low or very high required values for $K_{\rho\theta}$, would earn a "poor" rating, while intermediate values earn "good" ratings. This is shown in figure 2-11.

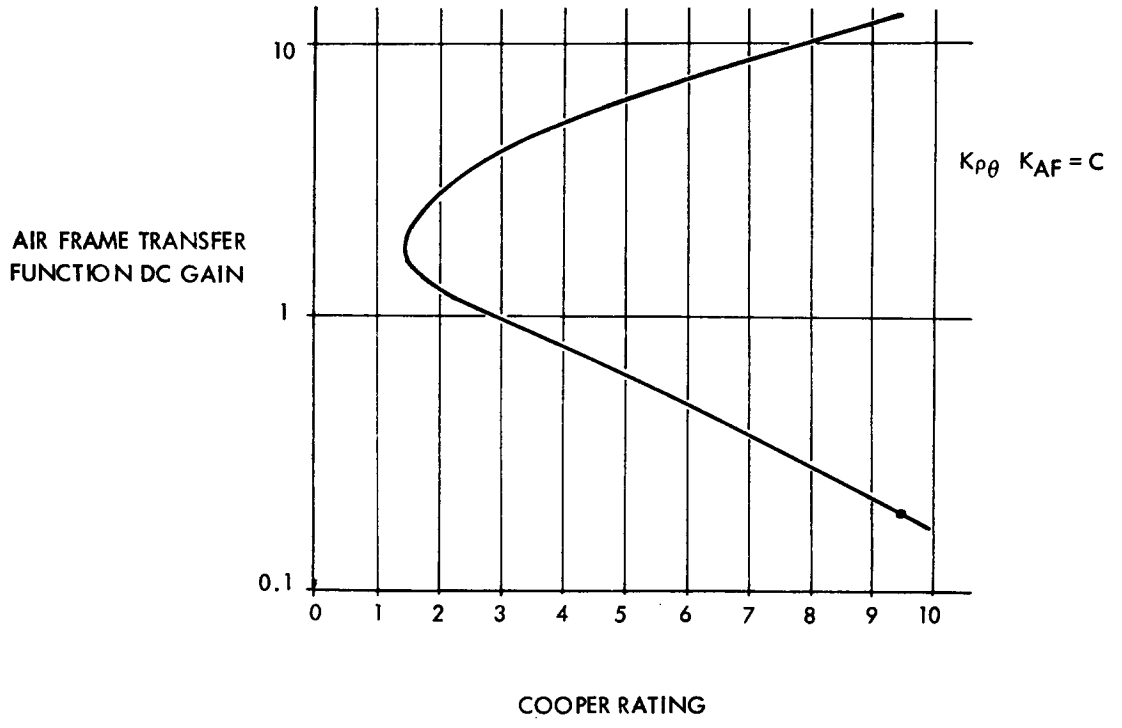

Figure 2-11. - Gain Requirements Versus Cooper Rating

These transfer functions suffice for steady-state tracking tasks involved in maneuvering the LESS but do not, of course, represent pilot characteristics under stress situations such as engine failure.

Assessing whether or not a vehicle has satisfactory handling qualities is a process conducted during test flights by engineering test pilots. It has been found through experience that test pilots comprise a highly trained group, and their ratings of a given vehicle are reasonably consistent. The standard method used for a number of years to rate vehicle handling qualities is the Cooper Rating scale. The Cooper scale forms the basis for a quantified weighting of a test pilot's evaluation. The basic Cooper scale is shown in table 2-1. Cooper ratings for a given vehicle depend upon the workload imposed on the pilot. Thus, deficiencies not especially objectionable when only pitch, yaw, and roll attitude are to be controlled might become very objectionable if a complicated guidance display must also be interpreted to obtain attitude commands. Failure to meet performance requirements despite intensive efforts will cause degraded opinion.

This implies that the Cooper rating is decremented by additional tasks in this fashion:

$$R = R_{BEST} - \sum \Delta R_{TASKS} \tag{2-2}$$

For example, the Cooper rating is heavily influenced by the value of pilot lead required, as shown in figure 2-12, and the vehicle is decremented for each T_L the pilot must generate. Adding more variables to the control task would cause further decrementing.

To be considered operational, a vehicle must consistently earn a Cooper rating of four or better.

Mathematical modeling of the one-body kinesthetic vehicle: The kinesthetic method of controlling the LESS results in a model with four simultaneous differential equations of motion if the following assumptions are used:

1. Single plane motion only

2. Vehicle center of gravity and pilot feet are coincident.

Figure 2-13 defines the nomenclature. The derivation of the equations are presented in Appendix C. Resulting from the derivation is the transfer function for the response of pilot attitude to his control input:

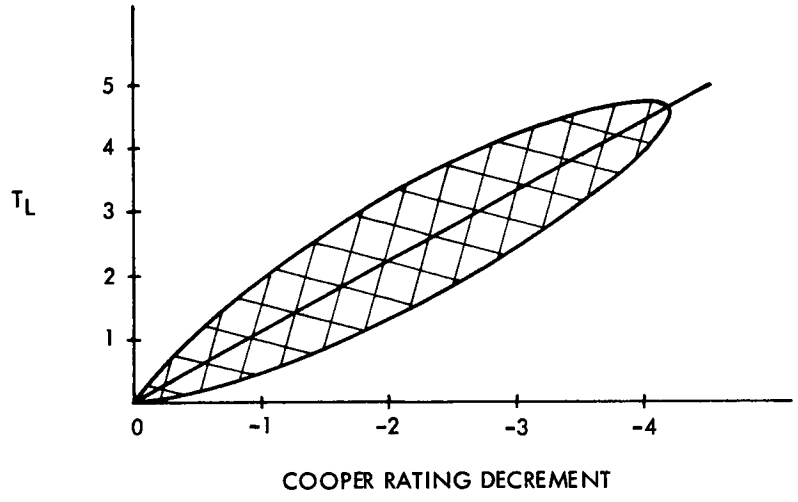

Figure 2-12. - Pilot Lead Versus Cooper Rating Decrement

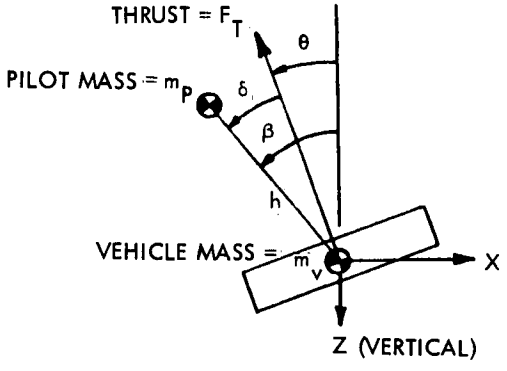

Figure 2-13. -. Dynamic Model for Kinesthetic Control

$$\frac{\beta}{\delta} = \frac{I_v}{I_p + I_v + \left(\frac{m_p m_v}{m_p m_v}\right) h^2} \left[\frac{s^2 + \frac{F_t h}{I_v}\left(\frac{m_p}{m_t} + 1\right)}{s^2} \right] \qquad (2\text{-}3)$$

Mathematical modeling of the two-body kinesthetic vehicle: This model is derived using the same assumptions as was used for the single body kinesthetic model, but is much more complex. A sketch of the vehicle geometry is shown in figure 2-14. A computer program was used to reduce the linearized equations to transfer functions evaluated at specific root locus point; hence, no general equation similar to Equation (2-3), above, is available. The derivation is shown in Appendix D.

Kinesthetic control analyses. -

Analysis of kinesthetic control with a one-body vehicle: This section discusses handling qualities questions for the LESS under kinesthetic control. That is, can a human pilot stabilize, control, and guide the LESS by himself, without the aid of stability augmentation systems? This question is amenable to the techniques of aircraft handling qualities analysis. It will be discussed here using test data and math models developed by McRuer, Ashkenas, et. al. as well as lunar flying vehicle flight test and visual simulator experience. The efforts presented here attempt to predict pilot opinion ratings of the kinesthetically controlled LESS. Vehicle constraints due to handling qualities requirements are identified and estimates made of excess pilot workload capacity for ancillary guidance tasks.

Figure 2-15 shows the two-body action-reaction characteristics that occur in the kinesthetic control concept. This effect is identical to the "tail-wags-dog" phenomenon encountered in launch vehicle control system design and depends in its essence upon the mass/moment of inertia ratios between pilot and airframe. It will shortly be shown that increasing vehicle inertia and mass (pilot is relatively fixed) degrades system bandwidth capabilities, hence makes for sluggish, conditionally stable systems. This is only one of the factors involved in the handling qualities problem.

Figure 2-16 shows attitude command histories for a typical LESS ascent to a 40-nautical mile trajectory, using a calculus of variations solution and a three-step approximation to the calculus of variations. Handling qualities studies of manned aircraft (for example, ref. 2-5) have shown pilots prefer the overall stabilization and control system damping ratio to be in excess of about 0.3. Values less than this degrade pilot opinion because the airframe is very oscillatory, and stability margins are small.

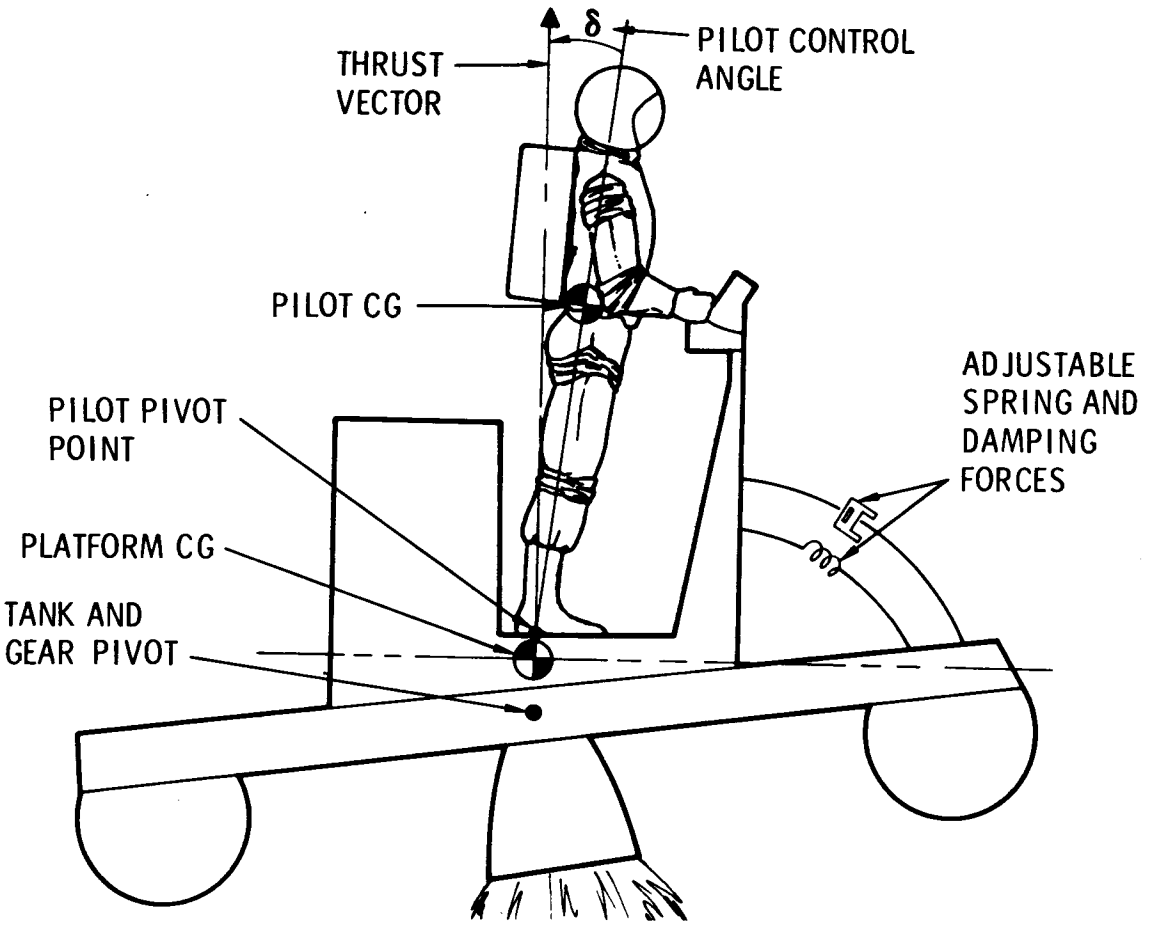

Figure 2-14. - Gimbaled Platform LESS

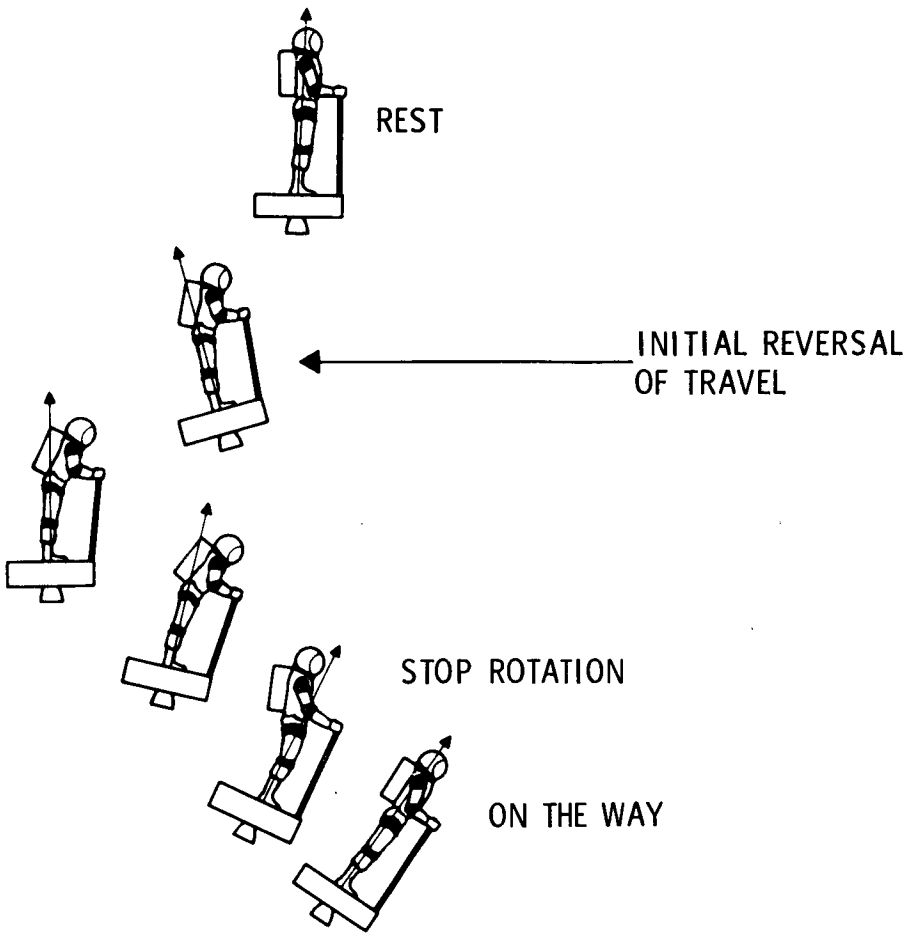

Figure 2-15. - LESS Kinesthetic Control
Action-Reaction Effect

An estimate to overall system bandwidth requirements may be made by assuming the guidance mode should have enough bandwidth to perform at least ten corrective maneuvers during the ascent. This makes for a guidance system bandwidth of at least:

$$\omega_{N_{GUIDANCE}} = \frac{2\pi 10}{400} = 0.156 \text{ radians/sec} \qquad (2\text{-}4)$$

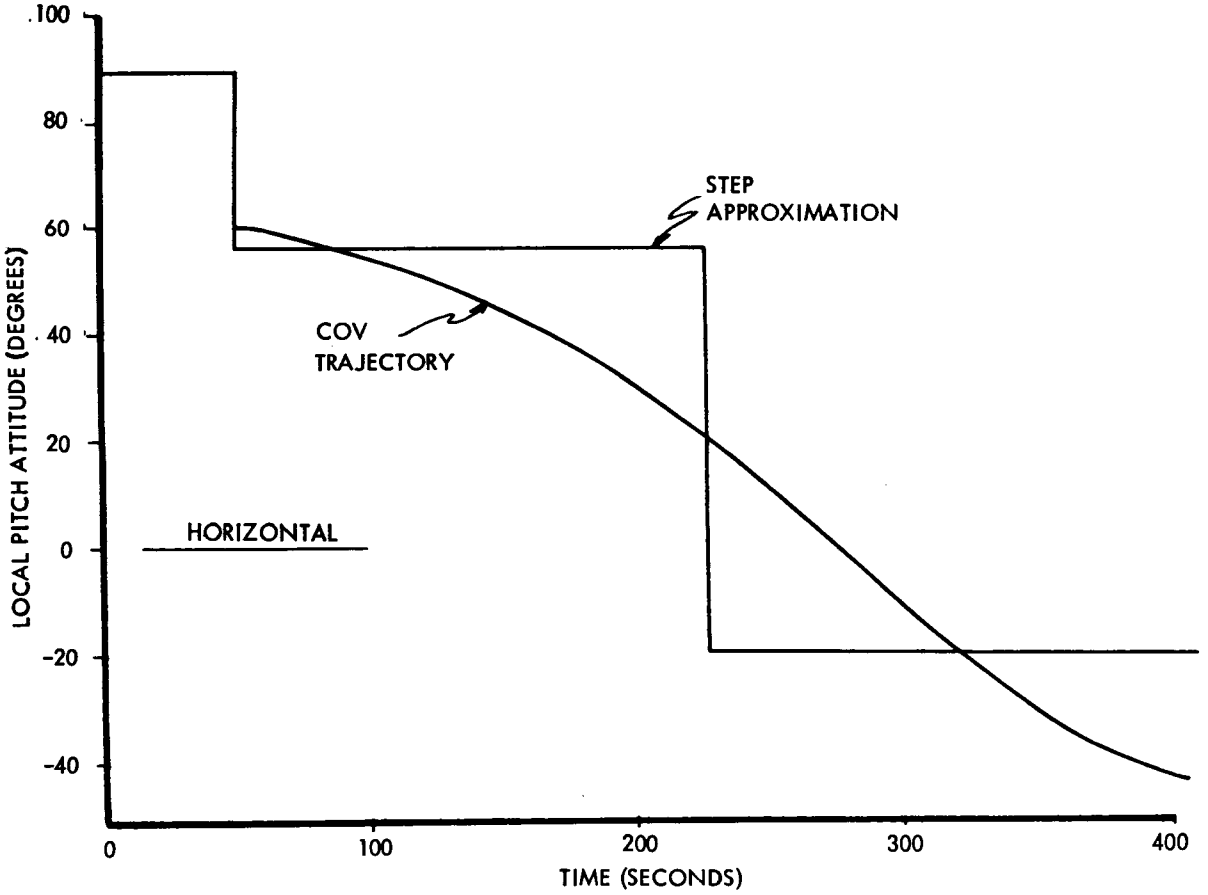

Figure 2-16. LESS Pitch Attitude Profile

The dynamics of the stabilization and control system should be well removed from those of the guidance system. Using the 10:1 separation rule:

$$\omega_{N_{SCS}} = 10\ \omega_{N_{GUIDANCE}} = 1.6\ \text{RAD/SEC} \qquad (2\text{-}5)$$

Taking another approach, the steps of the three-step approximation to the COV are approximately 175 seconds long. The two percent settling time is $4/\zeta\omega_N$. Considering that the settling time should be 1/10 of the step length:

$$\omega_{N_{SCS}} = \frac{4}{\zeta \times 175/10} = 0.76\ \text{RAD/SEC} \qquad (2\text{-}6)$$

The conclusion is that system bandwidth should be between 0.76 rad/sec and 1.6 rad/sec and system damping ratio ≥0.3. The higher bandwidth number will be used, for a conservative analysis.

By way of comparison, the Apollo SCS thrust vector control system and the Apollo SCS attitude TVC system characteristics are shown in table 2-6. Both vehicles perform roughly the same sort of burns as LESS, and hence the stated requirements seem reasonable.

For the Configuration C of LESS shown in the Contract Proposal table 2-7 lists pertinent parameters. This configuration is similar to figure 3-2 in this report.

TABLE 2-6. - TVC SYSTEM PERFORMANCE REQUIREMENTS

Vehicle	Bandwidth	Burn Time
Saturn S-II	0.5 ⟶ 1.5 rad/sec	~360 sec
Apollo ATVC (LM off)	0.8 ⟶ 1.3 rad/sec	~245 sec (TEI)
LESS	0.76 ⟶ 1.6 rad/sec	~400 sec

TABLE 2-7. - LESS CONFIGURATION C PARAMETERS
(EARLY VERSION OF FIGURE 3-1)

F_T = 1350 lb	h = 3.62 ft
m_p = 11.78 slugs	m_v = 71.2 slugs (full tanks)
I_p = 18.4 slug ft^2	I_v = 481.5 slug ft^2

Insertion of these numbers yields the transfer function:

$$\frac{\beta}{\delta} = \frac{0.685\ (S^2 + \overline{3.4^2})}{S^2} \qquad (2\text{-}7)$$

The pilots transfer function is similar to that derived in reference 2-7 from test data on subjects, with the following exceptions:

1. Reference 2-7 determined the transport delay to be 0.15 sec based on a one-axis tracking task and shirt-sleeve subject. Considering this analysis to be one plane of a three-axis overall task, it seems reasonable to double the above number to account for the added workload. Therefore, τ = 0.3 sec for this analysis.

2. A neuromuscular lag $1/T_N$ has been added, in accordance with reference 2-6.

With these restrictions in mind, the system block diagram is that shown in figure 2-17.

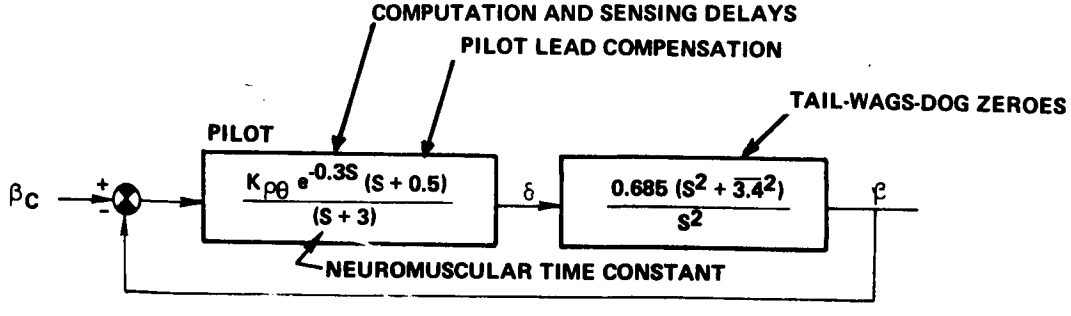

Figure 2-17. - LESS Kinesthetic Control Block Diagram

Considering the transport delay to be approximated by a first-order Padé approximation, the characteristic equation of loop closure becomes:

$$1 - \frac{0.685\ K_{p\theta}\ (S - 6.7)\ (S + 0.5)\ (S^2 + \overline{3.4}^2)}{S^2\ (S + 3)\ (S + 6.7)} = 0 \qquad (2\text{-}8)$$

The negative closure, corresponding to a zero degree locus, is used because of the right half plane root.

The root locus for this closure is shown in figure 2-18. The criteria for closure gain was a requirement for at least 6-db gain margin. As can be seen, the system is conditionally stable. It barely meets the system performance requirements. A pilot lead at -0.5 is required for the stabilization; and in accordance with figure 2-12, the basic Cooper rating is degraded by 1-1/2 to 2 points. An estimate of the Cooper rating for this system would be 5-6, since considerable pilot compensation is required to meet performance requirements.

The transport delay is now increased to 0.5 sec, representing pilot effort to accomplish a relatively simple guidance and navigation task. The root locus for this system is also shown in figure 2-18. It is noted that the very slight increase in transport delay cuts the system bandwidth in half, representing a tremendous system sensitivity to transport delay. Estimated Cooper rating for this system is 8-9, or totally unsatisfactory.

Figure 2-19 shows the various control variables to be discussed next. β is the pilot lean angle referenced to inertial space (i.e., the ground), while θ is the angle made by the thrust vector with respect to inertial space. Guided missiles, such as the Saturn V, have an instrument unit on the rocket body which essentially controls with respect to β. Pilots flying LFV type vehicles also tend to control to the angle made by their body with respect to the ground. A gyro horizon mounted to the LESS structure will reference to θ. Although the two variables differ only by lean angle, essential differences will be noted in system stability characteristics when controlled to either θ or β. A generic β root locus is shown on the bottom of figure 2-19, and it is noted to be similar to those shown in figure 2-18. If the LESS is controlled to a gyro horizon display, the block diagram shown in figure 2-20 results; and it is immediately noticed that the imaginary axis tail-wags-dog zeroes familiar to missile control system designers have moved from the imaginary axis to a conjugate pair of real zeroes. A generic root locus is shown in figure 2-20, and actual root loci for LESS Configuration C (an early version of figure 3-1) is shown in figure 2-21. Comparison of figure 2-21 with figure 2-18 shows less degradation with increasing pilot transport delay and also slightly better overall damping and bandwidth.

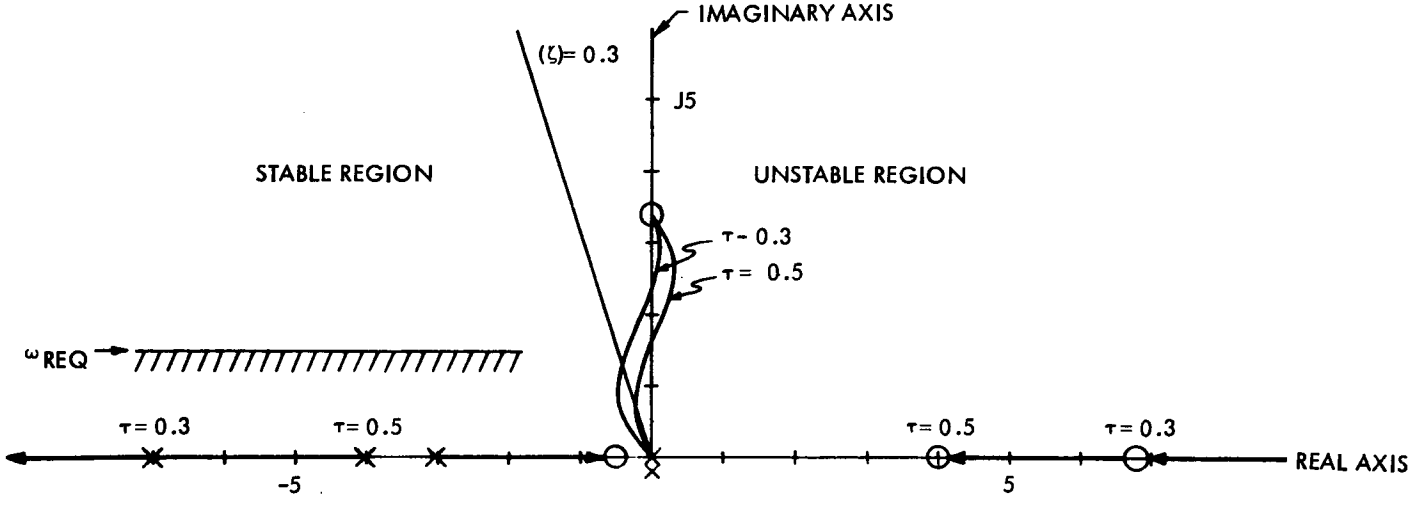

Figure 2-18. - LESS Kinesthetic Control Root Locus β Closure

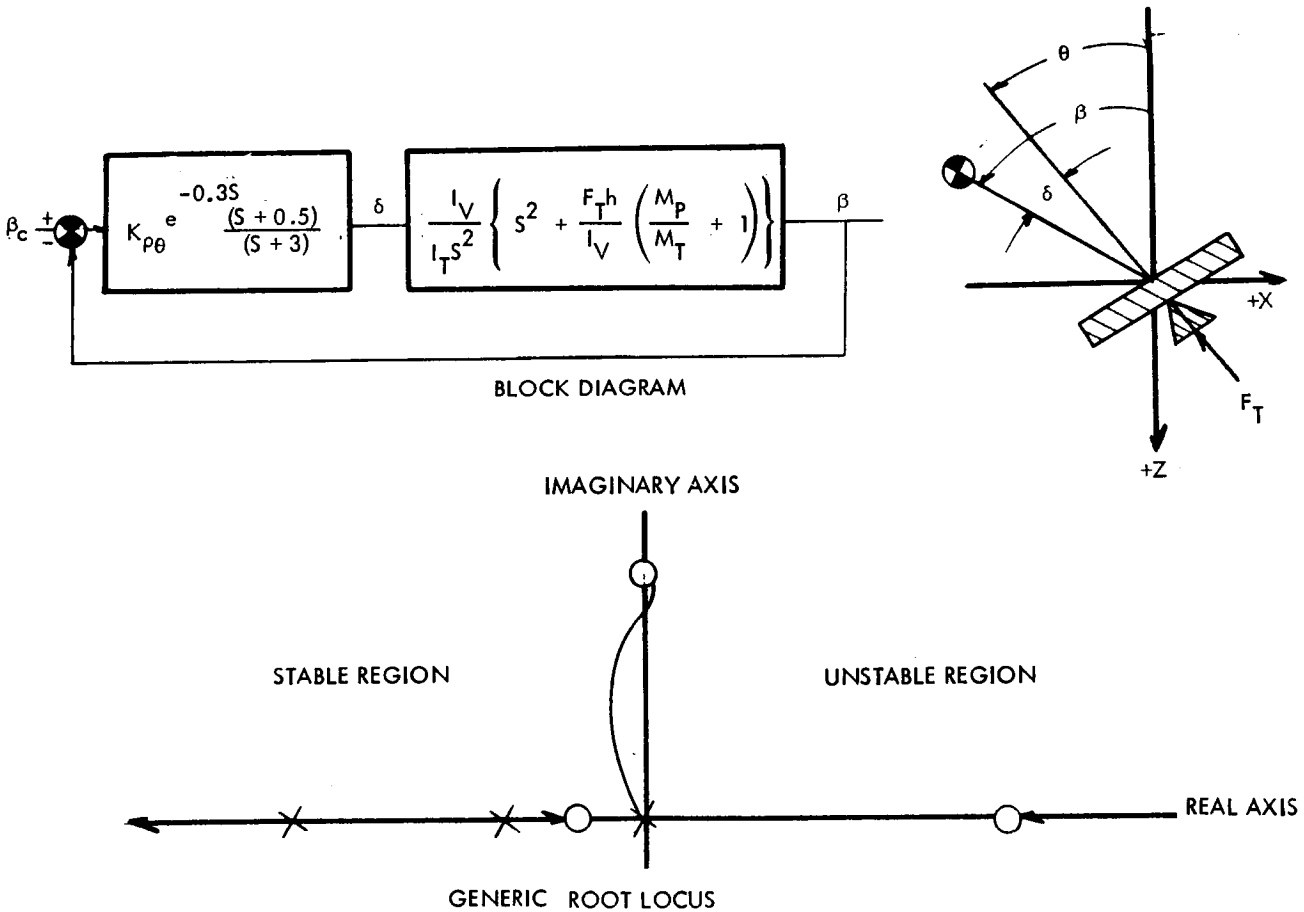

Figure 2-19. - LESS Kinesthetic Control β Closure

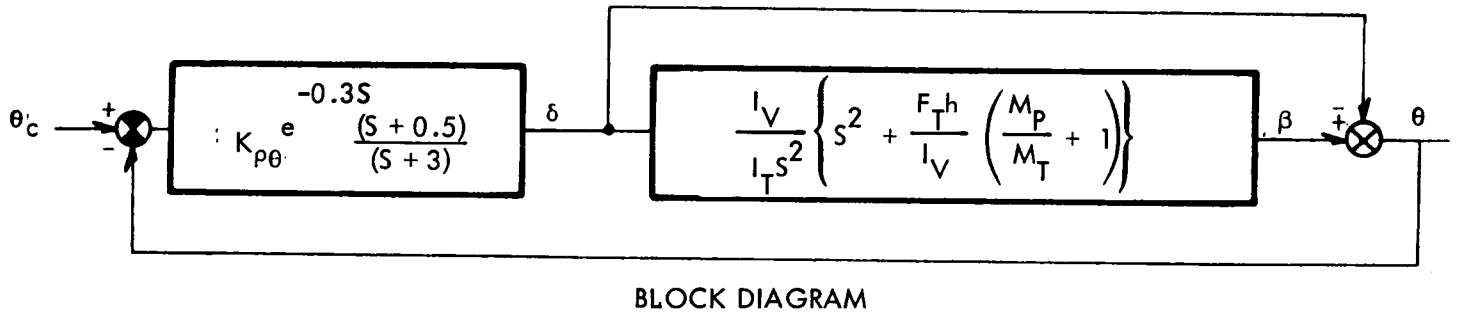

BLOCK DIAGRAM

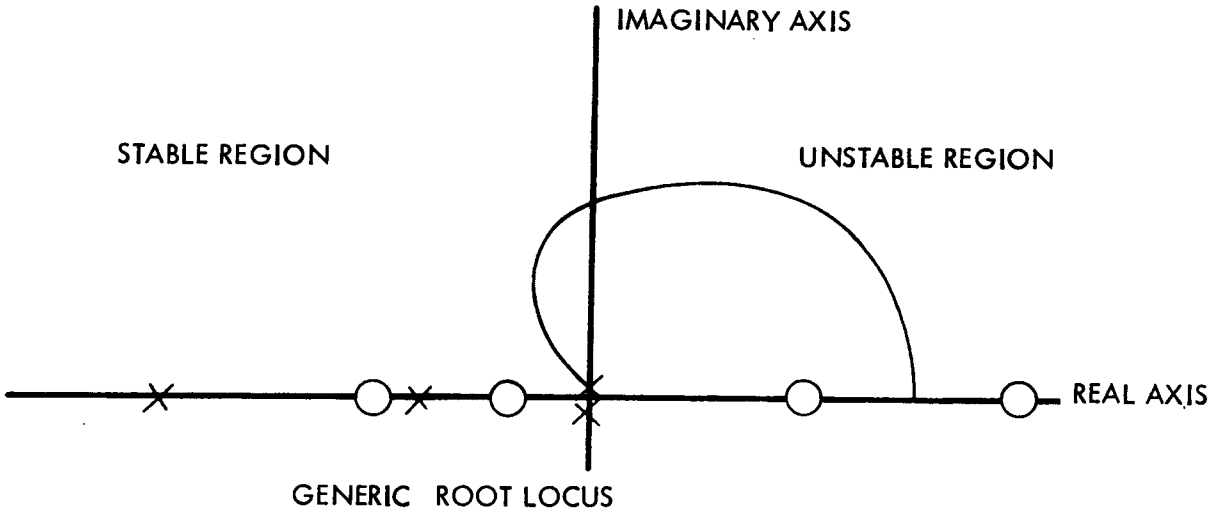

GENERIC ROOT LOCUS

Figure 2-20. - LESS Kinesthetic Control θ Closure Block Diagram

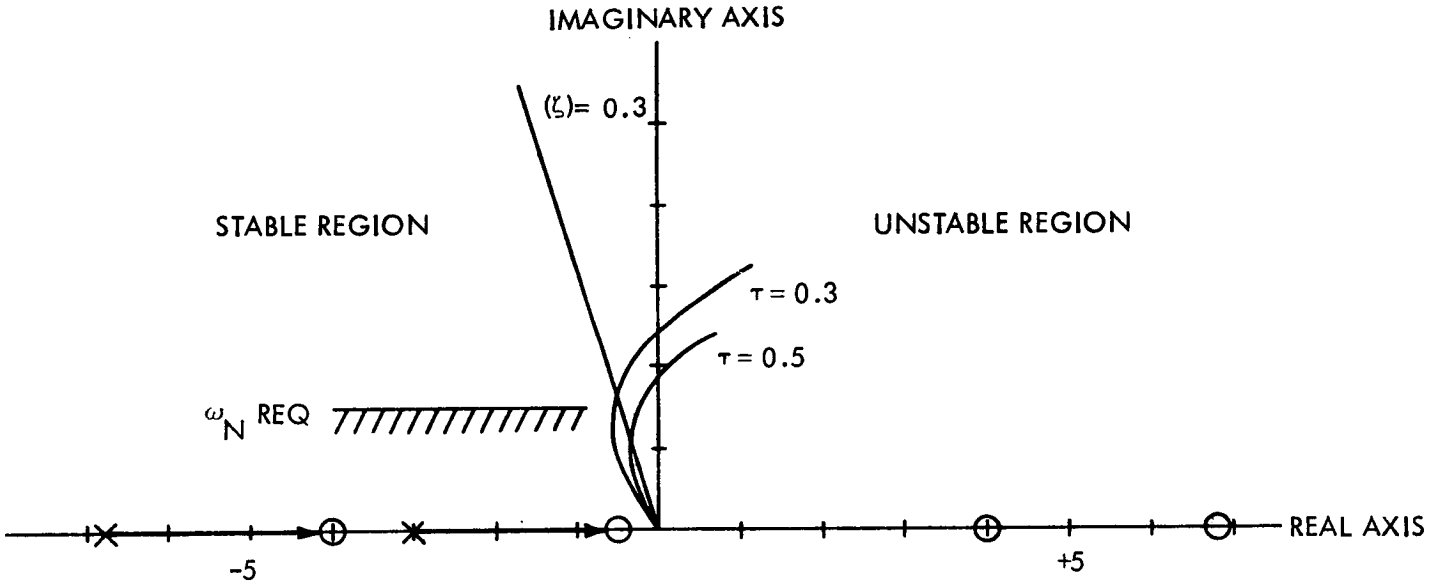

Figure 2-21. - LESS Kinesthetic Control θ Closure

Thus the conclusion is made that θ control, using a gyro horizon, is inherently superior from a controllability standpoint to schemes referencing the pilots body angle with respect to the ground.

The conclusions which may be drawn from this analysis are as follows:

1. Kinesthetic control is capable of meeting LESS stabilization and control performance requirements.

2. LESS handling qualities with kinesthetic control would be rated as "unacceptable-very poor" or a Cooper rating of 5-6 for LESS Configuration C (an early version of figure 3-1).

3. The basic control and stabilization task imposes a very heavy workload on the pilot.

4. Momentary distractions, incorrect control inputs, or increased pilot workload are likely to lead to loss of vehicle control.

5. Guidance, navigation, and display monitoring tasks must pose very low workloads for this control mode to be satisfactory.

6. Control to a gyro horizon display fixed to the LESS platform (θ control) is slightly more stable and poses a lower workload to the pilot than schemes which reference pilot body angles to inertial space (β control).

Analysis of kinesthetic control with a two-body vehicle: A brief investigation of the gimbaled-platform LESS was conducted using the matrix equation derived and shown in figure 2-22. The basic parameters from the previous analysis were used, along with various values of spring, dashpot constant, and pilot's transport delay. Expansion of the matrix shown in figure 2-22 yielded the system transfer functions shown in figure 2-23. A root locus analysis was then conducted using the pilot models from the previous analysis and the transfer functions from figure 2-23. The root loci are shown in figures 2-24 through 2-28 and are summarized in table 2-8.

The root loci show that the external spring masses (fuel tanks, etc.) form a dipole pair very much like a missile bending mode pair. A difference is that the frequency and damping ratio of this dipole pair can be easily adjusted with the spring-dashpot. This is clearly shown between figures 2-24 and 2-27. Figure 2-27 used a low spring rate and a small dashpot with the result that the system can go unstable at the dipole pair given sufficient system gain. Figure 2-24 shows that the dipole pair becomes unconditionally stable when the spring and dashpot are increased to the values shown.

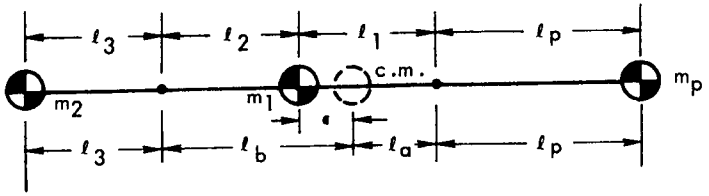

$$\ell_a = \ell_1 - \epsilon \qquad \ell_b = \ell_2 + \epsilon$$

$$\begin{bmatrix} I_V S^2 & \left[I_2 + m_2 \ell_3 (\ell_3 + \ell_b)\right] S^2 + \frac{m_2}{m_T} \ell_3 F_{T_1} + \left[\frac{m_p}{m_T}(\ell_1 + \ell_p) + \ell_2\left(1 - \frac{m_2}{m_T}\right)\right] F_{T_2} & \left[I_p + m_p \ell_p (\ell_p + \ell_a)\right] S^2 - \frac{m_p}{m_T} \ell_p \left(F_{T_1} + F_{T_2}\right) \\ \left[I_2 + m_2 \ell_3 (\ell_3 + \ell_b)\right] S^2 & \left[I_2 + m_2\left(1 - \frac{m_2}{m_T}\right)\ell_3^2\right] S^2 + B\ell_4^2 S + K\ell_4^2 + \frac{m_2}{m_T} \ell_3 F_{T_1} & \frac{m_2}{m_T} m_p \ell_p \ell_3 S^2 \\ \left[I_p + m_p \ell_p (\ell_p + \ell_a)\right] S^2 & \frac{m_2}{m_T} m_p \ell_p \ell_3 S^2 + \frac{m_p}{m_T} \ell_p F_{T_1} & \left[I_p + m_p \ell_p^2\left(1 - \frac{m_p}{m_T}\right)\right] S^2 - \frac{m_p}{m_T} \ell_p \left(F_{T_1} + F_{T_2}\right) \end{bmatrix} \begin{bmatrix} \theta \\ \rho = \lambda \\ \delta \end{bmatrix} = \begin{bmatrix} 0 \\ 0 \\ -1 \end{bmatrix}$$

Figure 2-22. - Gimbaled-Platform LESS Equations of Motion

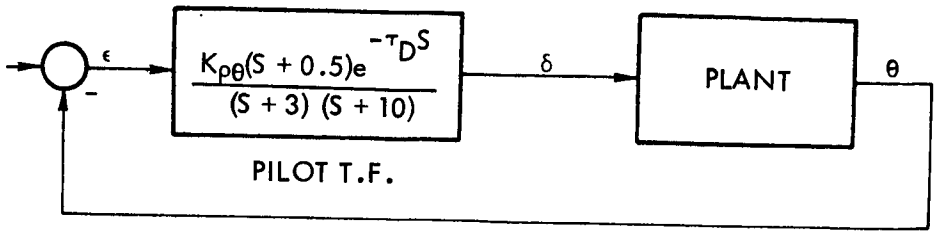

$0.3 \leq \tau_D \leq 0.50$ $\qquad e^{-\tau_D S} \simeq \frac{S - 2/\tau_D}{S + 2/\tau_D}$

$K_{p\theta} = 26.$ (NOMINAL)

PLANT: $\qquad (K = 4500. \qquad B = 500.)$

$$\frac{\theta}{\delta} = \frac{(S + 1.92)(S - 1.90)\left[S^2 + 2(0.20)(4.2) + \overline{4.2}^2\right]}{S^2\left[S^2 + 2(0.34)(6.6) + \overline{6.6}^2\right]}$$

$K = 10\,000. \qquad B = 1000.$

$$\frac{\theta}{\delta} = \frac{(S + 1.89)(S - 1.88)\left[S^2 + 2(0.28)(6.0) + \overline{6.0}^2\right]}{S^2\left[S^2 + 2(0.47)(9.7) + \overline{9.7}^2\right]}$$

Figure 2-23. - LESS Model for Study

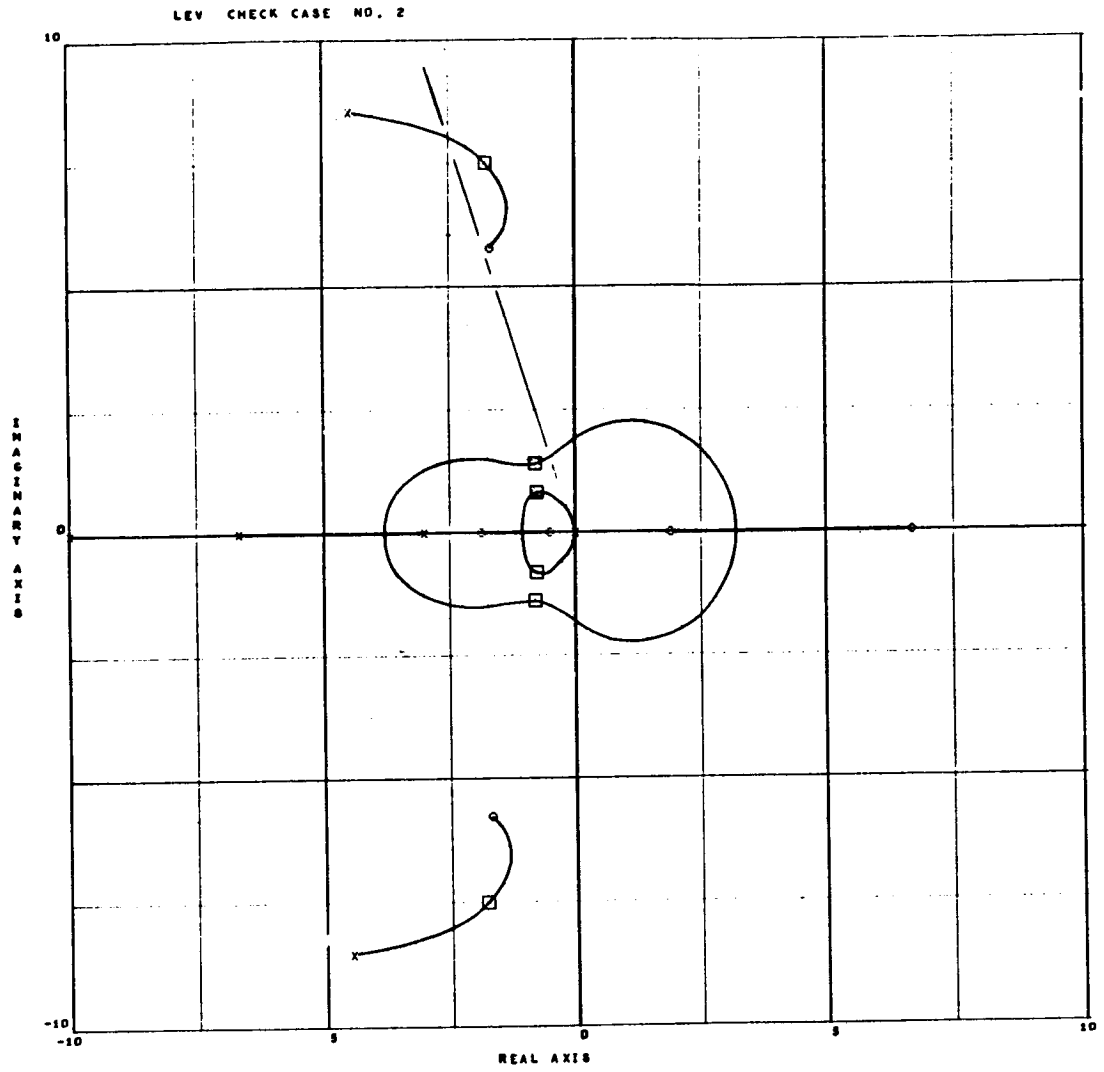

Figure 2-24. - Root Loci for the Gimbaled - Platform LESS, K = 10 000, B = 1000, τ_D = 0.30

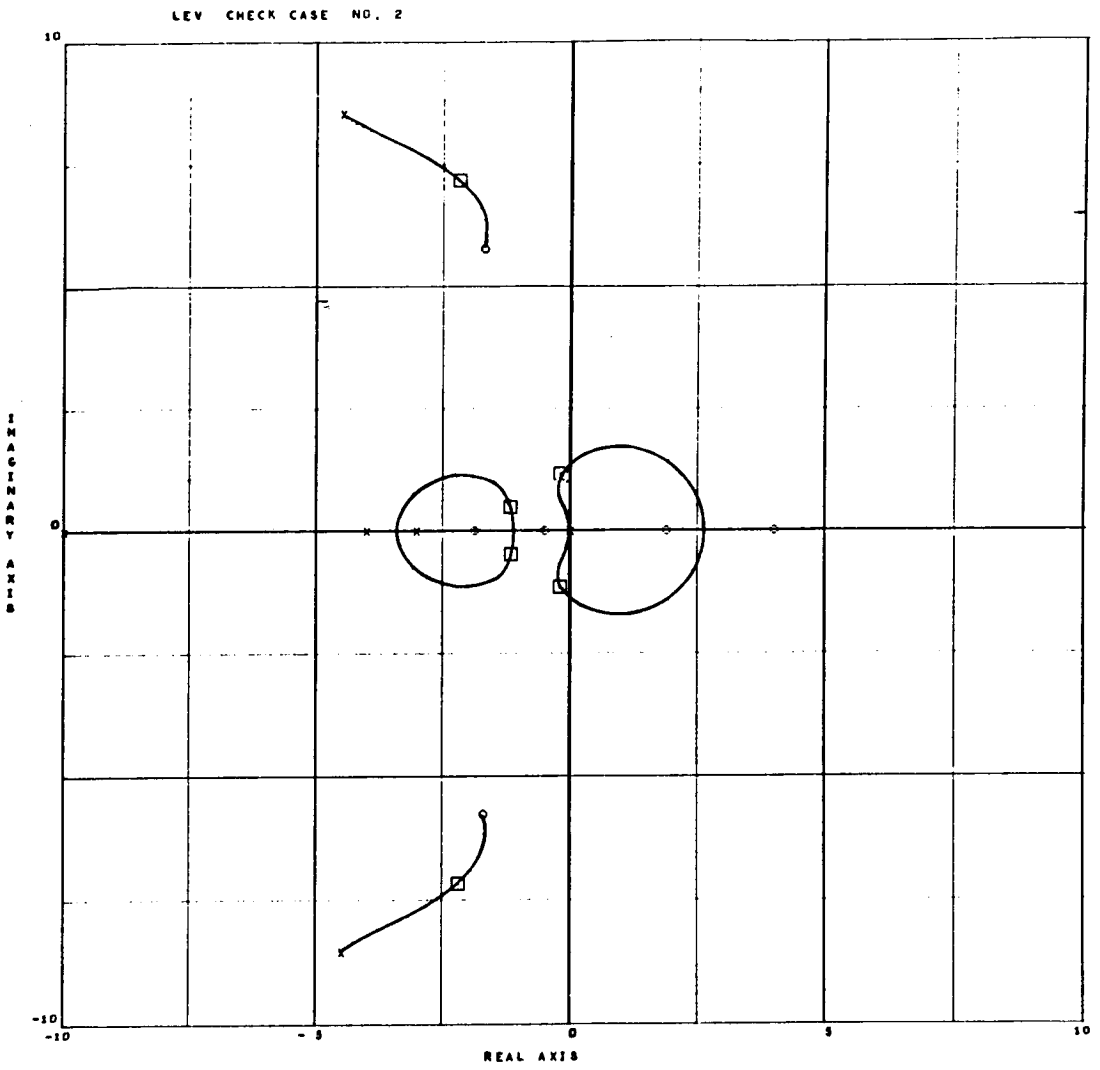

Figure 2-25. - Root Loci for the Gimbaled - Platform LESS, K = 10 000, B = 1000, τ_D = 0.50

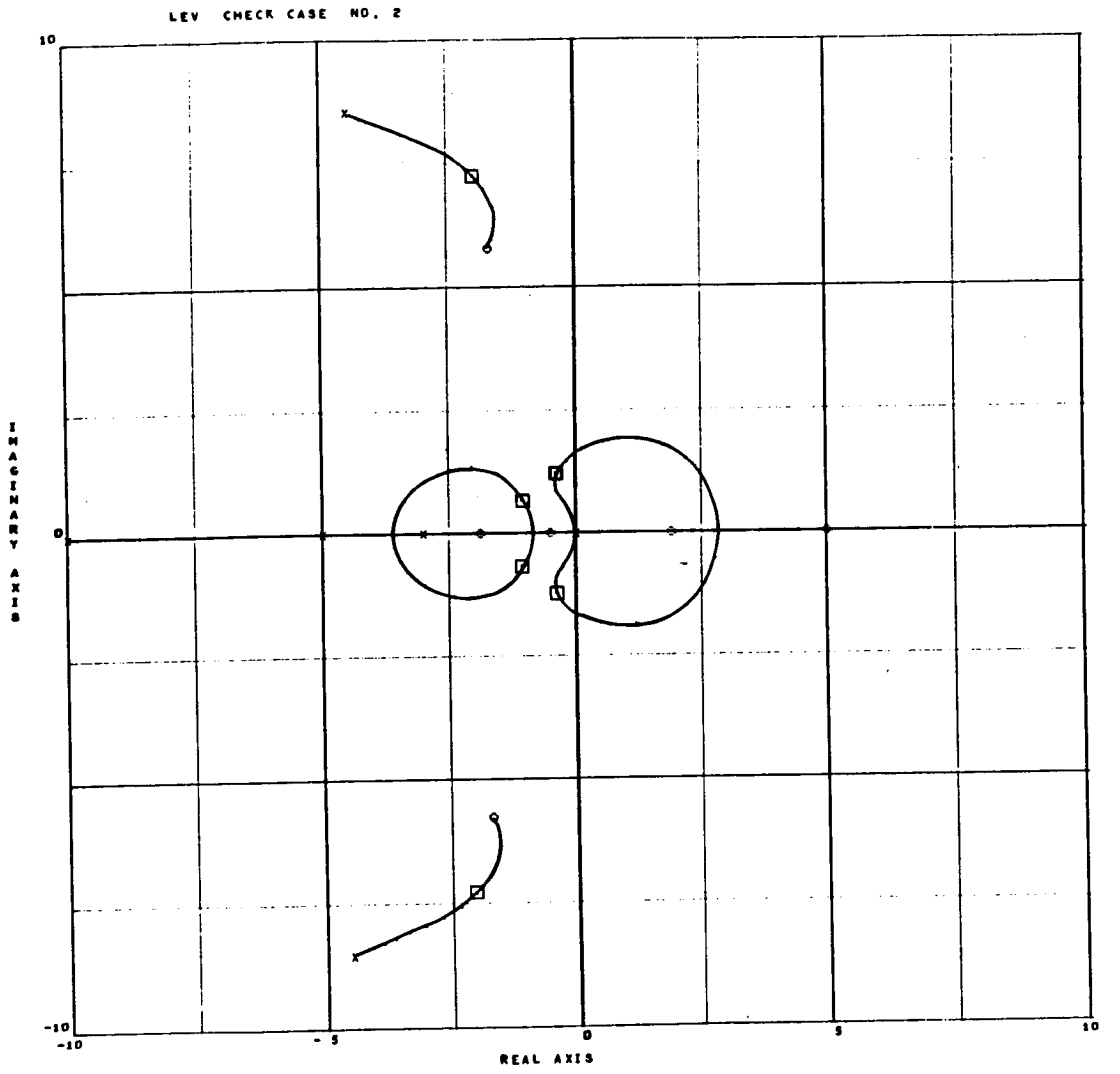

Figure 2-26. - Root Loci for the Gimbaled - Platform LESS, $K = 10\,000$, $B = 1000$, $\tau_D = 0.40$

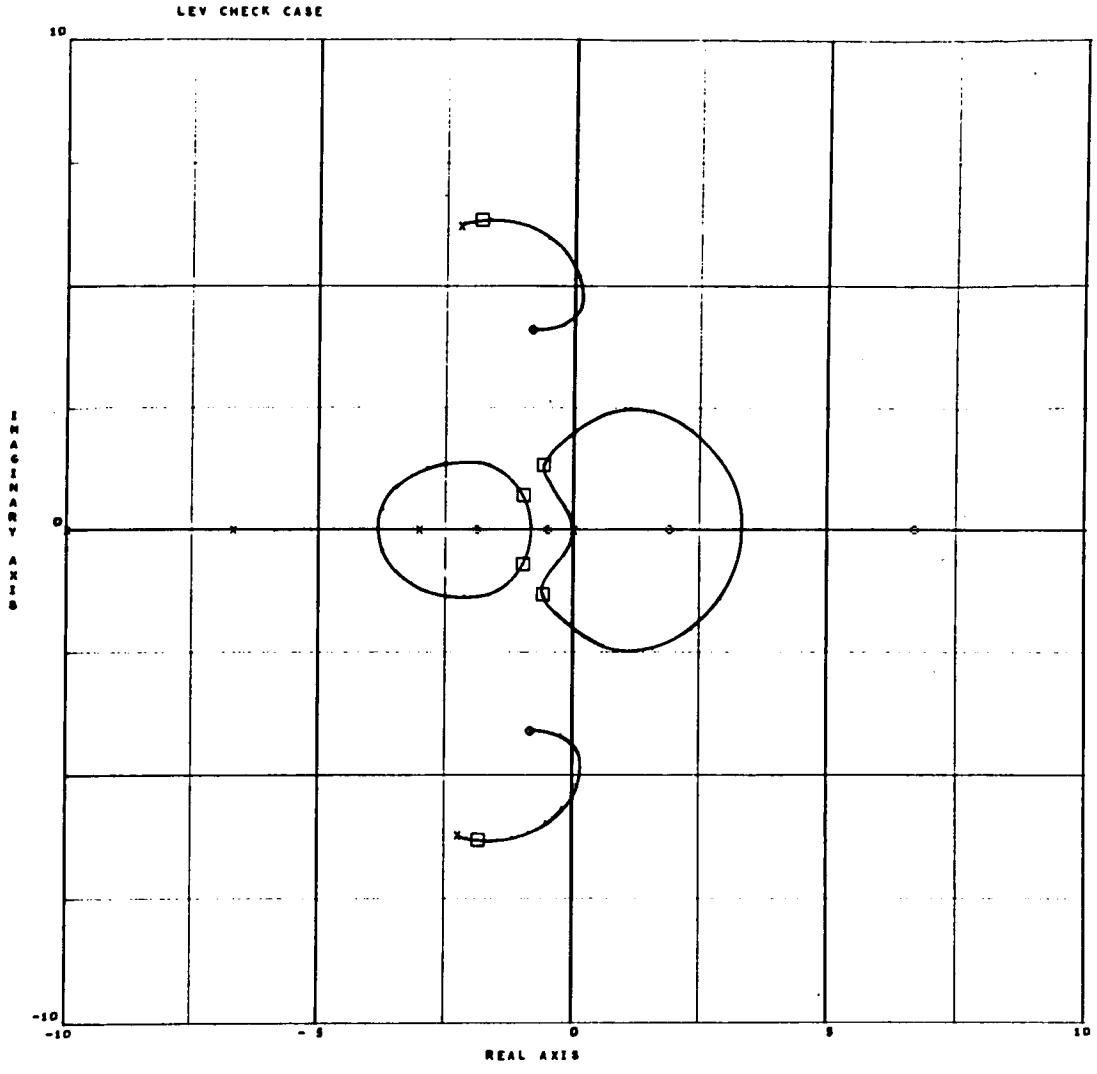

Figure 2-27. - Root Loci for the Gimbaled - Platform LESS, K = 4500, B = 500, τ_D = 0.30

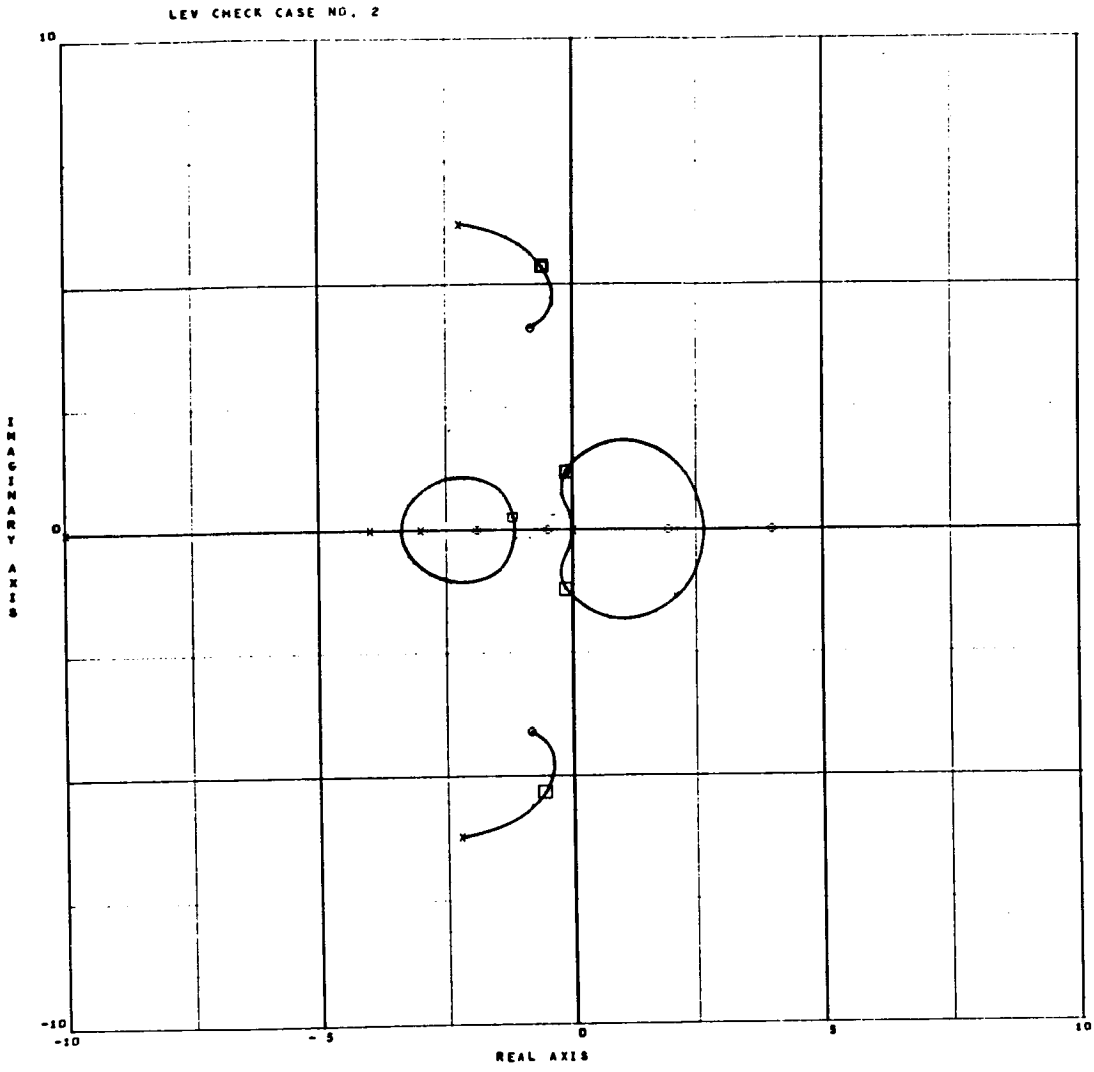

Figure 2-28. - Root Loci for the Gimbaled - Platform LESS, $K = 4500$, $B = 500$, $\tau_D = 0.50$

TABLE 2-8. - LESS CLOSED-LOOP TRANSFER FUNCTION ROOT VARIATIONS FOR PARAMETERIZATION OF τ_D, K, AND B. ($K_{\rho\theta}$ = 26.)

Case No.	τ_D (sec)	K (lb/ft)	B $\left(\frac{\text{lb-sec}}{\text{ft}}\right)$	Real Root at	Complex Roots					
					ω_1	ζ_1	ω_2	ζ_2	ω_3	ζ_3
1	0.30	10000.	1000.	39.3	1.10	0.681	1.61	0.503	7.72	0.230
2	0.40	10000.	1000.	37.4	1.25	0.842	1.28	0.289	7.58	0.266
3	0.50	10000.	1000.	36.3	1.25	0.927	1.18	0.150	7.50	0.290
4	0.30	4500.	500.	38.0	1.21	0.812	1.45	0.410	5.67	0.298
5	0.50	4500.	500.	34.9	1.23	0.976	1.20	0.116	5.39	0.110

Parameterization of pilot transport delays showed that the system suffered slightly less degradation with increasing transport delay and hence would be able to devote more of his workload to a guidance task. Thus it is concluded that the gimbaled platform configuration has advantages over the conventional kinesthetic configuration. It renders the system slightly less sensitive to transport delay and is capable of reducing pilot attitude gain requirements for very large, sluggish, vehicles. This would improve the configuration's Cooper rating. Gimbaling the platform does introduce design complexities which would weight against its stabilization and control advantages in a vehicle configuration tradeoff analysis.

The conclusions that may be drawn from this analysis are as follows:

1. The gimballed platform version of LESS Configuration C (an early version of figure 3-1) is slightly less sensitive to pilot transport delay than the ungimbaled version, and thus is capable of supporting a higher work loading.

2. Stabilization of the spring-mass mode of the gimbaled platform version of LESS is easily accomplished by adjustment of the spring-dashpot combination.

3. The gimbaled platform configuration is feasible, shows advantages over the conventional kinesthetic configurations, and should be investigated further. The gimbaled platform configuration does have design complexities that would weigh against it for an actual mechanization.

Hardwire control analysis. -

Analysis of the basic hardwire control system: The LESS Configuration C (an early version of figure 3-3) hardwire control system stability characteristics were examined and found to be capable of exceeding LESS control performance requirements. It is somewhat less sensitive to transport delay than the kinesthetic control mode and hence could tolerate a less sophisticated guidance and navigation display. An important advantage of the hardwire system is that handling qualities can be optimized by adjusting the hand controller gear ratio, leaving the airframe designer free to work to minimum envelope packaging constraints. It is estimated that the system is capable of a Cooper rating of 4.5, which is acceptable.

A hardwire control system, such as the Apollo direct mode manual TVC system, is defined here as one in which the engine is gimbaled directly by the hand controller, without use of gyro signals within the stabilization loop. Such systems are attractive when the engine is small because of their extreme simplicity. Larger engines require power boost systems and hence lose some simplicity.

In common with kinesthetic control means, the pilots visual, vestibular, and proprioceptive capabilities are used for sensing; and his neuromuscular system is used for actuation. Thus the hardwire system is very similar to kinesthetic control. It has an advantage in that thrust vector control is achieved by gimbaling small engines rather than by tilting the entire pilot. Intuitively, one would expect hardwire control to be preferable to kinesthetic for large moment of inertia vehicles, because larger control bandwidths are achievable when gimbaled mass is kept small. The system block diagram is shown in figure 2-29. Because the gimbaled engine is small, the quadratic zero pair discussed in the kinesthetic control analysis is not considered. The data shown in figure 2-29 is for the LESS Configuration C (an early version of figure 3-3) of the Contract Proposal. We have for the characteristic equation of the loop closure:

$$1 + \frac{1.82\, K_{\rho\theta}\, (S - 2/\tau)\, (S + 0.5)}{(S + 2/\tau)\, (S + 3)\, (S^2)} = 0 \qquad (2\text{-}9)$$

This characteristic equation is shown in figure 2-30 as a zero-degree root locus to account for stable control of a non-minimum phase system. The performance requirements derived for the kinesthetic control mode are shown as feathered lines in figure 2-30. To be satisfactory, the closed loop dominant roots must lie to the left of the 0.3 damping ratio line and above the 1.5 rad/sec bandwidth line. The transport delay parameter, τ, is a measure of pilot workload; and this parameter was varied in figure 2-30 to determine system degradation caused by increased pilot workload. As seen, τ of 0.3, which is representative of that required for a LESS three-axis control task, exceeds performance requirements, while increasing τ to 0.5 causes bandwidth to degrade to less than 1 rad/sec. This is slightly superior to the root loci for the kinesthetic system. One would expect a Cooper rating of about 4.5 for this system, provided the loop gain is optimized by adjusting hand controller gear ratio.

Analysis of hardwire compensation networks: The block diagram of the LESS attitude control system using hardwire control is shown in figure 2-31. The mathematical model of the pilot is that discussed in references 2-4 through 2-7 and 2-9 and has been used throughout the LFV and LESS studies with results that correlate well with those from flight simulators. Generic root loci for the system are shown in figure 2-32, with path reversal effects suppressed for clarity of presentation. Increasing the pilot's transport delay (representing increased workload) tends to make the system less stable and reduces achievable bandwidth. This is intolerable to the pilot, and he is forced to increase his lead compensation to restore the system bandwidth and damping ratio. This tends to degrade his opinion rating of the vehicle handling qualities.

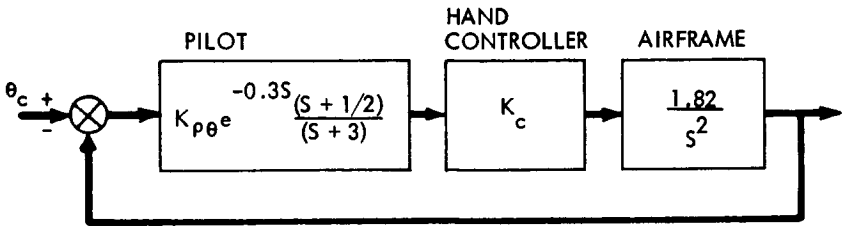

Figure 2-29. - LESS Hardwire Control Block Diagram

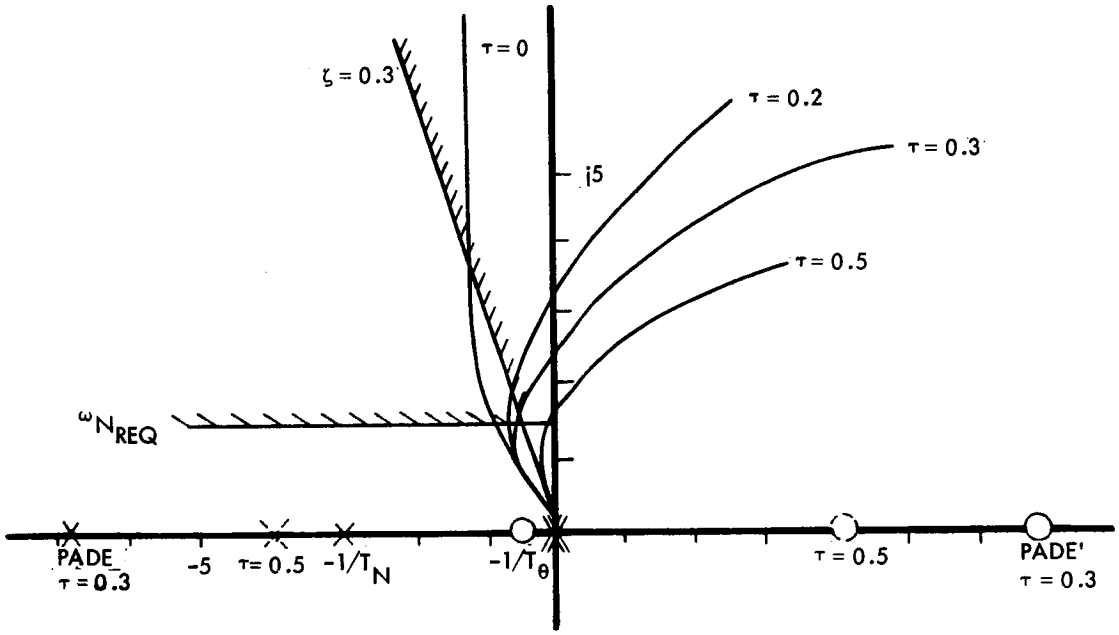

Figure 2-30. - LESS Hardwire Control System Root Loci

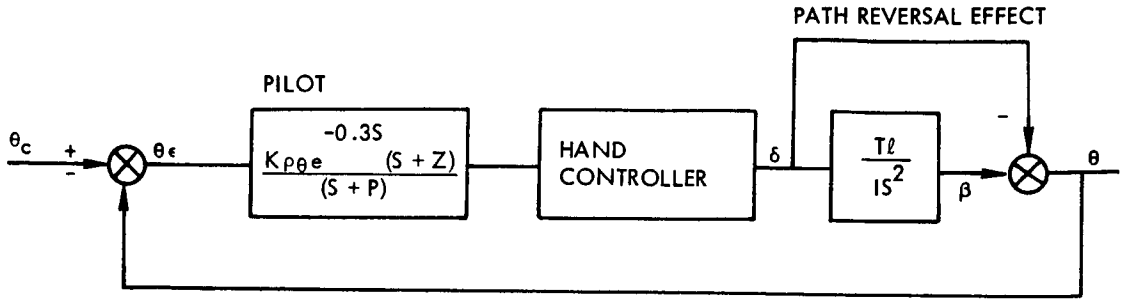

Figure 2-31. - LESS Hardwire Control System Block Diagram

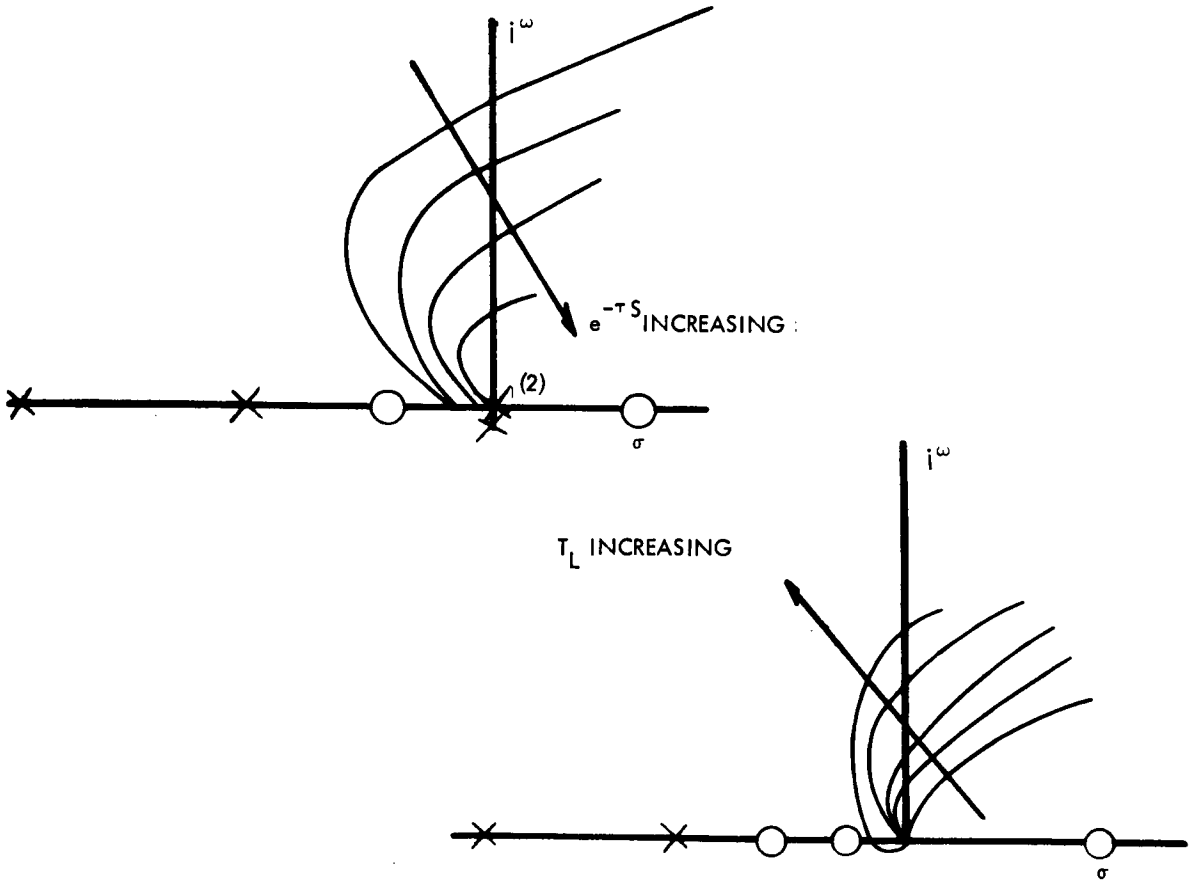

Figure 2-32. - Effects of Transport Delay and Lead Generation, S Plane

This section considers a method aimed at improving the hardwire Cooper rating by relieving the pilot of his attitude lead generation requirements. Use of gyros to do this would amount to stability augmentation and introduce complex, relatively unreliable components into the system. Thus consideration will only be given to the use of mechanical compensation networks (which consist of springs and dashpots) to improve matters. The network is inserted between the hand controller and nozzle, as shown in figure 2-33. Its function will be discussed in general terms and then a servoanalysis performed.

The basic hardwire system uses a straight link between engine and hand controller. A steady hand controller displacement produces a steady engine displacement, which amounts to constant angular acceleration. Vehicle angular velocity will increase until the hand controller is neutralized. Thus, as shown in figure 2-34, achieving proper pitchover rates involves accurately timing (mentally) controller displacements. This amounts to pilot lead generation and causes downrating of a vehicle.

If now a clock spring is placed around the engine gimbal to ensure a centering force, and a dashpot is placed in the hand controller link (fig. 2-35), a command now causes the engine to displace momentarily, but the clock spring returns it to center. LESS angular velocity is proportional to the integral of engine displacements, and hence the controller displacement commands angular rate. The system feels like a rate damped stability augmented system, and pilot opinion will improve because he no longer must generate an attitude lead (mental timing) function.

Thus the spring-dashpot system of figure 2-35 shows promise of obtaining the feel of a rate command system (which pilots prefer) without the use of gyros. This shows promise of improving the Cooper rating 1 to 2 points, making the possibility of an acceptable rating more likely.

However, it may be noticed that since the engine always returns to neutral, a constant external disturbing torque would require repeated hand controller inputs, eventually causing saturation and loss of control authority. Figure 2-35 shows one method of combating such disturbance torque inputs. A separate trimming device (like an airplane trim tab) is used to counteract the disturbing moments. Figure 2-36 shows another method for combating steady-state disturbance torques. The dashpot B of figure 2-35 is paralleled with a spring, K_2. This, in effect, allows steady-state engine displacements for disturbance suppression. Step response waveforms for this network are shown in figure 2-36. A step hand controller displacement causes an initial engine deflection which subsides to a steady-state displacement proportional to the ratio of K_2 and K_1. Vehicle rate is the integral of the engine displacement and is also shown. The steady-state δ yields a $\dot{\theta}$

OBJECTIVE:

TO UPGRADE HANDLING QUALITIES OF BASIC HARDWIRE SYSTEM

TECHNIQUE:

INTRODUCE A MECHANICAL COMPENSATION NETWORK TO DYNAMICALLY "MATCH" AIRFRAME DYNAMICS TO PILOT CAPABILITIES

SCHEMATIC:

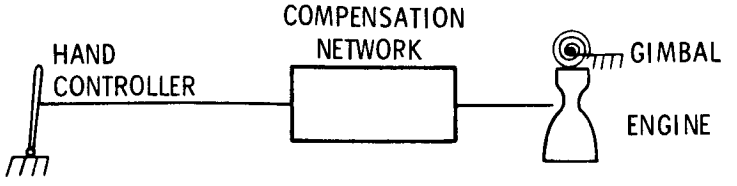

Figure 2-33. - Improvement of Basic Hardwire System

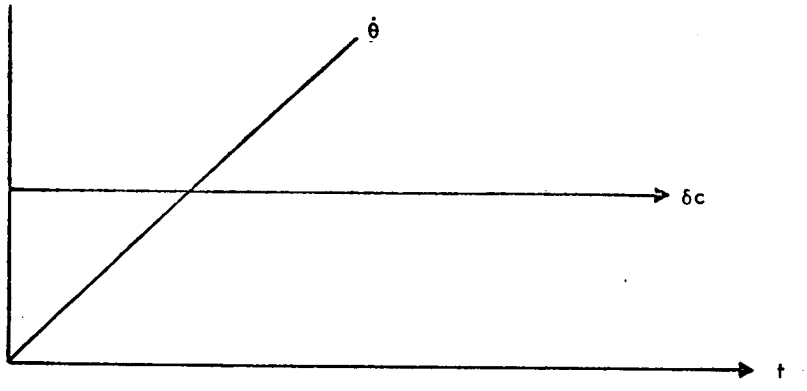

ACHIEVING DESIRED PITCHOVER RATE REQUIRES ACCURATE TIMING OF STICK DISPLACEMENT

POOR HANDLING QUALITIES

MAXIMUM RESISTANCE TO DISTURBANCE TORQUES

Figure 2-34. - Basic Hardwire Control System

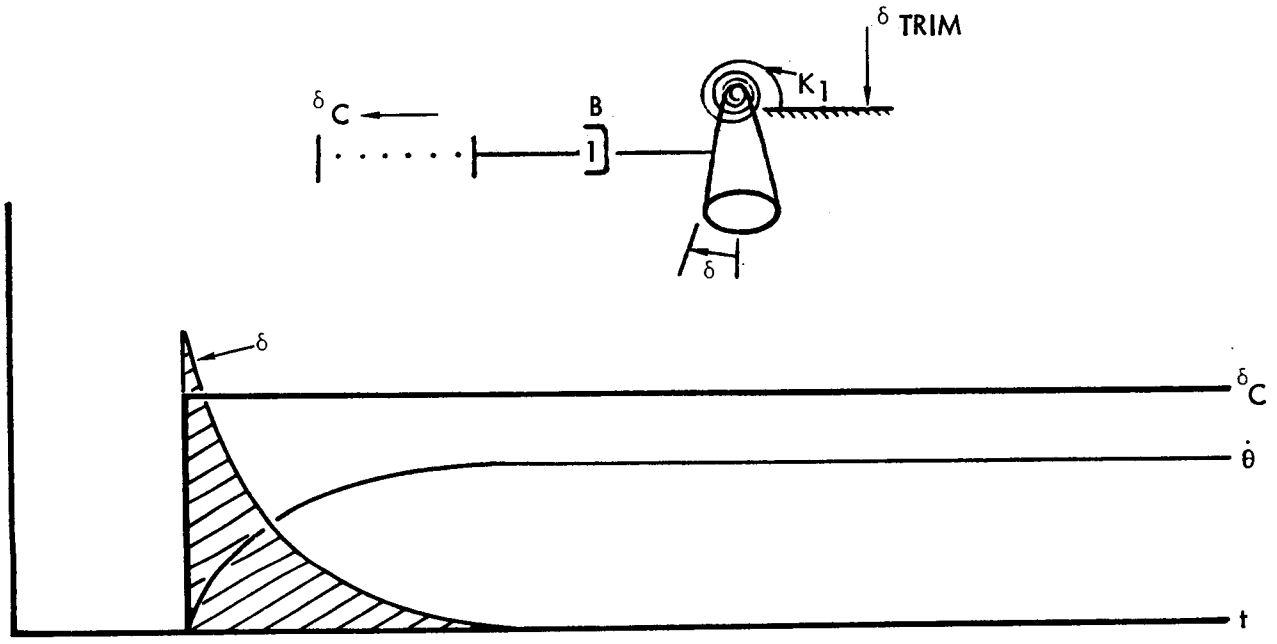

- STICK DISPLACEMENT COMMANDS VEHICLE RATE - HANDLING QUALITIES ARE IMPROVED OVER ACCEL. COMMAND SYSTEM
- SYSTEM SATURATES IF SUBJECTED TO STEADY STATE DISTURBANCE TORQUES (C.G. SHIFTS, ETC.)

Figure 2-35. - Hardwire Control System Network

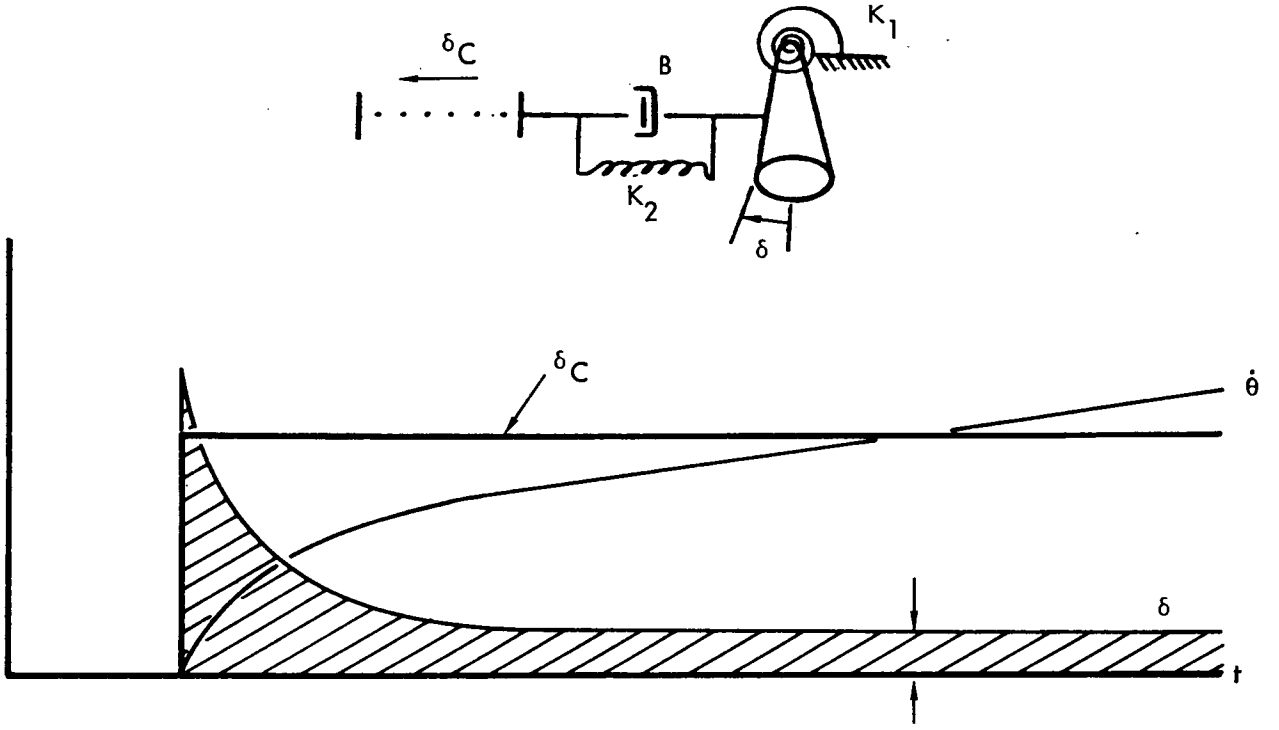

✓ ADDITION OF SPRING INCREASES SYSTEM D.C. GAIN TO FINITE VALUE-
RESISTANCE TO STEADY STATE DISTURBANCE TORQUES IMPROVED

Figure 2-36. - Hardwire Control System Network, Revised

that increases with time; and, therefore, this system is a hybrid between a straight hardwire system and the straight dashpot systems. This rather heuristic explanation of how the networks function will next be followed by an analysis of the problem, using servomechanism techniques.

Consider the simplified LESS attitude control system with disturbance inputs (center of gravity offsets, etc.) as shown in figure 2-37. A pure lead (dashpot only) network is shown.

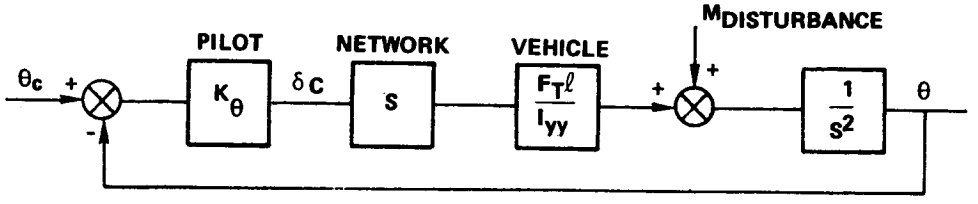

Figure 2-37. - Simplified LESS Attitude Control System With Disturbance Inputs

The system closed loop transfer function is, by inspection:

$$\frac{\theta}{\theta_c} = \frac{K_\theta F_T \ell}{I_{yy}\left(S + \frac{F_T \ell K_\theta}{I_{yy}}\right)} \qquad (2\text{-}10)$$

which shows good stable characteristics, as expected. However, the system response to a disturbance input, M_D, is:

$$\frac{\theta}{M_D} = \frac{1}{S\left(S + \frac{K_\theta F_T \ell}{I_{yy}}\right)} \qquad (2\text{-}11)$$

Equation (2-11) contains a free integration which would yield unbounded θ in response to a constant disturbance input, M_D. This is an unsatisfactory condition.

If a constant term is added to the compensator, the block diagram of figure 2-38 results:

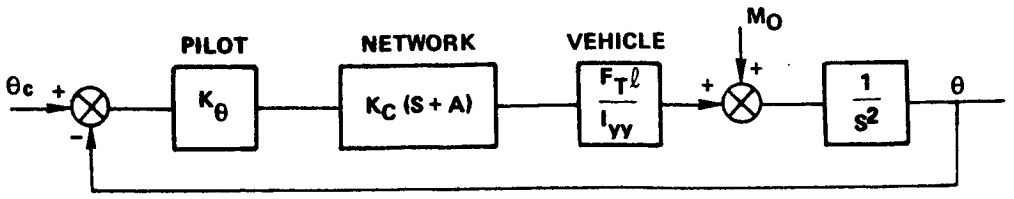

Figure 2-38. - Simplified LESS Attitude Control System With Lead Compensation

Again the system closed loop transfer function is:

$$\frac{\theta}{\theta_c} = \frac{K_\theta K_c F_T \ell (S + A)}{I_{yy}\left(S^2 + \frac{K_\theta K_c F_T \ell}{I_{yy}} S + \frac{K_\theta K_c F_T \ell A}{I_{yy}}\right)} \tag{2-12}$$

And the system disturbance input transfer function is:

$$\frac{\theta}{M_D} = \frac{1}{S^2 + \frac{K_\theta K_c F_T \ell}{I_{yy}} S + \frac{K_\theta K_c F_T \ell A}{I_{yy}}} \tag{2-13}$$

The system closed loop natural frequency and damping ratio are, by inspection:

$$\omega_N = \sqrt{\frac{K_\theta K_c F_T \ell A}{I_{yy}}} \tag{2-14}$$

$$\zeta = \frac{1}{2}\sqrt{\frac{K_\theta K_c F_T \ell}{I_{yy} A}} \tag{2-15}$$

And the disturbance rejection quotient is:

$$\frac{M_D}{\theta_c} = \frac{M_D/\theta_c}{\theta/\theta_c} = \frac{I_{yy}}{K_\theta K_c F_T \ell A} \tag{2-16}$$

Thus the conflict between stability and noise rejection capability becomes apparent. High natural frequency and good disturbance (noise) rejection require A to be a large number. Good damping ratio requires A to be a small number. Because the network is passive, $K_c A \leq 1$. Too large a requirement for K_θ degrades pilot opinion. Thus the degrees of freedom available to the network have been mapped out. Compensation network configurations and transfer functions are shown in figure 2-39.

CONFIGURATION

TRANSFER FUNCTION

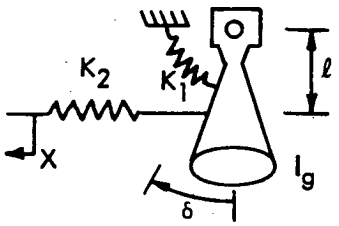

$$\frac{\delta}{X} = \frac{K_2 \ell / I_g}{S^2 + \frac{K_1 + \ell^2 K_2}{I_g}}$$

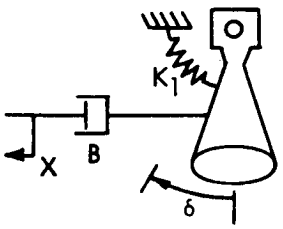

$$\frac{\delta}{X} = \frac{(B\ell/I_g)\,S}{S^2 + \frac{B\ell^2}{I_g}\,S + \frac{K_1}{I_g}}$$

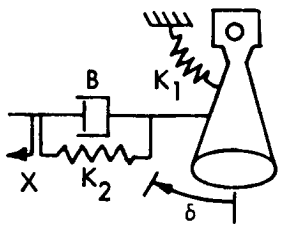

$$\frac{\delta}{X} = \frac{B\ell/I_g\,(S + K_2/B)}{S^2 + \frac{B\ell^2}{I_g}\,S + \frac{K_1 + K_2\ell^2}{I_g}}$$

$$\cong \frac{1}{\ell}\,\frac{(S + K_2/B)}{(S + K_2/B + K_1/B\ell^2)} \quad \text{for } I_g \approx 0$$

Figure 2-39. - Mechanical Hardwire Compensation Networks

The spring bypassed lead network was evaluated on the NR visual LFV simulator. Disturbing moments caused the hand controller to saturate when the bypass spring constant was set to zero. The value of the spring was increased to assist in rejecting the disturbing torques. When sufficient gain was added to successfully combat the disturbance torques, the test pilot remarked that the system was indistinguishable from a straight hardwire system. Several runs verified this finding. Thus it was concluded that this type of network was incapable of upgrading hardwire handling qualities.

However, the separate trimming type network was not evaluated due to lack of available time on the NR simulator and should be investigated further. The proper gain to use for the network will be discussed in the section of gain optimization.

Analysis of the neutral CG hardwire control system: An unusual configuration, the neutral-center-of-gravity LESS, is a special case of the general hardwire system but with interesting potentialities for LESS use due to its constantly level platform.

All of the LESS control systems discussed heretofore require a pitchover maneuver to allow a component of the main thrust vector to build up translation velocities. It is this requirement for pitchover maneuvers that gives rise to the handling qualities problem.

This section discusses a configuration that shows promise of avoiding these problems by placing the thrust vector gimbal through the system center of gravity. This decouples translation dynamics from rotation dynamics. The requirement for the pitchover maneuver disappears, and the platform remains level in regard to the ground. This has important advantages concerning decoupling G&N visual displays from vehicle motion without using gyros. The handling qualities problem is also different because the pilot remains vertical during flight. Two neutral center of gravity configurations are shown in figure 2-40. Theoretical aspects are discussed in the Lunar Flying Vehicle Final Report, reference 2-11.

It is never possible to get the thrust vector exactly through the center of gravity, of course; and hence a small bang-bang RCS is required to trim out residual drifts and center of gravity misalignments during flight. Gross center of gravity changes are compensated by changing the pilot's seat prior to flight. To perform an ascent, the pilot cranks the engines to the required two-step or three-step trajectory angles sequentially with respect to his centerline. He uses the bang-bang jets to trim out the drift rates resulting from center of gravity misalignments. If the vehicle is carefully designed and constructed, these should be small and hence require only occasional corrections.

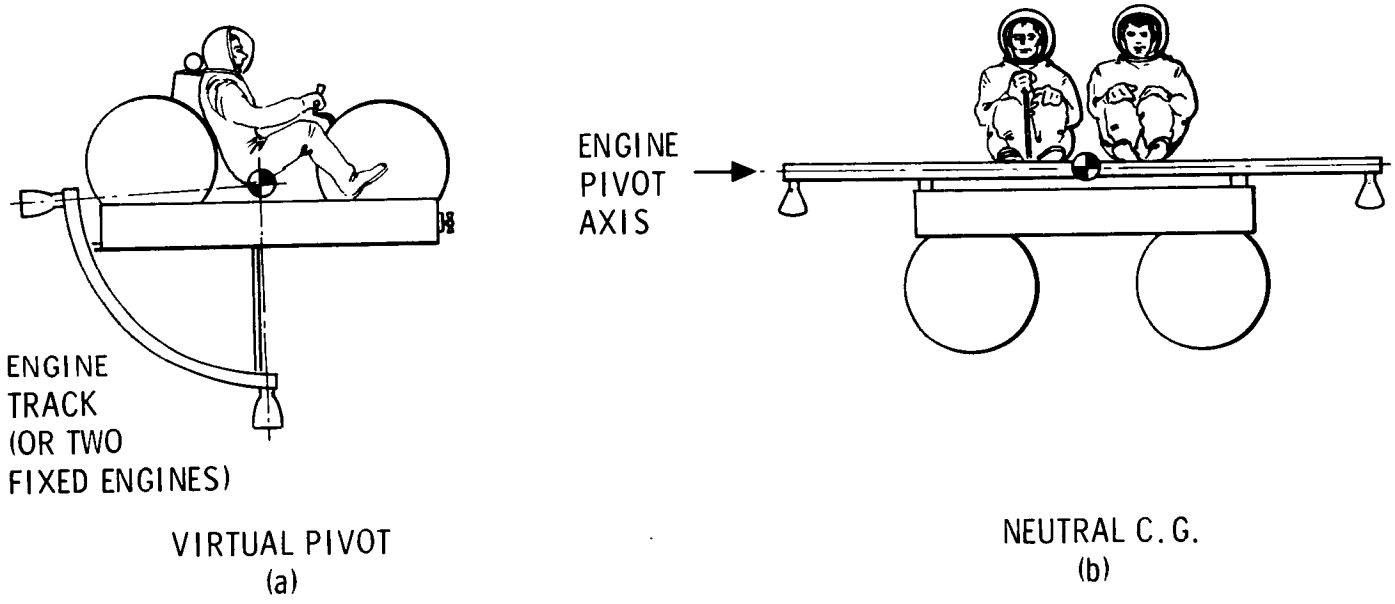

Figure 2-40. - Neutral Pivot Concepts

Although this configuration has much to recommend it from a guidance standpoint, the design complexities, including propulsion difficulties, are very real and tend to weigh against the scheme. But a feasible vehicle with a simple hardwire control and simple guidance qualities has so much promise that further investigations of this configuration are warranted. Until simulations are conducted, this configuration cannot be confidently said to have improved handling qualities. The advantages of level flight may be offset by the additional pilot tasks of controlling both thrust vector and platform attitude.

Analysis of hardwire reaction jet control: An alternate to gimbaling the boost propulsion system to provide attitude control moments is to pulse all or part of the propulsion differentially. Several potential advantages of pulsing are immediately apparent:

1. The problems of gimbaling are removed. These problems include gimbaling response in the presence of disturbing load torques; alignment of the engine within the gimbal system; reliable design of propulsion, control, and instrumentation lines across the gimbal interface, weight of the gimbaling system, and design constraints imposed by gimbaling.

2. A potential increase in reliability is possible if redundant pulse jets are used.

3. Several methods of improving handling qualities over that of a gimbaled hardwire system may be realized. The pulse jet system may use hardwire acceleration control with the pulse duration equal to rotation controller deflection duration, or proportional to the amount of rotation controller deflection. Shaping networks and stability augmentation systems may be easily adapted to the pulse jet system. Logic to remove interaxis coupling caused by vehicle cross products of inertia may be used.

4. The differential pulse jet system does not couple vehicle rotational and translational dynamics as does a gimbaled system. This coupling effect is objectionable for lunar flying vehicle missions.

5. Since the pulse jet system laterally translates the resultant thrust vector instead of rotating it as with a gimbaled system, a new approach to center of gravity alignment is available.

In view of these potential advantages, this section will provide analytical results for comparison with other systems. Disadvantages of individual versions of the differential pulse jet system will be stated during the analysis and used in the final system recommendations.

Two types of pulse jet configurations are feasible:

1. Fire one or more of the jets continuously to provide the major part of the boost thrust. Use the remainder of the jets for attitude stabilization and maneuvers.

2. Pulse all jets. Each pulse would use part of its on-time for boost and part for attitude stabilization.

A matrix showing a few of the possible configurations using these two types is presented in table 2-9. If jet redundancy is necessary to attain the required reliability, only configuration 1 is adequate; although configuration 3 could be acceptable if the central, continuously-operating jets were converted to pulse jets when the pulse system failed. The first two configurations are capable of controlling in yaw. If any of the other configurations were to be used, separate yaw control jets would be required for boost. These jets would produce control moments larger than that required for orbital operation, and could not be used for both purposes.

The first two configurations also provide greater capability for smooth operation. As jets are pulsed, they produce vibrations which may hinder the pilot's ability to operate the vehicle; the larger the number of jets, the more the pulses tend to overlap. Vibration isolation may be required to reduce the levels to those stipulated as tolerable for the pilot. If the jets are operated in such a manner that the vibration-excitation frequency is always at least twice the basic engine-pulse rate, the vibration forces can be reduced to tolerable levels by simple spring isolation on each engine or on the pilot seat. Reference 2-8 indicates that vibration levels in excess of 0.07 g in the frequency range from 3 to 25 Hz will impede pilot performance.

For reasons stated in the preceding paragraphs, the first configuration in table 2-9 seems to be the most acceptable. It provides jet redundancy, three-axis attitude control, and is capable of the smoothest operation. The jets are canted at a small angle so that each produces yaw torque along with either pitch or roll torque.

In its simplest form, a typical cycle of operation is shown in figure 2-41. Each pulse of each separate jet is initiated by a timing signal, in sequence, which provides the pulse duration necessary to maintain a minimum thrust-to-weight ratio. The pulse terminates unless a separate signal from the rotation controller causes the pulse to continue. If all jets are pulsed, the attitude control signal must be stored for use at the end of the boost pulse of the proper jets. If continuous boost propulsion is provided by part of the jets, the control signal is used immediately by the remaining jets. The logic for the two types of pulse configurations are quite different.

TABLE 2-9. - MATRIX OF DIFFERENTIAL PULSE JET CONFIGURATIONS
(ALL JETS RIGIDLY FIXED TO PLATFORM)

Configuration ○ Pulsed Jets ● Continuous Jets	① 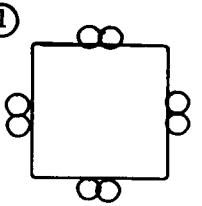	② 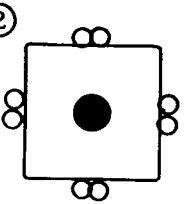	③ 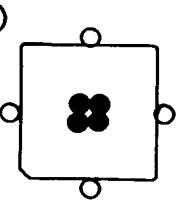	④ 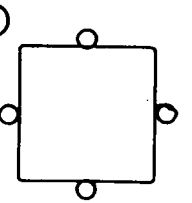	⑤ 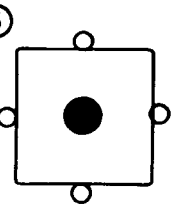
Total Jets	8	9	8	4	5
Total Pulsed	8	8	4	4	4
Total Continuous	0	1	4	0	1
Separate RCS for Yaw	No	No	Yes	Yes	Yes
Pulsed Jet Redundancy	Yes	Yes	No	No	No
Continuous Jet Redundancy	—	No	Yes	—	No

- MULTIJET SYSTEM
- PULSE PROVIDES BOOST AND CONTROL TORQUE
- THRUST PULSE IGNITION INITIATED BY TIMER
- THRUST PULSE TERMINATION INITIATED BY TIMER, BUT IS OVERRIDDEN BY ROTATION CONTROLLER SIGNAL

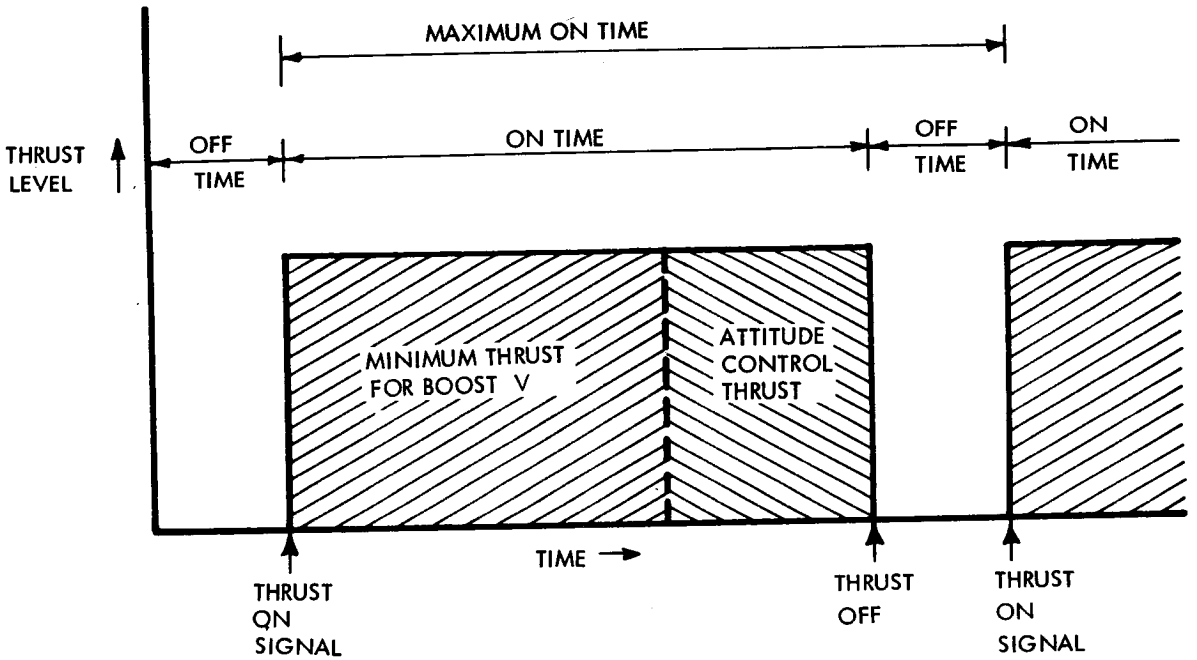

Figure 2-41. - Typical Duty Cycle of a Pulse Jet

The jet firing sequence for the first configuration in table 2-9 should be designed so that the boost portions of the pulses from the jets tend to counteract the torques produced by the preceding pulses: pulses should alternate across the platform. Two firing sequences which accomplish this are shown in figure 2-42, along with a diagram of the platform and jet arrangement. The cant angle of the jets is assumed to be less than the angle which points the jets through the axis containing the center of gravity. The first sequence allows jet-to-jet alternation of yaw torques, while the second sequence alternates every two pulses. Thus, the second sequence produces half the disturbance frequency in the yaw of the first. Other firing sequences exist, some with undesirable features.

Location of the jets at the corners of the platform, rather than as shown, would tend to increase the pitch and roll moments of more of the jets. For example, the roll moments of jets 1, 4, 5 and 8 are small as shown in the figure. If these jets were corner-located, their roll moment capability would greatly increase.

Operation during a single jet failure with the arrangement shown in figure 2-42 would require the diagonally opposite jet to nearly double its pulse duration for attitude control. For example, if the thrust of jet 1 failed off, the pulses of jets 4 and 5 would be balanced by increased pulse duration from jet 8, with a small amount of help from jet 2. If the thrust of jet 1 stayed on continuously, all jets except jet 7 would share the load of maintaining attitude.

It is not recommended that, in the event the thrust of a jet fails off, the opposing jet is turned off. To remove a jet from the system requires first that the failed jet be sensed and located, then that the mechanism for disabling the opposing jet be operated. Both the sensing and disabling logic must be quite complex and have additional reliability problems. The method was studied extensively under the lunar flying vehicle contract and was found to be undersirable. The concept of using all eight jets for control in each axis precludes the need for disabling a jet after a failure.

An example of the logic necessary to provide a pulse jet system for boost and attitude control is shown in figure 2-43. The system is sufficiently complex to warrant electrical components, rather than mechanical linkages.

The merits and demerits of a pulse jet boost and attitude control system have been briefly discussed. The method seems feasible. The major portion of the discussion dealt with pulse duration jet actuation with the premise that the pilot could comfortably handle such a system. The validity of the assumption remains to be proven by simulation. Since the pilot directly

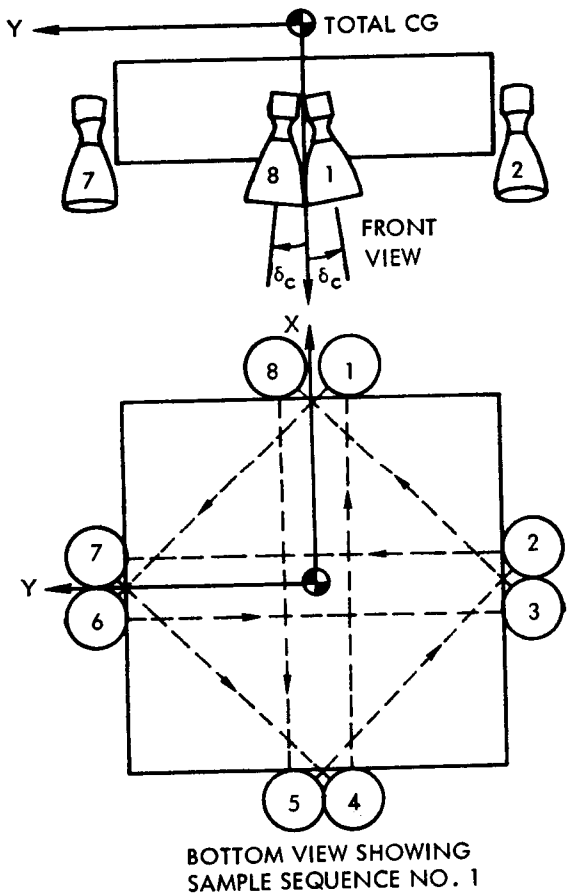

ENGINE FIRING ORDER	MOMENT DIRECTION BY RIGHT HAND RULE		
	ROLL	PITCH	YAW
SAMPLE SEQUENCE NO. 1			
1	+	+	+
6	-	-	-
3	+	-	+
8	-	+	-
5	-	-	+
2	+	+	-
7	-	+	+
4	+	-	-

SAMPLE SEQUENCE NO. 2			
1	+	+	+
5	-	-	+
2	+	+	-
6	-	-	-
3	+	-	+
7	-	+	+
8	-	+	-
4	+	-	-

Figure 2-42. - Pulse-Jet Engine Locations and Typical Firing Sequences

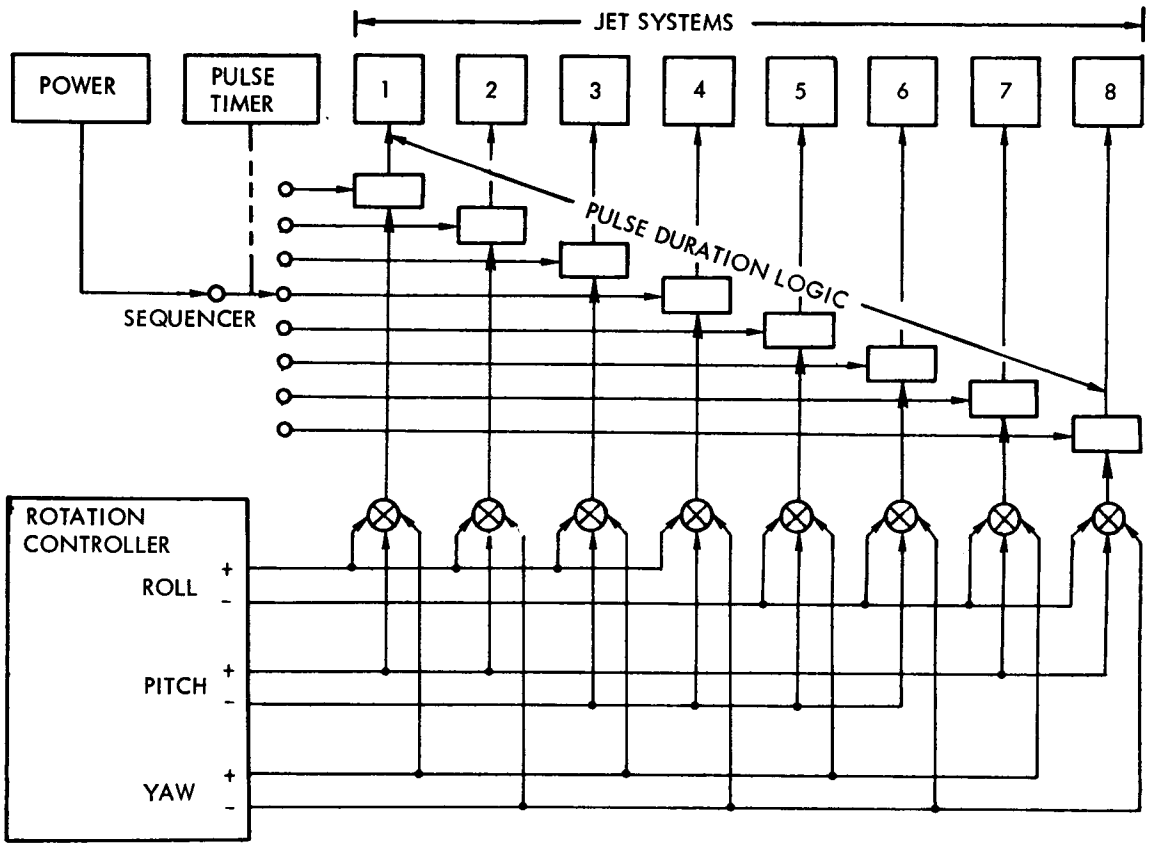

Figure 2-43. - Jet Sequencing and Modulation Logic

controls vehicle torques, the system is classed as hardwire, but it is clearly different from a gimbaled hardwire system and the pilot may feel the difference significantly.

The conclusions concerning the pulse jet system include the following:

1. The logic portion of the system is more complex than that of a hardwire gimbaled system, but may be more easily adapted to stability augmented (rate command) control simply by introducing feedback signals at the rotation controller outputs.

2. The hardwire portion of the system is simpler than a gimbaled system in that all jets are fixed and provide a rigid interface for propellant, control, and instrumentation lines. The system is more complex in that more engines are required than for a gimbaled system.

3. The problem of handling qualities of the pulse jet system is relatively unexplored. Both the pilot's ability to generate correct pulse lengths, and the effect of pulse-generated vibrations on the pilot require more study to be fully understood.

Analysis of the stability augmented control system. - The stability augmented system discussed here is similar to the Apollo SCS. The system provides rate damping and attitude hold. When the astronaut moves the hand controller, attitude feedback from the gyros is inhibited, while angular rate damping is maintained. The attitude loop is then closed through the astronaut, as is the translation loop.

Attitude hold with this system poses little workload to the pilot. A rate-damped maneuver with path control is the most difficult task to perform with this system. The task of the rate gyro is to suppress disturbance moments automatically, while also relieving the pilot of his lead generation task in attitude. A rate gyro gain of two was used to split the rigid body integration pole pair at the origin into a real pole at $-M_\delta K_\theta$ and one at the origin. The pilot, acting as a gain only (which earns favorable opinions), closes the loop to drive the poles together to form a dominant pair at $\zeta = 0.4$, $\omega_N = 2$. This is considerably in excess of that achievable with hardwire or kinesthetic control. It is interesting to note that system bandwidth is basically set by the pilot's neuromuscular pole, $-1/T_N$, and his transport delay.

Conclusions for the stability augmented control mode are that the convenience and performance capabilities of the stability-augmented system will

yield acceptable ratings from pilots. Thus the system is acceptable from a handling qualities standpoint for LESS. Use of stability augmentation should reduce the scope and intensity of the LESS flight training program from that required for a hardwire or a kinesthetic system. This savings in effort and cost deduct from the basic system costs. In a very tight system development program, the short pilot training program could constitute a very real advantage.

System gain optimization techniques. - Heuristic arguments quickly lead one to the conclusion that acceptable control authority lies between that which the pilot will rate "too sensitive" and that which is "too sluggish." Because of the nature of the system and the performance requirements demanded of it, system loop gain must be fixed:

$$\frac{K_\theta F_T \ell}{I_{yy}} = \text{Constant depending on bandwidth requirements} \qquad (2\text{-}17)$$

Hence if control authority (i.e., $F_T \ell / I_{yy}$) is too low, the pilot must increase his gain K_θ to compensate. If the required increase in K_θ is too large, he will complain the system is too "sluggish" and downrate it. The high value of K_θ causes difficulty with system higher order lags (especially transport delay) tending to go unstable.

Conversely, too high control authority (ref. 2-4 to 2-7) will force the pilot to reduce K_θ to very low values to avoid instability; and he will complain the system is too "sensitive." Thus there is a range in which his opinion, based on gain, will be good.

Data on extra atmospheric vehicles is extremely scarce. Many reports exist giving pilot transfer functions for all sorts of controlled objects, but very few give his Cooper ratings. Figure 2-44 represents the results of an extensive search for data on hardwire control system pilot opinion. Data was taken from reference 2-10 as well as from LFV flight articles, Apollo CSM simulations, and Langley simulations. NR test pilots have remarked that hardwire control of altitude with throttle degraded ratings one Cooper point. Hence the various LFV simulations used were uprated one point to try to cast their results in a LESS format.

It is noticed from the figure that the Cooper ratings form a bucket shaped optimization curve, with acceptable pilot ratings obtained between a $K_s T \ell / I$ of 0.3 and 1.3. An ideal hardwire design would, therefore, start

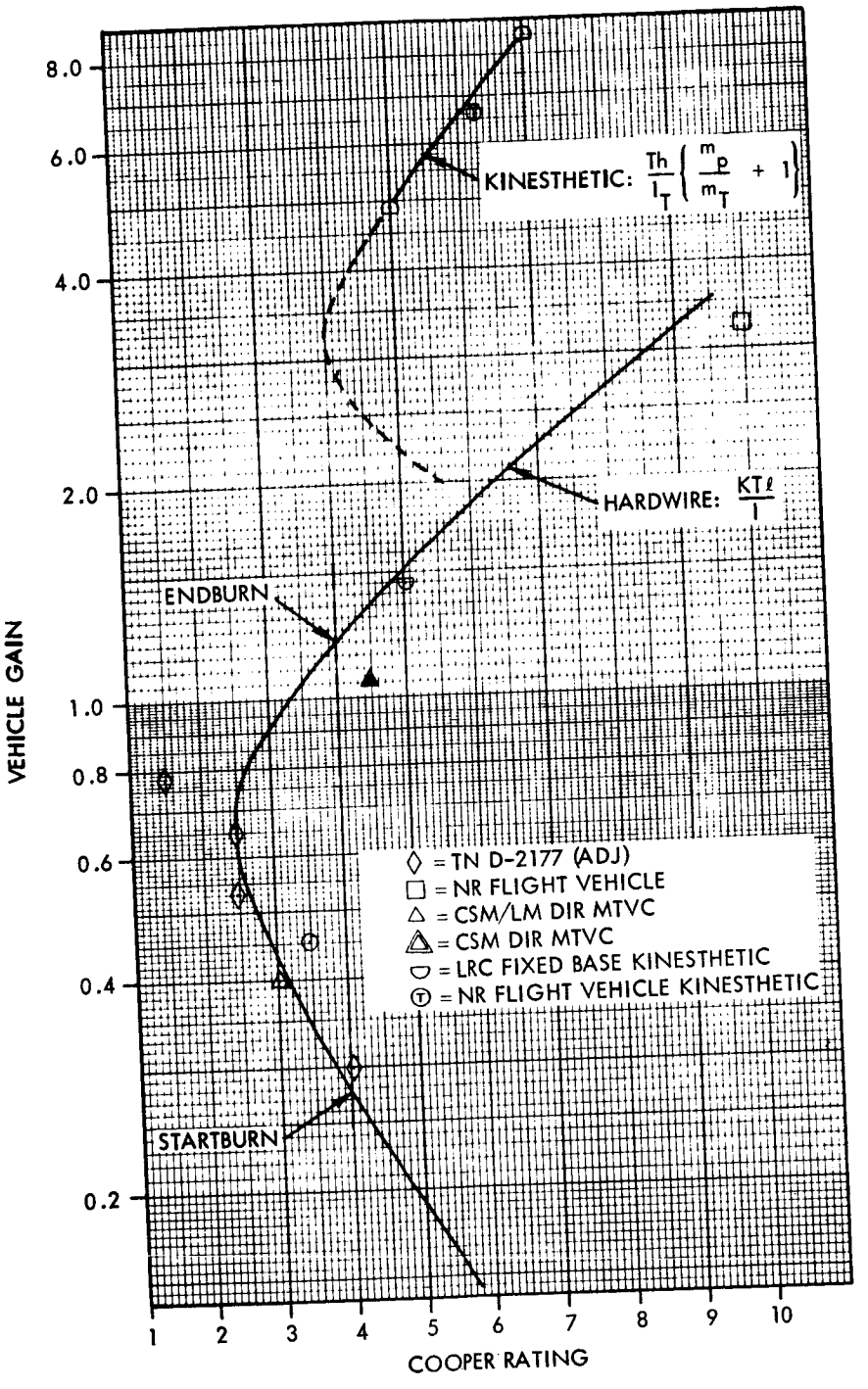

Figure 2-44. - System Gain Optimization Curves

with the airframe at start burn at the lower value. Then as fuel burned off and control authority increases, end burn takes place at the higher value. Acceptable Cooper ratings are obtained throughout.

Thus, even though the curve formed from many disparate sources, it seems as if the basis of an optimization theory has been formed. What is needed now is to check this optimization curve on a consistent simulator, using several qualified test pilots for opinion ratings. Such a check would give a solid basis for system design.

An advantage of hardwire controlled vehicles is that this system loop gain may be easily adjusted by changing the gear ratio in the rotational hand controller. Such an adjustment affects total nozzle throw or force required, and this must be allowed for in the design. Any gain from a shaping network should be included in the control authority parameter when designing the hand controller for optimum hardwire handling qualities.

A second curve, using the kinesthetic parameter discussed in the kinesthetic analysis has been plotted also in figure 2-44. Only a few points were available, and the dotted portion of the curve is added only to show (hopefully) that the curve will show an optimum when tested on a simulator. The dotted portion is not intended to represent actual numerical values, as none presently exist in this range.

The preceding discussion on gain optimization emphasizes a very important facet of hardwire control system design over kinesthetic control. Loop gain optimization is easily accomplished by changing the hardwire control system's hand controller gear ratio. However, the only parameter really available to change in a kinesthetic system is moment of inertia. Increasing moment of inertia makes for a larger envelope size and poses packaging and storage problems on the ELM. Thus a very important advantage of hardwire over kinesthetic is that the designer can set his sights for a minimum envelope design, optimizing the handling qualities by adjusting hand controller gear ratio, while to ensure good handling qualities on a kinesthetic system, the designer increases or decreases moment of inertia. This means practically moving fuel tanks in or out radically, which causes problems in ELM packaging.

The other control gain parameter which can be varied to compensate for the system gain change inevitably encountered with fuel consumption is thrust. At some expense in engine complexity, the engine can be step-throttled to reduced levels at the end of boost.

On the basis of the above discussions, the following conclusions may be reached:

1. Possibilities exist for improving the handling qualities of hardwire control systems for LESS by adjusting the hand controller gear ratio to the proper value or changing thrust.

2. Kinesthetic control handling qualities may be improved by changing vehicle inertia parameters, but these tend to affect the LESS packaging envelope.

3. The curves shown in figure 2-44 should be verified on a consistent simulation. Control authorities for the hardwire system should be investigated in the range between 0.3 and 3. Control authority for the kinesthetic system should be investigated in the range between 2 and 12. The evaluations should be made by trained test pilots and the control authority runs mixed to prevent the test pilot from spotting a trend. Fixed inertia points should be run with many samples to allow statistical smoothing of the data. Such data may be obtained with the NASA-LRC fixed base visual simulator.

4. The hardwire system shows promise of achieving acceptable handling qualities for LESS applications.

Tradeoffs between system gain factors. - In this section the factor of which the system gain is composed will be separately identified and analyzed. These factors are contained in the $(K_S T \ell / I)$ term, but also include maximum excursions of the rotation controller and the engine gimbal.

The requirements for maximum deflection and torque are based on those of the Apollo controller, which was the product of the most thorough human factors research available. During LESS boost the controller will require breakout torque in yaw for positive reaction jet switching, while engine gimbal deflections in pitch and roll require proportional torques with initial breakout torques. After boost, the controller will exhibit breakout torque in all three axes for reaction-jet control switching.

There are, therefore, two separate modes of operation in the pitch and roll axes: engine gimbaling during boost, and reaction-jet thrusting during orbital coast. To reliably implement the dual functions in a single-rotation controller may be beyond present technology, but two techniques are suggested:

1. Dual, side-by-side controllers. The advantages of using separate single-function controllers are that each is a simple three-axis component, many versions of which have been developed and used in the past. Among the disadvantages is that each controller may operate the same yaw reaction jets, each is located in a compromise position from the standpoint of the pilot, and two controllers add to the weight, cost, and power requirements of the vehicle.

2. Single controller with mode switching. This method is probably the simplest approach if stability augmented control is used and the controller deflections generate electrical signals. The controller could either be switched from gimbaling operation to reaction-jet operation manually by a toggle switch or automatically by the mode sequencing logic. If hardwire control is used, mode switching requires that the gimbal linkage be removed from the system after thrust termination. The reaction-jet linkage (either electrical or mechanical) may be operating during boost or be switched into the system with the same switch that removes the gimbal linkage.

The total excursion of the rotational controller in each axis has been set somewhat arbitrarily since it depends on mass properties as will be explained later. In the case of reaction-jet operation, very little deflection is necessary to provide the pilot with a positive indication that he has actuated the jets. The time duration of the deflection determines the on-time of the jet. If a pulse duration logic system is implemented, deflection becomes a proportional command and greater deflection range is needed. Controller excursion for gimbaling is proportional to the desired vehicle control torque. The maximum excursion required for hardwire stability should be sized for optimum sensitivity and may be quite small; however, compensation for center-of-gravity misalignments may dictate a larger excursion. Previous experience with hardwire controllers indicates that a spring return centering device is desirable which means that a separate method of aligning the nominal thrust vector to the center of gravity should be investigated. Controller use with a stability augmented gimbaling system requires that the maximum excursion be sized for optimum rotational rates.

Composite curves, showing LESS rotation controller characteristics for both main thruster (TVC) and reaction (RCS) control are shown in figures 2-45, 2-46, and 2-47 for roll, pitch, and yaw axes. Also shown in the figures in dashed lines are the requirements for Apollo.

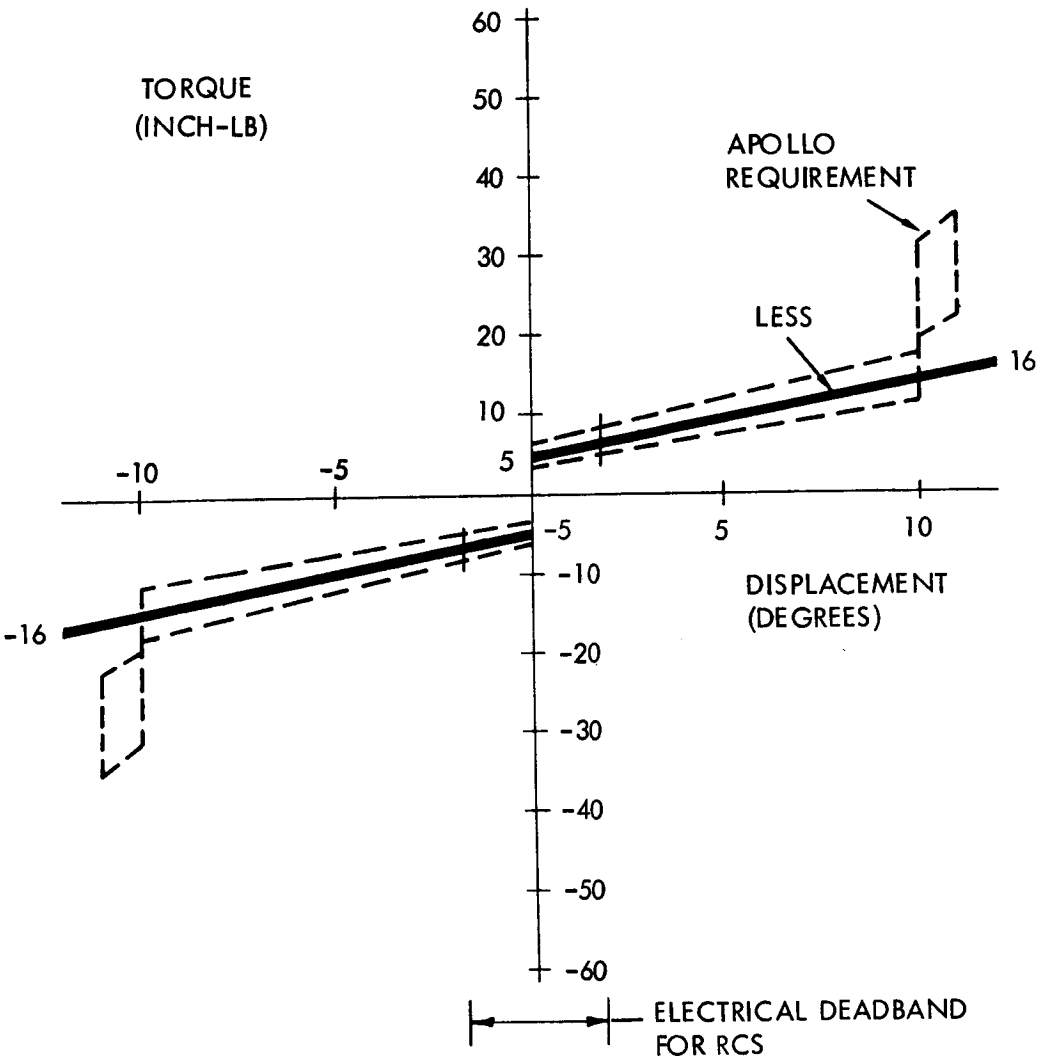

Figure 2-45. - Rotation Controller Torque Versus Displacement, Roll Axis

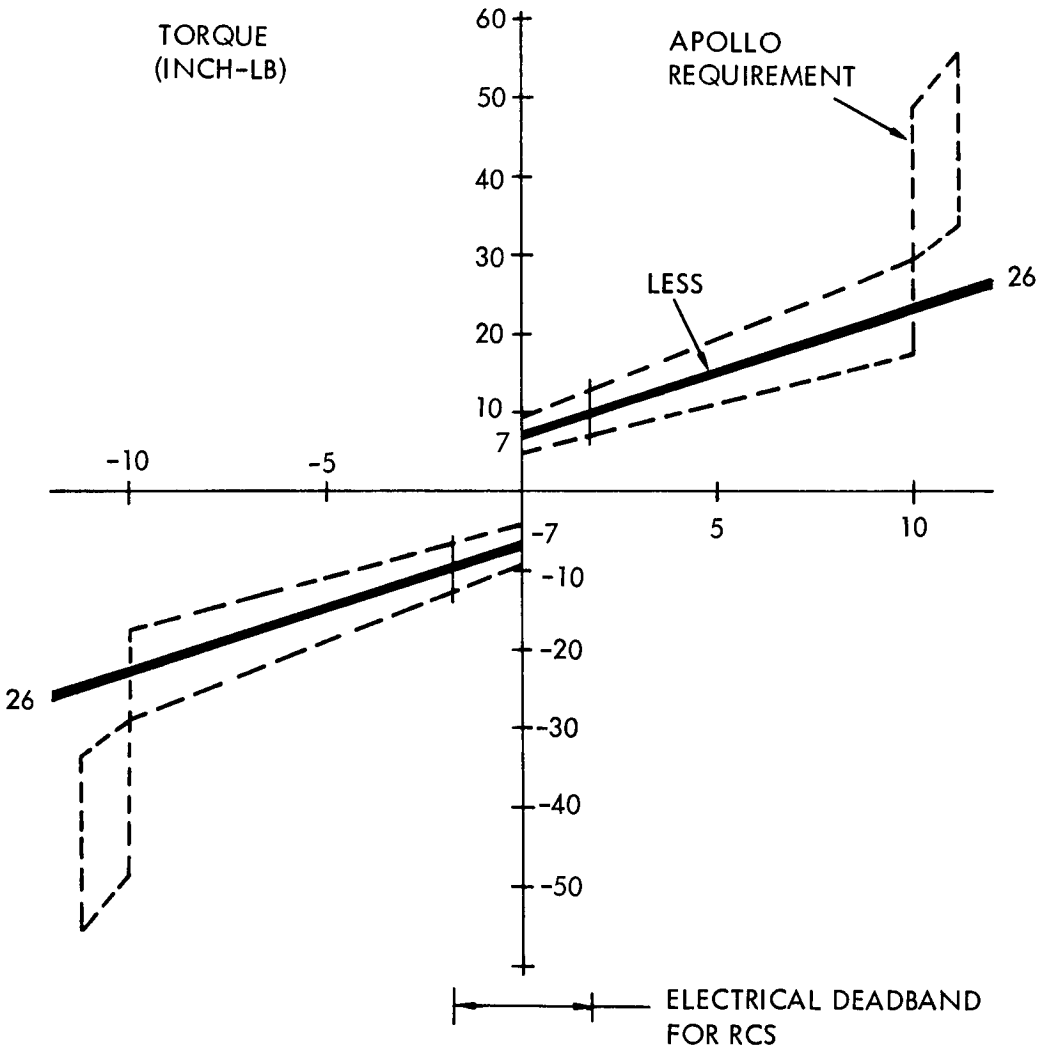

Figure 2-46. - Rotation Controller Torque Versus Displacement, Pitch Axis

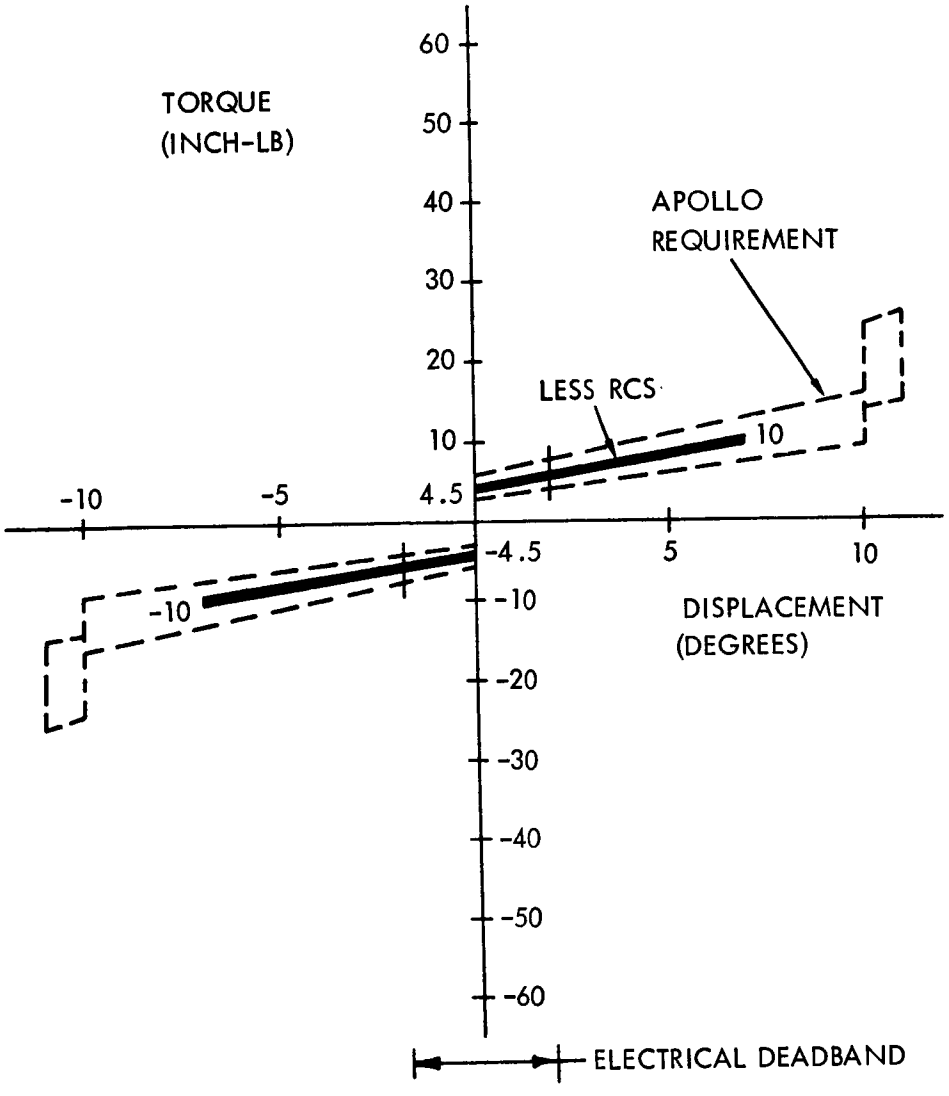

Figure 2-47. - Rotation Controller Torque Versus Displacement, Yaw Axis

Potentially, a conflict exists for hardwire control between the optimum sensitivity gear ratio from the controller to the engine gimbal, and the gear ratio which provides comfortable controller load torque. Typically, the load torque is generated by frictional and spring loads in the gimbal and linkage which are unsymmetrical about the null and are nonlinear. These torques must be minimized by the designer so that desirable torque characteristics may be built into the controller.

The first step in determining how severe is the conflict is to find the optimum controller sensitivity. Data will be generated for the gear ratio as a function of important parameters using the overall control sensitivity curve developed in the previous section and appearing in figure 2-44. Since the thrust, T, the moment of inertia, I, and the distance from the center of gravity to the gimbal, ℓ, for the vehicle is determined from other considerations, the gear ratio, K_S, is the parameter to be optimized. A proper value of K_S centers the control sensitivity about the peak pilot opinion rating: the start burn (launch) rating is equal to the end burn rating. The centering process is more easily accomplished if the data of figure 2-44 in the previous section are presented as shown in figure 2-48.

Table 2-10 presents the mass properties data (from an early configuration) to be used in the analysis. Start burn and end burn values of the term $(T\ell/I)$ are calculated from the table 2-10 data and are shown in table 2-11. Examination of the data shows that only a small area of the figure 2-48 sensitivity field is needed to investigate the particular vehicle characteristics of table 2-11.

The optimum controller-to-gimbal sensitivities (gear ratios) for various launch thrust-to-weight ratios for the pitch and roll axes are replotted in figure 2-49. The additional scale of pilot opinion rating at the top of the plot indicates that pilot opinion is nearly independent of launch thrust-to-weight. It also shows that the handling qualities are unsatisfactory.

Figure 2-44 in the previous section indicates a potential pilot opinion rating of 2.5, which is well within the acceptable handling qualities range. If only small variations in rating are allowed, then an acceptable hardware vehicle could be realized. Several methods of minimizing the parameter variations are apparent, but their implementation require further study:

1. Provide a programmed sensitivity gear ratio which tracks the optimum pilot opinion point.

2. While keeping thrust and gear ratio constant throughout flight, configure the vehicle so that the ratio of ℓ/I is constrained to the proper limits.

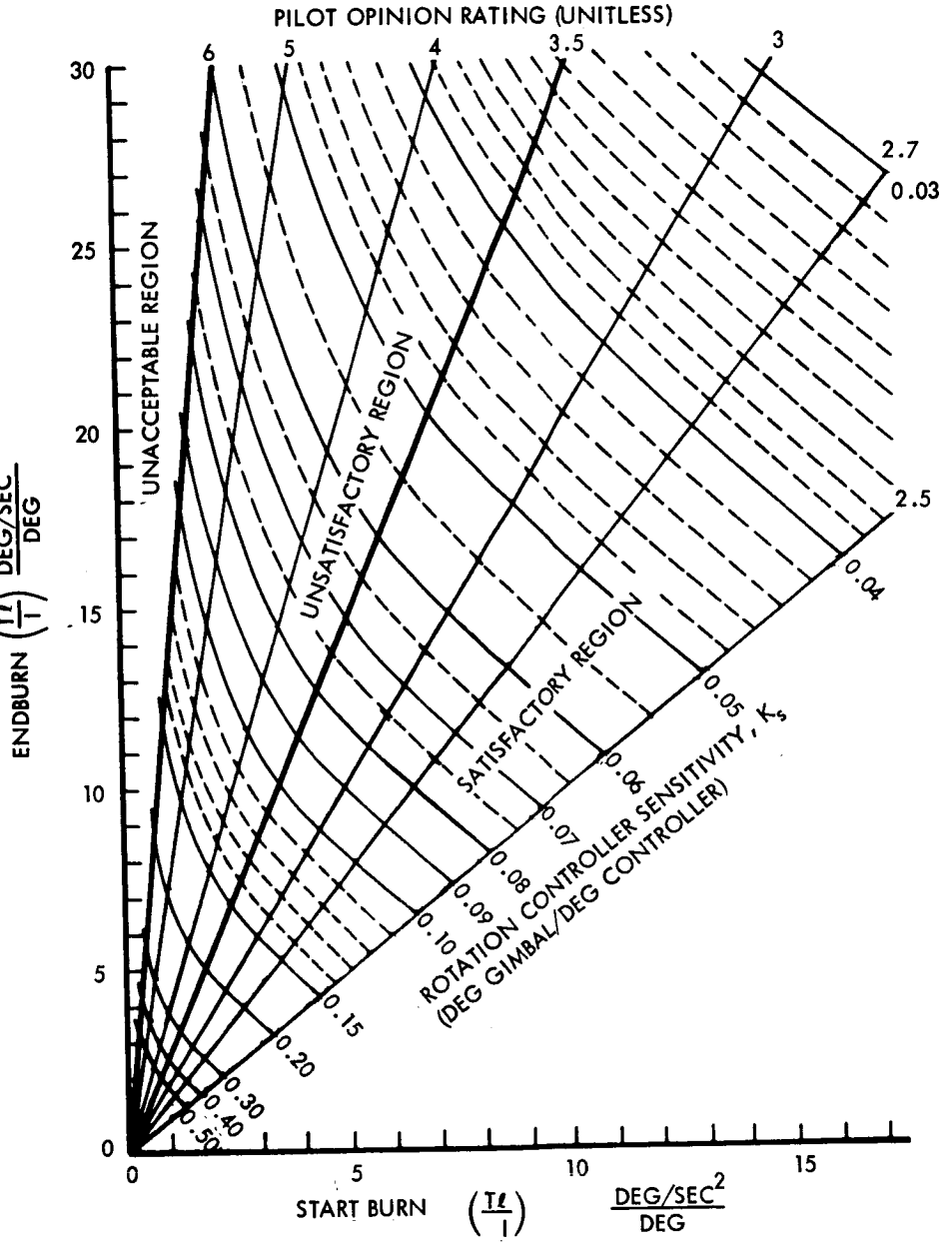

Figure 2-48. - Hardwire Control Pilot Opinion Rating and Sensitivity Curves

TABLE 2-10. - MASS PROPERTIES AND GEOMETRICAL DATA* FOR THE SYSTEM GAIN FACTORS STUDY

Parameter and Units	Start Burn	Mid Burn	End Burn
1000-lb Propellant--			
Weight - lbs	1975	1475	975
Moment arm - inches (ft)	10.5 (.875)	16.5 (1.375)	23.9 (1.99)
Pitch MOI - slug-ft^2	224	146	74
Roll MOI - slug-ft^2	270	166	77
1300-lb Propellant--			
Weight - pounds	2283	1633	983
Moment arm - inches (ft)	8.8 (.734)	15 (1.25)	23.7 (1.975)
Pitch MOI - slug-ft^2	258	167	75
Roll MOI - slug-ft^2	310	195	78
1600-lb Propellant--			
Weight - pounds	2595	1793	991
Moment arm - inches (ft)	7.4 (.616)	13.8 (1.15)	23.4 (1.95)
Pitch MOI - slug-ft^2	292	184	81
Roll MOI - slug-ft^2	359	221	85

*Reference configuration: Figure 3-1.

TABLE 2-11. - THRUST-TO-WEIGHT AND CONTROL SENSITIVITY DATA

Launch Thrust-to-Weight	End Burn Thrust-to-Weight	Launch T ℓ/I		End Burn T ℓ/I	
		Roll	Pitch	Roll	Pitch
1000-lb Propellant					
0.250	0.506	1.60	1.93	12.7	13.2
0.300	0.608	1.92	2.32	15.2	15.9
0.350	0.710	2.24	2.70	17.8	18.5
0.400	0.811	2.56	3.08	20.3	21.2
0.450	0.911	2.88	3.47	22.9	23.8
1300-lb Propellant					
0.250	0.581	1.35	1.62	14.4	15.0
0.300	0.698	1.62	1.95	17.3	18.1
0.350	0.814	1.89	2.28	20.2	21.2
0.400	0.930	2.16	2.60	23.1	24.2
0.450	1.047	2.43	2.92	26.0	27.1
1600-lb Propellant					
0.250	0.654	1.11	1.37	14.8	15.6
0.300	0.785	1.33	1.64	17.8	18.7
0.350	0.914	1.56	1.92	20.8	21.9
0.400	1.045	1.78	2.19	23.8	25.0
0.450	1.175	2.00	2.46	26.7	28.0

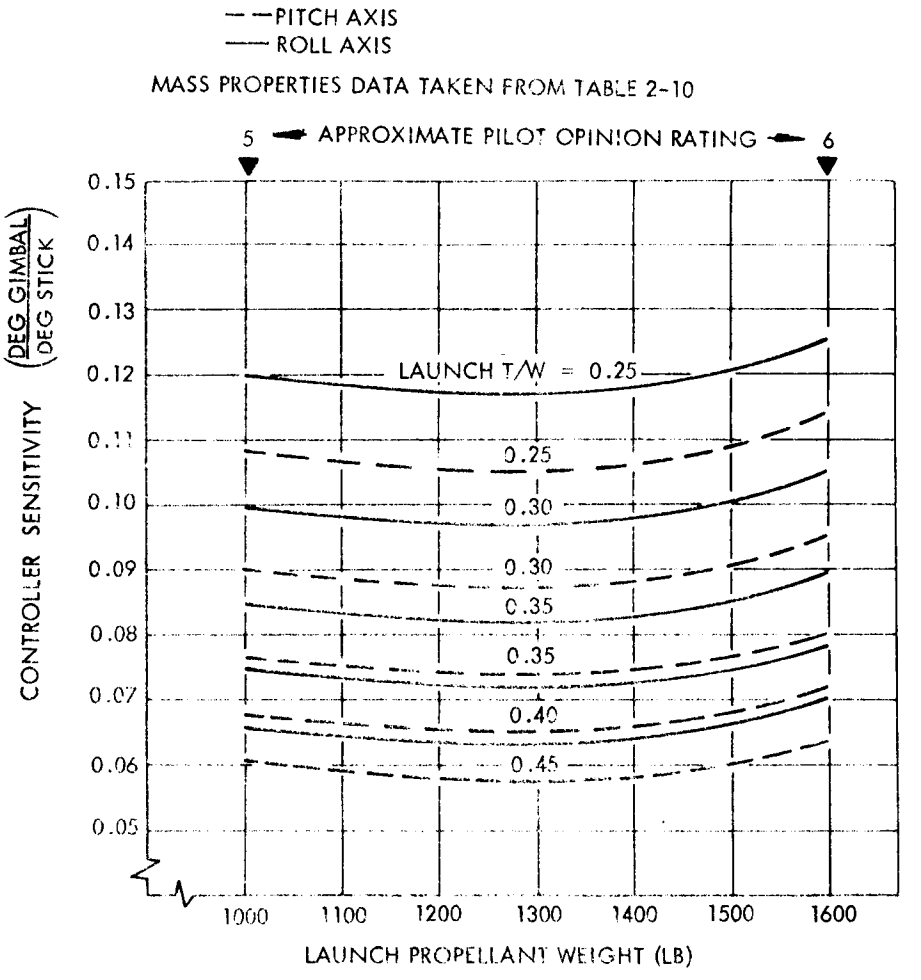

Figure 2-49. - Hardwire Stick Sensitivity Versus Propellant Loading

3. Program one or more step changes in thrust, so that the optimum region of the curve in figure 2-44 is traversed one or more times. The method is schematically shown in figure 2-50.

As a final guideline for vehicle design, once a value of $(T\ell/I)$ is determined for launch, a sensitivity gear ratio is set on the basis of handling qualities. This gear ratio will provide satisfactory handling qualities only until the value of $(T\ell/I)$ has tripled. The guideline is described pictorially in figure 2-51.

To further investigate the third suggested handling qualities improvement method, flight mechanics data was used, as seen in table 2-12. The values of $(T\ell/I)$ for start burn, the points just prior and just after thrust decrease, and end burn were calculated. To find the sensitivity gear ratio for the rotation controller, the start burn and end burn values of $(T\ell/I)$ were entered into the curves of figure 2-48. What occurred between start burn and end burn for each of the thrust decrease ratios could only be answered by further calculation. By using the propellant weight fraction data shown in figure 2-52 and the mass properties data in table 2-10, the intermediate values of $(T\ell/I)$ were computed. These values are shown in figure 2-53 for each thrust reduction ratio. The resulting estimated pilot opinion rating histories are shown in figure 2-54. The following observations can now be made:

1. Thrust reduction during boost may be used to improve hardwire pilot opinion ratings. Compare figures 2-54 and 2-49.

2. The optimum thrust reduction ratio, for the mass properties data utilized in this study, lies between 0.4 and 0.6. Ratios larger than 0.6 exhibit poor handling qualities at start burn and end burn. Ratios smaller than 0.4 produce poor handling qualities prior to thrust reduction. Further study of the small ratios may indicate that an intermediate, or three-level thrust history, will enhance handling qualities. Shifting the thrust reduction event to an earlier or later time penalizes total boost ΔV.

3. Decreasing the thrust reduction ratio increases the rotational controller sensitivity gear ratio. Large gear ratios are undesirable since they increase controller deflection load torques.

To complete the description of relationships between vehicle parameters, rotation controller sensitivity and deflection, and engine gimbal angle, the factor of total center of gravity alignment must be introduced. Typical hardwire control involves attitude oscillations about the desired attitude. These oscillations are caused by continuous control torque inputs by the

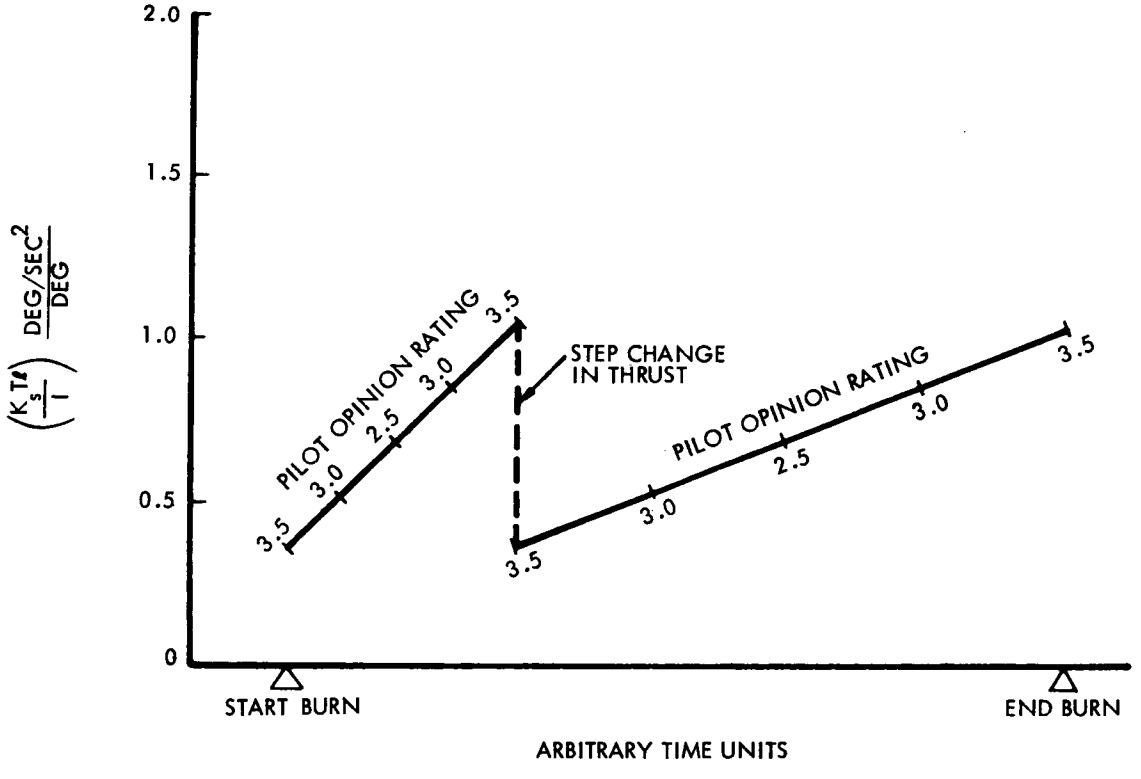

Figure 2-50. - Proposed Thrust Step Change Method for LESS Handling Qualities Improvement

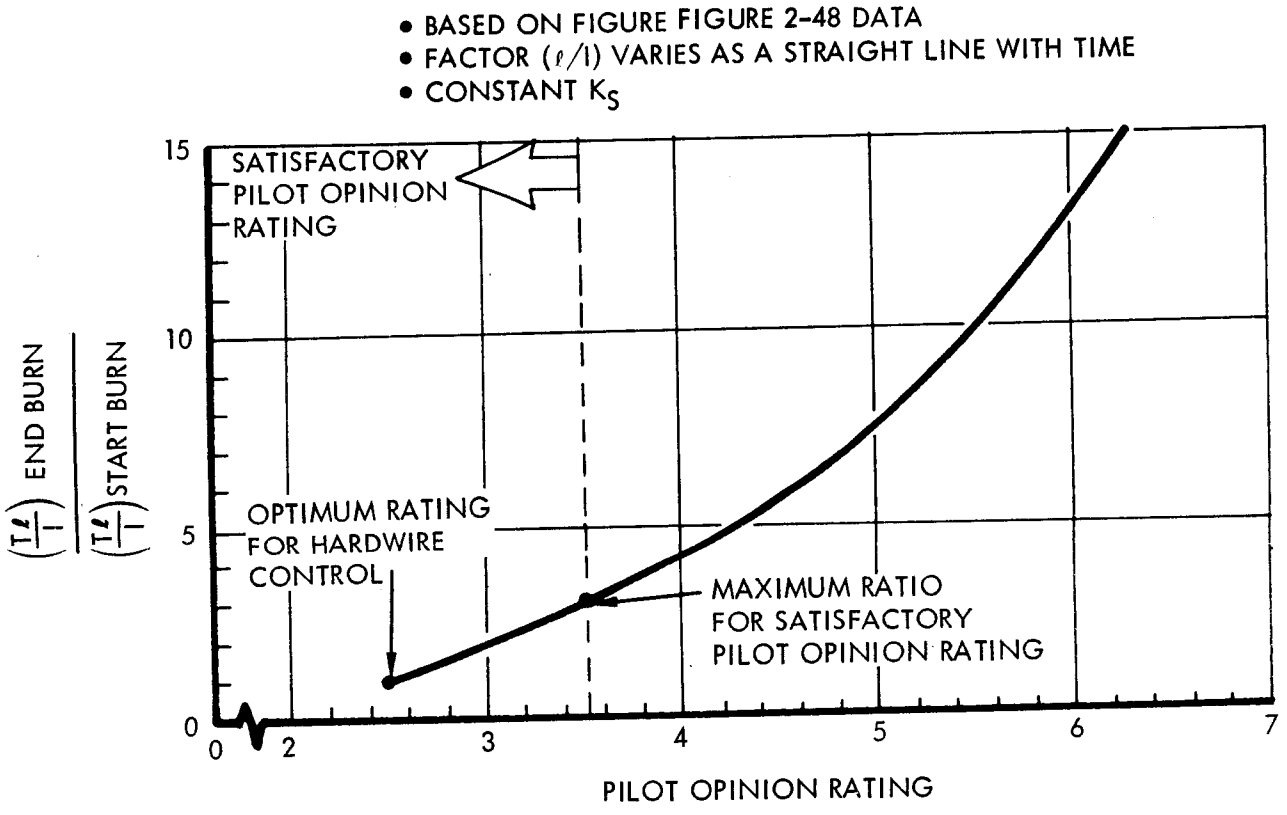

Figure 2-51. - Vehicle Configuration Guidelines for Improved Handling Qualities

TABLE 2-12. - OPTIMUM TWO-STEP TRAJECTORY THRUST SCHEDULE DATA

Ratio of Final to Initial Thrust Level (T_2/T_1)	Thrust-to-Weight Ratio Prior to Thrust Decrease, (T_1/W)	ΔV at Thrust Decrease, (1000 fps)	Total Boost ΔV (1000 fps)
1.0	0.375	2.20	7.216
0.8	0.395	2.67	7.070
0.6	0.422	3.60	6.935
0.4	0.450	3.95	6.830
0.2	0.490	4.75	6.725
0.1	0.530	5.42	6.670

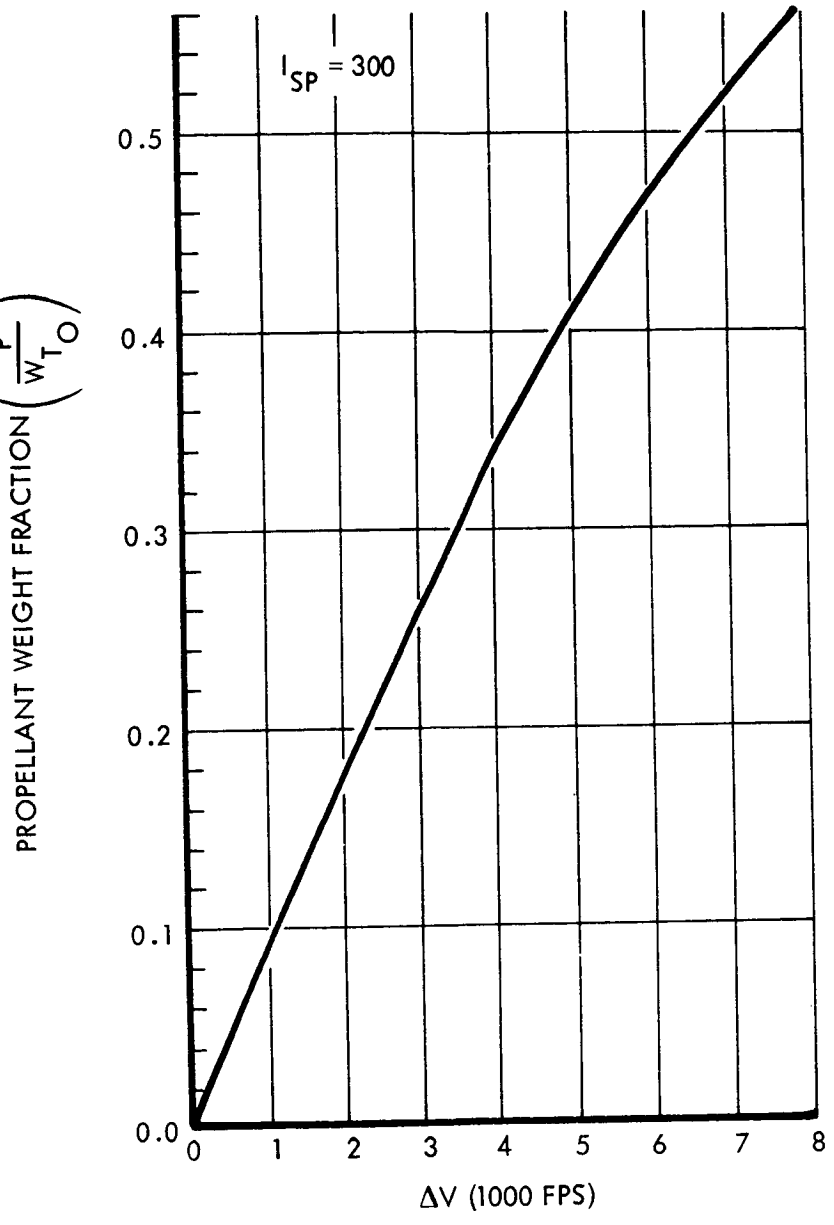

Figure 2-52. - Propellant Weight Fraction Versus Expended Boost ΔV, I_{SP} = 300

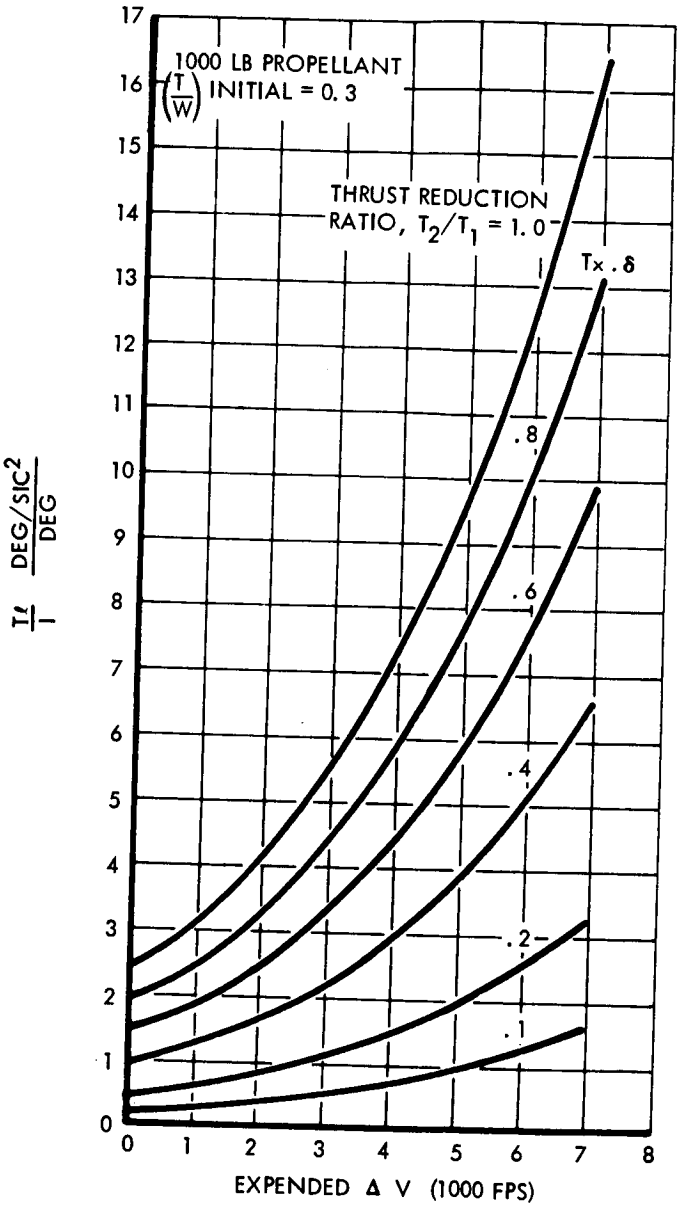

Figure 2-53. - $\frac{T\ell}{I}$ Versus Expended ΔV for Various Thrust Reduction Ratios

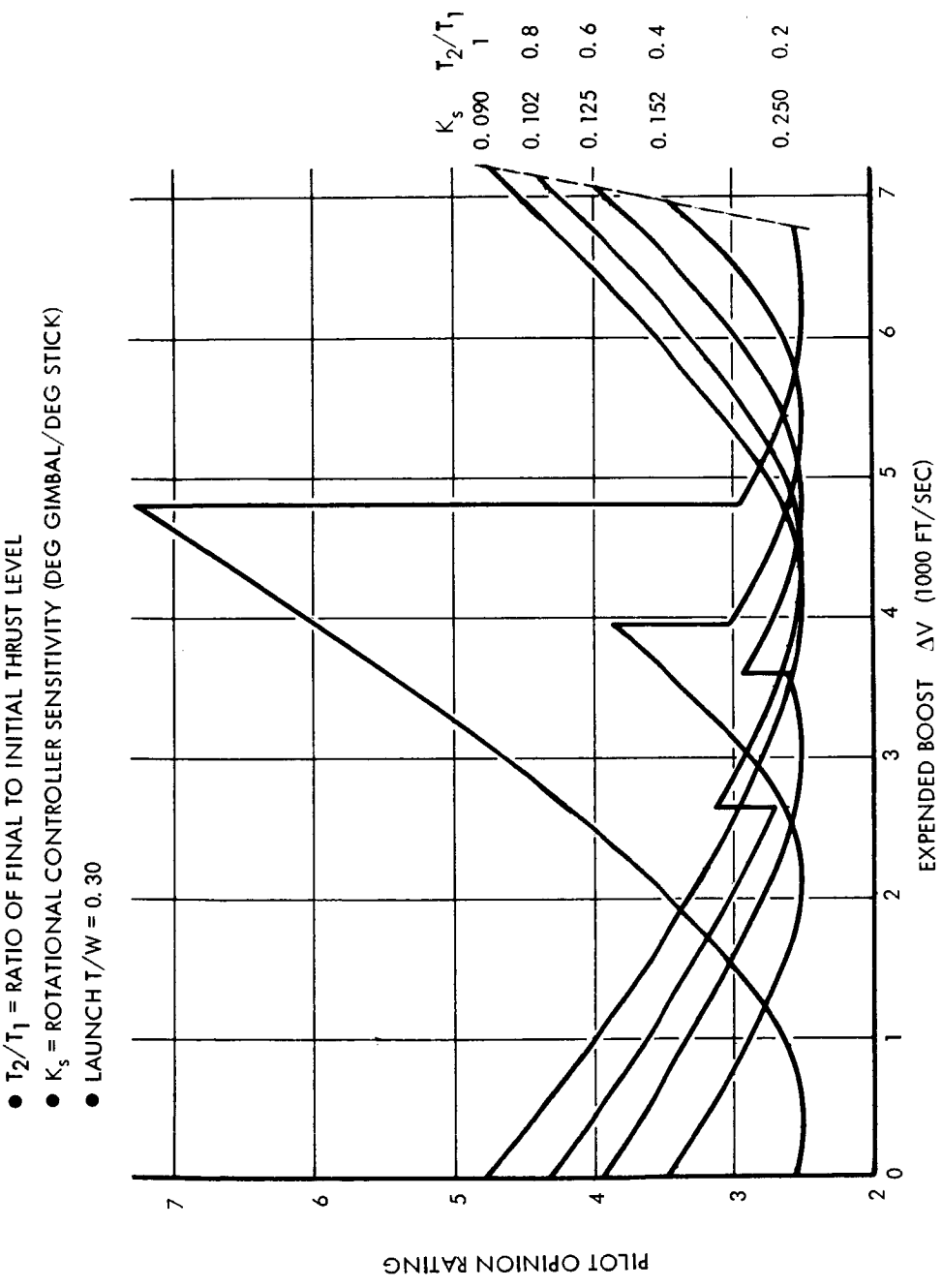

Figure 2-54. - Effect of Thrust-Level Switching on Pilot Opinion Rating

pilot, the average torque being zero. Since zero torque implies aligning the thrust vector through the total center of gravity, the center of gravity position is of importance for precision guidance. If the total center of gravity is off center an amount ΔX and ΔY feet, then the thrust vector must be misaligned ϵ_p degrees for stable attitude rate, where

$$\epsilon_p \cong \pm 57.3 \frac{\sqrt{\Delta X^2 + \Delta Y^2}}{\ell} \tag{2-18}$$

As an additional complication, both the rotation controller and the engine gimbal must be designed to include this misalignment without decreasing the deflection range needed for stabilization and maneuvers. The maximum gimbal travel required is then

$$\delta_{GIMBAL} = K_S \delta_{STICK} \pm \epsilon_p \tag{2-19}$$

and the maximum gimbal travel must be capable of producing a predetermined angular acceleration:

$$\ddot{\theta} \cong \left(\frac{T\ell}{I}\right) \delta_{GIMBAL}$$

The relationships between these factors are shown in figure 2-55 as a nomograph. In the figure, a particular example was chosen for illustrative purposes which uses the mass properties data for 1,000-pound propellant loading from table 2-10, and a launch thrust-to-weight ratio of 0.30. The maximum angular acceleration requirement was chosen to be 0.075 radians per second^2, which is one-half of the requirement for the lunar flying vehicle at launch. A pitch-plane total center of gravity misalignment corresponding to 0.5 degree thrust misalignment is shown. The remaining input data point, that of rotation controller sensitivity, was chosen to be 0.2 degrees of gimbal per degree of rotation controller. The results of the example show a 12-degree maximum rotation controller deflection and a 2.35-degree maximum gimbal angle suffices.

By entering compatible values of $(T\ell/I)$, angular acceleration, and thrust misalignment for various points during boost, maximum gimbal and rotation controller deflection history requirements may be determined. This operation is necessary to ensure adequate control capability throughout boost.

Manual stabilization and control techniques conclusions. - The detailed conclusions of this report section are given in the Guidance and Control Techniques Conclusions Summary section which follows.

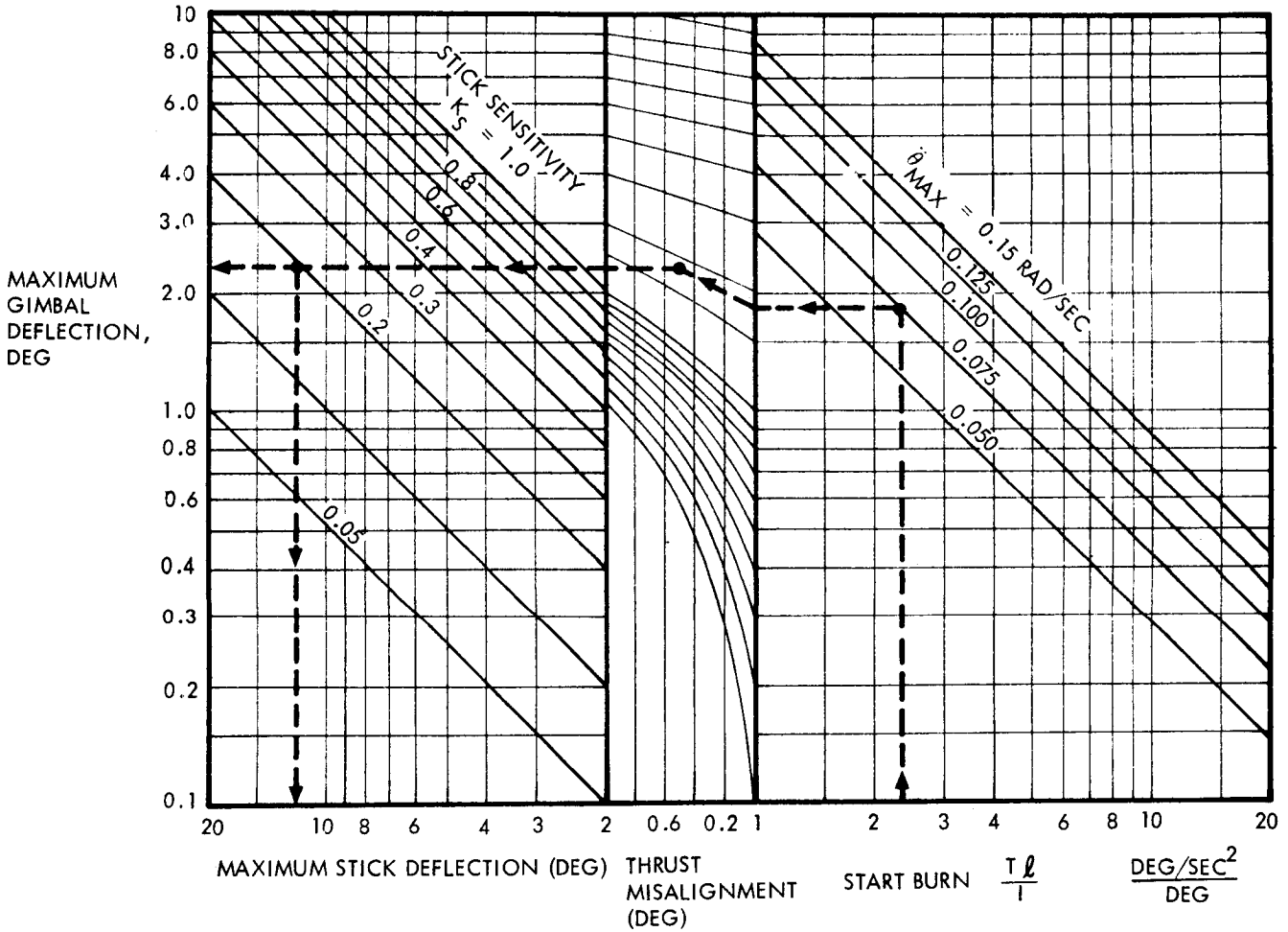

Figure 2-55. - Control Authority Relationships

Guidance and Navigation Concept Synthesis

Introduction and objectives. - The purpose of this effort was to identify guidance system concepts that are appropriate for the LESS. In keeping with the scope of this Phase A study, a broad variety of concepts were examined. Gross comparisons and tradeoffs were made to establish a relatively small family of preferred concepts.

Approach. - The LESS mission is an emergency or backup approach to the normal LM ascent and rendezvous. The availability of large quantities of LM propellants makes it virtually unnecessary to achieve fuel-optimal guidance and, therefore, permits less sophisticated guidance systems than either the primary or abort guidance system of the LM. The guidance system is required only to establish the LESS in a rendezvous-compatible orbit about the moon. In general, this orbit is clear and permits the CSM to perform the rendezvous within its ΔV constraints and within the time limitations of the spacesuit life support systems of the LESS crewmen. Injection into higher orbits than the LM (60 nm rather than approximately 10 nm) is utilized to reduce the guidance accuracy requirements even further.

With regard to safety and reliability, the presently conceived LESS does not operate in a fail-safe environment and requires the time-critical completion of several operations for success; therefore, the approach adopted is to employ "less guidance for LESS" and to achieve adequate safety and reliability through the use of simple systems and operations.

Guidance system requirements: The principal system requirements considered herein are minimizing the system complexity and maintaining sufficient accuracy. The word complexity is used qualitatively herein to refer to factors such as operational complication, ease of piloting, system weight, power, volume, cost, etc. System accuracy requirements may be inferred from the trajectory error sensitivity data in the Trajectories Section of this report using the error source data of G&C System Analysis Section. The approach employed in the study was to assess the accuracy capability of the subsystem concepts rather than to arbitrarily budget an accuracy requirement on each of the subsystems. The total thrust vector pointing errors must typically be maintained at a time-averaged value of less than 1.5 degrees to achieve a safe orbit with a nominal altitude of 60 nm.

System synthesis approach: The specific approach employed herein was to:

1. Identify the capabilities of existing systems external to the LESS (LM, CSM, and mission control center) to assist in the guidance functions.

2. Identify gross subsystem concepts.

3. Contrast qualitative merits of concepts to identify preferred approaches.

4. Integrate preferred subsystem candidates into complete system concepts that can be mechanized for simulation (NASA-LRC).

Anatomy of the problem: For the purpose of this report, guidance refers to control of the path or trajectory of the spacecraft center of mass. For LESS, this control consists of propulsion ignition timing, thrust vector steering, and propulsion cutoff control. Steering requires an attitude-reference sensing system and may employ additional trajectory measurements or navigation data to achieve the desired trajectory. The stabilization and control system consists of the devices used to control vehicle attitude dynamics and any additional stability-augmentation devices necessary to achieve adequate stability.

Assumptions and ground rules:

1. The LESS must be capable of being operated and flown satisfactorily by a single crewman in the event the second crewman is incapacitated; however, the two crewmen may share flight control tasks if they are both fit.

2. The LESS must achieve a clear orbit of the moon prior to the first propulsion system shutdown.

3. It is assumed that the LM voice communication and/or guidance and navigation updata link is operative and that the pre-ascent guidance targeting computations may be accomplished at the Mission Control Center and relayed to the LESS (i. e., an autonomous LESS guidance system is not required).

Guidance elements external to LESS. - To establish a minimum-complexity LESS guidance system, it is appropriate to examine functions that can be accomplished by other guidance equipment associated with the problem:

Mission Control Center at Houston (MCC/H): The existing voice link and guidance computer updata link in the LM can be utilized to transmit the LESS ascent guidance targeting data, as is the current procedure for all Apollo major thrusting maneuvers.

CSM: Sextant sighting and VHF range data can be utilized for landing (takeoff) site determination and for rendezvous guidance; however, the CSM guidance computer using the sextant and VHF range data does not provide sufficiently fast response to be of any assistance during the LESS ascent phase.

LM: The LM abort guidance system might be repackaged to provide for easy removability and, thereby, to permit its alternate use with the LESS. (This approach is evaluated further in this report.) The LM optics might also be of assistance in the alignment of LESS attitude reference systems. During ascent, the LM radar could track the LESS automatically and might be used via a communication link for closed-loop guidance. The technique might conceivably be worked out should a requirement for closed-loop guidance manifest itself.

Summary of stabilization and control system (SCS) concepts. - The SCS may be considered to be the plant function or controlled element in the guidance problem. For this reason, it is pertinent to summarize some of the properties of the candidate SCS concepts with respect to guidance prior to defining guidance subsystem concepts (table 2-13). An autopilot system is added to the manual SCS concepts for comparative purposes.

Based on the analyses given in the Manual Stabilization and Control System Section of this report, several of the SCS concepts are not as attractive as the others for the LESS application and will be deleted from further consideration. The systems deleted are the following:

1. Kinesthetic (two-body control): Analysis indicates that the small potential improvement in handling qualities, over those of the basic single-body kinesthetic control method, is not warranted by the increased complexity of the system (severe design constraints on the overall vehicle configuration), and the expected improvement is not sufficient to compete with hardwire control. For these reasons, no further effort in the guidance area on this system will be made.

2. Hardwire with compensation networks: The handling qualities anticipated for this system lie between those of the basic hardwire system and the stability-augmented system. Similarly, the mechanization penalties associated with adding compensation networks are probably a compromise between the two systems. It has been

TABLE 2-13. - SUMMARY OF STABILIZATION AND CONTROL SYSTEM CONCEPTS

SCS Concept	System Description and Possible Mechanizations	Pilot Handling Qualities (Estimated Cooper Rating for LESS Configuration C)	*Thrust Vector Pointing Error (1σ)	Dynamic Interaction W/Display	Comments (Pilot Work-loads, etc.)
Kinesthetic (one body)	Rocket engine not gimbaled; pitch and roll control achieved by pilot body motion and yaw control by RCS jets.	Emergency use only, to unacceptable, even for emergencies. 5-6	1.3°	The required body (head) motion will not permit simple visual display concepts.	Very demanding on pilot, requires complete attention to attitude control task.
Kinesthetic (two body)	Rocket engine not gimbaled; pitch and roll control achieved by pilot body motion. Undesirable frequencies filtered by network between two vehicle body masses. Yaw control is by RCS jets.	Emergency use only, to unacceptable, even for emergencies 5-6	1.3°	The required body (head) motion will not permit use of many visual display concepts.	Very demanding on pilot, requires nearly complete attention to attitude control task.
Hardwire (basic system)	Controller directly connected to rocket gimbal for pitch and roll. RCS jets provide yaw control.	Unpleasant characteristics, unacceptable for normal operations. (4-1/2)	1.2°	The large attitude excursions require fairly large display scale.	Very demanding on pilot, requires major attention to attitude control task.
Hardwire (with compensation networks)	Controller connected to rocket gimbal through passive compensation network for pitch and roll. RCS jets with network for yaw.	Unpleasant characteristics, unacceptable for normal operations. (4-1/2)	1.2°	The large attitude excursions require fairly large display scale.	Simulation studies do not confirm significant improvement in handling qualities over basic hardwire. Further study is recommended.

TABLE 2-13. - SUMMARY OF STABILIZATION AND CONTROL SYSTEM CONCEPTS - Concluded

SCS Concept	System Description and Possible Mechanizations	Pilot Handling Qualities (Estimated Cooper Rating for LESS Configuration C)	*Thrust Vector Pointing Error (1σ)	Dynamic Interaction W/Display	Comments (Pilot Workloads, etc.)
Hardwire (neutral c.g.)	Same as basic system except that rocket engine system is uncoupled from remainder of vehicle and can be pivoted about the c.g. Thrust vector is flown through pitch profile while remainder of vehicle remains in locally level attitude.	Unpleasant characteristics, unacceptable for normal operations. (4-1/2)	1.2°	Locally level vehicle attitude makes visual sighting devices more attractive for this concept.	Level vehicle attitude is attractive for simple visual attitude references.
Hardwire (reaction jet control)	Controller connected through logic to multi-jet system. Boost and attitude control by pulse duration modulation.	Potentially higher Cooper ratings than for basic hardwire.		Display scales similar to those of basic hardwire.	Most easily adapted to shaping networks or stability augmented control.
Stability-augmented system	Automatic control signals are added to manual control signals to enhance the stability and handling qualities of the vehicle. Requires the addition of some type of vehicle motion sensor such as rate gyro.	Good to satisfactory with some mildly unpleasant characteristics. (2-1/2)	0.3°	Negligible.	Pilot workload is more reasonable than above concepts, permitting greater attention to the utilization of additional displayed information.
Autopilot	Automatic closed-loop attitude control without pilot inputs. Greatest control system mechanization complexity of all concepts.	Not applicable.	0.2°	Negligible.	Minimizes pilot workload.

(*)Preliminary estimates are based on extrapolation from Apollo manual thrust vector control system simulation data and lunar flying vehicle simulation data. See Guidance Error Analysis Section for latest pointing error estimates.

recommended in the Stabilization and Control Section that further study of this mode be conducted to more firmly establish its position. In the absence of sufficient data to confirm the anticipated handling qualities improvement and since its performance is bounded by two other systems, it will be deleted from further guidance considerations.

3. Hardwire (neutral c. g.): The handling qualities improvement expected for the application of this concept to LESS is small compared with its complexity; the advantages of a level base for simple visual sight mounting are outweighed by the mechanization penalties.

Systems remaining for further consideration are the kinesthetic (basic), hardwire (basic), stability augmentation, and autopilot.

Thrust ignition and cutoff control concepts. - A family of potential concepts is listed in table 2-14 along with a discussion of their relative merits. The clock is found to provide the simplest basis for thrust ignition timing. The third and fourth concepts listed are operationally limited and are much more unwieldy than the first and second concepts. It is concluded that the clock for ignition and the ΔV meter for thrust cutoff constitute the least complex of the satisfactory approaches. The inertial guidance and navigation represents the most complex approach and is preferable only if steering accuracy necessitates this approach.

Attitude reference system concepts. - The attitude reference sensing devices are classified below as instrument or visual devices. For the manually controlled SCS concepts, the thrust vector pointing accuracy requirement necessitates that the pilot give his full attention to controlling the spacecraft. For this reason, integrated three-axis attitude displays are deemed necessary. Also, hybrid combinations of visual and instrument attitude reference systems are not given, primarily, because the resulting system generally possesses all the disadvantages of both types of systems.

Instrument attitude reference concepts: Present state-of-the-art attitude reference system technology has provided: gyroscopic devices, sun sensors, horizon scanners, and star sensors.

The star and horizon sensor devices are immediately rejected for the LESS application because of their relative complexity and sophistication when compared with the gyro, sun sensor, and visual display devices discussed in subsequent sections. The preferred concepts are summarized in table 2-15.

TABLE 2-14. - THRUST IGNITION AND CUTOFF CONTROL CONCEPTS

Clock	Requires an externally computed launch/cutoff time. Is simple to mechanize and is operationally easy to use. Excellent accuracy for obtaining on-time launch. Trajectory error sensitivity study indicates an unacceptable cutoff sensitivity to thrust-to-weight ratio errors.
ΔV Meter	Integrating accelerometer mounted along thrust axis of vehicle can provide very accurate measurement of characteristic velocity. Accuracies better than 0.1 percent are achievable with off-the-shelf hardware produced by several manufacturers. Hardware procurement costs are reasonable. Trajectory error sensitivity study indicates that this cutoff method is much less sensitive to thrust-to-weight ratio errors than the clock cutoff technique.
Line-of-Sight Angle to CSM	Requires external computation of angle and precise sighting equipment, and requires crew operation during a critical period. Appropriate for ignition time determination only. It is not appropriate for launches when CSM is out of sight of when visibility is limited by proximity to the sun.
Signal From CSM	For ignition control, communication from CSM through LM to PLSS is required. For ignition timing it is better to use this means to update clock setting and eliminate the potential problem of communication black-out. For cutoff control, the CSM astronaut may base the signal on the rate of change of his VHF range display. This technique is severely limited operationally by the maximum communication range of the CSM to the PLSS (less than 40 nautical miles). Ascent mission profile geometry may result in a considerable cutoff velocity error when using relative range rate as a basis for the cutoff.
Inertial Guidance and Navigation	The explicit navigation computations within this system provide the most accurate and flexible means of performing the thrust ignition and cutoff control functions. This system may possess greater complexity and refinement than is required or justifiable for the LESS.

TABLE 2-15. - INSTRUMENT ATTITUDE REFERENCE CONCEPTS

Concept	Description	SCS Applicability	Remarks
Free Gyros	Two 2-degree-of-freedom gimbaled free gyros. May use direct mechanical coupling to displays as with aircraft panel instruments. May not require power after initial spinup before launch.	All systems. Better for kinesthetic and hard-wire systems which do not require gyros to have electrical gimbal pickoff transducers.	Accuracies adequate, but poorest of gyro concepts. The technology is oldest, but none has been space qualified.
Rate Integrating Gyros	Three single-degree-of-freedom floated gyros. Electrically driven instruments are torqued providing electrical signals for stability augmentation and attitude display.	All systems. Best for stability augmented or autopilot systems, since electrical signals are available for mechanization.	Space-qualified hardware exists. May require appreciable warmup time and some temperature control. Can easily meet LESS accuracy requirements. Power consumption and complexity greater than free gyro concept.
Stable Platform	Three gimbal gyro-stabilized platform. Clever packaging and gimbal design may permit direct mechanical drive of attitude display. A very wide range of mechanization complexities are possible from a simple 3-axis attitude display (without gimbal transducers and torquers) to the refined inertial measurement unit of an inertial navigator.	All systems.	Attitude reference systems with appropriate characteristics have not been space-qualified, except for the larger more complex inertial measurement units used for inertial guidance.
Sun Sensors and Gyro	Two-axis solid-state solar-aspect detectors and single gyro for third axis. Multiple sun sensors can be used for multiple-step pitch profile, or detectors can be gimbaled for optimum pitch profile. The single gyro can be pendulously erected to local vertical	All systems.	Sun sensor mounting location requirements to obtain necessary FOV are more stringent than for gyros. Requires less complex pre-launch alignment than all-gyro system. Sun sensors require negligible power and provide electrical outputs for displays or automatic control. Many devices of this type have been space-qualified, and the technology is well established although this integrated sun sensor/gyro concept has not been developed.

Visual attitude reference concepts: Because of the less well-developed technology in the area of visual attitude reference devices (despite pioneering work at NASA-LRC), it was deemed advisable to return to basics, and the following approach was adopted:

1. Identify all the pertinent features of the visual environment that might be useful for visual attitude reference and define the attitude information that might be derived.

2. Contrast the relative advantages of the visual attitude-reference concepts to identify the superior techniques.

3. Combine the resulting attitude reference concepts into three-axis attitude display concepts.

Identification of visual references: The visually identifiable features of the lunar environment are listed in table 2-16 along with the attitude information that can be obtained, possible mechanization approaches, and relative advantages of the concept.

Visual attitude reference concept evaluation: Based on the remarks contained in table 2-16, the following visual attitude-reference concepts are judged to be inferior to the other concepts listed in the table.

1. Lunar terminator: poorly defined image is inferior to lunar horizon.

2. Earth: inferior to sun, not as bright, location is generally overhead providing no azimuth data.

3. Stars/planets: no particular advantage over solar and horizon, viewers and mechanizations are more cumbersome.

4. LM: less advantageous than forward landmarks.

5. Flare operationally more difficult than using the sun, landmarks, or horizon with no appreciable advantages over these references.

The remaining preferred visual attitude reference concepts are lunar horizon perpendicular to orbit plane, lunar horizon in orbit plane, lunar landmarks, solar viewer, and CSM.

The lunar landmarks and horizon located beyond the terminator (dark region of the moon) are included above, but considerable doubt remains at this time regarding their visibility. It may be observed that any of the attitude-reference concepts provides attitude information in no more than two axes; therefore, it becomes appropriate to investigate the feasibility of integrating the attitude reference concepts into complete three-axis displays.

TABLE 2-16. - ALTERNATIVE VISUAL ATTITUDE REFERENCE CONCEPTS

Visual Reference	Attitude Provided	System Description and Possible Mechanizations	SCS Concept Applicability	Remarks
Lunar Horizon (Perpendicular to orbit plane)	Pitch and roll	T-tube, mirror-reflected images of horizon segments perpendicular to orbit plane (mirrors/prisms).	All manual modes, slightly less appropriate for kinesthetic because of head motion required.	Most accurate for roll; less accurate for pitch. Probably requires sun illuminated horizon. Significant error at low altitudes due to terrain roughness.
Lunar Horizon (In orbit plane)	Pitch and roll	View forward (or rearward) horizon in plane of orbit, hinged wide-angle telescope, periscope, wire grid, recticle on plastic window, gunsight with virtually imaged recticle (Apollo COAS - type device).	All manual modes, less appropriate for kinesthetic because of head motion required.	Forward lunar horizon visibility past terminator (darkside of moon) is questionable (without dark adaption of eye). The aft horizon is well illuminated by the sun, but its use is subject to greater attitude errors than use of a forward landmark (this phenomena is discussed in a subsequent section). The simplest mechanizations have considerable parallax error for kinesthetic control because of required head motions. Significant error at low altitudes is due to terrain.
Lunar landmarks	Azimuth and pitch	Same type of devices as for lunar horizon use known landmarks near horizon to sight on. View can be shifted to more distant landmarks as vehicle flies over the landmarks used earlier in the boost.	Same as lunar horizon.	Same as for lunar horizon. The technique may be somewhat limited by the finite number of landmarks readily distinguishable.
Lunar Terminator	Pitch and roll	Same as lunar horizon (in orbit plane).	Same as lunar horizon.	Accuracy is poor because of lunar surface irregularities.
Solar Reference	Azimuth and pitch	Solar image filtered to reduce light intensity. May be viewed directly through periscope or imaged on ground-glass display. Variable intensity filtering will permit superposition of sun image into other displays (such as (T-tube). Non-spherical optics may be used to image the sun in unusual shapes such as a line.	Same as lunar horizon.	Daytime use only. Requires considerable filtering if crewman is to see other references also. Sunline can be considerably misaligned with control axes and can, therefore, introduce cross-coupling. The high light intensity and shape of the sun permits easy acquisition and imaging. Automatic solar-aspect sensing can also be easily accomplished, and many

TABLE 2-16. - ALTERNATIVE VISUAL ATTITUDE REFERENCE CONCEPTS - Concluded

Visual Reference	Attitude Provided	System Description and Possible Mechanizations	SCS Concept Applicability	Remarks
Solar Reference (Continued)				of these sensors have been space qualified. No azimuth available when sun is overhead.
Earth	Azimuth and elevation	Same devices as for lunar horizon (in orbit plane).	Same as lunar horizon.	Usually less desirable than sun because of sun's higher intensity. May be difficult to see because of proximity of sun. For some mission geometry, the earth may have a more favorable location for use as an attitude reference.
Stars and Planets	Yaw, pitch, and roll.	Wide-FOV telescope or sextant optics with extensive light shielding devices to permit dark adaption of eye. Drop filter into optical path whenever bright object enters FOV.	Same as lunar horizon.	Required light shielding around space helmet will be bulky and cumbersome. Reference is easily lost if bright object enters FOV and eye loses dark adaption. Complex gimbaling required to fly pitch profile.
CSM	Azimuth and elevation.	Same devices as for lunar horizon (in orbit plane).	All manual modes. Most appropriate for more stable fast-response systems.	Use for active steering w.r.t. CSM using classical collision-course guidance (proportional navigation). During latter portion of ascent in the near vicinity of the CSM, poor with some sun angles.
LM (on lunar surface)	Azimuth and elevation.	Same devices as for lunar horizon (in orbit plane).	Same as lunar horizon.	Errors in prior trajectory are perpetuated. Difficult to find a suitable means of using this reference.
Flare	Azimuth and elevation.	Flare shot from CSM or LM in direction of desired orbit plane. Track with same devices as lunar horizon (in orbit plane).	Same as lunar horizon.	Requires development and testing of space flare technology and deployment. Flare will probably have short life. Flare trajectory subject to deployment errors. Satisfactory use of flare will probably require deployment from CSM while some place overhead and hence, will result in CSM being phased appreciably ahead of LESS.
Balloon	Azimuth	Balloon inflated and deployed from LM during descent orbit phase. Track with same devices as lunar horizon (pitch).	Same as lunar horizon.	Balloon deployment errors propagated over the longer lunar mission stay-time can result in unfavorable phasing for rendezvous. Places tight constraint on ascent launch time. Possible visibility problem due to proximity of sun.

Visual attitude reference display integration: The visual attitude-reference concepts defined, in general, provide attitude information about no more than two axes. The poorer stability of some of the SCS concepts being considered requires that the pilot devote considerable attention to controlling all three axes of vehicle motion. Three-axis attitude displays, which require the pilot to do only a minimum amount of instrument scanning, are considered mandatory for these cases. The purpose of the following discussion is to integrate the visual concepts into three-axis displays.

Of the preferred visual attitude-reference concepts defined, only the solar viewer and lunar landmarks provide azimuth (yaw) references. For this reason the various possible combinations of concepts are classified according to whether they employ the sun or landmarks for the azimuth reference.

Table 2-17 presents some possible combinations of the visual attitude-reference concepts to achieve three-axis displays. Also included in the table is more definitive information on mechanization possibilities, whether the sight is directly coupled or gimbaled with respect to the vehicle, and the pitch steering profile that is most appropriate for the display. It may be noted that the solar viewer concepts can be implemented by facing the pilot toward the sun or by means of a periscope that enables the pilot to face in the direction of down-range flight.

Of the display concepts given in table 2-17, the following were judged to be inferior:

1.a - More complex than 1.b.

1.c - No significant advantage over other concepts.

2.b - More complex than 2.c.

2.d - Not so accurate as 2.b or 2.c; display more difficult to view than those of other concepts.

The following concepts are judged to be the superior approaches:

1.b - Minimum complexity of type 1 concepts, provides a "natural" display to pilot.

2.a, 2.c, and 2.e - Requires more detailed analysis to establish which of three is best.

TABLE 2-17. - INTEGRATION OF VISUAL ATTITUDE REFERENCE CONCEPTS TO OBTAIN ALL-ATTITUDE DISPLAY

	Attitude Reference			Sight Gimbaling	Pitch Profile	Cross-Coupling In Display	Mechanization
	Yaw (Azimuth)	Pitch (Elevation)	Roll (Roll)				
1.a	Landmark (near forward horizon)	Front horizon	Front horizon	Decoupled	Optimum program	Large	Wide-angle telescope or optical gunsight type devices.
b	Landmark (near forward horizon)	Front horizon	Front horizon	Coupled	N steps	Bad	Separate optics for each step.
c	Landmark (near forward horizon)	Front horizon	T-tube	Decoupled	Optimum program	Large	Add T-tube for roll reference; otherwise, same as 1.a. Improves roll-reference accuracy.
2.a	Solar viewer	Solar viewer	T-tube	Decoupled	Optimum program	Significant	Optical imaging.
b	Solar viewer	Solar viewer	T-tube	Coupled	Optimum program	Worse	Requires very-wide-angle sun imaging optics (multiple lenses) to image sun continuously through large pitch angle. Pip is driven to optimum program.
c	Solar viewer	Solar viewer	T-tube	Coupled	N steps	Worse	Separate sun-imaging optics and horizon mirrors may be utilized for each step.
d	Solar viewer	Solar viewer	Simple grids	Either	Either	Significant	Same as 2.a or b, but direct viewing of side horizon through simple grids replacing T-tube.
e	Solar viewer	T-tube	T-tube	Coupled	θ versus h or N steps	Worse	Sun is optically imaged as long narrow line for azimuth reference θ versus h is achieved with minor adjustment of T-tube arrangement.

Some factors affecting choice of lunar features for attitude reference: The lunar landmarks and horizon have been included in the visual attitude-reference concepts treated; however, some doubt exists regarding their visibility when located on the dark side of the terminator. The brightly illuminated region in front of the terminator may not permit the dark adaption of the eye necessary to see the features beyond the terminator even though these features are illuminated by earthshine. The Apollo 8 and 10 crewmen have given their opinions on this matter but were unable to be conclusive, as none of them viewed the terminator under these conditions.

Some interesting phenomena occur in using visual attitude-reference marks that are located at a finite distance with respect to the observer (fig. 2-56). If the ascent trajectory dispersions are significant compared with the distance to the reference mark, these dispersions produce a change in the direction of line of sight. As indicated in the figure, a reference mark ahead of the vehicle produces a favorable change in the line-of-sight direction, the thrust vector being turned back toward the preferred direction. Similarly, a reference mark behind the thrusting vehicle has the opposite effect and tends to increase or compound the effects of prior trajectory dispersions. On this basis, horizon and landmarks in the down-range direction appear to be distinctly preferable to those opposite the direction of flight. The choice of lunar landmarks may be made so as to maximize the beneficial effects of this phenomenon.

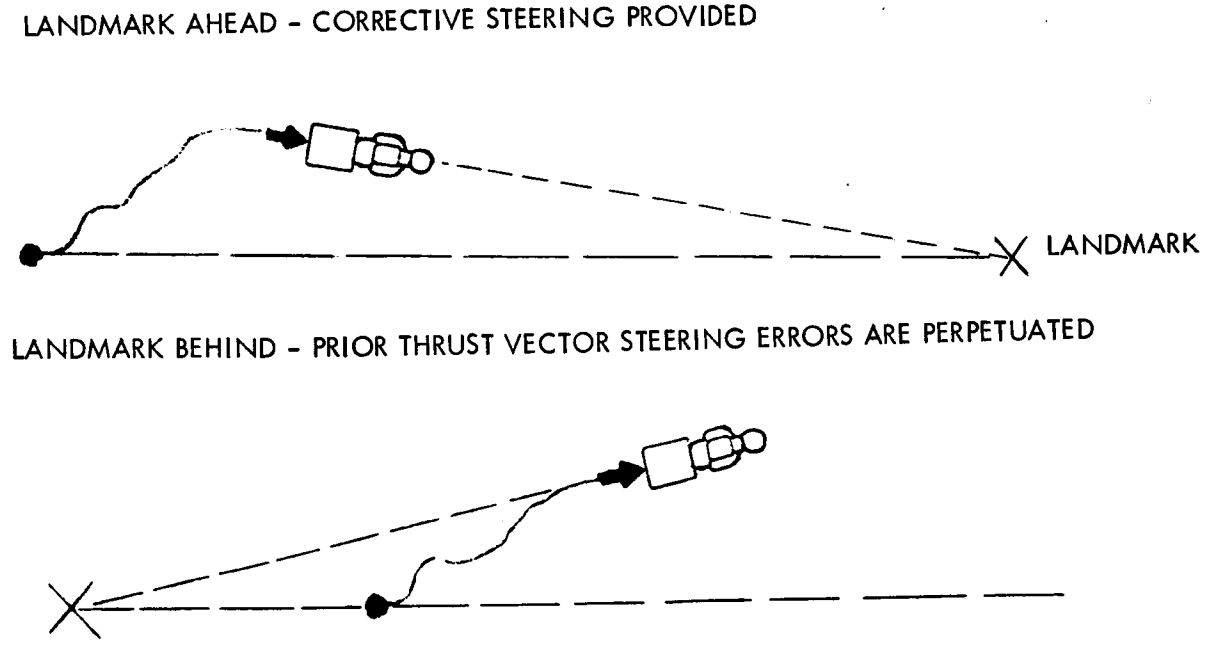

Figure 2-56. - Use of Landmarks at Finite Distance for Corrective Steering in Azimuth (top views)

Pitch profile requirements on visual displays: When steering the LESS to a horizon or solar attitude reference, the vehicle is required to pitch through relatively large angles. Table 2-18 presents typical values for these pitch angle requirements.

TABLE 2-18. - PITCH ATTITUDE CHANGE REQUIREMENTS FOR FRONTAL HORIZON AND SOLAR ATTITUDE REFERENCES

Steer to Frontal Horizon	
Standard 2-step	77°
90° 2-step	90°
Bent 2-step (angle between steps)	64°
3-step	90°
Optimum	102°
Steer to Sun (or inertial) reference	
Standard 2-step	98°
90° 2-step	90°
Bent 2-step (angle between steps)	79°
3-step	114°
Optimum	131.5°

It may be observed that the pilot's line of sight will have to turn through an appreciable angle without resorting to the use of mirrors or other indirect viewing schemes. The astronaut field-of-view limitations have been estimated and are given in figure 2-57. These data reflect the normal human eye deflection limits, normal head motion limits, and helmet-imposed limits. The pilot can perform normal attitude reference tracking tasks within the limits of eye fixation shown in the figure. These limits subtend an angle of 129 degrees. If an allowance of ±15 degrees is made as a design margin for attitude excursions and non-nominal positioning of the crewman on the vehicle, a usable range of approximately 100 degrees is left for the nominal pitch maneuvering. It may be seen from the table above that this 100 degrees of available field of view is exceeded by several possible pitch profiles. It is also noteworthy that the bent 2-step profile field-of-view requirements are smaller than for the other pitch profiles and do fall well within the available field of view requirements of the pilot.

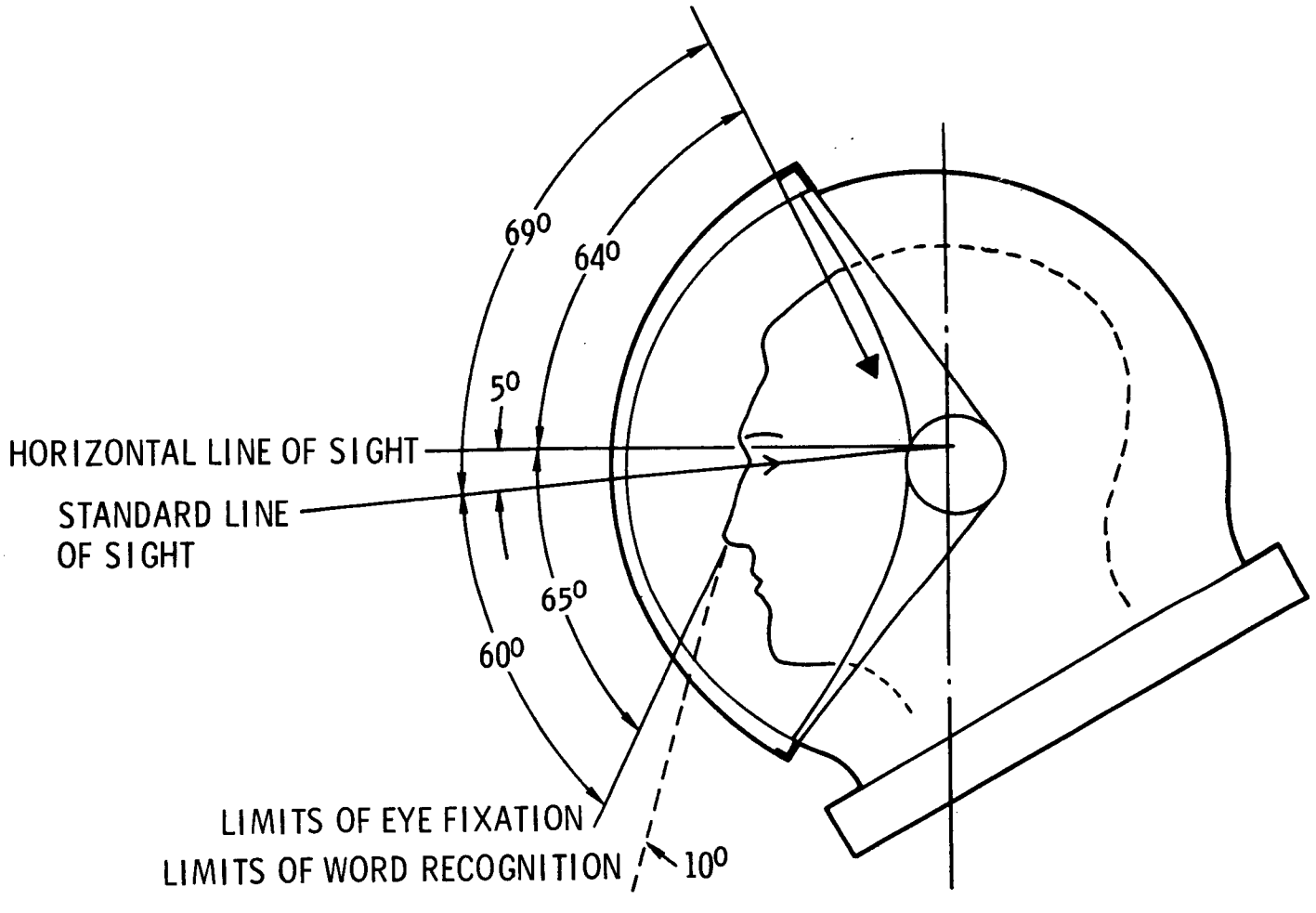

Figure 2-57. - Astronaut Field-of-View Limitations

Figure 2-58 depicts the hardwire configuration with the astronaut positioned to fly a bent 2-step trajectory using a frontal horizon reference. This position permits the pilot to fly both of the steps by moving the center of his vision ±32 degrees from his standard line of sight. The other pitch profiles more closely approach or exceed the limits of his field of view.

Figure 2-59 presents a similar diagram for the kinesthetic SCS system. When this system is used, the pilot stands erect to control the vehicle. It may be seen that all pitch profiles require that the pilot's field-of-view limits be exceeded. It is concluded that the direct-viewing frontal-horizon attitude-reference system used in conjunction with the kinesthetic control mode is not a workable concept. Mirrors or other devices might be employed to bend the line of sight; however, the inherent cross-coupling and additional pilot attention required to interpret such a display is believed to be excessive for the kinesthetic mode.

Cross-coupling between visual displays and controls. - During an optimum ascent trajectory, the LESS goes through a pitch angle of approximately 130 degrees with respect to a nonrotating reference. The spacecraft control axes, therefore, rotate through a large angle with respect to the visual frames of reference considered. The result is a severe change in the cross-coupling between the visual displays and the vehicle control axes. This cross-coupling is not a problem with the instrument display concepts, since these displays can readily be made to present information in vehicle body coordinates. The cross-coupling problem inherent in the visual display concepts are not without solution, and the following four concepts are offered as potential solutions to this problem:

1. The pilot may be able to mentally provide the necessary coordinate transformations. This approach will, of course, require considerable training (simulator experience) and a relatively stable SCS mode and would be enhanced by a natural nonimaged display, such as a horizon and landmark.

2. Transformation of the control signals into display axes with resolvers driven by a pitch-attitude programmer.

3. Same as 2, except, when flying the N-step pitch profile, the coordinate transformations can be mechanized with simple resistive networks rather than resolvers. Switching between networks can be accomplished at each step change.

4. Providing a controller with a gimbal and a shape that will permit the pilot to provide hand-control inputs in display coordinates. An example would be a controller shaped like a billiard ball and

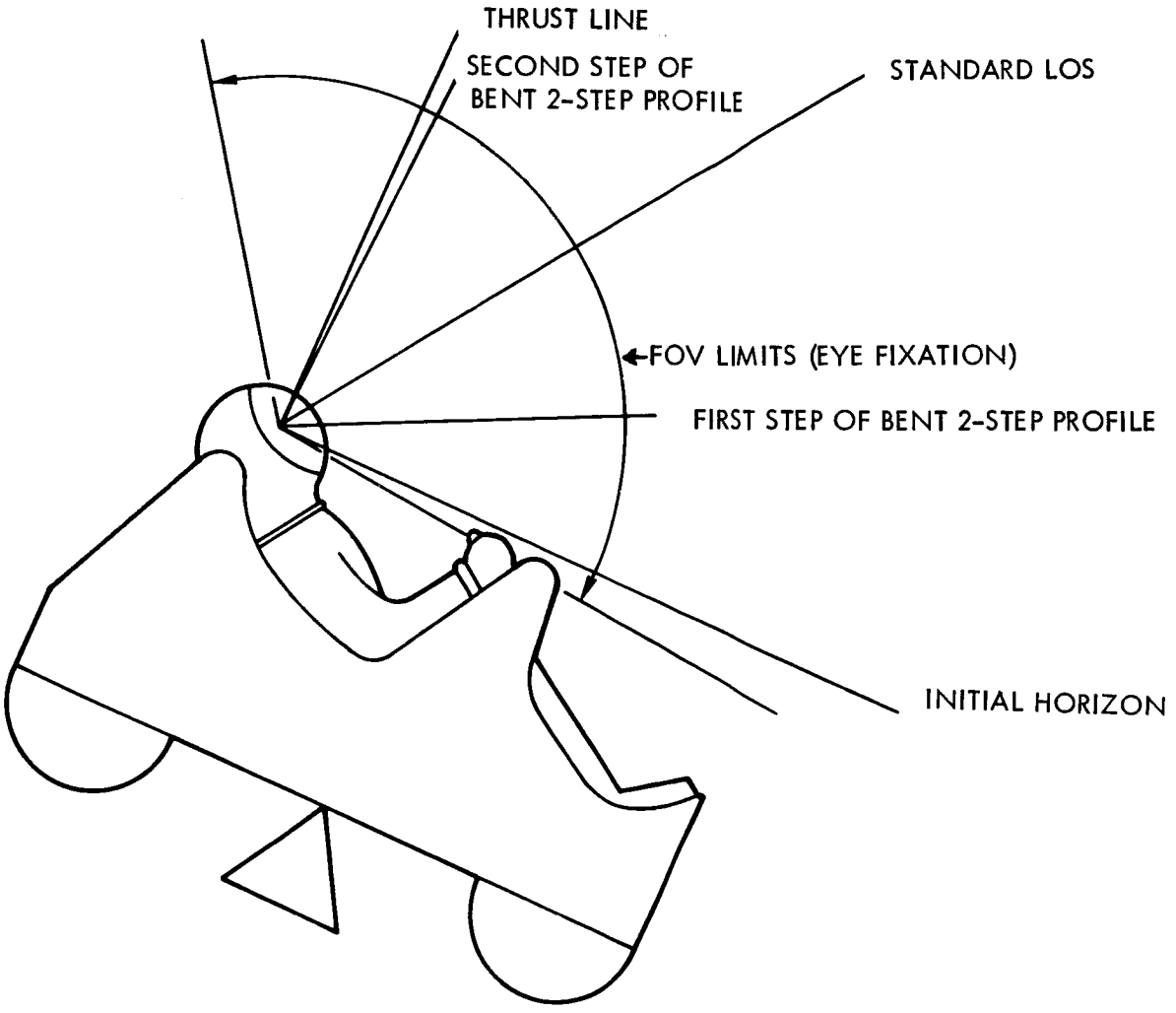

Figure 2-58. - Horizon-Viewing Limitations for Seated Pilot

gimbaled about its center. The SCS would be mechanized such that controller rotations about a display axis would provide spacecraft motion about that axis.

The severity of this cross-coupling between the visual displays and body control axes is not easily assessed but can be determined in a man-in-loop simulation. All of the above potential solutions to this problem ultimately lead to additional complexity, either in the training of the pilot or in system mechanization.

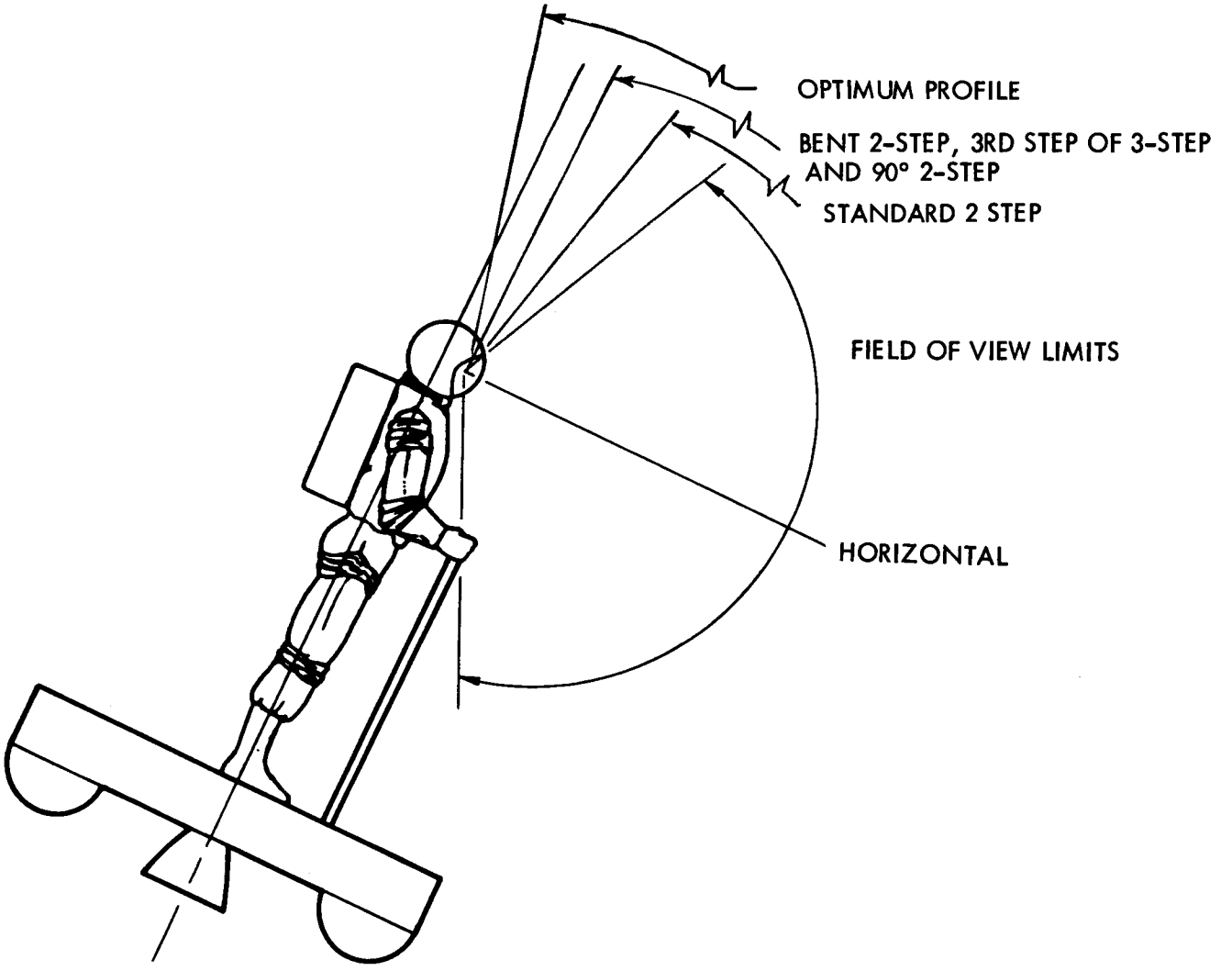

Figure 2-59. - Horizon-Viewing Limitations for Kinesthetic Control

Hybrid attitude reference systems. Attitude reference systems employing inertial sensors and visual cues may be used to embody the best features of both. For instance, a heading gyro might be used to augment the poor azimuth reference inherent in visual attitude reference systems. Such an approach appears to have the disadvantages of both system types as well as their advantages, however. The heading gyro requires alignment on the lunar surface and the visual reference still suffers from the limitations imposed by various lighting conditions, as well as inaccuracies because of surface roughness. For this reason, hybrid attitude reference systems are not given further consideration.

Guidance employing trajectory data. - The LESS ascent phase guidance may employ trajectory state vector data in a closed-loop fashion to greatly reduce the effects of thrust vector pointing errors inherent in the vehicle dynamics, the SCS, and attitude reference systems. Such an approach may be utilized to correct for the larger pointing errors of the less stable manually controlled SCS modes. The trajectory data may be sensed directly (as in a radar altimeter) or may be computed (as in inertial navigators).

Aircraft-type doppler navigators and concepts employing radar altimeters are excluded from consideration because of their higher complexity relative to the newer inertial navigators. The remaining concepts treated below are the simple visual sensing concepts and inertial navigation systems.

Visual sensing of trajectory data: Up to this point in the report, visual sensing has been restricted to attitude determination only. This section treats the visual sensing of trajectory state data. Such data may be employed to implement some form of closed-loop guidance.

The objects in the LESS visual environment that may be useful in sensing trajectory data are listed in table 2-19. Observations that require automatic computation to obtain meaningful steering information have been excluded because of the excessive complexity of such an approach. From the table, it is concluded that an altitude measurement using a T-tube (lateral horizons viewer) or sextant device is quite feasible. In fact, it is believed that the T-tube could be made to produce a null-seeking pitch display that yields a unique pitch attitude versus altitude steering profile. Such a sensor would permit the vehicle to be steered so as to achieve injection at a specified altitude. (The concept requires development, which was not possible in this study).

The reduction of lateral velocity errors inherent in the use of frontal landmarks for yaw attitude reference is attractive. The driftmeter approach is deemed to be excessively complex in light of its requirement for instrument stability and the workload imposed on the pilot. Observations of the CSM are useful if the computational capacity of a LESS-active rendezvous system were available.

TABLE 2-19. - VISUAL SENSING OF ASCENT TRAJECTORY DATA

Object Sighted	Measurement Made	Mechanization and Data Processing Required	Remarks
Lunar Horizon	Attitude	T-tube or sextant-type dual-image device permits direct reading of altitude.	Easily integrated with visual attitude sensors. Requires development.
Lunar Landmarks	Time crossing and drift angles	Aircraft-type driftmeter with gyroscopically stabilized sight required to provide necessary accuracy.	Doesn't read out useful steering data directly, but requires considerable pilot attention to interpret (compute) necessary steering corrections as a function of observed data. Sight must be stabilized to an accuracy greater than that required for a gyro instrument display if meaningful observations are to be made. The device presents primarily azimuth (out-of-plane) data; no pitch (in-plane) data are available. No known instruments of this type have been developed. Requires a relatively stable vehicle to permit pilot to divert attention from controlling vehicle attitude to reading the drift meter.
Lunar Landmarks	None	Steer vehicle toward pre-calculated landmark in forward field-of-view. As errors produce significant lateral drift (compared with distance to landmark), the vehicle is naturally steered in direction to compensate for the lateral velocity errors.	Corrective steering phenomena are inherent in forward landmark viewing visual attitude reference. Requires selection of landmarks at some specified range for maximum effectiveness.
CSM	Line-of-sight angles to CSM	Use observations with some form of proportional navigation during latter portions of ascent phase to reduce injection errors.	May be an effective way of reducing ascent phase injection errors if a LESS-active rendezvous scheme is implemented.

Inertial navigation systems: In recent years, numerous inertial navigators that have been developed might be appropriate for the LESS application should the accuracy requirements warrant an approach of this sophistication. The weight and power of these systems is of primary concern, since it is desirable to keep the dry weight of the LESS at a minimum. Although little emphasis has been placed on the reduction of weight in these systems, some state-of-the-art advances have been made. Table 2-20 is a brief summary of the weight and power of a family of autonavigators. The first system is representative of the state of the art existing approximately ten years ago. The last system utilizes electrostatic gyros and is at least four years and considerable dollars away from operational status. The table serves to indicate that the advances in circuit and instrument technology are resulting in orders-of-magnitude weight improvement. With regard to LESS application, it is clear that the weight of the first system is an extremely imposing penalty in contrast to the three-pound Micron system, It is obvious that the penalty for use of an inertial navigator in the LESS is strongly a function of the time period. If a LESS development program were implemented immediately, the lunar module abort guidance system development status could support a very accelerated vehicle development schedule. The Teledyne system might be available for a slower development program. The autonavigators listed in the table constitute a small fraction of the existing or near-term systems being developed and were selected to represent a wide variety of system types.

Use of LM abort guidance system: The mere existence of the LM abort guidance system (AGS) suggests the possibility of pirating this gear for use on the LESS. The AGS consists of three packages: (1) abort sensor assembly (ASA), a strapdown inertial measurement unit; (2) abort electronics assembly (AEA), the guidance computer and power supplies; and (3) data entry and display assembly (DEDA), the guidance system input-output device.

The concept would require reconnecting this gear to a new battery-pack power supply, aligning the gyros, insertion of new constants and targeting data into the computer, removal from the LM, and reinstallation on the LESS. To assess the feasibility of this approach, the following considerations must be made: environmental control, ease of removal and reinstallation, power required, program changes, alignment, etc. The principal problems associated with the concept are due to:

1. Removability The three major packages of the system are located in different places, two of which are accessible from the exterior of the LM only. The location, mounting, and connectors were not designed for quick removability and would have to be modified considerably.

TABLE 2-20. - INERTIAL NAVIGATOR SUMMARY

System	Status	Weight* (lb)	Power* (watts)	Comment
Apollo CSM (A-C Spark Plug)	Operational	173	398	3-gimbal platform
Carousel IV (A-C Spark Plug)	For Boeing 747	74	350	4-gimbal platform
H-419 (Honeywell Strapdown)	Operational	59	180	Early strapdown
Lunar Module Abort Guidance System (TRW and Hamilton Standard)	Operational	53.4	155	Existing strapdown
Teledyne Flight Reference System (AN/ASN-82)	In Test	12.3	84	4-gimbal platform
Micron (Autonetics)	Four years development required, components in test.	3	12	Strapdown with two electrostatic free gyros

*Physical properties data are for inertial measurement unit and guidance computer only; input or output devices and equipment for temperature control are not included.

2. Environmental control: The ASA and AEA are temperature controlled by mounting them on the coldplate of the LM environmental control system. Without the normal heat transfer to the coldplate, the gyro temperatures go out of specification tolerances in approximately one hour. Mounting the gyro package on a heat sink could provide several hours of lifetime, which would be sufficient for the LESS application.

It is concluded that LM AGS satisfies the functional requirements of the LESS mission, but that its present physical configuration is not amenable to the equipment transfer required for this application. Considerable physical redesign of the system is required to obtain the necessary ease of removal and to provide necessary environmental control.

Integration of guidance subsystem concepts. - The preferred guidance subsystem concepts have been defined and are summarized in figure 2-60. These subsystems are integrated to provide the complete guidance system concepts presented in table 2-21. These guidance system concepts constitute a family of competitive systems suitable for more detailed definition, analysis, and evaluation. Each stabilization and control concept has been matched with the more appropriate attitude-reference system and steering profile. These system concepts are analyzed further in the next section from the standpoint of mechanization penalties and guidance errors.

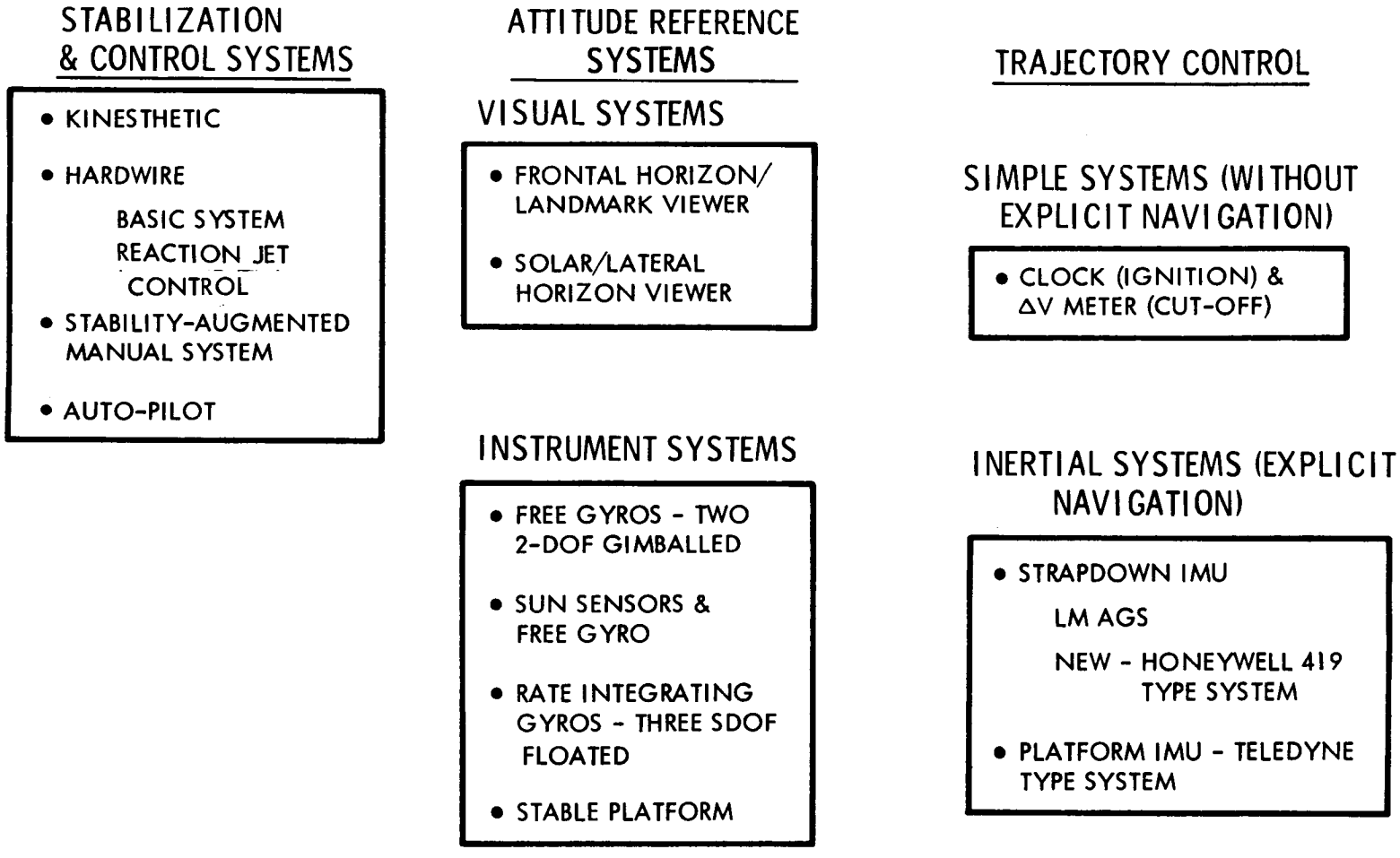

Figure 2-60. - Summary of Preferred Guidance and Control Subsystem Concepts

TABLE 2-21. - INTEGRATED GUIDANCE AND CONTROL CONCEPTS

SCS Mode	Attitude Reference System	Guidance	Steering Profile	Accuracy	Remarks
Kinesthetic	Three-axis gyro display	None	Optimum program	Probably marginal	No cross-coupling between displays and control. Display is insensitive to head motion. No steps in steering profile to aggravate manual stabilization. Best possible break for system with poor handling qualities.
Hardwire (basic system)	Frontal horizon/landmark viewer	None	Bent 2-step	Probably marginal	Combination of poor handling qualities and cross-coupling associated with displays expected to produce unacceptable pilot ratings. Minimum complexity attitude-reference systems.
Hardwire (basic system)	Three-axis gyro display	None	Optimum program	Probably acceptable	Gyro display is more flexible and less subject to visibility constraints.
Stability-Augmented Manual System	Integrating rate gyros with three-axis display and rate outputs for stability augmentation	None	Optimum program	Meets requirements	Best attitude reference display.
Stability-Augmented Manual System	Solar/lateral horizon viewer	None or θ Vsh	Bent 2-step or θ Vsh	Meets requirements	Enhanced stability combined with accurate but simple display.
Stability-Augmented Manual System	Frontal horizon/landmark viewer	None	Bent 2-step	Meets requirements	Minimum-complexity attitude-reference display.
Autopilot	Integrating rate gyros with rate output for stability augmentation	None	Optimum program	Meets requirements	Included to permit relative comparison with piloted systems.
Autopilot	Strapdown inertial G&N system	Inertial	Optimum program	Exceeds requirements	Included for further analysis to establish relative penalties of this more exotic approach.

Guidance and Control Systems Considerations

The previous two report sections have explored manual stabilization and control techniques and guidance and navigation system concepts appropriate for LESS. These techniques and concepts were integrated into the family of guidance and control system concepts summarized in table 2-21. It is the purpose of this section to present analyses relating to these total systems. A guidance error analysis has been performed to assess the accuracy capability of the various system concepts. Also, the mechanization aspects of these systems are considered in order to provide some insight into the relative weight and complexity penalties that might be incurred in their implementation.

Guidance error analysis. -

Objectives: The purpose of the guidance error analysis is to assess the ascent phase orbit injection error capability of the various G&C system configurations being considered for candidate LESS vehicle concepts.

Approach: In the interests of LESS vehicle safety, a high probability of successful orbit insertion is necessary. For this reason the orbit injection errors are assessed on a 3σ basis.

To establish the limits for safe injection a 5-nm margin for lunar mountain clearance is necessary. Also, an altitude margin of 10 nm is required for the rendezvous to provide the necessary altitude clearance for the CSM while on its rendezvous transfer orbit; therefore, if the nominal LESS orbit is a 60-nm circular orbit, an altitude uncertainty in the resulting orbit of -45 nm can be tolerated.

Error source magnitudes: The error sources affecting the LESS ascent guidance are summarized in table 2-22. They are classified into acceleration vector (thrust and weight) magnitude errors, pointing errors, and timing errors. In all cases, the magnitudes are based on the use of simple system hardware and do not require a special high level of quality control in manufacturing.

TABLE 2-22. - SOME GUIDANCE ERROR SOURCE MAGNITUDES (3σ)

Thrust-to-Weight Ratio (±4. 36%)

Thrust magnitude (due to engine, tankage and specific impulse tolerances) = ±4. 00 percent.

Initial weight (due to crew, PLSS tolerances, and propellant density variations) = ±1. 74 percent.

Thrust-Vector Pointing Error

Manual steering errors (when flying to a constant or slowly varying attitude reference)

Kinesthetic = ±1. 30 degrees.
Hardwire = ±1. 10 degrees.
Stability augmented system = ±0.40 degrees.

Multistep profile attitude maneuver rate errors

Kinesthetic and hardwire = ±2. 45 degrees per second.
Stability augmented = ±0. 54 degrees per second.

Thrust vector misalignment relative to engine = ±0.40 degrees.

Center-of-mass uncertainties = ±0. 78 inches.

(Compensation employed to produce a thrust vector pointing error = ±0. 40 degrees)

Thrust Ignition and Cutoff Error

Manual ignition and cutoff timing errors = ±1. 00 second.

ΔV meter cutoff accuracy (including accelerometer instrument and propulsion tailoff errors) = 0. 10 percent.

Thrust and weight errors: The thrust level tolerances have been estimated at 4 percent. This value includes engine, pressurization system, propellant temperature, and specific impulse variations. Simple pressure-fed engines and orifice flow rate control is assumed. The vehicle initial weight error (1.74 percent) includes crew weight variations (14 lb) and hardware tolerances and presumes that the propellant density variation due to temperature is not compensated. (Compensation through temperature measurement would avoid ±3 percent density variation.)

Hardware contribution to pointing errors: The thrust vector misalignment with respect to the vehicle is pertinent for the ungimbaled configurations and can easily be held to 0.4 degree (test data and higher quality control could reduce this to 0.1 degree).

The average vehicle lateral center-of-mass uncertainty (without compensation) is estimated at 0.78 inch. The dominant contribution is due to crew positioning uncertainties taken as 2 inches per crewman. In addition, the initial tanking tolerances (2 percent) and propellant consumption rate tolerances (2 percent) are included. For hardwire control with the gimbal-to-center-of-mass distance is assumed to be three feet, the resulting thrust vector misalignment is 1.24 degree (3σ). This is an excessively large error contribution to the system and must be improved. Potential means of improvement are:

1. Balancing of the vehicle/crew prior to liftoff (this is the preferred method).

2. Instrumentation of the gimbal or addition of accelerometers to provide a steering bias to be used in flight.

3. Design to achieve a large gimbal-to-center-of-mass distance. If necessary this can be achieved with a sliding engine translator or mechanical linkages providing a virtual gimbal point at some distance from the vehicle.

4. Finding better means of reducing the crew positioning error.

The choice of technique to minimize the thrust vector pointing error due to center-of-mass uncertainty involves design tradeoffs (see Design Section, later in this report). Any of these techniques can readily reduce the magnitude of this error source to 0.4 degree, and the remaining analysis will assume this value.

Langley Research Center simulation results for manual control errors: Recently obtained thrust vector pointing error data from the NASA-LRC fixed-base kinesthetic control mode simulator have been received and analyzed. The data contains 27 simulation runs of the LESS ascent phase. The vehicle configurations noted as A, B, and D were simulated. Four pilots participated in the runs. An "8-ball" attitude reference was employed. The standard two-step pitch profile was flown, and pointing-accuracy data were taken for each step.

Table 2-23 presents the statistical estimates of thrust vector pointing accuracy obtained from the simulation data based on all 27 simulation runs. The mean plus 3σ pitch angle error for both steps is 1.72 degree. This can produce a reduction in perigee altitude of -54 nm, based on the trajectory error sensitivity data in the Trajectories Section earlier in this report. It is noteworthy that the LRC pointing accuracy data (1.72 degree) is appreciably improved over conservative early NR estimates (4 degrees). The early NR estimates were extrapolated from Apollo and LFV simulation data and were based on smaller vehicles with poorer handling qualities.

TABLE 2-23.- LRC KINESTHETIC SIMULATOR THRUST VECTOR POINTING ACCURACY DATA

Angle	Step	Mean	1 Standard Deviation	Mean +3 Standard Deviations
Pitch	1	-0.110	0.509	1.64
Pitch	2	-0.230	0.524	1.80
Pitch	Both	-0.17	0.517	1.72
Roll	1	+0.176	0.363	1.27
Roll	2	+0.362	0.714	2.50

A statistical analysis of the three vehicle configurations is not performed because of the limited number of runs available for each case; however, an examination of the data indicates that the number of cases in which a one-degree pointing error was exceeded in at least one or more of the steps is as follows:

A - 3 times in 5 runs (60 percent)
B - 2 times in 11 runs (18 percent)
D - 3 times in 11 runs (27 percent)

These data tend to indicate that the pointing accuracy capability of the B and D configurations was better than that of Configuration A. This pointing accuracy data appears to correlate with the pilot handling qualities ratings for the various configurations which were better for Configuration B and poorer for Configuration A.

In light of the pointing accuracy variations achieved with the different vehicle configurations, it is believed that optimized handling qualities can yield even better pointing accuracies than those obtained over the entire group of simulation runs. On this basis it seems reasonable to expect that a 3σ manual controlling error contribution of 1.3 degree for kinesthetic controls is achievable. Similarly, the hardwire control mode might be expected to achieve an accuracy of 1.1 degree in light of its relative freedom from tail-wags-dog dynamics. This extrapolation of hardwire control accuracies from the kinesthetic mode data is extremely crude and is only done because no better source of data is available. (It is recommended that the hardwire control mode pointing accuracies be investigated more thoroughly in future man-in-loop simulation studies.)

Other errors: The timing error in performing manual switching is assumed to have an upper bound of 1.0 second. For pitch profile scheduling and propulsion sutoff, a ΔV meter accuracy of 0.1 percent is more than adequate. Instrumentation of this accuracy is readily available.

Gyro attitude reference system errors using contemporary equipment can easily be reduced to a small value compared with the other pointing errors inherent in the simple G &C systems. For this reason, the gyro errors are neglected in the present treatment.

Error analysis results: Table 2-24 is a summary of the effects of the individual error sources. The results are given in terms of injection orbit altitude uncertainties when targeted for a 60-nm circular orbit. It may be seen that the manual steering errors dominate for the kinesthetic and hardwire modes. The contribution of thrust-to-weight ratio errors is the next largest item. It must be recalled that the ΔV meter is used to schedule the pitch attitude profile in order to reduce the sensitivity to this level.

TABLE 2-24. - EFFECT OF INDIVIDUAL ERROR SOURCES

Error Source	Magnitude (3σ)	60-nm Injection Orbit Altitude Uncertainties (3σ)
Thrust/Weight (Launch T/W = 0.3)	4.36%	21 nm
Thrust Vector Pointing Errors		
Thrust vector alignment with respect to vehicle (fixed gimbal) or effect of cg uncertainty (gimbaled)	0.4°	13 nm
Manual steering errors		
Kinesthetic	1.3°	41 nm
Hardwire	1.1°	35 nm
Stability augmented	0.4°	13 nm
Autopilot	0.1°	3 nm
Step profile attitude maneuver rate errors		
Kinesthetic and hardwire	±2.45°/sec	19 nm
Stability augmented	±0.54°/sec	7 nm
Thrust Ignition and Cutoff Errors		
Manual ignition and cutoff timing errors	1.0 sec	12.5 nm
ΔV meter	0.1%	5.5 nm
Engine tailoff impulse	Negligible	

The total 3σ system injection uncertainties relative to a 60-nm target orbit are then as follows:

1. Kinesthetic control = ±51.2 nm
2. Hardwire control = ±46.4 nm
3. Stability augmented = ±28.4 nm
4. Simple autopilot = ±21.3 nm

These values are based on the error source values of table 2-24 and assume a 60-nm circular target orbit, a three-step ascent pitch profile and manual operation of the propulsion system cutoff. To gain some insight as to how reductions or removal of some of the error sources affect the overall accuracy, figure 2-61 presents the 3σ injected orbit altitude uncertainty versus manual steering errors for the kinesthetic and hardwire control modes. The figure demonstrates the dominance of the manual steering errors for the larger values, but also demonstrates that very significant accuracy improvement can be made through removal or reduction of some of the error sources. For example, the step attitude maneuver errors are appreciable if done on an open-loop basis, but can be reduced appreciably by flying to displayed pitch rate information or by flying a smooth, slowly varying pitch profile.

It may be concluded that, on the basis of the present error source estimates, the kinesthetic mode provides very marginal, if indeed acceptable, accuracy. It is conceivable that further improvements in the handling qualities of this system could improve its accuracy to an acceptable level. The hardwire accuracies are somewhat better. The stability augmented system and the simple autopilot (without inertial guidance) are even better, as would be expected.

The error analysis results are predicated on the use of simple systems and in some instances the estimated magnitudes of the error sources may still prove to be pessimistic. As discussed, some of the error sources are obtained from somewhat crude extrapolations, and further simulation is recommended to provide better bases for the estimates. Also, it has been shown in the Trajectories Section earlier in this report that the choice of an elliptic target orbit, rather than a circular orbit, further reduces the sensitivity to the various error sources. For example, the contribution of manual steering errors, as given in table 2-24, for the kinesthetic control mode, 1.3 degree, to orbital uncertainty was 41 nm for a circular target orbit. For an elliptical target orbit of 60 by 120 nm, this same 1.3 degree steering error would only cause a 15-nm error in final orbit.

In this light, the results obtained are encouraging and do serve to indicate that the simple systems considered herein have the potential of meeting the LESS mission requirements.

System mechanization considerations. - The purpose of this section is to explore some details of the mechanization of the various G&C system concepts previously identified. The principal results obtained are estimates of the weight penalties to mechanize the various concepts and a listing of the required system elements that may be used to make a qualitative assessment of relative complexity and reliability. Existing equipment characteristics are employed where practical, and all estimates are predicated on present

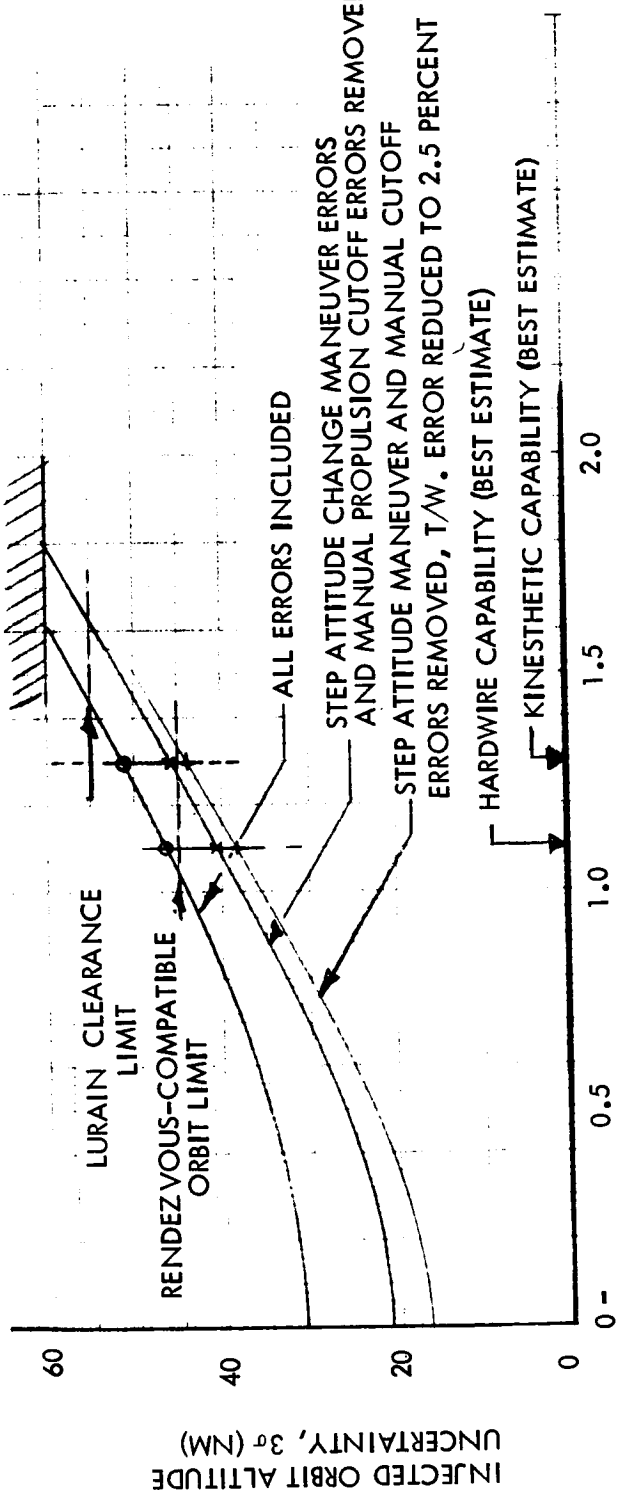

Figure 2-61. - Kinesthetic and Hardwire Injected Orbit Altitude Uncertainties (3σ), Sixty-Nautical-Mile Circular Target Orbit

state-of-the-art technology. (Appreciable weight reductions are possible using newer technology if more time and costs are allowable). Very little redundancy has been incorporated in response to the study goal of adequate reliability and safety through the employment of simple techniques and systems.

The use of fluidic control components offers interesting mechanization possibilities for the more complex systems, such as stability-augmentation. Potential reliability improvements are the principal advantage. The development status of these devices precludes their consideration for LESS at present.

Table 2-25 is a listing of the components and subsystems required to mechanize the eight integrated guidance and control concepts being considered. The hardwire configuration with reaction-jet attitude control is intentionally excluded, as the weight penalties associated with this concept are primarily associated with the propulsion system and are beyond the scope of this section. Estimates of the battery weight required to power the systems are made and added to the equipment weights to reflect the overall system weight requirement. The battery weight estimates assume an energy of 40 watt-hours per pound of battery weight. The equipment common to all systems consists of the ΔV meter, the control panel, the VHF ranging transponder, and the flashing beacon for CSM tracking.

Table 2-26 is a concise summary of the system weight totals for each of the eight guidance and control system concepts considered. Relative weight penalties may be assessed by comparing these totals. It must be recalled that these weights include the VHF ranging transponder and flashing beacon equipment required for the CSM active rendezvous. The remainder of the weight contains the G&C elements required for surface preparations, ascent, and coasting flight prior to docking.

The data summarized in table 2-26 give rise to the following conclusions:

1. The hardwire system has a weight penalty of approximately 17 lb over the kinesthetic system employing the same displays; however, the kinesthetic system requirement for larger moments of inertia to achieve suitable handling qualities probably produces a more severe structural weight penalty.

TABLE 2-25. - GUIDANCE AND CONTROL SYSTEM WEIGHT BREAKDOWN

System Breakdown	Weight (lb)	Power (watts)
1. Kinesthetic, Instrument ARS		
Instrument ARS Gyro Package: The search for aircraft panel display instruments driven by two-degree-of-freedom gyros yielded none that would satisfy the LESS maximum drift rate requirement of approximately one degree per hour. The Lunar Orbiter inertial reference unit manufactured by Sperry Gyro Co. and utilizing a variety of available gyros is selected. Several other manufacturers have similar packages, but do not have the testing or space operational experience available with this one. An allowance for gyro heater power is included. (13 lb, 20 watts, 7 x 10 x 7 in.)	25	41
Gyro Display Coupling Circuitry: The circuitry to approximately compute the euler angle signals from gyro body rate data is required to drive the 8-ball attitude display. (3 lb, 5 watts)		
Attitude Display: The display for the LESS ascent phase requires a display of approximately 140 degrees in pitch and ±15 degrees in roll and yaw. A special-purpose 3-axis display could be developed for these ranges that would provide a savings in weight and power over the 8-ball all-attitude indicator; however, the ready availability and pilot familiarity with 8-ball all-attitude indicators makes them preferable for this application. An advanced three-axis indicator manufactured by Lear Siegler (Instrument Division, Grand Rapids) is selected. (6 lb, 16 watts, 7 x 7 x 8 in.)		

TABLE 2-25. - GUIDANCE AND CONTROL SYSTEM WEIGHT BREAKDOWN - Continued

System Breakdown	Weight (lb)	Power (watts)
Gyro Alignment Device: This device is similar to the base of a surveyors transit. Bubble levels are used to find the local level, and a gunsight type of device is employed for azimuth sightings. The three readouts are set into the gyro display coupling electronics. (3 lb)		
Common equipment	35	67
ΔV Meter The ΔV meter includes the accelerometer, the velocity pulse counter electronics, and logic switches to signal pitch-step changes and propulsion cutoff. A Bell Aerosystems Model VI velocity meter is selected because of its small size, availability, and the company's proven capability with this type of system. (1 lb, 5 watts)		
Control Panel The panel provides a location for the following controls and displays: Attitude display (if utilized), a six-digit digital display for displaying time (prior to liftoff) and ΔV (during ascent), an increment/decrement switch for updating the ΔV meter setting, and the clock and rotary switches to power the gear and electrically configure the systems. (4 lb, 1 watt)		
Rendezvous Equipment		
VHF Transponder: A telecommunication link to permit the CSM VHF range measuring system to operate. Also provides a voice communication link between the CSM and LESS. (20 lb, 40 watts)		

TABLE 2-25. - GUIDANCE AND CONTROL SYSTEM
WEIGHT BREAKDOWN - Continued

System Breakdown	Weight (lb)	Power (watts)
Flashing Beacon: (10 lb, 21 watts)		
Equipment total	60	108
Battery weight	8	--
Total system weight	68	--
2. Hardwire, Frontal Horizon/Landmark ARS		
Hardwire SCS The weights are estimated from design drawings. Controller: 5 lb Linkage: 2 lb Gimbaled Propulsion Weight Penalty: 10 lb (Total) 17 lb	17	--
Frontal Horizon/Landmark Viewer: The Gemini rendezvous sight manufactured by Chicago Aerial Industries is selected for this application. The physical properties given are for two sights as they would be mechanized to fly the bent two-step pitch profile and include allowance for the adjustable mounting, optics covers, and electrical connectors. (12 lb, 150 watts, 5 x 6 x 10 in. per unit)	12	150
Common equipment (see 1. above)	35	67
Equipment total	64	217
Battery weight	11	--
Total system weight	75	--
3. Hardwire, Instrument ARS		
Hardwire SCS (see 2. above)	17	--
Instrument ARS (see 1. above)	25	41
Common equipment (see 1. above)	35	67
Equipment total	77	108
Battery weight	8	--
Total system weight	85	--

TABLE 2-25. - GUIDANCE AND CONTROL SYSTEM WEIGHT BREAKDOWN - Continued

System Breakdown	Weight (lb)	Power (watts)
4. Stability Augmented System, Frontal Horizon/ Landmark ARS		
Stability-augmented SCS	38	115
Hand Controller: Honeywell design for the LFV hand controller is selected due to astronaut familiarity and preference for Honeywell controllers employed in LM & CSM. (5 lb, 5 watts, 4.25 x 7.0 x 4.5 in.)		
Rate Gyro Package: For stability augmentation simple spring-restrained rate gyros are sufficient. Nortronics package utilizing 3 GR-H4 subminiature rate gyros. (2 lb, 10 watts)		
Gimbal Actuators: Modified Minute-man actuator manufactured by Cadillac Controls of Costa Mesa, Calif., (6 lb, 80 watts total for two actuators)		
Gimbaled Propulsion Weight Penalty: Additional weight added to engine and vehicle for gimbaling. (10 pounds.)		
Control Electronics: The stability augmented system control logic, actuator servo amplifiers, coasting flight RCS valve drivers, and associated power supplies are estimated to have the following properties: (15 lb, 20 watts, 6 x 6 x 8 in.)		
Frontal horizon/landmark viewer ARS (see 2, above)	12	150
Common equipment (see 1, above)	35	67
Equipment total	85	332
Battery weight	11	--
Total system weight	96	--

TABLE 2-25. - GUIDANCE AND CONTROL SYSTEM WEIGHT BREAKDOWN - Continued

System Breakdown	Weight (lb)	Power (watts)
5. Stability Augmented System, Solar/Lateral Horizon ARS Same as 4, but change display to Solar/Lateral Horizon Viewer	93	182
Solar/Lateral Horizon Viewer: This sight is estimated to weigh 20 pounds, including the necessary adjustments for sun angle variations, optics covers, and sun shielding.		
Battery weight	9	--
Total system weight	102	
6. Stability Augmented System, Instrument ARS		
Same as 4, but change display to Instrument ARS from 1, above.	98	223
Battery weight	11	--
Total system weight	109	--
7. Autopilot, gyro ARS		
Hand controller	5	5
Gimbal actuators	6	80
Gimballed propulsion weight penalty	10	--
Control logic	20	30
ARS gyro package	13	20
Common equipment (see 1. above)	35	67
Equipment total	89	202
Battery weight	10	--
Total system weight	99	--
8. Autopilot, Inertial Autonavigator		
Hand controller	5	5
Rate gyro package	2	10
Gimbal actuators	6	80
Gimballed propulsion weight penalty	10	--
Servo amplifiers	8	12
Control panel	4	1
Inertial guidance system	62	172

TABLE 2-25. - GUIDANCE AND CONTROL SYSTEM WEIGHT BREAKDOWN - Continued

System Breakdown	Weight (lb)	Power (watts)
Inertial navigation equipment has been discussed in a previous section with that title. The LM abort guidance system is selected as representative of present technology. TRW produces the system, and the strapdown inertial reference system is subcontracted to Hamilton Standard.		
Inertial Measurement Unit: (20.7 lb, 72 watts, 9 x 12 x 5 in.)		
Guidance Computer: (32.7 lb, 90 watts, 24 x 5 x 8 in.)		
Data Entry and Display Assembly: (8.4 lb, 10 watts, 6 x 6 x 6 in.)		
Rendezvous equipment	30	61
Azimuth alignment sight	2	--
Equipment total	129	341
Battery weight	16	--
Total system weight	145	--

TABLE 2-26. - GUIDANCE AND CONTROL SYSTEM WEIGHT SUMMARY

System	Basic Equipment Weight (lb)	Battery Weight (lb)	Total (Equipment and Batteries) (lb)
1. Kinesthetic, gyro ARS	60	8	68
2. Hardwire, frontal horizon/landmark reference	64	11	75
3. Hardwire, gyro ARS	77	8	85
4. Stability augmented, front horizon/ landmark reference	85	11	96
5. Stability augmented, solar/lateral horizon reference	93	9	102
6. Stability augmented, gyro ARS	98	11	109
7. Autopilot, gyro ARS	89	10	99
8. Autopilot, inertial autonavigator	129	16	145

2. The mechanization weight penalty to achieve the stability-augmented system requires approximately 24 lb over the equivalent hardwire system and approximately 41 lb more than the equivalent kinesthetic system. In addition the stability-augmented system is inherently less reliable because of the larger amount of electromechanical gear used in its mechanization (without redundancy).

3. The simplest possible autopilot system, which excludes the 8-ball display, actually weighs less than the stability-augmented system with the gyro ARS. The addition of the 8-ball to the autopilot system for pilot monitoring purpose makes these two systems approximately equivalent in weight.

4. The weight penalty of the inertially guided system over the hardwire with gyro ARS is approximately 60 lb.

5. The systems employing the frontal horizon/landmark viewer ARS concept enjoy approximately a 10- to 13-lb weight advantage over the systems employing the gyro ARS. The solar/lateral horizon viewer ARS has approximately a 7-lb weight advantage over the gyro ARS.

Guidance and control system comparison summary. - An abbreviated summary of the results obtained in the Guidance and Control Techniques section of this report are presented in table 2-27. Estimated pilot rating of handling qualities, injected orbit altitude uncertainties, and guidance and control system weights are given. It must be recalled that the system weight data include approximately 35 pounds of control panel and rendezvous equipment common to all systems. The injected orbit altitude uncertainties are not given for the visual attitude reference concepts, as no suitable data were available on the manual steering errors when these displays were employed. It is anticipated that the cross-coupling between the display and vehicle control axes and the effect of lunar surface roughness will produce larger manual steering errors than with the gyro attitude reference concepts; however, these effects may prove to be negligible. The magnitude of this error is not readily amenable to analytical estimation and is more properly the subject of a simulator investigation. It may be seen from the table that each successive system provides improved accuracy for moderate increases in system weight up to the autopilot (inertial navigator) system wherein appreciable increases are evident.

2. The mechanization weight penalty to achieve the stability-augmented system requires approximately 24 lb over the equivalent hardwire system and approximately 41 lb more than the equivalent kinesthetic system. In addition the stability-augmented system is inherently less reliable because of the larger amount of electromechanical gear used in its mechanization (without redundancy).

3. The simplest possible autopilot system, which excludes the 8-ball display, actually weighs less than the stability-augmented system with the gyro ARS. The addition of the 8-ball to the autopilot system for pilot monitoring purpose makes these two systems approximately equivalent in weight.

4. The weight penalty of the inertially guided system over the hardwire with gyro ARS is approximately 60 lb.

5. The systems employing the frontal horizon/landmark viewer ARS concept enjoy approximately a 10- to 13-lb weight advantage over the systems employing the gyro ARS. The solar/lateral horizon viewer ARS has approximately a 7-lb weight advantage over the gyro ARS.

Guidance and control system comparison summary. - An abbreviated summary of the results obtained in the Guidance and Control Techniques section of this report are presented in table 2-27. Estimated pilot rating of handling qualitites, injected orbit altitude uncertainties, and guidance and control system weights are given. It must be recalled that the system weight data include approximately 35 pounds of control panel and rendezvous equipment common to all systems. The injected orbit altitude uncertainties are not given for the visual attitude reference concepts, as no suitable data were available on the manual steering errors when these displays were employed. It is anticipated that the cross-coupling between the display and vehicle control axes and the effect of lunar surface roughness will produce larger manual steering errors than with the gyro attitude reference concepts; however, these effects may prove to be negligible. The magnitude of this error is not readily amenable to analytical estimation and is more properly the subject of a simulator investigation. It may be seen from the table that each successive system provides improved accuracy for moderate increases in system weight up to the autopilot (inertial navigator) system wherein appreciable increases are evident.

TABLE 2-27. - GUIDANCE, NAVIGATION, AND CONTROL SYSTEM COMPARISON SUMMARY (4)

System Description	Pilot Opinion Rating (1)	Orbit Injection Accuracy (2)	System Weight (3)	Concluding Comments
Kinesthetic Control Gyro attitude reference Optimum steering	5-6	51	68	Marginal handling qualities
Basic Hardware Control Frontal horizon/ landmark viewer Bent two-step steering	4.5		75	Marginal handling qualities unless optimized
Gyro attitude reference Optimum steering	4.5	46	85	Marginal handling qualities unless optimized
Stability Augmented Control Frontal horizon/ landmark viewer Bent two-step	2.5		96	Satisfactory handling qualities
Solar/lateral horizon viewer Bent two-step or θVsh	2.5		102	Satisfactory handling qualities
Gyro attitude reference Optimum steering	2.5	28	109	Satisfactory handling qualities
Autopilot Control Gyro attitude reference Optimum steering	Not applicable	21	99	Satisfactory handling qualities
Inertial navigator Optimum steering	Not applicable	Very small	145	Satisfactory handling qualities

Notes:
1 Pilot opinion ratings use Cooper scale.
2 Injected orbit altitude uncertainty, 3σ, in nautical miles.
3 System weight in pounds, including basic systems and batteries. Includes a ΔV meter, VHF transponder, flashing beacon, and control panel common to all systems (35 lb).
4 Primary LESS mission capability only and single-engine propulsion only.

Guidance and Control Techniques Conclusion Summary

The conclusions derived as a result of the analyses described in section 2.0 are summarized in the following paragraphs. For convenience these conclusions are grouped by the same titles used earlier in the report.

Manual stabilization and control system. - The major conclusion derived from the stabilization and control studies is that the hardwire control system provides adequate handling qualities for the basic LESS mission. Qualifications to this conclusion are that the pilot is capable of devoting a sufficiently large portion of his total workload to stabilization and maneuvering tasks, and that certain optimizations to the vehicle configuration be implemented. The kinesthetic control mode is not believed to be capable of providing adequate handling qualities. Detailed conclusions are as follows:

1. The simulations conducted to date have not provided sufficient data required for full confidence that all candidate control methods have been assessed.

2. Kinesthetic Control Conclusions:

   a. Single body kinesthetic control is capable of meeting LESS performance requirements, but imposes excessive pilot workload demands. The estimated Cooper rating is 5 to 6, which is unacceptable.

   b. To be even marginally acceptable, guidance, navigation and display monitoring tasks for single body kinesthetic control must impose very low workloads.

   c. The two-body kinesthetic control configuration is feasible from a stabilization standpoint and indicates potentially better handling qualities than the single-body vehicle.

3. Hardwire Control Conclusions:

   a. The basic hardwire control methods allows optimization of handling qualities with less impact or constraints on the overall vehicle configuration than does kinesthetic control. A Cooper rating of 4.5 is predicted for the basic hardwire control system.

b. Compensation networks for hardwire control have not been fully investigated; however, preliminary analytical and LFV visual simulator studies indicate no significant change in handling qualities over basic hardwire control.

c. Hardwire control with the engine gimbaled at the center of gravity (neutral center of gravity configuration) shows good potential for simplifying guidance, but has not been adequately studied by simulation.

4. Hardwire Reaction Jet Control:

a. Reaction jet control requires more complex logic and more engines than basic hardwire control, but eliminates the problems of gimbaled engines.

b. Preliminary handling qualities studies indicate that the reaction jet system is at least equal to basic hardwire control, but much more study is needed to fully assess the method.

c. The configuration is potentially more versatile than that of basic hardwire in that reliability may be increased, compensation networks and stability augmentation systems may be more easily installed, and correction for cross products of inertia and thrust misalignments may be devised.

d. At least one configuration of the reaction jet control method provides three-axis control moments without the use of auxiliary RCS.

5. Stability-augmented control has inherently better handling qualities than either kinesthetic or hardwire control, at the cost of more complex hardware. The basic mission requirements of LESS will not warrant the use of stability augmentation if the predicted qualities of hardwire control are borne out in subsequent studies.

6. Evaluation of optimization techniques for the parameters K_S (rotation controller sensitivity gear ratio), thrust, and the ratio of ℓ/I (distance from the center of gravity to the gimbal point over the moment of inertia), show that handling qualtities may be improved by their proper selection. Detailed examination of one of these parameters, thrust, using a particular set of mass properties data, showed that the Cooper rating of the hardwire system could be improved at least one point by using a step thrust decrease during boost (reference figure 2-54).

Guidance concept considerations

1. Mission Control Center can perform guidance targeting computations; the LESS guidance system need not perform these functions independently.

2. A clock and an integrating accelerometer (ΔV meter) are found to provide the simplest adequate means for controlling thrust ignition and cutoff, respectively.

3. Pirating the LM abort guidance system for use on the LESS is not practical without considerable physical redesign to facilitate easier removal and reinstallation.

4. Existing inertial navigators would impose severe weight and complexity penalties on the LESS; however, there is some indication that lightweight inertial navigators may become available in the future, which would not impose a severe weight penalty on the LESS.

Guidance/attitude reference system. - The gyro-driven all-attitude display is preferred over a visual attitude reference system. Some conclusions supporting this preference are:

1. Suitable visible reference features providing yaw or azimuth information are less available than for pitch or roll. The sun and lunar landmarks are found to be the best yaw references. Neither of these types of references is completely adequate for the full range of sun angles during stay-times up to 14 days.

2. Solar viewing systems require a periscope to accommodate the range of sun angles and pitch profiles.

3. Two preferred visual attitude reference concepts have been identified which provide all-attitude information. These concepts are the solar/lateral horizon viewer and the frontal horizon/landmark viewer.

4. The large pitch-attitude changes required during ascent make it difficult to keep the visual reference within the pilot's field of view. A direct view of the frontal horizon is not available throughout the ascent for the kinesthetic mode. The most attractive solution to this problem combines the bent 2-step profile, the hardwire SCS mode, and a partially reclined couch to keep the horizon well within the pilot's field of view. Surface roughness at the launch site may induce an error with this system, however.

5. Of the three-axis visual display concepts, the frontal horizon/ landmark viewer is the preferred concept. The mechanization employs the Gemini rendezvous alignment sight with virtually imaged reticle.

6. All visual displays have inherent cross-coupling due to the non-orthogonality of vehicle axes and line of sight. Methods to minimize the cross-coupling are available, but entail a mechanization penalty.

7. The principal disadvantage of the gyro-driven ARS is its requirement for alignment prior to launch. The gyro attitude reference system is found to have a relatively small weight penalty when compared to the visual ARS concepts.

8. The gyro ARS is less subject to visibility variations, cross coupling problems and astronaut field of view limitations than are the visual ARS concepts.

9. Hybrid attitude-reference systems employing both gyro and visual techniques are generally undesirable, as the resulting system usually has the disadvantages of both system types.

Guidance error analysis. -

1. The simplest adequate method to compensate the system sensitivity to thrust or weight errors is the use of a ΔV meter. The ΔV meter is used to schedule the ascent pitch profile as well as for propulsion cutoff.

2. Scheduling the ascent pitch profile as a function of altitude is found to compensate the system sensitivity to thrust and weight errors even better than scheduling as a function of ΔV; however, the mechanization penalty to provide a special altimeter for this purpose is not warranted.

3. Errors in the total vehicle center-of-mass location can easily produce excessive thrust vector pointing errors for some gimbaled engine configurations. The errors in lateral positioning of the crew with respect to the vehicle are found to dominate in this problem. The following design techniques may be employed to reduce the thrust vector pointing error to acceptable levels:

a. Design crew couches to minimize the errors in positioning the crewmen on the vehicle.

b. Maximize the distance between the center of mass and the engine gimbal to minimize corrective gimbal angle required. If necessary, a system of linkages could be employed to produce a virtual gimbal at some distance from the vehicle.

c. Provide a system to permit balancing accurately prior to launch.

d. Instrument the engine gimbal to provide a measurement of the thrust vector pointing error.

4. The manual contribution to thrust vector pointing errors dominates the orbital injection errors for the kinesthetic and hardwire modes. The stability-augmented and autopilot modes can be designed to allow vehicle hardware errors to dominate (thrust level, center of mass, or engine thrust vector alignment errors).

5. Simulation data from NASA-LRC indicates that kinesthetic control mode thrust vector pointing accuracy is appreciably better than previous NR estimates, which were based on simple extrapolations from Apollo manual thrust vector control and LFV simulation data. The NASA-LRC vehicle configuration identified as B had the best pointing accuracy; Configuration D was intermediate; and Configuration A was worst. The best pointing accuracies appear to correlate with the pilot ratings of handling qualities on these vehicle configurations.

6. Guidance error analysis of 60-nm cirular orbit injection accuracies using latest available NASA-LRC data indicates that the kinesthetic mode is possibly acceptable, but marginal, and the hardwire mode is somewhat better. However, small improvements anticipated in the kinesthetic system handling qualities may improve its accuracy to an acceptable level. Elliptical target orbits can be employed to desensitize the variation of perilune altitude with boost errors, but the higher resulting apolune altitudes cause higher CSM energy expenditures for subsequent transearth injection. At present, use of elliptical target orbits is therefore not recommended. Subsequent in-depth analyses of specific systems and missions (i.e. landing sites, stay-times, total mission profiles, etc.) may show an overall advantage, but such studies are well beyond the scope of the present effort.

Guidance and control system mechanization considerations. -

1. The hardwire system has a weight penalty of approximately 17 lb over the kinesthetic system with similar displays; however, the kinesthetic system is expected to have a larger structural weight penalty than this in order to achieve the larger moments of inertia required for good handling qualities.

2. The mechanization weight penalty to employ the stability-augmented system requires approximately 24 lb over the equivalent hardwire system and approximately 41 lb more than the equivalent kinesthetic system. In addition, the stability-augmented system is inherently less reliable because of the larger amount of electromechanical gear used in its mechanization, unless redundancy is provided.

3. The simplest possible autopilot system, which excludes the 8-ball display, actually weighs less than the stability-augmented system with the gyro ARS. The addition of the 8-ball to the autopilot system for pilot monitoring purpose makes these two systems approximately equivalent in weight.

4. The weight penalty of the inertially guided system over the hardwire with gyro ARS is approximately 60 lb.

5. The systems employing the frontal horizon/landmark viewer ARS concept enjoy approximately a 10- to 13-lb weight advantage over the systems employing the gyro ARS. The solar/lateral horizon viewer ARS has approximately a 7-lb weight advantage over the gyro ARS.

Overall guidance and control techniques. - A family of guidance and control concepts has been conceived and analyzed. A simple summary of these systems is given in table 2-28. All systems concepts appear to be marginal or better from a guidance accuracy consideration. Moderate increases in system weight and complexity are found to produce favorable increases in system accuracy. Based on the analyses conducted, the basic hardwire system with gyro attitude reference and ΔV meter for ascent pitch profile scheduling and engine cutoff appears to be slightly more attractive for the basic LESS mission than the other system concepts.

Computer programs used in this and the preceding section are identified briefly in Appendix E.

Symbols and Definitions

Symbol	Definition and Units
A	Compensation network natural frequency, radians/sec
B	Dashpot constant coefficient, lb/ft/sec
F_T	Thrust force magnitude, lb (used in dynamics equations in place of T)
h	Distance from pilot feet to pilot cg, ft
I	Total moment of inertia about centroid, slug-ft^2
I_g	Engine moment of inertia about its gimbal, slug-ft^2
I_P, I_V, I_T	Pilot, vehicle, and total moments of inertia about their respective cg's
K, K_1, K_2	Compensation network spring constants, lb/ft
K_C	Compensation network gain constant, sec
K_S	Sensitivity constant, degrees gimbal per degree of rotation controller deflection
K_{AF}	Vehicle airframe gain, unitless
$K_{\rho\theta}, K_\theta$	Dynamic and steady-state pilot gain constants, unitless
ℓ	Distance from total cg to gimbal point measured along vehicle centerline, ft.
M_D	Disturbance moment, ft-lbs
M_P, M_V, M_T	Pilot, vehicle, and total masses, respectively, slugs
P	Denominator root (pole) in pilot transfer function, radians/sec

Symbol	Definition and Units
R	Pilot opinion rating, unitless
S	Laplace complex frequency operator, radians/sec
T	Thrust force, lb
T_L	Pilot lead time constant, seconds
T_N	Pilot neuromuscular lag time constant, seconds
T_1, T_2	Initial and final thrust forces, lb
t	Time, seconds
W	Total weight, lb
W_P	Propellant weight, lb
W_{T_o}	Total launch weight, lb
X, Z	Local horizontal and vertical axes of a central force field frame of reference, X positive in downrange direction and Z positive down, feet
ΔX, ΔY	Forward or lateral total cg offset from nominal, feet
Z	Numerator root (zero) in pilot transfer function, radians/sec
β	Total lean angle of the pilot from vertical, positive in right-hand sense, degrees
β_C	Commanded pilot lean angle, degrees
δ	Engine gimbal angle from nominal, or pilot lean angle from thrust vector; both are positive in right-hand sense, degrees
δ_C	Commanded pilot lean angle or gimbal angle, degrees
ϵ_P	Resultant total cg offset from nominal, feet
ζ	Damping ratio, unitless

Symbol	Definition and Units
θ	Pitch attitude angle from vertical, measured positive in the right-hand sense, degrees
θ_ϵ	Pitch attitude error from commanded value, degrees
θ_C	Pitch attitude command angle, degrees
T, T_D	Pilot transport delay time constant, seconds
ω_N	Natural frequency, radians/sec.

3.0 PARAMETRIC AND CONCEPTUAL DESIGN DATA

The design considerations supporting systems analysis and leading to overall system feasibility determination are discussed in this section. Parametric data of importance are provided in key systems areas so that future tradeoffs with different assumptions or groundrules can be conducted. It is here that the more practical aspects of integrated performance and working interfaces are seen. The conceptual designs described cover a range of vehicle weights corresponding to a family of vehicle concepts rather than any one "best" concept. When NASA-LRC simulations have been completed and more information will be available as to choice of guidance and control concept, it will be possible to refine the conceptual design, choosing from configuration features illustrated in this study.

Operations on the lunar surface provide a number of problems, but the key item appears to be accomplishing the necessary tasks with minimum astronaut effort and time.

The adaptation of a LESS vehicle to the long-range lunar surface flyer mission is an attractive possibility from two standpoints. First, it promises to provide a substantial increase in available range as compared to the smaller lunar roving vehicle (LRV) for which Phase B definition studies were recently completed. This should be of tremendous potential interest to mission planners and could possibly make the flyer mode more competitive with the roving vehicle exploration mode. The main operational problems appear to be the source of propellants and the safety considerations relative to need for a rescue concept. With a second (logistic) launch per mission, these conditions could be alleviated and a second escape/rescue vehicle could be provided.

A second reason for interest in the long range flyer version of LESS is in the added use or multi-mission aspect it provides. The two requirements appear mutually compatible and similar so that the dual-mission capability is a realistic possibility which merits further consideration.

Weight, Balance, and Design Integration

Objectives. - The primary objectives of this portion of the study were the investigation of various vehicle configurations to determine the practical application of theoretical analysis, and to provide design data feedback required for guidance and control analysis. In the accomplishment of these objectives, several promising design concepts and approaches were devised for various control modes and packaging constraints. In conjunction with these concepts, the required subsystems and structures were investigated to the extent necessary to establish their rough requirements; approximate weight, size, and power feasibility. The guidance and control subsystems which have major impact on vehicle capability and configuration were studied in considerably more detail and are covered in a separate section of this report.

Approach. - Since the vehicle payload of the two suited astronauts is known and fixed, the vehicle size is determined primarily by the amount of propellant necessary to reach the desired orbital altitude. Preliminary performance data revealed that for the simple two-step profile, approximately 1600 pounds of propellant would be required, while for the optimum trajectory with the lightest possible vehicle, approximately 1000 pounds is necessary. Therefore, these two extremes of propellant loading have been used in the design analysis. Where possible, data were generated such that any propellant capacity between these two extremes could be utilized.

The approaches taken in the development of vehicle design concepts are described below.

The layouts are intended to illustrate the feasibility of vehicles resulting from parametric analysis, to show possible solutions to various design problems and to illustrate general configurations resulting from requirements of mission, performance, and astronaut capabilities. For this phase A study, a refinement of configuration concepts and design features into a single recommended vehicle design has not been attempted. Subsystem details have been defined only in those areas which are critical to the overall vehicle performance and/or configuration. Other subsystems have been identified and approximations of their weight, size, and power requirements made based on present technology. In such areas as LM interfaces, propulsion, and structures, this study benefited considerably from detailed analyses of a similar, though smaller, lunar flying vehicle.

Design integration ground rules and assumptions.

1. Major emphasis has been placed on vehicle simplicity, light weight, and minimum size. The single engine propulsion system utilized is a result of this philosophy.

2. The PLSS will provide environmental control for the astronauts as well as voice communication during the escape mission.

3. Stowage on the basic or extended lunar module (ELM) descent stage is desired, if possible.

4. Changes to the LM to accommodate the LESS stowage and surface operations as well as the CSM for rendezvous and recovery will be minimized.

5. The LM failures which cause use of the LESS are not specifically defined, but propellants are assumed to be available.

6. Nominal orbital altitude at end boost is 60 nm.

7. Provision is for two crewmen but one crewman may be incapacitated.

8. Main propulsion system will not be restartable; single burn from surface to orbit.

9. Attitude control after shut-off of main engine is required.

10. Desired time from take-off to rendezvous is less than four hours.

11. One astronaut can accomplish unloading, deployment and servicing.

Typical design configuration concepts. - Based on the parametric analysis of performance, guidance, control and visibility requirements and conditions, several conceptual designs of typical vehicles have been prepared. These concepts include kinesthetic, hardwire, and stability-augmented types of vehicle control. Two basic types of guidance systems illustrated are optical sights where the pilot controls vehicle orientation by alignment with landmarks, horizon, or the sun; and all-axis attitude indication and accumulated error instruments. The functional analysis of these guidance and control concepts are covered in detail in another section of this report.

Variations between configurations are primarily those dictated by the different guidance and control concepts, although other variations in seating arrangement, instrumentation/displays, and structural design are evident.

These differences are intended to show possible alternatives and no attempt has been made to select "best" overall arrangements or to prepare a single recommended vehicle design drawing which incorporates all of the necessary and desirable features selected from possible alternatives. This follows from the interdependance of so many variables and the uncertainties of the basic guidance and control mode to be utilized.

Previous analysis showed that at least 1000 pounds and as much as 1600 pounds of propellant are required for the expected range of vehicle weight, trajectories, and orbital altitudes. For a typical configuration, flying a "bent two-step" profile to a 60 nm circular orbit, with engine thrust reduction to 10 percent during boost, calculations show a propellant requirement of 1160 pounds. The layouts reflect this range of propellant requirements and resulting tank sizes in that 1000- and 1600-pound sizes as well as the 1160-pound size are shown. Thus, if later groundrules change and influence weights, the resulting effects on design should still be apparent.

Figures 3-1 through 3-10 show approaches to various vehicle and control methods as well as possible methods of stowing a candidate vehicle on the LM or ELM and the subsequent deployment and servicing on the lunar surface.

Figure 3-1 is a two-man kinesthetic control vehicle and was configured with four fuel tanks extended along the X and Y axes on truss structure booms. Propellant tanks were positioned at a distance from the center line which results in near optimum moments of inertia and resultant handling qualities, at least initially. This concept shows 1000-pound and 1600-pound capacity fuel tanks suspended below the structural booms and an alternate tank position above the booms. The alternate tank position is shown as a possible method of minimizing the vehicle vertical center of gravity shift as the fuel load is expended.

The vehicle has a lightweight aluminum structure consisting of a reinforced honeycomb deck plate over a tubular truss structure and mounting four fuel tanks and four pressurant tanks symmetrically about a single fixed position constant thrust engine. The deck plate is equipped with a form-fitting passenger crew couch arranged to support one man and his life support equipment in a predetermined position to trim the vehicle balance.

The pilot station display panel is equipped with two hand grips. The left hand grip is fixed to provide for pilot balance. The right hand handle is the RCS controller for directional (yaw) control and stabilization following engine burnout. The flight control attitude indicator is mounted directly above the display panel and is fitted with an adjustable glare guard.

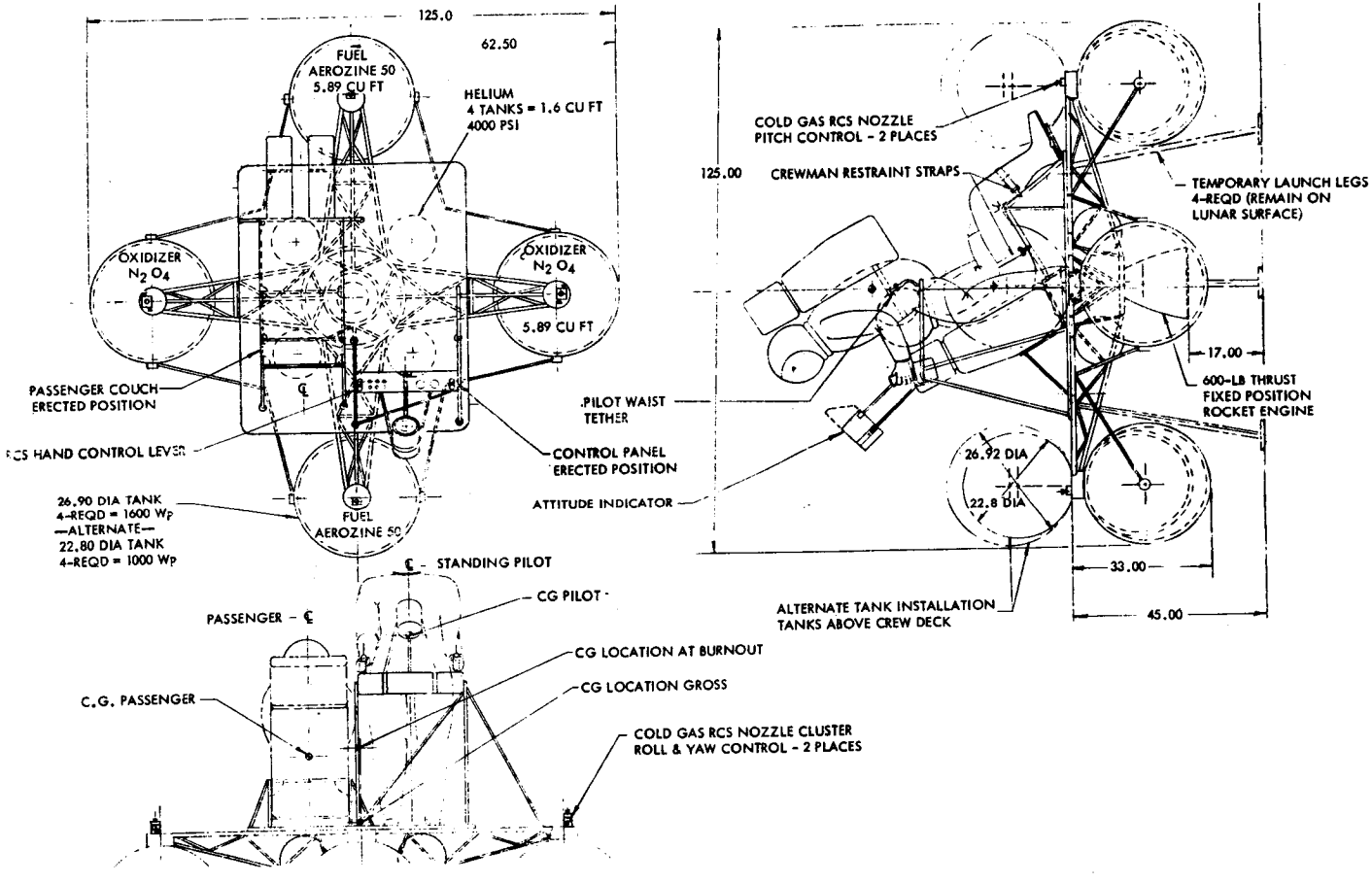

Figure 3-1. LESS Kinesthetic Control Concept

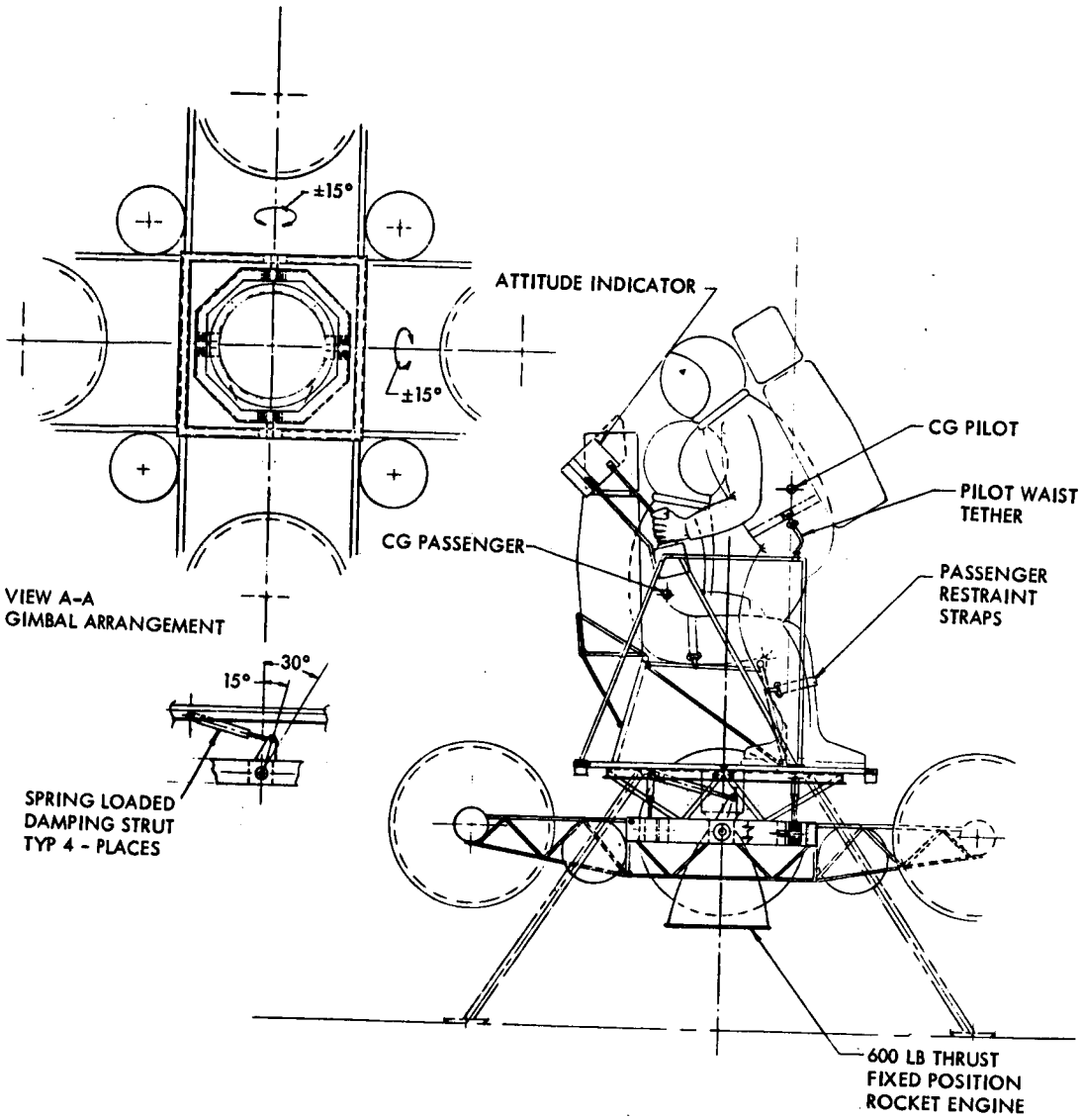

Figure 3-2. LESS Three-Body Kinesthetic Control Concept (Sheet 1 of 2)

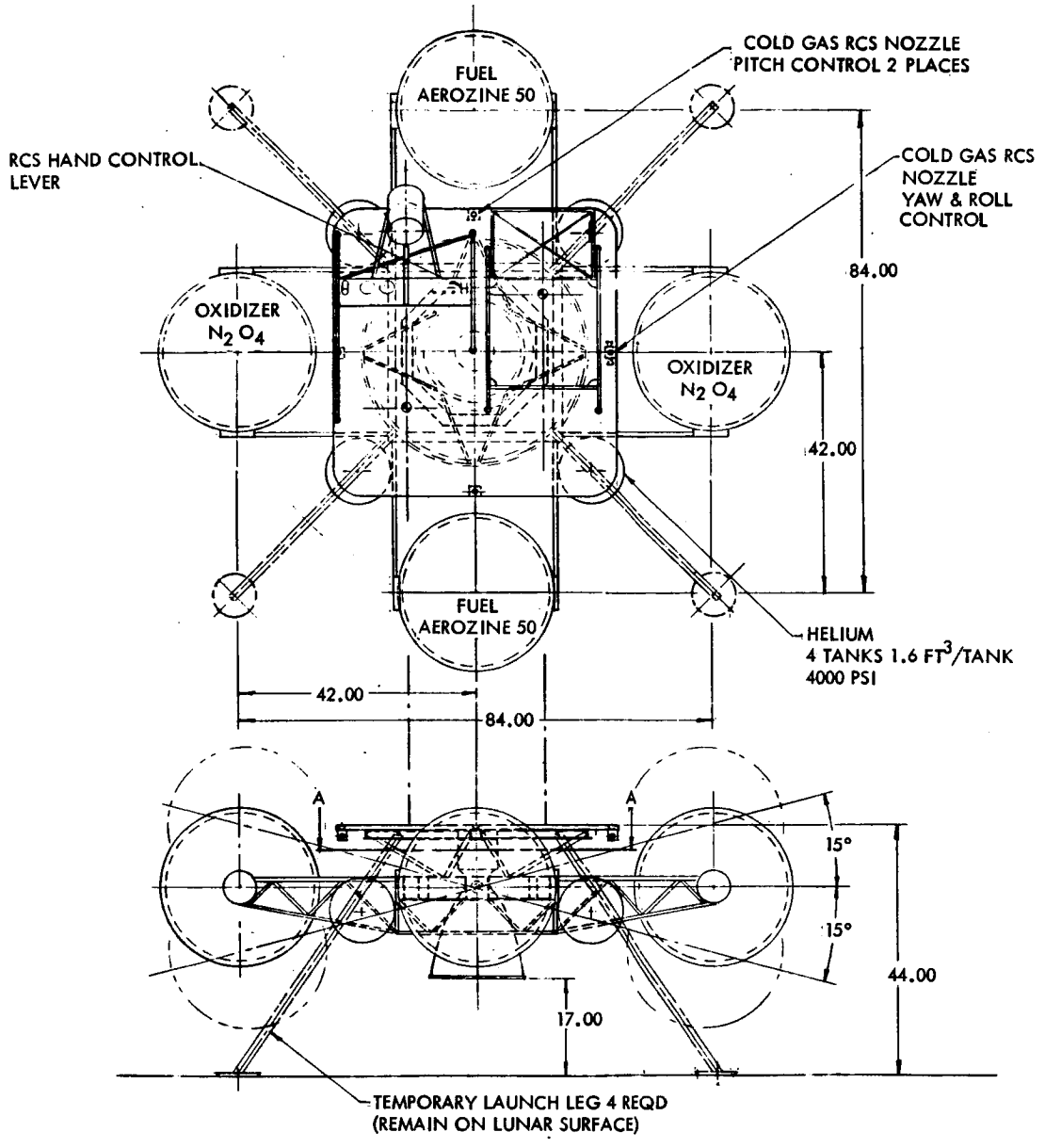

Wp TOTAL	1000 LB	1600 LB
FUEL	AEROZINE 50	AEROZINE 50
OXIDIZER	N_2O_4	N_2O_4
TANK DIA	12.8	26.9
TANK VOL	3.58 FT^3	5.89 FT^3
W_O/TANK	322 LB	530 LB
W_P/TANK	202 LB	330 LB

Figure 3-2. LESS Three-Body Kinesthetic Control Concept (Sheet 2 of 2)

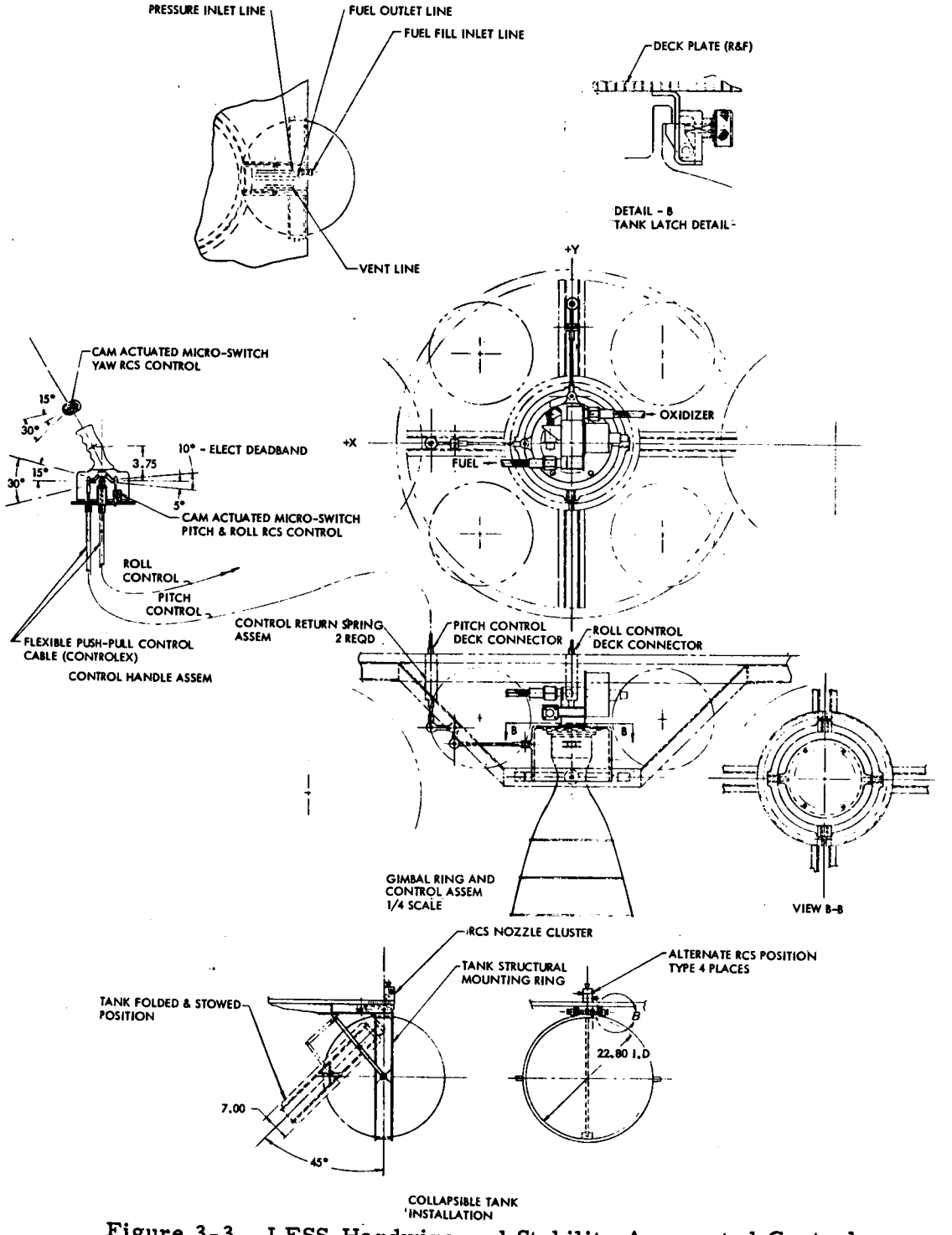

Figure 3-3. LESS Hardwire and Stability Augmented Control Representative Concepts (Sheet 1 of 2)

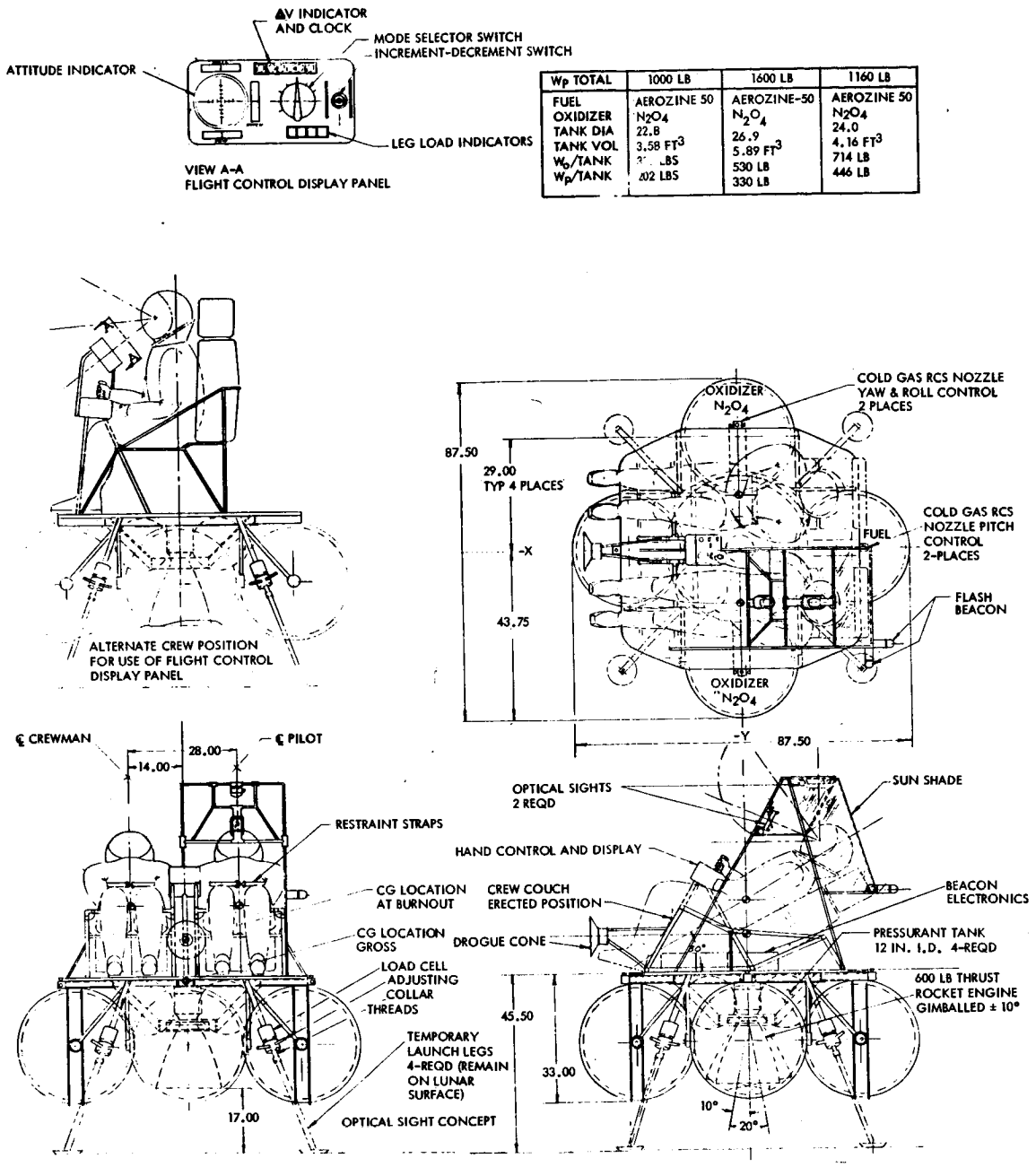

W_P TOTAL	1000 LB	1600 LB	1160 LB
FUEL	AEROZINE 50	AEROZINE-50	AEROZINE 50
OXIDIZER	N_2O_4	N_2O_4	N_2O_4
TANK DIA	22.8	26.9	24.0
TANK VOL	3.58 FT^3	5.89 FT^3	4.16 FT^3
W_O/TANK	[illegible] LBS	530 LB	714 LB
W_P/TANK	402 LBS	330 LB	446 LB

Figure 3-3. LESS Hardwire and Stability Augmented Co
Representative Concepts (Sheet 2 of 2)

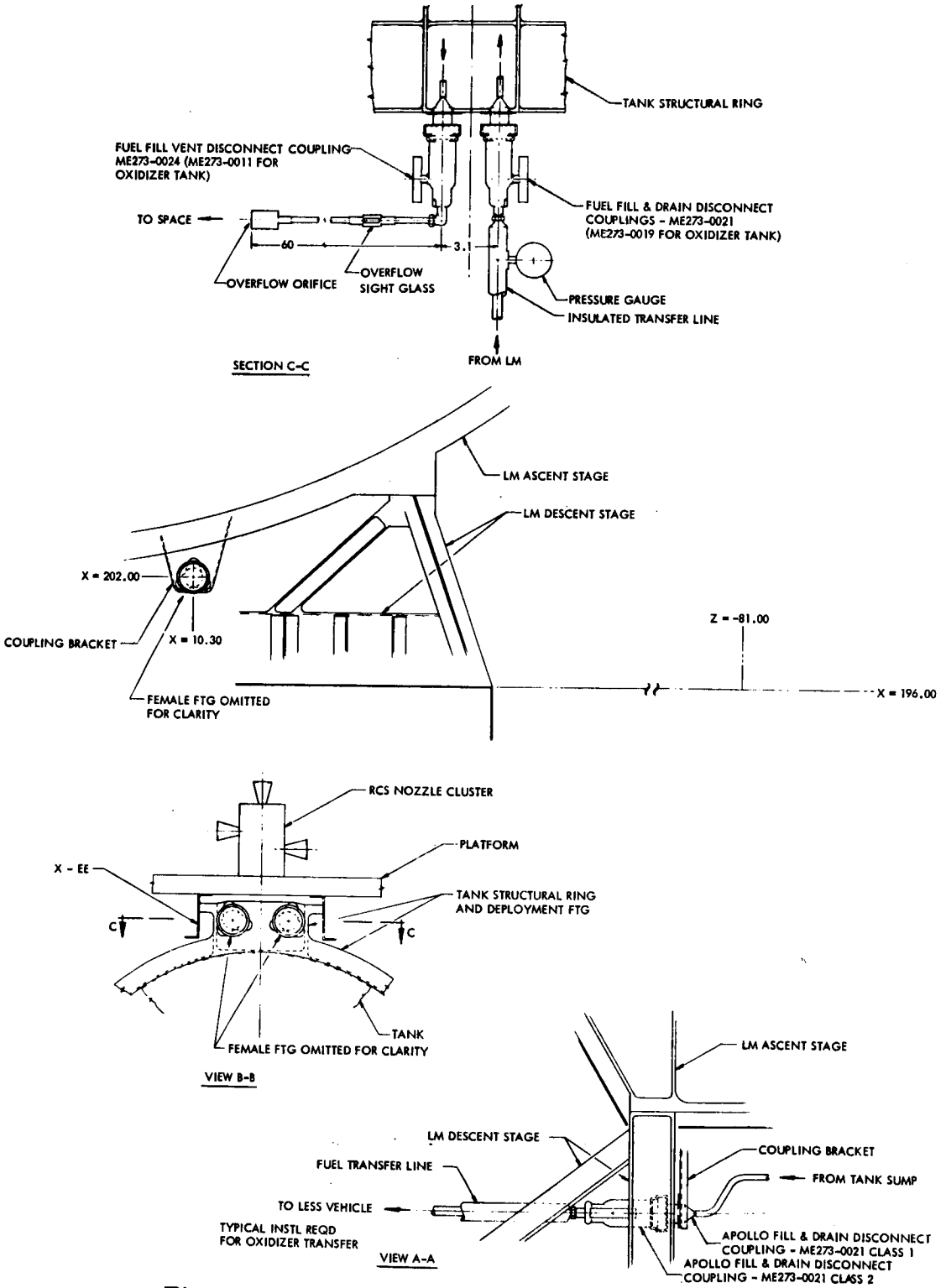

Figure 3-4. Lunar Surface Servicing (Sheet 1 of 3)

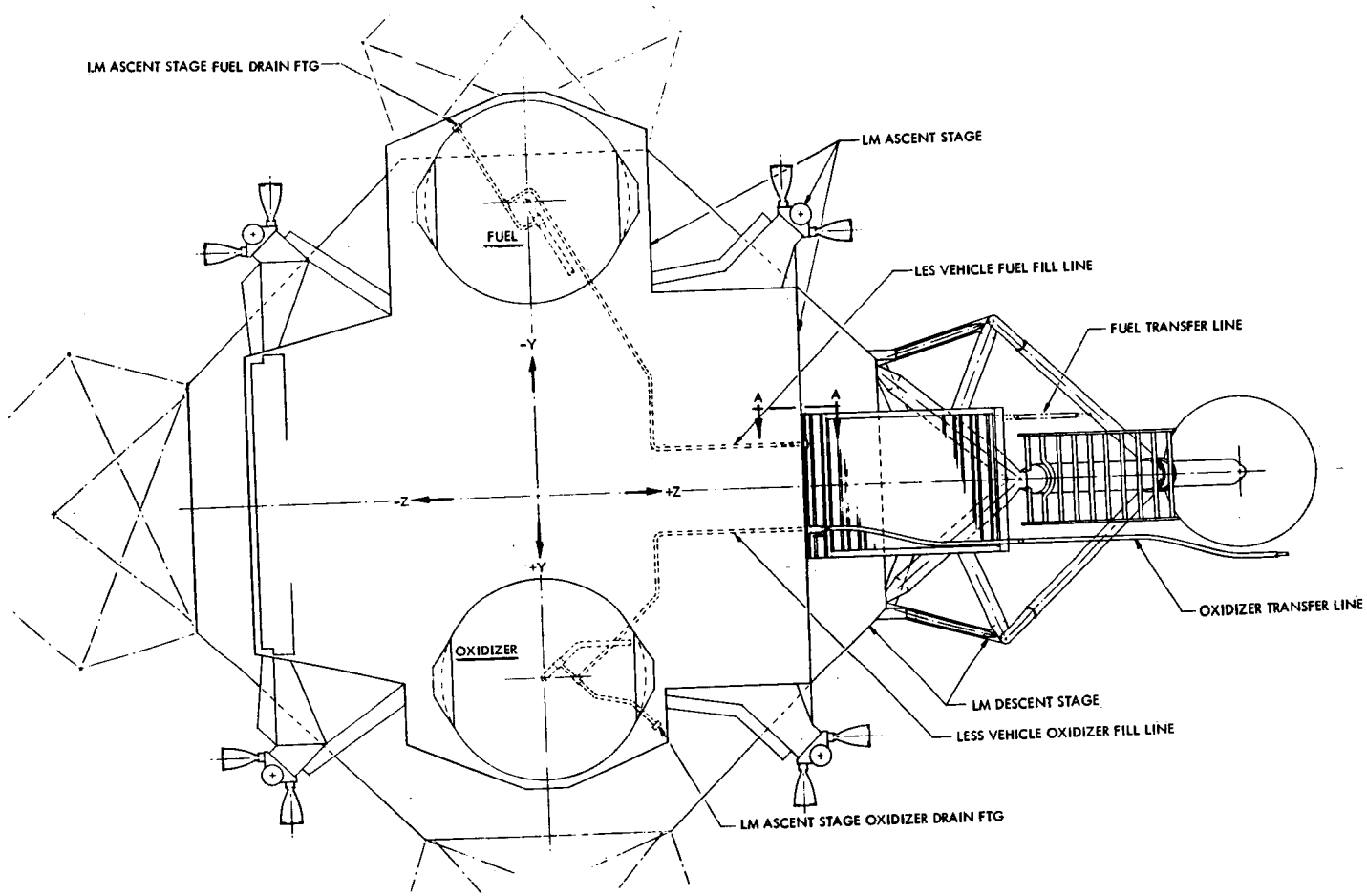

SECTION D-D

Figure 3-4. Lunar Surface Servicing (Sheet 2 of 3)

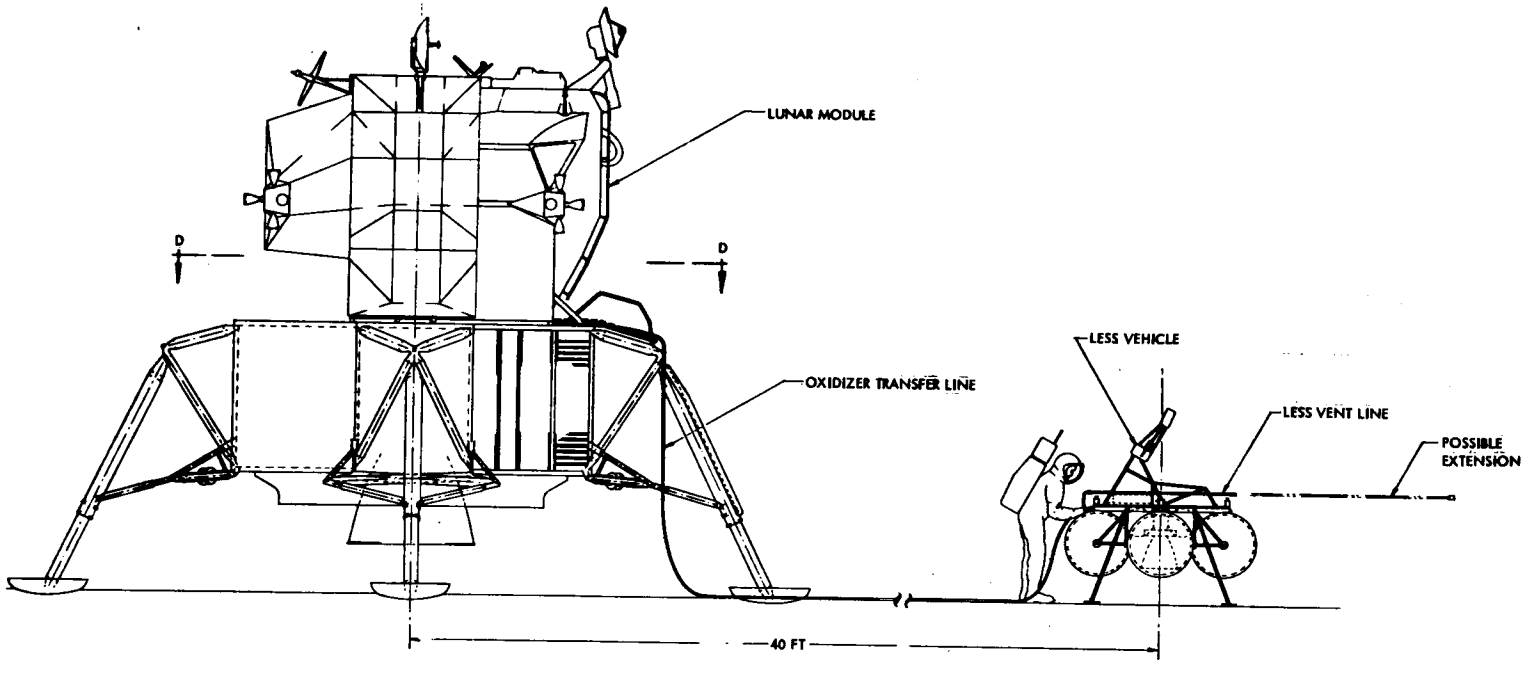

Figure 3-4. Lunar Surface Servicing (Sheet 3 of 3)

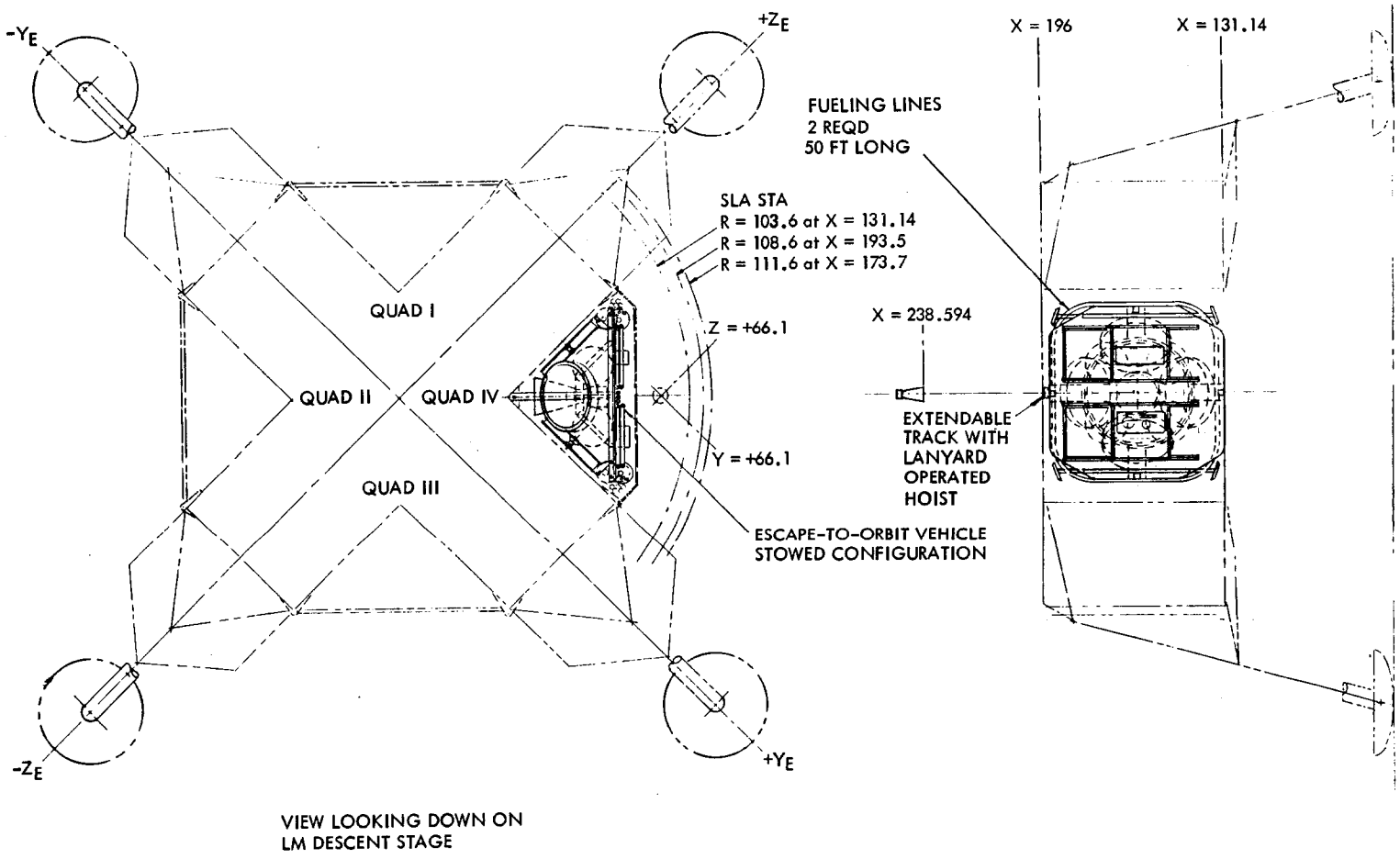

Figure 3-5. LESS Lunar Module Storage

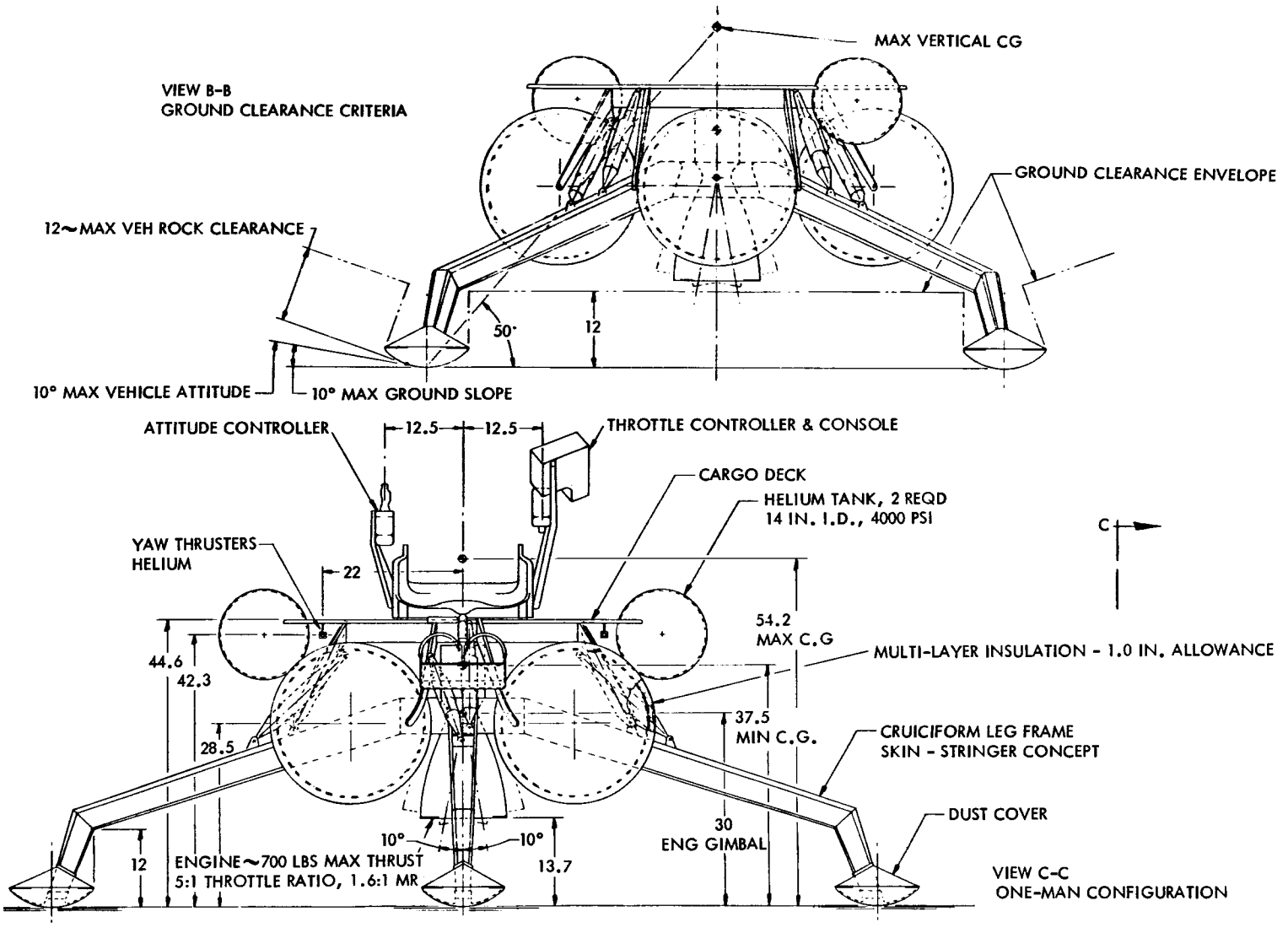

Figure 3-6. Long Range Lunar Flying Vehicle (Sheet 1 of 2)

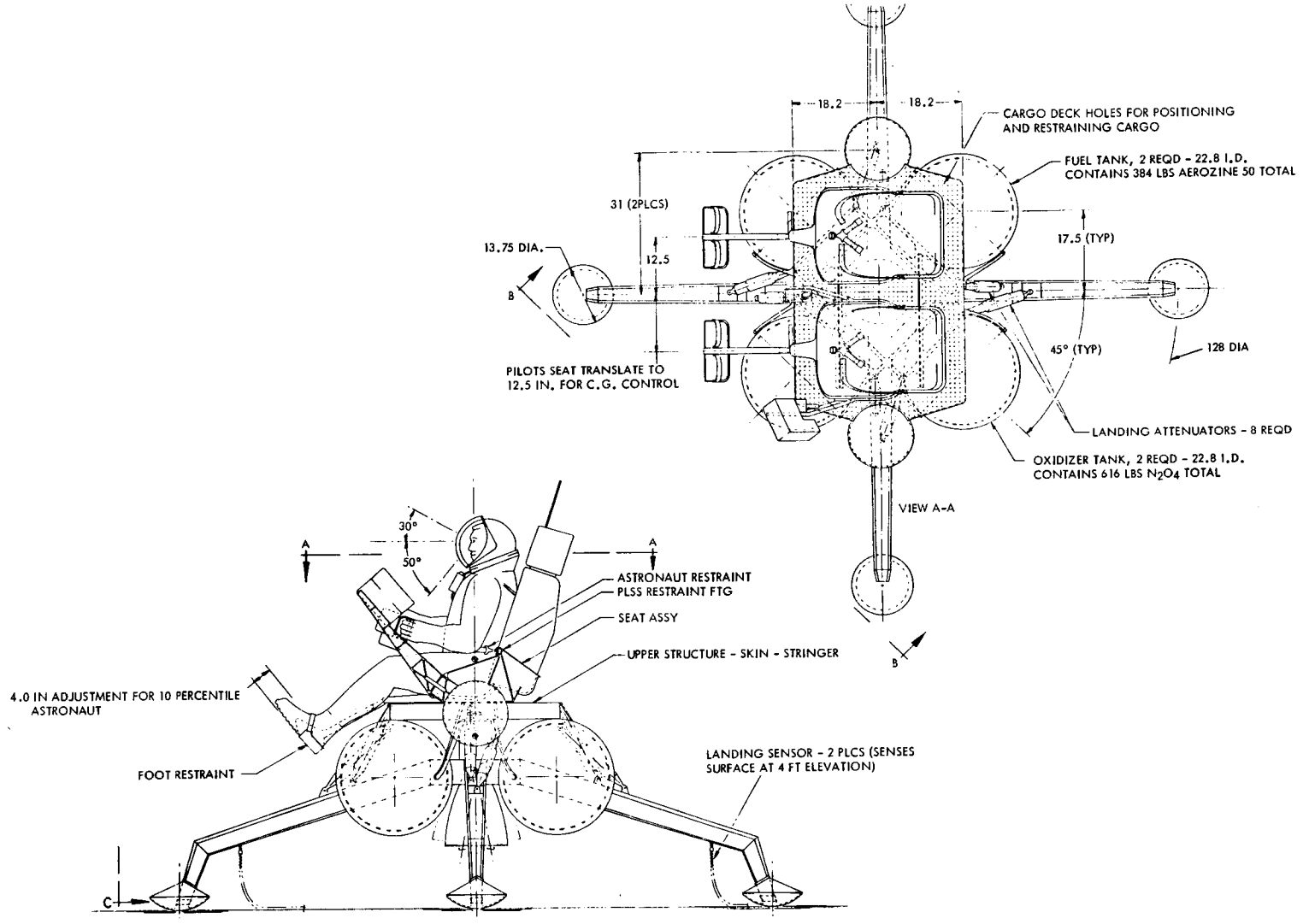

Figure 3-6. Long Range Lunar Flying Vehicle (Sheet 2 of 2)

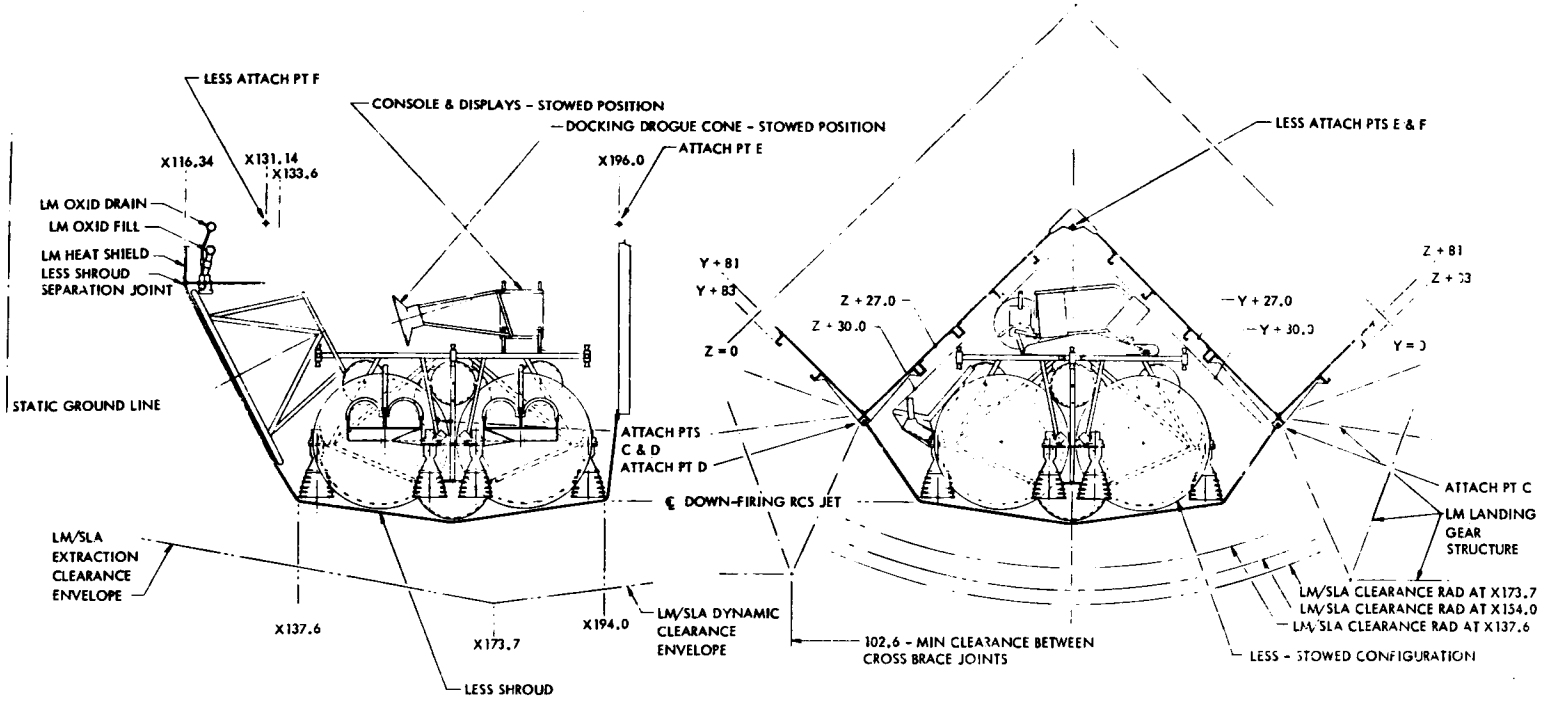

Figure 3-7. LESS Stability-Augmented Pulse-Mode Propulsion Concept
(Sheet 1 of 2)

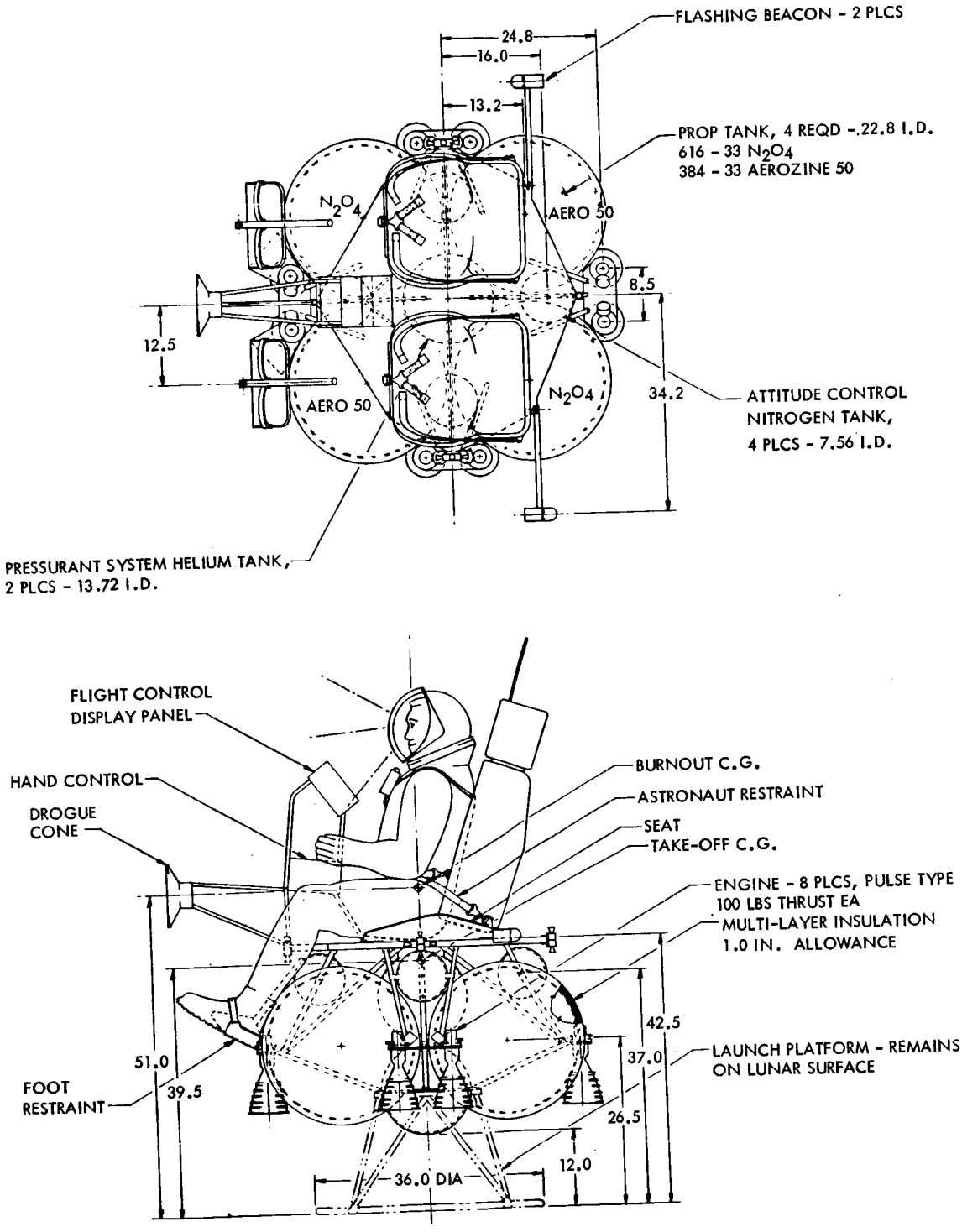

Figure 3-7. LESS Stability-Augmented Pulse-Mode Propulsion Concept
(Sheet 2 of 2)

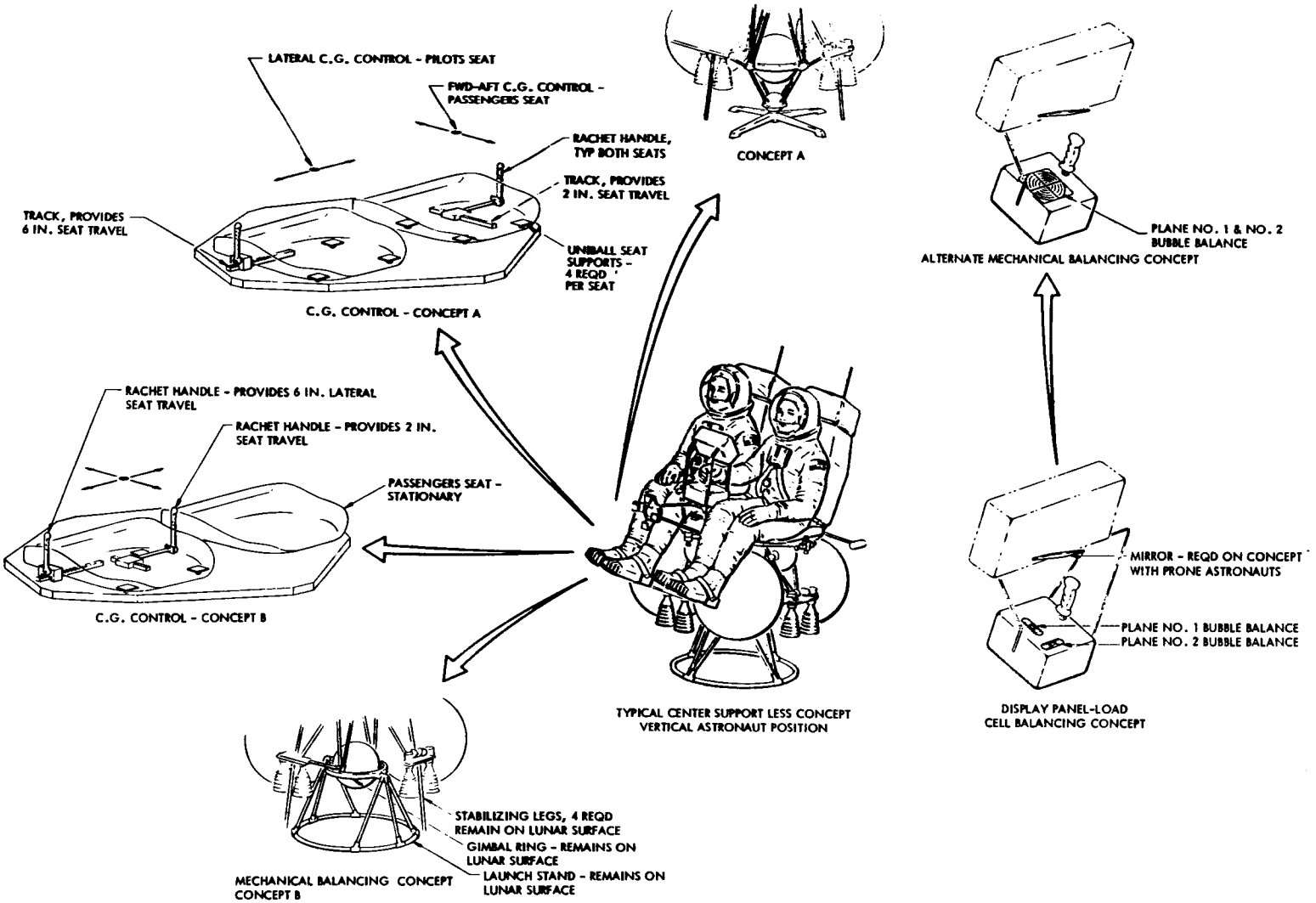

Figure 3-8. LESS Level and Balance Methods (Sheet 1 of 2)

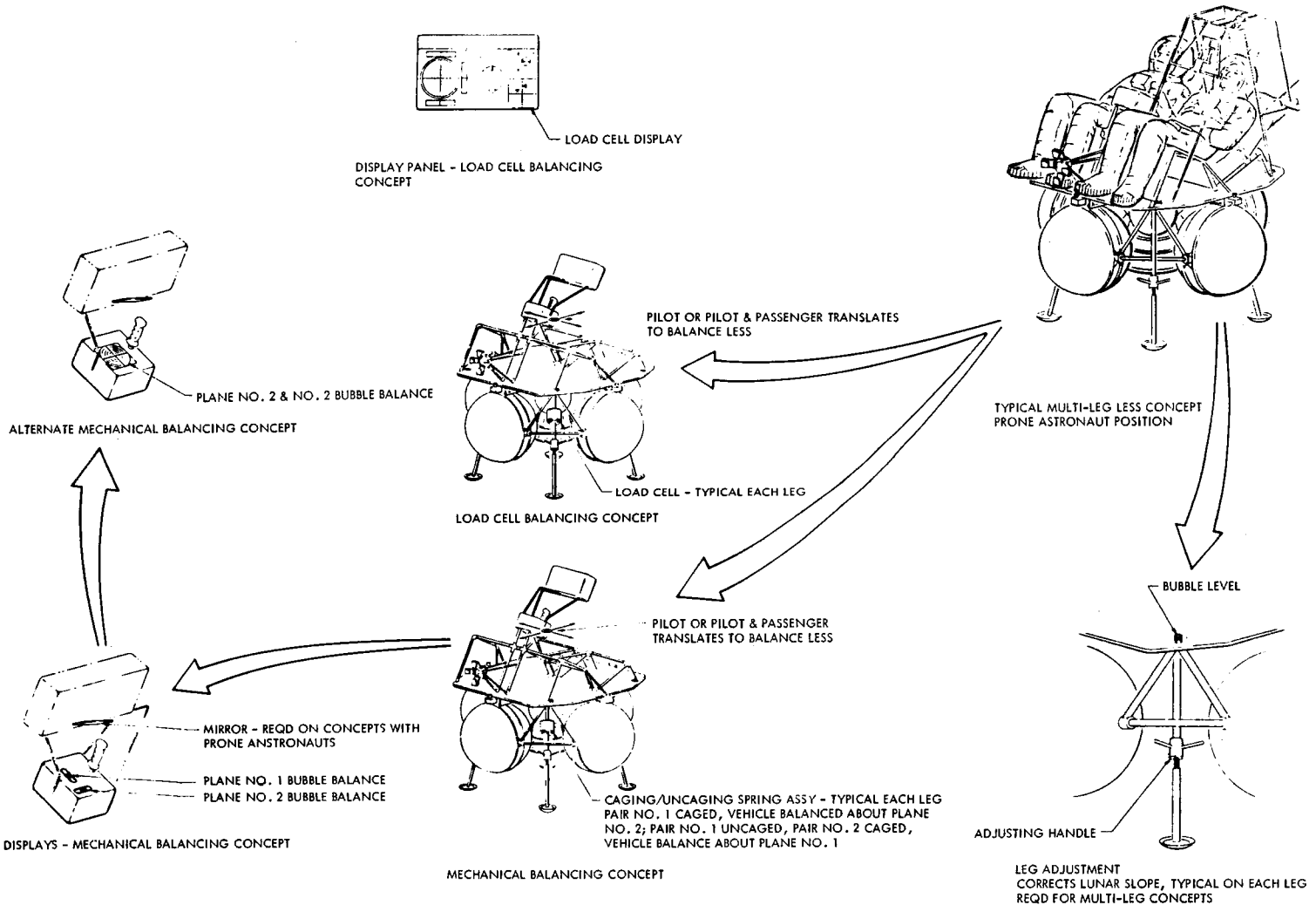

Figure 3-8. LESS Level and Balance Methods (Sheet 2 of 2)

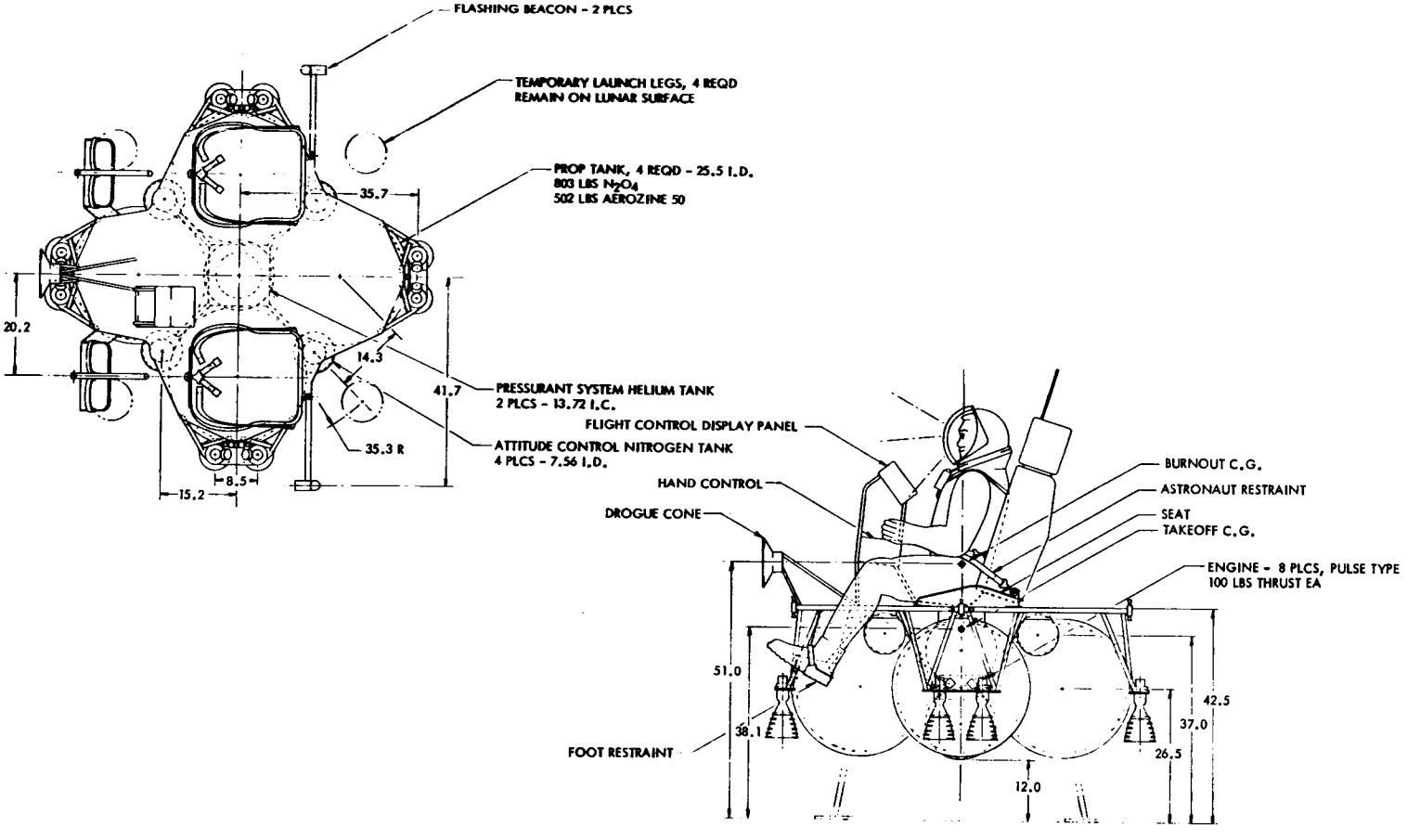

Figure 3-9. LESS Mechanical Control Pulse-Mode Propulsion Concept
(Sheet 1 of 2)

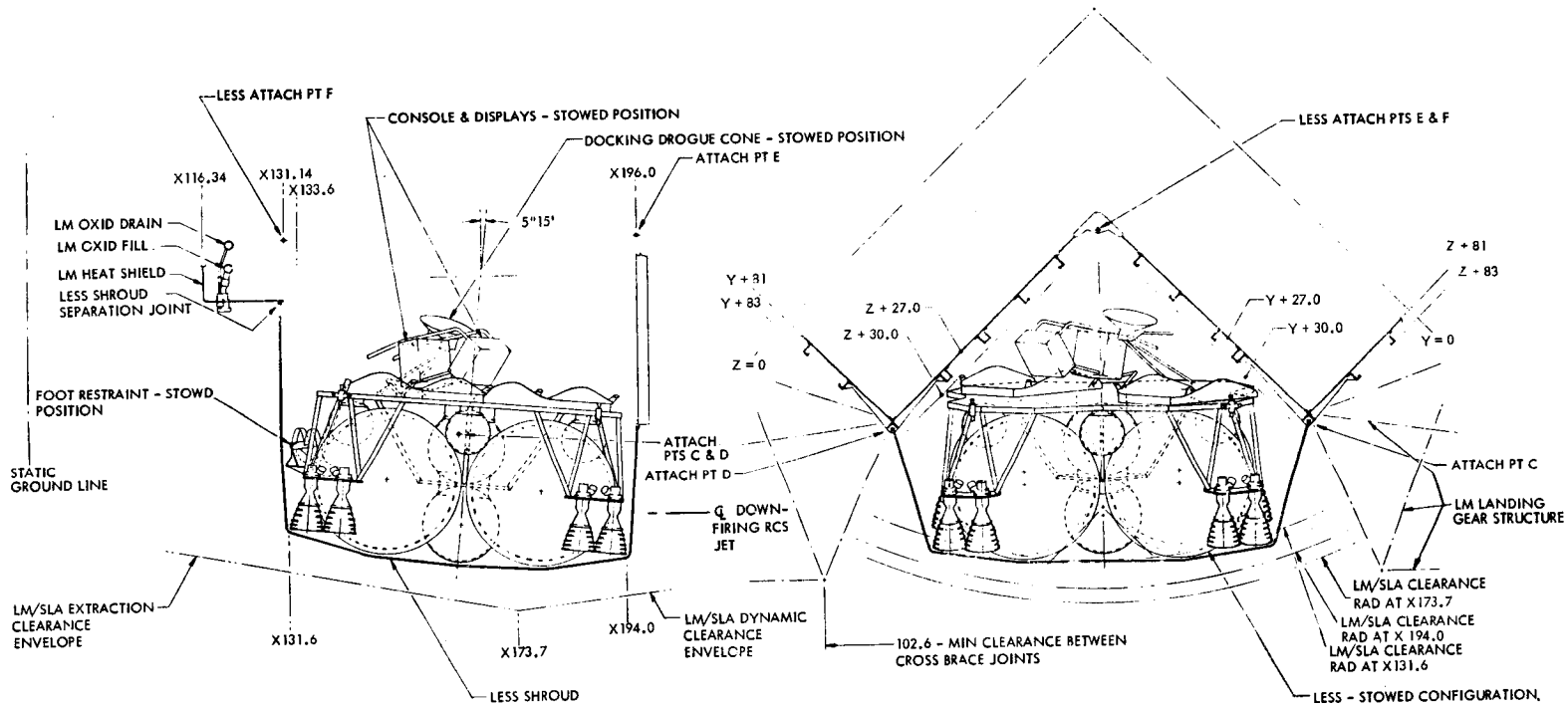

Figure 3-9. LESS Mechanical Control Pulse-Mode Propulsion Concept
(Sheet 2 of 2)

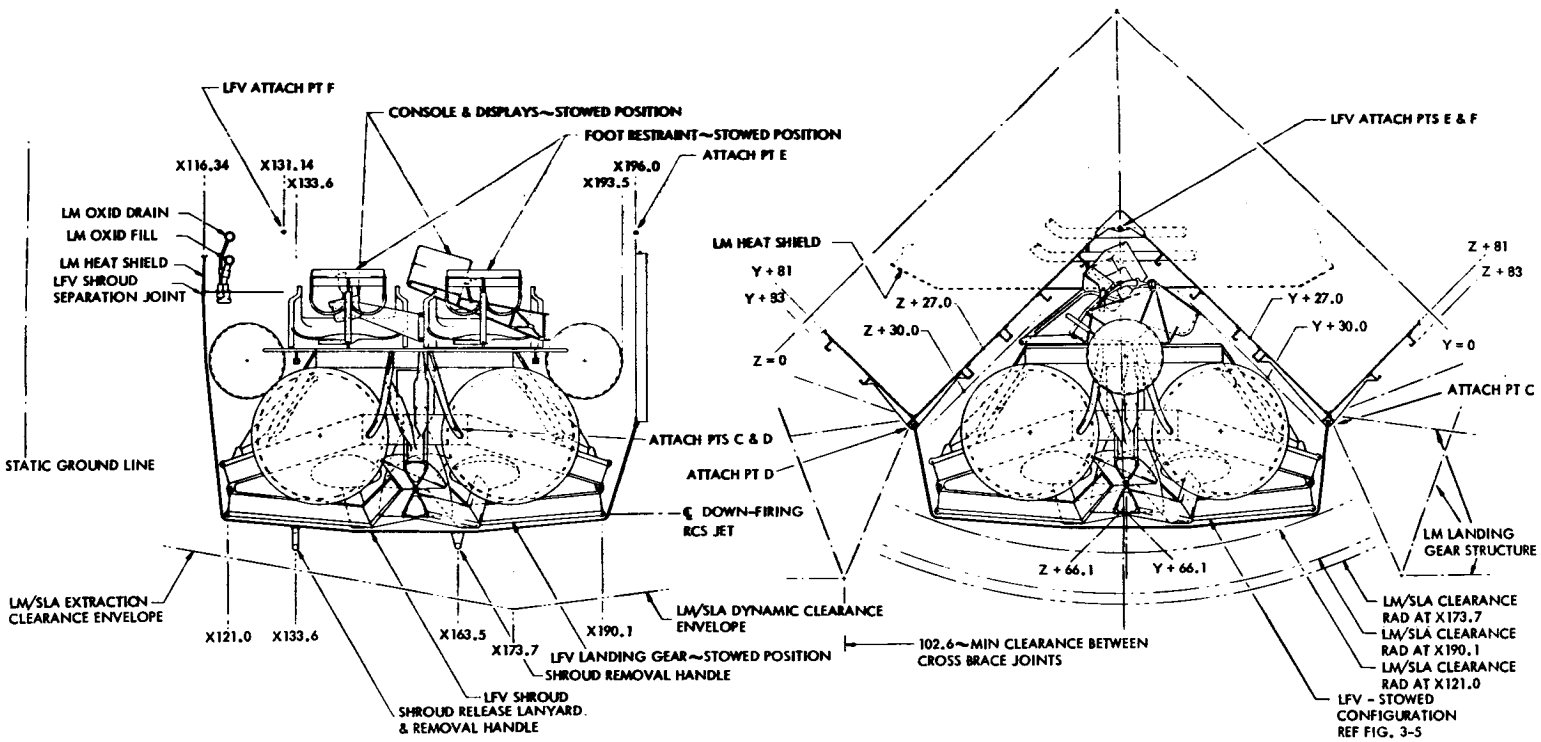

Figure 3-10. LESS/LRF Lunar Module Storage

The LESS vehicle is supported by four adjustable and jettisonable launch legs which can be adjusted to level the vehicle and compensate for an uneven surface and to assist in thrust vector-center of gravity alignment. Cold gas RCS jets are shown to provide yaw control during boost and all-attitude control later. They could be used also for docking translation (if required) when properly located relative to the center of gravity.

Figure 3-2 illustrates an approach to a three-body kinesthetic control vehicle, which analysis revealed has possibilities for improved handling qualities. The three separate bodies of this concept are the pilot and his life support equipment as body 1. Body 2 consists of the passenger crewman, the crew deck, passenger seat, flight controls, engine and engine thrust structure. Body 3 consists of the four propellant tanks, three H_e pressurant tanks, one GN_2 supply tank, battery and the tubular truss support structure. Body 2 is mounted on body 3 by a gimbal arrangement that allows each body to move independently of the other ±15 degrees. This relative movement is controlled by two opposed spring loaded double acting damping struts on each gimbal axis. The improvement in handling qualities obtained must be balanced by the increased configuration complexity required.

Figure 3-3 shows a typical configuration for hardware engine gimbal movement for attitude control (direct link, pilot to engine). The vehicle deck plate is of reinforced honeycomb supported on a Z-bar engine thrust structure. The single engine is attached to the structure by a gimbal assembly and capable of excursions through as much as 20-degree cone angle, although 10 degrees should be enough. The four propellant tanks are symmetrical about the engine. On the X and Y axes four 12-inch diameter H_e pressurant tanks were used for this concept, mounted to the engine thrust structure 45 degrees to the X and Y axes. This tank arrangement was selected to minimize cross products of inertia. Tank locations shown provide lower moments of inertia than either figure 3-1 or figure 3-2. In these previous kinesthetic control concepts little attention was paid to LM stowage constraints; the hardwire case appeared to be the first which might be configured to fit on LM/ELM. Propellant tank size shown is the large 1600-pound (26.9 inches in diameter) size, which is indicative of a worst case volume requirement.

Figure 3-3 illustrates the use of visual sight type of guidance control which for a "bent two-step" trajectory requires a reclined pilot position to maintain horizon sightings throughout the trajectory without pilot or sight movement. In this reclined position and with the expected sun position (from the back) a sun shade will be required. A possible arrangement of such a screen is shown. An alternate crew position (more upright) is shown which is applicable to the alternative all-attitude indicator instrument type guidance concept.

The crew deck is equipped with two lightweight, form-fitted crew couches designed to position the man's body and life support equipment in the balance of the vehicle. The pilot's hand controller is mounted between the crew couches within reach of both crewmen. The hand control and displays shown would be similar for either hardwire or stability augmented controls. View A-A shows one arrangement of an attitude indicator, meter, clock, mode switch, and increment/decrement switch. This attitude display panel is mounted on a tripod arrangement from the side arm control console and has provisions to slide to one side during pilot boarding.

The RCS thruster configuration shown is a minimum eight thruster arrangement to provide pitch, roll, and yaw control as well as translation during final docking. Refined system analysis could show that additional thrusters provide sufficient improved handling to justify more complexity.

The vehicle is supported on the lunar surface by four temporary launch legs which are expected to be jettisoned at lift-off. However, further study might indicate that hazards of dropping these light legs is not justified by the weight saved. Each leg is equipped with a screw jack for vehicle leveling and may incorporate load cells to calibrate vehicle balance before launch. Flashing beacons aligned along the flight path of a two-step trajectory are mounted to the A frame to facilitate tracking by the CSM. On the front of the vehicle between the crewmen is shown a lightweight drogue, a device which can be utilized to latch onto the CSM docking probe to facilitate retention of the LESS vehicle while the crewmen dismount and enter the CM hatch. Also shown is a proposed method of mechanizing the hardwire control. Some of the inherent design problems of hardwire controls have been studied by NR in conjunction with such other projects as the AMU backpack, the lunar flying vehicle, and are currently being investigated by NR under contract from NASA-LRC for the flying lunar excursion experimental platform (FLEEP, NAS1-9516).

The mechanism shown is a typical gimbal ring assembly equipped with precision bearings and actuated by a hand control through a low friction push-pull and rod bell crank arrangement. In order to describe the hardwire control, some assumptions had to be made: an engine weight of 25 pounds; angular accelerations of $0.05\ \pi$ rad/sec^2; total engine excursion of ±5 degrees; control handle deflections of ±15 degrees, with a 3:1 mechanical lever advantage from control handle to engine gimbal, and a spring-loaded bungee calibrated to a breakout force of 5 inch-pounds and capable of returning to the null position.

The subsequent calculations show a torque of 33.4 inch-pounds at the engine gimbal and 11.1 inch-pounds at the bell crank pivot due to the 3:1 reduction. Adding to this, a restraining force of 12 inch-pounds results in a 23.39 inch-pounds of torque at the control handle pivot. This torque load

would be classed as a medium workload for short periods of time. More information on hardwire controls will be available as the current FLEEP study progresses.

To avoid the necessity of developing the 600- to 700-pound thrust engine for the single-engine LESS vehicle, the eight engine concepts illustrated in figures 3-7 and 3-9 were generated utilizing highly developed RCS engines. The most notable change is the resulting envelope, much smaller than that shown in figure 3-3; this resulted when the single center engine was removed allowing the four propellant tanks to move inboard. Moving the tanks inboard and positioning the crew 45 degrees to the tank centerline then allowed the crewmen to be positioned better on the upper deck. This has the advantage of providing a more compact vehicle with less moment of inertia change during propellant depletion.

The structural concept of the upper honeycomb deck and lower truss of figure 3-3 was retained with modification. The four tanks are attached to the engine thrust structure which is trussed to the upper deck and launch stand. Truss structure was again considered for the docking drogue cone, flight central display panel, and hand controller.

The eight engines are mounted in pairs, 90 degrees apart on the vehicle pitch and roll axis. Pairing is necessary for redundancy since engine failure causes a large thrust vector change. The engines are non-gimbaled, and vehicle attitude during ascent is maintained by differential pulsing. Should an engine fail, the opposite engine could be shut down and the flight would continue utilizing the six remaining engines. After the desired orbit has been achieved, all engines are shut down and the vehicle utilizes the cold gas RCS. Initially, the LESS is the passive vehicle (the Apollo CSM being active) during which time the LESS must only retain position and orientation; after the CSM is within close range (perhaps 10 to 15 feet), either vehicle could be the passive vehicle. Visibility for final docking of LESS to the CSM probe could be difficult when controlled from the CSM unless a docking target were extended from LESS into the CSM field of view.

The four propellant tanks of figure 3-7 contain 1160 pounds of N_2O_4/Aerozine 50 at a mixture ratio of 1.6 to 1.0 in the 24-inch-inner-diameter tanks. Figure 3-9 shows tankage containing 1300 pounds and the pilot position rotated 45 degrees to eliminate cross coupling of inertias which cannot be tolerated with hardwire control. This arrangement represents the worst stowage condition for the pulse mode engine concept. Calculations of propellant requirement are shown in the propulsion subsystem section of this report. The tanks were positioned inward until minimum clearance (one inch) exists; the central area was then used to stow the helium pressurant in two 13.72-inch inner diameter tanks. The nitrogen supply for RCS was then located in four 7.56-inch inner diameter tanks located on the vehicle centerline.

Due to the engine locations, the launch legs utilized on the previous designs could not be considered because of the possibility that the legs would interfere with the engines during lift-off. The central launch platform illustrated consists of a 36-inch diameter ring which is trussed up to the separation ring located on the meridian of the lower helium tank, and the loads are then trussed out to the engine thrust structure. The concepts discussed for balancing and leveling would also apply to this arrangement.

It should be noted that the compact arrangement of figure 3-7 is best suited for stability-augmented control. The location of the vehicle principal axes, offset from the control axes (pilot orientation), results in cross products of inertia. When a pure pitch, yaw, or roll maneuver is commanded, the vehicle responds with the desired rotation plus small rotations about the other axes from the cross products of inertia. Stability augmentation removes these undesired responses without pilot corrections.

The vehicles stow on the LM very well with encroachment into the LM RCS exhaust area. A design innovation that provides considerable improvement in stowage is the use of expandable propellant tanks which are collapsed and folded for stowage (discussed in Stowage and Structures Sections). Tank collapsing would only be required if the tanks increase considerably in diameter or the area under the LM RCS exhaust is restricted. The stowage concept illustrated in figures 3-7 and 3-9 requires folding the display panel assembly, foot rests, the drogue cone, and removal of the launch platform. The configuration is interesting because of the ready availability of engines and the compactness for stowage. It may well be a prime candidate if a crash development program were to be required with the least possible component and system uncertainties.

Subsystem analysis philosophy. - For this conceptual study where detail design definition of a singular LESS vehicle is not appropriate, the vehicle subsystems which do not significantly influence the concept feasibility were studied only to the minor extent necessary to establish weight and size approximations. Among these subsystems are electrical power, environmental control, and communication/data. The structural design was also investigated only to the extent required to determine the practicality of the structural concept shown on the drawings and to assure that the structural weight estimates made are realistic. The guidance/control and propulsion subsystems were studied in more detail since feasibility and performance are established by these subsystems.

Guidance and control systems. - The guidance and control systems analysis is covered in a previous section and will not be discussed again here. In the design of vehicle concepts, the control and handling qualities requirements have been a primary influencing factor, along with the constraints of packaging for LM stowage, and configurations compatible with visibility and boarding constraints. Two arrangements for kinesthetic control (figs. 3-1

and 3-2) and two for hardwire control (figs. 3-3 and 3-9) have been conceived. The hardwire control concepts are applicable to stability augmented control without noticeable difference in configuration.

Propulsion subsystem. - The LESS propulsion subsystem is required to provide the linear impulse necessary to boost the vehicle in the lunar gravity field and attain orbital velocity at 60 nm altitude, and the angular impulse necessary to maintain stable attitude as required of the powered trajectory (thrust vector control), the orbital coast phase, and the docking phase. The nominal mission studied utilizes CSM-active rendezvous with either LESS-active or CSM-active final docking. An alternative requirement studied included the additional propulsion requirements for LESS-active rendezvous and docking.

The LESS is to utilize LM ascent stage propellants (NTO and A-50) and is intended to be stowed in the LM descent stage corner compartments (if possible). The propulsion subsystem then must be designed as compactly as possible to aid in resolving the stowing constraints. The LESS vehicle and LM systems must contain provisions for propellant servicing on the lunar surface as well as for simplified checkout and flight preparation of the propulsion subsystem.

The LESS propulsion subsystem interface must be compatible with the pilot controls and the attitude/TVC control system (kinesthetic, manual hardwire, and other types were considered) with respect to gimbaling torques and swing, response rates, and related design factors.

Programmatic aspects require the propulsion subsystem to be considered from two schedule viewpoints. The nominal schedule would probably call for an operational date three to four years from start of a Phase C. The alternate schedule might require development as rapidly as possible, perhaps in a fraction of the nominal time.

The LESS ideal velocity requirements are a function of thrust and are as shown in figure 3-11 for a constant thrust trajectory and in figure 3-12 for a dual thrust level trajectory. Both utilize a "bent two-step" pitch steering profile. For the alternate case of LESS-active rendezvous and docking, additional energies of 600 and 200 fps, respectively, were used.

Since ascent stage propellants are to be used, non-optimum trajectory and engine performance are permitted if beneficial effects on dry weight, stowing dimensions, and simplicity of operations are obtained. The LM payload during transport to the lunar surface may be the primary variable to be optimized.

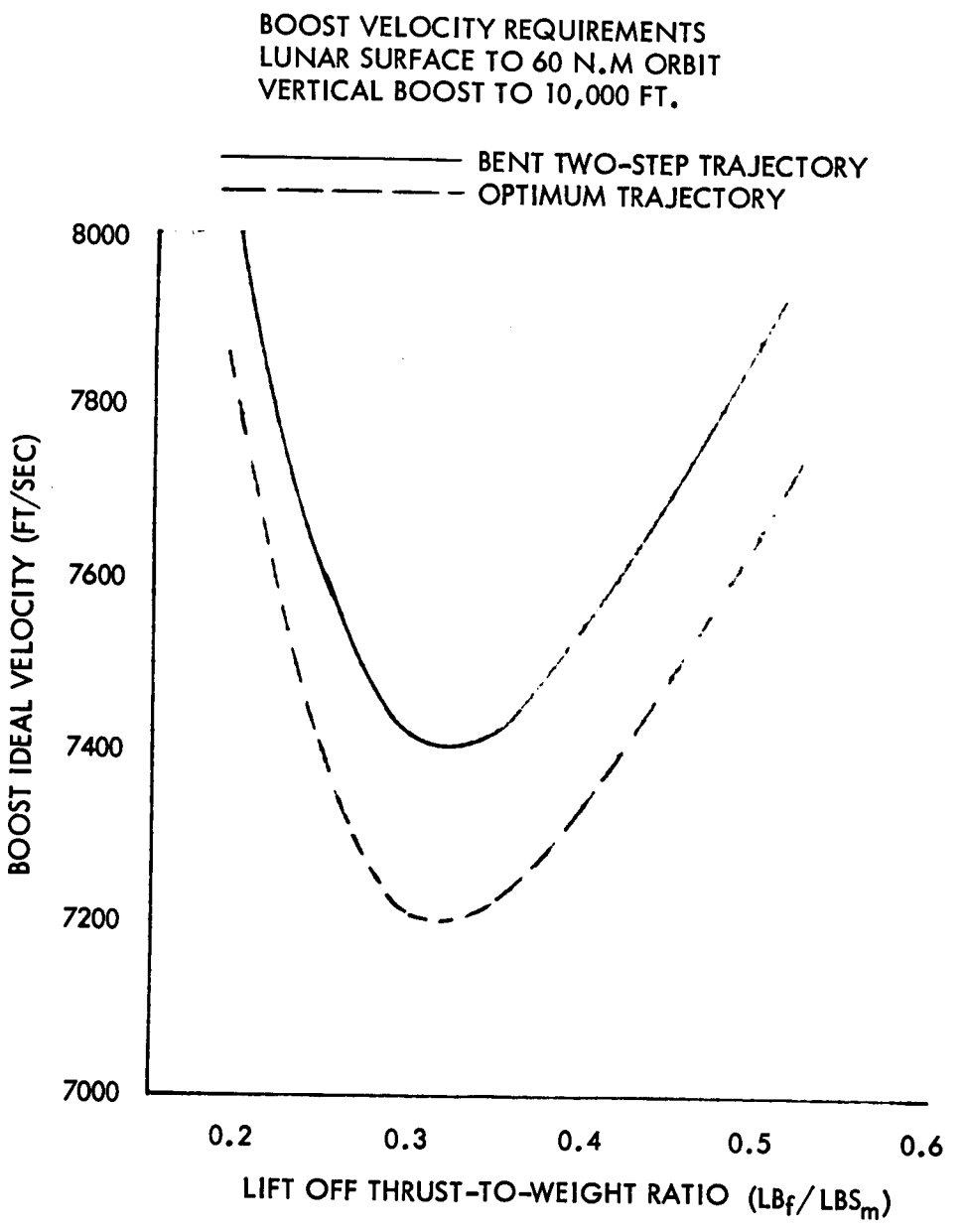

Figure 3-11. - Boost Velocity Requirements

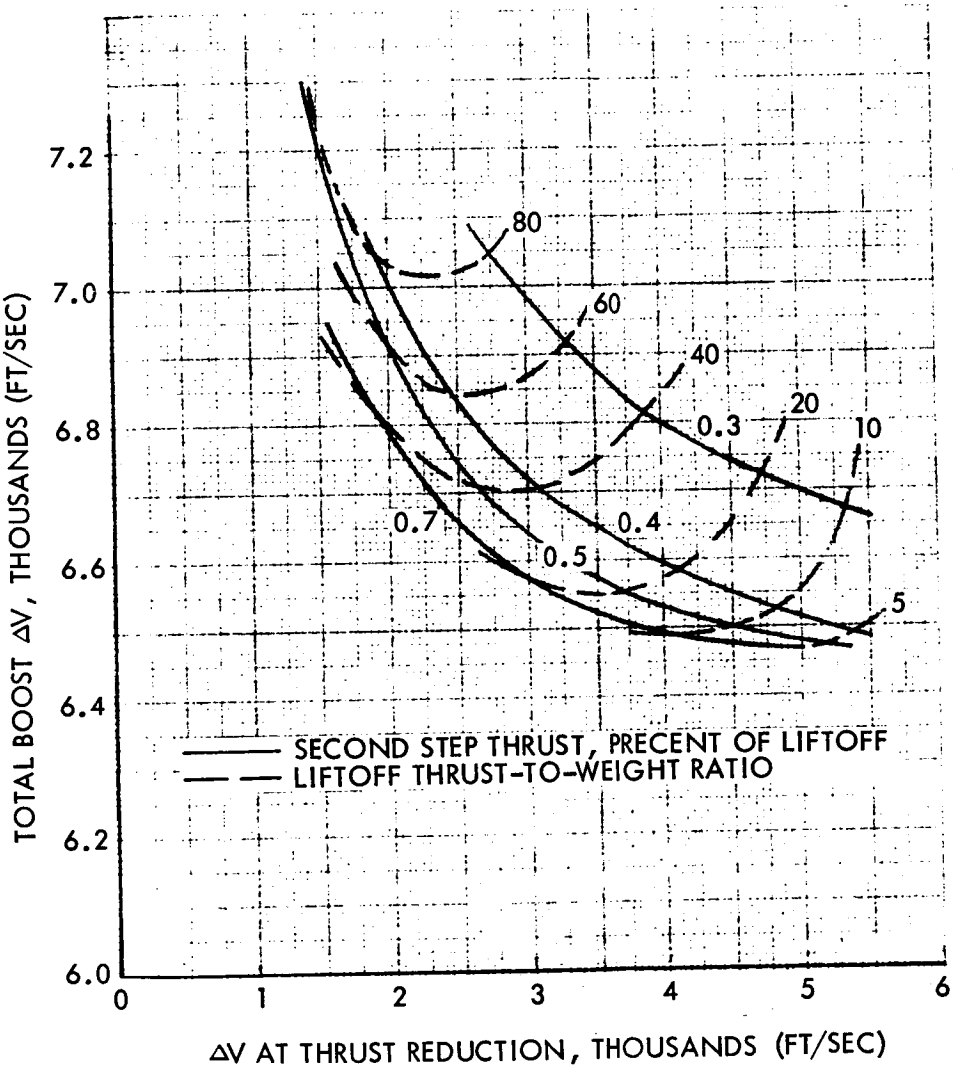

Figure 3-12. - Optimum Two-Step Thrust Schedules for Boost

Candidate concepts. - As stated before, propulsion is one of the subsytems which has a substantial bearing on the vehicle configuration. The primary or basic variations in propulsion candiate concepts were established to compare single versus multiple engines, available versus "new" engines and fixed dual-thrust and pulsed thrust control modes. The resulting matrix of primary candiates is shown in table 3-1. The Apollo R4D engine is the Marquardt radiation-cooled engine used for RCS on the SM and LM. It has a molybdenum chamber and an L605 nozzle extension, a weight installed of 7 pounds and a specific impulse of 273 seconds. The 325-pound engine considered is an uprated Rocketdyne RS2101, a space-rated version of their PBPS RS1401 engine. It has a beryllium interregenerative plus radiation cooled chamber and L605 extension, a weight of 17 pounds and a specific impulse of 290. The new single engines are considered to also be of the RS1401 type with predicted dimensions, weights and specific impulses as shown in figures 3-13, 3-14, and 3-15.

A third possibility, the use of a proportional throttling single engine, was not studied separately since its energy requirements and performance would be similar to the dual thrust case. Its advantage would only apply if the same engine were to be used on a lander or flyer version of LESS. Disadvantages would be the increased engine complexity and development cost and time.

TABLE 3-1. - PROPULSION CONCEPT BASIC MATRIX

Number of engines	1		4	8
Thrust control	Fixed	Dual 5 to 1	Pulsed	
Total thrust	To be Optimized (600 ~ 700)		1300	800
Engine status	New Development		PRE-PFRT 325 lb_F	APOLLO R4D 100 lb_F

Propellant feed system concepts. - All of the propulsion concepts utilize NTO/A-50 propellants at a mixture ratio of 1.6. This permits the use of the Apollo type of feed system, a very mature and well-developed concept. Figure 3-16 illustrates its application to the LESS. At this mixture ratio, the tanks are of equal size. Helium is passed through two series redundant regulators rather than four series/parallel since recent review of failure

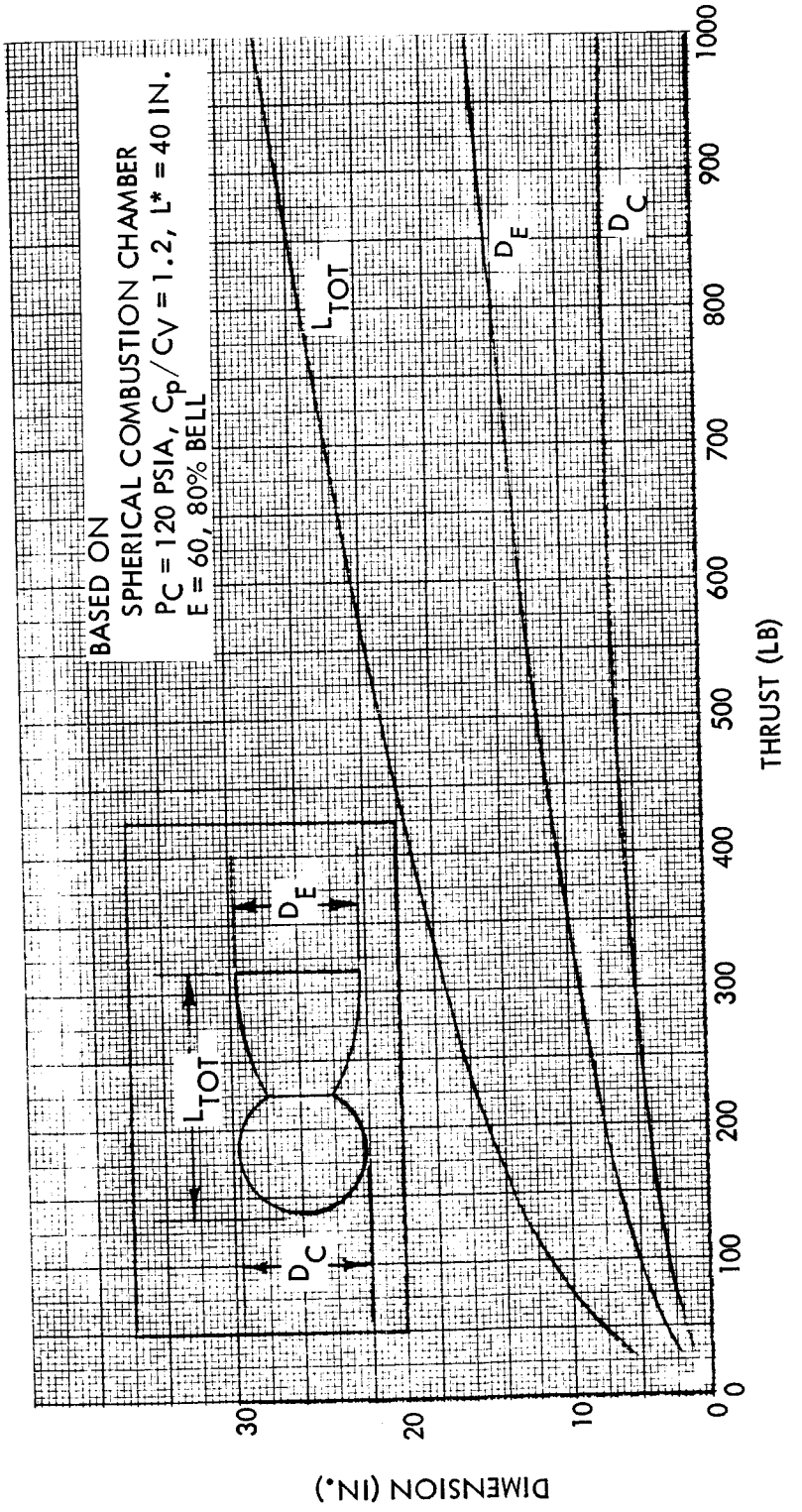

Figure 3-13. - Parametric Engine Dimensions

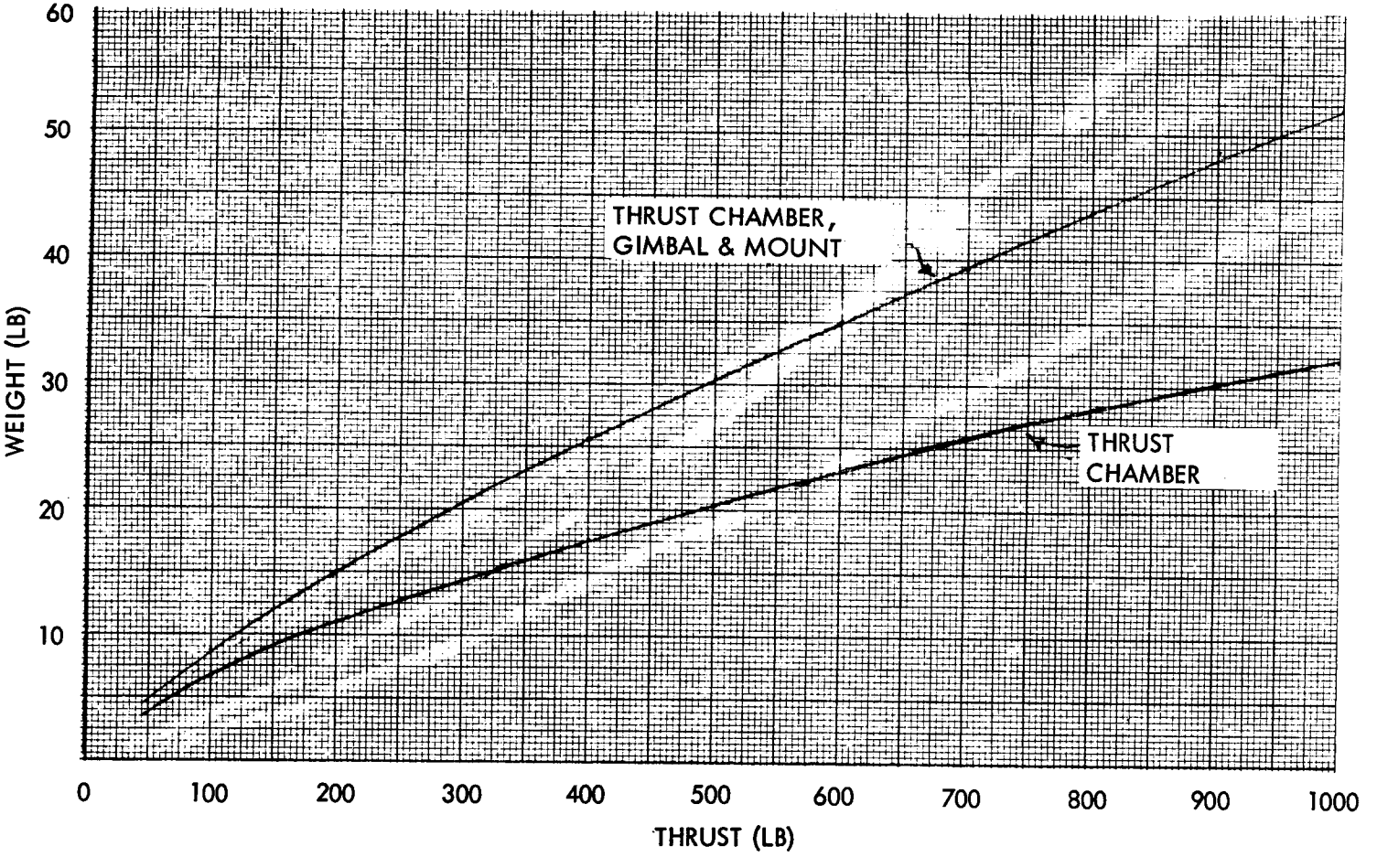

Figure 3-14. - LESS Propulsion Weights

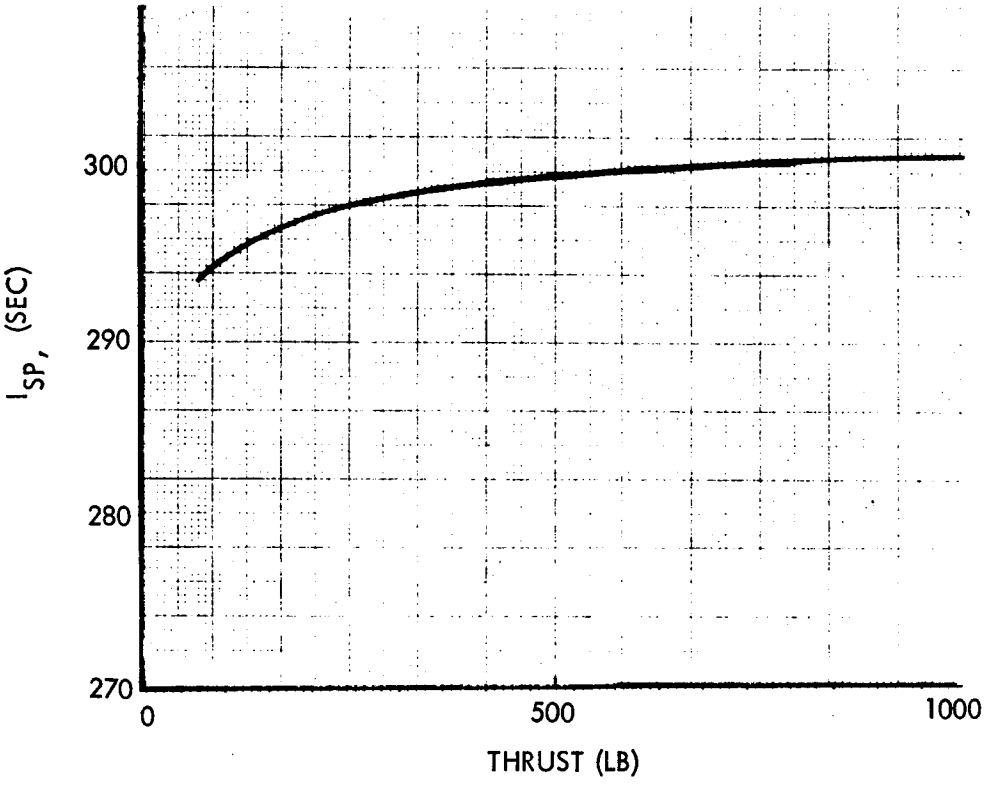

Figure 3-15. - Typical Specific Impulse Variation With Engine Size

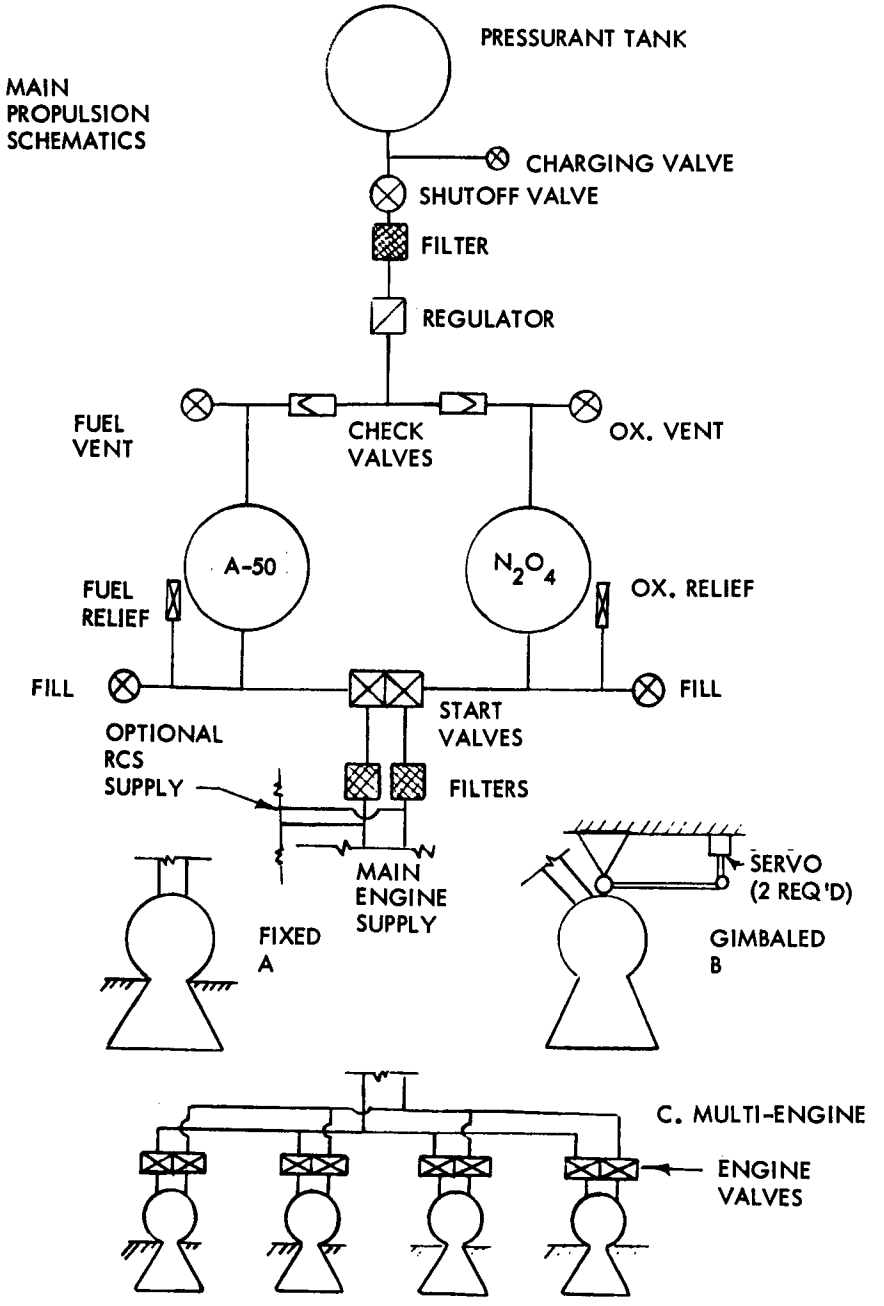

Figure 3-16. - Main Propulsion Schematics

rates has shown the series design enhances reliability. The tanks could include capillary barrier internals (screen sump) to permit tap-off of RCS supply in zero-g for those concepts which might use bipropellant RCS. The number of propellant tanks is a variable primarily dictated by stowage configuration dimensions. A four-tank arrangement is most compact and a parallel feed manifold (as in the LM descent stage) was selected for each pair (oxidizer and fuel). Series feed designs as used in the SPS would entail excessive lateral center of gravity excursion and introduce operational difficulties and delays in servicing.

RCS system concepts. - For those concepts utilizing the main engine TVC for pitch/yaw control and the RCS for roll, a cold nitrogen gas system such as shown in figure 3-17 could be utilized. Helium could be used by tapping off the main tank pressurization system. However, a 30-percent weight penalty would result. The only advantage would be use of a common regulator which also has disadvantages related to reliability. Multiple helium vessels were chosen as being more suitable for the configuration and an additional nitrogen vessel entails no weight disadvantages. The weight of a multiple vessel helium/nitrogen system is the same as for a single vessel of the same capacity except for minor installation secondary structure and connecting lines.

Another RCS concept which could be utilized, particularly in an active LESS rendezvous is the bipropellant RCS. This concept becomes attractive only when a considerable amount of maneuvering and/or propellant settling has to be done with the RCS engines.

A typical bipropellant RCS system is shown in figure 3-18. An independent feed system is shown. However, an alternate concept utilizing main tank tap-off is shown in figure 3-16. For roll control only, four engines are required. For three-axis control, 12 engines were used for both bipropellant and cold gas systems. Fewer engines could be used, but they generally result in undesirable couples from a stability and control standpoint.

Propulsion system concepts comparison. - Candidate single engine concepts studied are defined in table 3-2 as concepts 1, 2, 3, 6, 7 and 8. Concepts 6, 7, and 8 are the same as 1,2, and 3 except for the additional requirement for rendezvous and docking. Numbers 1 and 3 both utilize gimbaled engine TVC for pitch and yaw with cold gas and bipropellant RCS systems as variations to be compared. Number 2 uses a fixed engine with bipropellant RCS over-ride of any main engine thrust misalignment. The basis and results of estimates used for sizing the RCS systems are shown in table 3-3.

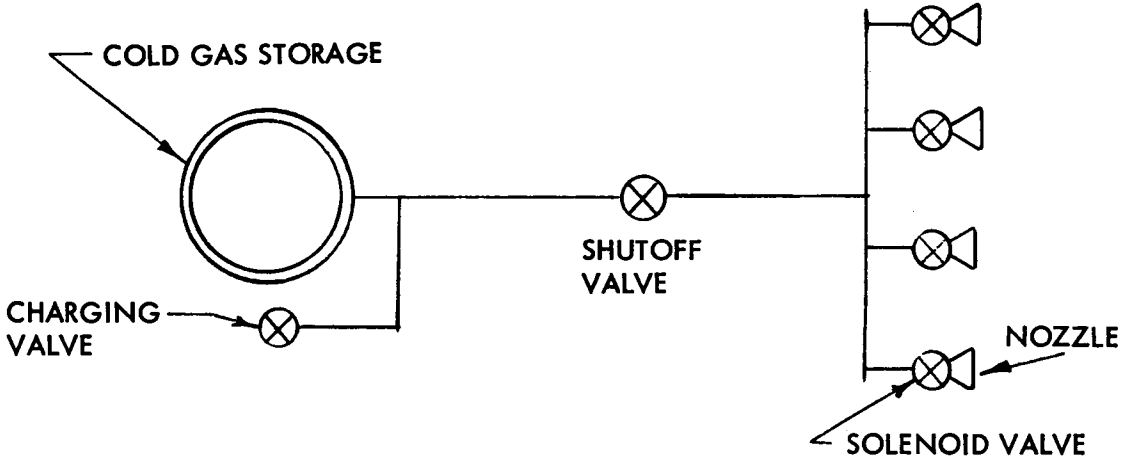

Figure 3-17. - Cold Gas Reaction Control System Schematic

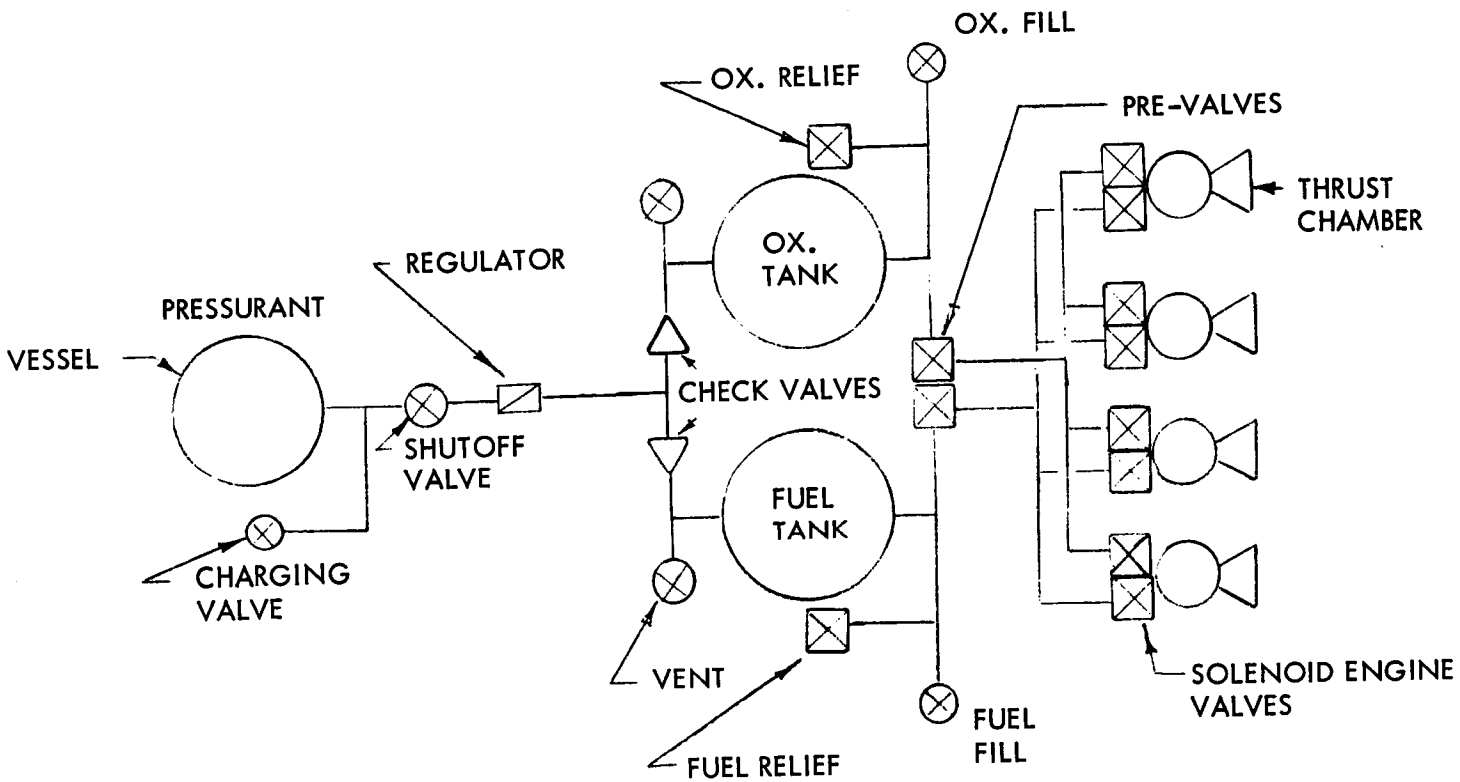

Figure 3-18. - Bipropellant Reaction Control Schematic (Independent Feed System)

TABLE 3-2. - CANDIDATE CONCEPT DEFINITION

Concept Identification	1	2	3	4	5	6	7	8	9	10
Fixed Thrust	1-1	2-1	3-1			6-1	7-1	8-1		
Dual Thrust	1-2	2-2	3-2	4-2	5-2	6-2	7-2	8-2	9-2	10-2
Rendezvous										
CSM	X	X	X	X	X					
Main Engines						X	X	X	X	X
Docking										
CSM	X	X	X	X	X					
RCS						X	X	X	X	X
Main Engines										
Number	1	1	1	4	8	1	1	1	4	8
Thruster				325	100				325	100
Roll Control										
Cold Gas RCS	X				X	X				
Bipropellant RCS		X	X				X	X		
Pulsed Main Engines				X	X				X	X
Pitch-Yaw Control										
Gimbal TVC	X		X			X		X		
RCS Override		X			X		X			
Pulsed Main Engine				X	X				X	X
Coast RCS										
Cold Gas	X			X	X	X			X	X
Bipropellant		X	X	X		X	X			X

TABLE 3-3. - RCS CHARACTERISTICS

Characteristics	Concept No. 1	2	3	4	5	6	7	8	9	10
Total Impulse (lb-sec)										
Pitch and Yaw Control	-	24 800.00	-	-	-	-	26 190.00	-	-	-
Roll Control	41.00	41.00	41.00	41.00	41.00	41.00	43.00	43.00	41.00	41.00
Acquisition	21.00	21.00	21.00	21.00	21.00	21.00	21.00	21.00	21.00	21.00
Rotation	335.00	2 120.00	261.00	335.00	335.00	335.00	2 120.00	261.00	335.00	335.00
Attitude Hold	1.00	2.00	1.00	1.00	-	1.00	-	1.00	1.00	1.00
Delta V (ft/sec)	-	-	-	-	-	3700.00	5 400.00	5400.00	-	-
Total	398.00	26 984.00	324.00	398.00	398.00	4098.00	33 774.00	5726.00	398.00	398.00
Engine Thrust (lb)	1.25	50.00	0.75	1.25	1.25	1.25	50.00	0.75	1.25	1.25
Pulse Rate										
Roll	5.3	0.25	5.3	5.3	5.3	5.3	0.25	5.3	5.3	5.3
Pitch and Yaw	-	7.0	-	25.4	87.5	-	7.0	-	25.4	87.5
Weight Propellants (lb)	6.0	93.0	1.5	6.0	6.0	61.00	116.0	21.00	21.0	6.00
Weight System (lb)	20.0	140.0	12.00	20.0	20.0	130.00	170.00	38.00	20.0	20.00

NOTES:

RCS Requirements and Assumptions

1. Center of gravity excursion due to propellant imbalance:
   Lateral 1 to 2.5 in.
   Fore and aft 1 to 7.75 in.
2. Vehicle Inertia - 500 slug-ft^2, all axes
   Moment Arm - 2.5 ft
3. Mission Profile:
   5 to 10 minutes for boost
   30 minutes for tracking and prerendezvous
   60 to 90 minutes for rendezvous intercept
4. Disturbances
   Roll - 0.2 ft-lb
   Pitch and Yaw - 0.5 degree thrust misalignment
5. Attitude Profile
   Acquisition rate - 2 deg/sec
   Rotation Maneuver - one at 180 degrees, each axis
6. System Impulse/Weight Ratio -
   Cold gas 30 seconds

The types of main propulsion considered are fixed thrust, two-level, and throttlable. The fixed thrust propulsion system (fig. 3-19) requires only a start valve for control. Throttlable engine systems using external control (fig. 3-20) require a start valve and a flow control valve. If a variable area injector such as shown in figure 3-21 is used for throttling, the flow control valve is optional. For externally controlled dual thrust systems (fig. 3-22), there are two possible control arrangements. One method is the use of two independently controlled sets of propellant manifold; the other consists of one master start valve with another set of valves downstream controlling the additional propellant manifold.

Dual thrust level can also be produced by a variable area injector of the type used successfully in the LM descent stage. Figures 3-21 and 3-23 show such an injector, which uses a single moving sleeve simultaneously controlling the fuel and oxidizer entering the combustion chamber. With a two-position control, the injector could operate in a dual thrust mode. The LM-type injector offers good cooling and injection velocity at both thrust levels, and fast response time. This type of injector has been used successfully for thrusts from 500 to 10 500 pounds, so should present no scaling difficulties. Development time may be slightly longer than for other dual-thrust systems.

The advantage of a fixed thrust system is its relative simplicity. Combustion and cooling processes can be optimized more easily for a single thrust level rather than a range of levels. These properties make the single thrust level system the most reliable; development time is relatively short (~ 24 months). The major disadvantages of the single thrust propulsion system are the added ΔV requirement and the increased burnout acceleration which affects manual control characteristics (handling qualities).

Throttleable engines offer the greatest flexibility in thrust program and consequently the lowest ΔV requirement. Combustion chamber cooling is good if a fuel bleed independent of the throttle is supplied to the chamber wall. More controls are needed than with a fixed thrust engine. Precise machining is required for injector stability. With external control, there is a longer response time than for injector control due to the longer distance from control to combustion. External control causes varying injector velocities which limit the range of stable combustion to about 5:1. For variable area injectors, a range of 15:1 is obtainable.

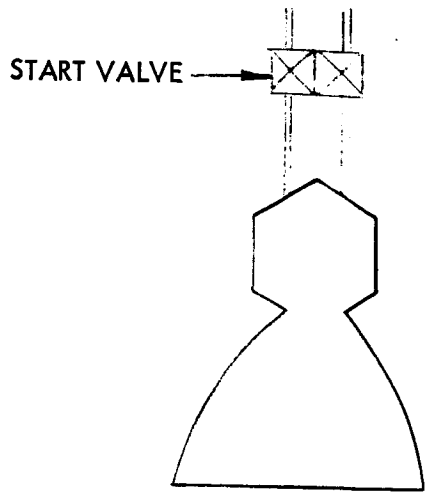

Figure 3-19 - Fixed Thrust
Engine Schematic

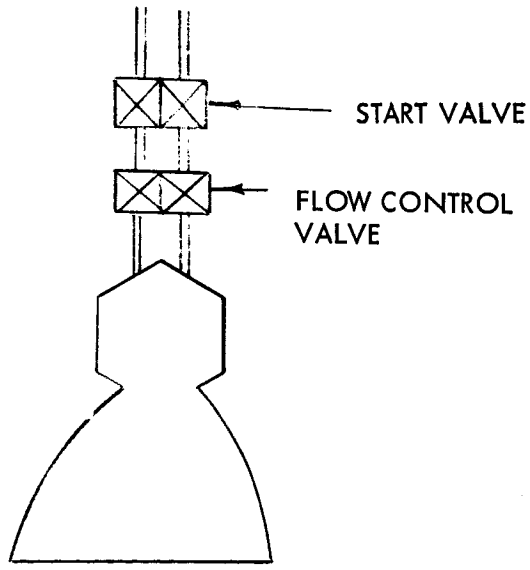

Figure 3-20. - Externally-Throttled
Engine Schematic

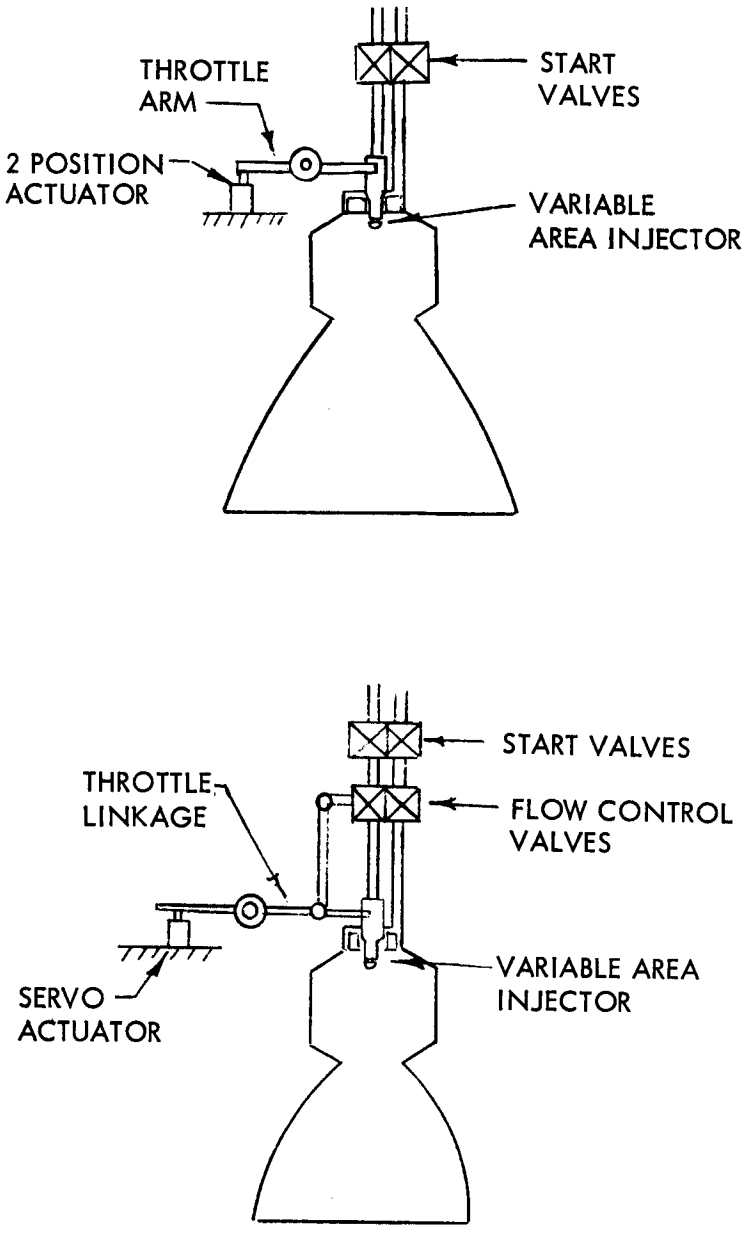

Figure 3-21. - Variable Area Injector Engine Schematic

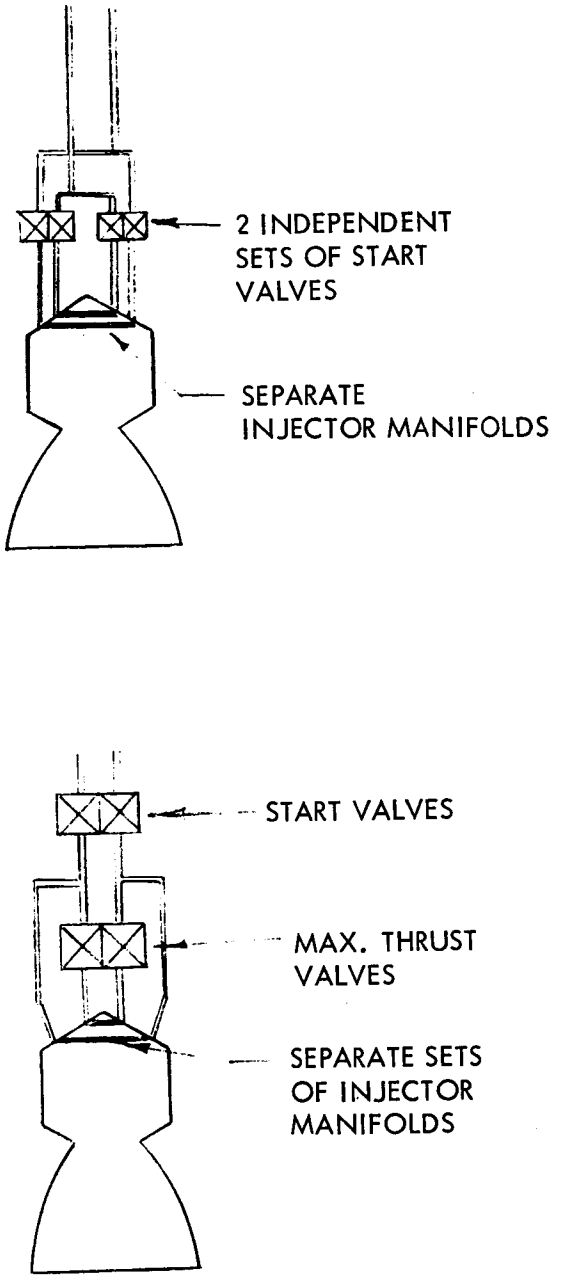

Figure 3-22. - External Valve, Dual Thrust Engine Control Schematic

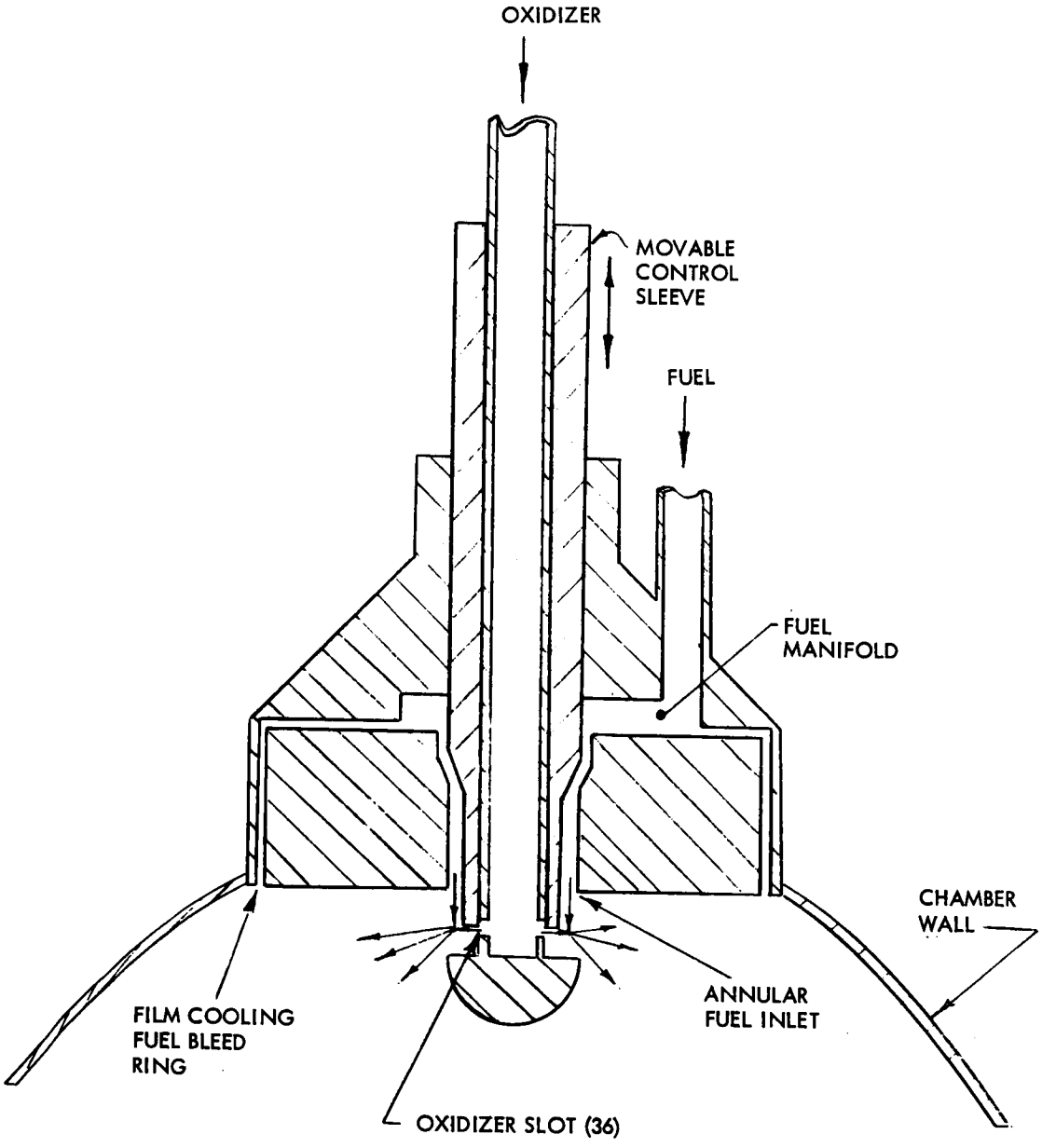

Figure 3-23. Variable Area Injector Schematic

The two-thrust mode propulsion system is the type favored from a trajectory and handling qualities viewpoint without excessive complexity. Control is accomplished by using only two throttle positions. For external control this is simply an on-off control of one set of valves. With independent valves, there is more precise control as one set of valves is not upstream of another, and both sets of valves can be located closer to the engine. Pressure drop is reduced since flow is through only one set of valves. The primary advantage of this system is relatively simple thrust control, using well-proven components. The major disadvantages are flexibility problems caused by extra plumbing and poor cooling at the lower thrust level.

In summary, trajectory-mission requirement analysis favors the dual thrust mode propulsion system. The TRW-variable area injector probably could be used for this system with success. It has been proven reliable and safe on the lunar module, and involves a simple control and plumbing system. If development time for application to the LESS should prove longer than desired, the two sets of independent propellant start valves would be most in keeping with mission requirements and very short development time.

Multiple engine concepts. - The multiple engine concepts use either 4 or 8 engines with 1 or 2 engines outboard in each quadrant. The engines are canted in roll pairs 2 to 3 degrees. The pulsing capability of the engines permits them to be pulled off for short intermittent periods to obtain pitch, yaw, and roll control. For main thrust reduction, they may all be pulsed off at a rate/duration corresponding to the throttle ratio desired. The arrangement introduces vibration disturbances but a preliminary investigation (see reference 2-11) indicates the difficulties are not insurmountable.

The reliability of the system must be considered by noting that the failure of one engine requires the shutdown of the opposite one to maintain control moments. For concept 4-2, table 3-2, there would be no control in the plane of the failed engine and no failures are permitted. With a single engine realiability estimated at 0.998 after a 2-year development period, the 4-engine arrangement has a crew safety of only 0.984. The 8-engine arrangement (concept 5-2, table 3-2) permits one failure without loss of control; however, the shutdown of the opposite engine leaves only 600 pounds thrust. As long as the vehicle gross weight does not exceed 2400 pounds (using a F_o/W_o minimum = 0.25) then one failure is allowable during the lift-off phase.

No other failures in the same plane can be permitted during the entire ascent and the allowance for other failures depends on the point in the trajectory and the minimum allowable thrust. Assuming "other plane" failures are permitted, crew safety of the combination is 0.9999 and is superior to the single and four engine designs.

Table 3-4 shows the results of calculations to determine the usable propellant required to achieve a 60 nm orbit based on the various ΔV values necessary. The engine specific impulse depending on concept, vehicle weights, propulsion system weight and engine thrust level. The cases shown correspond to the propulsion concepts shown in table 3-2. The ΔV values shown in table 3-4 are those associated with a bent two-step profile at a t/w = 0.3 as shown by figure 3-11 (7400 ft/sec) and a simple two-step profile (8200 ft/sec). Table 3-5 presents similar data based on the dual thrust ΔV requirements shown in figure 3-12 and a bent two-step launch trajectory. Table 3-6 shows calculation of propulsion system component sizes and weights for selected cases based on the propellant requirements determined from table 3-5 data. Table 3-7 shows an evaluation of selected propulsion system concepts. Results show that based on this evaluation, Concept 1-2 rates best with 5-2 a close second. A tabulation of these concepts or cases (from table 3-2) is as follows:

	Case 1-2	Case 5-2
Thrust	two level	two level
Rendezvous and docking	CSM active	CSM active
Number of engines	1	8
Thrust level	approximately 700 pounds	100 pounds each
Roll Control	cold gas RCS (N_2)	Pulsed main engines or cold gas RCS
Pitch-yaw control	Gimbal TVC	Pulsed main engine
Post boost attitude control	cold gas RCS (N_2)	Cold gas RCS (N_2)

TABLE 3-4. - USABLE PROPELLANT REQUIREMENT CALCULATION
SINGLE THRUST LEVEL
(Propulsion Payload 940 lb)

Case	Delta V	I_{SP}	LM Load	Gross	Burned	Thrust	Usable
1-1	7400.0	297.0	150.9	2428.0	171.1	728.4	1310.9
2-1	7400.0	297.0	180.4	2706.1	211.5	811.8	1554.5
3-1	7400.0	297.0	141.9	2411.3	168.0	723.4	1303.4
4-1	7400.0	290.0	192.1	2667.1	216.2	800.1	1504.9
5-1	7400.0	273.0	182.6	2719.1	207.9	815.7	1565.2
6-1	8000.0	297.0	290.5	2914.7	262.5	874.4	1651.2
7-1	8200.0	297.0	192.5	3020.1	229.6	906.0	1850.5
8-1	8200.0	297.0	153.1	2693.7	184.4	808.1	1569.3
9-1	8200.0	290.0	205.0	2944.2	233.3	883.3	1763.9
10-1	8200.0	273.0	196.1	3014.1	225.9	904.2	1841.1

TABLE 3-5. - USABLE PROPELLANT REQUIREMENT
DETERMINATION DUAL THRUST LEVEL
(Propulsion Payload 940 lb)

Case	Delta V	I_{SP}	LM Load	Gross	Burned	Thrust	Usable
1-2	6672.0	297.0	151.4	2273.2	168.6	681.0	1158.6
2-2	6672.0	297.0	187.6	2507.9	214.6	751.1	1353.3
3-2	6672.0	297.0	142.2	2257.2	165.2	676.4	1152.0
4-2	6554.0	290.0	180.2	2369.8	198.7	1300.0	1225.1
5-2	6637.0	273.0	171.6	2442.0	191.7	800.0	1304.3
6-2	7272.0	297.0	298.8	2769.4	267.8	829.9	1500.6
7-2	7472.0	297.0	203.9	2812.5	236.6	842.5	1635.9
8-2	7472.0	297.0	157.5	2537.0	185.7	759.9	1411.3
9-2	7350.0	290.0	192.3	2617.1	214.4	1300.0	1455.7
10-2	7482.0	273.0	185.2	2731.7	209.7	800.0	1574.9

TABLE 3-6. PROPULSION SYSTEM COMPONENT WEIGHTS AND SIZES
(Propulsion Payload 940 lb)

Case 1-1						
Volume	Diameter	Wall	Dry Weight	No. Tanks		
Oxidizer System						
4.907	25.3	0.025	14.0	2		
Fuel System						
5.010	25.5	0.025	14.1	2		
Helium System						
0.459	11.5	0.115	10.6	3		
Nitrogen System						
0.408	11.0	0.110	9.7	1		
Main Engine System			35.0			
RCS Engine System			9.0			
Delta V	I_{SP}	LM Load	Gross	Burned	Thrust	Usable
7400	297	150.5	2419.1	170.6	725.7	1302.5

TABLE 3-6. - PROPULSION SYSTEM COMPONENT WEIGHTS AND SIZES - Continued

Case 2-1						
Volume	Diameter	Wall	Dry Weight	No. Tanks		
Oxidizer System						
5.814	26.8	0.025	15.1	2		
Fuel System						
5.936	27.0	0.025	15.3	2		
Helium System						
0.407	11.0	0.110	9.7	4		
Main Engine System			30.0			
RCS Engine System			47.0			
Delta V	I_{SP}	LM Load	Gross	Burned	Thrust	Usable
7400	297	180.0	2694.2	210.8	808.2	1543.3

TABLE 3-6. - PROPULSION SYSTEM COMPONENT WEIGHTS AND SIZES - Continued

Case 3-1						
Volume	Diameter	Wall	Dry Weight	No. Tanks		
Oxidizer System						
4.879	25.2	0.025	13.9	2		
Fuel System						
4.981	25.4	0.025	14.1	2		
Helium System						
0.342	10.4	0.104	8.4	4		
Main Engine System			35.0			
RCS Engine System			14.0			
Delta V	I_{SP}	LM Load	Gross	Burned	Thrust	Usable
7400	297	141.5	2402.6	167.5	720.8	1295.1

TABLE 3-6. - PROPULSION SYSTEM COMPONENT WEIGHTS AND SIZES - Continued

Case 4-1						
Volume	Diameter	Wall	Dry Weight	No. Tanks		
Oxidizer System						
5.629	26.5	0.025	14.9	2		
Fuel System						
5.747	26.7	0.025	15.1	2		
Helium System						
0.526	12.0	0.120	11.9	3		
Nitrogen System						
0.408	11.0	0.110	9.7	1		
Main Engine System			68.0			
RCS Engine System			9.0			
Delta V	I_{SP}	LM Load	Gross	Burned	Thrust	Usable
7400	290	191.6	2655.7	215.5	796.7	1494.2

TABLE 3-6. - PROPULSION SYSTEM COMPONENT WEIGHTS AND SIZES - Continued

Case 5-1						
Volume	Diameter	Wall	Dry Weight	No. Tanks		
Oxidizer System						
5.851	26.8	0.025	15.2	2		
Fuel System						
5.974	27.0	0.025	15.3	2		
Helium System						
0.547	12.2	0.122	12.3	3		
Nitrogen System						
0.408	11.0	0.110	9.7	1		
Main Engine System			56.0			
RCS Engine System			9.0			
Delta V	I_{SP}	LM Load	Gross	Burned	Thrust	Usable
7400	273	182.1	2706.5	207.1	811.9	1553.3

TABLE 3-7. CONCEPT EVALUATION

Case	1-1	1-2	2-1	2-2	3-1	3-2	4-1	4-2	5-1	5-2
Utility										
LM Load	151	152	180	188	142	142	192	180	183	172
Flexibility	Low	Mod	Low	Mod	Low	Mod	High	High	High	High
*Crew Safety	.998	.998	.998	.998	.998	.998	.984	.984	.9999	.9999
Resource Requirements										
Development Time (months)	24	28	24	28	24	28	18	18	12	12
Cost 10^6	12	15	12	15	12	15	3	3	1	1
Concept										
Rating Rank	4	1	5	5	5	3	6	6	5	2

*Main engine system only

Depending on other factors such as development time available, packaging for LM stowage, alternate usage design, and available funding, either of these concepts could be selected. Figures 3-1 and 3-7 show configurational layouts incorporating these propulsion concepts.

Figure 3-24 shows the thrust to weight ratio which yields minimum weight. From this curve, it can be seen that the minimum gross weight optimizes at about 0.36 thrust to weight while the optimum for minimum propellant optimizes at about 0.4 thrust to weight.

Environmental control subsystem. - For maximum simplicity, the use of an active environmental control system for the LESS vehicle is undesirable. However, certain subsystem components have temperature limitations which would be exceeded during exposure of the vehicle to the lunar environment while awaiting possible usage. Two such components are the battery and the attitude display gyro package. One alternative is to store these components within the LM temperature controlled environment until needed. However, this increases the astronaut assembly requirements, lengthens the preparation time required, which may be critical, and increases the possibility of failure due to a bad connection. The other alternative is to provide a simple, passive or semi-passive means of temperature control, or combinations of both approaches.

Temperature control of vehicle on lunar surface: Two figures are constructed to illustrate the problems involved in passive temperature control of the vehicle on the moon's surface.

Figure 3-25 assumes a 460-pound aluminum vehicle covered with a one-inch thick superinsulation blanket. It is assumed that the outside surface coating on the blanket is such that the average outside surface temperature is equal to that of the surface of the Moon and the inside surface temperature is equal to the average temperature of the vehicle. It is assumed that, based on these blanket surface temperatures, all of the heat transmitted through the blanket is absorbed by the mass of the vehicle resulting in an average vehicle temperature. This average temperature was computed for each 15 degrees of solar inclination assuming a starting vehicle temperature of 70 F at sunrise.

Figure 3-26 is based on the same approach, except that the surface of the moon is held constant at -250 F during the lunar night. The vehicle is assumed to start at 70 F at sunset. A constant coefficient of heat conduction is assumed for the blanket.

The above approach is based on a rather simplified heat balance, but it does permit bracketing of the cooling and heating requirements.

In the case of cooling of the vehicle during the hot lunar day, the extra heat gain above a certain temperature could be picked up by the change of state

CONCEPT 1-2
DUAL THRUST SINGLE ENGINE
I_{SP_1} = 297 SEC
I_{SP_2} = 275 SEC
PROPULSION PAYLOAD = 940 LB
60-NM ORBIT

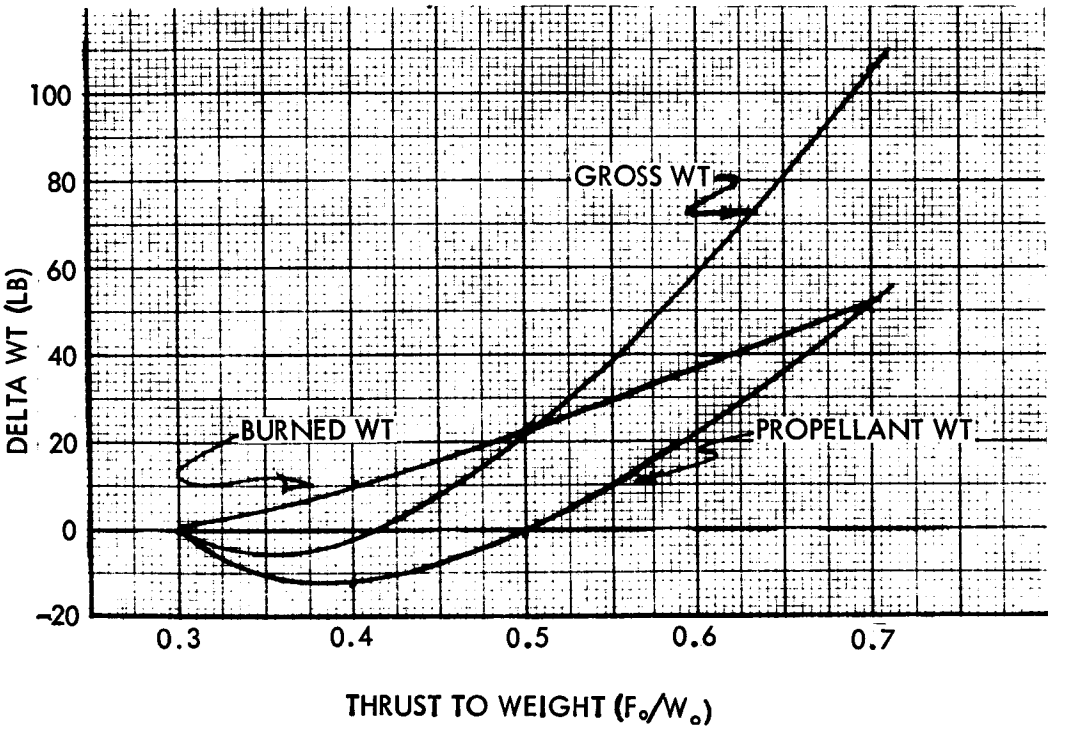

Figure 3-24. - Propulsion System Weight Optimization

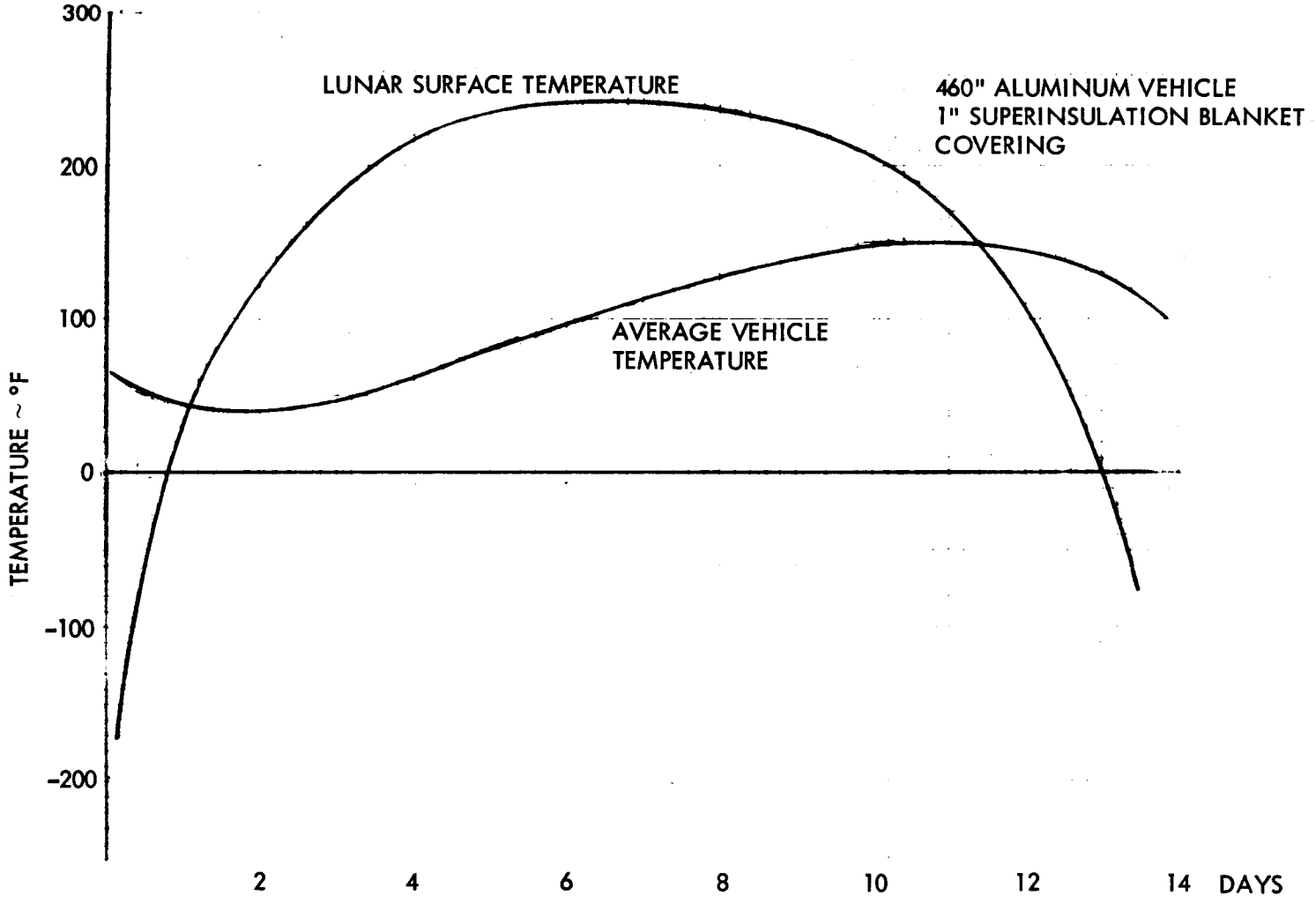

Figure 3-25. - Dormant Vehicle Temperature (Lunar Daytime Cycle)

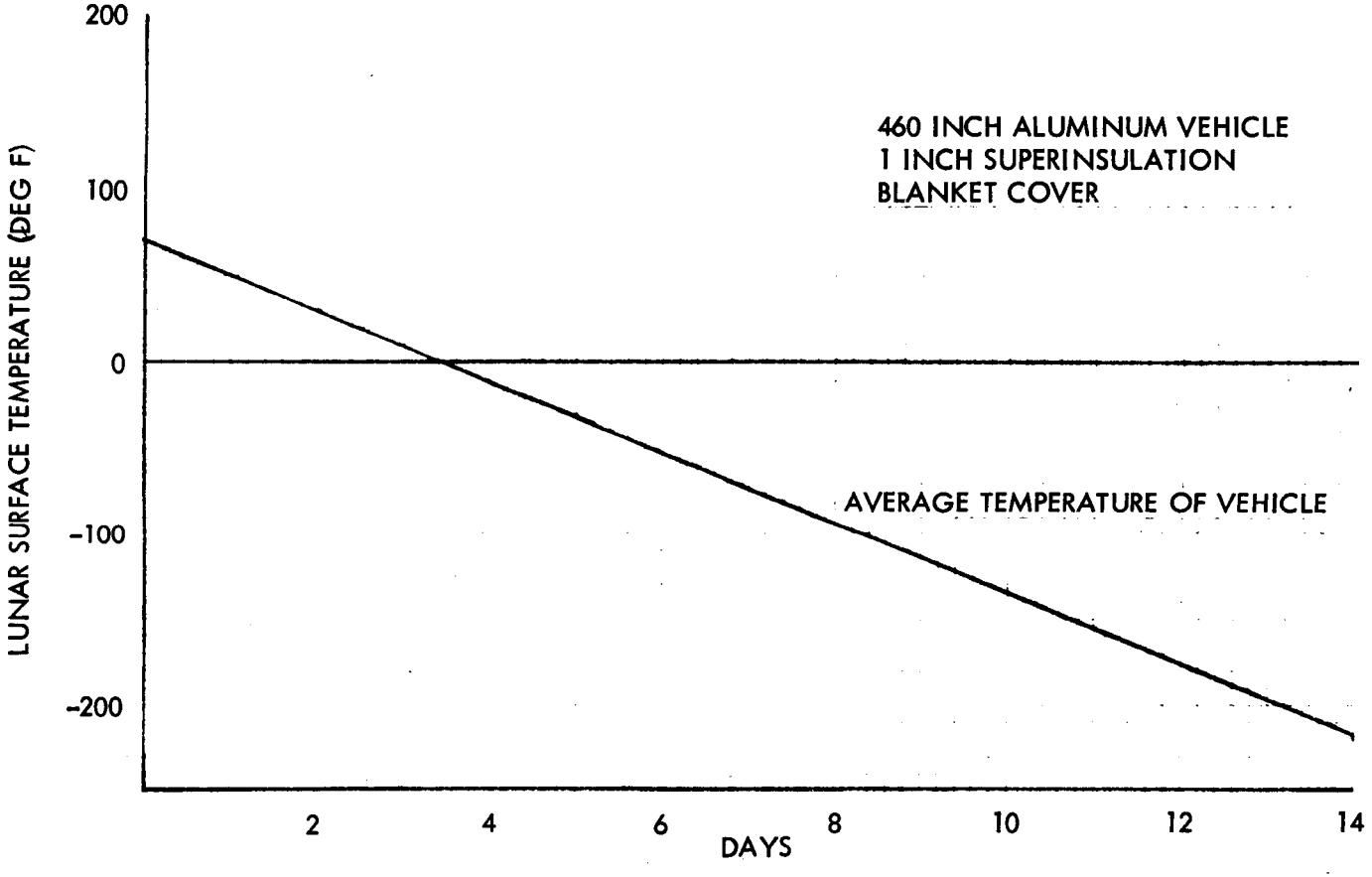

Figure 3-26. - Dormant Vehicle Temperature (Lunar Night Cycle)

of a body of fluid. For instance, if water were sublimed, it would take about 4 pounds of water (table 3-8) to keep the vehicle below 100 F under the superinsulation blanket. Another example is phosphorium chloride (PH_4Cl), in table 3-9, which has a melting point of 82 F. Melting of about 17 pounds of this liquid will keep the maximum average vehicle temperature near 82 F and require no venting of gases.

If it is required to heat the vehicle during the lunar night, about 50 watts would maintain the vehicle at 70 F with a -250 F lunar surface temperature.

The results of this analysis indicate that a vehicle landing at lunar sunrise could be passively temperature-controlled with a properly optimized superinsulation blanket plus a small change of state type heat sink. For missions involving stowage during the lunar night, however, some sort of heating would be required.

Electronic equipment cooling. - During the escape mission, the need for electronic equipment cooling is illustrated in figure 3-27. This figure was constructed by assuming that no cooling is accomplished and all power dissipated goes into heating the mass of the electronics packages. The initial package temperature was assumed to be 75 F and resulting temperature versus time was plotted. The maximum equipment temperature of 120 F and the activity timelines for the mission are also plotted in the figure.

As can be seen by examining figure 3-27, only the displays and controls packages could run for the mission time without overheating. The VHF transponder and the gyro package exceed the 120 F maximum temperature early in the mission.

Several approaches can be applied to maintain the proper temperature.

By the use of effective heat transfer conduction to the primary structure, a certain amount of cooling could be accomplished. The low operating temperature of system components restrict the amount of heat that can be radiated to space. The approximate total continuous power load of 100 to 150 watts into the 350-pound structure for four hours would raise the structure temperature from 75 F to approximately 95 F assuming a balance of external heat input and losses. Proper surface coatings to cause heat loss to surface could result in an acceptable passive system.

A combination system might prove to be the optimum design. This combination system might be to use the primary structure of possibly part of the fuel as a heat sink during non-flight operation and then use the PLSS heat transport loop to cool a coldplate network in series with the wet-suit during

TABLE 3-8. - POTENTIAL MATERIALS HAVING LOW MELTING TEMPERATURES

Material	Melt Temperature (Deg F)	λ (Btu/lb)	ρ Solid (lb/ft^3)	ρ Liquid (lb/ft^3)	ρλ (Btu/ft^3)	Boiling Temperature (Deg F)
Glycol Ethylene, $C_2H_6O_2$	+11 F	78		70	5 400(ℓ)	387
n-Dodecane, $C_{12}H_{26}$	15	92		46.9	4 310(ℓ)	418
Aniline, $C_6H_5NH_2$	21	48		65	3 120(ℓ)	364
Butyric Acid (n-), $C_4H_8O_2$	22	54		60	3 250(ℓ)	328
Cyanogen Chloride, CNCl	23	65		76	4 950(ℓ)	54
Hydrogen Perioxide, H_2O_2	28	122		90	11 000(ℓ)	304
Water, H_2O	32	143		63	8 900(ℓ)	212
Benzene, C_6H_6	42	54		55	3 000(ℓ)	176
Formic Acid, CH_2O_2	47	105		76	8 000(ℓ)	212
Acrylic Acid, $C_3H_4O_2$	54	66		66	4 380(ℓ)	286
Dioxane, $C_4H_8O_2$	52	62		65	4 050(ℓ)	214

flight conditions. The coldplate network would be connected downstream of the wet-suit outlet and upstream of the pump assembly. The estimated electronic load of 166.9 watts would equal 166.9 times 3.41, or 569 Btu per hour. Since the capacity of the sublimator is about 2180 Btu per hour as previously calculated, 2180 minus 569 equals 1611 Btu per hour, which leaves ample capacity for metabolic needs. There might be some question of whether or not the present pump will accommodate the extra pressure drop of the coldplate network in series with the wet suit. The present PLSS could be modified to provide two additional quick disconnects that could be connected when the crewman mounts the vehicle and prepares for flight.

Another alternative method of cooling the electronic equipment is to use the liquid transport and feed water loops of the PLSS to cool a coldplate network. The sublimator design point heat load for the transport water circuit is to cool the transport water to 45 F maximum with inlet conditions of 4.0 pounds per minute minimum and a temperature of 54.1 minimum.

TABLE 3-9. - POTENTIAL MATERIALS HAVING MEDIUM MELTING TEMPERATURES

Material	Melting Temperature (Deg F)	λ (Btu/lb)	ρ Solid (lb/ft^3)	ρ Liquid (lb/ft^3)	ρλ (Btu/ft^3)	Boil Temperature (Deg F)
Transit Heet 60	60	100	98	98	9 300	
p-Xylene, $C_6H_4(CH_3)2$	61	71		53.7	3 820(ℓ)	281
Acetic Acid, CH_3COOH	62	78		65.4	5 100(ℓ)	244
n-Hexadecane, $C_{16}H_{34}$	64	101	48.3		4 880(ℓ)	549
Glycerol, $C_3H_5(OH)_3$	64	86		78.6	6 750(ℓ)	553
Polyethylene Glycol (Carbowax 600)	68-77	63				
n-Heptadecane, $C_{17}H_{36}$	72	72	48		3 450(ℓ)	577
Sodium Chromate, $Na_2CrO_4 \cdot 1OH_2O$	73	71	93		6 600(ℓ)	
Phosphonium Chloride, PH_4Cl	82	324				
n-Octadecane	82	105		48	5 050(ℓ)	602
Calcium Chloride, $CaCl_2 \cdot 6H_2O$	84	73	105		7 650(ℓ)	
Transit Heet 86	86	130				
Nitrogen Pentoxide	86	138	102		14 000(ℓ)	116.6
Sodium Sulphate, $NA_2SO_4 \cdot 1OH_2O$	88	92		92		
n-Nanodecane, $C_{19}H_{40}$	90	81		48	3 885(ℓ)	626
Technical Eicosane, $C_{20}H_{42}$	92-98	66-78	48		3 200/ 3 780(ℓ)	401
Dibasic Sodium Phosphate, $NA_2HPO_4 \cdot 12H_2O$	96	120		95	11 400(ℓ)	
1-Tetradecanol, $CH_3(CH_2)_{12} \cdot CH_2O_4$	100	99	52	51	5 199(ℓ)	507
Octacosane, $C_{28}H_{58}$	142	109				

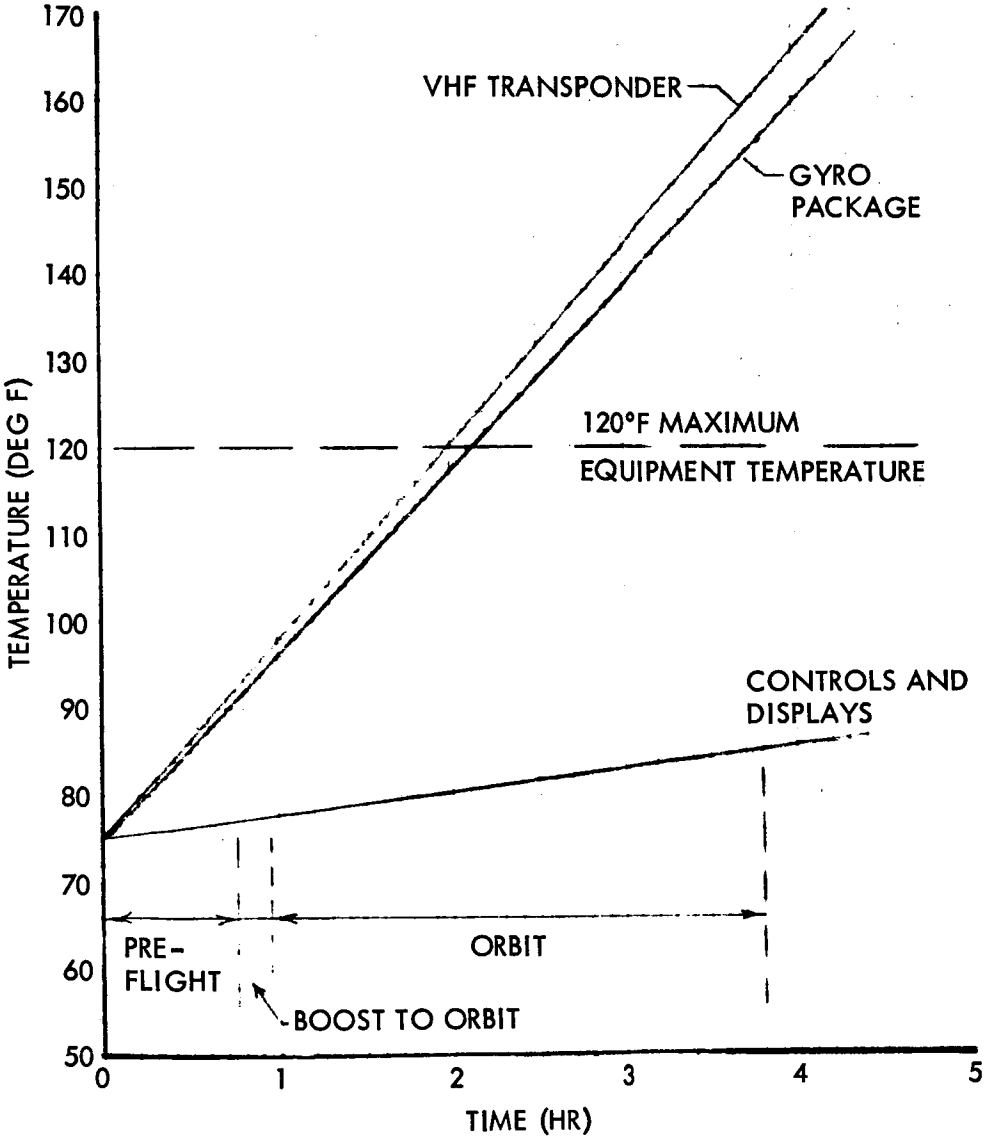

Figure 3-27. - Electronic Equipment Temperatures

$$H = W_{cp} \Delta T$$

$$H = (4.0 \text{ lbs/min})(60 \text{ min/hr})(1 \text{ Btu/lbs-F})(54.1 \text{ F} - 45 \text{ F})$$

$$H = 2180 \text{ Btu/hr}$$

$$\frac{2180}{3.41} = 640 \text{ watts}$$

With a probable load of 160 watts, the sublimator should be of ample capacity. A four-hour load of 160 watts will require about 2.5 pounds of water. A coldplate network could probably be designed to simulate the pressure drop of the wet suit which would not require the development of a new pump. The primary undesirable feature of this concept is in the interconnection of equipment cooling with the astronaut life support system. Some degradation of backpack reliability and safety is bound to result from the possibility of fluid leakage or other malfunction of the equipment circuit. Some risk to astronaut safety is involved in pushing the limits of the backpack capability including the time required to rendezvous and enter the CM. Life support by the PLSS/ oxygen purge system (OPS) provides a maximum of 7200 Btu of heat removal and an equivalent quantity of oxygen. The 4-hour capability of the PLSS is based on a metabolic rate of 1200 Btu per hour. Work rates in excess of either of these figures for any length of time will result in less than a 5.5 hour operational life for the PLSS/OPS system. About 45 minutes of activity could be required using the PLSS prior to escape. Therefore, time to accomplish transfer from the LESS to the CM after rendezvous and docking may be critically time-dependent or require that an umbilical from the CM be connected to the PGA before transfer. Present design of the PGA inlet and exhaust gas connectors presents the potential of loss of the pressure within the suit if connection is inadvertently misaligned since the PGA connector check valve is depressed prior to the umbilical connector making a seal with the connector "O" rings. It is also very difficult to hook up a gas connector which is flowing gas with the PGA connector and shut off valves are not presently found in the distal end of the CM gas umbilical hoses.

Both the PGA gas connectors and umbilical PGA connectors may be modified with the addition of an appropriately positioned rotary on-off valve to permit interconnection to be completed before flowing gas through the umbilical connector or potentially causing loss of PGA integrity due to inlet and exhaust connector manipulation.

Any movement of the crewman during transfer will perturbate the LESS unless a rigid docking relationship exists between the LESS and the CSM. The most likely docking method, and that implied by the docking drogue shown on configuration drawings, is that of hard docking the LESS to the CM at the LM docking probe. The normal LM drogue would not be used because of excessive weight and forces required, but instead a light-weight drogue with spring-loaded arms which would latch onto the CM probe at impact thus holding the LESS while crew members transferred from LESS to the CM hatch. Prior to release of restraints on the LESS, safety lines anchored to the CM will be attached to the crew members. Handholds will be provided on the CM to aid in crew transfer and CM hatch entry in minimum time.

It is noted that the ability to connect the astronaut suit to an extended umbilical, without first requiring an entry into the LM or CSM pressurized cabin, would be a useful improvement in advanced missions and even for basic LM missions. This would save crew time and would not require an extra cabin pressurization followed later (after umbilical hookup) by depressurization to eject backpacks.

Communications subsystem. - As a study ground rule, the backpack communication system will be utilized during the escape mission. An S-band earth communications system or long-range VHF link to the CSM would be necessary to avoid loss of communication during most of the escape trajectory. For the rendezvous of the LESS and CSM, a VHF ranging transponder is considered necessary to obtain range and range rate data. The CSM already has the capability to receive and utilize this VHF data (rendezvous techniques are analyzed elsewhere in this report).

Electrical power subsystem. - The logical source of electrical power for this vehicle, where a small to moderate amount of power is required for a few hours, is a battery. Since, for this application, cyclic (charge-discharge) operation will not be required, a secondary battery will be adequate. Silver-zinc oxide batteries such as used in the Apollo CM entry and post-landing possess high energy-to-weight ratios of 30 to 50 watt hours/pound. Low temperatures, below 80 F, will reduce the capacity (reduction is 60 percent at 0 F). To ensure maximum capacity when utilization is required, storage in the dry charged state within the LM is desirable. The electrolyte could be injected by the astronauts when required by applying pressure at a specified point to break a seal and allow flow of electrolyte into the battery. The silver-zinc-oxide batteries are currently available in a variety of sizes and would present no development problems. Advanced type batteries show promise of doubling the power to weight ratio achievable with silver-zinc. Of these, the acid type lithium-copper-flouride battery has demonstrated energy density of over 100 watt hours/pound. However, for the LESS vehicle, the conventional batteries do not present a critical weight problem.

Table 3-10 shows the power users and approximate level and duration required. The summation of these for the various concepts were used with an assumption of a silver-zinc oxide battery with a 50-watt hour/pound capability to arrive at the estimated battery weights shown in table 3-11. Cabling and electrical equipment weights were estimated in a gross manner. Individual components, wire sizes, and lengths were not identified.

Reliability and safety considerations. - Three candidate lunar escape vehicle/systems configurations were examined with respect to differences in equipment options and concepts affecting mission accomplishments and safety. All three configurations have minimum equipment requirements in common; for example, cold gas RCS, hypergolic main propulsion system, simple pilot flight aids, basic system controls and minimum electrical power supply. The mission reliability of these equipment items for all three concepts is essentially equal. Design alternatives for some of this equipment including the electrical power supply are discussed with regard to effects on reliability and crew safety.

Equipment differences of the three concepts, and the associated reliability considerations and remarks are listed in table 3-12. Each configuration as indicated is assumed for discussion purposes to have two or more levels of increasing design sophistication including levels of pilot support or flight aids. An assumed acceptable minimum of pilot support equipment is listed for the configuration which is the minimum vehicle. Since it is the least complex, it is the most reliable from the stnndpoint of successful equipment operation. The most complex configuration is -8C, equipped with engine gimbal system and controls, automated flight stabilization, and the capability to integrate increasing levels of automated guidance and navigation support functions. The -9 configuration, basically a -7 type vehicle with a three-body, two rotational degree of freedom propulsion tankage support refinement, is limited to and remains dependent upon the kinesthetic flight skills of the pilot.

While more complex hardware and additional equipment provide increased opportunity for failures, some combination other than the most simple design may represent the acceptable minimum to accommodate pilot limitations within a given set of anticipated mission profiles. The additional equipment and design sophistication is expected to increase the prelaunch checkout work load with the advantage of reducing pilot demands during flight. The passenger can support the prelaunch preparation of the escape vehicle but his contributions to pilot flight workload reduction appear to be minimal (one-man operation was an objective).

The more complex -8 vehicle configurations have the capability to be operated in a degraded mode if the stabilization function fails. The -8 minimum design provides for manual thrust vector control supported by a 'fly to' pilot instrument display. For backup capability the 'fly to' instruments can

TABLE 3-10. - ELECTRICAL POWER REQUIREMENTS

Concept	Warmup		Operating		Total
	Watts	Hours	Watts	Hours	Watt Hours
Kinesthetic					
All axis attitude gyros	60	1	60	4	300
display	0	0	15	4	60
Beacon	0	0	15	4	60
VHF transponder	0	0	30	4	120
Engine valves	0	0	200	0.1	1
					541
Hardwire Control					
With Sight Guidance					
Same as kinesthetic except:					
Add sight illumination	300	0.2	300	0.5	+210
Add hand controller	0	0	5	4	+20
Eliminate attitude system	-60	1	-75	4	-360
					311
Hardwire Control					
With Attitude Display Guidance					
Same as kinesthetic except:					
Add hand controller	0	0	5	4	+20
					561
Stability Augmented					
Same as kinesthetic except:					
Add stability augmentation gyros	225	0.2	100	4	+445
Add gimbal actuators	0	0	80	4	+320
Add control logic	0	0	20	4	+ 80
					1386

TABLE 3-11. - ESTIMATED BATTERY WEIGHTS

Concept	Total Watt-Hours Required	Battery Weight (lb)
Kinesthetic	541	11
Hardwire with sight guidance	311	9
Hardwire with attitude display guidance	561	12
Stability augmented with attitude display guidance	1386	28

be designed to operate independently of any integrated error readouts or navigation function equipments that might be provided. With exception of the automated guidance and flight control equipped vehicle, the other concepts are subject to the effects of the pilots visual time response accommodation inadequacy with sudden, extreme changes in illumination expected during flight. The kinesthetically controlled vehicle is most sensitive to this condition since the pilot workload is very high and momentary distractions could lead to unrecoverable loss of control. The more sophisticated levels of automated flight control, while subject to greater opportunity of equipment failure, provide a better chance of lunar escape in the event of kinesthetic skill impairment of the pilot by exhaustion or trauma.

The cold gas reaction control system for yaw, orbital attitude control, and docking maneuvers will be operated by a hand controller which also may be used for the vectoring of the main propulsion engine in the -8 configuration by means of a function switch-over. (A separate left hand control may be utilized for RCS functions.) The mechanical advantage and nominal pilot inputs available through a hand control may be inadequate for direct drive "hardwire" coupling to the gimbaled engine. Augmentation can be provided by the autopilot type of electromechanical devices or a cold gas-powered servo system. The automated flight stabilization mode could possibly utilize hardwire as a backup operation. The minimal remaining mode of operation is kinesthetic control requiring the pilot to be in a standing position if all other modes appear inoperable during preflight checkout.

Preparation of the lunar escape vehicle and its checkout prior to flight represents a considerable amount of disciplined effort by both crew members for the least complex system. Confirmation of some equipment status may not require more than "go, no-go" type indicators where corrective action is not possible. Visual inspection and observation of control responses may be part of prelaunch checkout. Adjustments such as weight balance, flight system alignment, and clock setting should be held to a minimum by appropriate design approaches and mission planning.

Battery-supplied electrical power is considered essential to successful mission completion for all of the candidate vehicles. Principal failure modes are internal cell shorting and internal open circuits. Other modes of failure include loss of electrolyte and loss of activated battery charge from standing. Other considerations include extremes of temperature which have a significant effect on available power or result in battery failure. To enhance satisfactory operation of LESS electrical dependent equipment, the input voltage requirements should reflect a wider tolerance to voltage variations.

Since batteries are a high weight item, simple one-for-one redundancy for reliability is considered objectionable particularly in applications where they represent a higher fraction of vehicle weight in one mission type of

TABLE 3-12. - LUNAR ESCAPE SYSTEMS
RELIABILITY

Type	Configuration Assumptions	Reliability Considerations	Remarks
Kinesthetic -7A (Fig 3-2)	Minimum pilot aids: 3-axis gyro attitude indicator; clock/ event timer; 2-way radio communication with CSM.	Least complexity. Most reliable from mechanical simplicity standpoint	1. Assumes loss of gyro-supported pilot aids will not prevent successful rendezvous. 2. Piloting work load very high. Momentary distractions cause loss of control. Assumes that pilot aids can be utilized without increasing the hazard of vehicle control loss. 3. Prelaunch checkout workload a minimum.
-7B	Additional pilot aids: 3-axis "fly to" integrated error displays; ΔV integrator.	Added complexity of pilot flight aid instrumentation. More complex than -7A.	1. Same as 1 and 2 above. Additional pilot aid serves to reduce trajectory errors. 2. Additional pilot aids require added checkout time.
Hardwire -8A (Fig 3-1)	Engine gimbal, wire drive, propellant flexible feed.	Propulsion system complexity is increased over that for -7 systems. If system jammed in near null position pilot may be	1. Hardwire manually operated system may require power augmentation if mechanical hand control rotation and leverage is marginal.

TABLE 3-12. - LUNAR ESCAPE SYSTEMS RELIABILITY - Continued

Type	Configuration Assumptions	Reliability Considerations	Remarks
Hardwire -8A (Continued)	Pilot aid complement same as either 7A or 7B	able to fly by kinesthetic method by assuming "standing" position before launch. Thrust vector must be accurately aligned through CG for guidance accuracy.	2. Additional checkout effort and time required over -7A, -7B to confirm freedom of movement, desired response. 3. System reduces instability characteristic of the high, off center kinesthetically controlled system and flight work load demand on pilot. 4. System permits more attention directed to trajectory control of the vehicle. 5. System aids reduction of trajectory error.
Augmented Hardwire -8B	Pilot aids: Complement of -7B plus auto pilot, alignment controls and displays. Assumes a simple pitch control program. Servo driven	Complexity of above systems increased by autopilot and simple pitch control program. If autopilot function fails design approach should permit operation as a -8A type configuration.	Further reduction of flight work load on pilot. Additional functions to be checked out before launch. More attention can be directed to trajectory control of vehicle during flight.

TABLE 3-12. - LUNAR ESCAPE SYSTEMS RELIABILITY - Continued

Type	Configuration Assumptions	Reliability Considerations	Remarks
Augmented Hardwire -8B (Continued)	hardwire system with manual override capability during thrusting		
-8C	Pilot aids: Same as -8B with more sophisticated programming of flight trajectory.	Complexity of -8B increased by additional automation or simple guidance for flight path control. If system fails design approach should permit operation in manual mode. The -7 pilot aids should be functionally independent of autopilot system.	Minimizes flight work load on pilot. Additional set up and checkout of system needed before launch. Reduction in trajectory error to a minimum. Reduced hazard of sudden light contrast affecting pilot visual accuity necessary to track flight instruments.
Kinesthetic 3-Body -9 (Fig 3-3)	Two-axis suspension of propulsion system tankage, mechanical damping system, plus flexible propellant lines to engine. Pilot aids: Same as -7A or -7B configuration.	Tankage suspension system adds its complexity to the simple kinesthetic -7 configurations. Flexible nature may require securing until after removal from the LM.	Remarks same as for -7 configuration. Suspension system requires checkout for damage and nominal mechanical function. System may provide some reduction in sensitivity to kinesthetic overcontrol hazard existing in the -7 configuration. System sensitivity reduction will change with propellant consumption.

operations. The substitution of cells or bypassing defective cells requires test or monitoring circuits and somewhat elaborate switching capabilities. The LESS application will not readily accommodate this requirement. The more complex LESS configurations will permit reduction of electrical loading to equipment classified as mission essential for continuation of the mission in a degraded mode of operations. Unless backup battery weight is acceptable the LESS battery should have sufficiently high survival design requirements that are compatible with the potential failure effect on the LESS mission.

Weight and balance. - Lunar escape system configurations selected for study were the kinesthetic, hardwire and stability-augmented control, and the kinesthetic three-body models. For each concept, a configuration design drawing was prepared showing 90 percentile crew members, basic structure, equipment, engine, and propulsion tankage arrangements (with some variations) for design propellant loadings of 1000 and 1600 pounds, the expected range of propellant requirements. Each configuration studies utilizes a cold gas (nitrogen) reaction control system, helium for tank pressurization, and a single liquid rocket engine.

Mass properties analysis consisted of determining parametrically the various concept weights, centers of gravity, and moments of inertia for propellant design loadings of 1000 to 1600 pounds. The factors were generated to support stabilization and control dynamic response tradeoffs. The analysis was performed by first determining each configuration's base point weight; the base point in each case is for a 1000-pound propellant design load. Parametric subsystem weight data, as a function of propellant weight, were applied to these basepoint data. Vehicle mass properties were then determined and presented as a function of propellant design weight.

For the weight breakdown tables a propellant weight of 1160 pounds is used which represents that required for this weight vehicle flying a bent two-step trajectory with dual thrust level.

The crewman weight used in this study represents a 90 percentile man (192 pounds, and 72.2 inches tall), space suit (63 pounds), portable life support system (82 pounds), and an oxygen purge system (38 pounds), for a total of 375 pounds. Mass properties were derived for each position as depicted by the configuration design drawings.

Parametric weight/balance and inertias, kinesthetic models (fig. 3-1). - Low and high propellant tank configurations were considered. The pilot is standing and the passenger is seated with his back inclined at an angle, or approximately 26 degrees to the vertical center line. Both are positioned such that their centers of gravity lie nominally in the YZ plane of the vehicle, thereby minimizing pitch and yaw inertia values. The parametric mass properties data included are given in tables 3-13 through 3-15 and figures 3-28 through 3-35.

TABLE 3-13. - LESS WEIGHT STATEMENT KINESTHETIC-LOW TANK TYPICAL CONFIGURATION

Item	Weight (lb)
Structure	70.2
Platform	46.0
Guard Rail	3.0
Passenger Seat	2.0
Truss Structure	19.2
Controls	31.0
Control Panel and Instrumentation	6.0
RCS Hand Controller	2.0
Hand Hold	2.0
Attitude Indicator Installation	21.0
Electrical System	21.0
Battery	11.0
Cabling and Equip.	10.0
Engine and Mount	25.0
Reaction Control System	20.0
Propellant System	74.0
Tanks, Insulation and Mounts (4)	64.0
Plumbing, Etc.	10.0
Pressurization System	41.0
Tanks - Helium	31.0
Plumbing, Etc.	10.0
Beacon	15
VHF Transponder	10
Docking Mechanism	20
Vehicle Dry Weight	327.2
Residual Propellant	10.0
Helium Pressurant	3.0
Residual Nitrogen	.5
Crew + PLSS + OPS and Suits (2)	750.0
Vehicle at Burnout	1090.7
Fuel	446
Oxidizer	714
Nitrogen - RCS Consumable	5.5
Gross Weight	2256.2

TABLE 3-14. - KINESTHETIC MODELS-LOW TANK CONFIGURATION MASS CHARACTERISTICS SUMMARY

Propellant Load / Condition	Weight (lb)	CG ~ (In.)			Inertia (Slug-ft^2)		
		X	Y	Z	I_{xx}	I_{yy}	I_{zz}
1000 lb Propellant							
Burnout	1083.5	0	0	-23.5	197.6	195.0	113.0
Midburn	1586.3	0	0	-9.9	486.0	426.0	361.9
Gross	2089.0	0	0	-4.7	678.1	560.7	610.8
1300 lb Propellant							
Burnout	1105.0	0	0	-22.7	208.8	206.1	119.6
Midburn	1757.8	0	0	-6.5	576.1	498.9	443.1
Gross	2410.5	0	0	-1.3	813.1	661.3	766.6
1600 lb Propellant							
Burnout	1128.0	0	0	-21.9	220.8	218.1	126.8
Midburn	1930.8	0	0	-3.5	662.4	568.0	524.9
Gross	2733.5	0	0	+1.4	941.8	755.6	923.0

TABLE 3-15. - KINESTHETIC MODELS-HIGH TANK CONFIGURATION MASS CHARACTERISTICS SUMMARY

Propellant Load/ Condition	Weight (lb)	CG (In.)			Inertia (Slug-ft^2)		
		X	Y	Z	I_{xx}	I_{yy}	I_{zz}
1000 lb Propellant							
Burnout	1083.5	0	0	-25.1	180.0	175.2	113.0
Midburn	1586.3	0	0	-19.3	357.9	295.7	361.9
Gross	2089.0	0	0	-18.1	513.2	393.4	610.8
1300 lb Propellant							
Burnout	1105.0	0	0	-24.7	183.8	181.2	119.6
Midburn	1757.8	0	0	-18.3	409.4	332.2	443.1
Gross	2410.5	0	0	-17.5	610.2	458.4	766.6
1600 lb Propellant							
Burnout	1128.0	0	0	-24.3	190.3	187.7	126.8
Midburn	1930.8	0	0	-17.5	462.5	368.1	524.9
Gross	2733.5	0	0	-17.3	707.9	521.7	923.0

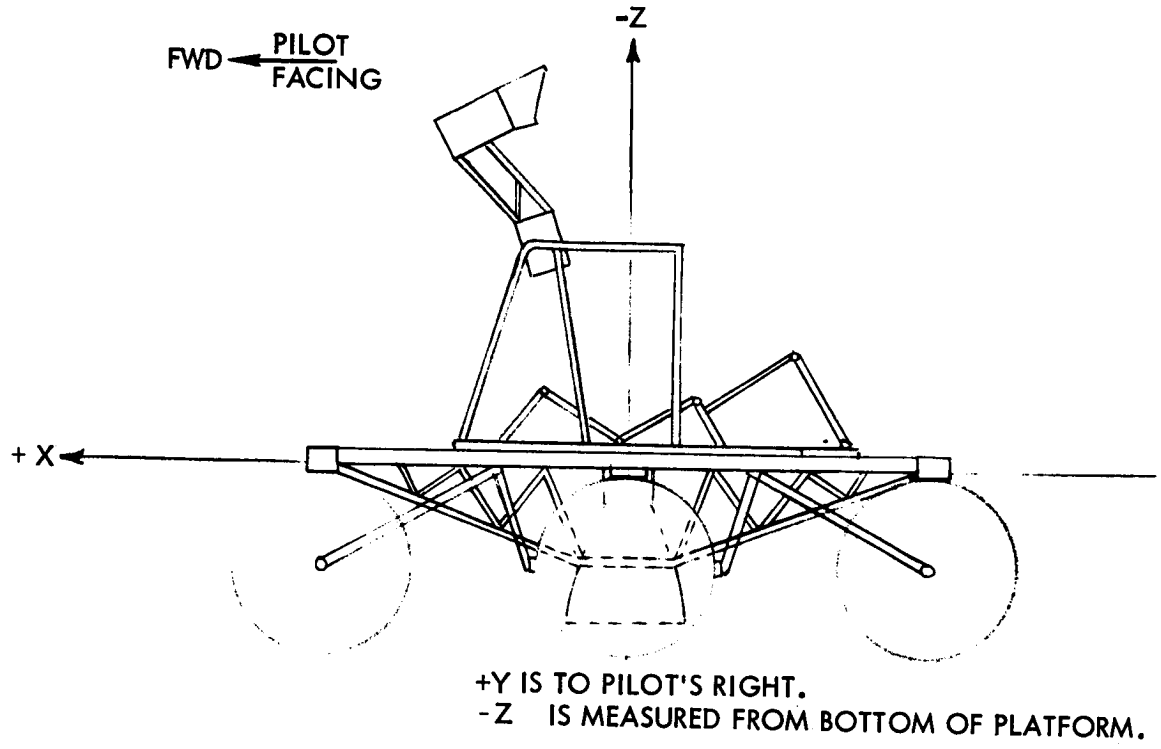

Figure 3-28. - LESS Kinesthetic Model Coordinate System

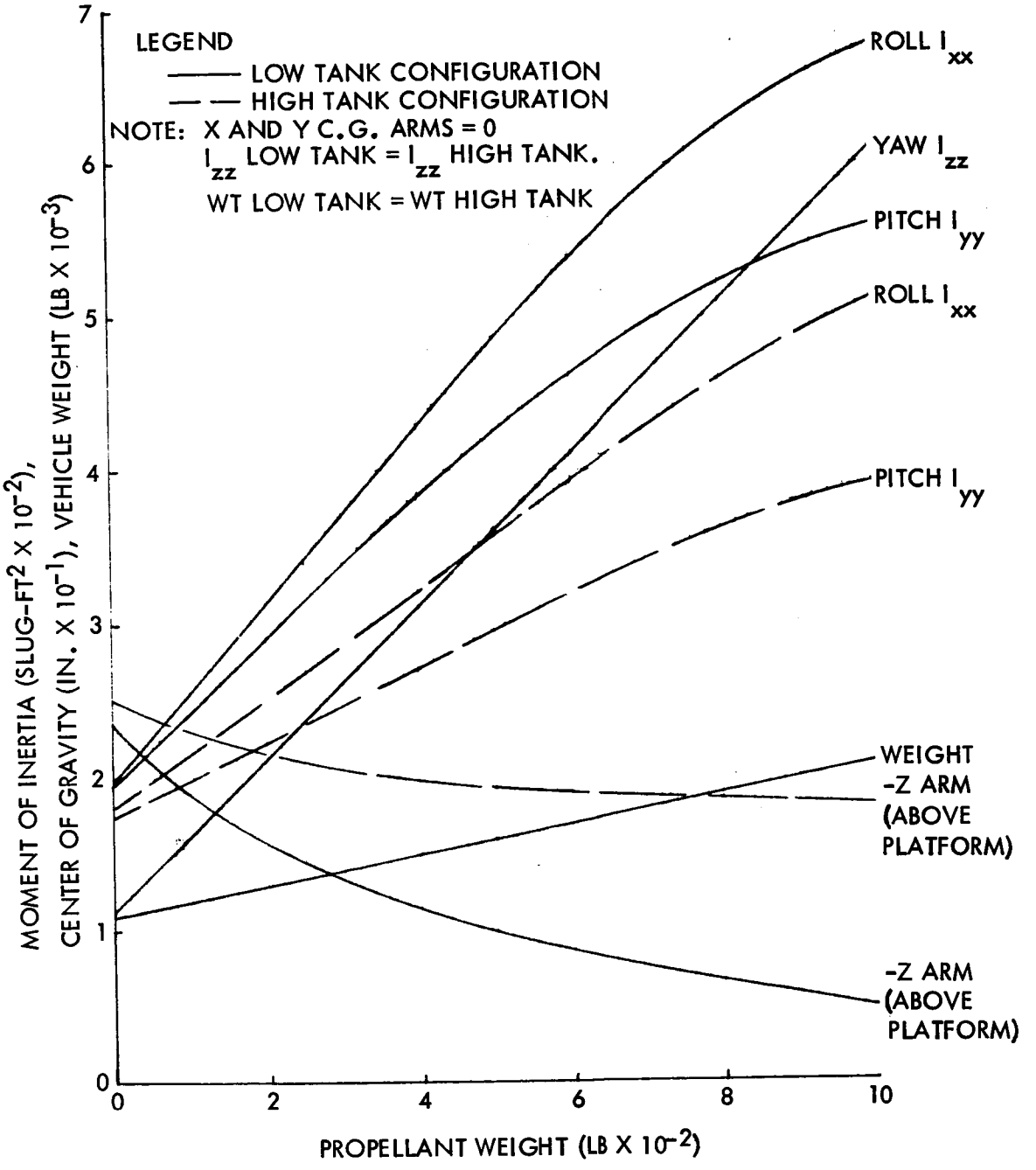

Figure 3-29. - LESS Kinesthetic Model Mass Characteristics Versus Propellant Weight (Base Point 1000 Lb Propellant Loading

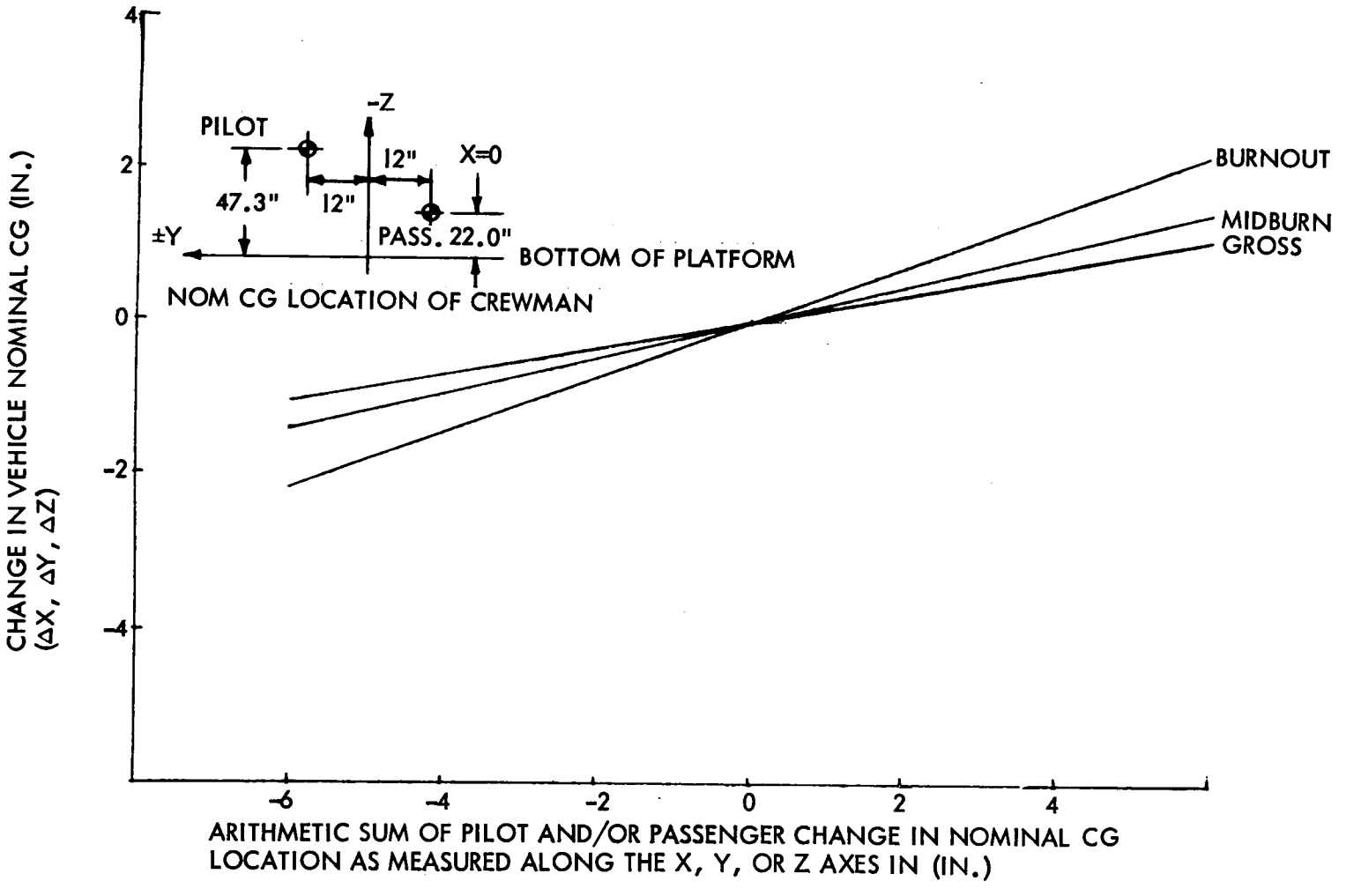

Figure 3-30. - LESS Kinesthetic Model Effect of Pilot and/or Passenger Movement on Vehicle Center of Gravity

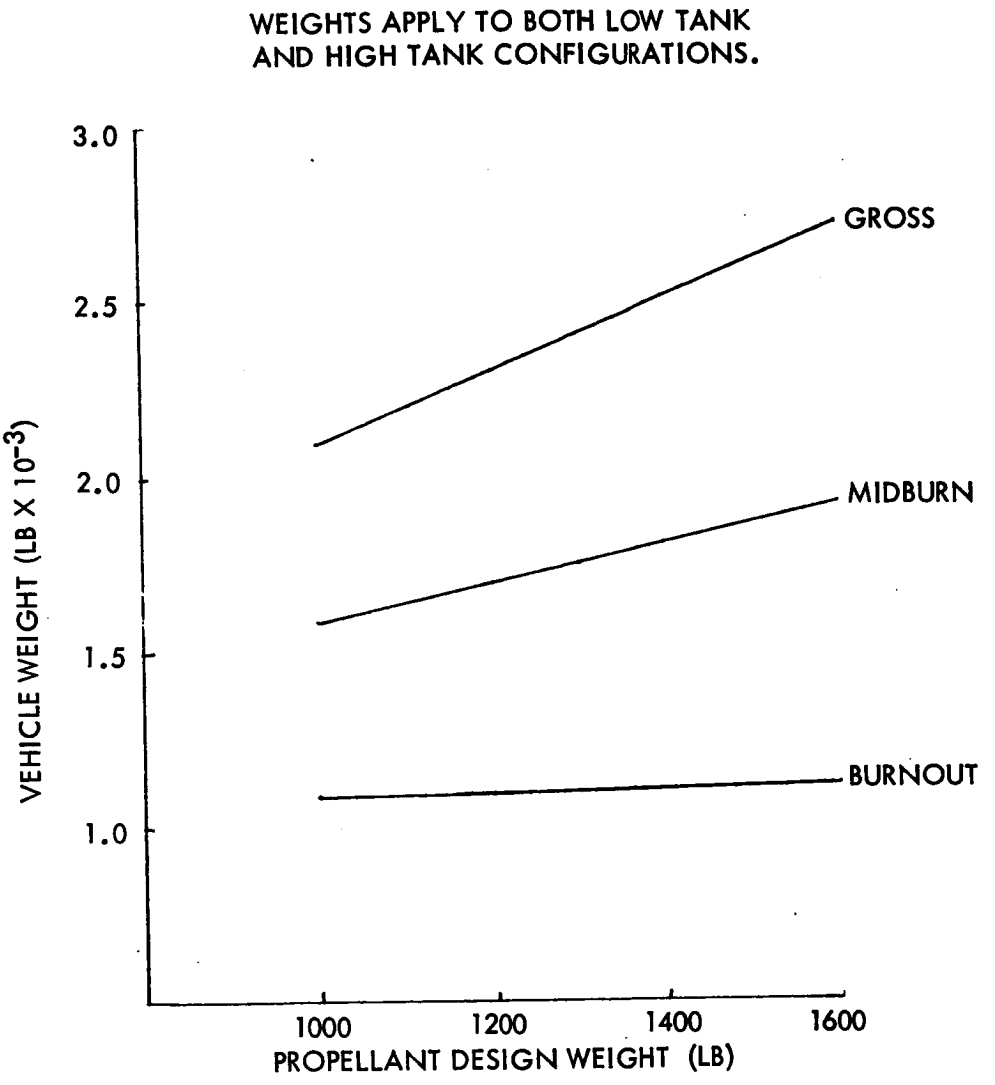

Figure 3-31. - LESS Kinesthetic Model Effect of Propellant Design Weight on Vehicle Weight

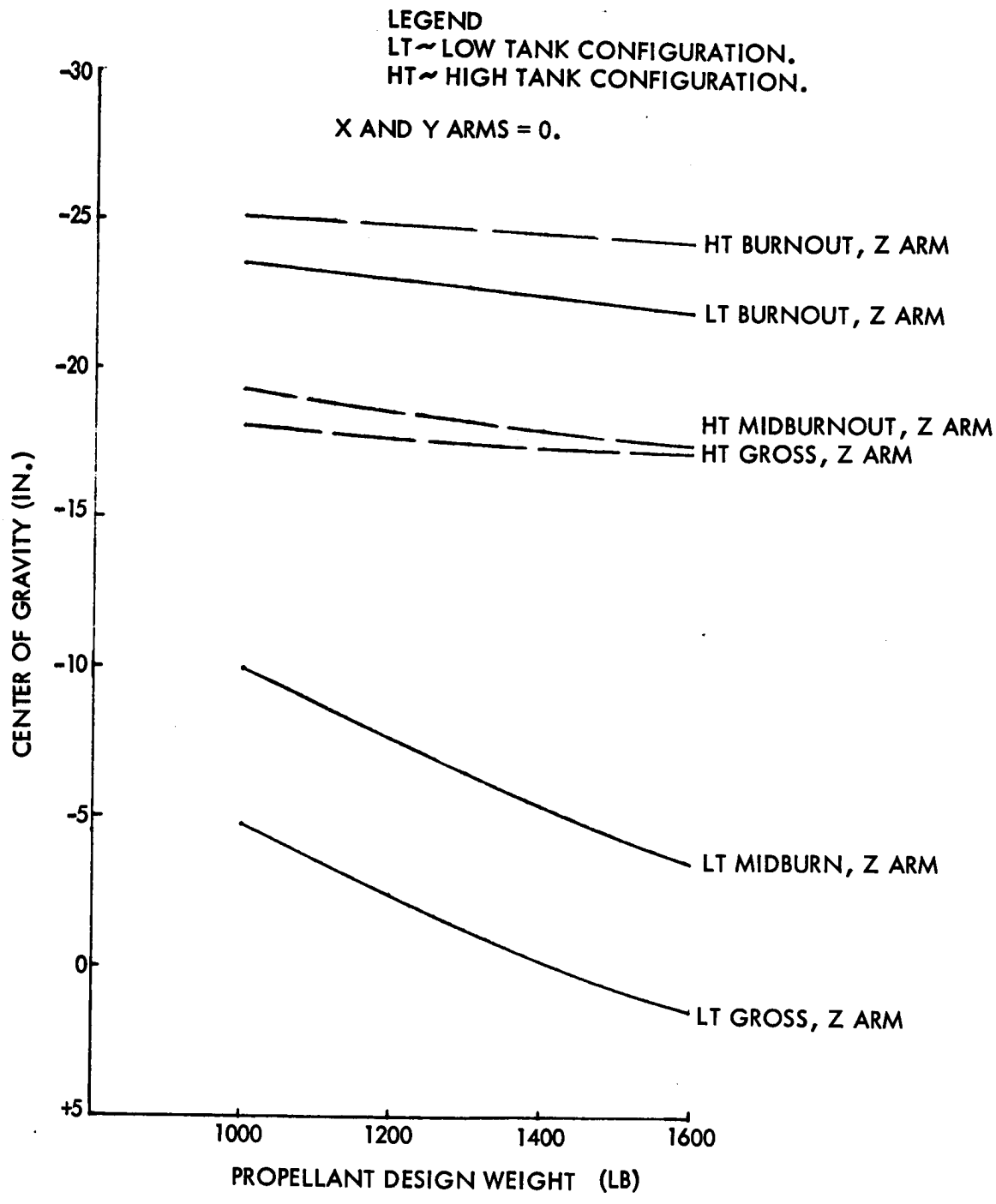

Figure 3-32. - LESS Kinesthetic Model Effect of Propellant Design Weight on Vehicle Center of Gravity

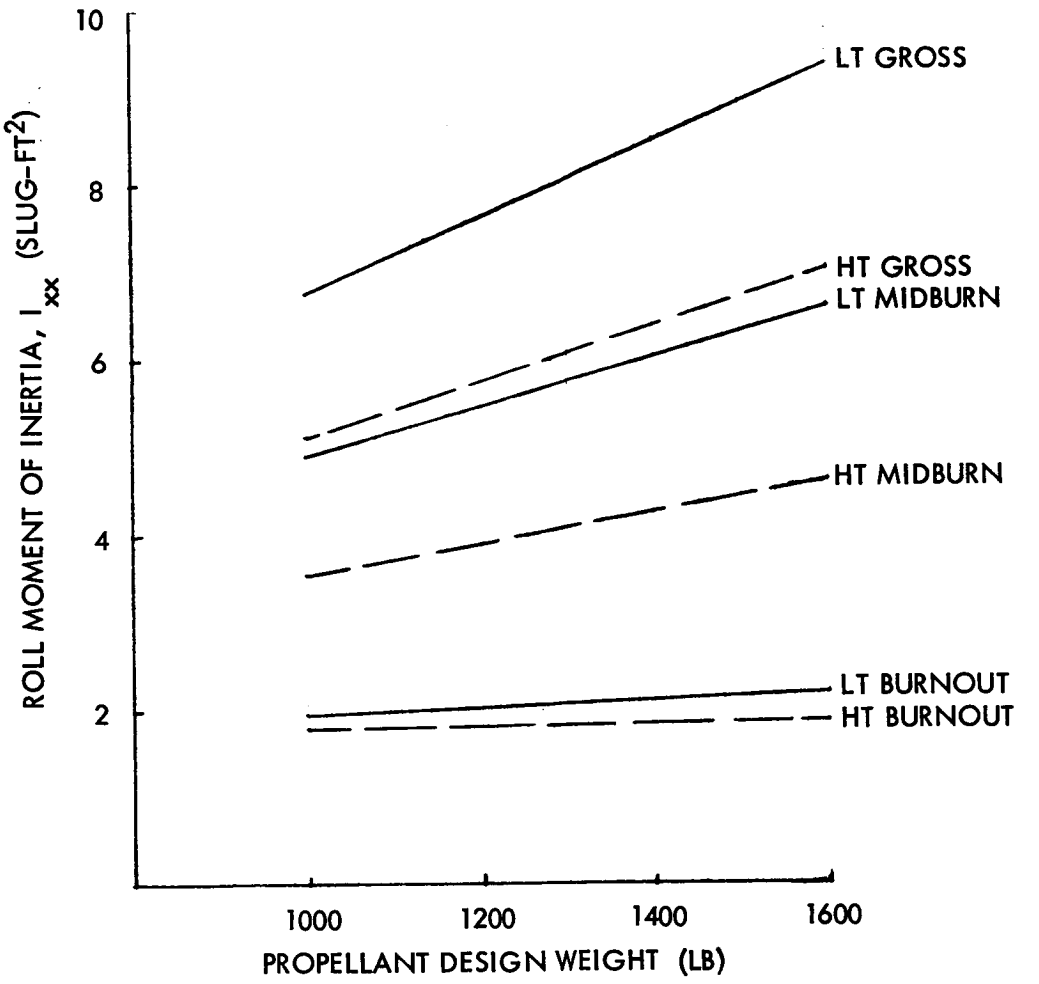

Figure 3-33. - LESS Kinesthetic Model Effect of Propellant Design Weight on Vehicle Roll Moment of Inertia

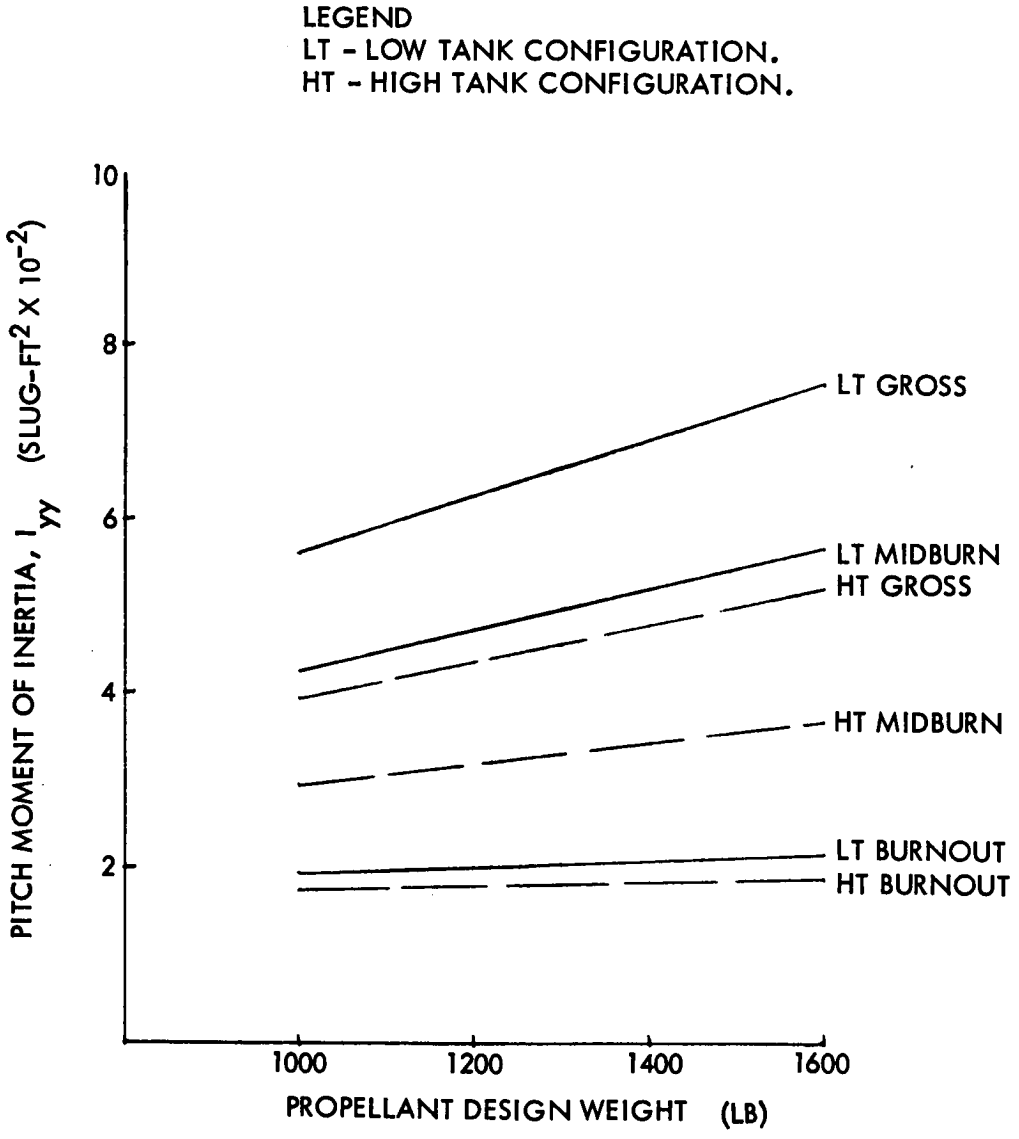

Figure 3-34. - LESS Kinesthetic Model Effect of Design Weight on Vehicle Pitch Moment of Inertia

NOTE: DATA APPLIES TO LOW AND HIGH TANK CONFIGURATIONS.

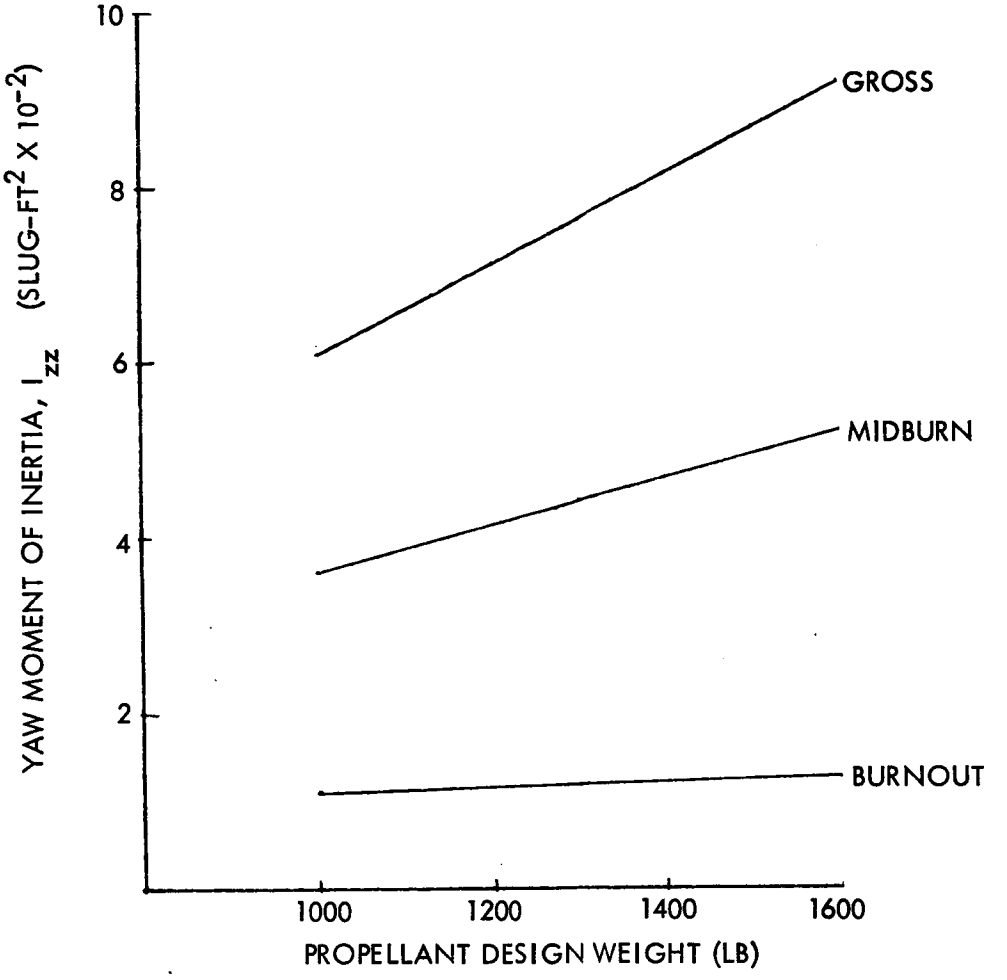

Figure 3-35. - LESS Kinesthetic Model Effect of Propellant Design Weight on Vehicle Yaw Moment of Inertia

Hardwire and stability-augmented control models (fig. 3-3): Parametric mass properties were generated for the hardwire control model only. For the stability-augmented model, a weight statement is presented showing the weight differential to the hardwire concept. The pilot is also seated in a reclined position to favor use of visual sighting devices in a bent two-step profile, their backs making an angle of approximately 60 degrees to the vertical centerline. Both are positioned such that their centers of gravity lie nominally in the vehicle YZ plane, thereby minimizing pitch and yaw inertia values. The parametric mass properties data included are given in tables 3-16 through 3-18, and in figures 3-36 through 3-41.

Kinesthetic three-body model (fig. 3-2): Mass characteristic data were generated for the 1000-pound propellant design load only. Data for the platform associated mass, body structure associated mass, and the total vehicle are presented. The pilot is standing and the passenger is seated in an upright position. Their center of gravity locations, with respect to the vehicle centerline, are 10 inches aft for the pilot and 10 inches forward for the passenger. Mass properties data included are given in tables 3-19 through 3-21 and in figures 3-42 through 3-44.

Balance and center of gravity position. - The requirement to balance the vehicle statically about the thrust vector is desirable for all configurations and may be a necessity for hardware or stability-augmented concepts unless center of gravity offsets can be shown to be less than a determinable amount. If the vehicle is not balanced with the center of gravity on the center line, the engine must be gimbaled, or differentially thrusted (for pulsing engine versions) to align the thrust vector through the center of gravity. This will result in the vehicle platform being tilted with respect to the vehicle thrust vector structure. Since the flight trajectory corresponds to the thrust vector, the angle between thrust line and vehicle center line then becomes an error in the trajectory if the guidance equipment is referenced to the vehicle. For more sophisticated systems such as the stability augmented control system, this angle can be measured and incorporated into the guidance system to eliminate the error. If this complexity is included, the vehicle need only be balanced to minimize gimbal angle, perhaps to within two or three inches of center of gravity uncertainty if as much as 10 to 15 degrees of gimbal are available.

For the simplified guidance and control concepts which are the objective for this vehicle, a method of accurate center of gravity positioning may be necessary. The center of gravity of the empty vehicle would have been determined very accurately on Earth, the combined center of gravity of the two astronauts would be known very accurately and the major errors would be the propellant loading variation and slight changes in crew mass and position. A method for accomplishing vehicle balance if required is illustrated in figure 3-8. This concept involves vehicle leveling in two planes to correct for

TABLE 3-16. - LESS WEIGHT STATEMENT
HARDWIRE CONTROL MODEL - BASE POINT CONFIGURATION

Item	Weight (lb)	
Structure		56.0
Platform	35.0	
Seats	5.0	
Thrust and truss structure	16.0	
Guidance and Controls		57.5
Control panel pedestal	4.0	
Control panel and instrumentation	6.0	
Hand controller	5.5	
Attitude indicator and display panel	27.0	
Hardwire gimbal mechanism	15.0	
Electrical System		15.0
Battery	5.0	
Cabling and equipment	10.0	
Engine		40.0
Thrust chamber	23.0	
Gimbal	15.0	
Mount	2.0	
Reaction Control System		20.0
Propellant System		74.0
Tanks, insulation and mounts (4)	64.0	
Plumbing, etc.	10.0	
Pressurization System		41.0
Tanks - Helium	31.0	
Plumbing, etc.	10.0	
Beacon		15.0
VHF transponder		10.0
Docking mechanism		20.0
Vehicle dry weight		348.5
Residual Propellant		10.0
Helium Pressurant		3.0
Residual Nitrogen		0.5
Crew + PLSS + OPS and Suits (2)		750.0
Vehicle at burnout		1112.0
Fuel		446.0
Oxidizer		714.0
Nitrogen - RCS Expendable		5.5
Gross Weight		2278.0

TABLE 3-17. - LESS WEIGHT SUMMARY—
STABILITY-AUGMENTED CONTROL MODEL

Component/Condition	Weight (lb)
Hardwire Control Model Dry Weight	348.5
Less:	
Gimbal System - Hardwire	-15.0
Plus:	
Gimbal Actuator Installation	25.0
Stability Augmentation Package	11.0
Additional Battery Weight	17.0
Vehicle Dry Weight	386.5
Residual Propellants and Gases	13.5
Crew + PLSS and Suits (2)	750.0
Vehicle at Burnout	1150.0
Propellant	*1200.0
Nitrogen - RCS Expendable	5.5
Gross Weight	2355.5
*Increased from 1160 pounds due to increased vehicle weight	

the lunar surface slope; this requires two bubble levels on the LESS installed perpendicular to the theoretical thrust vector and screw adjustments in each of the launch legs or launch stand. The vehicle center of gravity can now be determined by use of load cells in the legs. Display of the load cell outputs on the pilot's console where it can be seen while the crew are in final flight position is required. Also required is the inclusion of a mechanism to facilitate movement of pilot and/or passenger seat position in both the x and the y axes to obtain uniform load cell readings.

Guidance error analysis shows that for a typical configuration, center of gravity positioning to within 1/4 to 1/2 inch with reasonable dimensions on engine location is required. With accurate calibration on Earth before the mission (which may involve static engine firing in a vacuum chamber) the vehicle center of gravity can be positioned to within ±0.1 inch. Achievement of this accuracy requires balancing with the same astronauts scheduled for

TABLE 3-18. - HARDWIRE CONTROL MODEL
MASS CHARACTERISTICS SUMMARY

Propellant Load/Condition	Weight (lb)	CG (in.)			Inertia (slug-ft^2)		
		X	Y	Z	I_{XX}	I_{YY}	I_{ZZ}
1000 lb Propellant							
Burnout	1129.5	0	0	-12.7	99.9	132.1	131.4
Midburn	1632.3	0	0	-3.2	228.3	246.0	222.2
Gross	2135.0	0	0	+0.1	300.4	297.2	313.1
1300 lb Propellant							
Burnout	1151.0	0	0	-12.2	105.5	137.7	134.2
Midburn	1803.8	0	0	-0.6	270.6	275.6	252.3
Gross	2456.5	0	0	+2.7	358.4	336.2	370.3
1600 lb Propellant							
Burnout	1174.0	0	0	-11.6	111.6	143.8	137.3
Midburn	1976.8	0	0	-0.5	280.6	279.3	282.5
Gross	2779.5	0	0	+4.2	405.9	371.1	427.8

that particular mission seated in suits and backpacks. This calibration would have to be accomplished with uniformly loaded propellant tanks. In actual servicing on the lunar surface, particularly if expandable tanks are utilized, variation between propellant tank loadings can be expected. With the typical tank center 30 inches from vehicle center line, a 1 percent variation in oxidizer loading will result in a center of gravity movement of approximately 0.1-inch. A 2 percent loading uncertainty (0.2-inch) when combined with nominal vehicle variation of 0.1-inch, if in the same direction might approach or exceed that allowed for orbit insertion accuracy in some configurations. More detail analysis and loading tests of the actual system and vehicle design would be required to determine if loading errors of less than 2 percent are achievable. Figure 3-38 shows that a pilot and or passenger movement of over 1 inch is required to correct for a 0.2-inch vehicle center of gravity variation for a minimum weight vehicle in takeoff condition.

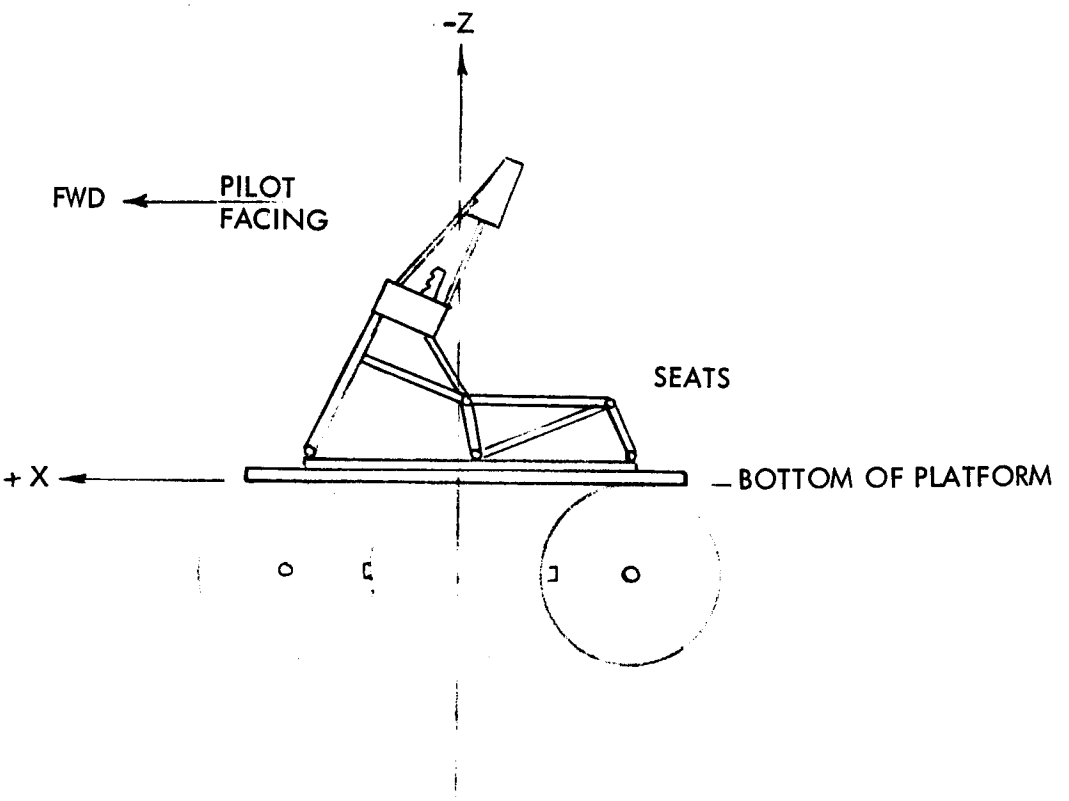

Figure 3-36. - LESS Hardwire Control Model Coordinate System

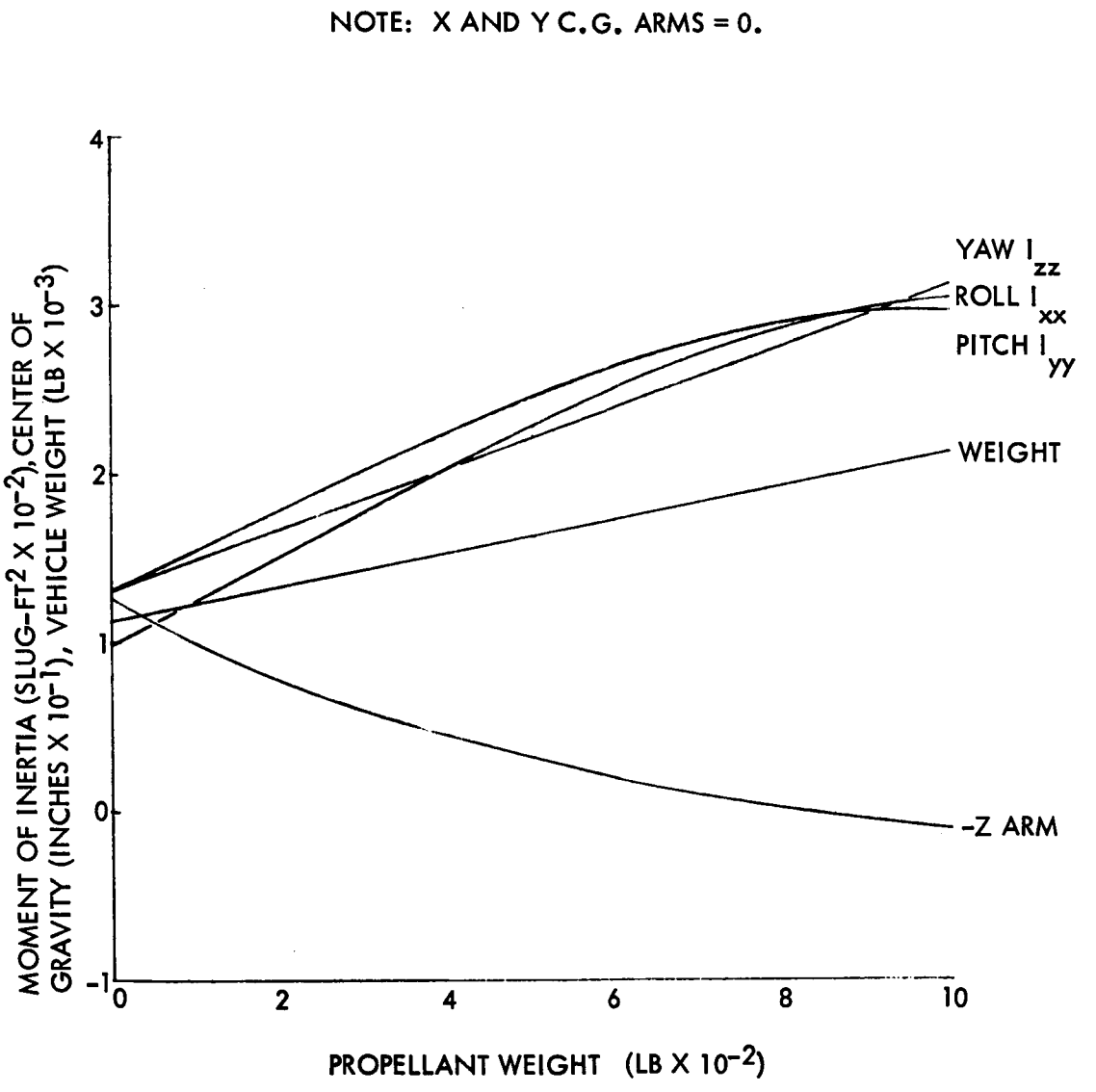

Figure 3-37. - LESS Hardwire Control Model Mass Characterisitics Versus Propellant Weight (Base Point 1000 lb Propellant Loading)

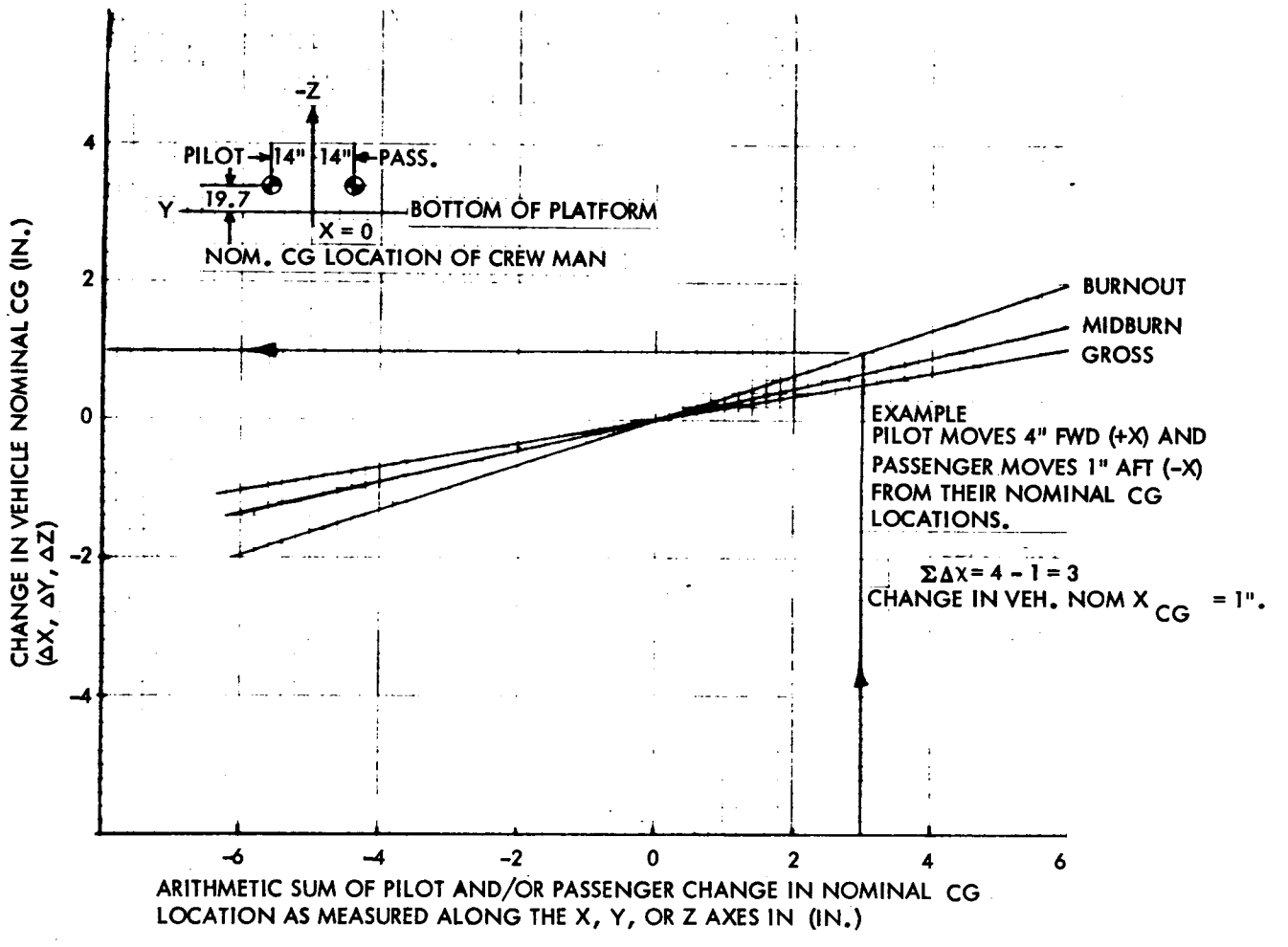

Figure 3-38. - LESS Hardwire Control Model Effect of Pilot and/or Passenger Movement on Vehicle Center of Gravity

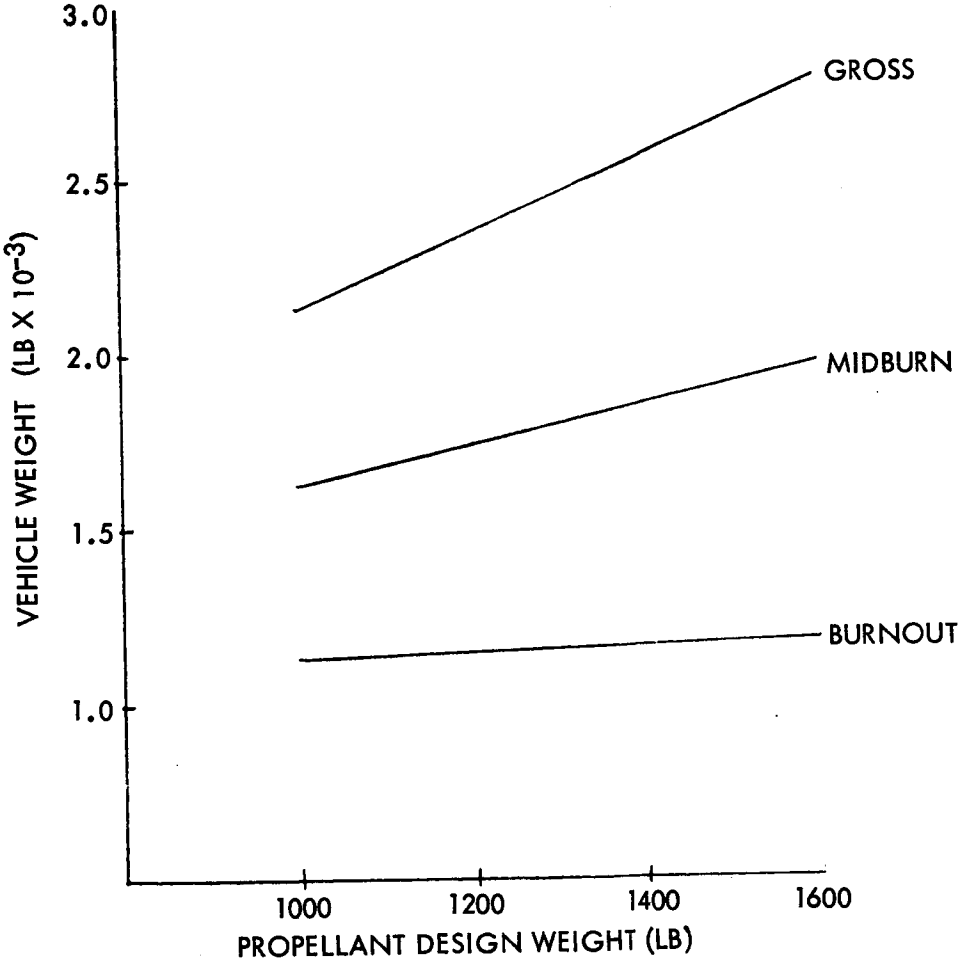

Figure 3-39. - LESS Hardwire Control Model Effect of Propellant Design Weight on Vehicle Weight

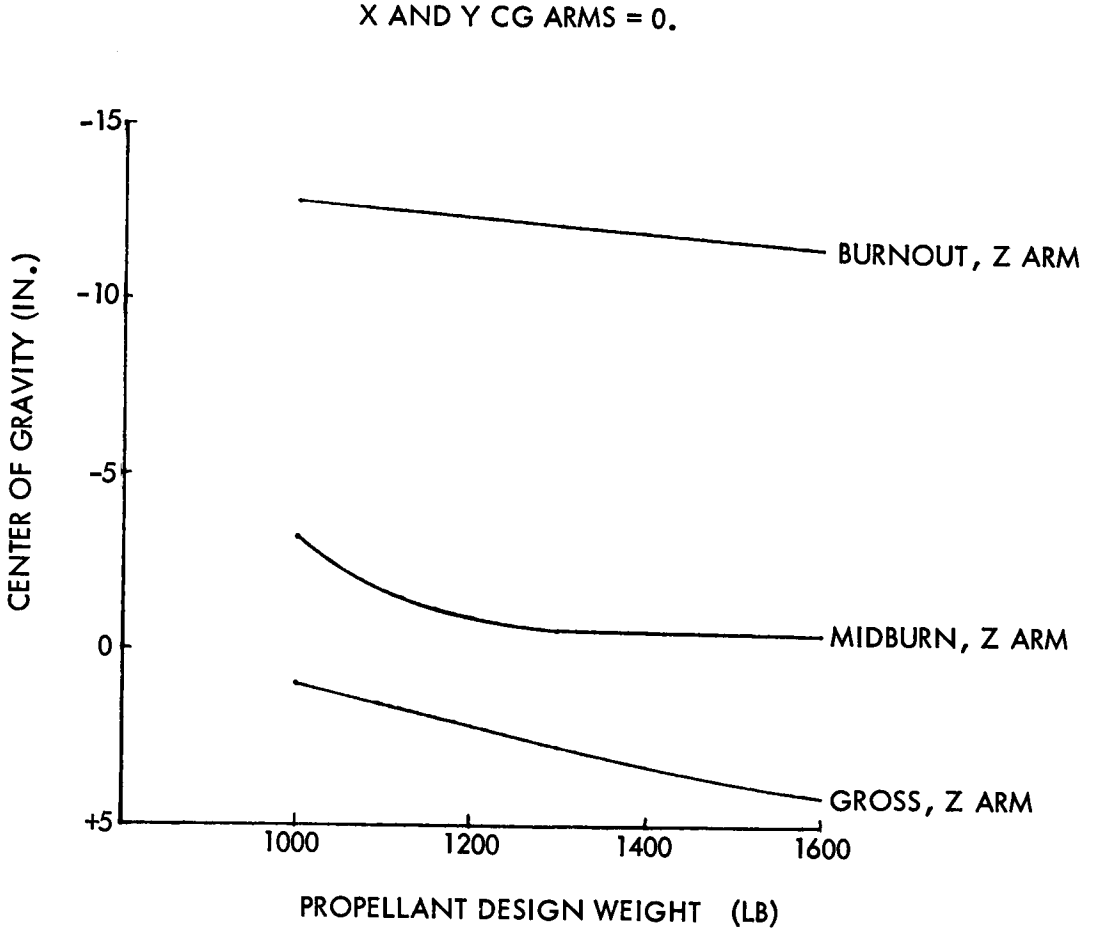

Figure 3-40. - LESS Hardwire Control Model Effect of Propellant Design Weight on Vehicle Center of Gravity

I_{xx} ~ ROLL MOM. OF INERTIA .
I_{yy} ~ PITCH MOM. OF INERTIA.
I_{zz} ~ YAW MOM. OF INERTIA.

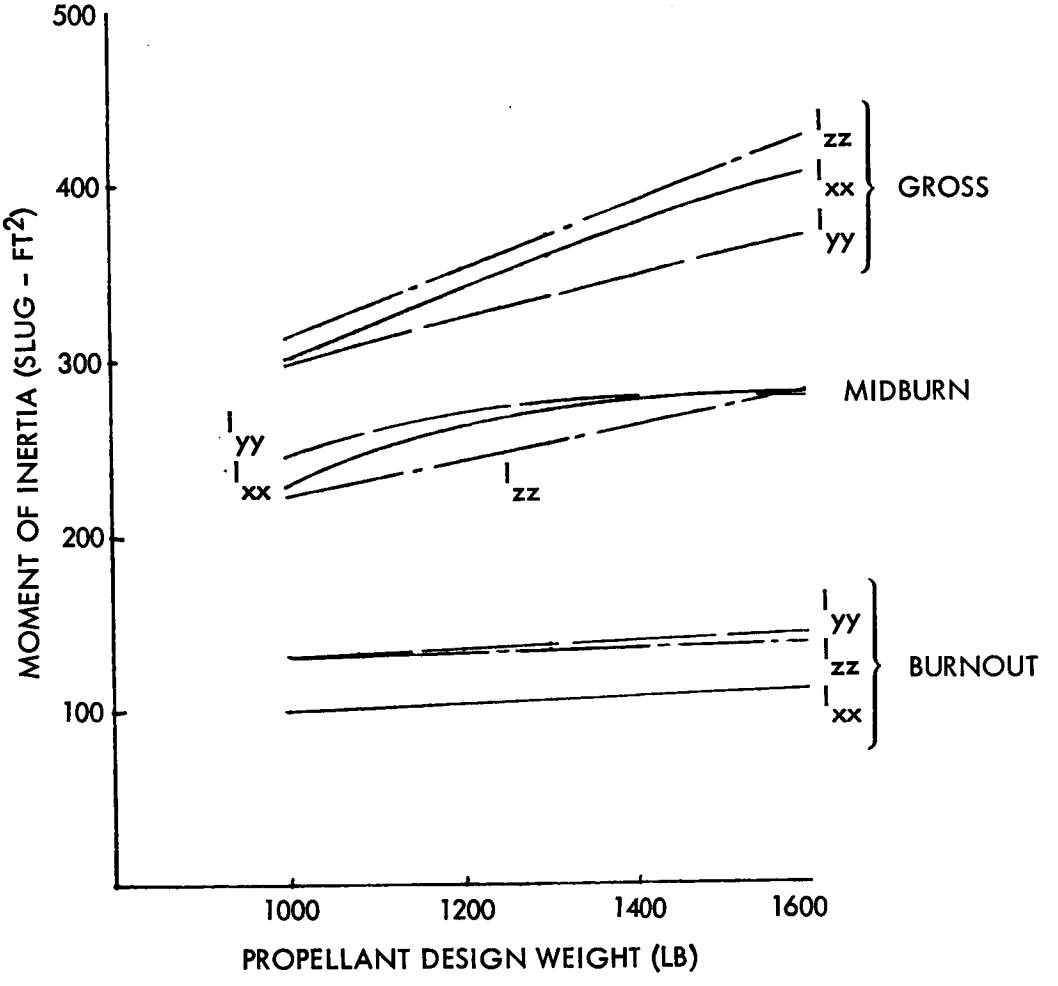

Figure 3-41. - LESS Hardwire Control Model Effect of Propellant Design Weight on Vehicle Moment of Inertia

TABLE 3-19. - LESS WEIGHT STATEMENT:
KINESTHETIC CONTROL THREE-BODY MODEL

Item		Weight (lb)
Structure		62.2
Platform and support truss	40.6	
Guard rail	3.0	
Passenger seat	2.5	
Basic body	6.5	
Propellant tank support trusses	9.6	
Controls		52.7
Control panel and instrumentation	6.0	
RCS hand controller	2.0	
Hand hold	2.0	
Attitude indicator installation	21.0	
Damping struts - spring loaded	5.2	
Platform gimbal	16.5	
Electrical System		21.0
Battery	11.0	
Cabling and equipment	10.0	
Engine and Mount		25.0
Reaction Control System		20.0
Propellant System		74.0
Tanks, insulation and mounts (4)	64.0	
Plumbing, etc.	10.0	
Pressurization System		41.0
Tanks - helium	31.0	
Plumbing, etc.	10.0	
Beacon		15.0
VHF transponder		10.0
Docking Mechanism		20.0
Vehicle dry weight		340.9
Residual Propellant		10.0
Helium Pressurant		3.0
Residual Nitrogen		0.5
Crew + PLSS + OPS and Suits (2)		750.0
Vehicle at burnout		1104.4
Fuel		446.0
Oxidizer		714.0
Nitrogen - RCS Consumable		5.5
Gross Weight		2270.9

TABLE 3-20. - LESS KINESTHETIC CONTROL THREE-BODY MODEL MASS CHARACTERISTICS SUMMARY (1000 LB PROPELLANT LOAD)

Condition	Weight (lb)	CG (in.)			Inertia (slug-ft^2)		
		X	Y	Z	I_{XX}	I_{YY}	I_{ZZ}
Burnout	1097.5	0	0	36.2	213.2	218.7	120.4
Midburn	1600.0	0	0	23.4	453.8	415.4	311.3
Gross	2103.0	0	0	18.4	604.8	522.4	502.2

There are other methods of balance sensing and adjustment which may be better than the leveling-load cell concept illustrated. One of these utilizes a ball and socket or gimbal ring support system in place of launch legs. This method allows slight tilting of the vehicle around both axes if it is not balanced. Level sensing could be accomplished with a single bubble (tire balance type) mounted on the vehicle structure in such a position that the pilot could see it while in the normal seated position (a disposable mirror could be used for convenience). Seat adjustment would then be made to obtain balance. Another mechanical method is to use identical calibrated springs in the four legs, compressed fully while leveling the vehicle to bubble levels. After mounting the vehicle, the crew would remotely release the spring tie-downs and observe the new platform bubble level readings. When load is equalized in all legs by shifting the seats, the vehicle platform should again be level and center of gravity in proper position. Several other methods are possible; during the next LESS vehicle development phase, the concept which provides the required accuracy with minimum astronaut effort and time may be determined.

Structures. - The structural analysis performed in this study was limited to a review of the conceptual drawings and a brief analysis of the feasibility of expandable tank concepts.

The type of structure utilized in most conceptual layouts consists of a honeycomb/plate deck with truss supports of engine, tanks, displays and equipment. The primary advantage of this type structural design is simplicity and ease of manufacturing where no high acceleration loads are present at concentration points. (In the Lunar Flying Vehicle Study where 8g landing loads are a requirement, skin-stringer construction was found to be lighter.)

TABLE 3-21. - LESS KINESTHETIC CONTROL THREE-BODY MODEL PLATFORM AND BODY-ASSOCIATED MASS CHARACTERISTICS (1000 LB PROPELLANT LOAD)

Gimbal Axis	Weight (lb)	Center of Gravity (in.)			Inertia (slug-ft^2)	
		X	Y	Z	I_{xx}	I_{yy}
PLATFORM ASSOCIATED MASS CHARACTERISTICS IN PITCH AND ROLL.						
Pitch (1)	882.3	0	0	-45.5	--	108.8
Roll (2)	891.8	0	0	-45.0	108.0	--
(1) Pitch condition does not include roll gimbal ring. (2) Roll condition includes roll gimbal ring.						
BODY STRUCTURE ASSOCIATED MASS CHARACTERISTICS IN PITCH AND ROLL.						
Burnout						
Pitch (2)	215.2	0	0	+1.8	--	24.8
Roll (2)	205.7	0	0	+1.9	25.6	--
Midburn						
Pitch (1)	717.7	0	0	+3.8	--	98.4
Roll (2)	708.2	0	0	+3.9	143.3	--
Gross						
Pitch (1)	1220.7	0	0	+1.1	--	171.1
Roll (2)	1211.2	0	0	+1.1	259.7	--
(1) Pitch condition includes roll gimbal ring. (2) Roll condition does not include roll gimbal ring.						

The use of expandable tanks greatly facilitates stowage aboard the LM descent stage (fig. 3-6). Since the tanks are not filled when stowed on the LM, the use of the collapsed and folded tank concept is particularly pertinent. Although collapsible tanks are not known to have been in any other aircraft or space vehicles, the positive expulsion diaphragm propellant technology, which is well developed, is applicable. Positive expulsion tank bladders developed for these propellants could be used with a flexible retainer to limit expansion to the desired final spherical shape and absorb all or part of the internal pressure loads. Metal mesh or fiberglass cloth material could be used to withstand the 300 psi internal pressure and still be capable of folding into a metal hoop such as shown in figure 3-3. The fiberglass cloth or mesh could be formed into a composite tank material with Teflon or a fluoro-elastomer on the inside.

A brief analysis has shown that tank wall thickness of 0.020- to 0.025-inch is sufficient (Viton A) which results in a tank weight not significantly greater than a metal tank. Calculation of the effect of dynamic loads during launch from the lunar surface show that tank material thickness requirement is not significantly increased for vehicle thrust to weight of 0.3.

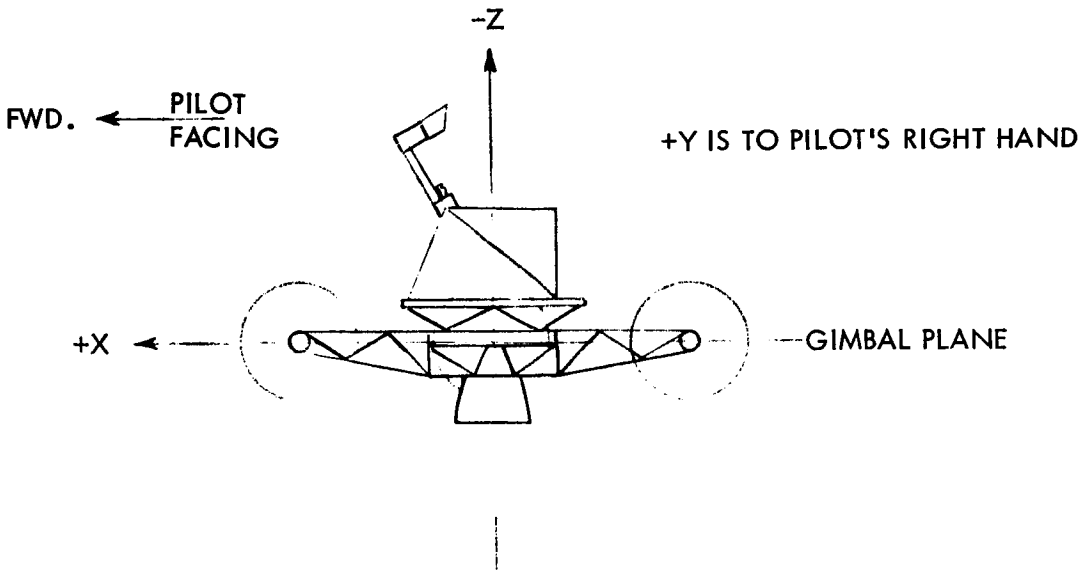

Figure 3-42. - LESS Kinesthetic Control Model Coordinate System (Decoupled Mode)

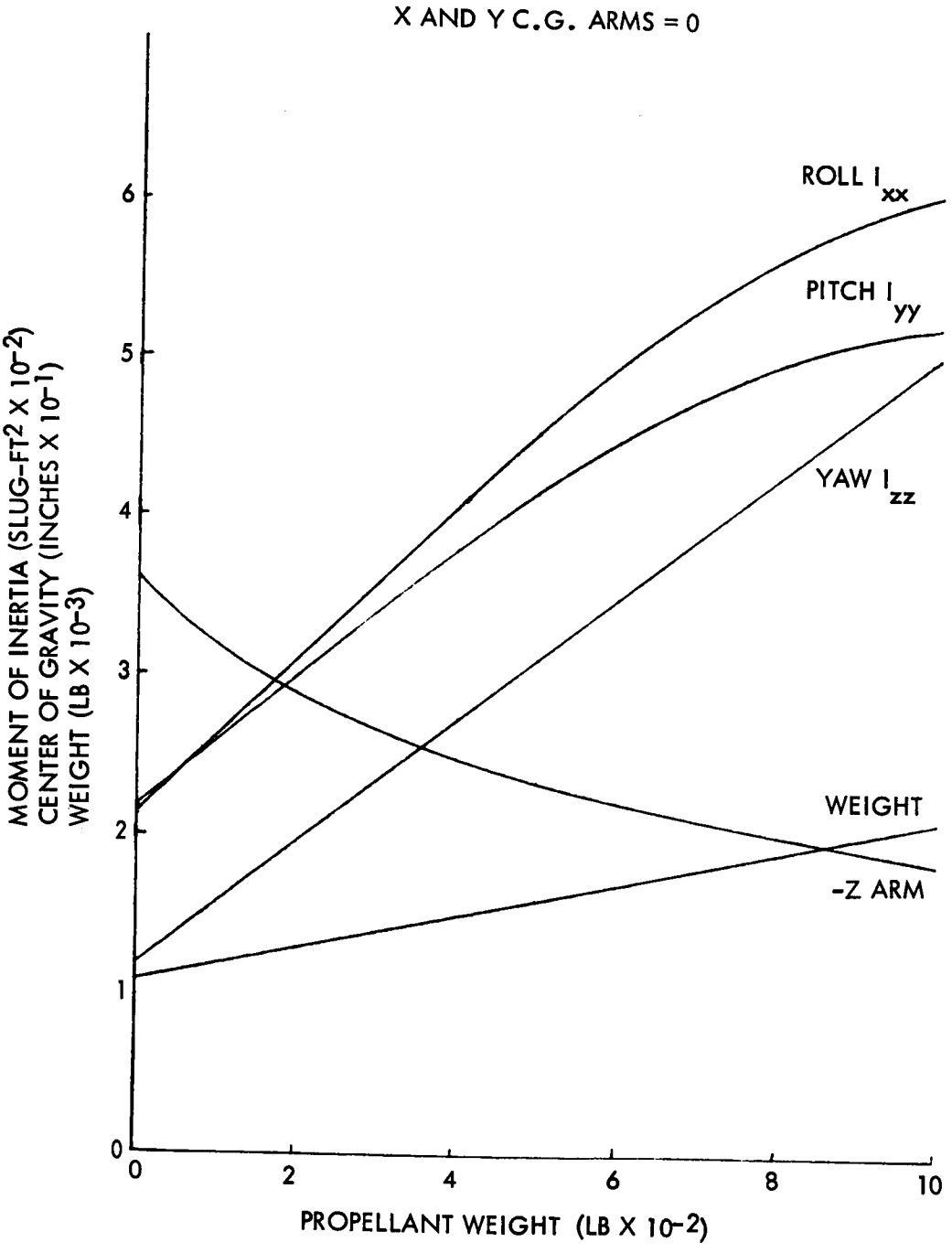

Figure 3-43. - LESS Kinesthetic Control Three-Body Model Mass Characteristics Versus Propellant Weight (1000 lb Propellant Mode)

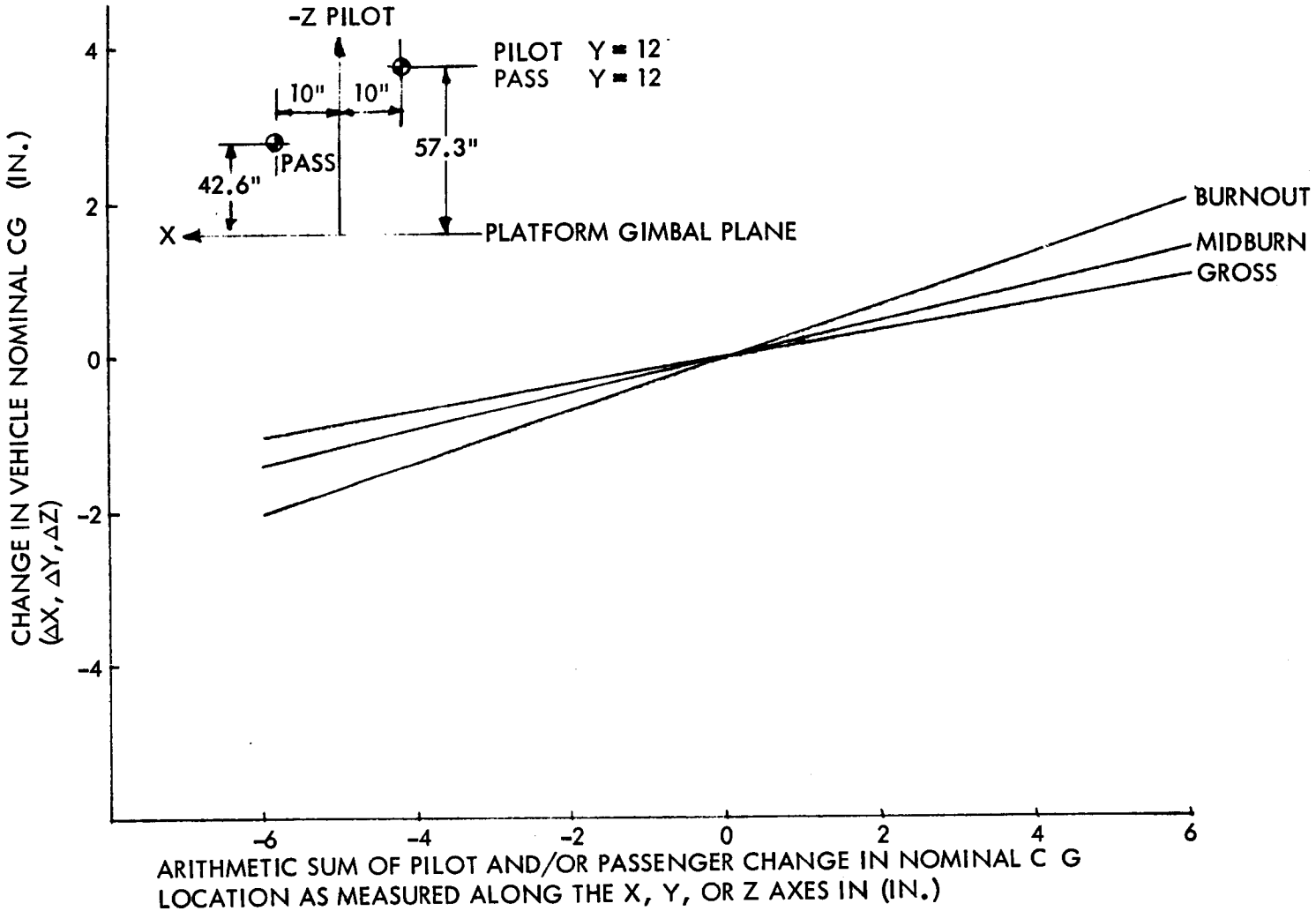

Figure 3-44. - LESS Kinesthetic Three-Body Model Effect of Pilot and/or Passenger Movement on Vehicle Center of Gravity

Another concept variation utilizes a single-layer metalic convoluted diaphragm of the type developed for cyrogenic propellant positive expulsion. Bell Aircraft has produced tanks of this type for the Air Force under AF04-611-8183. The problem with this concept is to find material which is ductile enough to be convoluted, to straighten into a sphere with internal pressure and to withstand operating pressures of 300 psi. A candidate material is Inconel 718 which has a yield strength of 180,000 psi. Required material thickness for a 27-inch diameter tank with 300 psi internal pressure is 0.014-inch, which results in weight of less than 10 pounds not including supports and fittings. With the required support hoop and fittings, the weight is estimated to be approximately 20 pounds which compares to 16 pounds for a conventional spherical titanium tank.

Stowage on the lunar module. - Figure 3-45 shows potential storage areas on the LM into which the LESS must fit. The 32 by 70 by 90-inch rectangular area on the rear deck of the descent stage appears to be the area most compatible with vehicle shape, but during the Lunar Flying Vehicle Study NASA stated that a LM ground rule is that all equipment be stowed below the ascent-descent separation plane. This is to eliminate the possibility of interference during a descent abort where translation of the ascent stage could result in interference of the engine with something stowed on the upper deck area. Therefore, study stowage investigations have concentrated on the Quads I and IV areas. (Recent information from NASA MSC has shown plans to use Quad IV for MESA experiments and equipment stowage).

Figure 3-5 shows the configuration of figure 3-1, with collapsed tanks stowed in a LM quad. Even with the large (1600-pound) propellant tanks, (collapsed and folded) this configuration stows within the available area provided the equipment and seats above the LESS deck are folded into the deck. Without the expandable propellant tanks the vehicle can not be stowed without encroachment into the area under the LM RCS exhaust. Stowage within this jet encroachment area is another approach as indicated in figure 3-10, which shows the long range flyer version of LESS stowed without collapsed tanks. Use of this area under the RCS downward firing jet is undesirable because it reduces the jet effectiveness and causes an increased LM RCS propellant requirement. This propellant increase must be compared with the complexity and development costs of the expandable tank concept, if that is the choice. Another, or poor fourth, stowage method utilizes detached propellant tanks which are stowed in another LM quad. This greatly complicates the surface assembly which the astronaut must do, increases workload, and poses the possibility of contamination and improper connections.

Conceptual design conclusions. - From the conceptual design studies conducted it can be concluded that a vehicle capable of performing the LESS

mission is feasible from a design and construction standpoint. The weight, balance, subsystems integration, and stowage on the LM present problems, but all have one or more apparent solutions. Additional design conclusions are described below.

The guidance and control techniques to be employed can affect the vehicle configuration and packaging. Hardwire and stability-augmented control techniques, particularly with gyro displays, tend to permit more compact layouts.

Design for best handling qualities with manual stability modes tends to complicate design of hardwire controls and engine gimbal arrangements.

Use of RCS jets for powered boost attitude control offers advantages in potential hardwire control simplification and reduced guidance system center of gravity variation sensitivity.

Weight penalties for pure RCS couples are excessive so downward-only firing is feasible. However, this configuration leads to the multi-engine pulsing configuration using Apollo RCS engines which requires only a 100-pound propellant penalty, eliminates gimbaling and thrust misalignment guidance errors, and promises availability and packaging gains as well. It does appear to violate the groundrule calling for simplicity in all systems.

Optimum thrust-to-weight at takeoff is in the order of 0.3 for minimum energy and good control. Reduction of thrust (2 levels) to 10 to 20 percent later in boost flight helps improve handling qualities and substantially decreases total energy requirements, particularly if takeoff thrust-to-weight is increased to 0.4. The thrust reduction should come at about 60 percent of final velocity gained.

Stepped thrust capability is not difficult to provide but requires longer engine development.

With single main engine configurations, it is most practical to use cold gas jets for yaw control. Nitrogen gas provides lowest system weights and is also adequate for RCS functions in orbital coast phases. Multiple gas jets are desirable for 3-axis translation as well as rotation couples for precise docking maneuvers, if required.

A design objective should be to achieve good handling qualities with manual control modes and practical geometric layouts. However, large changes in inertia with the high mass of propellants aboard from start to end burn are difficult to accommodate (stepped thrust reduction is a major help). Desirable moment arms from engine gimbal to center of gravity with conventional hardware control are most difficult to provide, yet are needed to avoid guidance angle errors resulting from gimbal angles to correct for small center of gravity offsets.

Backpack (PLSS) recharge time of approximately one hour appears excessively long under likely emergency conditions requiring haste in abort preparations.

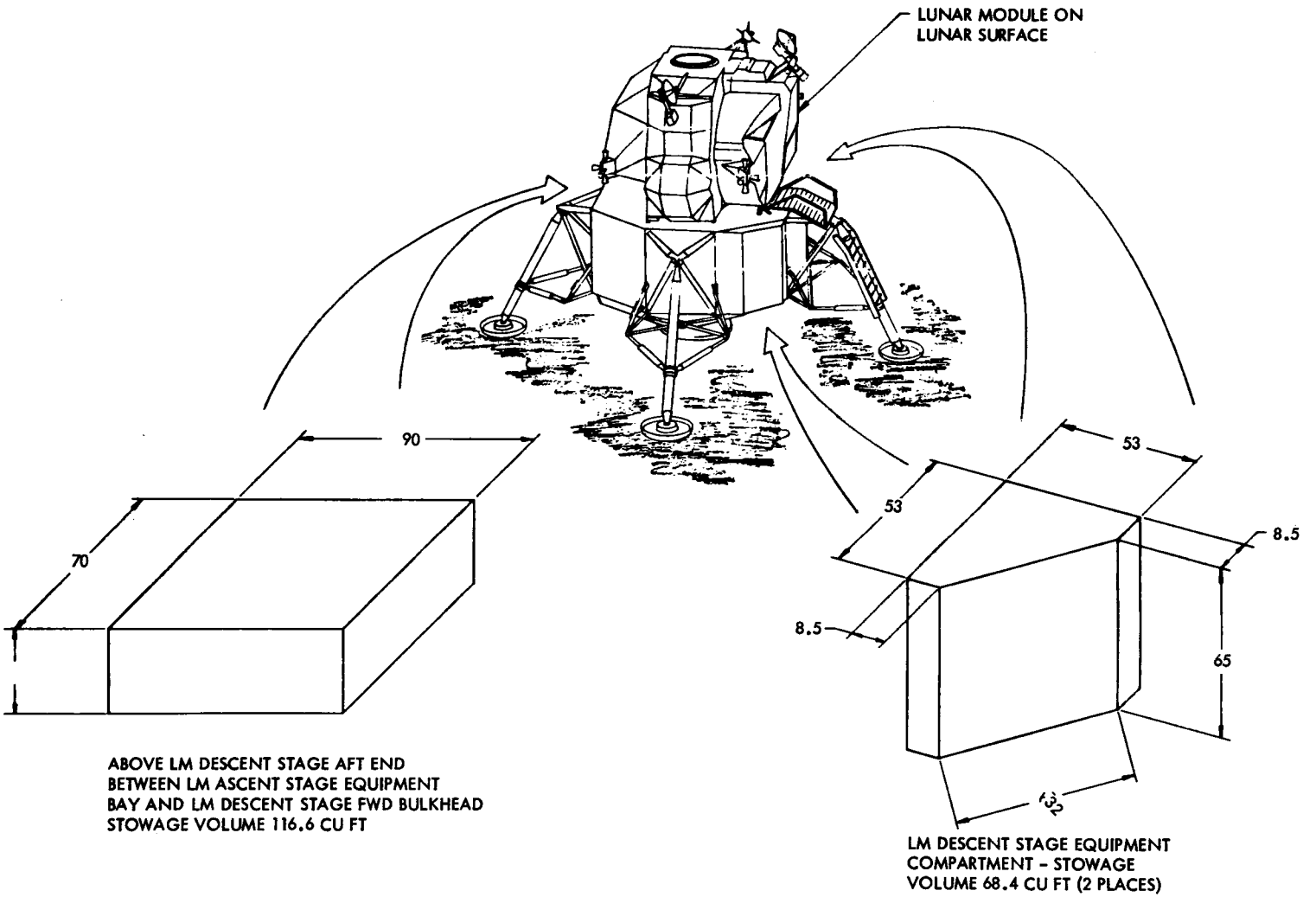

LUNAR MODULE STOWAGE PROVISIONS

Figure 3-45. Available Lunar Module Stowage Areas (Sheet 1 of 2)

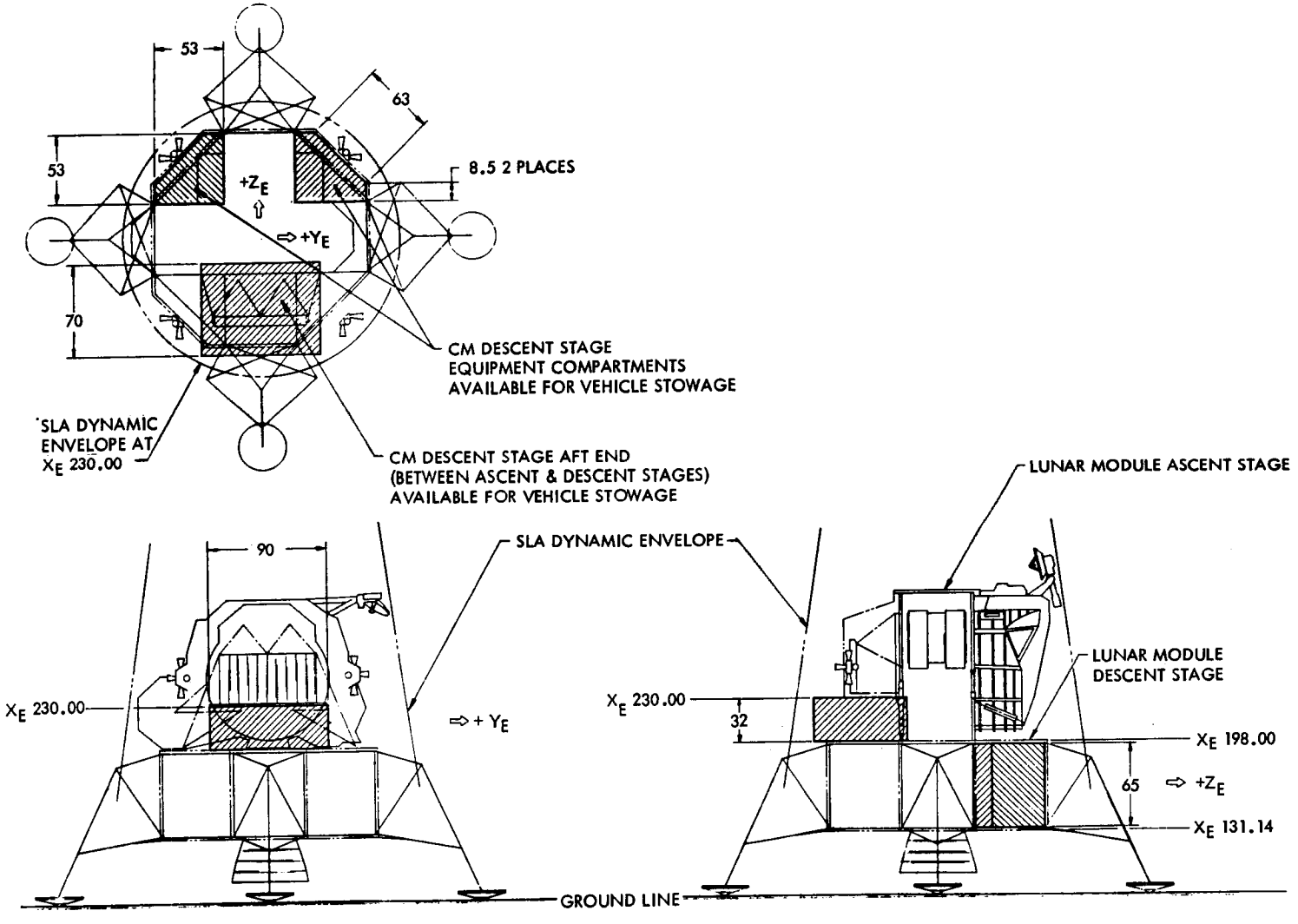

LUNAR MODULE DELIVERY VEHICLE CONFIGURATION

Figure 3-45. Available Lunar Module Stowage Areas (Sheet 2 of 2)

Redevelopment of the spacesuit-to-umbilical connector to permit coupling in vacuum appears very desirable as a safety improvement both for the LESS and other potential missions.

Three areas which warrant considerable effort in future studies or related research are: balance and center of gravity control methods refinement to require a minimum of astronaut time and effort; vehicle design for stowage on LM with reduced amount of equipment folding; research on improved locations for stowage on LM/ELM; and research into the collapsible tank concept to prove feasibility for this and other applications.

Surface Operations

Objective. - The unloading, setup and servicing of the LESS are critical to the feasibility and practicality of the emergency vehicle concept. Unless the LESS can be unloaded, assembled, fueled, aligned/balanced, checked out and launched within a relatively short period of time and without fatiguing the crew, the vehicle may not serve its intended purpose. Part of the surface operations can be performed before an emergency occurs when time will not be as critical and crew workload can be spread over a longer period. The objective of this effort was to examine these operations to determine their requirements in terms of time, effort, and equipment.

Approach. - The approach taken in the analysis of surface operations involves study of the LM vehicle, constraints dictated by astronaut capabilities, and suit restrictions. Surface operations analysis relied heavily on past Space Division contract and research studies; in particular, the recently completed Lunar Flying Vehicle Study where similar problems of deployment, setup, checkout, and servicing were studied.

Several assumptions must be made which influence the analysis of surface operations:

1. The carrier vehicle is the LM or extended LM with configuration of the present LM.
2. The backpacks can be fully recharged shortly before launch.
3. The LM ascent stage propellants are available for transfer and the drain ports have not been uncovered by overturning the LM.
4. Unloading and servicing of the LESS must be accomplished by one man.
5. Changes to the LM vehicle to accommodate LESS stowage or servicing will be minimal.
6. No pyrotechnic devices will be used for LESS release, deployment, or separation.

Operational tasks and timeline estimates. - Table 3-22 shows the general sequence of surface operations and an estimate of the time required. Considerable time is involved both before and after a decision has been reached to use the LESS. During future studies, effort should concentrate on reduction of these tasks and time required particularly that required after the decision to use LESS.

Guidance and control system preparation and alignment. - The launch preparation required for the G&C system involves system assembly, the updating of ascent guidance targeting variables, and alignment of gyro attitude reference systems, if used. Very little G&C system assembly is anticipated, with the possible exception of such components as gyros which may require storage in a tightly controlled temperature environment.

The ascent phase targeting parameters which will probably require updating to the specific conditions existing at the time of launch include the following:

1. Launch time - set into clock

2. ΔV meter settings

3. Pitch profile parameters - note or adjust parameters such as angles of pitch profile steps and step change ΔV values

4. Visual attitude reference parameters - note or adjust to proper sun angle, note memorize landmark to be tracked, etc.

As discussed elsewhere in the report, these targeting parameters are all computed at the Mission Control Center at Houston, and voice-linked to the crewmen. The data will be recorded as is presently done in the Apollo program as a backup to the on-board guidance computer solutions.

Attitude reference system alignment. - Several methods of aligning the gyro attitude reference before launch have been considered. The alignment methods can be classified into two broad groups: those in which attitude is completely determined from optical sightings of external references, and those methods which employ leveling of the entire vehicle or attitude reference system (ARS) alignment unit, and determine only azimuth from an external reference. A third method not belonging to either group which was considered is to initialize the ARS on the LM navigation base, utilizing star

TABLE 3-22. LESS DEPLOYMENT/PREPARATION PROCEDURE

Item	Time Estimate (min)
1. Remove protective cover, place beneath vehicle	2
2. Release deployment mechanism	1
3. Unlatch lower attach points	1
4. Swing out, rotating around top supports	2
5. Snap out legs and tanks, check to insure that locks are in place	3
6. Release upper attach points	1
7. Lower to surface and detach cables	4
8. Drag to take-off area 30 to 40 ft from LM in LM shadow	5
9. Level vehicle by leg screw jack adjustment	5
10. Obtain thermal protection blanket from stowage	5
11. Obtain propellant lines from storage and deploy. remove dust cover and attach to LESS fill fittings place LM ends in retainers near LMA drain fittings	7 10
12. Activate LESS battery and check condition on indicator	2
13. Check condition of vehicle subsystems and helium pressure	2
14. Remove battery and stow in LM vehicle	2
15. Deploy insulation cover over vehicle and activate sublimator coding	3
(This concludes normal procedure - steps 16 and subsequent steps are necessary only upon LM problems and decision to use LESS)	Total time this phase 45
16. Connect fuel lines to LM drain connector	2
17. Pressurize LM tanks	3

TABLE 3-22. LESS DEPLOYMENT/PREPARATION PROCEDURE – Continued

	Item	Time Estimate (min)
18.	Open fuel drain valve, fill tanks (LESS tanks will expand with pressure)	5
19.	Watch vent sight glass and close drain valve when liquid is observed	2
20.	Wait 15 seconds, then again open fuel drain valve. Close when liquid is observed in sight glass	2
21.	Repeat step 19	2
22.	Disconnect fuel line at LESS connection and carry fuel line end 15 to 20 feet away from LESS	3
23.	Connect oxidizer line to LM Ox. drain connector	2
24.	Open oxidizer drain valve, fill tanks (LESS tanks will expand with pressure)	5
25.	Watch sight glass and close drain valve when liquid is observed	2
26.	Wait 15 seconds, then again open oxidizer drain valve. Close when liquid is observed in sight glass	2
27.	Repeat step 25	2
28.	Disconnect oxidizer line at LESS connection and carry away from LESS vehicle	3
29.	Activate guidance and control systems and align in accordance with latest data	10
30.	Set launch timer in accordance with earth control data	3
31.	Recharge PLSS from LM supplies and wait in LM until 15 minutes before launch time	45
32.	Egress from LM and board LESS vehicle , attach crew restraints 10 minutes prior to launch time	15
33.	Pressurize LESS tanks	3
34.	Activate all systems, check status and condition	3
35.	Update timer and guidance systems	3

TABLE 3-22. LESS DEPLOYMENT/PREPARATION PROCEDURE - Continued

Item	Time Estimate (min)
36. If all systems are "go" launch at time "0" or on ground command	3
	Total time this phase 120
37. In case vehicle systems operational difficulty results in delay and missed launch opportunity, correct problem, then reenter LM, recharge PLSS and await next launch opportunity.	

sightings with the LM alignment telescope and the LM computer to determine the navigation base attitude, and then physically transferring the gyro package and strapdown attitude computer, while operating, to the LESS.

External attitude references which might be used are the sun, earth, known stars, the orbiting CSM using either radar or optical tracking, and distinguishable features of the lunar surface or sighting targets set out a few hundred feet from the LESS. The directions to surface sighting targets (man-made or natural lunar surface features) must be determined after LESS deployment from sightings of the targets and known celestial bodies.

The advantages and disadvantages of the three alignment techniques mentioned above are summarized in Table 3-23. Any of the methods can give more than adequate alignment accuracy for the LESS. However, method II (leveling, with azimuth only from an external reference) is judged to be the simplest alignment procedure, and is therefore preferred.

Leveling of the azimuth optical sight base on the vehicle would be accomplished with bubble levels, probably a spheroidal two axis level. Leveling accuracy comparable to that obtained with a surveying transit, 0.1 degree or better, should be achievable. The potential gravity direction error due to lunar mascons is estimated to be one milliradian or less since the largest gravity anomalies on Earth are a few tenths of a milliradian.

TABLE 3-23. COMPARISON OF ATTITUDE ALIGNMENT METHODS

Complete Attitude Determination from External References
Requires optical telescope or gunsight, compatible with helmet faceplate, and with elevation and azimuth angle resolvers. Requires two optical sightings and computations to determine vehicle attitude. Computations could be performed by ground control center using the LM voice link. Does not require leveling vehicle or alignment telescope base.
Azimuth Measurement from External Reference, and Leveling
Requires leveling vehicle, or adjustable telescope base with pitch and roll angle resolvers. Requires telescope or azimuth only gunsight, compatible with helmet faceplate, and azimuth angle resolver. Requires computation or knowledge of external reference azimuth. Direction cosine matrix of ARS in launch attitude easily obtained by sending delta attitude pulse trains to the measured azimuth and equivalent tilt angles to the ARS attitude DDA. No special computations required for attitude initialization.
Alignment by LM G&N SYSTEM
Requires LM G&N system, or several portions thereof, operative. Requires modification of LM navigation base to mount ARS gyro package and probably addition to LM computer I/O section for interface with ARS. Requires transport of ARS gyro package with portable power supply from LM to LESS vehicle, and connection with other LESS systems. No alignment equipment required on LESS.

Lateral accelerometers mounted on the ARS gyro package could be used to determine the gyro package tilt angles directly, in place of angle resolvers on the telescope base tilt mechanism. The use of accelerometers is excessively complex unless they are required for some other system such as an inertial autonavigator.

The external azimuth reference remains to be chosen. The characteristics of various techniques for azimuth determination are compared in Table 3-24. A variation of method 1 (radar tracking of the CSM) which was briefly considered is to acquire the CSM after lift-off. However, the radar is excessively complex unless it is required primarily for some other function such as LESS-active rendezvous.

From the comparisons of Table 3-24, method 6 (sightings on a precalibrated surface target) is considered to be the preferred method. Decisive factors were the relative ease of sighting and the elimination of the requirement for real time computation of the reference azimuth. If earthshine does not provide sufficient visibility at night, a star sighting can be done.

TABLE 3-24. AZIMUTH SIGHTING TARGET CHARACTERISTICS

I. Rendezvous Radar Tracking of Orbiting CSM.
Rendezvous radar might otherwise not be required.
CSM only 2 degree-4 degree above horizon at lift-off--may not be visible and quick alignment required.
Possible ground clutter from side lobes.
May have significant boresighting errors.
Would require accurate leveling of vehicle.
Provides check of CSM downrange position before launch and maintains knowledge of position during ascent.
II. Optical Sighting of Orbiting CSM.
Same visibility problem as with radar.
Uncertain detection and acquisition capabilities.
Quick alignment required to launch in time.

TABLE 3-24. AZIMUTH SIGHTING TARGET CHARACTERISTICS - Continued

III. Sun Sighting
Sighting should be conducted at low sun angles since azimuth data is not available with sun near high noon. Requires light filter. Somewhat less accurate than sighting on point target.
IV. Earth Sighting
Unsuitable for azimuth determination at small longitudes. Always in view. Large apparent diameter (1.9 degree) might degrade sighting accuracy.
V. Sighting on Known Star
Difficult during daylight with helmet on. Requires star recognition. Probably best sighting accuracy.
VI. Sighting on Precalibrated Surface Target
Easy during daylight, can probably be done at night from earthshine. Requires prior azimuth determination from sun, star or earth sighting. Azimuth angle does not vary with time; hence, target launch plane azimuth angle can be precomputed.

Predetermination of the surface target azimuth from the LESS could be done by a star, sun or earth sighting, and could be done with the LESS alignment telescope or with the LM alignment optical telescope (AOT). Using the

LM AOT would permit daylight star sightings for the surface target azimuth determination with much less severe sighting problems than with the LESS azimuth alignment sight. However, the displacement of the LESS from the LM would introduce a parallax error which would be difficult to determine and compensate for precisely. Since LM landings will be accomplished in daylight near the terminator, a good azimuth reference will be obtainable from a sun sighting immediately after LESS deployment. Hence, a sun sighting is the preferred method of determining the surface target azimuth.

The azimuth sighting instrument can be essentially a gunsight. While a more sophisticated system which presented a collimated image at the cross hairs to the astronaut might allow slightly better alignment accuracy, a simple gunsight type instrument should permit alignment accuracies on the order of 0.1 degree, which is adequate. For the initial sun sighting to determine the surface target azimuth, an auxiliary ring on the rear sight and a removeable light filter incorporating a ring having the apparent diameter of the sun for the front sight would be adequate. The overall sighting system would thus be simple and light.

In summary, the preferred concept for ARS alignment is an azimuth, sighting of a precalibrated surface target with a simple gunsight type of instrument mounted on a level base. The base would be leveled with bubble levels. The surface target azimuth from the LESS would be determined after LESS deployment by sun and target sightings. Alternately, if the surface target could not be sufficiently well seen by earthshine at night, a star sighting could be taken for azimuth alignment with LM or earth-based computation of the star-launch plane offset. The gyro package tilt angles would be determined either from angle resolvers on the tilt mechanism for the levelled sighting instrument base, with respect to launch site local level and the desired launch azimuth.

Unloading and deployment. - Several concepts have been considered for removal of the LESS from the LM. In each method, the first step is the removal of a protective cover which is held in place by pins which are released by the pulling of a single lanyard. The cover will have a handle molded in for ease of handling by one man. The cover will be extremely light but awkward to handle. This cover will be placed on the surface under the vehicle and utilized as a sled to move the vehicle to the launch area and then used as a takeoff pad to prevent dust and rocks from being kicked up by the engine exhaust at takeoff. Figures 3-46 and 3-47 show two of the possible methods for lowering the LESS to the surface. The first is a system of cables and pulleys arranged to first lower the vehicle to a horizontal position with a stop while the legs are snapped in place then dropped to the surface and the cables detached. Figure 3-48 shows a boom concept which reduces

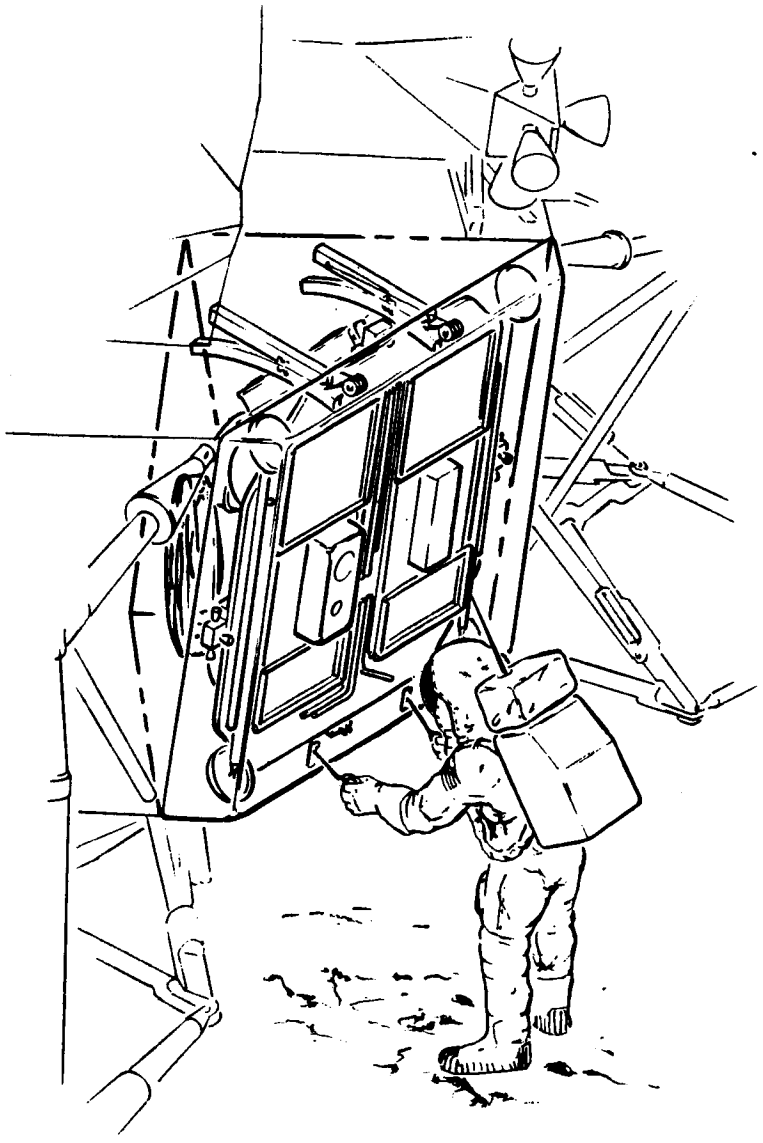

Figure 3-46. - LESS Unloading Concept

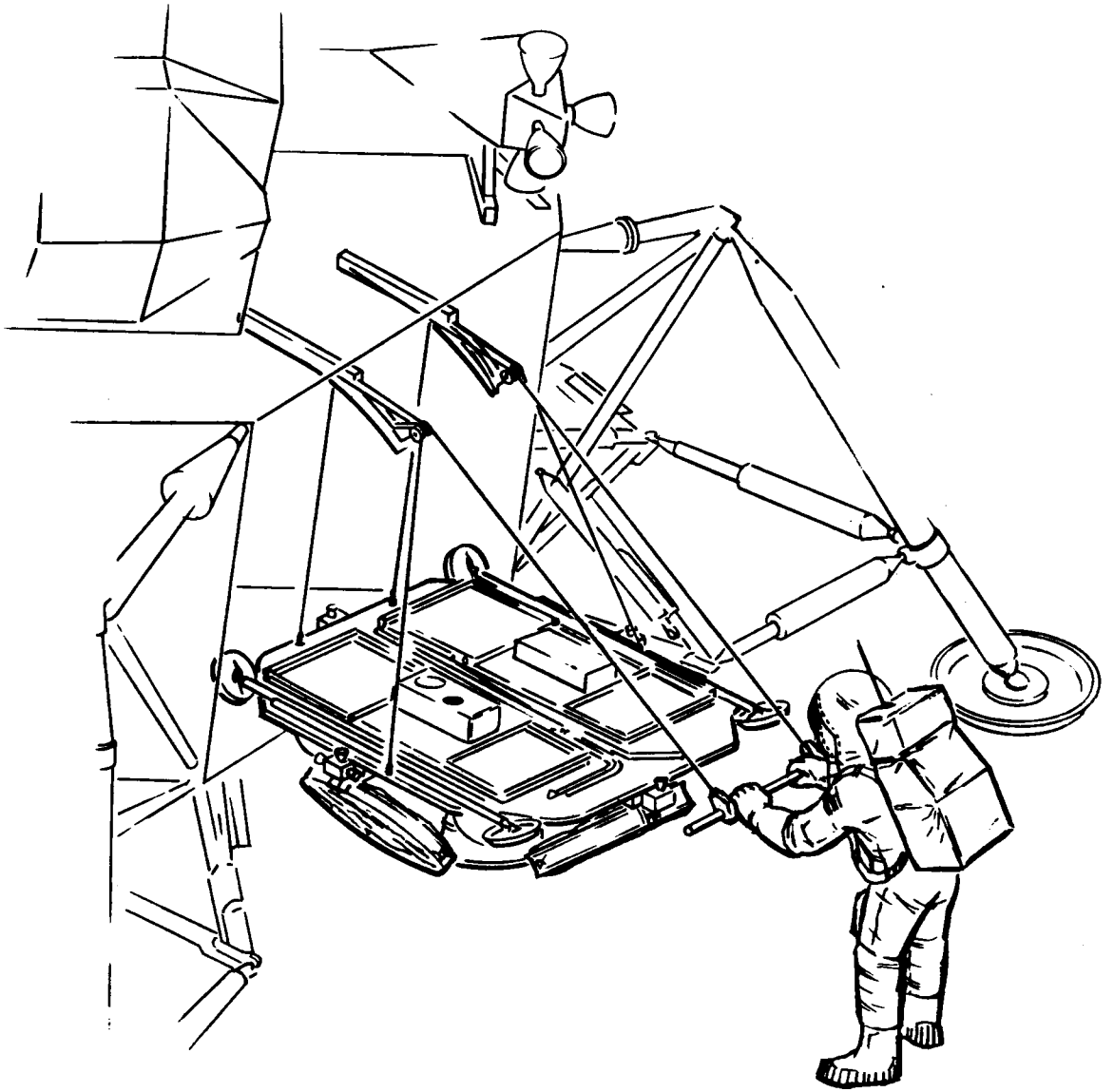

Figure 3-47. - Lowering LESS to Lunar Surface Concept

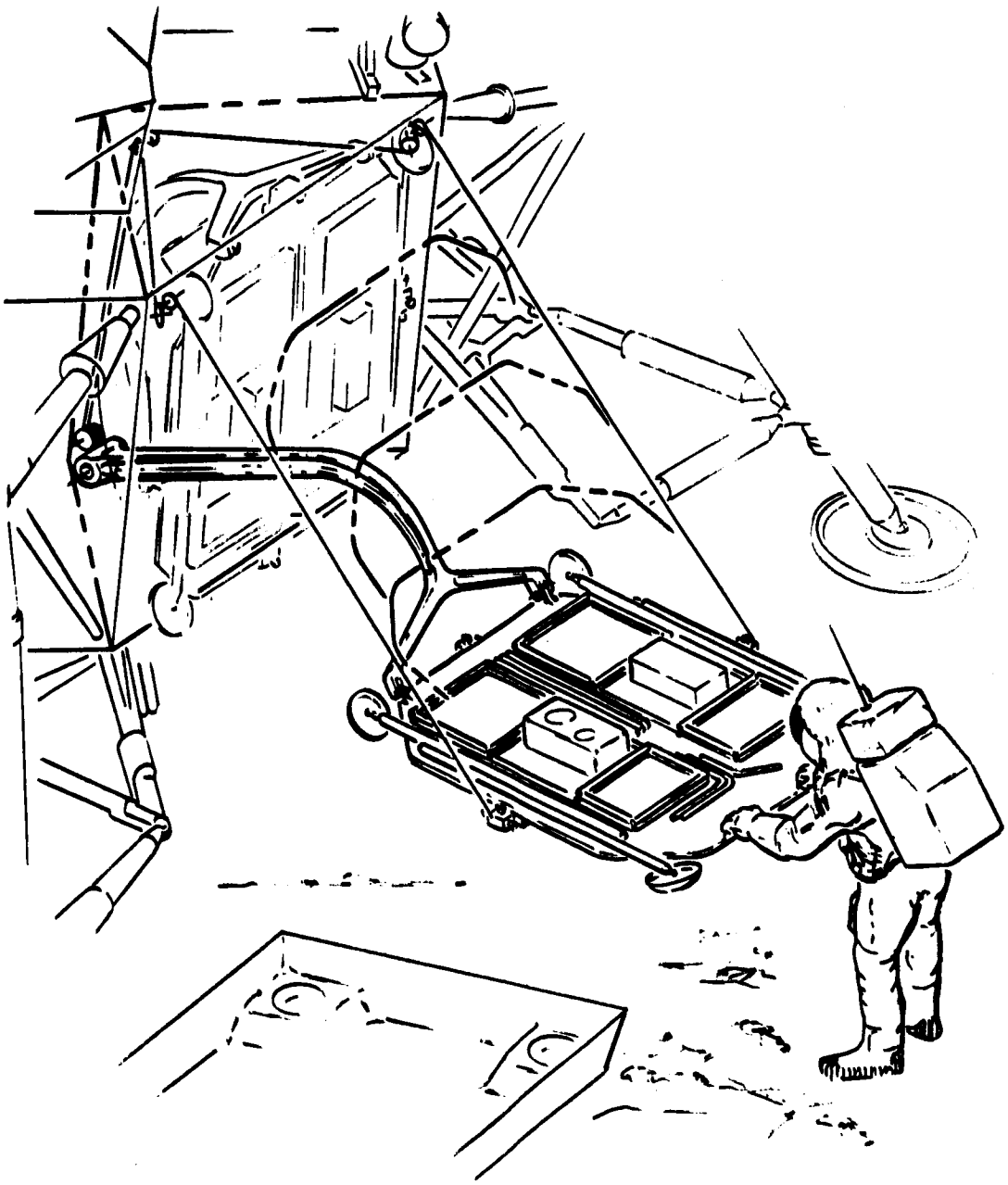

Figure 3-48. - LESS Boom Deployment Concept

the complexity, lessens the chance of cables becoming snagged, is simpler for the astronaut to operate and provides a more positive stop for leg deployment. During the LFV study another method resulted from a study of several alternatives. Although the vehicle is different, this concept (fig. 3-49) is a possibility for the LESS vehicle.

Propellant transfer. - Figure 3-4 illustrates the propellant servicing of the LESS vehicle and lunar module modifications required. The configuration represents an escape-to-orbit mission rather than a surface flyer mission: the propellant source is the LM ascent stage rather than the descent stage. As would be expected, changes are required in the ascent stage plumbing, but these are minimal, and the additional hardware required is existing Apollo with no advance in the present technology. Considerable analysis of lunar surface fueling and transfer of propellants from the LM during the recent LFV study. This LFV fueling data has been utilized and adopted to the LESS.

The LM ascent stage has fill and drain fittings located forward and outboard of the oxygen tank (+ Z, + Y) and aft and outboard of the fuel tank (- Z, - Y) at approximately the separation plane X = 200. Without modifying the lunar module, these locations would be difficult to utilize on the lunar surface by a suited astronaut; the fittings are buried under the ascent stage tank structure and are in close proximity to the descent stage upper structure. The astronaut would also have difficulty reaching the area of the fittings. He would have to ascend the boarding ladder on the + Z leg, walk along the upper-outboard edge of the descent stage (climb over the landing gear to reach the fuel tank fitting), then connect the fittings which would now be located around his feet; obviously, this procedure is unworkable. If ladders were added to the + Y and - Y legs, he could ascend these ladders to a convenient height to connect the fittings. This procedure has the disadvantage in the additional weight involved and the connectors would still be somewhat buried and difficult to manipulate by a suited astronaut.

Consideration of the above difficulties led to the concept illustrated: adding additional drain lines and connectors to the "porch" area which can be serviced from the present boarding ladder. The drain line extensions would be connected to the present drain lines, near the tank sumps then routed as illustrated in View D-d (This routing avoids piercing any pressurized structure and would have minimal impact on the LM). In addition to the two lines, the only additional hardware are the two couplings and coupling attach bracket. These couplings are presently used in the Apollo as the fill couplings for the service module RCS system. They are the male-half, or flight-half, and have the part number ME 273-0021 class 1 for the fuel fitting and ME 273-0019 class 1 for the oxidizer fitting.

The two propellant lines between the LM and LESS are flexible, insulated, and would be between 0.5 and 0.75 in inner diameter. A female-half fitting from the Apollo RCS is attached to each end (ME 273-0021 class 2 for the fuel line and ME 273-0019 class 2 for the oxidizer line) and a pressure gauge is also included at the LESS end. The length of line would be dictated by LESS take-off safety clearance. The 40 feet of spacing illustrated provides approximately 20 feet of vehicle clearance. This is about 50 percent of that provided in the Phase B Lunar Flying Vehicle Study (NAS 9-9045) just concluded by NR, but in the LFV study, endangering the LFV astronauts on both multiple take-offs and landings and damage to the LM by rocks from the LFV engine plume had to be considered. Since it is desirable to minimize the line length, and the LFV study represents a conservative maximum, it is felt that the value selected is a good compromise.

Each of the four tanks on the LESS vehicle has provisions for filling and overflow. The overflow or vent line consists of the female coupling (ME 273-0011 class 2 for the fuel tanks and ME 273-0024 class 2 for the oxidizer tanks), sight-glass, overflow orifice and five feet of line. This assembly enables the astronaut to know when the tank is full (when he observes fluid flowing) and vents the propellants away from his person.

A typical fueling operation would be to remove the oxidizer fill and vent lines from the LESS protective shroud and attach the LESS couplings, securing the vent line and closing both valves. The astronaut would now walk to the LM, ascend the ladder, attach the LM coupling, and secure the line to the porch and open the LM valve. He would then return to the LESS, open the vent line valve, then the fill line valve and adjust each while observing the line pressure. The astronaut will continue to monitor the pressure gauge and overflow sight-glass until fluid flow is observed (the tank is now filled except for the ullage cavity); he will now close both valves. The vent line is removed from the first tank and attached to the second tank as is the fill line (the couplings onboard the LESS will close when the female half is removed). He will then open the two valves and fill the second tank as before. After completion of the oxidizer transfer, the two lines are removed from the proximity of the LM and LESS and the fuel transfer is completed identically to that outlined for the oxidizer system. After removing the fuel fill and vent lines from the LESS, the astronaut will open the helium valves to pressurize the four tanks and the LESS fueling operation is complete.

It should be noted that the above system was one of many studied during the LFV Study and selected as the recommended concept for the Phase B study. The only differences are the source, LM ascent stage instead of the descent stage, and filling two tanks each instead of one. This fueling procedure would suffice for single tanks or multiple tanks with a parallel feed system to the engine. On multiple tanks with a series feed, a single fill point is utilized; the sump tanks is filled first and when filled the tank overflows into the storage

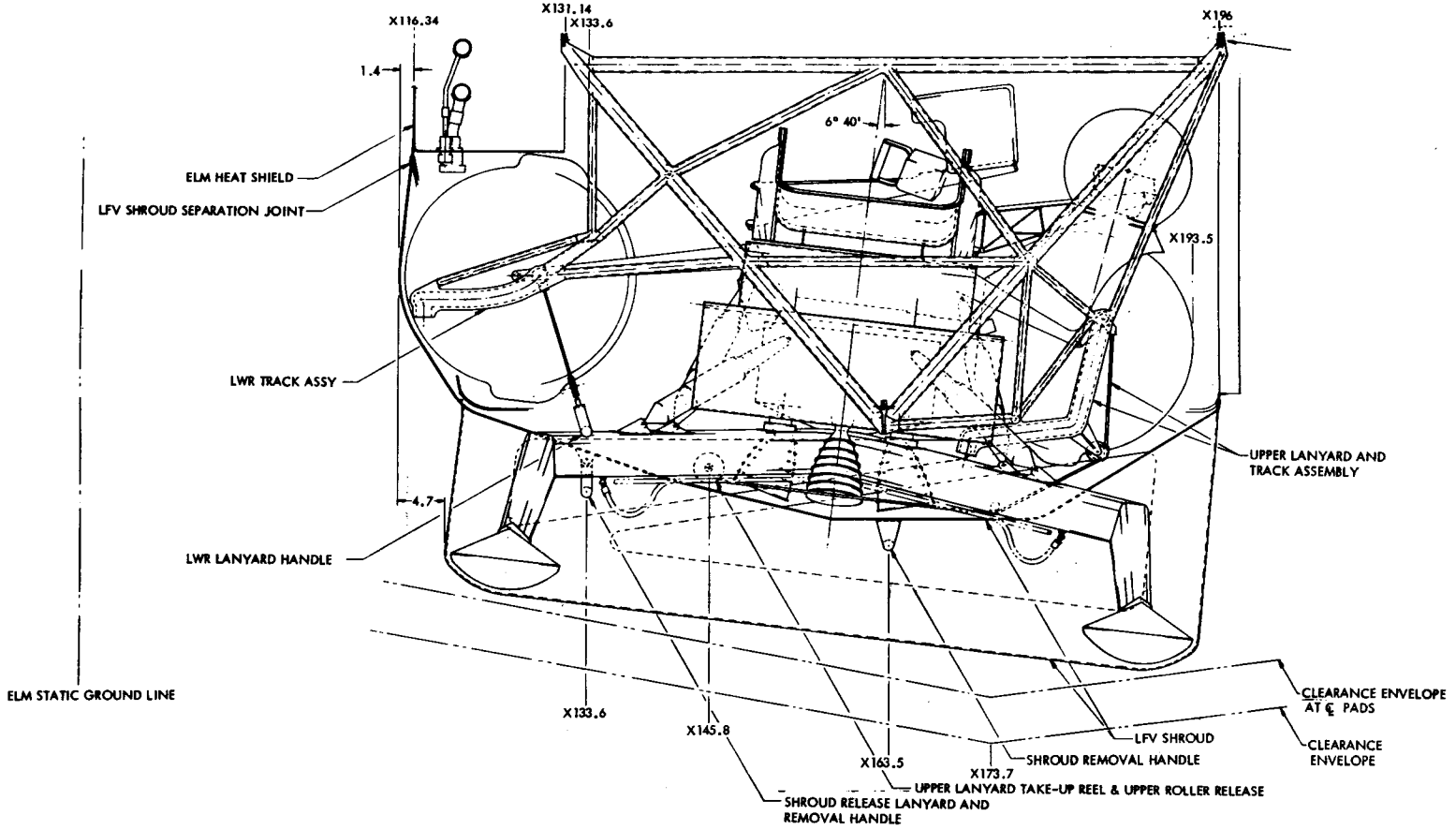

Figure 3-49. LESS Stowage in Lunar Module (Sheet 1 of 2)

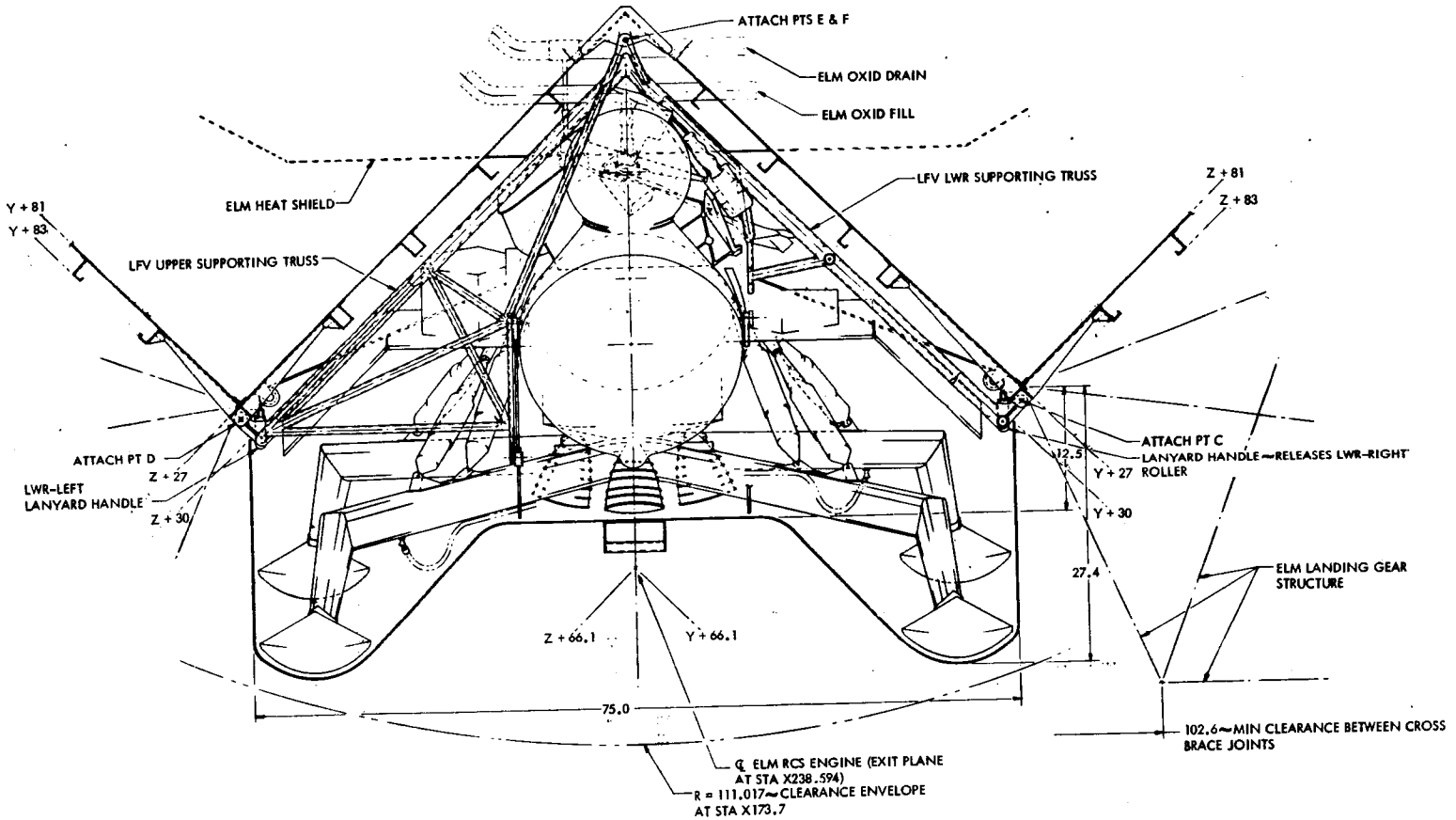

Figure 3-49. LESS Stowage in Lunar Module (Sheet 2 of 2)

tank filling each storage tank in series. This is the system employed by the Apollo service module main propulsion engine and was examined for use in the LESS study and LFV study for four-tank configurations. NR's experience from the Apollo fueling suggested that the series feed approach should not be recommended for lunar surface operations. One problem is the ability to trap the correct amount of ullage gas in the sump tank prior to propellant transfer. This has been a problem on the Apollo service module and prolongs the fueling operation even with the extensive fueling facilities available at the launch site. The problems would be worse on the lunar surface with the decrease in the gravity force and minimal facilities. The series feed concept introduces a second problem, the shifting center of gravity and inertia as the propellant is being consumed.

The parallel feed system is not without fault, particularly in the ability to drain simultaneously from the two tanks; should one tank drain out first ullage gas would be fed into the engine, causing a premature shutdown. This can be avoided by proper design of the manifold system, bubble screens at the tank outlet and perhaps by the use of valves.

It is assumed that the propellant transferring head would be the helium pressure within the LM ascent stage. Should this not be available a pump could be installed in the two transfer lines. These pumps need not be large and would be battery powered, but the fueling transfer would be prolonged. An alternate backup would be lunar gravity. However, only seven feet of head, equivalent to 14 inches on Earth, is available which would require large diameter lines introducing weight and stowage problems. Also, should the LM be tilted, additional problems are introduced.

Servicing equipment. - Several pieces of servicing equipment which will be required have been identified. This equipment will add to the Apollo-LM load but is not shown as LESS weight since it will be left on the lunar surface. This equipment is shown in table 3-25. The weights shown are only estimates since the detail design of this equipment obviously is not complete.

Astronaut capabilities, protection, and safety. - Of primary importance during the LESS surface operations is the protection and safety of the astronauts and the design of equipment requiring effort and dexterity well within their capabilities and the space suit/backpack metabolic heat removal limits. This requires a careful analysis since the more automated methods require more complicated, costly, and heavy equipment. With the rather simple surface operations equipment suggested as one alternative, the weight of equipment added to the LM load is over 120 lb. This, together with the LESS vehicle weight of approximately 350 lb, represents a sizable reduction in the payload available for experiments, lunar mobility, or staytime extension shelter and expendables.

TABLE 3-25. LESS GSE REQUIREMENTS AND WEIGHTS

Component	Weight (lb)
LM stowage boom, cables, latches, pulleys, etc.	20
LM stowage cover/takeoff pad	8
LM propellant drain line extensions (2 - 5 lb ea)	10
LM half transfer quick disconnects (2 - 2 lb ea)	4
LM emergency transfer pumps (2 - 10 lb ea)	20
LM valves and miscellaneous	5
Fuel and oxidizer lines (insulated) with valves (2 - 50 feet)	20
Propellant line quick disconnect fittings (4 - 2 lb ea)	8
Boarding ladder (1 - 2 step)	4
Vent line extension (12 feet)	3
Takeoff stand or legs	18
Guidance alignment targets	5
	125

Equipment design is limited by considerations for astronaut safety which prevent his having to get under the LESS during deployment to unfold legs or to release lines. A positive stop must be designed so that accidental release is not possible while takeoff legs are being unfolded or the stand being put in place. Another safety consideration is the prevention of propellant spillage on the astronauts during the transfer/filling operation. Any spillage of Aerozine-50 on the PGA could result in fire when the crewman enters the LM and is exposed to an oxygen rich environment and is also highly toxic. Kennedy Space Center personnel indicate that making and breaking Apollo-type hypergolic connectors periodically result in some fuel or oxidizer spillage which would be more likely to occur with the absence of a line purge capability. These disconnects were developed and qualified to produce essentially no leakage during operation.

More development to prevent leakage or other equipment to protect the astronaut from spray or accidental spillage may be necessary. A possible solution is to provide the PGA-attired astronaut with a fuel handler's overgarment during the fueling operation which is then discarded and left on the lunar surface. Fuel contamination could still occur with poor doffing procedures and such a garment would significantly effect already existing marginal biomechanical abilities and mobility.

Conclusions - surface operations. - Preliminary deployment of LESS upon LM/ELM landing will take approximately 45 minutes. Upon need for abort with LESS, another two hours will be required for servicing and checkout. Considerable analysis and design of the LM stowage, deployment, and servicing are warranted by the importance this has to the success of the mission and practicality of the LESS concept, preparation workloads and time required.

Servicing provisions for the LESS will require only minor LM drain system plumbing changes and the addition of propellant quick disconnect and valves.

Long-Range Lunar Surface Flying Vehicle Application

Objective. - The objectives of this analysis were to determine the feasibility of using the basic LESS configuration as a long range lunar surface flying vehicle, to establish the performance capability, and to compare the structural and system differences. An additional part of this study was to analyze the effects of conversion to a long-range flying vehicle on the capability to perform the basic LESS escape mission.

Approach. - The approach to this effort was to determine flying vehicle requirements from the LFV study results and convert a representative LESS configuration to a LESS/long range flyer (LESS/LRF) by structural modifications and the addition of equipment as dictated by lunar flying vehicle (LFV) requirements. Flying vehicle requirements were taken from the very recent Phase B LFV Study, and other related lunar studies, in-house simulator, and tethered flight test results. A weight estimate was compiled for the LESS/LRF and performance computed based on the range of propellant quantities required for the escape mission.

The basic specifications for a lunar flying vehicle from the LFV study were utilized as the most appropriate and up-to-date available:

1. Landing criteria of 20 degrees tip-over safety margin, 7 fps vertical and 2 fps horizontal velocities, three degrees per second attitude

rate, ±10 degrees initial vehicle attitude, ±10 degrees ground slope, 4 g's maximum lateral and 8 g's maximum vertical deceleration, hard-surface landing, no-slide condition and 12-inch engine nozzle ground clearance.

2. Astronaut to fly vehicle in sitting position.

3. Payloads up to 380 pounds considered (additional astronaut or scientific equipment). Cargo location adjusted for vehicle balance, but pilot can translate up to 12 1/2 inches to balance single payloads.

4. One-man unloading from LM, deployment, fueling, checkout, loading and flying.

5. Four-gear, integral leg-frame, eight-attenuator with omni-landing capability.

6. Stability-augmented control, engine gimbaled for pitch and roll control with thrusters for yaw control.

Configurations and design concepts. - The configuration of a flying vehicle will depend on the selection of an approach from several basic alternatives: design of an LFV with no influence from the LESS vehicle or mission; design of a LRF (long range flyer) starting with and adapting a LESS vehicle configuration, but not the LESS mission requirements (fig. 3-6 resulted from this approach); design for both the LESS and LFV missions interchangeably, and design of an LFV and then adopt the design to the LFV mission (fig. 3-50, from the LFV study).

The approach taken in this study was to take the typical LESS configuration (fig. 3-3), and convert this vehicle with minimum changes to perform the long range flyer mission. This resulted in the configuration illustrated by figures 3-6 and 3-51. The capability of this vehicle to perform the LESS mission, the equipment removals and/or additions, and penalties to the LESS mission vehicle design were examined briefly.

The structural concept shown in fig. 3-6 is similar to that selected for the LFV study: standard aerospace structure with heavy use of skin-stringer concepts. The vehicle consists of two basic sections, attenuated and non-attenuated, and connected by the eight attenuators. The payload, astronauts and all vehicle components are attenuated with the exception of the engine assembly; the engine and gimbal actuators are attached through Lord shock-mounts to the cruciform leg-frame. The upper structure consists of 3 1/2-inch-deep beams stabilized by the cargo deck skin. The beams pick up the eight upper attenuator attach points, eight tank support arms, pilot's seat

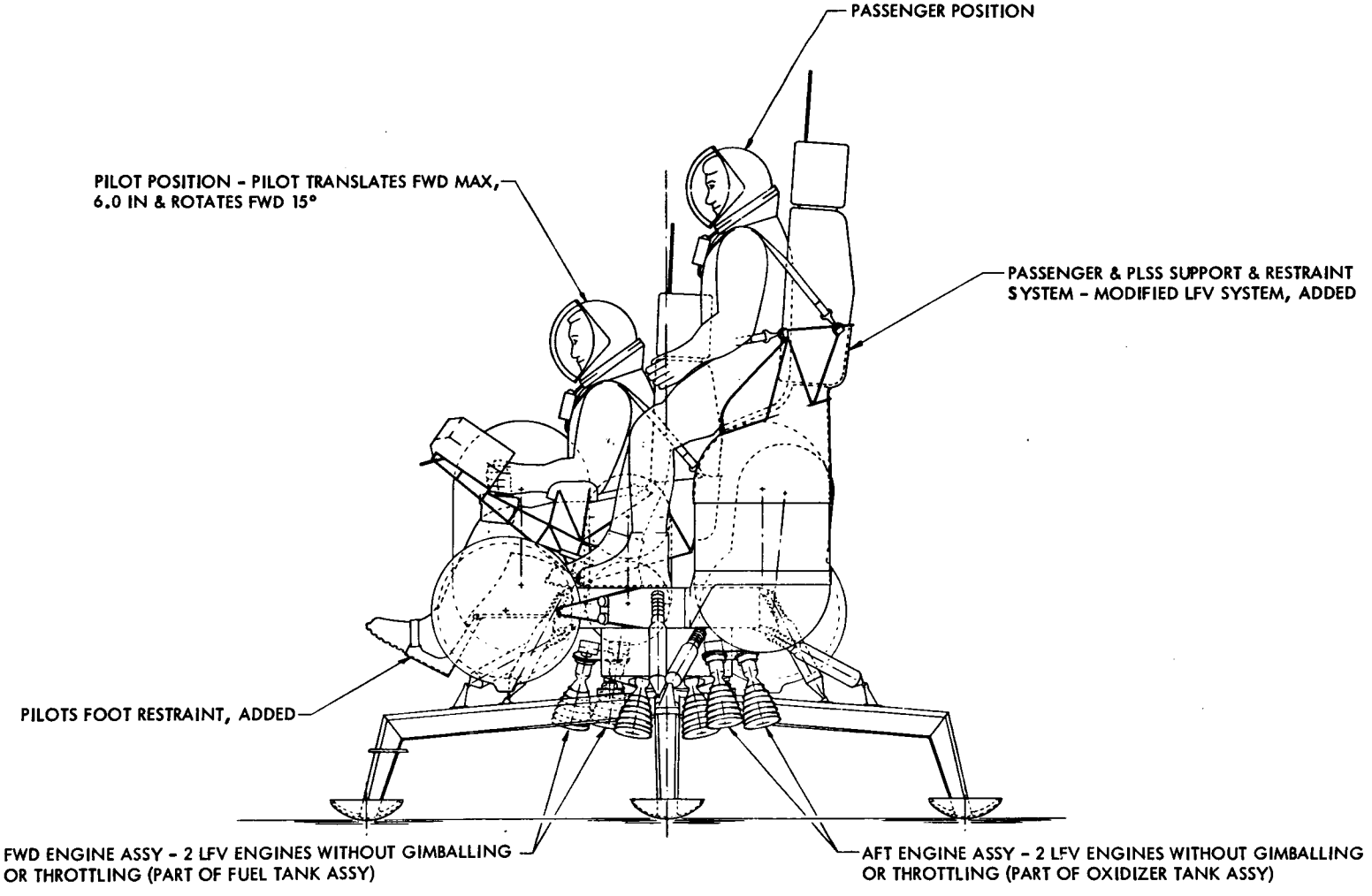

Figure 3-50. Lunar Flying Vehicle Modified for LESS Missions
(Sheet 1 of 2)

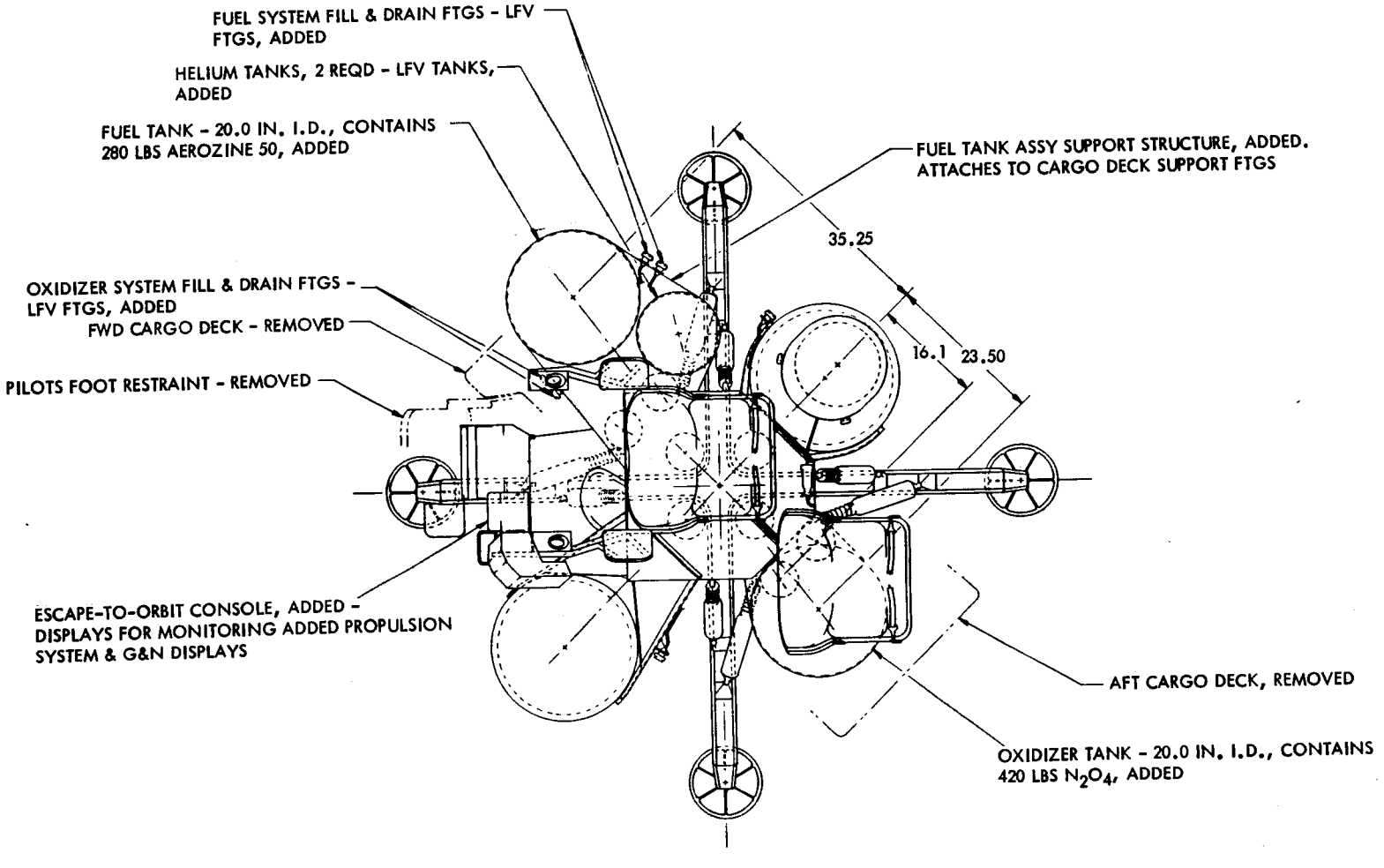

Figure 3-50. Lunar Flying Vehicle Modified for LESS Missions
(Sheet 2 of 2)

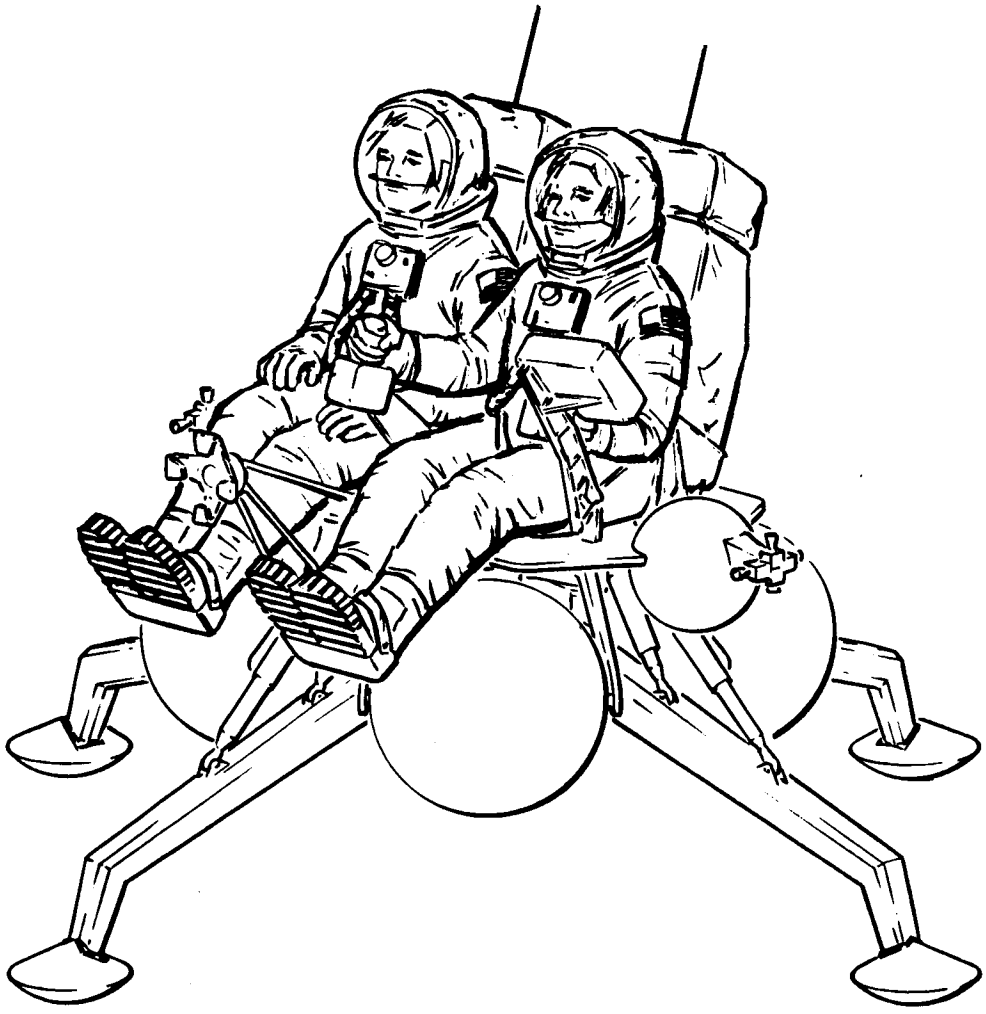

Figure 3-51. - LESS/Long Range Flyer Concept

tracks and the uniformly distributed loads imposed by the cargo. The cruciform leg-frame is composed of two upper caps and the lower cap; these are connected by three skin sections to form a triangular section. The section depth and width and cap areas increase toward the center as the landing bending loads increase. The landing pads are an integrally stiffened section, rigidly attached to the end of the leg-frame.

Many structural approaches were investigated on the Phase B LFV study. The forcing considerations were landing criteria and loads, engine quantity, arrangement and gimbal pattern, propellant tank quantity, arrangement and geometry, and pilot position. Upper structural assemblies of platform-truss, pure truss and skin-stringer were investigated and evaluated against vehicle weight, stowage envelope, ease of deployment and manufacturing costs. Similar considerations and evaluations were performed on the landing gear members. In platform concepts it was difficult to obtain sufficient bending stiffness within the weight limit. The pure truss concepts were attractive from weight considerations but were bulky, which produced problems in LM stowage and attenuation clearances. The truss concepts were considered before investigating the integral leg-frame, when the attenuation was being performed at the landing pads. The truss concepts are most incompatible with the integral leg-frames.

The integral leg-frame was developed as a means of decreasing the required maximum attenuation stroking. For a given velocity and landing attitude, the attenuator spring rate is determined by a minimum weight vehicle (one astronaut, no payload and no propellant, for 840 pounds), the maximum allowable deceleration (8 g's) and the vehicle landing on 4 pads. The maximum attenuator stroke is determined from the maximum energy to absorb the maximum weight vehicle (two astronauts and full propellant load, totaling 2358 pounds), the vehicle landing on a single pad and applying the above attenuator spring weight. The second case will produce attenuator 11.77 greater than the first (2358/840 x 4/1), or 11.29 greater than first expected. The second case would dictate the vehicle ground clearance line which locates the vehicle center of gravity, resulting footprint diameter and ease of LM stowage. Since difficulty was being experienced in stowing the vehicle, several attempts were made on concepts where all or several of the attenuators would be utilized on any landing; this eliminates or reduces the 4-to-1 multiplication factor. Concepts were examined wherein the attenuators were replaced with actuators hydraulically driving, tension cables activating or compression rods activating a single central attenuator. These concepts had the problems of weight and stability, and inability to attenuate vehicle torsion. These problems led to the integral leg-frame and four perpendicular attenuators but this arrangement also required a separate system to attenuate torsion. The four attenuators were then canted but the vehicle was found to be unstable (under combined torsion and horizontal loading the vehicle would "wind-down", then go over-center). This led to the eight attenuators illustrated. The NR landing

dynamics program was used to determine the attenuator angles and offsets shown in figure 3-52; these same values were applied to the figure 3-6 configuration.

The seated pilot evolved during two years of design activity. Originally, the LFV was controlled kinesthetically which required a standing pilot for all feasible control concepts. When gimbaled engines with mechanical hardwire and stability augmented control modes were investigated the standing pilot presented one serious problem, that of having two methods of control: the primary, or direct hardwire gimbaled engines and inadvertent kinesthetic control by the pilot. Unless the pilot is fixed so that he is part of the payload, he can introduce advertent/inadvertent kinesthetic control moments. If he is not aware of these moments he would continue to correct by means of the primary system with the chance that the primary system can become saturated, whereafter control could be lost. When the standing pilot was considered, the landing g's were lower and difficulty was experienced in trying to provide adequate landing restraint; when the criteria for landing g's increased to the present values, restraint appeared impossible. During this time, difficulty was also being experienced in stowing the LFV within the LM descent bay without excessive dismantling of the LFV; this problem could be improved if the gear length were decreased, which required a lower center of gravity.

The pilot's position was determined by required visibility, ingress and egress and the vehicle general configuration; the final arrangement was then approved by Life Science personnel and confirmed (with minor changes) after the full-scale mockup was investigated. The seat, displays, and controls are illustrated in figure 3-53. The seat provides the necessary support for the pilot and his PLSS, and has an adjustable footrest for 10th to 90th percentile astronauts. The seat is form-fitting and includes one-inch of padding under and one-half inch of padding along-side the astronaut with one-half inch padding around the backpack. The pilot is restrained from moving back or sideways by the seat and up or forward by the crouch straps illustrated. The backpack is restrained separately since it was undesirable to impose these loads on the pilot. Originally, the backpack support was higher and pilot shoulder straps were included, but these were felt to be unnecessary and affected the LFV stowage, therefore producing the configuration illustrated. The footrest and foot restraint were reduced to the present envelope to improve visibility and still provide adequate support. The instep strap and locking handle would be opened until the astronaut's feet are in position, then locked by rotating the handle downward along the center support. Besides the adjustment lock for astronaut size, the center support can be rotated to aid ingress and egress and LFV stowage. The flight console on the earlier concepts was a one-piece unit which was required to be rotated to enable ingress and egress. Concern was expressed with this and stowage difficulties were experienced. Therefore, the walk-through concept was generated; the two supporting arms are rotated sideways to enable stowage. One primary requirement for the controls was to have them identical to or very similar

to the Apollo command module and lunar module. The attitude controller and throttle control are modified Apollo hardware, ME 901-0172. The display panel provides displays for vehicle attitude, thrust-to-weight ratio, propellant tank quantity, high and low pressure, landing light indicator, timer and timer reset button, switch and light for testing status of electrical power (systems A and B), circuit breaker switch and vehicle power switch. On multiple engine concepts a handle mechanically operating the throttle valves is included to shut off the propellant flow to any engine that has failed.

On lunar flyer missions servicing is required between flights to replenish the propellant and helium supply. The refueling is discussed in the previous surface operations section. During the LFV study, the problem of replenishing the helium supply was examined quite extensively, to determine if sufficient helium should be included for all LFV flights, or resupplied, separate tanks for oxygen and fuel systems, and if the tanks should be installed charged, or transferred from the LM system. Due to the helium system weight, number of flights per LM landing and ability to store the LFV for later use it was decided to recharge the helium tank (or tanks) after each flight. To have adequate pressure and avoid the problem of high pressure gas transfer it was decided not to utilize the LM supply, but to have fully charged tanks available. From weight considerations and to minimize EVA time a single tank was used for both oxygen and fuel. When the LESS vehicle was modified for the LRF mission the four pressurant tanks were reduced to two and moved outboard to be accessible. A single tank would be desirable but would be large and produce center of gravity problems (on the two-tank LFV vehicles the single tank can be used to provide center of gravity balance). The helium tanks would be designed for a quick structural disconnect (to minimize EVA time) and would incorporate Apollo transfer couplings.

The LFV study devoted considerable time in examining the engine quantity and location and control method and arrangement. Configurations were examined where the engine gimbal was located above the center of gravity to provide stability and control improvements, but presented difficult thermal and structural problems; therefore, the below-center of gravity family of concepts was pursued. The arrangements of multiple engines where the engines are widespread offer advantages in stowage and control, but are difficult to recover should an engine fail, and have large specific impulse losses under failed engine conditions. Reliability analysis indicates that the single engine is most reliable unless the pilot can recover and continue to fly after one engine has failed. Since the NR simulator program indicated that the pilot could not recover with kinesthetic and hard-wire control, the multiple engines were only considered on stability augmented concepts; further, in these concepts the engine reliability was much better than for single engine versions.

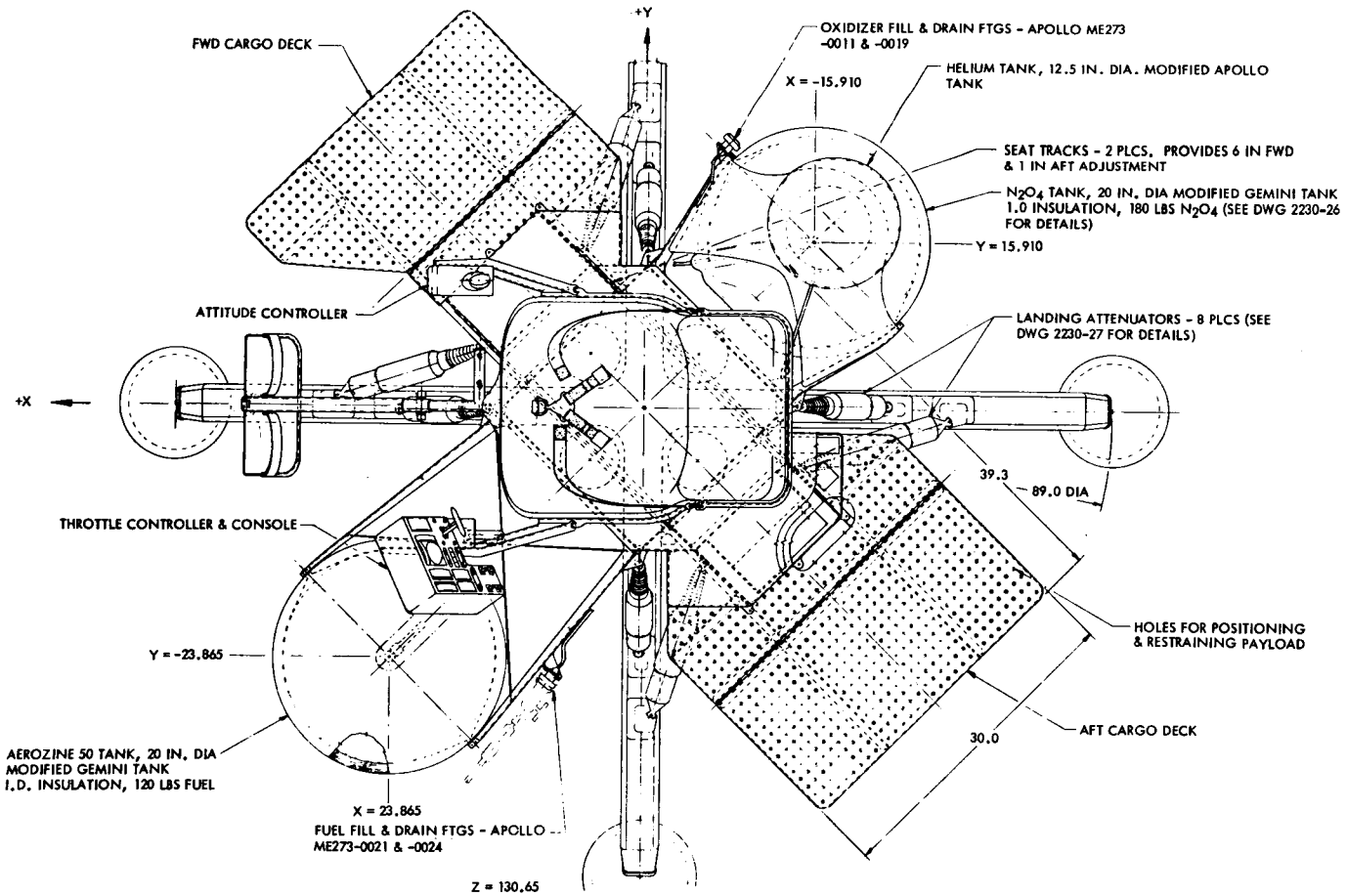

Figure 3-52. Lunar Flying Vehicle Selected Concept (Sheet 1 of 2)

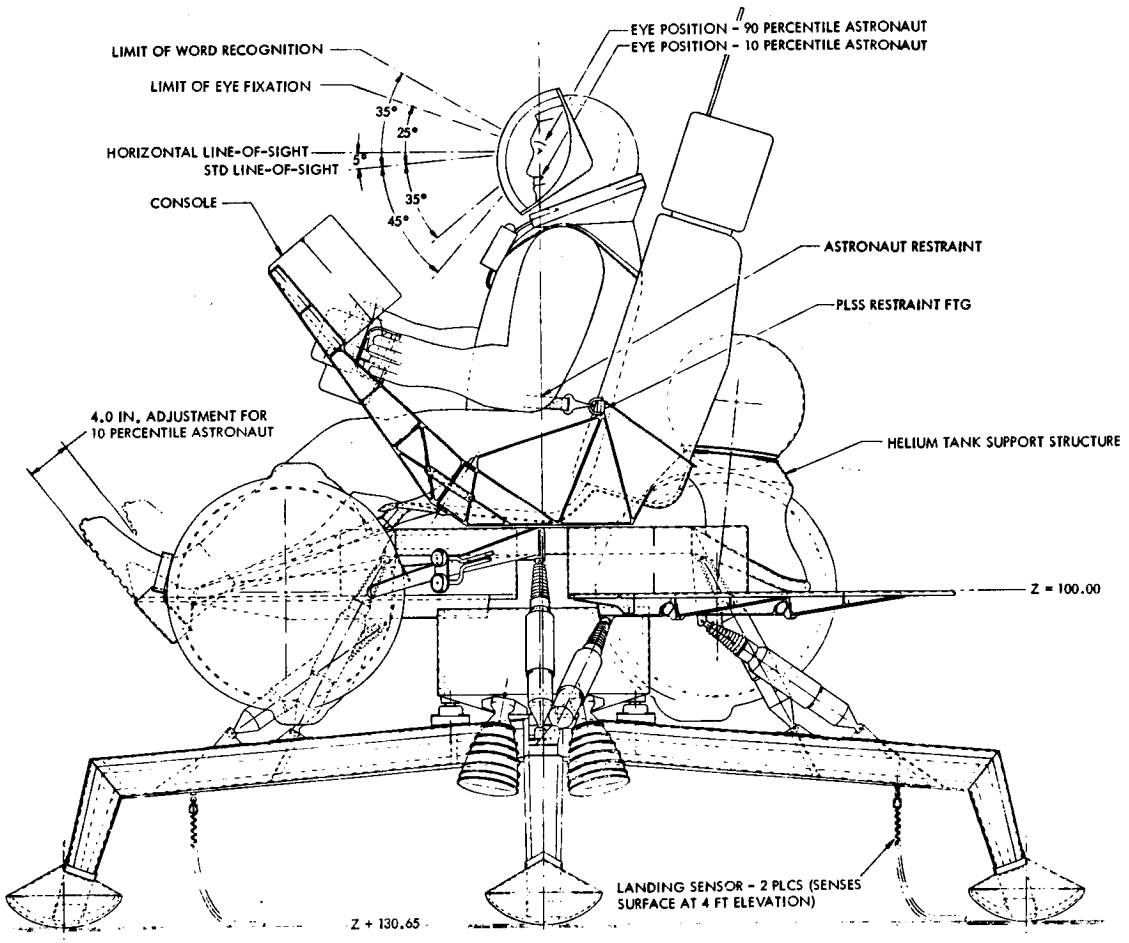

Figure 3-52. Lunar Flying Vehicle Selected Concept (Sheet 2 of 2)

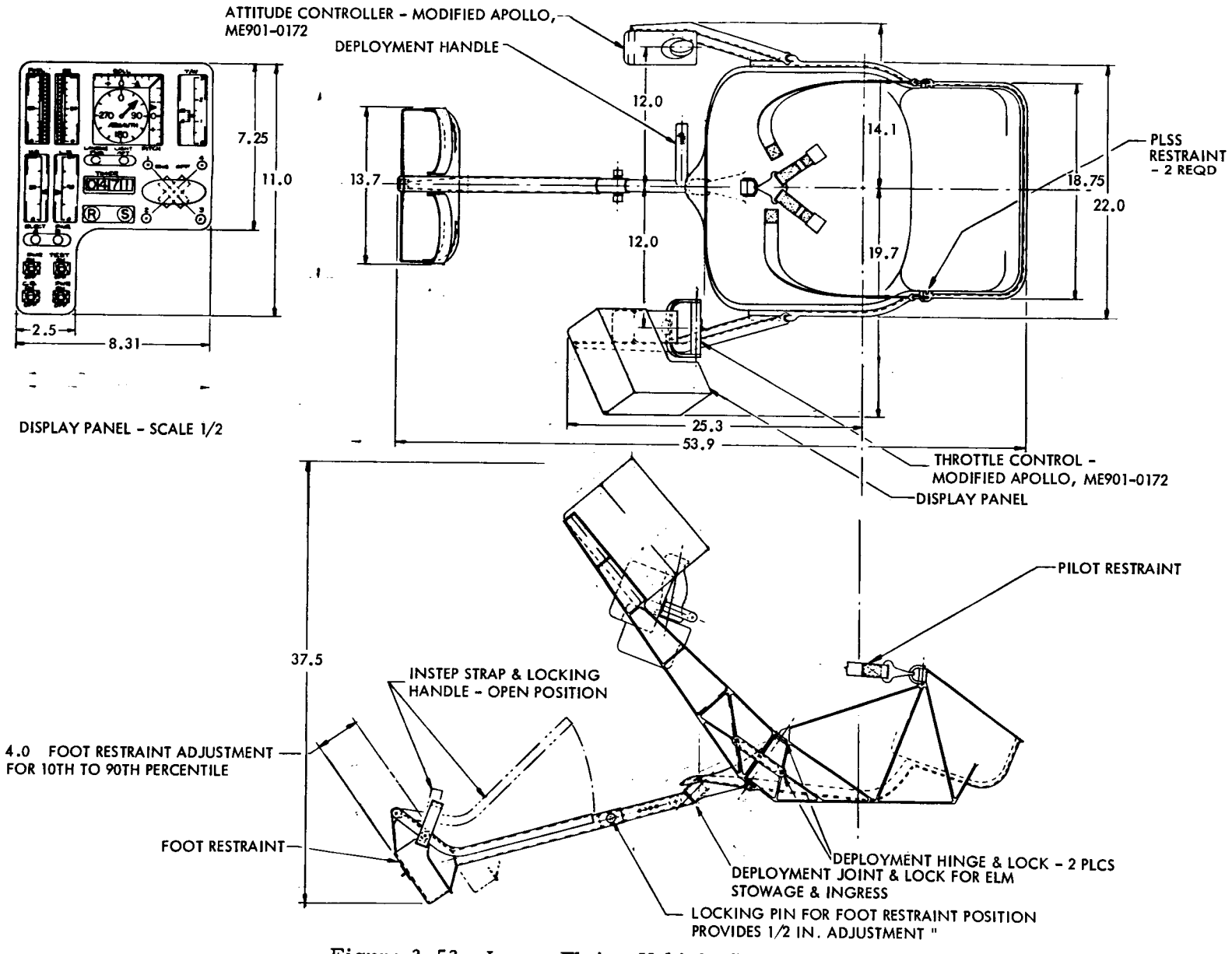

Figure 3-53 Lunar Flying Vehicle Seats and Displays

Arrangements with the engines in-line (two, three and four engines), triangular pattern and four engines in both square and diamond patterns were investigated. All investigated arrangements were workable, the advantages were in vehicle envelope (affecting stowage) which depended upon structural concept, tank quantity and arrangement, etc. Control investigations included individual 2-axis gimbals and concepts where the engines are rigidly mounted to the thrust structure which is then gimbaled or translated to provide the control moment. These latter concepts offered packaging advantages but produced excessive actuator forces under one-engine-out situations.

As can be seen on the LFV concepts included in this study, the engine (or engines) are mounted to the leg-frame rather than the attenuated structure. This has advantages in the vehicle envelope when large attenuations are required. The engine thrust structure is shock mounted to the leg-frame and the shock mounts and leg-frame deflections would provide engine assembly attenuation so that the g's are expected to be less than 20, which are well within the limits of the engine, throttle valve, bearings and actuators.

On LFV missions the primary purpose was to transport miscellaneous payloads. Since the vehicle should remain balanced at all times attention must be given to this problem. In all cases the cargo would be loaded to provide a balanced configuration where possible, but when a single package is being transported the pilot's seat must be translated to correct the center of gravity. It was assumed that this correction is required in one plane only, since the cargo center of gravity can be positioned correctly in the second plane. Should the center of gravity be off the nominal thrust vector the engines must be gimbaled to correct for this offset. In figure 3-12 the maximum allowable engine gimbal is approximately 7-1/2 degrees before clearance problems during attenuation are encountered; since 2-1/2 degrees are required for one-engine-out correction or actuator failure and ±5 degrees are required for control authority, the vehicle must be balanced to within 1/2 inch. On the LESS vehicle the thrust vector must also be within 1/2-inch for orbit insertion accuracy. For these configurations a cargo balancing device must be included which requires bubble levels on the vehicle and a ball joint pivot or knife edge on the landing pads to perform this balancing. It is expected that on a given LFV flight the astronaut would know the required seat location from predetermined program data, so the only problem would be deviations from this program and picking up such unknown objects as rocks. When the astronaut adds unknown objects to the LFV, he would be required to weigh this payload and determine the seat and payload location.

One of the tasks on the LFV study was to modify the LFV to an escape-to orbit vehicle; this configuration is included in this study report for general information as illustrated on figure 3-50. The main changes from the LFV baseline (fig. 3-12) are the addition of four engines, two propellant tanks, one helium tank, the second seat and additional guidance displays and the removal of

the two cargo decks. The two propulsion packages would have been assembled and checked out on earth, requiring only the cross-coupling of propellant lines and attaching to the cargo deck fittings. The forward package contains the fuel tank, helium tank and two engines with the aft package containing the oxidizer tank, second seat and two engines. These four engines are identical to the 100-pound thrust LFV engines, except they do not include gimbaling or throttling. During ascent the LFV gimbaled engines would be throttled down so that the added propulsion system is depleted first; in this way vehicle control is maintained throughout the mission.

LESS/LRF Performance. - The performance of a modified LESS as a long range lunar surface-to-surface flyer is shown in figure 3-54. Two trajectory profiles were considered: modified ballistic and constant altitude. The modified ballistic mode consists of a boost segment followed by a reduced thrust coast phase until apolune at the midpoint of the trajectory. The modified ballistic trajectory is symmetrical about the midpoint. The constant altitude trajectory consists of a modified ballistic ascent and descent with a patched constant altitude segment. These two profiles are shown in figure 3-54. Several simplifying assumptions were made:

1. flat moon
2. constant lunar g
3. constant specific impulse
4. instantaneous pitch maneuvers between trajectory segments

Some results can be taken from the LFV study. The optimum boost tip angle (angle between local vertical and thrust vector) for the modified ballistic mode is approximately 40 degrees. The optimum tip angle for the constant altitude segment is 60 degrees. However, human factors dictate a shallower pitch angle. The pilot can fly the vehicle at a 45 degree pitch angle with a small decrease in performance. The modified ballistic mode is more efficient than the constant altitude, but it is extremely sensitive to errors in trajectory variables. In view of the precision required in pointing and thrust maneuvers of relatively low altitudes, the mode is not considered safe enough to justify the performance gain.

Figure 3-55 presents the propellant requirements of the outbound leg for a maximum range trajectory. This curve is based on the assumption that the ratio of the initial (lift-off weight) to final weight of the outbound leg is equal to that of the return leg, $(W_p/W_I)_{LEG\ 1} = (W_p/W_I)_{LEG\ 2}$. This is a good first order approximation if the thrust to weight time history of the outbound leg is approximately equivalent to that of the return leg.

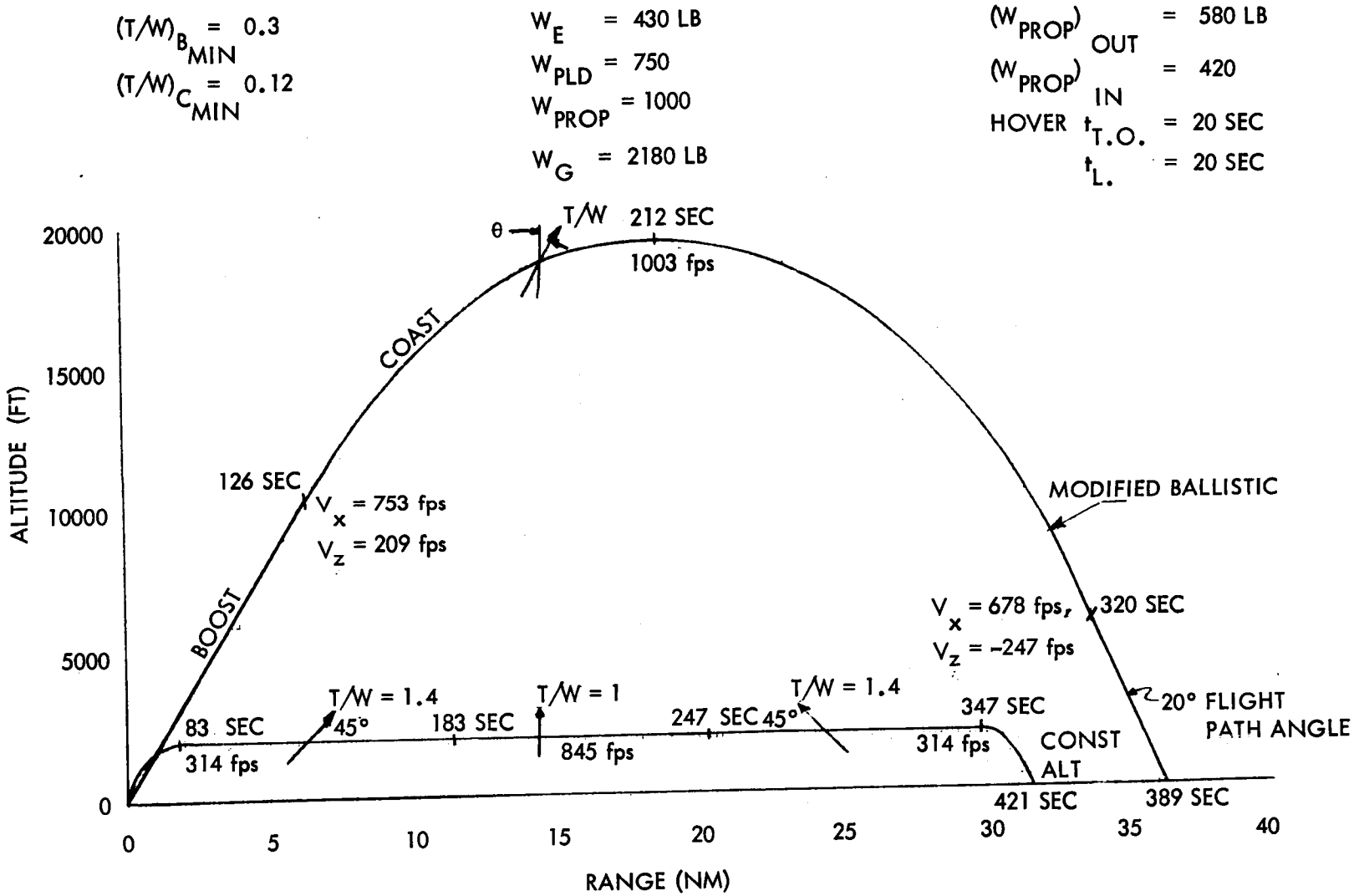

Figure 3-54. - Trajectory Profiles

$$\frac{W_{PROP}}{W_{LIFT-OFF}} = 1 - \sqrt{\frac{W_e + W_{PLD}}{W_{LIFT-OFF}}}$$

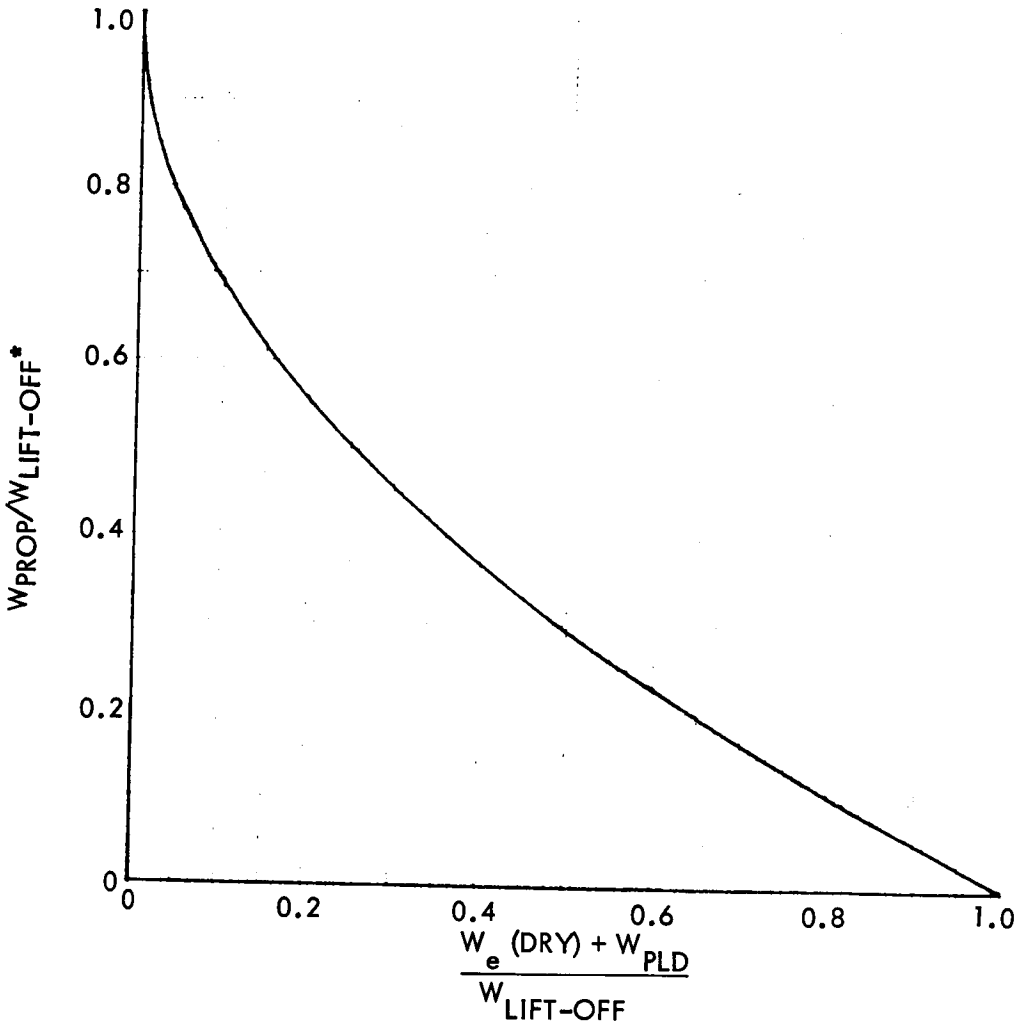

*USED IN CONJUNCTION WITH FIGURE 3-56 IN DETERMINING MAXIMUM RADIUS OF OPERATION $(W_p/W_{lo})_{FIG\ 3-55} = (W_p/W_{lo})_{FIG\ 3-56}$

Figure 3-55. - Outbound Leg Propellant Requirement for Maximum Range (Round Trip)

*SEE FIGURE 3-54 FOR MAXIMUM RADIUS OF OPERATION
$W_{PROP}/W_{LIFT-OFF}$ (W_p/W_{lo}) FIG 3-55 = (W_p/W_{lo}) FIG 3-56

$(T/W)_B = 0.3$
$(T/W)_c = 0.12$
$\theta = \pm 45°$
H = 1000 FT (PERF. NOT SENSITIVE TO H)
V_{CRUISE} = OPT
I_{SP} = 297
HOVER & RESERVES = 5% W_{PROP}

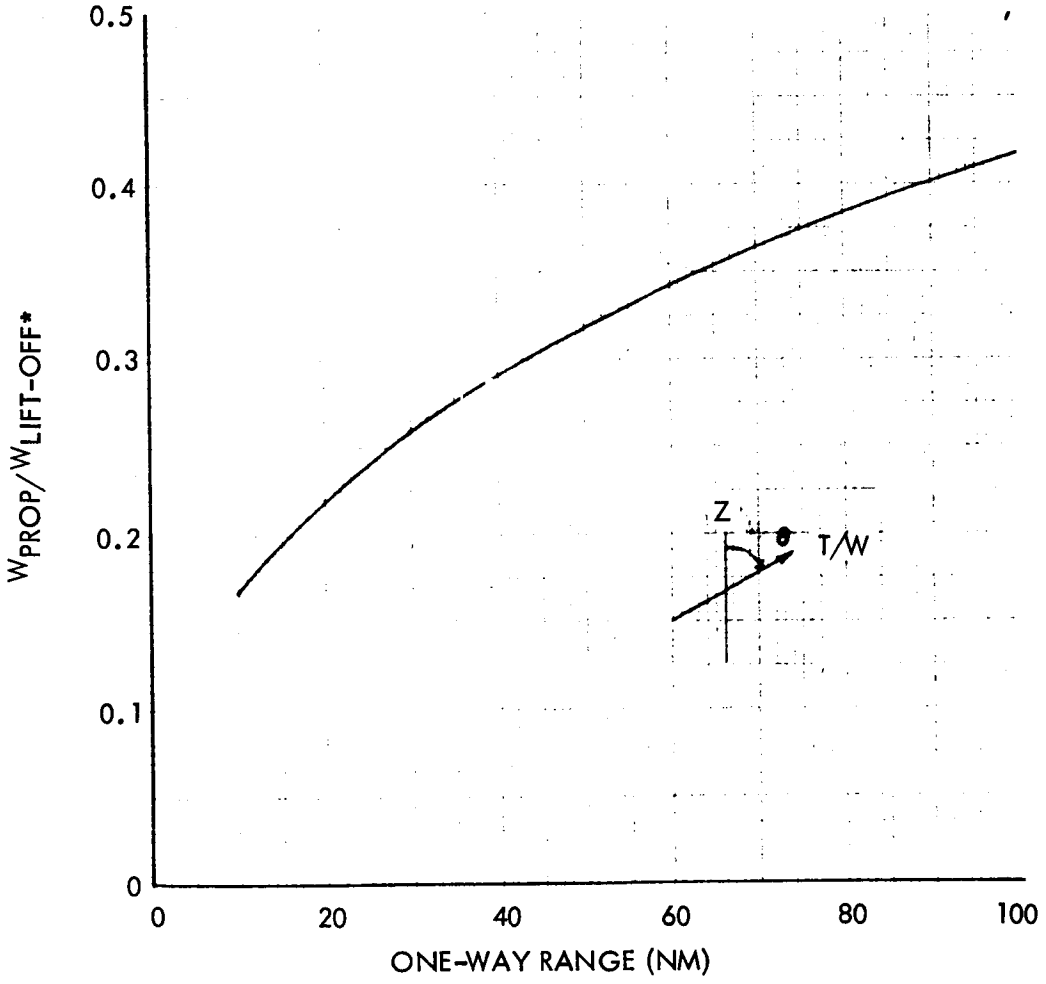

Figure 3-56. - Constant Altitude Propellant Requirement

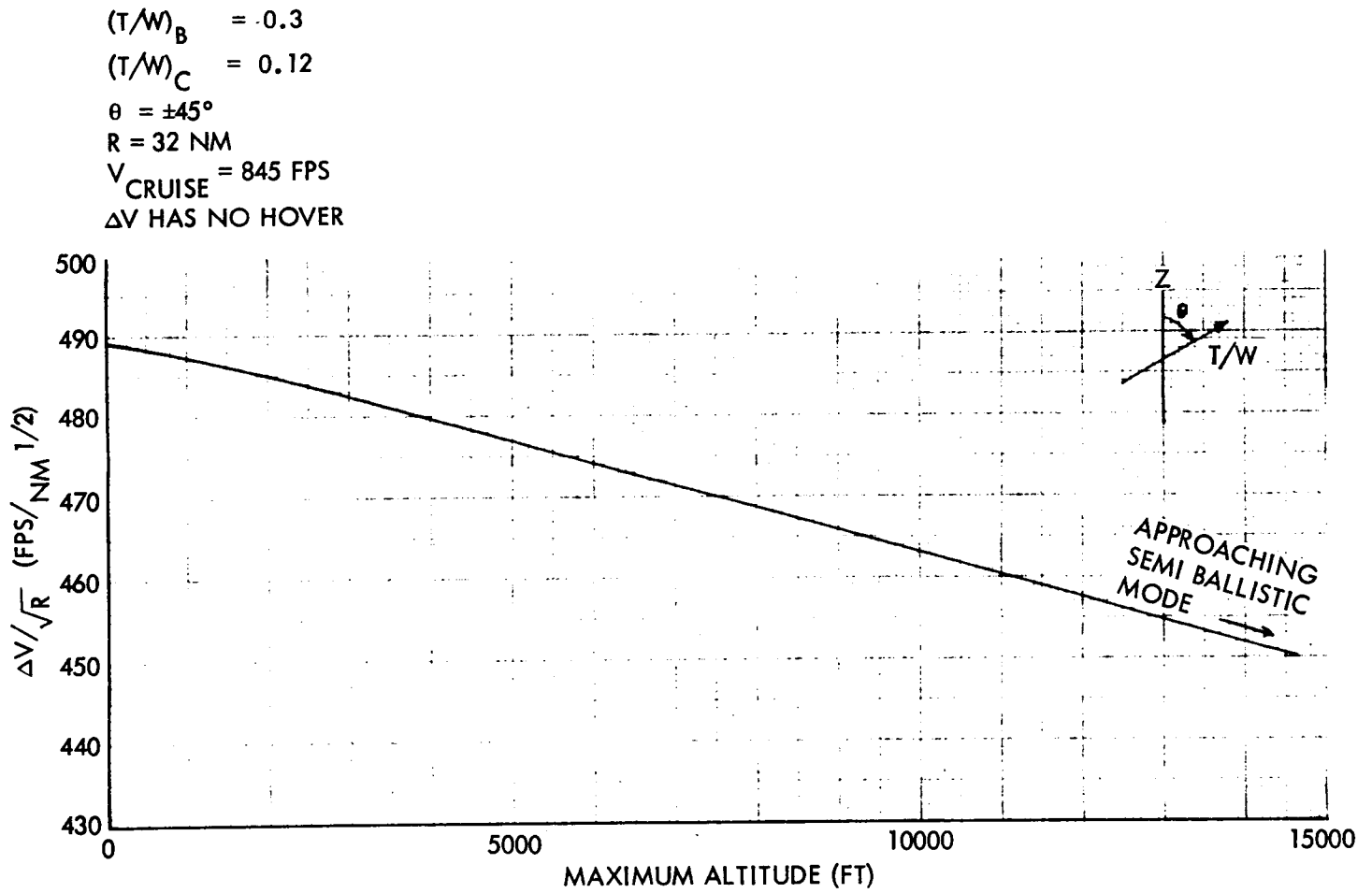

Figure 3-57. - Performance Variation With Respect to Maximum Altitude for Constant Altitude Trajectories

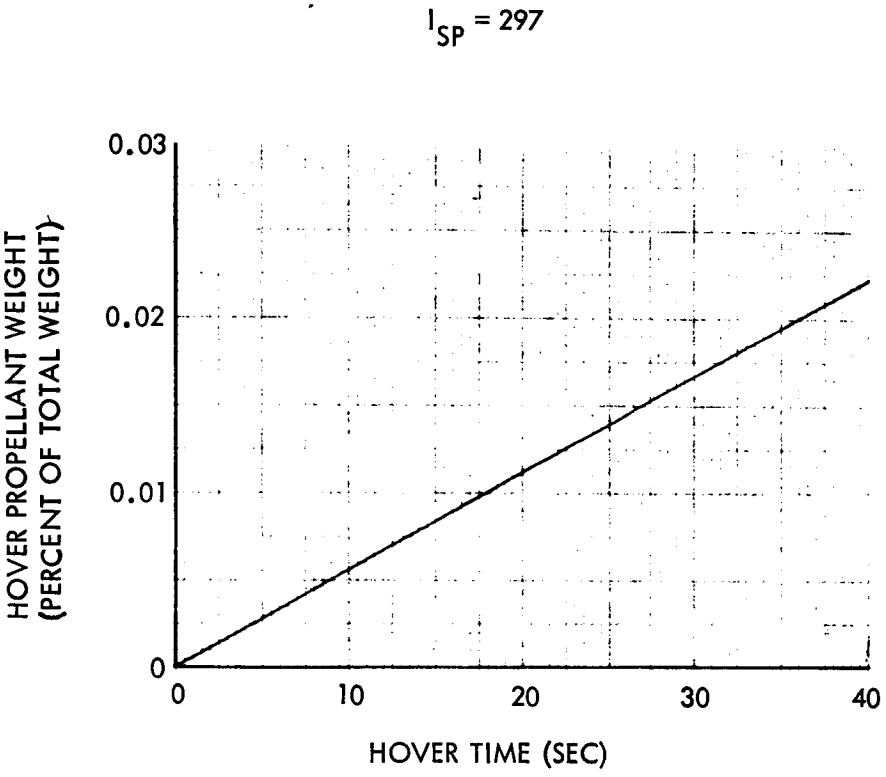

Figure 3-58. - Hover Propellant Requirements

After obtaining $W_{prop}/W_{liftoff}$ from figure 3-55, the maximum range can be determined from figure 3-56, $(W_p/W_{LO})_{Figure\ 3-55} = (W_p/W_{LO})_{Figure\ 3-56}$. This figure can also be used to obtain the propellant required for a given one-way range. A digital computer program was used to determine this curve. The curve was based on an altitude of 1000 feet, but the performance is not sensitive to altitude (figure 3-57).

Depending on the experience of the pilot, a certain amount of propellant must be expended for takeoff and landing hovers. Hover propellant as a function of time is shown in figure 3-58. A range penalty due to hover time can be determined by taking the product of cruise velocity and hover time.

The constant altitude segment consists of three phases: an acceleration to the cruise velocity, cruise at a constant velocity, and a deceleration phase. The optimum cruise velocity as a function of pitch angle is given in figure 3-59. For a 30 nm range with a 45-degree pitch angle, the optimum cruise velocity is 740 fps. For an altitude on the order of 600 feet altitude trajectory, this velocity may be too fast for the pilot to identify lunar landmarks along the path of the trajectory. The effect of reducing the cruise velocity on the performance is shown in figure 3-60. For a 30 nm trajectory, the cruise velocity can be reduced from 740 fps to 500 fps with an increase of 300 fps in characteristic velocity.

LESS/LRF subsystems. -

Communications: During the LESS long range flyer surface mission, communication with the flyer vehicle occupants will be required at all times. Several methods were considered for accomplishing this requirement, including surface emplaced relay stations, CSM usage by limiting surface flights to periods when the CSM was within range, use of lunar communication satellites, and use of a direct to earth S-band link utilizing the 85-foot Goldstone receiving antenna. The best system consistent with minimum LESS/LRF weight, safety, and maximum flexibility appears to be through use of a direct communications with earth through use of an S-band transceiver and semi-directional antenna and a high frequency intercom (such as proposed by RCA) to relay backpack output through the S-band to earth. Sufficient gain can be obtained with a directional antenna which has a 90-degree cone angle and therefore requires only approximate pointing by the LESS/LRF crew. With this equipment and approximate orientation of the antenna before take-off and again after landing, continuous communication between astronauts and Earth is possible. The crew uses their normal backpack communicators with no special controls or switching connections. Communication between the LM or CSM and LESS/LRF by the backpack VHF is possible only when within line-of-sight, after which an astronaut in the LM or CSM could receive communications through the earth relay.

$$\frac{V_{C_{OPT}}}{\sqrt{R}} = \left(\frac{g\,T/W \text{ SIN } \theta}{2\,T/W - 1}\right)^{1/2}$$

$$T/W = 1./\text{COS}\,\theta$$

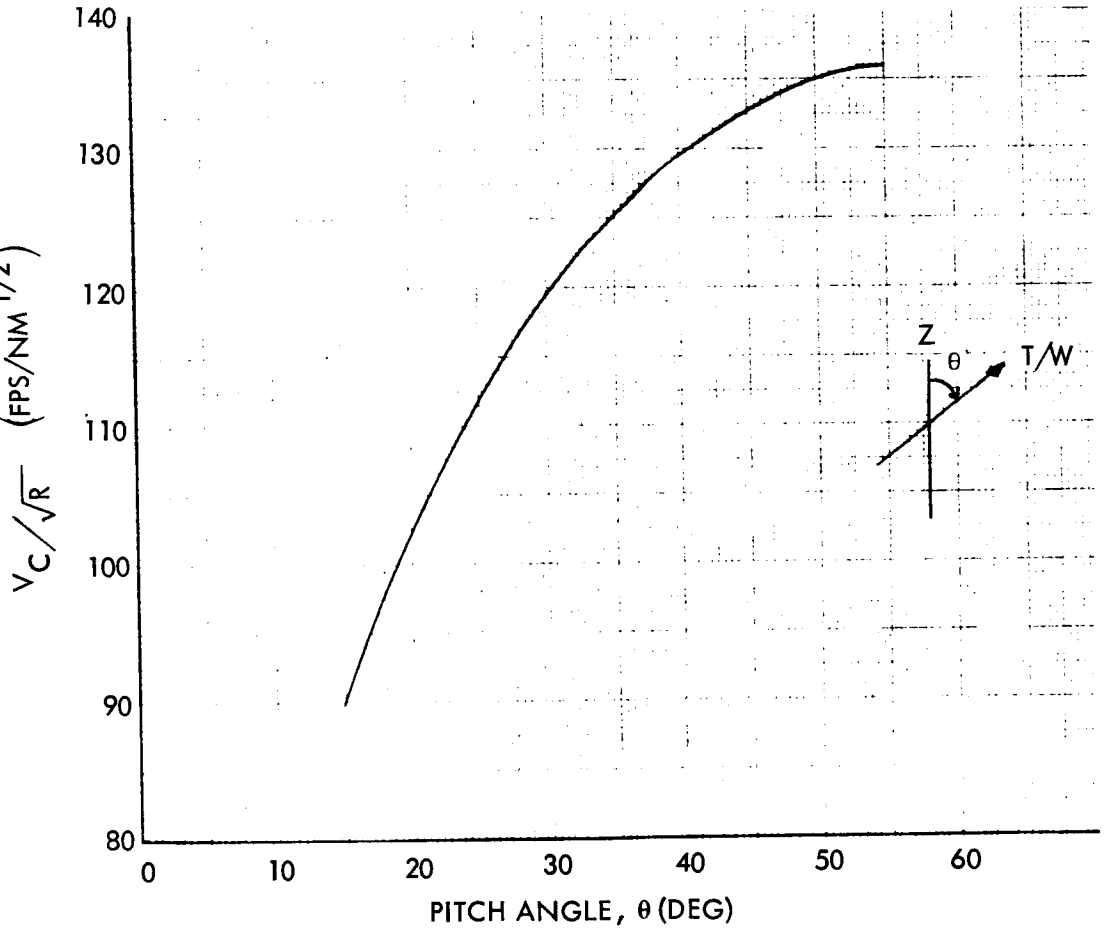

Figure 3-59. - Normalized Optimum Cruise Velocity for Constant Altitude Trajectories

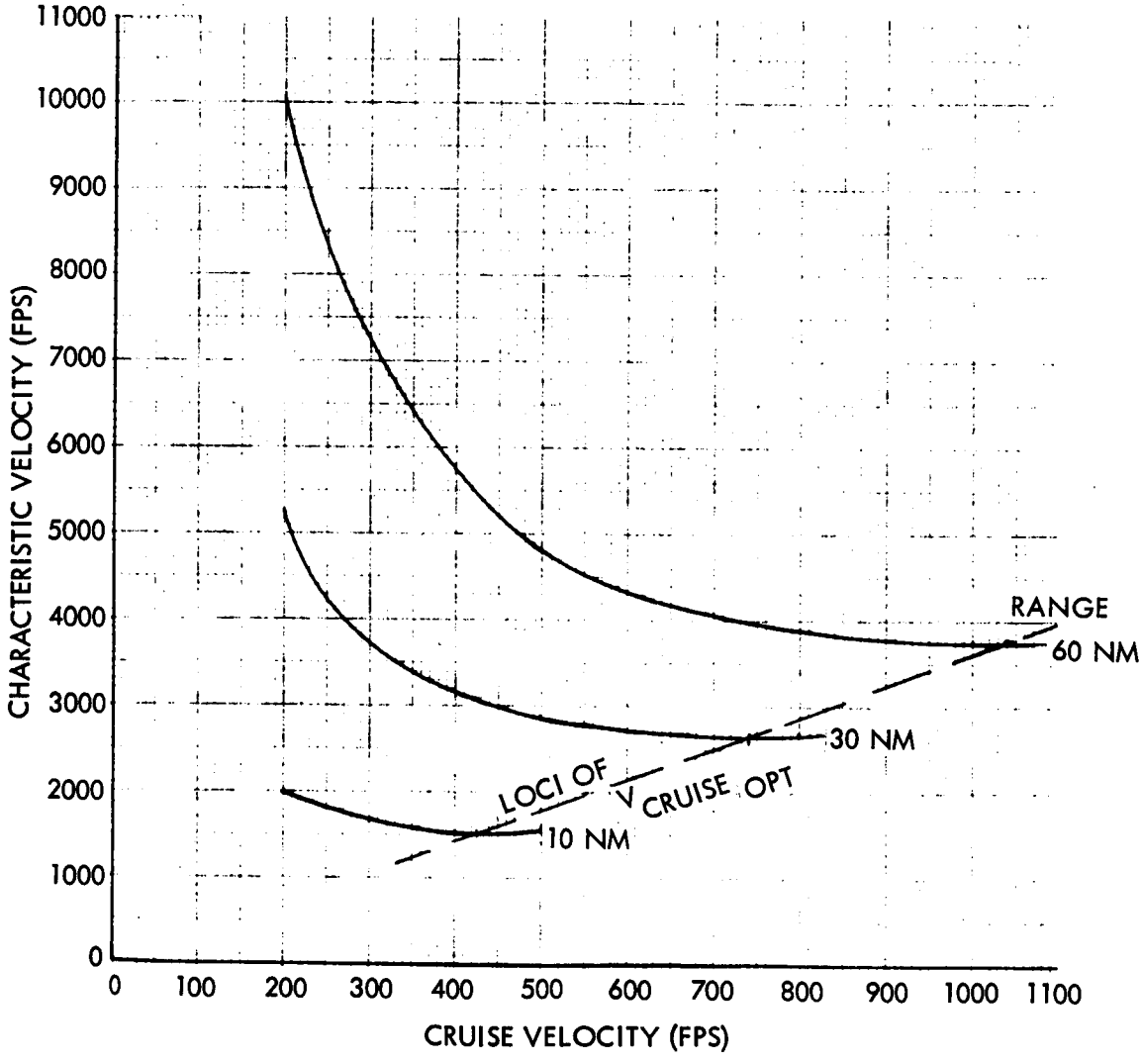

Figure 3-60. - Constant Altitude Non-Optimum Trajectories

Estimated weight, volume and power of the LESS/LRF equipment are shown in table 3-26.

TABLE 3-26. - LESS/LRF COMMUNICATION SYSTEM

Item	Weight (lb)	Volume (cu. in.)	Power (dc) (watts)
S-Band transmitter/receiver	6.0	168	32
Power converter	1.5	41	2
Antenna	2.5	24	-
Multiplexer	2.0	122	-
High frequency transmitter/receiver/relay	1.0	30	3
High frequency antenna	0.2	-	-
Cabling and connectors	2.0	-	-
Total	15.2	385	37

Electrical power: The electrical power system will be similar to that of the stability-augmented version of the LESS with the additional power requirement due to the added communications (37 watts). Since the total mission time will be limited by the backpack capability, a four-hour maximum time has been utilized. Present PLSS maximum time is less than four hours, but with improved versions, up to six hours should be possible in the near future. The addition of 148 watt hours (37 x 4) to the LESS basic 1386 watt hours makes a LESS/LRF total of 1534. This total power requirement results in a battery weight of approximately 30 pounds. Additional battery packs of this size will be required for each anticipated LESS/LRF operation. The battery could be recharged between flights if an active power source is available. However, if the battery is to be recharged the depth of discharge must be reduced with consequent increase in battery weight of 50 percent, for a total of 45 pounds. A more careful mission analysis may result in a reduction in battery weight since this analysis assumes continuous operation of all equipment, which is conservative.

Propulsion: The propulsion system for the LESS/LRF would be similar to the basic escape vehicle except that the engine must be throttlable through a range down to 10 percent maximum thrust and a method of thrust control must be provided. The detail propulsion system analysis of the LFV phase B study contract is applicable except that a much larger engine or engines will be

required. The result of using a throttlable rather than basic LESS two-level thrust engine is a slight weight increase and an increase in engine development time. The multiple pulsing engine concept shown in figure 3-8 offers many advantages for the LESS/LRF application. Among these are use of existing Apollo RCS engines, engine-out capability, reduced vehicle height, easier boarding, and a more compact vehicle, improving stowage capability.

Environmental control: Control of LESS/LRF vehicle temperatures, while awaiting usage on the lunar surface is similar in general to that of the basic LESS vehicle, and the use of an insulation blanket cover and sublimating water cooler concept are applicable. In the case of the long-range flyer mission, the primary difference is the stay time at the exploration site with the propellant tanks over half full. It is advisable, if possible, to shut down electronic equipment to conserve power and prevent heat generation. However, some equipment such as the S-band transmitter/receiver and VHF relay equipment must operate and some method of cooling appears to be required. The use of the insulation blanket to cover the vehicle while not in use is advisable to reflect solar radiation and that from the surrounding hot lunar surface. The primary structure can absorb some heat, and a water bottle sublimater could be used as recommended during inactive storage of the LESS. However, another possibility is utilization of the partial fuel and oxidizer aboard the vehicle. Although propellant temperatures cannot be raised too high, a considerable heat sink is available. Figure 3-61 shows a parametric presentation of the effect on fuel temperature of dissipating electronic heat into the fuel and oxidizer. The figure is based on the assumption of using a weighted average specific heat. The 1000- and 1600-pound propellant capacity are shown for use in iteration and while fully fueled before flight.

Figure 3-61 shows that (assuming a limiting temperature of about 100 F for the oxidizer) there is ample capacity for dissipating electronic heat into the fuel. However, dissipation of electronic waste heat into the fuel requires some sort of heat transport loop. The usual fluid systems with heat exchanger, pumps, and controls might not be the optimum application for a vehicle of this sort which otherwise lends itself to passive temperature control.

It is believed that this might be a good application for the "heat pipe." The "heat pipe" consists of a wick lined "evaporator" and "condenser" section connected by a wick-lined pipe. Steam produced in the evaporator section flows to the condenser section where it is condensed and wicked back to the evaporator along the walls of the connecting pipe. This cycle operates at a ΔT between the evaporator and the condenser of about one half a degree Fahrenheit.

With the evaporator located at electronic boxes and the condenser located in the fuel tanks, a relatively passive system may be feasible.

Guidance and navigation: The longer range radius capability of the LESS for the lunar surface flight (up to 60 nm) compared to the original LFV

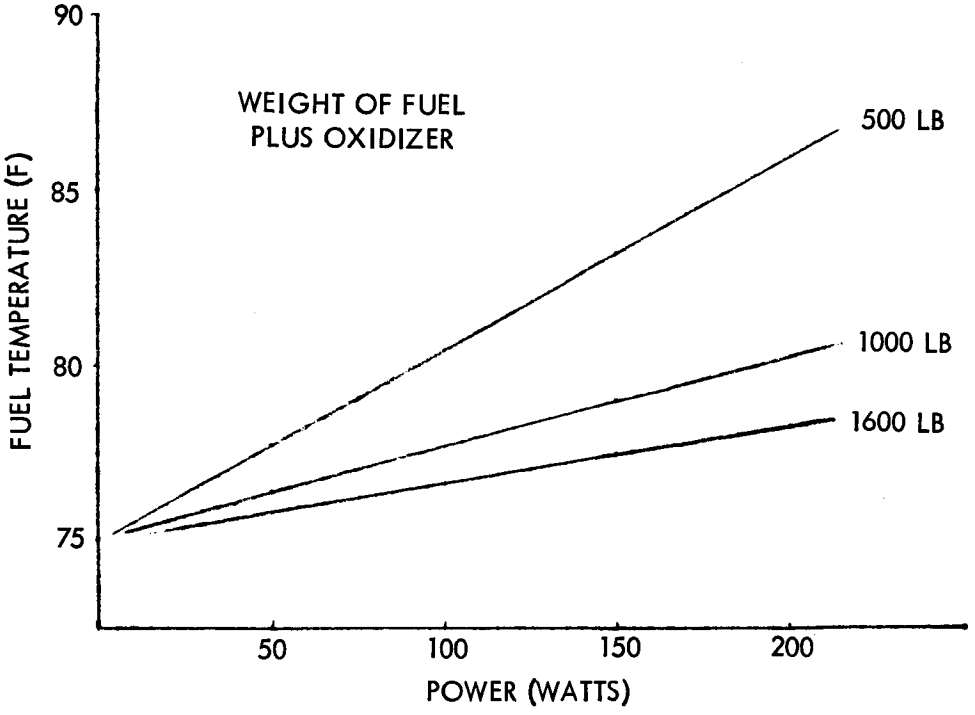

Figure 3-61. - Fuel Temperature Versus Power Dissipated After Four Hours

concept (5 nm), requires that some improvement in navigation capability be added to ensure reaching the desired landing sites on both outbound and return legs.

The basic LESS attitude gyro reference system and display is suitable for LFV applications. Ground alignment of the attitude reference system (ARS) for the outbound leg will be the same procedure as for the basic LESS mission. Azimuth alignment (if needed) for the return flight can be accomplished with either a sun sighting or a known terrain feature sighting before return launch. Azimuth direction to the landmark could be determined after landing at the remote site by taking an azimuth sighting to the landmark and recording the yaw indication on the attitude display.

Powered ascent would be a programmed pitch maneuver as on the basic LESS mission.

For terminal descent and soft landing, the basic LESS or LFV G&N system could be augmented with a landing radar to measure altitude and perhaps altitude rate. LFV simulations have shown that an altitude indication to the pilot considerably reduces the propellant consumption during terminal descent as well as increasing mission safety. For the long-range flyer, this improvement seems advisable. (The utility of a Doppler altitude rate measurement, although theoretically attractive, is questionable because of the high sensitivity of the measurement to pitch attitude.) It is estimated that with landing radar, over 500 ft/sec ΔV could be saved.

For the return flight landing at the lunar base, use of the LM rendezvous radar to track the LESS and provide range, altitude and azimuth indications via voice link could aid the pilot in homing on the landing site and providing a backup for the landing radar. A relatively lightweight transponder in the LESS would be required.

Terminal maneuvering to reach the landing site can be manually piloted. A downviewing mirror mounted to the pilot's left would allow the pilot to keep track of the landing site during descent braking and terminal maneuvering from semiballistic flights. For constant altitude hover mode flights, the downviewing mirror probably would not be necessary for terminal maneuvering. With this flight mode, retrobraking (at 20,000- to 40,000-foot range from the landing site) would be initiated at a specified time after launcher by reference to landmarks. It can be assumed that fairly accurate maps will be available from orbital and/or surface surveys by the time the LESS/LRF is operational.

Visual acquisition of the landing site would be aided by a da-glo orange or red cloth laid out on the ground. A 20-foot square would probably be adequate for recognition from 10,000 feet, which is adequate range to initiate terminal maneuvering to remove maximum dispersions estimated to be on the order of one-half nautical mile.

Stabilization and Control. - Since one of the most natural secondary or alternate missions of the LESS is for lunar surface transportation, it is appropriate to consider the necessary design changes for this application. Prior efforts for the LFV contract have established certain criteria necessary to the performance of each sortie. In the area of stabilization and control, these criteria are summarized and contrasted with LESS requirements in Table 3-27. Data in the table for the LFV also include a new requirement for navigational displays which is implied by the fact that an LESS surface mission may have nearly ten times the range of the original LFV mission.

Beginning with mission requirements, use of an LESS for many flights (sorties) implies an increased stress on safety. A single-engine version of the LFV was rejected for two major reasons: development time for a sufficiently reliable engine was greater than for several redundant engines; and the complexity of a single engine when yaw RCS, redundant valving and control lines, and other safety features were added, was comparable to multi-engine versions. These reasons may apply to LESS for LFV missions also. A high reliability LESS engine, to be used for a single, emergency, unthrottled flight, would not necessarily meet the reliability requirements for an LFV mission when throttling is added and many normal flights are conducted, unless the actual experience with the LESS had proven conclusively that adequate reliability had been achieved.

If the pilot stabilization task with LESS for its primary mission is compared to the surface mission stabilization task, a major difference is noted: the requirement for landing. The pilot's ability to land depends on how closely his control of three-axis attitude and translation is, with only rotation controller commands at his disposal. A tradeoff exists between the pilot's control of these variables and landing gear construction. To minimize landing gear weight and size, reliable data on stabilization are necessary. The difficulty of controlling for a landing using various control methods is shown schematically in figure 3-62. With kinesthetic and hardwire control methods, the pilot has only angular acceleration at his disposal, yet he must use it to produce a translation in order to reach his destination. The procedure involves a prediction, on the part of the pilot, as to the propagated results of each of his commands. As seen in figure 3-62, his predictions are necessary to control a variable which is four integrations removed. The task is difficult at best, but is greatly magnified if it must be simultaneously carried out in three axes. With the use of a shaping network, the task was slightly simplified by eliminating one of the integrals part of the time. The stability augmentation system completely eliminated one of the integrals for commands, and eliminates one more for stability. With the control method involving a stabilized platform and hardwire control to engines gimbaled at the c.g., only two integrals remain; a system comparable to accelerating an automobile. Thus, the landing task imposes two additional integrations in each axis, above those inherent in the primary LESS mission.

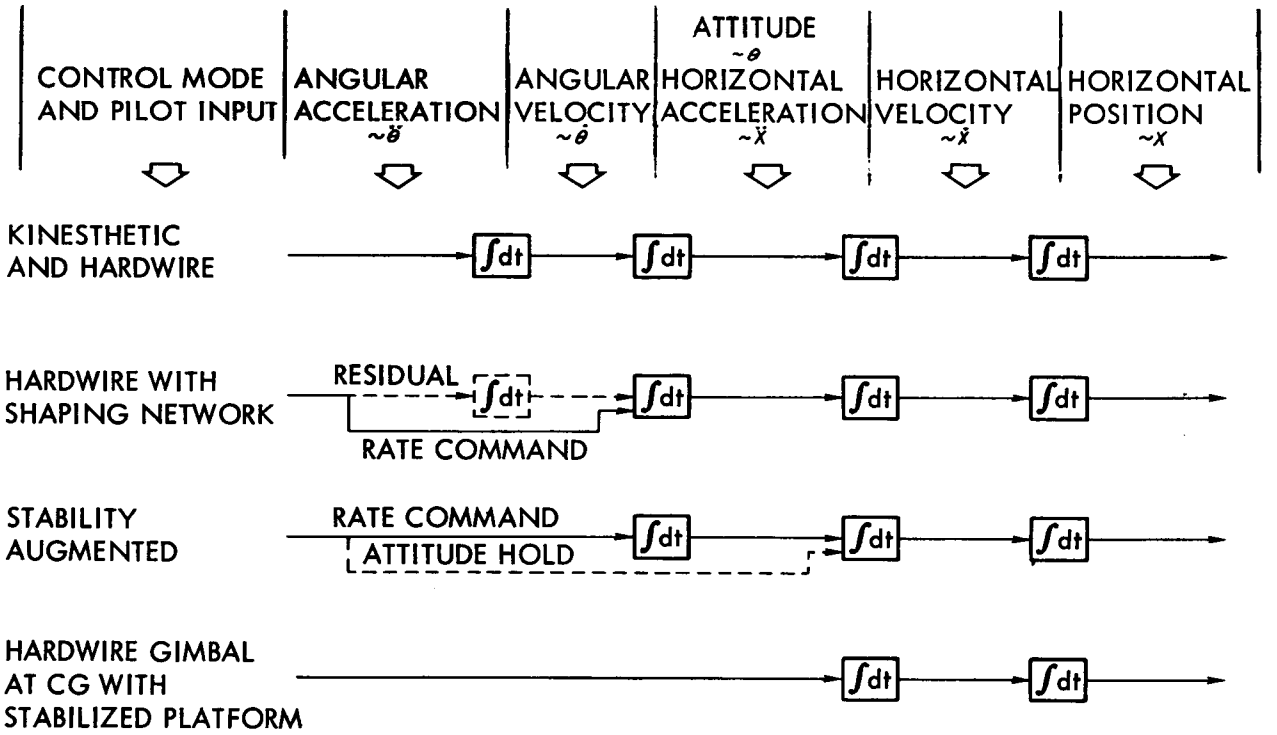

Figure 3-62. - Comparison of Predicted Tasks for Various Control Methods

TABLE 3-27. - LRF APPLICATIONS OF LESS
(COMPARISON OF REQUIREMENTS)

Area	LESS	LFV
Mission	• Single flight to orbit • Reliability unspecified	• Many flights near surface • Mission success: 0.99 Crew safety: 0.999 to 0.9999
Guidance	• Accurate launch vertical • Zero roll and yaw during flight • Accurate azimuth determination • Pitch plane tilt profile critical • ΔV cutoff critical	• Long distance navigation necessary • 5.3:1 thrust throttle range • Communication with LM or earth
Stability	• Pilot controls attitude • Hardwire control recommended • Orbital attitude control	• Pilot controls horizontal position • Hardwire control not feasible, stability augmentation recommended • 6 DOF landing variables critical
	• Pitch, yaw, roll attitude • ΔV indicator • Clock • Mode selector switch and logic	• Pitch, yaw, roll attitude • Propellant weight • Thrust-to-weight • Failure indicators • Additional displays for navigation (Required for LRF)

Another difference between LESS and LESS/LRF lies in the type of decision the pilot must make after the onset of a failure. The LESS/LRF pilot must decide whether the failure sufficiently reduces the chance of mission success and crew safety to cause him to return to his base. To aid in arriving at this decision, in-flight measurements are taken and automatically displayed. The failure displays, together with attitude, propellant remaining, and thrust-to-weight ratio displays comprise all of the in-flight data and pilot needs for the short-range mission.

The range LESS is capable of, however, takes the pilot out of the immediate area surrounding the LM and navigational displays become necessary. The navigational information, if provided by radar and combined with

the existing rate gyro measurements, may be displayed in rectilinear coordinates giving horizontal position from base as well as altitude.

One of the major handling qualities-degrading influences of the LFV was the throttle control. Throttling engines is an acceleration method of control when the valve is connected directly to the control. If radar is added to the onboard equipment, it could also provide altitude rate feedback for a much-desired rate command throttle.

Of the various LESS configurations studied in this report, most have gimbaled single engines for hardwire control or single fixed engines for kinesthetic control. Since the lunar surface mission requires stability augmented control as a minimum for handling qualities, the gimbaled engine is no longer directly linked to the controller and must therefore be power actuated. The addition of a two-axis actuation system and a throttling mechanism to an engine which has to have an extremely high reliability represents a compromise to basic LESS design.

An alternative which appears simpler is in modifying the hardwire reaction jet control system which was described elsewhere in this report and illustrated by figure 3-10. The configuration used eight engines, rigidly positioned, and pulsed to provide combined boost and three-axis control torque thrusting. Although this configuration has not yet been simulated, it has been studied both here and under the LFV contract and is an acceptable candidate.

It is therefore concluded that, unless future studies find that hardwire control is unsatisfactory for the basic LESS mission and that stability-augmented control must be used, the most attractive candidate control configuration for the long-range lunar flying vehicle adaptation of LESS may be the hardwire reaction jet system.

LESS/LRF weights: A weight estimate for the configuration shown in figure 3-5 is given in table 3-28. These estimates were derived using the weight estimates made for the figure 3-3 configuration modified where necessary due to necessary design changes. The basis for landing gear weights and other flying vehicle structural and system additions and modifications was the Lunar Flying Vehicle Study.

LESS/LRF stowage: Since the LESS/LRF must be transported to the lunar surface, the ground-rule was assumed that the vehicle must be capable of being stowed and deployed from the lunar module. Further, the LESS/LRF must be stowed within Quad I or IV of the descent stage. These specifications are conservative as the stowage considerations are dependent on the time period involved and unmanned landing vehicles could be available for transporting the LESS/LRF; these vehicles would not be as restrictive for stowage space as the present LM/ELM.

TABLE 3-28. LESS/LRF WEIGHT STATEMENT

	Weight (lb)	
Body Structure		(66.4)
Carry-through structure	41.0	
Payload platforms	20.0	
Fuel and oxidizer tank supports	16.3	
Engine compartment	-	
Secondary structure	2.0	
Environmental Protection		(26.4)
Insulation	26.4	
Landing Gear		(86.4)
Structural legs	35.6	
Landing pads	9.7	
Attenuators (including attachments)	40.6	
Landing sensors	0.5	
Main Propulsion System		(139.0)
Engine and accessories	43.0	
Fuel tank	20.0	
Fuel and oxidizer system	10.0	
Oxidizer tank	20.0	
Pressurization system	38.0	
Reaction control system	8.0	
Power Source		(16.6)
Batteries	16.6	
Power Conversion and Distribution	(8.0)	(8.0)
Power equipment	8.0	
Guidance and Navigation		(29.9)
Guidance output	29.9	
Stability Augmentation (Incl. Actuators)	26.0	

TABLE 3-28. LESS/LRF WEIGHT STATEMENT - Continued

	Weight (lb)	
Personnel Provisions		(17.0)
Accommodations for personnel	9.2	
Furnishings	7.8	
Crew Station Controls and Panels		(23.5)
Pedestal	2.0	
Instrument power	12.0	
Crew station controls	9.5	
Communications		(15.2)
	Vehicle Dry Weight	(454.2)
Payload		(750.0)
Crew	375.0	
Scientific payload or astronaut	375.0	
Residual Propellant		(33.0)
Residual fuel	11.5	
Residual oxidizer	18.5	
Residual helium	3.0	
Propellant	Burnout Weight	(1237.2)
		(1160.0)
	Max takeoff weight	(2397.2)

During the LFV study, other areas were investigated for stowage. One was aft of the ascent stage (below the aft equipment compartment) with the vehicle attached to the descent stage. This area can accommodate vehicles of large planform but only 32 inches deep. It would produce problems during ground prelaunch operations as the LM requires servicing of the aft equipment compartment and access is obtained through the SLA to this region. Also, the basic groundrule was established that the LFV (or LESS) must not be attached to the ascent stage (to minimize weight should LM abort during descent be required); this requires attaching to the descent stage. This in turn violates a current LM requirement where no part of the ascent or descent stage can protrude beyond the separation plane (again due to descent abort dynamics considerations).

The descent stage bays cannot generally assume large loads, but form fittings are provided (or contemplated) and were used as the only points of attachment. To these four points a truss structure would be built out to accept the LESS/LRF. The vehicle has to be translated out (to clear the LM), then translated and rotated down to the lunar surface. During this operation the astronaut must not be endangered, overtaxed, required to expend excessive EVA time, and must be capable of doing it alone. These requirements require the use of aids (tracks, cables, lanyards, etc.) that he can operate remotely.

Figure 3-7 shows the LESS/LRF stowed in the LM quad stowage envelope, which is a 90 degree segment, 77 inches high (between the LM heat shield and the upper bulkhead) and inside the conical envelope defined by the SLA dynamic clearance and LM/SLA extraction clearance. To meet this envelope, the vehicle requires folding of some of the components; the landing gear, display panel and support, attitude controller and support, and the two foot restraints must be folded. Completely removing a component was avoided due to the difficulty of one-man assembly. Folding was employed instead.

The shroud has the requirement of protecting the vehicle from the LM down-firing jet (located at Y = 66.1 and Z = 66.1) plume from the descent stage engine and rocks that could be thrown up from the landing engine. The shroud illustrated achieves these objectives and also offers micrometeoroid protection during translunar cruise. The shroud is enwrapped continuously around the perimeter and retained by a series of pins; the pins are released by a lanyard. Various pyrotechnics were ruled out for safety reasons.

After the shroud is removed, the LESS/LRF would be released by a lanyard operating releasing pins. Two pairs of parallel tracks control the LESS/LRF motion during removal as shown in figure 3-46. Prior to final removal the four legs are deployed, then the vehicle is lowered to the surface.

Usage of the dual purpose LESS/LRF for the basic escape mission. - Design of the vehicle modified to perform both the long-range surface flyer and the escape to orbit mission results in some compromises in performance of the basic escape mission. Structural weight is increased since landing gear must be added and the structure designed to absorb the landing loads of up to 8 g's vertical and 4 g's lateral. The landing gear or part of it could be dropped off on ascent to minimize weight but this still adds some tare weight. Separation of the lower half of the gear at the fold joints (fig. 3-7) will reduce vehicle weight by only 25 pounds at most since much of the weight is in the attenuators attached to the upper leg sections. A preferred concept if the gear is to be dropped involves design of the main engine/gear support ring in two parts with a horizontal split line. The gear would be supported from the bottom half which could be separated by pulling pins prior to escape usage.

The upper pin points of the landing load attenuators would also be disconnected and the attenuators laid down against the lower legs. Before release of the attenuators, however, four support rods must be installed to add firm attachment between engine support ring and platform. These solid rods will be pieces of GSE which will be snapped in place. These rods will be required even if the gear is not dropped off, since accurate balance and thrust vector-vehicle alignment cannot be accomplished if flexing of the attenuators were permitted. The advantages of this concept are a stable vehicle support during liftoff with the vehicle sitting on the entire support ring surface, and possible dropping of the entire gear structure with a weight saving of approximately 85 pounds.

When used for the escape mission, some pieces of subsystem equipment such as the S-band communication equipment (23 pounds) could be removed resulting in some additional weight saving. Without the landing gear and S-band communication equipment, the vehicle would be only slightly heavier than a stability-augmented vehicle designed for the escape mission only.

Within the small differences involved, performance differences between the LESS and the LESS/LRF is strictly a function of the difference in gross weight and the resultant increase in propellant requirement to achieve the required ΔV. For each pound of gross weight increase, slightly less then one pound of additional propellant is required.

Conclusions. - Since propellant for the escape mission is not critical (assuming 5000 pounds available from the LM), the weight added by conversion to also permit use as a surface flying vehicle does not significantly effect the performance of the escape to orbit mission. The complexity added to the vehicle by making the landing gear drop off for the escape mission does not appear to be justified. The added propellant required to carry the added 85 pounds increases the tank diameter requirement approximately 1/2-inch, which requires a minimal tank weight increase and should not hinder LM stowage to any great extent.

The effects on escape mission reliability and mission success probability after first using the vehicle as a surface flyer have not been evaluated, but some degradation is expected since the possibility of damage and equipment failure exists and increases with total surface usage time.

The design and development of one vehicle to perform both the surface flyer and escape missions appears to be highly desirable in view of the great similarity in vehicle requirements and the lack of significant degradation of

escape mission performance by incorporation of flyer capability. The best concept to avoid degradation of escape probability by previous vehicle surface usage may be the delivery of two identical vehicles with one being used for the surface flyer missions and the other held ready for rescue in case of flyer failure or mishap while on an extended mission and/or for use if needed for escape to orbit.

The LESS modified to perform as a long range flyer has a range radius potential of about 40 nm with 1200 pounds of propellant or 60 nm with 1600 pounds of propellant. Ranges of these magnitudes should permit substantial exploration accomplishment.

4.0 STUDY CONCLUSIONS

The analyses, test data, tradeoffs, and design studies accomplished have shown that the basic LESS concept of a simple escape vehicle is feasible. This overall conclusion is based on the following key supporting conclusions:

1. Simple manual control modes may suffice.
2. Simple boost profiles are acceptable.
3. Estimated orbital errors are acceptable, but should be confirmed by further simulation testing.
4. Initial targeting functions can be performed by MCC and transmitted via LM/ELM updata link.
5. CSM-active rendezvous requires no changes.
6. Present CSM energy budget is adequate.
7. PLSS lifetime is not exceeded (4 hours).
8. One man can deploy and set up LESS.
9. Stowage of LESS on LM/ELM is possible.
10. LM/ELM changes are minimal for stowage and defueling.
11. LESS adapts well to alternative missions.

More detailed conclusions resulting from the major task areas of the study are as follows:

Parametric Operational Information (Section 1.0)

Total ΔV requirements vary from 6200 fps to 8000 fps in the range studied, depending upon type of boost profile used, target altitudes, and thrust and weight relationships. Reduced thrust level, in contrast to fixed thrust, in the latter part of the ascent profile reduces the ΔV required.

The bent two-step trajectory profile combines near-minimum energy with simple profile steps and is particularly suitable for hardwire control with visual attitude reference sighting concepts.

A ΔV meter to signal both pitch change steps and thrust cutoff reduces trajectory errors due to expected variations in thrust/weight ratio.

Sensitivity of perilune altitude to boost errors is reduced if elliptical, rather than circular, target orbits are used; however, the total CSM energy required for rendezvous and subsequent transearth injection is increased slightly because of injection at nonoptimum orbital conditions.

CSM orbit plane changes should be made after LESS boost to minimize required energy for correction of out-of-plane LESS ascents.

The CSM will be able to track the LESS and prepare to initiate the rendezvous trajectory within approximately one quarter orbit after burnout using CSM optics, VHF ranging, and computing capabilities. A VHF ranging transponder and a flashing-light beacon will be required on LESS.

LESS boost dispersions will likely exceed the field of view of the sextant (1.8 degrees) so that initial acquisition by the scanning telescope with its 60-degree field of view will be required. To assure good viewing conditions, LESS boost should be planned so that line-of-sight range to the CSM at end boost is between 10 and 50 nm and so that neither the moon's lighted surface nor the sun is in the background when the LESS is viewed from the CSM. Depending on LESS target orbit altitude necessary to assure a clear perilune under the influence of boost errors, the CSM orbit of 60 nm may be lowered slightly (or raised) to be compatible with these requirements.

CSM-active rendezvous can be accomplished with the LM rescue ΔV budget and requires no changes to the CSM. A relatively simple LESS concept can be employed.

A hybrid LESS-active mode of rendezvous, wherein the CSM does the tracking and computing and relays the propulsion maneuver requirements by voice link to the LESS for execution, appears feasible and may be an attractive alternative, although the LESS becomes more complex.

CSM-active docking is feasible and minimizes LESS complexity; however, damage or contamination to spacesuits from CSM-RCS jet impingement is a potential problem. Alternative LESS-active docking is feasible at the expense of complications to the LESS. Another potential solution is to disable one or more of the offensive jets.

The LESS should be docked to the CSM nose to hold the vehicle steady in position for a short-path crew transfer. It would be desirable to be able to hook up the spacesuits of the LESS crew to an extended umbilical prior to entering the CSM as a safety improvement. This saves a pressure-depressure cycle of the CSM and permits independence from the backpack at the earliest time.

A wide range of sun angles, varying with surface staytime, will be encountered. This will affect vehicle sighting, landmark visibility, and glare and contrast with navigation instruments. Simple visual sighting concepts are generally characterized by their limited conditions for use and thus tend to be inappropriate for this application.

Visibility from one vehicle to the other will be a problem at various times during a mission because of sun glare from the lunar surface or looking too close to the sun. Visibility limitations will therefore be a factor to be considered in planning specific missions although it is believed that, in most instances, the mission could be completed in spite of lapses in visual contact.

Guidance and Control Techniques (Section 2.0)

Kinesthetic control vehicles tend to be very simple in concept. Consideration of desirable inertia values makes their packaging more difficult. The analysis and some of the test data indicate marginal stability and control characteristics and resulting guidance accuracy. The NASA-LRC simulation data to date, however, have indicated that further improvement in handling qualities and guidance accuracies is possible.

The hardwire mode appears more controllable and should be an acceptable mode for LESS vehicles with good guidance displays. Vehicle layout and packaging is easier than with the kinesthetic mode, because there is more freedom to adjust vehicle geometry without adversely affecting vehicle handling qualities.

A multiple-engine pulse mode concept has advantages for hardwire control in that trimming out c.g. offsets does not cause guidance errors. Early (existing) engine availability is also a feature, although the concept appears to violate the ground rule to employ simplest possible subsystems.

A relationship between control torques available and inertia of the vehicle has been postulated for evaluating vehicle manual handling qualities. Statistical data are needed from simulator testing such as that being performed at NASA-LRC to confirm and establish values of these parameters,

which then can be utilized in future design optimization. Limited data and correlations with theoretical analysis so far indicate that the relationships will prove valuable. Methods such as reducing thrust level or changing controller gains were found to considerably improve the manual-handling-quality potential of some vehicle configurations.

In the LESS mission, pilot attention is divided between two functions: maintaining vehicle stability and performing guidance tasks. Concentration on one function detracts from the attention available for the other. Simple visual attitude reference concepts generally demand high pilot concentration and, therefore, require good vehicle stability. Conversely, a manual stability mode tends to require a better instrument display, such as an all-attitude gyro horizon, to minimize pilot attention. This type of display is also superior under a wide range of sun angle conditions and is generally recommended for LESS.

A hardwire control mode with all-attitude gyro display appears to be the best choice for simple but adequate vehicle configurations. Its ability to provide acceptable trajectory accuracy is believed to be adequate for the LESS mission based on analysis, but is yet to be proved in simulations. Typical gross weight for this concept to 60 nm orbit is 2275 pounds, with 1160 pounds of propellants, 365-pound dry weight, and a 750-pound payload (two crewmen).

Design (Section 3.0)

Several arrangements appear feasible for LM or ELM stowage of LESS. A collapsible tank concept shows promise for easing the stowage problems, but requires development. Stowage of some configurations on LM/ELM Quad I may be within the RCS exhaust. Analyses by the vehicle contractor may be required to determine the effects on LM control dynamics.

The most compact vehicle appears to be one employing multiple Apollo RCS engines operating in the pulse mode, which permits tanks to be clustered in the vehicle center and minimizes lateral c.g. and inertia change during flight. This configuration also provides the necessary high reliability through redundancy for the long-range flyer adaptation where increased safety may be required (normal, rather than emergency use).

Minor changes in the LM/ELM ascent stage propellant tank drains are needed to provide for LESS fueling. Initial LESS deployment and setup requires approximately 45 minutes; and checkout for launch requires two

hours. Several balancing concepts to determine the c.g. accurately (if needed) appear feasible. Recharging of the backpacks is a major element in preparation time.

The long-range flyer adaptation of LESS is feasible and provides an order-of-magnitude increase in mission radius (40 to 60 nm) over the smaller vehicle concept recently studied for NASA-MSC. The weight-increase changes for this alternate mission, in turn, require only modest increases in propellants for the escape mission. Landing gear and structure (designed for the criteria imposed during the recent Phase B Lunar Flying Vehicle Study), throttled engines, stability augmentation, and a telecom package are the primary design changes for long-range flyer missions. The concept also has potential merit as a surface rescue vehicle, future landing site reconnaissance vehicle, and other alternative applications.

5.0 RECOMMENDATIONS

As a direct result of this study and related studies, the following recommendations are made:

1. It is recommended that additional simulation effort be supported for manual stability modes with emphasis on hardwire control. Gimbaled and reaction-jet or clustered-engine concepts should be investigated to establish pointing accuracies, handling qualities, and ultimate orbital injection accuracies. A recommended convenient approach is to assess the manual error contributions from simulation data and to combine these with other analytical errors. It is suggested that the following factors be considered in planning further simulations.

   a. High-frequency stability effects are best studied with flight vehicles such as FLEEP at NASA-LRC. Longer term effects on guidance during simulated boost should employ fixed-base visual simulators such as those in operation at NASA-LRC, with duplication of the high frequency-induced pilot workload.

   b. If possible, constant inertia data should be taken, preferably with many data points, using the same pilots, to obtain a good statistical sampling.

2. The Apollo program represents a possible opportunity to obtain excellent data on visibility limitations under extreme lunar viewing conditions. The most profitable way to obtain definitive data would be to schedule specific visibility experiments in early Apollo flights.

3. It is recommended that the long-range flyer adaptation of LESS be studied and defined in more detail because of its potential for greatly increased lunar exploration support. Its use as a surface rescue vehicle to improve mission safety and as a future landing site reconnaissance vehicle should also be considered along with alternative application possibilities.

Specific recommendations for LESS development are contained in Appendix F.

6.0 REFERENCES

1-1 CSM/LM Spacecraft Operational Data Book, Vol. II. LM Data Book, SNA-8-D-027 (June 1968), pp. 3.2-3.

1-2 Bioastronautics Data Book, Paul Webb, M.D., Editor, NASA SP-3006 (1964), p. 310.

1-3 Lunar Atlas, Vol. 1. United States Air Force (February 1960).

1-4 Guidance System Operations Plan for Manned CM Earth Orbital and Lunar Mission Using Program Colossus, MIT Laboratory Report R-577, (December 1967); see Section 5.4.4.5, "Stable Orbit Rendezvous."

1-5 Apollo Operations Handbook, Vol. II, Procedures, NR SD, SD 69-57 (17 April 1969).

1-6 Mission Evaluation 104 Study Analysis Report, NR SD, SD 69-73, Section 7.7 (February 1969).

1-7 A Manual Method for Space Rendezvous Navigation and Guidance, AIAA Guidance, Control and Flight Dynamics Conference, Pasadena, California. Pre-print No. 68-859 (12 August 1968).

1-8 Rendezvous Navigation and Guidance Using a Hand-Held, Self-Powered Digital Computer, AIAA Guidance, Control, and Flight Dynamics Conference, Pasadena, California, Pre-print No. 68-860 (12 August 1968).

1-9 Nishizaka, T.J. "Docking Mechanisms Applicable to Logistics Spacecraft Systems," AIAA Journal of Spacecraft and Rockets (September 1968), p. 1112.

1-10 Chiarappa, Daniel. Analysis and Design of Space Vehicle Flight Control Systems, Vol. VIII, Rendezvous and Docking, NASA CR-827 (July 1967), para. 22.

1-11 Ward and Williams. "Orbital Docking Dynamics," AIAA Journal (June 1963).

1-12 Grubin, C. Docking Dynamics for Rigid-Body Spacecraft, IAS Paper No. 62-43 (January 1962).

1-13 Heilfron, J., and F.H. Kaufman. Rendezvous and Docking Techniques, ARS No. 2460-62 (July 1962).

1-14 Beasley, G.P., R.F. Brissendon, W.H. Straly, and R.W. Ailhock. "Retrieving the Tethered Astronaut," Astronautics and Aeronautics (January 1965), para. 72.

1-15 Freeman, B. The Reaction Control System Facility (Building 289-S&ID Downey) Operational Capabilities Evaluation and Analysis. NR SD, SID 66-1905 (May 1967).

2-1 Hewes, D.E. Studies of Piloting Problems of One-Man Flying Units Operated in Simulated Lunar Gravity, Second National Conference on Space Maintenance and Extravehicular Activities, Las Vegas, Nevada (6-8 August 1968).

2-2 Hefner, W., and G.C. McGee. Stability, Control, and Flight Performance Characteristics of Small, Manned Propulsion Devices, NR SD, SD 69-405 (30 June 1969).

2-3 Satterlee, C.E. Flight Evaluation of a Kinesthetically Controlled Flying Vehicle, Bell Aerosystems Company, Report 2369-927001 (March 1969).

2-4 Pilot Dynamics and Aircraft Handling Qualities, AIAA Professional Study Series, International Hotel, Los Angeles, California (10-11 August 1968).

2-5 Ashkenas, I.L., D.T. McRuer, and C.L. Guerre. A Systems Analysis View of Longitudinal Handling Qualities, Wright-Patterson AFB, Ohio, WADD-TR-60-63 (January 1960).

2-6 McRuer, D.T. and E.S. Drendel, Dynamic Response of Human Operators, Wright-Patterson AFB, Ohio, WADC-TR-56-524 (1957).

2-7 Study of the Mechanism of Human Balancing for Potential Application to the Control of Vehicles, Part II: Toward a Math Model of Vertical Balance in Earth Gravity, Bethpage, New York, Grumman Engineering Report RM 369 (July 1967).

2-8 Linder, G.S. Effects of Mechanical Vibration on Humans, NR SD, NA 59-1420 (September 1959).

2-9 Bergeron, H.P., and J. Adams. Measured Transfer Functions of Pilots During Two-Axis Tasks With Motion, NASA TN D-2177 (March 1964).

2-10 Boisseau, P. C., et al. Preliminary Investigation of the Handling Qualities of a Vehicle in a Simulated Lunar Gravitational Field, NASA TN D-2636 (February 1965).

2-11 Study of One-Man Lunar Flying Vehicle, NR SD, SD 69-419 (31 August 1969).

APPENDIX A. COMPUTER PRINTOUT FOR BENT TWO-STEP TRAJECTORY WITH TWO-STEP THRUST

This appendix contains a computer printout of a trajectory to 60 nm orbit used as the basis for some simulation studies at NASA-LRC. It reflects a two-step thrust schedule with the first step charcterized by a liftoff thrust-to-weight ratio of 0.3 pounds per pound and the second step representing a reduction in thrust to one-third liftoff value. The parameters for thrust reduction are based on LESS handling quality considerations (see the Guidance and Control section). A modified bent two-step steering profile is employed. It is initiated by a 10-second vertical boost followed by two constant attitude steps corresponding to the thrust level steps. The pitch maneuvers were simulated assuming a pitching acceleration of minus one degree per second squared to a maximum value of minus five degrees per second, followed by a pitching acceleration of one degree per second squared to a pitch rate of zero.*

Table A-1 contains a definition of the elements in the print format. Those elements which are meaningless to this particular problem are not defined and distinctions are not made among those elements for which the simplifying assumptions result in equal values.

Each page of computer printout (Table A-2) contains a block of headings followed by three blocks of data conforming to the headings. On the bottom of each page is some descriptive information relating to the case and to the segment of the trajectory presently being computed. For convenience of analysis, this trajectory has been divided into segments ("stages") that correspond to the key phases of the boost. As is evident from the headings, the program was designed to solve boost problems on the earth. The following constants were used to approximate the characteristics of the moon:

Gravitational parameter ($\mu = .17314 \times 10^{15}$ ft^3/sec^2)
Radius = 5,702,400 feet (spherical)
Spin rate = 0
No gravitational anomalies

*A trajectory informally transmitted to LRC on 18 September 1969 had the same properties except that the pitch maneuvers were approximated with a constant pitch rate.

TABLE A-1. - PRINT FORMAT DEFINITION

A	B	C		D	E	F
TIME	INCLINATION	GAMMA GEOC	1	AZIMUTH GEOC	WEIGHT	ALTITUDE
STAGE TIME	AIRSPEED	GAM A GEOC	2	AZI A GEOC	FLOW RATE	RADIUS
THRUST	VEL EARTH FIX	GAM A GEOD	3	AZI A GEOD	LATITUDE GEOC	LONGITUDE
MACH NO.	VEL INERTIAL	GAMMA INERT	4	AZIMUTH INERT	LATITUDE GEOD	HOUR ANGLE
DYNAMIC PRESS	VEL WIND	GAMDOT GEOC	5	AZIDOT GEOC	VEL THEO	ETA X
RANGE TOTAL	LIFT	VELDOT GEOC	6	PSI	VEL DRAG	ETA Y
RANGE GRT-CIR	DRAG	ALPHA	7	THETA	VEL GRAV	ETA Z
ENERGY	SIDEFORCE	BETA	8	PHI	AERO HEAT	ETA TOTAL
ANGULAR MOMENTUM	RADIUS PERIGEE	RADIUS APOGEE	9	VEL PERIGEE	VEL APOGEE	VEL CIRCULAR

Element	Heading	Description	Units
A1	TIME	Time since beginning of problem	Seconds
A2	STAGE TIME	Time since beginning of stage	Seconds
A3	THRUST	Vehicle thrust	Pounds
A4	MACH NO.	NA	
A5	DYNAMIC PRESS	NA	
A6	RANGE TOTAL	Integral of vehicle subpoint trace	Nm
A7	RANGE GRT-CIR	Surface range from vehicle subpoint to reference point (ignore for small displacements)	Nm
A8	ENERGY	Specific energy	Ft^2/sec^2
A9	ANGULAR MOMENTUM	Specific angular momentum	Ft^2/sec
B1	INCLINATION	Angle between trajectory plane and equator plane	Degrees
B2	AIRSPEED	Vehicle speed with respect to moon	Ft/sec
B3	VEL EARTH FIX	Same as B2	Ft/sec
B4	VEL INERTIAL	Same as B2	Ft/sec
B5	VEL WIND	NA	
B6	LIFT	NA	
B7	DRAG	NA	
B8	SIDEFORCE	NA	
B9	RADIUS PERIGEE	Distance from the center of the moon to the instantaneous perilune	Feet
C1	GAMMA GEOC	Flight path angle, positive above the local horizontal	Degrees
C2	GAM A GEOC	Same as C1	
C3	GAM A GEOD	Same as C1	
C4	GAMMA INERT	Same as C1	
C5	GAMDOT GEOC	Rate of change of flight path angle	Deg/sec
C6	VELDOT GEOC	Rate of change of speed	Ft/sec^2
C7	ALPHA	Pitch angle of attack	Degrees
C8	BETA	Yaw angle of attack	Degrees
C9	RADIUS APOGEE	Distance from the center of the moon to the instantaneous apolune	Feet

TABLE A-1. - PRINT FORMAT DEFINITION - Continued

Elements	Heading	Description	Units
D1	AZIMUTH GEOC	Azimuth with respect to meridian	Degrees
D2	AZI A GEOC	Same as D1	
D3	AZI A GEOD	Same as D1	
D4	AZIMUTH INERT	Same as D1	
D5	AZIDOT GEOC	Rate of change of azimuth	Deg/sec
D6	PSI	Thrust azimuth with respect to meridian	Degrees
D7	THETA	Pitch attitude with respect to the local horizontal, positive above the horizontal	Degrees
D8	PHI	Roll attitude	Degrees
D9	VEL PERIGEE	Speed at instantaneous perilune	Ft/sec
E1	WEIGHT	Vehicle weight	Pounds
E2	FLOW RATE	Propulsion system flow rate	Pounds/sec
E3	LATITUDE GEOC	Latitude, positive north of equator	Degrees
E4	LATITUDE GEOD	Same as E3	
E5	VEL THEO	Characteristic velocity	Ft/sec
E6	VEL DRAG	NA	
D7	VEL GRAV	Velocity losses due to gravity	Ft/sec
D8	AERO HEAT	NA	
E9	VEL APOGEE	Speed at instantaneous apolune	Ft/sec
F1	ALTITUDE	Distance above the moon	Feet
F2	RADIUS	Distance from the center of the moon	Feet
F3	LONGITUDE	Longitude, positive counterclockwise	Degrees
F4	HOUR ANGLE	Same as F3	
F5	ETA X	Load factor in vehicle longitudinal direction	Unitless
F6	ETA Y	NA	
F7	ETA Z	NA	
F8	ETA TOTAL	Same as F5	
F9	VEL. CIRCULAR	Instantaneous circular velocity	Ft/sec

TABLE A-2. - BENT TWO-STEP TRAJECTORY, TWO-STEP THRUST PRINTOUT

TIME	INCLINATION	GAMMA GEOC	1	AZIMUTH GEOC	WEIGHT	ALTITUDE
STAGE TIME	AIRSPEED	GAM A GEOC	2	AZI A GEOD	FLOW RATE	RADIUS
THRUST	VEL EARTH FIX	GAM A GEOD	3	AZI A GEOD	LATITUDE GEOC	LONGITUDE
MACH NO.	VEL INERTIAL	GAMMA INERT	4	AZIMUTH INERT	LATITUDE GEOD	HOUR ANGLE
DYNAMIC PRESS	VEL WIND	GAMDOT GEOC	5	AZIDOT GEOC	VEL THRO	ETA X
RANGE TOTAL	LIFT	VELDOT GEOC	6	PSI	VEL DRAG	ETA Y
RANGE GRT-CIR	DRAG	ALPHA	7	THETA	VEL GRAV	ETA Z
ENERGY	SIDEFORCE	BETA	8	PHI	AERO HEAT	ETA TOTAL
ANGULAR MOMENTUM	RADIUS PERIGEE	RADIUS APOGEE	9	VEL PERIGEE	VEL APOGEE	VEL.CIRCULAR
0.0	0.999999E-02	0.999999E-02	1	0.0	0.100000E 04	0.0
0.0	0.999999E-02	0.999999E-02	2	0.0	0.100000E 01	0.570246E 07
0.300000E 03	0.999999E-02	0.999999E-02	3	0.270000E 03	0.500000E 01	0.0
0.0	0.999999E-02	0.999999E-02	4	0.0	0.500000E 01	0.0
0.0	0.0	-0.144653E 04	5	-0.185146E 02	0.0	0.300000E 00
0.0	0.0	0.432766E 01	6	-0.900001E 02	0.0	0.0
0.324031E 00	0.0	-0.187754E-04	7	0.900000E 02	0.0	0.0
-0.303626E 08	0.0	0.0	8	0.0	0.0	0.300000E 00
0.0	0.0	0.570246E 07	9	0.0	0.327693E-08	0.551023E 04
0.100000E 02	0.999999E 02	0.999999E 02	1	0.0	0.989999E 03	0.218103E 03
0.100000E 02	0.437739E 02	0.999999E 02	2	0.0	0.100000E 01	0.570261E 07
0.300000E 03	0.437739E 02	0.999999E 02	3	0.273414E 03	0.499999E 01	0.360000E 03
0.0	0.437739E 02	0.999999E 02	4	0.0	0.499999E 01	0.0
0.0	0.0	-0.364674E 01	5	-0.340342E 00	0.970080E 02	0.303030E 00
0.264776E-07	0.0	0.442558E 01	6	-0.900001E 02	0.0	0.0
0.324031E 00	0.0	-0.187754E-04	7	0.900000E 02	-0.532441E 02	0.0
-0.303626E 08	0.0	0.0	8	0.0	0.0	0.303030E 00
0.0	0.0	0.570246E 07	9	0.0	0.143447E-04	0.551012E 04

END OF STAGE 1 MET WITH STOP NUMBER 1 = 0.100000E 02 , EXECUTION TIME = 1 MIN 0 SEC,

STAGE 1 BENT 2-STEP WITH 2-STEP THRUST T/W =0.3 60NM ORBIT 9/12 CASE 1
IC SECOND VERTICAL BOOST PAGE 1

TABLE A-2. - BENT TWO-STEP TRAJECTORY, TWO-STEP THRUST PRINTOUT - Continued

TIME	INCLINATION	GAMMA GEOC	1	AZIMUTH GEOC	WEIGHT	ALTITUDE
STAGE TIME	AIRSPEED	GAM A GEOC	2	AZI A GEOC	FLOW RATE	RADIUS
THRUST	VEL EARTH FIX	GAM A GEOD	3	AZI A GEOD	LATITUDE GEOC	LONGITUDE
MACH NO.	VEL INERTIAL	GAMMA INERT	4	AZIMUTH INERT	LATITUDE GEOC	HOUR ANGLE
DYNAMIC PRESS	VEL WIND	GAMCCT GEOC	5	AZICCT GEOC	VEL THEO	ETA X
RANGE TOTAL	LIFT	VELCCT GEOC	6	PSI	VEL DRAG	ETA Y
RANGE GRT-CIR	DRAG	ALPHA	7	THETA	VEL GRAV	ETA Z
ENERGY	SIDEFORCE	BETA	8	PHI	AERO HEAT	ETA TOTAL
ANGULAR MOMENTUM	RADIUS PERIGEE	RADIUS APOGEE	9	VEL PERIGEE	VEL APOGEE	VEL.CIRCULAR
0.1[illegible]E 02	0.[illegible]E 02	0.[illegible]E 02	1	0.0	0.989999E 03	0.2181C3E C3
0.0	0.4377[illegible]E 02	0.[illegible]E 02	2	0.0	0.1000C0E 01	0.5702[illegible]E C7
0.3[illegible]E C3	0.4377[illegible]E 02	0.[illegible]E 02	3	0.273414E 03	0.499999E 01	0.3600C0E C3
0.0	0.4377[illegible]E 02	0.[illegible]E 02	4	0.0	0.499999E 01	0.0
0.0	0.0	-0.729347E 01	5	-0.103862E 07	0.970C80E 02	0.3C3031E CC
.244776E-07	0.0	-0.532441E 01	6	-0.900001E 02	0.0	0.0
0.324031E CC	0.0	-0.[illegible]E 02	7	0.0	-0.532441E 02	0.0
-0.3[illegible]E C8	0.0	0.0	8	0.0	0.0	0.303031E CC
0.0	0.0	0.5702[illegible]E 07	9	0.0	0.143440E-04	0.551C12E C4
0.14[illegible]E 02	0.175[illegible]E 03	0.[illegible]E 02	1	0.270000E 03	0.985999E C3	0.42855[illegible]E C3
0.4000[illegible]E 01	0.414822E 02	0.[illegible]E 02	2	0.270000E 03	0.100000E 01	0.5702[illegible]E C7
0.3000[illegible]E C3	0.414822E 02	0.[illegible]E 02	3	0.270000E 03	0.499999E 01	0.360C[illegible]E C3
0.0	0.414822E 02	0.[illegible]E 02	4	0.270000E 03	0.499999E 01	0.360CC0E C3
0.0	0.0	-0.114[illegible]E C1	5	-0.260256E-04	0.136086E 03	0.3042[illegible]E CC
0.3158[illegible]E-03	0.0	0.44[illegible]E C1	6	-0.900002E 02	0.0	0.0
0.324031E CC	0.0	-0.[illegible]E C1	7	0.819999E 02	-0.745384E 02	0.0
-0.3[illegible]E C8	0.0	-0.[illegible]E-05	8	0.0	0.0	0.3042[illegible]E CC
0.1[illegible]E C8	0.[illegible]E CC	0.[illegible]E 07	9	0.154614E 08	0.184314E 01	0.551CC2E C4
0.180[illegible]E 02	0.175[illegible]E 03	0.[illegible]E 02	1	0.270000E 03	0.981998E 03	0.707544E C3
0.8[illegible]E 01	0.785723E 02	0.[illegible]E 02	2	0.270000E C3	0.100000E 01	0.5703[illegible]E C7
0.3[illegible]E C3	0.785723E 02	0.[illegible]E 02	3	0.270000E 03	0.499999E 01	0.3600C0E C3
0.0	0.785723E 02	0.[illegible]E 02	4	0.270000E 03	0.499999E 01	0.360CCCE C3
0.0	0.0	-0.283[illegible]E C1	5	-0.151461E-04	0.175323E 03	0.3054[illegible]E CC
0.469716E-02	0.0	0.412981E C1	6	-0.900002E 02	0.0	0.0
0.324031E CC	0.0	-0.175[illegible]E C2	7	0.624791E 02	-0.957231E 02	0.0
-0.3[illegible]E C8	0.0	-0.223242E-04	8	0.0	0.0	0.3054[illegible]E CC
0.777004E C8	0.175[illegible]E 02	0.5703[illegible]E 07	9	0.443793E 07	0.136229E 02	0.5509[illegible]E C4

STAGE 2 BENT 2-STEP WITH 2-STEP THRUST T/W =0.3 6CNN CRRIT 9/12 CASE 1
PITCH AT THOCT = -1EPS2 TO THOCT = -5DEG PAGE 2

TABLE A-2. - BENT TWO-STEP TRAJECTORY, TWO-STEP THRUST PRINTOUT - Continued

TIME	INCLINATION	GAMMA GEOC	1	AZIMUTH GEOC	WEIGHT	ALTITUDE
STAGE TIME	AIRSPEED	GAM A GEOC	2	AZI A GEOC	FLOW RATE	RADIUS
THRUST	VEL EARTH FIX	GAM A GEOD	3	AZI A GEOD	LATITUDE GEOC	LONGITUDE
MACH NO.	VEL INERTIAL	GAMMA INERT	4	AZIMUTH INERT	LATITUDE GEOC	HOUR ANGLE
DYNAMIC PRESS	VEL WIND	GAMDOT GEOC	5	AZIDOT GEOC	VEL THEO	ETA X
RANGE TOTAL	LIFT	VELDOT GEOC	6	PSI	VEL DRAG	ETA Y
RANGE GRT-CIR	DRAG	ALPHA	7	THETA	VEL GRAV	ETA Z
ENERGY	SIDEFORCE	BETA	8	PHI	AERO HEAT	ETA TOTAL
ANGULAR MOMENTUM	RADIUS PERIGEE	RADIUS APOGEE	9	VEL PERIGEE	VEL APOGEE	VEL.CIRCULAR
0.198850E 02	0.175000E 03	0.741916E 02	1	0.270000E 03	0.980114E 03	0.858570E 03
0.988498E 01	0.862810E 02	0.741916E 02	2	0.270000E 03	0.100000E 01	0.570226E 07
0.300000E 03	0.862810E 02	0.741916E 02	3	0.270000E 03	0.499999E 01	0.359999E 03
0.0	0.862810E 02	0.741916E 02	4	0.270000E 03	0.499999E 01	0.359999E 03
0.0	0.0	-0.332097E 01	5	-0.214695E-04	0.193868E 03	0.306087E 00
0.103883E-01	0.0	0.406384E 01	6	-0.900002E 02	0.0	0.0
0.324031E 00	0.0	-0.211374E 02	7	0.530542E 02	-0.105503E 03	0.0
-0.303544E 08	0.0	-0.197286E-04	8	0.0	0.0	0.306087E 00
0.134053E 09	0.520173E 02	0.570399E 07	9	0.257710E 07	0.235021E 02	0.550982E 04

END OF STAGE 2 MET WITH STOP NUMBER 7 = 0.988497S4E 01 , EXECUTION TIME = 1 MIN 2 SEC,

STAGE 2 BENT 2-STEP WITH 2-STEP THRUST T/W =0.2 6CAA ORBIT 9/12 CASE 1
PITCH AT THDOT = -1DPS2 TO THDOT = -5DPS PAGE 2

TABLE A-2. - BENT TWO-STEP TRAJECTORY, TWO-STEP THRUST PRINTOUT - Continued

TIME	INCLINATION	GAMMA GEOC	1	AZIMUTH GEOC	WEIGHT	ALTITUDE
STAGE TIME	AIRSPEED	GAMMA GEOC	2	AZI A GEOC	FLOW RATE	RADIUS
THRUST	VEL EARTH FIX	GAMMA GEOD	3	AZI A GEOC	LATITUDE GEOC	LONGITUDE
MACH NO.	VEL INERTIAL	GAMMA INERT	4	AZIMUTH INERT	LATITUDE GEOD	HOUR ANGLE
DYNAMIC PRESS	VEL WIND	GAMDOT GEOC	5	AZIDOT GEOC	VEL THEO	ETA X
RANGE TOTAL	LIFT	VELDOT GEOC	6	PSI	VEL DRAG	ETA Y
RANGE DOT-CIR	DRAG	ALPHA	7	THETA	VEL GRAV	ETA Z
ENERGY	SIDEFORCE	BETA	8	PHI	AERO HEAT	ETA TOTAL
ANGULAR MOMENTUM	RADIUS PERIGEE	RADIUS APOGEE	9	VEL PERIGEE	VEL APOGEE	VEL.CIRCULAR
0.198866E 02	0.175[illegible]E 03	0.741916E 02	1	0.270000E 03	0.983113E 03	0.859970E 03
0.0	0.862881E 02	0.741916E 02	2	0.270000E 03	0.100000E 01	0.570326E 07
0.300000E 03	0.862881E 02	0.741916E 02	3	0.270000E 03	0.499999E 01	0.359999E 03
0.0	0.862881E 02	0.741916E 02	4	0.270000E 03	0.499999E 01	0.359999E 03
0.0	0.0	-0.332096E 01	5	-0.213242E-04	0.193868E 03	0.306087E 00
0.0	0.0	0.406384E 01	6	-0.900002E 02	0.0	0.0
-0.113883E-01	0.0	0.0	7	0.530542E 02	-0.105503E 03	0.0
0.324031E 00	0.0	-0.211374E 02	8	0.0	0.0	0.306087E 00
-0.335544E 08	0.0	-0.197286E-04	9	0.257710E 07	0.235021E 02	0.550982E 04
0.134053E 09	0.522173E 02	0.570390E 07				
0.238850E 02	0.175000E 03	0.604375E 02	1	0.270000E 03	0.976113E 03	0.120673E 04
0.400000E 01	0.103393E 03	0.604375E 02	2	0.270000E 03	0.100000E 01	0.570360E 07
0.300000E 03	0.103393E 03	0.604375E 02	3	0.270000E 03	0.499999E 01	0.359999E 03
0.0	0.103393E 03	0.604375E 02	4	0.270000E 03	0.499999E 01	0.359999E 03
0.0	0.0	-0.327327E 01	5	-0.449904E-04	0.223341E 03	0.307341E 00
0.345781E-01	0.0	0.469891E 01	6	-0.900033E 02	0.0	0.0
0.324031E 00	0.0	-0.193833E 02	7	0.410542E 02	-0.125095E 03	0.0
-0.335544E 08	0.0	-0.899864E-04	8	0.0	0.0	0.307341E 00
0.290948E 09	0.244478E 03	0.570437E 07	9	0.119009E 07	0.510045E 02	0.550965E 04
0.248850E 02	0.175000E 03	0.572797E 02	1	0.270000E 03	0.975113E 03	0.129724E 04
0.500000E 01	0.108241E 03	0.572797E 02	2	0.270000E 03	0.100000E 01	0.570369E 07
0.300000E 03	0.108241E 03	0.572797E 02	3	0.270000E 03	0.499999E 01	0.359997E 03
0.0	0.108241E 03	0.572797E 02	4	0.270000E 03	0.499999E 01	0.359997E 03
0.0	0.0	-0.330310E 01	5	-0.515593E-04	0.243234E 03	0.307657E 00
0.438876E-01	0.0	0.500218E 01	6	-0.900004E 02	0.0	0.0
0.324031E 00	0.0	-0.167255E 02	7	0.405542E 02	-0.129649E 03	0.0
-0.335544E 08	0.0	-0.699521E-04	8	0.0	0.0	0.307656E 00
0.333715E 09	0.321671E 03	0.570448E 07	9	0.103744E 07	0.585006E 02	0.550961E 04

STAGE 3 BENT 2-STEP WITH 2-STEP THRUST T/W =0.2 60NM CRBIT 9/12 CASE 1
COMPLETE PITCH MANEUVER TO THDOT = 0 AT THDOT = 1DPS2 PAGE 3

TABLE A-2. - BENT TWO-STEP TRAJECTORY, TWO-STEP THRUST PRINTOUT - Continued

TIME	INCLINATION	GAMMA GEOC	1	AZIMUTH GEOC	WEIGHT	ALTITUDE
STAGE TIME	AIRSPEED	GAM A GEOC	2	AZI A GEOC	FLOW RATE	RADIUS
THRUST	VEL EARTH FIX	GAM A GEOD	3	AZI A GEOD	LATITUDE GEOC	LONGITUDE
MACH NO.	VEL INERTIAL	GAMMA INERT	4	AZIMUTH INERT	LATITUDE GEOD	HOUR ANGLE
DYNAMIC PRESS	VEL WIND	GAMDOT GEOC	5	AZIDOT GEOC	VEL THEO	ETA X
RANGE TOTAL	LIFT	VELDOT GEOC	6	PSI	VEL DRAG	ETA Y
RANGE GRT-CIR	DRAG	ALPHA	7	THETA	VEL GRAV	ETA Z
ENERGY	SIDEFORCE	BETA	8	PHI	AERO HEAT	ETA TOTAL
ANGULAR MOMENTUM	RADIUS PERIGEE	RADIUS APOGEE	9	VEL PERIGEE	VEL APOGEE	VEL.CIRCULAR
0.248850E 02	0.175000E 03	0.572797E 02	1	0.270000E 03	0.975113E 03	0.129724E 04
0.0	0.108241E 03	0.572797E 02	2	0.270000E 03	0.100000E 01	0.570369E 07
0.300000E 03	0.108241E 03	0.572797E 02	3	0.270000E 03	0.499999E 01	0.359997E 03
0.0	0.108241E 03	0.572797E 02	4	0.270000E 03	0.499999E 01	0.359997E 03
0.0	0.0	-0.303016E 01	5	-0.515593E-04	0.243234E 03	0.307657E 00
0.435876E-01	0.0	0.500219E 01	6	-0.900004E 02	0.0	0.0
0.324031E 00	0.0	-0.167255E 02	7	0.405542E 02	-0.129649E 03	0.0
-0.303499E 08	0.0	-0.699921E-04	8	0.0	0.0	0.307657E 00
0.333715E 09	0.321671E 03	0.570448E 07	9	0.103744E 07	0.585006E 02	0.550961E 04
0.408850E 02	0.175000E 03	0.314115E 02	1	0.269998E 03	0.959112E 03	0.290173E 04
0.160000E 02	0.210683E 03	0.314115E 02	2	0.269998E 03	0.100000E 01	0.570530E 07
0.300000E 03	0.210683E 03	0.314115E 02	3	0.269998E 03	0.499999E 01	0.359978E 03
0.0	0.210683E 03	0.314115E 02	4	0.269998E 03	0.499999E 01	0.359978E 03
0.0	0.0	-0.757861E 00	5	-0.158077E-03	0.402925E 03	0.312789E 00
0.356808E 00	0.0	0.716361E 01	6	-0.900020E 02	0.0	0.0
0.324031E 00	0.0	0.514274E 01	7	0.405542E 02	-0.185585E 03	0.0
-0.303250E 08	0.0	-0.201443E-03	8	0.0	0.0	0.312789E 00
0.102585E 10	0.304068E 04	0.570643E 07	9	0.337375E 06	0.179770E 03	0.550883E 04
0.568850E 02	0.175000E 03	0.232889E 02	1	0.269994E 03	0.943112E 03	0.482121E 04
0.320000E 02	0.329983E 03	0.232889E 02	2	0.269994E 03	0.100000E 01	0.570722E 07
0.300000E 03	0.329983E 03	0.232889E 02	3	0.269994E 03	0.499999E 01	0.359939E 03
0.0	0.329983E 03	0.232889E 02	4	0.269994E 03	0.499999E 01	0.359939E 03
0.0	0.0	-0.317256E 00	5	-0.266245E-03	0.565302E 03	0.318096E 00
0.991735E 00	0.0	0.767168E 01	6	-0.900054E 02	0.0	0.0
0.648262E 00	0.0	0.172653E 02	7	0.405542E 02	-0.223820E 03	0.0
-0.302826E 08	0.0	-0.167530E-03	8	0.0	0.0	0.318096E 00
0.172984E 10	0.865445E 04	0.570882E 07	9	0.199978E 06	0.303011E 03	0.550795E 04

STAGE 4 BENT 2-STEP WITH 2-STEP THRUST T/W =0.3 60NM CRFIT 9/12
CONSTANT PITCH ANGLE

CASE 1
PAGE 4

TABLE A-2. - BENT TWO-STEP TRAJECTORY, TWO-STEP THRUST PRINTOUT - Continued

TIME	INCLINATION	GAMMA GEOC	1	AZIMUTH GEOC	WEIGHT	ALTITUDE
STAGE TIME	AIRSPEED	GAM A GEOC	2	AZI A GEOC	FLOW RATE	RADIUS
THRUST	VEL EARTH FIX	GAM A GEOD	3	AZI A GEOD	LATITUDE GEOC	LONGITUDE
MACH NO.	VEL INERTIAL	GAMMA INERT	4	AZIMUTH INERT	LATITUDE GEOD	HOUR ANGLE
DYNAMIC PRESS	VEL WIND	GAMDOT GEOC	5	AZIDOT GEOC	VEL THEO	ETA X
RANGE TOTAL	LIFT	VELDOT GEOC	6	PSI	VEL DRAG	ETA Y
RANGE GRT-CIR	DRAG	ALPHA	7	THETA	VEL GRAV	ETA Z
ENERGY	SIDEFORCE	BETA	8	PHI	AERO HEAT	ETA TOTAL
ANGULAR MOMENTUM	RADIUS PERIGEE	RADIUS APOGEE	9	VEL PERIGEE	VEL APOGEE	VEL.CIRCULAR
0.728850E 02	0.175[illegible]E 03	0.196767E 02	1	0.269989E 03	0.927112E 03	0.708768E 04
0.488000E 02	0.455[illegible]E 03	0.196767E 02	2	0.269989E 03	0.100000E 01	0.570948E 07
0.300000E 03	0.455[illegible]E 03	0.196767E 02	3	0.269989E 03	0.499993E 01	0.359880E 03
0.0	0.455[illegible]E 03	0.196767E 02	4	0.269989E 03	0.499998E 01	0.359880E 03
0.0	0.0	-0.195286E 00	5	-0.376113E-03	0.734458E 03	0.323585E 00
0.195343E 01	0.0	0.703912E 01	6	-0.900105E 02	0.0	0.0
0.180413E 01	0.0	0.268775E 02	7	0.405542E 02	-0.254563E 03	0.0
-0.302215E 08	0.0	-0.222252E-03	8	0.0	0.0	0.323585E 00
0.244614E 10	0.173322E 05	0.571171E 07	9	0.141133E 06	0.428268E 03	0.550681E 04
0.898850E 02	0.175000E 03	0.177739E 02	1	0.269982E 03	0.911113E 03	0.973576E 04
0.640000E 02	0.583738E 03	0.177739E 02	2	0.269982E 03	0.100000E 01	0.571213E 07
0.300000E 03	0.583738E 03	0.177739E 02	3	0.269982E 03	0.499996E 01	0.359801E 03
0.0	0.583738E 03	0.177739E 02	4	0.269982E 03	0.499996E 01	0.359801E 03
0.0	0.0	-0.877872E-01	5	-0.487774E-03	0.898489E 03	0.329268E 00
0.324702E 01	0.0	0.814766E 01	6	-0.900175E 02	0.0	0.0
0.328856E 01	0.0	0.227803E 02	7	0.405542E 02	-0.281802E 03	0.0
-0.311405E 08	0.0	-0.122601E-03	8	0.0	0.0	0.329268E 00
0.317523E 10	0.292644E 05	0.571516E 07	9	0.108501E 06	0.555581E 03	0.550554E 04
0.124985E 03	0.175000E 03	0.166561E 02	1	0.269974E 03	0.895112E 03	0.128028E 05
0.800000E 02	0.715641E 03	0.166561E 02	2	0.269974E 03	0.100000E 01	0.571520E 07
0.300000E 03	0.715641E 03	0.166561E 02	3	0.269974E 03	0.499993E 01	0.359701E 03
0.0	0.715641E 03	0.166561E 02	4	0.269974E 03	0.499993E 01	0.359701E 03
0.0	0.0	-0.554206E-01	5	-0.601187E-03	0.106950E 04	0.335152E 00
0.487771E 01	0.0	0.833693E 01	6	-0.900262E 02	0.0	0.0
0.490349E 01	0.0	0.238581E 02	7	0.405542E 02	-0.306875E 03	0.0
-0.308386E 08	0.0	-0.226084E-03	8	0.0	0.0	0.335152E 00
0.391760E 10	0.446677E 05	0.571525E 07	9	0.877055E 05	0.694985E 03	0.550405E 04

STAGE 4 BENT 2-STEP WITH 2-STEP THRUST T/W =0.3 6DAY ORBIT 9/12 CASE 1
CONSTANT PITCH ANGLE PAGE 5

TABLE A-2. - BENT TWO-STEP TRAJECTORY, TWO-STEP THRUST PRINTOUT - Continued

TIME	INCLINATION	GAMMA GEOC	1	AZIMUTH GEOC	WEIGHT	ALTITUDE
STAGE TIME	AIRSPEED	GAM A GEOC	2	AZI A GEOC	FLOW RATE	RADIUS
THRUST	VEL EARTH FIX	GAM A GEOD	3	AZI A GEOD	LATITUDE GEOC	LONGITUDE
MACH NO.	VEL INERTIAL	GAMMA INERT	4	AZIMUTH INERT	LATITUDE GEOC	HOUR ANGLE
DYNAMIC PRESS	VEL WIND	GAMDOT GEOC	5	AZIDOT GEOC	VEL THEO	ETA X
RANGE TOTAL	LIFT	VELDOT GEOC	6	PSI	VEL DRAG	ETA Y
RANGE GRT-CIR	DRAG	ALPHA	7	THETA	VEL GRAV	ETA Z
ENERGY	SIDEFORCE	BETA	8	PHI	AERO HEAT	ETA TOTAL
ANGULAR MOMENTUM	RADIUS PERIGEE	RADIUS APOGEE	9	VEL PERIGEE	VEL APOGEE	VEL.CIRCULAR
0.128885E 03	0.175000E 03	0.160816E 02	1	0.269963E 03	0.879112E 03	0.163285E 05
0.969000E 02	0.859565E 03	0.160816E 02	2	0.269963E 03	0.100000E 01	0.571872E 07
0.300000E 03	0.859565E 03	0.160816E 02	3	0.269963E 03	0.499986E 01	0.359580E 03
0.0	0.859565E 03	0.160816E 02	4	0.269963E 03	0.499986E 01	0.359580E 03
0.0	0.0	-0.280983E-01	5	-0.716357E-03	0.124359E 04	0.341253E 00
0.685975E 01	0.0	0.852697E 01	6	-0.900367E 02	0.0	0.0
0.685846E 01	0.0	0.244125E 02	7	0.405542E 02	-0.330748E 03	0.0
-0.299142E 08	0.0	-0.175253E-03	8	0.0	0.0	0.341253E 00
0.467380E 10	0.637861E 05	0.572409E 07	9	0.732730E 05	0.816513E 03	0.550236E 04
0.136885E 03	0.175000E 03	0.157562E 02	1	0.269951E 03	0.863112E 03	0.203573E 05
0.112000E 03	0.988503E 03	0.157562E 02	2	0.269951E 03	0.100000E 01	0.572275E 07
0.300000E 03	0.988503E 03	0.157562E 02	3	0.269951E 03	0.499975E 01	0.359438E 03
0.0	0.988503E 03	0.157562E 02	4	0.269951E 03	0.499975E 01	0.359438E 03
0.0	0.0	-0.135262E-01	5	-0.833298E-03	0.142088E 04	0.347575E 00
0.917142E 01	0.0	0.871628E 01	6	-0.900491E 02	0.0	0.0
0.917647E 01	0.0	0.247580E 02	7	0.405542E 02	-0.353938E 03	0.0
-0.297661E 08	0.0	-0.227166E-03	8	0.0	0.0	0.347575E 00
0.544444E 10	0.868975E 05	0.572579E 07	9	0.626528E 05	0.950192E 03	0.550642E 04
0.152885E 03	0.175000E 03	0.156256E 02	1	0.269937E 03	0.847113E 03	0.249344E 05
0.128000E 03	0.112951E 04	0.156256E 02	2	0.269937E 03	0.100000E 01	0.572733E 07
0.300000E 03	0.112951E 04	0.156256E 02	3	0.269937E 03	0.499969E 01	0.359274E 03
0.0	0.112951E 04	0.156256E 02	4	0.269937E 03	0.499969E 01	0.359274E 03
0.0	0.0	-0.335520E-02	5	-0.951950E-03	0.161149E 04	0.354144E 00
0.118451E 02	0.0	0.891099E 01	6	-0.900634E 02	0.0	0.0
0.118261E 02	0.0	0.249286E 02	7	0.405542E 02	-0.376777E 03	0.0
-0.255926E 08	0.0	-0.123998E-03	8	0.0	0.0	0.354144E 00
0.623700E 10	0.114219E 06	0.572647E 07	9	0.544966E 05	0.108863E 04	0.549822E 04

STAGE 4 BENT 2-STEP WITH 2-STEP THRUST T/W =0.2 SCAM ORBIT 9/12 CASE 1
CONSTANT PITCH ANGLE PAGE 6

TABLE A-2. - BENT TWO-STEP TRAJECTORY, TWO-STEP THRUST PRINTOUT - Continued

TIME	INCLINATION	GAMMA GEOC		AZIMUTH GEOC	WEIGHT	ALTITUDE
STAGE TIME	AIRSPEED	GAM A GEOC		AZI A GEOC	FLOW RATE	RADIUS
THRUST	VEL EARTH FIX	GAM A GEOD		AZI A GEOD	LATITUDE GEOC	LONGITUDE
MACH NO.	VEL INERTIAL	GAMMA INERT		AZIMUTH INERT	LATITUDE GEOD	HOUR ANGLE
DYNAMIC PRESS	VEL WIND	GAMCCT GEOC		AZICCT GEOC	VEL THEO	ETA X
RANGE TOTAL	LIFT	VELOCT GEOC		PSI	VEL DRAG	ETA Y
RANGE GRT-CIR	DRAG	ALPHA		THETA	VEL GRAV	ETA Z
ENERGY	SIDEFORCE	BETA		PHI	AERO HEAT	ETA TOTAL
ANGULAR MOMENTUM	RADIUS PERIGEE	RADIUS APOGEE		VEL PERIGEE	VEL APOGEE	VEL.CIRCULAR
0.168885E 03	0.175000E 03	0.156347E 02	1	0.269920E 03	0.831112E 03	0.301099E 05
0.144000E 03	0.127369E 04	0.156347E 02	2	0.269920E 03	0.100000E 01	0.573259E 07
0.300000E 03	0.127369E 04	0.156347E 02	3	0.269920E 03	0.499936E 01	0.359088E 03
0.0	0.127369E 04	0.156347E 02	4	0.269920E 03	0.499936E 01	0.359088E 03
0.0	0.0	0.414055E-02	5	-0.107242E-02	0.178554E 04	0.360962E 00
0.0	0.0	0.911245E 01	6	-0.900796E 02	0.0	0.0
0.148771E 02	0.0	0.249195E 02	7	0.405542E 02	-0.399497E 03	0.0
0.148527E 02	0.0	-0.150808E-04	8	0.0	0.0	0.360962E 00
-0.298902E 08	0.0	0.574429E 07	9	0.480245E 05	0.122404E 04	0.549574E 04
0.703128E 10	0.146410E 06					
0.184888E 03	0.175000E 03	0.157469E 02	1	0.269902E 03	0.815112E 03	0.359371E 05
0.160000E 03	0.142115E 04	0.157469E 02	2	0.269902E 03	0.100000E 01	0.573833E 07
0.300000E 03	0.142115E 04	0.157469E 02	3	0.269902E 03	0.499904E 01	0.358880E 03
0.0	0.142115E 04	0.157469E 02	4	0.269902E 03	0.499904E 01	0.358880E 03
0.0	0.0	0.991854E-02	5	-0.119461E-02	0.197317E 04	0.368047E 00
0.192726E 02	0.0	0.982190E 01	6	-0.900977E 02	0.0	0.0
0.182556E 02	0.0	0.248052E 02	7	0.405542E 02	-0.422263E 03	0.0
-0.291627E 08	0.0	-0.175543E-03	8	0.0	0.0	0.368047E 00
0.784891E 10	0.193583E 06	0.575946E 07	9	0.427541E 05	0.136421E 04	0.549295E 04
0.200885E 03	0.175000E 03	0.159460E 02	1	0.269882E 03	0.799112E 03	0.424730E 05
0.176000E 03	0.157204E 04	0.159460E 02	2	0.269882E 03	0.100000E 01	0.574487E 07
0.300000E 03	0.157204E 04	0.159460E 02	3	0.269882E 03	0.499861E 01	0.358649E 03
0.0	0.157204E 04	0.159460E 02	4	0.269882E 03	0.499861E 01	0.358649E 03
0.0	0.0	0.145451E-01	5	-0.131856E-02	0.216452E 04	0.375417E 00
0.220373E 02	0.0	0.958407E 01	6	-0.901178E 02	0.0	0.0
0.220298E 02	0.0	0.244682E 02	7	0.405542E 02	-0.445203E 03	0.0
-0.280025E 08	0.0	-0.122752E-03	8	0.0	0.0	0.375417E 00
0.868836E 10	0.226305E 06	0.576417E 07	9	0.383708E 05	0.150649E 04	0.548982E 04

TABLE A-2. - BENT TWO-STEP TRAJECTORY, TWO-STEP THRUST PRINTOUT - Continued

TIME	INCLINATION	GAMMA GEOC	1	AZIMUTH GEOC	WEIGHT	ALTITUDE
STAGE TIME	AIRSPEED	GAM A GEOC	2	AZI A GEOC	FLOW RATE	RADIUS
THRUST	VEL EARTH FIX	GAM A GEOD	3	AZI A GEOD	LATITUDE GEOC	LONGITUDE
MACH NO.	VEL INERTIAL	GAMMA INERT	4	AZIMUTH INERT	LATITUDE GEOD	HOUR ANGLE
DYNAMIC PRESS	VEL WIND	GAMDOT GEOC	5	AZIDOT GEOC	VEL THEO	ETA X
RANGE TOTAL	LIFT	VELDOT GEOC	6	PSI	VEL DRAG	ETA Y
RANGE GRT-CIR	DRAG	ALPHA	7	THETA	VEL GRAV	ETA Z
ENERGY	SIDEFORCE	BETA	8	PHI	AERO HEAT	ETA TOTAL
ANGULAR MOMENTUM	RADIUS PERIGEE	RADIUS APOGEE	9	VEL PERIGEE	VEL APOGEE	VEL.CIRCULAR
0.216885E 03	0.175000E 03	0.162102E 02	1	0.269860E 03	0.783113E 03	0.497785E 05
0.192000E 03	0.172655E 04	0.162102E 02	2	0.269860E 03	0.100000E 01	0.575217E 07
0.300000E 03	0.172655E 04	0.162102E 02	3	0.269860E 03	0.499804E 01	0.358396E 03
0.0	0.172655E 04	0.162102E 02	4	0.269860E 03	0.499804E 01	0.358396E 03
0.0	0.0	0.183709E-01	5	-0.144418E-02	0.235974E 04	0.383087E 00
0.261762E 02	0.0	0.576876E 01	6	-0.501399E 02	0.0	0.0
0.261672E 02	0.0	0.243440E 02	7	0.405542E 02	-0.468413E 03	0.0
-0.286095E 08	0.0	-0.226691E-03	8	0.0	0.0	0.383087E 00
0.953630E 10	0.275131E 04	0.577670E 07	9	0.346610E 05	0.165082E 04	0.548634E 04
0.232885E 03	0.175000E 03	0.165308E 02	1	0.269836E 03	0.767112E 03	0.579185E 05
0.208000E 03	0.188470E 04	0.165308E 02	2	0.269836E 03	0.100000E 01	0.576031E 07
0.300000E 03	0.188470E 04	0.165308E 02	3	0.269836E 03	0.499731E 01	0.358119E 03
0.0	0.188470E 04	0.165308E 02	4	0.269836E 03	0.499731E 01	0.358119E 03
0.0	0.0	0.216227E-01	5	-0.157145E-02	0.255899E 04	0.391077E 00
0.306946E 02	0.0	0.100079E 02	6	-0.501640E 02	0.0	0.0
0.306955E 02	0.0	0.240234E 02	7	0.405542E 02	-0.491971E 03	0.0
-0.282813E 08	0.0	-0.694263E-04	8	0.0	0.0	0.391077E 00
0.104077E 11	0.339672E 04	0.577139E 07	9	0.314744E 05	0.179710E 04	0.548246E 04
0.248885E 03	0.175000E 03	0.168559E 02	1	0.269810E 03	0.751112E 03	0.669624E 05
0.224000E 03	0.204681E 04	0.168559E 02	2	0.269810E 03	0.100000E 01	0.576936E 07
0.300000E 03	0.204681E 04	0.168559E 02	3	0.269810E 03	0.499639E 01	0.357818E 03
0.0	0.204681E 04	0.168559E 02	4	0.269810E 03	0.499639E 01	0.357818E 03
0.0	0.0	0.244553E-01	5	-0.170033E-02	0.276244E 04	0.399408E 00
0.355977E 02	0.0	0.112588E 02	6	-0.501902E 02	0.0	0.0
0.355910E 02	0.0	0.236543E 02	7	0.405542E 02	-0.515941E 03	0.0
-0.279155E 08	0.0	-0.179646E-04	8	0.0	0.0	0.399408E 00
0.112988E 11	0.393657E 04	0.577663E 07	9	0.287022E 05	0.194519E 04	0.547816E 04

STAGE 4 BENT 2-STEP WITH 2-STEP THRUST T/W =0.3 ACAN CRPIT 9/12
CONSTANT PITCH ANGLE

CASE 1
PAGE 8

TABLE A-2. - BENT TWO-STEP TRAJECTORY, TWO-STEP THRUST PRINTOUT - Continued

TIME	INCLINATION	GAMMA GEOC	1	AZIMUTH GEOC	WEIGHT	ALTITUDE
STAGE TIME	AIRSPEED	GAM A GEOC	2	AZI A GEOC	FLOW RATE	RADIUS
THRUST	VEL EARTH FIX	GAM A GEOD	3	AZI A GEOD	LATITUDE GEOC	LONGITUDE
MACH NO.	VEL INERTIAL	GAMMA INERT	4	AZIMUTH INERT	LATITUDE GEOD	HOUR ANGLE
DYNAMIC PRESS	VEL WIND	CAMCCT GEOC	5	AZICCT GEOC	VEL THEO	ETA X
RANGE TOTAL	LIFT	VELCCT GEOC	6	PSI	VEL DRAG	ETA Y
RANGE CRT-CIR	DRAG	ALPHA	7	THETA	VEL GRAV	ETA Z
ENERGY	SIDEFORCE	BETA	8	PHI	AERO HEAT	ETA TOTAL
ANGULAR MOMENTUM	RADIUS PERIGEE	RADIUS APOGEE	9	VEL PERIGEE	VEL APOGEE	VEL.CIRCULAR
0.264888E 03	0.175051E 03	0.173117E 02	1	0.269781E 03	0.735112E 03	0.769842E 05
0.240000E 03	0.221364E 04	0.173117E 02	2	0.269781E 03	0.100000E 01	0.577938E 07
0.300000E 03	0.221364E 04	0.173117E 02	3	0.269781E 03	0.499524E 01	0.357454E 03
0.0	0.221364E 04	0.173117E 02	4	0.269781E 03	0.499524E 01	0.357454E 03
0.0	0.0	0.269701E-01	5	-0.183076E-02	0.297027E 04	0.408101E 00
0.0	0.0	0.165222E 02	6	-0.902184E 02	0.0	0.0
0.408826E 02	0.0	0.232425E 02	7	0.405542E 02	-0.540375E 03	0.0
0.408826E 02	0.0	-0.691399E-04	8	0.0	0.0	0.408101E 00
-0.275004E 08	0.0	0.582892E 07	9	0.262640E 05	0.209484E 04	0.547341E 04
0.122106E 11	0.464918E 04					
0.280885E 03	0.175000E 03	0.177616E 02	1	0.269751E 03	0.719113E 03	0.880626E 05
0.256000E 03	0.238359E 04	0.177616E 02	2	0.269751E 03	0.100000E 01	0.579046E 07
0.300000E 03	0.238359E 04	0.177616E 02	3	0.269751E 03	0.499381E 01	0.357145E 03
0.0	0.238359E 04	0.177616E 02	4	0.269751E 03	0.499381E 01	0.357145E 03
0.0	0.0	0.292419E-01	5	-0.196264E-02	0.318267E 04	0.417181E 00
0.0	0.0	0.107990E 02	6	-0.902488E 02	0.0	0.0
0.465782E 02	0.0	0.227526E 02	7	0.405542E 02	-0.565314E 03	0.0
0.465797E 02	0.0	-0.224784E-03	8	0.0	0.0	0.417181E 00
-0.270601E 08	0.0	0.585291E 07	9	0.240989E 05	0.224576E 04	0.546817E 04
0.131442E 11	0.545427E 04					
0.296885E 03	0.175000E 03	0.182464E 02	1	0.269719E 03	0.703112E 03	0.100281E 06
0.272000E 03	0.255866E 04	0.182464E 02	2	0.269719E 03	0.100000E 01	0.580268E 07
0.300000E 03	0.255866E 04	0.182464E 02	3	0.269719E 03	0.499210E 01	0.356772E 03
0.0	0.255866E 04	0.182464E 02	4	0.269719E 03	0.499210E 01	0.356772E 03
0.0	0.0	0.313231E-01	5	-0.209585E-02	0.339985E 04	0.426674E 00
0.0	0.0	0.110904E 02	6	-0.902813E 02	0.0	0.0
0.526653E 02	0.0	0.229078E 02	7	0.405542E 02	-0.590794E 03	0.0
0.526667E 02	0.0	-0.224166E-03	8	0.0	0.0	0.426674E 00
-0.265645E 08	0.0	0.588141E 07	9	0.221601E 05	0.239750E 04	0.546241E 04
0.141107E 11	0.636310E 04					

STAGE 4 BENT 2-STEP WITH 2-STEP THRUST T/W =0.3 ECAM ORBIT 9/12 CASE 1
CONSTANT PITCH ANGLE PAGE 9

TABLE A-2. - BENT TWO-STEP TRAJECTORY, TWO-STEP THRUST PRINTOUT - Continued

TIME	INCLINATION	GAMMA GEOC	1	AZIMUTH GEOC	WEIGHT	ALTITUDE
STAGE TIME	AIRSPEED	GAM A GEOC	2	AZI A GEOC	FLOW RATE	RADIUS
THRUST	VEL EARTH FIX	GAM A GEOD	3	AZI A GEOD	LATITUDE GEOC	LONGITUDE
MACH NO.	VEL INERTIAL	GAMMA INERT	4	AZIMUTH INERT	LATITUDE GEOD	HOUR ANGLE
DYNAMIC PRESS	VEL WIND	GAMDOT GEOC	5	AZIDOT GEOC	VEL THEO	ETA X
RANGE TOTAL	LIFT	VELDOT GEOC	6	PSI	VEL DRAG	ETA Y
RANGE GRT-CIR	DRAG	ALPHA	7	THETA	VEL GRAV	ETA Z
ENERGY	SIDEFORCE	BETA	8	PHI	AERO HEAT	ETA TOTAL
ANGULAR MOMENTUM	RADIUS PERIGEE	RADIUS APOGEE	9	VEL PERIGEE	VEL APOGEE	VEL.CIRCULAR
0.312885E 03	0.175000E 03	0.187632E 02	1	0.269684E 03	0.687112E 03	0.113730E 06
0.288000E 03	0.273857E 04	0.187632E 02	2	0.269684E 03	0.100000E 01	0.581612E 07
0.300000E 03	0.273857E 04	0.187632E 02	3	0.269684E 03	0.499003E 01	0.356375E 03
0.0	0.273857E 04	0.187632E 02	4	0.269684E 03	0.499003E 01	0.356375E 03
0.0	0.0	0.322521E-01	5	-0.223033E-02	0.362204E 04	0.436610E 00
0.591564E 02	0.0	0.113574E 02	6	-0.503159E 02	0.0	0.0
0.591577E 02	0.0	0.217910E 02	7	0.405542E 02	-0.616843E 03	0.0
-0.260191E 08	0.0	-0.665709E-04	8	0.0	0.0	0.436610E 00
0.150814E 11	0.738877E 06	0.991547E 07	9	0.204112E 05	0.254948E 04	0.545609E 04
0.328885E 03	0.175000E 03	0.193098E 02	1	0.269647E 03	0.671112E 03	0.128502E 06
0.304000E 03	0.292356E 04	0.193098E 02	2	0.269647E 03	0.100000E 01	0.583099E 07
0.300000E 03	0.292356E 04	0.193098E 02	3	0.269647E 03	0.498757E 01	0.355952E 03
0.0	0.292356E 04	0.193098E 02	4	0.269647E 03	0.498757E 01	0.355952E 03
0.0	0.0	0.350572E-01	5	-0.236592E-02	0.384946E 04	0.447019E 00
0.660560E 02	0.0	0.117211E 02	6	-0.903526E 02	0.0	0.0
0.660564E 02	0.0	0.212444E 02	7	0.405542E 02	-0.643484E 03	0.0
-0.254201E 08	0.0	-0.172130E-03	8	0.0	0.0	0.447019E 00
0.160876E 11	0.854648E 06	0.955665E 07	9	0.188237E 05	0.270986E 04	0.544918E 04
0.344885E 03	0.175000E 03	0.198644E 02	1	0.269608E 03	0.655113E 03	0.144655E 06
0.320000E 03	0.311374E 04	0.198644E 02	2	0.269608E 03	0.100000E 01	0.584709E 07
0.300000E 03	0.311374E 04	0.198644E 02	3	0.269608E 03	0.498468E 01	0.355504E 03
0.0	0.311374E 04	0.198644E 02	4	0.269608E 03	0.498468E 01	0.355504E 03
0.0	0.0	0.367587E-01	5	-0.250248E-02	0.408236E 04	0.457937E 00
0.733686E 02	0.0	0.120628E 02	6	-0.903916E 02	0.0	0.0
0.733686E 02	0.0	0.216657E 02	7	0.405542E 02	-0.670734E 03	0.0
-0.247436E 08	0.0	-0.176561E-04	8	0.0	0.0	0.457936E 00
0.171229E 11	0.958367E 06	0.866635E 07	9	0.173751E 05	0.285466E 04	0.544162E 04

STAGE 4 BENT 2-STEP WITH 2-STEP THRUST T/W =0.3 CONV CRRIT 0/12
CONSTANT PITCH ANGLE

CASE 1
PAGE 10

TABLE A-2. - BENT TWO-STEP TRAJECTORY, TWO-STEP THRUST PRINTOUT - Continued

TIME	INCLINATION	GAMMA GEOC	1	AZIMUTH GEOC	WEIGHT	ALTITUDE
STAGE TIME	AIRSPEED	GAM A GEOC	2	AZI A GEOC	FLOW RATE	RADIUS
THRUST	VEL EARTH FIX	GAM A GEOD	3	AZI A GEOD	LATITUDE GEOC	LONGITUDE
MACH NO.	VEL INERTIAL	GAMMA INERT	4	AZIMUTH INERT	LATITUDE GEOC	HOUR ANGLE
DYNAMIC PRESS	VEL WIND	GAMDOT GEOC	5	AZIDOT GEOC	VEL THRO	ETA X
RANGE TOTAL	LIFT	VELDOT GEOC	6	PSI	VEL DRAG	ETA Y
RANGE GET-CTR	DRAG	ALPHA	7	THETA	VEL GRAV	ETA Z
ENERGY	SIDEFORCE	BETA	8	PHI	AERO HEAT	ETA TOTAL
ANGULAR MOMENTUM	RADIUS PERIGEE	RADIUS APOGEE	9	VEL PERIGEE	VEL APOGEE	VEL.CIRCULAR
.3504845 03	.1756[illegible] 03	0.2043195 02	1	0.269571E 03	0.541513E 03	.1608125 07
.3345095 03	.3292225 04	0.2043195 02	2	0.269571E 03	.1013[illegible]E 01	0.5863215 07
.3300065 03	.3292225 04	.2043195 02	3	0.269571E 03	.498161E 01	.3555735 03
[illegible]	.3292225 04	.2043195 02	4	0.269571E 03	0.498161E 01	.3555735 03
[illegible]	[illegible]	.3523435-01	5	-0.262777E-02	0.429989E 04	0.4683745 00
[illegible]	[illegible]	.1235145 02	6	-0.904290E 02	[illegible]	[illegible]
0.8142305 02	[illegible]	0.2011225 02	7	0.405542E 02	-0.696141E 03	0.0
0.8042265 02	[illegible]	-0.1705165-02	8	0.0	0.0	0.4683745 00
-.2411155 08	0.0	0.6561725 07	9	0.161595E 05	0.298407E 04	0.5434145 04
.1808865 11	0.1115285 07					

END OF STAGE 4 MET WITH STEP NUMBER 2[illegible] = 0.429989C6E C4 , EXECUTION TIME = 1 MIN 5 SEC,

STAGE 4 BENT 2-STEP WITH 2-STEP THRUST T/W =0.3 6CAN CRBIT 9/12 CASE 1
CONSTANT PITCH ANGLE PAGE 10

TABLE A-2. - BENT TWO-STEP TRAJECTORY, TWO-STEP THRUST PRINTOUT - Continued

TIME	INCLINATION	GAMMA GEOC	1	AZIMUTH GEOC	WEIGHT	ALTITUDE
STAGE TIME	AIRSPEED	GAM A GEOC	2	AZI A GEOC	FLOW RATE	RADIUS
THRUST	VEL EARTH FIX	GAM A GEOD	3	AZI A GEOD	LATITUDE GEOC	LONGITUDE
MACH NO.	VEL INERTIAL	GAMMA INERT	4	AZIMUTH INERT	LATITUDE GEOD	HOUR ANGLE
DYNAMIC PRESS	VEL WIND	CAMDOT GEOC	5	AZIDOT GEOC	VEL THEO	ETA X
RANGE TOTAL	LIFT	VELDOT GEOC	6	PSI	VEL DRAG	ETA Y
RANGE CRT-CIR	DRAG	ALPHA	7	THETA	VEL GRAV	ETA Z
ENERGY	SIDEFORCE	BETA	8	PHI	AERO HEAT	ETA TOTAL
ANGULAR MOMENTUM	RADIUS PERIGEE	RADIUS APOGEE	9	VEL PERIGEE	VEL APOGEE	VEL.CIRCULAR
0.359484E 03	0.175000E 03	0.204319E 02	1	0.269571E 03	0.640513E 03	0.160812E 06
0.0	0.329222E 04	0.204319E 02	2	0.269571E 03	0.333333E 00	0.586321E 07
0.100000E 03	0.329222E 04	0.204319E 02	3	0.269571E 03	0.498161E 01	0.355073E 03
0.0	0.329222E 04	0.204319E 02	4	0.269571E 03	0.498161E 01	0.355073E 03
0.0	0.0	-0.219147E-01	5	-0.262777E-02	0.429989E 04	0.156125E 00
0.824336E 02	0.0	0.295835E 01	6	-0.904290E 02	0.0	0.0
0.804026E 02	0.0	0.201223E 02	7	0.405542E 02	-0.696141E 03	0.0
-0.241105E 08	0.0	-0.170916E-03	8	0.0	0.0	0.156125E 00
0.180886E 11	0.111938E 07	0.666172E 07	9	0.161595E 05	0.298407E 04	0.543414E 04
0.363484E 03	0.175000E 03	0.203259E 02	1	0.269560E 03	0.639180E 03	0.165407E 06
0.400000E 01	0.330438E 04	0.203259E 02	2	0.269560E 03	0.333333E 00	0.586780E 07
0.100000E 03	0.330438E 04	0.203259E 02	3	0.269560E 03	0.498069E 01	0.354951E 03
0.0	0.330438E 04	0.203259E 02	4	0.269560E 03	0.498069E 01	0.354951E 03
0.0	0.0	-0.330250E-01	5	-0.263666E-02	0.432009E 04	0.156451E 00
0.823817E 02	0.0	0.311245E 01	6	-0.904396E 02	0.0	0.0
0.823820E 02	0.0	0.122242E 02	7	0.325542E 02	-0.703153E 03	0.0
-0.240473E 08	0.0	-0.120726E-03	8	0.0	0.0	0.156450E 00
0.181816E 11	0.113286E 07	0.666708E 07	9	0.160488E 05	0.299677E 04	0.543201E 04
0.367484E 03	0.175000E 03	0.201415E 02	1	0.269550E 03	0.637846E 03	0.169950E 06
0.800000E 01	0.331746E 04	0.201415E 02	2	0.269550E 03	0.333333E 00	0.587238E 07
0.100000E 03	0.331746E 04	0.201415E 02	3	0.269550E 03	0.497975E 01	0.354830E 03
0.0	0.331746E 04	0.201415E 02	4	0.269550E 03	0.497975E 01	0.354830E 03
0.0	0.0	-0.618791E-01	5	-0.264774E-02	0.434316E 04	0.156778E 00
0.843683E 02	0.0	0.327559E 01	6	-0.904501E 02	0.0	0.0
0.843693E 02	0.0	-0.715918E 01	7	0.129823E 02	-0.710107E 03	0.0
-0.239816E 08	0.0	-0.120873E-03	8	0.0	0.0	0.156778E 00
0.182907E 11	0.114986E 07	0.667102E 07	9	0.159281E 05	0.301267E 04	0.542585E 04

STAGE 5 BENT 2-STEP WITH 2-STEP THRUST T/W =0.3 ASAP ORBIT 9/12 CASE 1
PITCH AT THDOT = -1DPS2 TO THDOT = -5DPS CUT T BY 2/3 PAGE 11

TABLE A-2. - BENT TWO-STEP TRAJECTORY, TWO-STEP THRUST PRINTOUT - Continued

TIME	INCLINATION	GAMMA GEOC	1	AZIMUTH GEOC	WEIGHT	ALTITUDE
STAGE TIME	AIRSPEED	CAM A GEOC	2	AZI A GEOC	FLOW RATE	RADIUS
THRUST	VEL EARTH FIX	CAM A GEOD	3	AZI A GEOD	LATITUDE GEOC	LONGITUDE
MACH NO.	VEL INERTIAL	GAMMA INERT	4	AZIMUTH INERT	LATITUDE GEOD	HOUR ANGLE
DYNAMIC PRESS	VEL WIND	GAMEQT GEOC	5	AZIEQT GEOC	VEL THEO	ETA X
RANGE TOTAL	LIFT	VELEQT GEOC	6	PSI	VEL DRAG	ETA Y
RANGE GRT-CIR	DRAG	ALPHA	7	THETA	VEL GRAV	ETA Z
ENERGY	SIDEFORCE	BETA	8	PHI	AERO HEAT	ETA TOTAL
ANGULAR MOMENTUM	RADIUS PERIGEE	RADIUS APOGEE	9	VEL PERIGEE	VEL APOGEE	VEL.CIRCULAR
0.369379E 03	0.175000E 03	0.200112E 02	1	0.269545E 03	0.637214E 03	0.172151E 06
0.989575E 01	0.332395E 04	0.200112E 02	2	0.269545E 03	0.333333E 00	0.587455E 07
0.100000E 03	0.332395E 04	0.200112E 02	3	0.269545E 03	0.497929E 01	0.354772E 03
0.0	0.332395E 04	0.200112E 02	4	0.269545E 03	0.497929E 01	0.354772E 03
0.0	0.0	-0.755436E-01	5	-0.265357E-02	0.434973E 04	0.156933E 00
0.853130E 02	0.0	0.312420E 01	6	-0.904552E 02	0.0	0.0
0.853123E 02	0.0	-0.165016E 02	7	0.350356E 01	-0.713374E 03	0.0
-0.239499E 08	0.0	-0.171379E-03	8	0.0	0.0	0.156933E 00
0.183456E 11	0.115715E 07	0.607211E 07	9	0.158541E 05	0.302129E 04	0.542669E 04

END OF STAGE 5 MET WITH STOP PARAM T = 0.98957548E 01 , EXECUTION TIME = 1 MIN 7 SEC.

STAGE 5 BENT 2-STEP WITH 2-STEP THRUST T/W =0.3 ACAM ORBIT 9/12 CASE 1
PITCH AT THDOT1 = -1DPS2 TO THDOT2 = -5DPS CUT T BY 2/3 PAGE 11

TABLE A-2. - BENT TWO-STEP TRAJECTORY, TWO-STEP THRUST PRINTOUT - Continued

TIME	INCLINATION	GAMMA GEOC	1	AZIMUTH GEOC	WEIGHT	ALTITUDE
STAGE TIME	AIRSPEED	GAM A GEOC	2	AZI A GEOC	FLOW RATE	RADIUS
THRUST	VEL EARTH FIX	GAM A GEOD	3	AZI A GEOD	LATITUDE GEOC	LONGITUDE
MACH NO.	VEL INERTIAL	GAMMA INERT	4	AZIMUTH INERT	LATITUDE GEOD	HOUR ANGLE
DYNAMIC PRESS	VEL WIND	GAMDOT GEOC	5	AZIDOT GEOC	VEL THRO	ETA X
RANGE TOTAL	LIFT	VELDOT GEOC	6	PSI	VEL DRAG	ETA Y
RANGE GRT-CIR	DRAG	ALPHA	7	THETA	VEL GRAV	ETA Z
ENERGY	SIDEFORCE	BETA	8	PHI	AERO HEAT	ETA TOTAL
ANGULAR MOMENTUM	RADIUS PERIGEE	RADIUS APOGEE	9	VEL PERIGEE	VEL APOGEE	VEL.CIRCULAR
0.369379E 03	0.175000E 03	0.200112E 02	1	0.269545E 03	0.637214E 03	0.172151E 06
0.0	0.333333E 04	0.200112E 02	2	0.269545E 03	0.333333E 00	0.587455E 07
0.100000E 03	0.333333E 04	0.200112E 02	3	0.269545E 03	0.497929E 01	0.354772E 03
0.0	0.333333E 04	0.200112E 02	4	0.269545E 03	0.497929E 01	0.354772E 03
0.0	0.0	-0.155436E-01	5	-0.265357E-02	0.434973E 04	0.156933E 00
0.853138E 02	0.0	0.312426E 01	6	-0.904552E 02	0.0	0.0
0.853123E 02	0.0	-0.165076E 02	7	0.350356E 01	-0.713374E 03	0.0
-0.239499E 08	0.0	-0.171379E-03	8	0.0	0.0	0.156933E 00
0.183456E 11	0.115715E 07	0.607211E 07	9	0.158541E 05	0.302129E 04	0.542669E 04
0.373379E 03	0.175000E 03	0.196693E 02	1	0.269534E 03	0.635881E 03	0.176673E 06
0.400000E 01	0.333522E 04	0.196693E 02	2	0.269534E 03	0.333333E 00	0.587906E 07
0.100000E 03	0.333522E 04	0.196693E 02	3	0.269534E 03	0.497831E 01	0.354649E 03
0.0	0.333522E 04	0.196693E 02	4	0.269534E 03	0.497831E 01	0.354649E 03
0.0	0.0	-0.914556E-01	5	-0.266606E-02	0.436994E 04	0.157262E 00
0.873135E 02	0.0	0.277452E 01	6	-0.904658E 02	0.0	0.0
0.873138E 02	0.0	-0.281697E 02	7	-0.849644E 01	-0.720181E 03	0.0
-0.238884E 08	0.0	-0.681940E-04	8	0.0	0.0	0.157262E 00
0.184463E 11	0.117499E 07	0.607288E 07	9	0.157141E 05	0.304038E 04	0.542661E 04
0.374379E 03	0.175000E 03	0.195775E 02	1	0.269531E 03	0.635547E 03	0.177793E 06
0.500000E 01	0.333755E 04	0.195775E 02	2	0.269531E 03	0.333333E 00	0.588019E 07
0.100000E 03	0.333755E 04	0.195775E 02	3	0.269531E 03	0.497806E 01	0.354618E 03
0.0	0.333755E 04	0.195775E 02	4	0.269531E 03	0.497806E 01	0.354618E 03
0.0	0.0	-0.918595E-01	5	-0.266914E-02	0.437500E 04	0.157345E 00
0.878151E 02	0.0	0.276752E 01	6	-0.904685E 02	0.0	0.0
0.878152E 02	0.0	-0.285739E 02	7	-0.899644E 01	-0.721864E 03	0.0
-0.238736E 08	0.0	-0.682333E-04	8	0.0	0.0	0.157345E 00
0.184933E 11	0.117946E 07	0.607291E 07	9	0.156794E 05	0.304521E 04	0.542629E 04

STAGE 6 BENT 2-STEP WITH 2-STEP THRUST T/W =0.3 SCAM CRRIT S/12 CASE 1
COMPLETE PITCH MANEUVER TO THDOT = 0 AT THDOT = 10DPS2 PAGE 12

TABLE A-2. - BENT TWO-STEP TRAJECTORY, TWO-STEP THRUST PRINTOUT - Continued

TIME	INCLINATION	GAMMA GEOC	1	AZIMUTH GEOC	WEIGHT	ALTITUDE
STAGE TIME	AIRSPEED	GAM A GEOC	2	AZI A GEOC	FLOW RATE	RADIUS
THRUST	VEL EARTH FIX	GAM A GEOD	3	AZI A GEOD	LATITUDE GEOC	LONGITUDE
MACH NO.	VEL INERTIAL	GAMMA INERT	4	AZIMUTH INERT	LATITUDE GEOD	FOUR ANGLE
DYNAMIC PRESS	VEL WIND	GAMDOT GEOC	5	AZIDOT GEOC	VEL TRUE	ETA X
RANGE TOTAL	LIFT	VELDOT GEOC	6	PST	VEL DRAG	ETA Y
RANGE ORT-CIR	DRAG	ALPHA	7	THETA	VEL GRAV	ETA Z
ENERGY	SIDEFORCE	BETA	8	PHI	ACCEL HEAT	ETA TOTAL
ANGULAR MOMENTUM	RADIUS PERIGEE	RADIUS APOGEE	9	VEL PERIGEE	VEL APOGEE	VEL CIRCULAR
.3723766E 03	.175 E 03	-.1557755E 02	1	.2465316 02	.6355475E 03	.1777 3 E6
	.2337666 04	.1557755 02	2	.2465316 02	.3333333E 00	.5885 E7
.1 E 03	.2337666 04	.1557755 02	3	.2465316 02	.4973 65 1	.3546161 03
	.2337666 04	.155775E 02	4	.2465316 02	.4973 6E 1	.3546161 03
		-.5185666E-01	5	-.2669146E-02	.4225 E 04	.1573455 00
		.2767692E 01	6	-.9246856E 02		
.8781516E 02		-.2857396E 02	7	-.8996446E 01	-.7219646E 03	
.8781526E 02		-.6623306E-04	8			.1573455E 00
-.2387366E 08		.6672616E 07	9	.1567946E 05	.3045216E 04	.5426296E 04
.1849326E 11	.1179466E 07					
.4 637 E 03	.1756666E 03	-.1675322E 02	1	.2695446E 03	.6248806E 03	.2115696E 06
.3 666E 02	.3433756E 04	-.1675322E 02	2	.2695446E 03	.3333336E 00	.5913666E 07
.1 E 03	.3433756E 04	-.1675322E 02	3	.2695446E 03	.4969136E 01	.3536156E 03
	.3433756E 04	-.1675322E 02	4	.2695446E 03	.4969136E 01	.3536156E 03
		-.8456756E-01	5	-.2769546E-02	.4532376E 04	.1633616E 00
		.3216576E 01	6	-.9355556E 02		
.1 41826E 03		-.2574666E 02	7	-.8996436E 01	-.7714796E 03	
.1 4194E 03		-.2263166E-03	8			.1633616E 00
-.2339156E 08						
.1944456E 11	.1331226E 07	.6673736E 07	9	.1467686E 05	.3245456E 04	.5416866E 04
.4383766E 03	.1756666E 03	-.1416716E 02	1	.2693546E 03	.6142136E 03	.2412546E 06
.6 E 02	.2543676E 04	-.1416716E 02	2	.2693546E 03	.3333336E 00	.5943616E 07
.1 E 03	.2543676E 04	-.1416716E 02	3	.2693546E 03	.4959236E 01	.3525726E 03
	.2543676E 04	-.1416716E 02	4	.2693546E 03	.4959236E 01	.3525726E 03
		-.7726186E-01	5	-.2872776E-02	.4723546E 04	.1628166E 00
		.3616416E 01	6	-.9266576E 02		
.1212186E 03		-.2316356E 02	7	-.8996436E 01	-.8134416E 03	
.1212166E 03		-.1821446E-04	8			.1628166E 00
-.2285326E 08						
.2 4186E 11	.1E 1546E 07	.6674446E 07	9	.1353816E 05	.3361326E 04	.5397276E 04

STAGE 2 BENT 2-STEP WITH 2-STEP THRUST T/W = 2 6CAN ORBIT 9/12 CASE 1
CONSTANT PITCH ANGLE PAGE 13

TABLE A-2. - BENT TWO-STEP TRAJECTORY, TWO-STEP THRUST PRINTOUT - Continued

TIME	INCLINATION	GAMMA GEOC	1	AZIMUTH GEOC	WEIGHT	ALTITUDE
STAGE TIME	AIRSPEED	GAM A GEOC	2	AZI A GEOC	FLOW RATE	RADIUS
THRUST	VEL EARTH FIX	GAM A GEOD	3	AZI A GEOD	LATITUDE GEOC	LONGITUDE
MACH NO.	VEL INERTIAL	GAMMA INERT	4	AZIMUTH INERT	LATITUDE GEOD	HOUR ANGLE
DYNAMIC PRESS	VEL WIND	GAMDCT GEOC	5	AZIDCT GEOC	VEL THEO	ETA X
RANGE TOTAL	LIFT	VELDCT GEOC	6	PSI	VEL DRAG	ETA Y
RANGE ERT-CIR	DRAG	ALPHA	7	THETA	VEL GRAV	ETA Z
ENERGY	SIDEFORCE	BETA	8	PHI	AERO HEAT	ETA TOTAL
ANGULAR MOMENTUM	RADIUS PERIGEE	RADIUS APOGEE	9	VEL PERIGEE	VEL APOGEE	VEL.CIRCULAR
0.470379E 03	0.175000E 03	0.118218E 02	1	0.269260E 03	0.603546E 03	0.267075E 06
0.960000E 02	0.366482E 04	0.118218E 02	2	0.269260E 03	0.333333E 00	0.596947E 07
0.100000E 03	0.366482E 04	0.118218E 02	3	0.269260E 03	0.494517E 01	0.351487E 03
0.0	0.366482E 04	0.118218E 02	4	0.269260E 03	0.494517E 01	0.351487E 03
0.0	0.0	-0.695414E-01	5	-0.297874E-02	0.487366E 04	0.165687E 00
0.138918E 03	0.0	0.358738E 01	6	-0.907394E 02	0.0	0.0
0.138918E 03	0.0	-0.206162E 02	7	-0.899643E 01	-0.848499E 03	0.0
-0.222888E 08	0.0	-0.126015E-03	8	0.0	0.0	0.165687E 00
0.214130E 11	0.169318E 07	0.607485E 07	9	0.126466E 05	0.352486E 04	0.538556E 04
0.502379E 03	0.175000E 03	0.971484E 01	1	0.269164E 03	0.592880E 03	0.289324E 06
0.128000E 03	0.379792E 04	0.971484E 01	2	0.269164E 03	0.333333E 00	0.599172E 07
0.100000E 03	0.379792E 04	0.971484E 01	3	0.269164E 03	0.492973E 01	0.350359E 03
0.0	0.379792E 04	0.971484E 01	4	0.269164E 03	0.492973E 01	0.350359E 03
0.0	0.0	-0.621755E-01	5	-0.308725E-02	0.504577E 04	0.168668E 00
0.157320E 03	0.0	0.432610E 01	6	-0.908364E 02	0.0	0.0
0.157320E 03	0.0	-0.187112E 02	7	-0.899643E 01	-0.877388E 03	0.0
-0.216844E 08	0.0	-0.185062E-04	8	0.0	0.0	0.168668E 00
0.224297E 11	0.150952E 07	0.607501E 07	9	0.117463E 05	0.369213E 04	0.537555E 04
0.534379E 03	0.175000E 03	0.783968E 01	1	0.269063E 03	0.582213E 03	0.308162E 06
0.160000E 03	0.394138E 04	0.783968E 01	2	0.269063E 03	0.333333E 00	0.601056E 07
0.100000E 03	0.394138E 04	0.783968E 01	3	0.269063E 03	0.491165E 01	0.349187E 03
0.0	0.394138E 04	0.783968E 01	4	0.269063E 03	0.491165E 01	0.349187E 03
0.0	0.0	-0.550654E-01	5	-0.319809E-02	0.522100E 04	0.171758E 00
0.176454E 03	0.0	0.463957E 01	6	-0.909370E 02	0.0	0.0
0.176454E 03	0.0	-0.168361E 02	7	-0.899643E 01	-0.900813E 03	0.0
-0.210387E 08	0.0	-0.717427E-04	8	0.0	0.0	0.171758E 00
0.234685E 11	0.215467E 07	0.607491E 07	9	0.108919E 05	0.386318E 04	0.536712E 04

STAGE 7 BENT 2-STEP WITH 2-STEP THRUST T/W =0.3 ECAN ORBIT 9/12
CONSTANT PITCH ANGLE

CASE 1
PAGE 14

TABLE A-2. - BENT TWO-STEP TRAJECTORY, TWO-STEP THRUST PRINTOUT - Continued

TIME STAGE TIME THRUST MACH NO. DYNAMIC PRESS RANGE TOTAL RANGE GRT-CIR ENERGY ANGULAR MOMENTUM	INCLINATION AIRSPEED VEL EARTH FIX VEL INERTIAL VEL WIND LIFT DRAG SIDEFORCE RADIUS PERIGEE	GAMMA GEOC CAM A GEOC CAM A GEOC GAMMA INERT CAMECT GEOC VELOCT GEOC ALPHA BETA RADIUS APOGEE	1 2 3 4 5 6 7 8 9	AZIMUTH GEOC AZI A GEOC AZI A GEOC AZIMUTH INERT AZIOCT GEOC PSI THETA PHI VEL PERIGEE	WEIGHT FLOW RATE LATITUDE GEOC LATITUDE GEOC VEL THRU VEL DRAG VEL GRAV AERO HEAT VEL APOGEE	ALTITUDE RADIUS LONGITUDE HOUR ANGLE ETA X ETA Y ETA Z ETA TOTAL VEL.CIRCULAR
0.566376E 03	0.175000E 03	0.618734E 01	1	0.268958E 03	0.571547E 03	0.323866E 06
0.192000E 03	0.429432E 04	0.618734E 01	2	0.268958E 03	0.333333E 00	0.602622E 07
0.140000E 03	0.429432E 04	0.618734E 01	3	0.268958E 03	0.489168E 01	0.347968E 03
0.0	0.429432E 04	0.618734E 01	4	0.268958E 03	0.489168E 01	0.347968E 03
0.0	0.0	-0.492621E-01	5	-0.331397E-02	0.539948E 04	0.174964E 00
0.0	0.0	0.491891E 01	6	-0.910411E 02	0.0	0.0
0.196348E 03	0.0	-0.151828E 02	7	-0.899643E 01	-0.919442E 03	0.0
0.196348E 03	0.0	-0.181328E-03	8	0.0	0.0	0.174964E 00
-0.213405E 08	0.0	0.607458E 07	9	0.100789E 05	0.403905E 04	0.536015E 04
0.245295E 11	0.243375E 07					
0.508837E 03	0.175000E 03	0.474725E 01	1	0.268851E 03	0.568808E 03	0.336482E 06
0.224000E 03	0.425564E 04	0.474725E 01	2	0.268851E 03	0.333333E 00	0.603887E 07
0.140000E 03	0.425564E 04	0.474725E 01	3	0.268851E 03	0.486655E 01	0.346701E 03
0.0	0.425564E 04	0.474725E 01	4	0.268851E 03	0.486655E 01	0.346701E 03
0.0	0.0	-0.418033E-01	5	-0.342552E-02	0.558132E 04	0.178291E 00
0.0	0.0	0.517519E 01	6	-0.911489E 02	0.0	0.0
0.217934E 03	0.0	-0.137437E 02	7	-0.899643E 01	-0.933902E 03	0.0
0.217934E 03	0.0	-0.721712E-04	8	0.0	0.0	0.178291E 00
-0.196144E 08	0.0	0.607398E 07	9	0.935292E 04	0.421682E 04	0.535452E 04
0.256129E 11	0.276321E 07					
0.633379E 03	0.175000E 03	0.350814E 01	1	0.268740E 03	0.551213E 03	0.346429E 06
0.256000E 03	0.442556E 04	0.350814E 01	2	0.268740E 03	0.333333E 00	0.604882E 07
0.140000E 03	0.442556E 04	0.350814E 01	3	0.268740E 03	0.483894E 01	0.345383E 03
0.0	0.442556E 04	0.350814E 01	4	0.268740E 03	0.483894E 01	0.345383E 03
0.0	0.0	-0.350701E-01	5	-0.354129E-02	0.576665E 04	0.181748E 00
0.0	0.0	0.541929E 01	6	-0.9126 3E 02	0.0	0.0
0.238544E 03	0.0	-0.125146E 02	7	-0.899643E 01	-0.944775E 03	0.0
0.238544E 03	0.0	-0.152148E-03	8	0.0	0.0	0.181748E 00
-0.188396E 08	0.0	0.607316E 07	9	0.856137E 04	0.429956E 04	0.535611E 04
0.267193E 11	0.312127E 07					

STAGE 2 BENT 2-STEP WITH 2-STEP THRUST T/W =0.3 ECAN CRRIT 9/12 CASE 1
CONSTANT PITCH ANGLE PAGE 15

TABLE A-2. - BENT TWO-STEP TRAJECTORY, TWO-STEP THRUST PRINTOUT - Continued

TIME	INCLINATION	GAMMA GEOC	1	AZIMUTH GEOC	WEIGHT	ALTITUDE
STAGE TIME	AIRSPEED	GAM A GEOC	2	AZI A GEOC	FLOW RATE	RADIUS
THRUST	VEL EARTH FIX	GAM A GEOD	3	AZI A GEOD	LATITUDE GEOC	LONGITUDE
MACH NO.	VEL INERTIAL	GAMMA INERT	4	AZIMUTH INERT	LATITUDE GEOD	HOUR ANGLE
DYNAMIC PRESS	VEL WIND	GAMDOT GEOC	5	AZIDOT GEOC	VEL THEO	ETA X
RANGE TOTAL	LIFT	VELDOT GEOC	6	PSI	VEL DRAG	ETA Y
RANGE CRT-CIR	DRAG	ALPHA	7	THETA	VEL GRAV	ETA Z
ENERGY	SIDEFORCE	BETA	8	PHI	AERO HEAT	ETA TOTAL
ANGULAR MOMENTUM	RADIUS PERIGEE	RADIUS APOGEE	9	VEL PERIGEE	VEL APOGEE	VEL.CIRCULAR
0.662379E 03	0.175000E 03	0.245869E 01	1	0.268624E 03	0.539546E 03	0.353899E 06
0.288000E 03	0.460259E 04	0.245869E 01	2	0.268624E 03	0.333333E 00	0.605629E 07
0.100000E 03	0.460259E 04	0.245869E 01	3	0.268624E 03	0.480754E 01	0.344013E 03
0.0	0.460259E 04	0.245869E 01	4	0.268624E 03	0.480754E 01	0.344013E 03
0.0	0.0	-0.295488E-01	5	-0.365773E-02	0.595561E 04	0.185241E 00
0.260508E 03	0.0	0.564168E 01	6	-0.913755E 02	0.0	0.0
0.260938E 03	0.0	-0.114551E 02	7	-0.899643E 01	-0.952608E 03	0.0
-0.179965E 08	0.0	-0.235817E-03	8	0.0	0.0	0.185341E 00
0.278489E 11	0.354859E 07	0.607215E 07	9	0.784788E 04	0.458634E 04	0.534681E 04
0.694379E 03	0.175000E 03	0.158783E 01	1	0.268505E 03	0.528880E 03	0.359157E 06
0.320000E 03	0.478649E 04	0.158783E 01	2	0.268505E 03	0.333333E 00	0.606155E 07
0.100000E 03	0.478649E 04	0.158783E 01	3	0.268505E 03	0.477199E 01	0.342589E 03
0.0	0.478649E 04	0.158783E 01	4	0.268505E 03	0.477199E 01	0.342589E 03
0.0	0.0	-0.245354E-01	5	-0.377418E-02	0.614834E 04	0.189079E 00
0.284159E 03	0.0	0.584936E 01	6	-0.914945E 02	0.0	0.0
0.284158E 03	0.0	-0.105842E 02	7	-0.899643E 01	-0.957898E 03	0.0
-0.171084E 08	0.0	-0.182220E-03	8	0.0	0.0	0.189079E 00
0.290024E 11	0.404922E 07	0.607055E 07	9	0.716246E 04	0.477724E 04	0.534449E 04
0.726379E 03	0.175000E 03	0.885050E 00	1	0.268383E 03	0.518213E 03	0.362464E 06
0.352000E 03	0.497681E 04	0.885050E 00	2	0.268383E 03	0.333333E 00	0.606488E 07
0.100000E 03	0.497681E 04	0.885050E 00	3	0.268383E 03	0.473192E 01	0.341109E 03
0.0	0.497681E 04	0.885050E 00	4	0.268383E 03	0.473192E 01	0.341109E 03
0.0	0.0	-0.194396E-01	5	-0.388983E-02	0.634500E 04	0.192971E 00
0.308833E 03	0.0	0.604384E 01	6	-0.916171E 02	0.0	0.0
0.308832E 03	0.0	-0.988147E 01	7	-0.899643E 01	-0.961114E 03	0.0
-0.161637E 08	0.0	-0.128731E-03	8	0.0	0.0	0.192971E 00
0.301801E 11	0.466207E 07	0.606961E 07	9	0.650143E 04	0.497234E 04	0.534302E 04

STAGE 7 BENT 2-STEP WITH 2-STEP THRUST T/W =0.3 ECAM ORBIT 9/12
CONSTANT PITCH ANGLE

CASE 1
PAGE 16

TABLE A-2. - BENT TWO-STEP TRAJECTORY, TWO-STEP THRUST PRINTOUT - Concluded

TIME	INCLINATION	GAMMA GEOC	1	AZIMUTH GEOC	WEIGHT	ALTITUDE
STAGE TIME	AIRSPEED	GAM A GEOC	2	AZI A GEOC	FLOW RATE	RADIUS
THRUST	VEL EARTH FIX	GAM A GEOD	3	AZI A GEOD	LATITUDE GEOC	LONGITUDE
MACH NO.	VEL INERTIAL	GAMMA INERT	4	AZIMUTH INERT	LATITUDE GEOC	HOUR ANGLE
DYNAMIC PRESS	VEL WIND	CAMCCT GEOC	5	AZICCT GEOC	VEL THEO	ETA X
RANGE TOTAL	LIFT	VELCCT GEOC	6	PSI	VEL DRAG	ETA Y
RANGE CRT-CIR	DRAG	ALPHA	7	THETA	VEL GRAV	ETA Z
ENERGY	SIDEFORCE	BETA	8	PHI	AERO HEAT	ETA TOTAL
ANGULAR MOMENTUM	RADIUS PERIGEE	RADIUS APOGEE	9	VEL PERIGEE	VEL APOGEE	VEL.CIRCULAR
[illegible]	[illegible]	[illegible]	1	[illegible]	[illegible]	[illegible]
[illegible]	[illegible]	[illegible]	2	[illegible]	[illegible]	[illegible]
[illegible]	[illegible]	[illegible]	3	[illegible]	[illegible]	[illegible]
[illegible]	[illegible]	[illegible]	4	[illegible]	[illegible]	[illegible]
[illegible]	[illegible]	[illegible]	5	[illegible]	[illegible]	[illegible]
[illegible]	[illegible]	[illegible]	6	[illegible]	[illegible]	[illegible]
[illegible]	[illegible]	[illegible]	7	[illegible]	[illegible]	[illegible]
[illegible]	[illegible]	[illegible]	8	[illegible]	[illegible]	[illegible]
[illegible]	[illegible]	[illegible]	9	[illegible]	[illegible]	[illegible]
[illegible]	[illegible]	[illegible]	1	[illegible]	[illegible]	[illegible]
[illegible]	[illegible]	[illegible]	2	[illegible]	[illegible]	[illegible]
[illegible]	[illegible]	[illegible]	3	[illegible]	[illegible]	[illegible]
[illegible]	[illegible]	[illegible]	4	[illegible]	[illegible]	[illegible]
[illegible]	[illegible]	[illegible]	5	[illegible]	[illegible]	[illegible]
[illegible]	[illegible]	[illegible]	6	[illegible]	[illegible]	[illegible]
[illegible]	[illegible]	[illegible]	7	[illegible]	[illegible]	[illegible]
[illegible]	[illegible]	[illegible]	8	[illegible]	[illegible]	[illegible]
[illegible]	[illegible]	[illegible]	9	[illegible]	[illegible]	[illegible]

END OF STAGE 7 MET WITH STEP NUMBER 20 = [illegible] , EXECUTION TIME = 1 MIN 10 SEC,
CONVERGENCE REACHED, MISS= [illegible] FPS USED = [illegible]
CONVERGENCE REACHED, MISS= [illegible] FPS USED = [illegible]

STAGE 7 BENT 2-STEP WITH 2-STEP THRUST T/W =[illegible] GDAM CRIT 9/12 CASE 1
CONSTANT PITCH ANGLE PAGE 14

APPENDIX B.
DERIVATION OF LUNAR FLYING PLATFORM SIMULATOR EQUATIONS OF MOTION

Introduction

In this section the equations of motion for the lunar flying platform simulator, as described in table 2-5, will be derived. In comparison, the equations of motion describing a flying version of the simulator will also be derived. Both the simulator and its flying equivalent differ from other vehicles in that the pilot and vehicle centers of gravity are nominally coincident. Both derivations are simplified by the following assumptions:

1. Air bearing pads on the simulator produce frictionless translation

2. The pilot is a rigid member, pivoting about the soles of his shoes

3. Motion occurs in the pitch plane only

A diagram which defines the nomenclature and geometry for both simulations is shown in figure B-1. The flying version does not include the air bearing dolly.

Definitions. -

F_T is the thrust force magnitude.

h is the distance from the pilot pivot to either the pilot or vehicle center of gravity.

I_p, I_v are the moments of inertia about the pilot and vehicle respectively.

ℓ_1 is the distance from the pilot pivot radially to the spherical surface.

ℓ_2 is the distance from the spherical surface to the pad dolly center of gravity

m_p, m_v, m_d, m_T are the pilot, vehicle, pad dolly, and total masses, respectively.

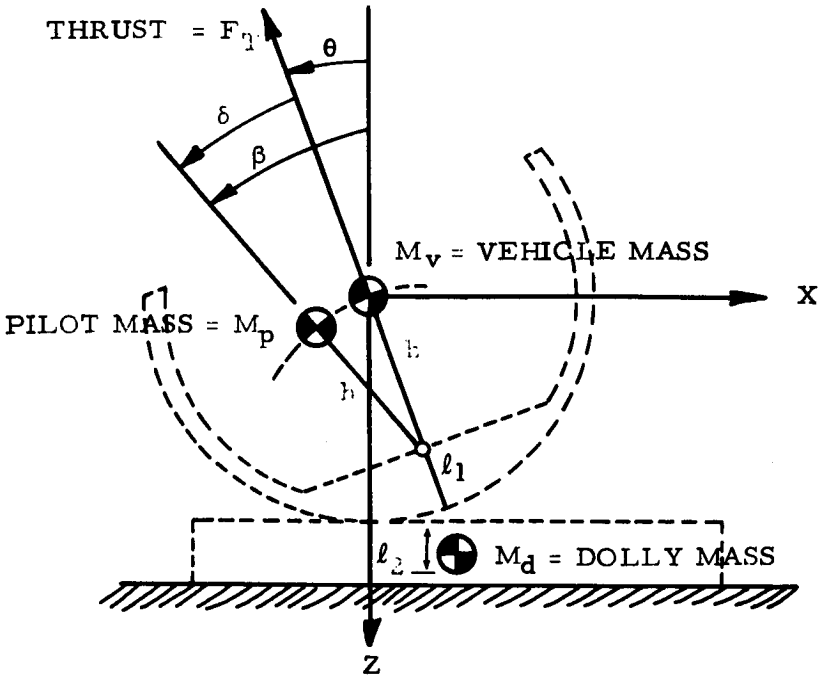

Figure B-1. Dynamic Model for Kinesthetic Control

x, z are the local horizontal and vertical axes of a central force field frame of reference.

β is the total lean angle of the pilot from vertical (positive in the right hand sense).

θ is the thrust vector orientation from vertical (positive in the right hand sense).

δ is the pilot control input angle, the difference between β and θ (positive in the right hand sense).

Lagrangian formulation of equations of motion for the flying vehicle. -

Constraints:

$$\beta = \theta + \delta \tag{B-1}$$

$$\bar{r}_p = [x + h\sin\theta - h\sin\beta]\,\bar{i} + [z + h\cos\theta - h\cos\beta]\,\bar{k} \tag{B-2}$$

$$\bar{r}_v = x\bar{i} + z\bar{k} \tag{B-3}$$

Velocities:

$$v_p^2 = [\dot{x} + h\dot{\theta}\cos\theta - l\dot{\beta}\cos\beta]^2 + [\dot{z} - h\dot{\theta}\sin\theta + h\dot{\beta}\sin\beta]^2 \qquad \text{(B-4)}$$

$$v_v^2 = \dot{x}^2 + \dot{z}^2 \qquad \text{(B-5)}$$

Kinetic energy:

$$T = \frac{1}{2}\left|m_p v_p^2 + m_v v_v^2 + I_p\dot{\beta}^2 + I_v\dot{\theta}^2\right| \qquad \text{(B-6)}$$

Potential energy:

$$V = -m_T g z - m_p g h(\cos\theta - \cos\beta) \qquad \text{(B-7)}$$

Forces not derivable from a potential: External forces and moments are derived by either

$$Q_i = \sum_j \bar{F}_j \cdot \frac{\partial r_j}{\partial q_i} \qquad \text{(B-8)}$$

or

$$Q_i = \sum_j \bar{M}_j \cdot \frac{\partial \lambda_j}{\partial q_i} \qquad \text{(B-9)}$$

where $\bar{F}_j$ and $\bar{M}_j$ are the forces and moments acting on the jth body. The generalized variable is q_i. Evaluating the individual terms:

$$\bar{F}_p = 0 \qquad \text{(B-10)}$$

$$\bar{F}_v = [-F_T \sin\theta]\bar{i} + [-F_T \cos\theta]\bar{k} \qquad \text{(B-11)}$$

$$\bar{M}_p = [-F_T h \sin\delta]\bar{j} \qquad \text{(B-12)}$$

$$\bar{M}_v = [F_T h \sin\delta]\bar{j} \qquad \text{(B-13)}$$

$$\bar{\lambda}_p = \beta\bar{j} \tag{B-14}$$

$$\bar{\lambda}_v = \theta\bar{j} \tag{B-15}$$

Note that $\bar{r}_p$ and $\bar{r}_v$ are stated in equations (B-2) and (B-3). Because the pilot's feet are not pin joints to the vehicle, they apply the moment $\bar{M}_p$ and receive the reaction $\bar{M}_v$. Evaluating the forces and moments:

$$Q_x = -F_T \sin\theta \tag{B-16}$$

$$Q_z = -F_T \cos\theta \tag{B-17}$$

$$Q_\theta = F_T h \sin\delta \tag{B-18}$$

$$Q_\beta = -F_T h \sin\delta \tag{B-19}$$

Description of the Lagrangian: The generalized form of the equations of motion to be used is:

$$\frac{d}{dt}\left\{\frac{\partial L}{\partial \dot{q}_i}\right\} - \frac{\partial L}{\partial q_i} = Q_i \tag{B-20}$$

where the Lagrangian, L, is

$$L = T - V = \frac{1}{2} m_p \left[\dot{x} + h\dot{\theta}\cos\theta - h\dot{\beta}\cos\beta\right]^2 + \frac{1}{2} m_p \left[\dot{z} - h\dot{\theta}\sin\theta + h\dot{\beta}\sin\beta\right]^2 + \frac{1}{2} m_v \left[\dot{x}^2 + \dot{z}^2\right] + I_p\dot{\beta}^2 + I_v\dot{\theta}^2 + m_T gz + m_p gh(\cos\theta - \cos\beta) \tag{B-21}$$

from substituting Equations (B-4) through (B-7).

Exact equations of motion for the flying vehicle:

$$m_T\ddot{x} + m_p h\left[\ddot{\theta}\cos\theta - \dot{\theta}^2\sin\theta - \ddot{\beta}\cos\beta + \dot{\beta}^2\sin\beta\right] + F_T\sin\theta = 0 \tag{B-22}$$

$$m_T\ddot{z} + m_p h\left[-\ddot{\theta}\sin\theta - \dot{\theta}^2\cos\theta + \ddot{\beta}\sin\beta + \dot{\beta}^2\cos\beta\right] - m_T g + F_T\cos\theta = 0 \tag{B-23}$$

$$(I_v + m_p h^2)\ddot{\theta} - m_p h^2\cos\delta\ddot{\beta} + m_p h(\ddot{x}\cos\theta - \ddot{z}\sin\theta) + m_p h^2\dot{\beta}^2\sin\delta + m_p hg\sin\theta = F_T h\sin\delta \tag{B-24}$$

$$(I_p + m_p h^2)\ddot{\beta} + m_p h(-\ddot{x}\cos\beta + \ddot{z}\sin\beta) - m_p h^2\cos\delta\ddot{\theta} - m_p h^2\dot{\theta}^2\sin\delta - m_p hg\sin\beta = -F_T h\sin\delta \tag{B-25}$$

Linearizing procedures: The exact equations, (B-22) through (B-25) may be linearized by using an expansion including the first two terms of a Taylor's series. This represents small perturbations about a fixed operating point, denoted by the subscript (o). The operating point selected for this linearization represents a pitch tilt angle (θ_o) which produces a -x acceleration. To further simplify the linearized equations, first term series approximations for sine and cosine perturbed arguments are retained. The resulting list of linearizing substitutions which include operating point terms are as follows:

$$\theta \Rightarrow \theta_o + \theta \tag{B-26}$$

$$\beta \Rightarrow \theta_o + \beta \tag{B-27}$$

$$\ddot{x} \Rightarrow -\frac{F_T}{m_T}\sin\theta_o + \ddot{x} \tag{B-28}$$

$$\ddot{z} \Rightarrow g - \frac{F_T}{m_T}\cos\theta_o + \ddot{z} \tag{B-29}$$

$$\sin\theta \Rightarrow \sin\theta_o + \theta\cos\theta_o \tag{B-30}$$

$$\cos\theta \Rightarrow \cos\theta_o - \theta\sin\theta_o \tag{B-31}$$

$$\sin\beta \Rightarrow \sin\theta_o + \beta\cos\theta_o \tag{B-32}$$

$$\cos\beta \Rightarrow \cos\theta_o - \beta\sin\theta_o \tag{B-33}$$

Linearized equations of motion for the flying vehicle:

$$m_T\ddot{X} + m_p h \cos\theta_o\ddot{\theta} - m_p h \cos\theta_o\ddot{\beta} + F_T \cos\theta_o\theta = 0 \qquad \text{(B-34)}$$

$$m_T\ddot{Z} - m_p h \sin\theta_o\ddot{\theta} + m_p h \sin\theta_o\ddot{\beta} - F_T \cos\theta_o\theta = 0 \qquad \text{(B-35)}$$

$$(I_v + m_p h^2)\ddot{\theta} - m_p h^2\ddot{\beta} + m_p h (\cos\theta_o\ddot{X} - \sin\theta_o\ddot{Z}) + \frac{m_p}{m_T} F_T h\theta = F_T h\delta \qquad \text{(B-36)}$$

$$(I_p + m_p h^2)\ddot{\beta} - m_p h^2\ddot{\theta} + m_p h (-\cos\theta_o\ddot{X} + \sin\theta_o\ddot{Z}) - \frac{m_p}{m_T} F_T h\beta = -F_T h\delta \qquad \text{(B-37)}$$

Derivation of the β/δ transfer function: The four linearized equations (B-34) through (B-37) may be used in obtaining the transfer function which shows the response of pilot attitude to his control input, β/δ. The simplest procedure is to add equations (B-36) and (B-37) to eliminate $\ddot{X}$ and $\ddot{Z}$, then eliminate θ and $\ddot{\theta}$ using equation (B-1). In Laplace transform domain the final form is:

$$\frac{\beta}{\delta} = \frac{I_v}{(I_p + I_v)} \left(\frac{S^2 + \frac{F_T h}{I_v}\left[\frac{m_p}{m_T}\right]}{S^2} \right) \qquad \text{(B-38)}$$

Lagrangian formulation of equations of motion for the simulator. -

Constraints:

$$\beta = \theta + \delta \qquad \text{(B-39)}$$

$$r = h + \ell_1 \qquad \text{(B-40)}$$

$$\bar{r}_p = [X + h\sin\theta - h\sin\beta]\bar{i} + [h\cos\theta - h\cos\beta]\bar{k} \qquad \text{(B-41)}$$

$$\bar{r}_v = X\bar{i} \qquad \text{(B-42)}$$

$$\bar{r}_d = [X + r\theta]\bar{i} + [r + \ell_2]\bar{k} \qquad \text{(B-43)}$$

Velocities:

$$v_p^2 = [\dot{X} + h\dot{\theta}\cos\theta - h\dot{\beta}\cos\beta]^2 + [-h\dot{\theta}\sin\theta + h\dot{\beta}\sin\beta]^2 \quad \text{(B-44)}$$

$$v_v^2 = \dot{X}^2 \quad \text{(B-45)}$$

$$v_d^2 = [\dot{X} + r\dot{\theta}]^2 \quad \text{(B-46)}$$

Kinetic energy:

$$T = \frac{1}{2}\left\{m_p v_p^2 + m_v v_v^2 + m_d v_d^2 + I_p\dot{\beta}^2 + I_v\dot{\theta}^2\right\} \quad \text{(B-47)}$$

Potential energy:

$$V = -m_p gh(\cos\theta - \cos\beta) \quad \text{(B-48)}$$

Forces not derivable from a potential:

$$\overline{F}_p = 0 \quad \text{(B-49)}$$

$$\overline{F}_v = [-F_T \sin\theta]\overline{i} \quad \text{(B-50)}$$

$$\overline{F}_d = 0 \quad \text{(B-51)}$$

$$\overline{M}_p = -F_T h \sin\delta \quad \text{(B-52)}$$

$$\overline{M}_v = F_T h \sin\delta \quad \text{(B-53)}$$

$$\overline{\lambda}_p = \beta \quad \text{(B-54)}$$

$$\overline{\lambda}_v = \theta \quad \text{(B-55)}$$

Note that $\overline{r}_p$, $\overline{r}_v$, and $\overline{r}_d$ are stated in equations (B-41) through (B-43). Evaluating the forces and moments:

$$Q_X = -F_T \sin\theta \quad \text{(B-56)}$$

$$Q_Z = 0 \tag{B-57}$$

$$Q_\theta = F_T h \sin \delta \tag{B-58}$$

$$Q_\beta = -F_T h \sin \delta \tag{B-59}$$

Lagrangian:

$$L = T - V = \frac{1}{2} m_p [\dot{X} + h\dot{\theta} \cos \theta - h\dot{\beta} \cos \beta]^2 + \frac{1}{2} m_p [-h\dot{\theta} \sin \theta + h\dot{\beta} \sin \beta]^2$$

$$+ \frac{1}{2} m_v \dot{X}^2 + \frac{1}{2} m_d [\dot{X} + r\dot{\theta}]^2 + \frac{1}{2} I_p \dot{\beta}^2 + \frac{1}{2} I_v \dot{\theta}^2 + m_p gh (\cos \theta - \cos \beta) \tag{B-60}$$

Exact equations of motion for the simulator:

$$m_T \ddot{X} + (m_p h \cos \theta + m_p r)\ddot{\theta}$$

$$+ m_p h [-\dot{\theta}^2 \sin \theta - \ddot{\beta} \cos \beta + \dot{\beta}^2 \sin \beta] + F_T \sin \theta = 0 \tag{B-61}$$

$$(I_v + m_p h^2 + m_d r^2)\ddot{\theta} - m_p h^2 \cos \delta \ddot{\beta}$$

$$+ (m_p h \cos \theta + m_d r)\ddot{X} + m_p h^2 \dot{\beta}^2 \sin \delta + m_p hg \sin \theta = F_T h \sin \delta \tag{B-62}$$

$$(I_p + m_p h^2)\ddot{\beta} - m_p h \cos \beta \ddot{X}$$

$$- m_p h^2 \cos \delta \ddot{\theta} - m_p h^2 \dot{\theta}^2 \sin \delta - m_p hg \sin \beta = - F_T h \sin \delta \tag{B-63}$$

Linearized equations of motion for the simulator:

$$m_T \ddot{X} + (m_p h \cos \theta_o + m_d r)\ddot{\theta} - m_p h \cos \theta_o \ddot{\beta} + F_T \cos \theta_o \theta = 0 \tag{B-64}$$

$$(I_v + m_p h^2 + m_d r^2)\ddot{\theta} - m_p h^2 \ddot{\beta}$$

$$+ (m_p h \cos \theta_o + m_d r)\ddot{X} + \left(\frac{m_p}{m_T} F_T h \sin^2 \theta_o + m_p hg \cos \theta_o\right)\theta = F_T h \delta \tag{B-65}$$

$$(I_p + m_p h^2)\ddot{\beta} - m_p h^2 \ddot{\theta} - m_p h \cos\theta_o \ddot{X}$$

$$- \left(\frac{m_p}{m_T} F_T h \sin^2\theta_o + m_p hg \cos\theta_o\right)\beta = -F_T h\delta \qquad \text{(B-66)}$$

Derivation of the β/δ transfer function: The procedure used for eliminating $\ddot{X}$ from the linearized β and θ equations for the flying vehicle will not work for the simulator equations. Instead, $\ddot{X}$ is eliminated by substitution of equation (B-64) into equations (B-65) and (B-66), which are subsequently added together. Next eliminate θ and $\ddot{\theta}$ by substitution of equation (B-39). In Laplace transform domain, the final form is:

$$\frac{\beta}{\delta} = \frac{I'_v}{I'_T}\left(\frac{S^2 + \frac{F_T h}{I'_v}\left[\frac{m_p}{m_T}\right] C_1}{S^2 - C_2}\right) \qquad \text{(B-67)}$$

where

$$I'_v = I_v + \frac{m_d}{m_T} r^2 \left[m_p\left(1 - \frac{h}{r}\cos\theta_o\right) + m_v\right] \qquad \text{(B-68)}$$

$$I'_T = I_p + I_v + \frac{m_d}{m_T} r^2 (m_p + m_v) \qquad \text{(B-69)}$$

$$C_1 = \sin^2\theta_o + \left(\frac{m_T g}{F_T} - \frac{m_d}{m_p}\frac{r}{h}\right)\cos\theta_o \qquad \text{(B-70)}$$

$$C_2 = \frac{F_T r}{I'_T}\left(\frac{m_d}{m_T}\right)\cos\theta_o \qquad \text{(B-71)}$$

APPENDIX C.
DERIVATION OF SINGLE-BODY KINESTHETIC EQUATIONS OF MOTION

For the point stability analysis to follow, assume moments of inertia, masses and lever arms to be constant. The nomenclature is shown in figure C-1.

Definitions

F_T	is the thrust force magnitude.
h	is the distance from pilot feet to pilot center of gravity.
I_P, I_V, I_T	are moments of inertia about pilot, vehicle, and total centers of gravity, respectively.
M_P, M_V, M_T	are the pilot, vehicle, and total masses, respectively.
X, Z	are the local horizontal and vertical axes of a central force field frame of reference.
β	is the total lean angle of the pilot from vertical (positive on the right-hand sense).
θ	is the thrust vector orientation from vertical (positive in the right-hand sense).
δ	is the pilot control input angle, the difference between β and θ (positive in the right-hand sense).

The kinetic energy of the system is:

$$T = \frac{1}{2}\left\{ m_p v_p^2 + m_v v_v^2 + I_p \dot{\beta}^2 + I_v \dot{\theta}^2 \right\} \qquad \text{(C-1)}$$

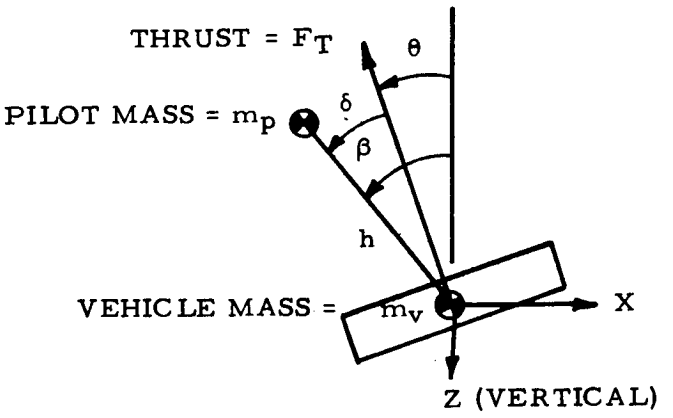

Figure C-1. Dynamic Model For Kinesthetic Control

And the potential energy of the system is:

$$V = -g\left\{m_v Z + m_p (Z - h\cos\beta)\right\} \tag{C-2}$$

where h is taken positive as shown. Forces not derivable from a potential are:

$$Q_x = -F_T \sin\theta \tag{C-3}$$

$$Q_z = -F_T \cos\theta \tag{C-4}$$

$$Q_\theta = F_T\, h \sin\delta \tag{C-5}$$

The velocities of the particles are:

$$v_v^2 = \dot{X}^2 + \dot{Z}^2 \tag{C-6}$$

$$v_p^2 = v_{px}^2 + v_{pz}^2 = \left[\dot{X} - h\,\dot{\beta}\cos\beta\right]^2 + \left[\dot{Z} + h\,\dot{\beta}\sin\beta\right]^2 \tag{C-7}$$

The Lagrangian is:

$$L = T - V = \frac{1}{2} m_p \left[\dot{X}^2 + \dot{Z}^2 - 2h\dot{\beta}\dot{X}\cos\beta + 2h\dot{\beta}\dot{Z}\sin\beta + h^2\dot{\beta}^2\right]$$

$$+ \frac{1}{2}\left[I_p\dot{\beta}^2 + m_v(\dot{X}^2 + \dot{Z}^2) + I_v\dot{\theta}^2\right] + m_v gZ + m_p gZ - m_p gh\cos\beta \qquad (C\text{-}8)$$

Using Lagrange's equation and performing the required operations:

$$\frac{d}{dt}\left(\frac{\partial L}{\partial \dot{q}_i}\right) - \frac{\partial L}{\partial q_i} = \sum_i Q_i \qquad (C\text{-}9)$$

$$(I_p + m_p h^2)\ddot{\beta} + m_p h(\ddot{Z}\sin\beta - \ddot{X}\cos\beta) - m_p gh\sin\beta = 0 \qquad (C\text{-}10)$$

$$I_v\ddot{\theta} = F_T h\sin\delta \qquad (C\text{-}11)$$

$$(m_p + m_v)\ddot{X} - m_p h\ddot{\beta}\cos\beta + m_p h\dot{\beta}^2\sin\beta = -F_T\sin\theta \qquad (C\text{-}12)$$

$$(m_p + m_v)\ddot{Z} + m_p h\ddot{\beta}\sin\beta + m_p h\dot{\beta}^2\cos\beta - (m_p + m_v)g = -F_T\cos\theta \qquad (C\text{-}13)$$

Linearized Equations of Motion

Linearizing procedure. - The exact equations may be linearized by using an expansion including the first two terms of a Taylor's series. This represents small perturbations about a fixed operating point, denoted by the subscript (o). The operating point selected for this linearization represents a pitch tilt angle (θ_o) which produces a -X acceleration. To further simplify the linearized equations, first-term series approximations for sine and cosine perturbed arguments are retained. The resulting list of linearizing substitutions which include operating point terms are as follows.

$$\theta \rightarrow \theta_o + \theta \tag{C-14}$$

$$\beta \rightarrow \theta_o + \beta \tag{C-15}$$

$$X \rightarrow -\frac{F_T}{m_T} \sin \theta_o + \ddot{X} \tag{C-16}$$

$$Z \rightarrow g - \frac{F_T}{m_T} \cos \theta_o + \ddot{Z} \tag{C-17}$$

$$\sin \theta \rightarrow \sin \theta_o + \theta \cos \theta_o \tag{C-18}$$

$$\cos \theta \rightarrow \cos \theta_o - \theta \sin \theta_o \tag{C-19}$$

$$\sin \beta \rightarrow \sin \theta_o + \beta \cos \theta_o \tag{C-20}$$

$$\cos \beta \rightarrow \cos \theta_o - \beta \sin \theta_o \tag{C-21}$$

If small angle perturbations are made about an operating point and the unperturbed equations are subtracted, we are left with the following linear differential equations:

$$(I_p + m_p h^2) \ddot{\beta} - \frac{m_p h F_T}{m_T} \cos^2 \theta_o \beta + m_p h \sin \theta_o \ddot{Z}$$

$$- \frac{m_p h F_T}{m_T} \sin^2 \theta_o \beta - m_p h \cos \theta_o \ddot{X} = 0 \tag{C-22}$$

$$I_v \ddot{\theta} = F_T h \delta \tag{C-23}$$

$$m_T \ddot{X} - m_p h \cos \theta_o \ddot{\beta} = -F_T \theta \cos \theta_o \tag{C-24}$$

$$m_T \ddot{Z} + m_p h \ddot{\beta} \sin \theta_o = F_T \theta \sin \theta_o \tag{C-25}$$

Finally, Laplace transforming and casting into matrix format we have:

$$\begin{bmatrix} (I_v + I_p + m_p h^2)S^2 & -m_p h \cos\theta_o S^2 & m_p h \sin\theta_o S^2 \\ -\frac{m_p}{m_T} h F_T & & \\ -m_p h \cos\theta_o S^2 & m_T S^2 & 0 \\ + F_T \cos\theta_o & & \\ m_p h \sin\theta_o S^2 & 0 & m_T S^2 \\ -F_T \sin\theta_o & & \end{bmatrix} \begin{bmatrix} \beta \\ X \\ Z \end{bmatrix} = \begin{bmatrix} I_v S^2 + F_T h \\ F_T \cos\theta_o \\ -F_T \sin\theta_o \end{bmatrix} \delta \qquad \text{(C-26)}$$

The matrix equation is solved in standard fashion to yield the desired transfer function:

$$\frac{\beta}{\delta} = \left[\frac{I_v}{I_p + I_v + \frac{m_p m_v}{m_p + m_v} h^2} \right] \left[\frac{S^2 + \frac{F_T h}{I_v}\left(\frac{m_p}{m_p + m_v} + 1\right)}{S^2} \right] \qquad \text{(C-27)}$$

APPENDIX D. DERIVATION OF TWO-BODY KINESTHETIC EQUATIONS OF MOTION

Discussion

The equations of motion for the LESS are derived in this section based upon the geometrical model shown in figure D-1. The mass M_2 represents the center of gravity of the LESS base structure containing the propellant tanks. Mass M_1 represents the center of gravity of the platform and passenger that is decoupled from the base at pivot 2. The center of gravity location of the pilot is represented by M_p pivoted about his ankles (pivot 1). The model was made general by allowing for thrusters to be located on either M_1 or M_2.

The equations of motion are derived by the energy method. A set of non-independent coordinates (θ, δ, β) are used to define the angular position of M_1 and M_p. This allows introduction of an undetermined multiplier λ associated with the constraint equation

$$F(\theta, \delta, \beta) = \theta + \delta - \beta = 0 \tag{D-1}$$

The multiplier λ turns out to have the dimensions of torque and is physically interpreted as a torque about the pivot 1. This torque is a measure of the amount of effort the pilot must exert in controlling the vehicle. Lagrange's equation then takes the form

$$\frac{d}{dt}\left(\frac{\partial T}{\partial \dot{q}_i}\right) - \frac{\partial T}{\partial q_i} + \frac{\partial V}{\partial q_i} + \frac{\partial R}{\partial q_i} = Q_i + \lambda \frac{\partial F}{\partial q_i} \tag{D-2}$$

where

T = kinetic energy of system

V = potential energy of system

R = Rayleigh's dissipation function

Q = generalized force not derivable from a potential function

F = equation of constraint

$i = x, z, \theta, \beta, \rho$

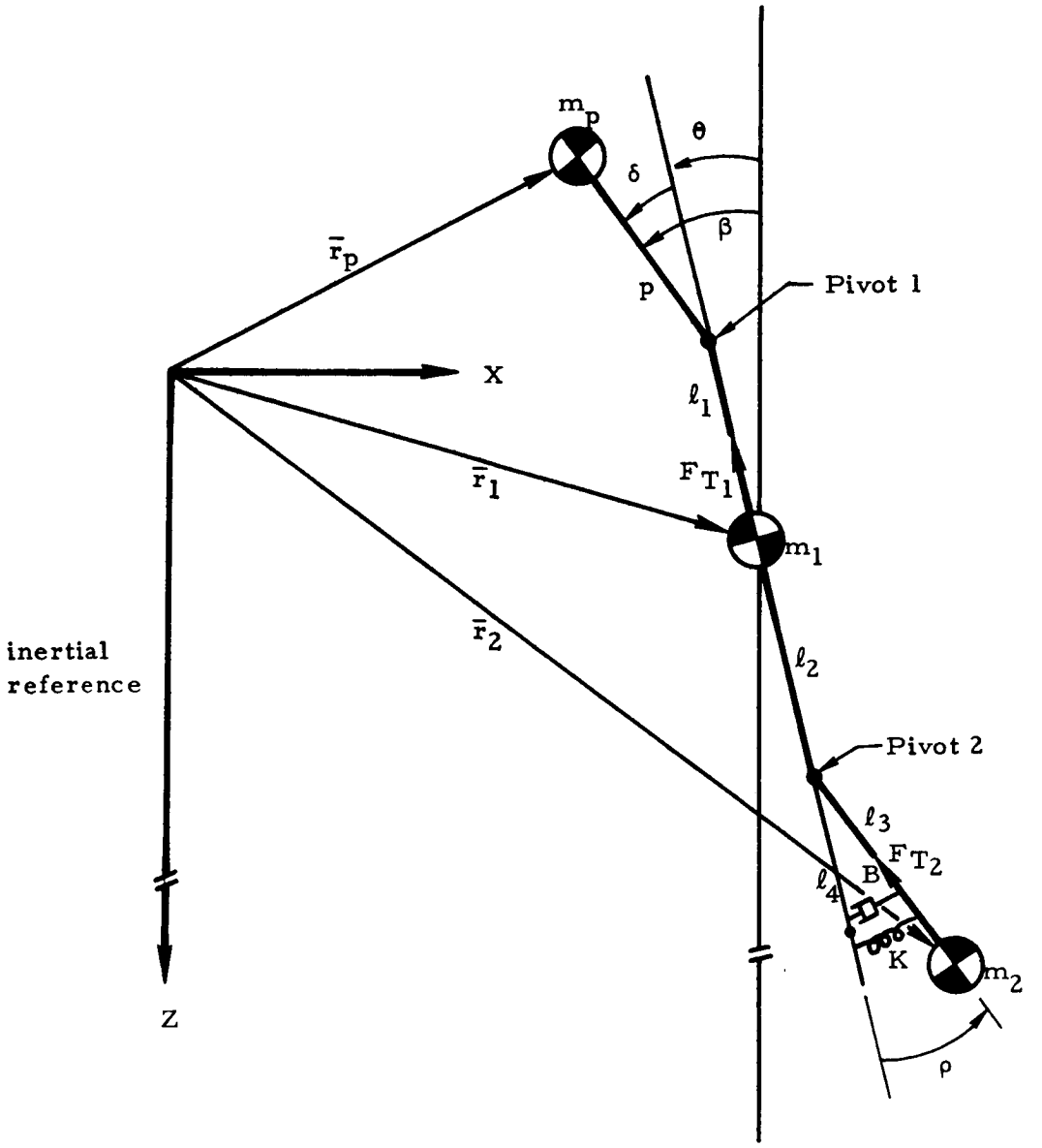

Figure D-1. LESS Goemetrical Model (Pitch Plane)

Lagrange's equation is applied for each coordinate. The constraint equation (D-1) is applied to the β coordinate to obtain an equation for the δ coordinate giving the pilot's motion relative to the platform.

It is noted that the three rotational equations (D-46), (D-52), and (D-58) all contain the terms in $\ddot{x}$ and $\ddot{z}$. Equations (D-46) and (D-58), for θ and δ, contain the torque λ applied in reaction as expected from the physics of the situation.

The rotational dynamics of the vehicle are decoupled from the translational dynamics by the use of equations (D-35) and (D-39). The necessary linearized expressions are developed as equations (D-62), (D-63), and (D-64). Substitution of those expressions into the three rotational equations is accomplished with equations (D-65) and (D-68). Note also that λ, in equation (D-66), is eliminated from equation (D-46) by substitution of equation (D-65). The final three equations for the rotational dynamics result as (D-65), (D-67), and (D-68), for δ, θ, and ρ, respectively.

The coefficients in the rotational equations are quite involved. This results principally from the arbitrary choice of M_1 as the reference point of the system rather than the system center of mass. Note that the vectors $\bar{r}_2$ and $\bar{r}_p$, equations (D-4) and (D-5), are expressed in terms of the M_1 coordinates plus the appropriate system geometry. In equation (D-69) an expression is developed for ϵ, the longitudinal location of the center of gravity, by summing first mass moments. Our expression for the "locked up" inertia, I_v, of the system about the center of mass is then developed as equation (D-70). It may now be recognized that the θ coefficient in equation (D-67) for the θ coordinate is I_v. It is also noted that the expression for ϵ shows up frequently in the rotational equations. If the geometry is redefined to accommodate the center of mass as shown in figure 2-22, then the rotational equations may be expressed more simply as given in the matrix accompanying the figure.

Position Coordinates of M_1, M_2, and M_p

$$\bar{r}_1 = x\,\hat{x} + z\,\hat{z} \tag{D-3}$$

$$\bar{r}_2 = \left[x + \ell_2 \sin\theta + \ell_3 \sin(\theta+\rho)\right]\hat{x} + \left[z + \ell_2 \cos\theta + \ell_3 \cos(\theta+\rho)\right]\hat{z} \tag{D-4}$$

$$\bar{r}_p = \left[x - \ell_1 \sin\theta - \ell_p \sin\beta\right]\hat{x} + \left[z - \ell_1 \cos\theta - \ell_p \cos\beta\right]\hat{z} \tag{D-5}$$

Generalized Forces

$$Q_i = \sum_j^j \overline{F}_j \cdot \frac{\partial \overline{r}_j}{\partial q_i} \tag{D-6}$$

$$\overline{F}_1 = - F_{T1} \sin\theta \, \hat{x} - F_{T1} \cos\theta \, \hat{z} \tag{D-7}$$

$$\overline{F}_2 = - F_{T2} \sin(\theta + \rho) \, \hat{x} - F_{T2} \cos(\theta + \rho) \, \hat{z} \tag{D-8}$$

$$Q_x = \overline{F}_1 \cdot \frac{\partial \overline{r}_1}{\partial x} + \overline{F}_2 \cdot \frac{\partial \overline{r}_2}{\partial x} = - F_{T1} \sin\theta - F_{T2} \sin(\theta + \rho) \tag{D-9}$$

$$Q_z = \overline{F}_1 \cdot \frac{\partial \overline{r}_1}{\partial z} + \overline{F}_2 \cdot \frac{\partial \overline{r}_2}{\partial z} = - F_{T1} \cos\theta - F_{T2} \cos(\theta + \rho) \tag{D-10}$$

where

$$\frac{\partial \overline{r}_1}{\partial x} = \frac{\partial \overline{r}_2}{\partial x} = \hat{x}, \quad \frac{\partial \overline{r}_1}{\partial z} = \frac{\partial \overline{r}_2}{\partial z} = \hat{z} \tag{D-11}$$

$$Q_\theta = \overline{F}_1 \cdot \frac{\partial \overline{r}_1}{\partial \theta} + \overline{F}_2 \cdot \frac{\partial \overline{r}_2}{\partial \theta} \tag{D-12}$$

$$\frac{\partial r_1}{\partial \theta} = 0 \tag{D-13}$$

$$\frac{\partial r_2}{\partial \theta} = \left[\ell_2 \cos\theta + \ell_3 \cos(\theta + \rho)\right] \hat{x} - \left[\ell_2 \sin\theta + \ell_3 \sin(\theta + \rho)\right] \hat{z} \tag{D-14}$$

$$Q_\theta = - F_{T2} \, \ell_2 \sin\rho \tag{D-15}$$

$$Q_\beta = \overline{F}_1 \cdot \frac{\partial \overline{r}_1}{\partial \beta} + \overline{F}_2 \cdot \frac{\partial \overline{r}_2}{\partial \beta} \tag{D-16}$$

$$\frac{\partial \overline{r}_1}{\partial \beta} = \frac{\partial \overline{r}_2}{\partial \beta} = 0 \tag{D-17}$$

$$\therefore \; Q_\beta = 0 \tag{D-18}$$

$$Q_\rho = \overline{F}_1 \cdot \frac{\partial \overline{r}_1}{\partial \rho} + \overline{F}_2 \cdot \frac{\partial \overline{r}_2}{\partial \rho} \tag{D-19}$$

$$\frac{\partial \overline{r}_1}{\partial \rho} = 0 \tag{D-20}$$

$$\frac{\partial \overline{r}_2}{\partial \rho} = \left[\ell_3 \cos(\theta + \rho)\right] \hat{x} - \left[\ell_3 \sin(\theta + \rho)\right] \hat{z} \tag{D-21}$$

$$Q_\rho = 0 \tag{D-22}$$

Kinetic Energy

$$T = \frac{1}{2}\left[I_1 \dot{\theta}^2 + I_2 (\dot{\theta} + \dot{\rho})^2 + I_\rho \dot{\beta}^2 + m_1 v_1^2 + m_2 v_2^2 + m_p v_p^2 \right] \tag{D-23}$$

$$\dot{\overline{r}}_1 = \dot{x}\,\hat{x} + \dot{z}\,\hat{z} \tag{D-24}$$

$$v_1^2 = \dot{\overline{r}}_1 \cdot \dot{\overline{r}}_1 = \dot{x}_1^2 + \dot{z}_1^2 \tag{D-25}$$

$$\dot{\bar{r}}_2 = \left[\dot{x} + \dot{\theta}\ell_2 \cos\theta + (\dot{\theta} + \dot{\rho})\,\ell_3 \cos(\theta + \rho)\right]\hat{x}$$

$$+ \left[\dot{z} - \dot{\theta}\ell_2 \sin\theta - (\dot{\theta} + \dot{\rho})\,\ell_3 \sin(\theta + \rho)\right]\hat{z} \qquad \text{(D-26)}$$

$$v_2^2 = \dot{\bar{r}}_2 \cdot \dot{\bar{r}}_2 \qquad \text{(D-27)}$$

$$v_2^2 = \dot{x}^2 + \dot{z}^2 + \dot{\theta}^2\,\ell_2^2 + (\dot{\theta} + \dot{\rho})^2\,\ell_3^2 + 2\dot{\theta}\ell_2\,(\dot{x}\cos\theta - \dot{z}\sin\theta)$$

$$+ 2\dot{\theta}\,(\dot{\theta} + \dot{\rho})\,\ell_2\ell_3 \cos\rho + 2\,(\dot{\theta} + \dot{\rho})\,\ell_3\left[\dot{x}\cos(\theta + \rho) - \dot{z}\sin(\theta + \rho)\right] \qquad \text{(D-28)}$$

$$\dot{\bar{r}}_p = \left[\dot{x} - \dot{\theta}\,\ell_1 \cos\theta - \dot{\beta}\,\ell_p \cos\beta\right]\hat{x} + \left[\dot{z} + \dot{\theta}\ell_1 \sin\theta + \dot{\beta}\,\ell_p \sin\beta\right]\hat{z} \qquad \text{(D-29)}$$

$$v_p^2 = \dot{\bar{r}}_p \cdot \dot{\bar{r}}_p \qquad \text{(D-30)}$$

Potential Energy

$$V = -m_1 g\,(\bar{r}_1 \cdot \hat{z}) - m_2 g\,(\bar{r}_2 \cdot \hat{z}) - m_p g\,(\bar{r}_p \cdot \hat{z}) + \frac{1}{2}K\,(\ell_4\,\rho)^2$$

$$= -m_1 g z - m_2 g\left[z + \ell_2 \cos\theta + \ell_3 \cos(\theta + \rho)\right]$$

$$- m_p g\left[z - \ell_1 \cos\theta - \ell_p \cos\beta\right] + \frac{1}{2}K\,(\ell_4\,\rho)^2 \qquad \text{(D-31)}$$

$$V = -m_T g z - m_2 g\left[\ell_2 \cos\theta + \ell_3 \cos(\theta + \rho)\right]$$

$$+ m_p g\left[\ell_1 \cos\theta + \ell_p \cos\beta\right] + \frac{1}{2}K\,(\ell_4\rho)^2 \qquad \text{(D-32)}$$

Dissipation Function

$$R = \frac{1}{2} B \, (\ell_4 \dot{\rho})^2 \tag{D-33}$$

x - Coordinate

$$\frac{\partial T}{\partial x} = \frac{\partial V}{\partial x} = \frac{\partial R}{\partial \dot{x}} = \frac{\partial F}{\partial x} = 0 \tag{D-34}$$

Then by equation (D-1):

$$m_T \ddot{x} + m_2 \left[\ddot{\theta} \ell_2 \cos \theta - \dot{\theta}^2 \ell_2 \sin \theta + (\ddot{\theta} + \ddot{\rho}) \ell_3 \cos (\theta + \rho) \right.$$

$$\left. - (\dot{\theta} + \dot{\rho})^2 \ell_3 \sin (\theta + \rho) \right] - m_p \left[\ddot{\theta} \ell_1 \cos \theta - \dot{\theta}^2 \ell_1 \sin \theta \right.$$

$$\left. + \ddot{\beta} \ell_p \cos \beta - \dot{\beta}^2 \ell_p \sin \beta \right] = - F_{T1} \sin \theta - F_{T2} \sin (\theta + \rho) \tag{D-35}$$

Linearized equation (substitute $\theta + \delta$ for β)

$$M_T \ddot{x} + \left[m_2 (\ell_2 + \ell_3) - m_p (\ell_1 + \ell_p) \right] \ddot{\theta} + m_2 \ell_3 \ddot{\rho} - m_p \ell_p \ddot{\delta}$$

$$= - (F_{T1} + F_{T2}) \theta - F_{T2} \rho \tag{D-36}$$

z - Coordinate

$$\frac{\partial T}{\partial z} = \frac{\partial R}{\partial \dot{z}} = \frac{\partial F}{\partial z} = 0 \tag{D-37}$$

$$\frac{\partial V}{\partial z} = - M_T \, g \tag{D-38}$$

Then by equation (D-1):

$$m_T \ddot{z} - m_2 \left[\ddot{\theta}\, \ell_2 \sin\theta + \dot{\theta}^2 \ell_2 \cos\theta + (\ddot{\theta} + \ddot{\rho})\, \ell_3 \sin(\theta + \rho)\right.$$

$$\left. + (\dot{\theta} + \dot{\rho})^2 \ell_3 \cos(\theta + \rho)\right] + m_p \left[\ddot{\theta}\, \ell_1 \sin\theta + \dot{\theta}^2 \ell_1 \cos\theta\right.$$

$$\left. + \ddot{\beta}\, \ell_p \sin\beta + \dot{\beta}^2 \ell_p \cos\beta\right] - m_T g$$

$$= - F_{T1} \cos\theta - F_{T2} \cos(\theta + \rho) \qquad \text{(D-39)}$$

Linearized equations.

$$m_T \ddot{z} = m_T g - (F_{T1} + F_{T2}) \qquad \text{(D-40)}$$

θ Coordinate

$$\frac{\partial T}{\partial \dot{\theta}} = I_1 \dot{\theta} + I_2 (\dot{\theta} + \dot{\rho}) + m_2 \left[\ell_2^2 \dot{\theta} + (\dot{\theta} + \dot{\rho}) \ell_3^2 + \ell_2 (\dot{x} \cos\theta - \dot{z} \sin\theta)\right.$$

$$\left. + (2\dot{\theta} + \dot{\rho}) \ell_2 \ell_3 \cos\rho + \ell_3 (\dot{x} \cos(\theta + \rho) - \dot{z} \sin(\theta + \rho))\right]$$

$$+ m_p \left[\ell_1^2 \dot{\theta} - \ell_1 (\dot{x} \cos\theta - \dot{z} \sin\theta) + \dot{\beta} \ell_1 \ell_p \cos(\beta - \theta)\right] \qquad \text{(D-41)}$$

$$\frac{d}{dt}\left(\frac{\partial T}{\partial \dot{\theta}}\right) = I_1 \ddot{\theta} + I_2 (\ddot{\theta} + \ddot{\rho}) + m_2 \left[\ell_2^2 \ddot{\theta} + (\ddot{\theta} + \ddot{\rho}) \ell_3 + \ell_2 (\ddot{x} \cos\theta - z \sin\theta)\right.$$

$$- \dot{\theta} \ell_2 (\dot{x} \sin\theta + \dot{z} \cos\theta) + (2\ddot{\theta} + \ddot{\rho}) \ell_2 \ell_3 \cos\rho$$

$$\left. - (2\dot{\theta} + \dot{\rho})\, \dot{\rho}\, \ell_2 \ell_3 \sin\rho + \ell_3 \left[\, \ddot{x} \cos(\theta + \rho) - \ddot{z} \sin(\theta + \rho) \,\right]\right.$$

$$- (\dot{\theta} + \dot{\rho})\, \ell_3 \,(\dot{x} \sin(\theta + \rho) + \dot{z} \cos(\theta + \rho))\Big] + m_p \Big[\ell_1^2\, \ddot{\theta}$$

$$- \ell_1 (\ddot{x} \cos\theta - \ddot{z} \sin\theta) + \ell_1\, \dot{\theta}\, (\dot{x} \sin\theta + \dot{z} \cos\theta)$$

$$+ \ddot{\beta}\, \ell_1 \ell_p \cos(\beta - \theta) - \dot{\beta}\, (\dot{\beta} - \dot{\theta})\, \ell_1 \ell_p \sin(\beta - \theta)\Big] \qquad \text{(D-42)}$$

$$\frac{\partial T}{\partial \theta} = m_2 \Big[-\ell_2\, \dot{\theta}\, (\dot{x} \sin\theta + \dot{z} \cos\theta) - (\dot{\theta} + \dot{\rho})\, \ell_3 \left(\dot{x} \sin(\theta + \rho) + \dot{z} \cos(\theta + \rho)\right)\Big]$$

$$+ m_p \Big[\ell_1\, \dot{\theta}\, (\dot{x} \sin\theta + \dot{z} \sin\theta) + \dot{\theta}\dot{\beta}\, \ell_1 \ell_p \sin(\beta - \theta)\Big] \qquad \text{(D-43)}$$

$$\frac{\partial V}{\partial \theta} = m_2\, g \Big[\ell_2 \sin\theta + \ell_3 \sin(\theta + \rho)\Big] - m_p\, g\, \ell_1 \sin\theta \qquad \text{(D-44)}$$

$$\frac{\partial R}{\partial \theta} = 0, \frac{\partial F}{\partial \theta} = 1 \qquad \text{(D-45)}$$

Substituting into equation (1) and using $\beta = \theta + \delta$

$$I_1\, \ddot{\theta} + I_2\, (\ddot{\theta} + \ddot{\rho}) + m_2 \Big[\ell_2^2\, \ddot{\theta} + \ell_3^2\, (\ddot{\theta} + \ddot{\rho}) + \ell_2\, (\ddot{x} \cos\theta - \ddot{z} \sin\theta)$$

$$+ (2\ddot{\theta} + \ddot{\rho})\, \ell_2 \ell_3 \cos\rho - (2\dot{\theta} + \dot{\rho})\, \dot{\rho}\, \ell_2 \ell_3 \sin\rho + \ell_3\, (\ddot{x} \cos(\theta + \rho)$$

$$- \ddot{z} \sin(\theta + \rho))\Big] + m_p \Big[\ell_1^2 \ddot{\theta} - \ell_1\, (\ddot{x} \cos\theta - \ddot{z} \sin\theta)$$

$$+ (\ddot{\theta} + \ddot{\delta})\, \ell_1 \ell_p \cos\delta - (\dot{\theta} + \dot{\delta})^2 \sin\delta\Big] + m_2\, g\, \ell_2 \sin\theta$$

$$+ m_2\, g\, \ell_3 \sin(\theta + \rho) - m_p\, g\, \ell_1 \sin\theta = -F_{T2} \ell_2 \sin\rho + \lambda \qquad \text{(D-46)}$$

The above equation is the complete expression for the θ - Coordinate.

ρ - Coordinate

$$\frac{\partial T}{\partial \dot{\rho}} = I_2 (\dot{\theta} + \dot{\rho}) + m_2 \left[(\dot{\theta} + \dot{\rho}) \ell_3^2 + \dot{\theta} \ell_2 \ell_3' \cos \rho + \ell_3 (\dot{x} \cos (\theta + \rho) - \dot{z} \sin (\theta + \rho)) \right] \tag{D-47}$$

$$\frac{d}{dt}\left(\frac{\partial T}{\partial \dot{\rho}}\right) = I_2 (\ddot{\theta} + \ddot{\rho}) + m_2 \left[(\ddot{\theta} + \ddot{\rho}) \ell_3^2 + \ddot{\theta} \ell_2 \ell_3 \cos \rho - \dot{\theta}\dot{\rho} \ell_2 \ell_3 \sin \rho \right.$$

$$+ \ell_3 \left[\ddot{x} \cos (\theta + \rho) - \ddot{z} \sin (\theta + \rho) \right] - \ell_3 (\dot{\theta} + \dot{\rho}) \left[\dot{x} \sin (\theta + \rho) \right.$$

$$\left. \left. + \dot{z} \cos (\theta + \rho) \right] \right] \tag{D-48}$$

$$\frac{\partial T}{\partial \rho} = m_2 \left[-\dot{\theta} (\dot{\theta} + \dot{\rho}) \ell_2 \ell_3 \sin \rho - (\dot{\theta} + \dot{\rho}) \ell_3 (\dot{x} \sin (\theta + \rho) + \dot{z} \cos (\theta + \rho)) \right] \tag{D-49}$$

$$\frac{\partial V}{\partial \rho} = m_2 g \ell_3 \sin (\theta + \rho) + K \ell_4^2 \rho \tag{D-50}$$

$$\frac{\partial R}{\partial \dot{\rho}} = B \ell_4^2 \dot{\rho}, \frac{\partial F}{\partial \rho} = 0 \tag{D-51}$$

Substituting into equation (1)

$$I_2 (\ddot{\theta} + \ddot{\rho}) + m_2 \left[(\ddot{\theta} + \ddot{\rho}) \ell_3^2 + \ddot{\theta} \ell_2 \ell_3 \cos \rho + \dot{\theta}^2 \ell_2 \ell_3 \sin \rho \right.$$

$$+ \ell_3 \left[\ddot{x} \cos (\theta + \rho) - \ddot{z} \sin (\theta + \rho) \right] + B \ell_4^2 \dot{\rho}$$

$$\left. + K \ell_4^2 \rho + m_2 g \ell_3 \sin (\theta + \rho) = 0 \right. \tag{D-52}$$

β-Coordinate

$$\frac{\partial T}{\partial \dot{\beta}} = m_p \left[\ell_p^2 \dot{\beta} - \ell_p (\dot{x} \cos\beta - \dot{z} \sin\beta) + \dot{\theta} \ell_1 \ell_p \cos(\beta - \theta) \right] + I_p \dot{\beta} \tag{D-53}$$

$$\frac{d}{dt}\left(\frac{\partial T}{\partial \dot{\beta}}\right) = I_p \ddot{\beta} + m_p \left[\ell_p^2 \ddot{\beta} - \ell_p (\ddot{x} \cos\beta - \ddot{z} \sin\beta) + \ell_p \dot{\beta} (\dot{x} \sin\beta + \dot{z} \cos\beta) \right.$$

$$\left. + \ddot{\theta} \ell_1 \ell_p \cos(\beta - \theta) - \dot{\theta}(\dot{\beta} - \dot{\theta}) \ell_1 \ell_p \sin(\beta - \theta) \right] \tag{D-54}$$

$$\frac{\partial T}{\partial \beta} = -\dot{\beta} \ell_p (\dot{x} \sin\beta + \dot{z} \cos\beta) - \dot{\theta} \dot{\beta} \ell_1 \ell_p \sin(\beta - \theta) \tag{D-55}$$

$$\frac{\partial V}{\partial \beta} = -m_p g \ell_p \sin\beta \tag{D-56}$$

$$\frac{\partial R}{\partial \dot{\beta}} = 0 \quad , \quad \frac{\partial F}{\partial \beta} = -1 \tag{D-57}$$

substituting into equation (1) and using $\beta = \theta + \delta$,

$$I_p(\ddot{\theta} + \ddot{\delta}) + m_p \left[\ell_p^2 (\ddot{\theta} + \ddot{\delta}) - \ell_p \left(\ddot{x} \cos(\theta + \delta) - \ddot{z} \sin(\theta + \delta) \right) \right.$$

$$\left. + \ddot{\theta} \ell_1 \ell_p \cos\delta + \dot{\theta}^2 \ell_1 \ell_p \sin\delta \right] - m_p g \ell_p \sin(\theta + \delta) = -\lambda \tag{D-58}$$

by use of the constraint equation to eliminate β, we have effectively arrived at the equation for the relative coordinate δ with "driving torque" λ.

Linearization of the Equations of Motion

To linearize and decouple the rotational dynamics from the translational motion, we must find expressions for the terms

$$\ddot{x} \cos\theta - \ddot{z} \sin\theta \tag{D-59}$$

$$\ddot{x} \cos(\theta + \rho) - \ddot{z} \sin(\theta + \rho) \tag{D-60}$$

$$\ddot{x} \cos\beta - \ddot{z} \sin\beta = \ddot{x} \cos(\theta + \delta) - \ddot{z} \sin(\theta + \delta) \tag{D-61}$$

In terms of δ, θ, and ρ as follows:

$$\ddot{x}\cos\theta - \ddot{z}\sin\theta = -\frac{m_2}{m_T}\left[(\ell_2 + \ell_3)\ddot{\theta} + \ell_3\ddot{\rho}\right]$$

$$+\frac{m_p}{m_T}\left[(\ell_1 + \ell_p)\ddot{\theta} + \ell_p\ddot{\delta}\right] - g\theta - \frac{F_{T_2}}{m_T}\rho \qquad \text{(D-62)}$$

$$\ddot{x}\cos\beta - \ddot{z}\sin\beta = -\frac{m_2}{m_T}\left[(\ell_2 + \ell_3)\ddot{\theta} + \ell_3\ddot{\rho}\right]$$

$$+\frac{m_p}{m_T}\left[(\ell_1 + \ell_p)\ddot{\theta} + \ell_p\ddot{\delta}\right] - g(\theta + \delta)$$

$$+\left(\frac{F_{T_1} + F_{T_2}}{m_T}\right)\delta - \frac{F_{T_2}}{m_T}\rho \qquad \text{(D-63)}$$

$$\ddot{x}\cos(\theta + \rho) - \ddot{z}\sin(\theta + \rho) = -\frac{m_2}{m_T}\left[(\ell_2 + \ell_3)\ddot{\theta} + \ell_3\ddot{\rho}\right]$$

$$+\frac{m_p}{m_T}\left[(\ell_1 + \ell_p)\ddot{\theta} + \ell_p\ddot{\delta}\right]$$

$$-g(\theta + \rho)\frac{F_{T_1}}{m_T}\rho \qquad \text{(D-64)}$$

Linearization of δ-Coordinate

$$\left\{ I_p + m_p \ell_p (\ell_1 + \ell_p) - \frac{m_p}{m_T} \ell_p \left[m_p (\ell_1 + \ell_p) - m_2 (\ell_2 + \ell_3) \right] \right\} \ddot{\theta}$$

$$+ \frac{m_2 m_p}{m_T} \ell_p \ell_3 \ddot{\rho} + \frac{m_p}{m_T} \ell_p F_{T_2} \rho$$

$$+ \left[I_p + m_p \ell_p^2 \left(1 - \frac{m_p}{m_T} \right) \right] \ddot{\delta} - \frac{m_p}{m_T} \ell_p \left(F_{T_1} + F_{T_2} \right) \delta = - \lambda \quad \text{(D-65)}$$

Linearization of θ-Coordinate

$$I_1 \ddot{\theta} + I_2 (\ddot{\theta} + \ddot{\rho}) + m_2 \ell_2^2 \ddot{\theta} + m_2 \ell_3^2 (\ddot{\theta} + \ddot{\rho})$$

$$- \frac{m_2^2}{m_T} \ell_2 \left[(\ell_2 + \ell_3) \ddot{\theta} + \ell_3 \ddot{\rho} \right] + \frac{m_2 m_p}{m_T} \ell_2 \left[(\ell_1 + \ell_p) \ddot{\theta} \right.$$

$$\left. + \ell_p \ddot{\delta} \right] - \frac{m_2}{m_T} \ell_2 F_{T_2} \rho + m_2 \ell_2 \ell_3 (2\ddot{\theta} + \ddot{\rho})$$

$$- \frac{m_2^2}{m_T} \ell_3 \left[(\ell_2 + \ell_2) \ddot{\theta} + \ell_3 \ddot{\rho} \right] + \frac{m_2 m_p}{m_T} \ell_3 \left[(\ell_1 + \ell_p) \ddot{\theta} \right.$$

$$\left. + \ell_p \ddot{\delta} \right] + \frac{m_2}{m_T} \ell_3 F_{T_1} \rho + m_p \ell_1^2 \ddot{\theta} + \frac{m_2 m_p}{m_T} \ell_1 \left[(\ell_2 + \ell_3) \ddot{\theta} + \right.$$

$$+ \ell_3 \ddot{\rho}\Big] - \frac{m_p^2}{m_T} \ell_1 \Big[(\ell_1 + \ell_p)\ddot{\theta} + \ell_p \ddot{\delta}\Big] + \frac{m_p}{m_T} \ell_1 F_{T_2} \rho$$

$$+ m_p \ell_1 \ell_p (\ddot{\theta} + \ddot{\delta}) + F_{T_2} \ell_2 \rho + \Bigg\{\Bigg[\Big[I_p + m_p \ell_p^2$$

$$+ \frac{m_p m_2}{m_T} \ell_p (\ell_2 + \ell_3) - \frac{m_p^2}{m_T} \ell_p (\ell_1 + \ell_p) + m_p \ell_1 \ell_p\Big]\ddot{\theta}$$

$$+ \frac{m_p m_2}{m_T} \ell_p \ell_3 \ddot{\rho} + \frac{m_p}{m_T} \ell_p F_{T_2} \rho$$

$$+ \left[I_p + m_p \ell_p^2 - \frac{m_p^2}{m_T} \ell_p^2\right]\ddot{\delta} - \frac{m_p}{m_T} \ell_p \left(F_{T_1} + F_{T_2}\right) \delta \Bigg\} = 0 \qquad \text{(D-66)}$$

where

$$\Big\{\qquad\Big\} = -\lambda$$

$$\Big\{I_1 + I_2 + I_p + m_p (\ell_1 + \ell_p)^2 + m_2 (\ell_2 + \ell_3)^2 - \frac{1}{m_T}\Big[m_p (\ell_1 + \ell_p)$$

$$-m_2 (\ell_2 + \ell_3)\Big]^2\Big\}\ddot{\theta} + \Big\{I_2 + m_2 \ell_3 (\ell_2 + \ell_3) + \frac{m_2}{m_T} \ell_3 \Big[m_p (\ell_1 + \ell_p)$$

$$- m_2 (\ell_2 + \ell_3)\Big]\Big\}\ddot{\rho} + \Big\{\frac{m_2}{m_T} \ell_3 F_{T_1} + \Big[\frac{m_p}{m_T} (\ell_1 + \ell_p)$$

$$+ \ell_2 \left(1 - \frac{m_2}{m_T}\right)\Big] F_{T_2}\Big\} \rho + \Big\{I_p + m_p \ell_p (\ell_1 + \ell_p) -$$

$$- \frac{m_p}{m_T} \ell_p \left[m_p (\ell_1 + \ell_p) - m_2 (\ell_2 + \ell_3) \right] \Bigg\} \ddot{\delta} - \frac{m_p}{m_T} \ell_p \left(F_{T_1} + F_{T_2} \right) \delta = 0 \qquad \text{(D-67)}$$

Linearization of the ρ -Coordinate

$$\Bigg\{ I_2 + m_2 \ell_3 (\ell_2 + \ell_3) + \frac{m_2}{m_T} \ell_3 \left[m_p (\ell_1 + \ell_p) - m_2 (\ell_2 + \ell_3) \right] \Bigg\} \ddot{\theta} + \left[I_2 + m_2 \left(1 - \frac{m_2}{m_T} \right) \ell_3^2 \right] \ddot{\rho}$$

$$+ B \ell_4^2 \rho + \left[K \ell_4^2 + \frac{m_2}{m_T} \ell_3 F_{T_1} \right] \rho + \frac{m_2 m_p}{m_T} \ell_p \ell_3 \ddot{\delta} = 0 \qquad \text{(D-68)}$$

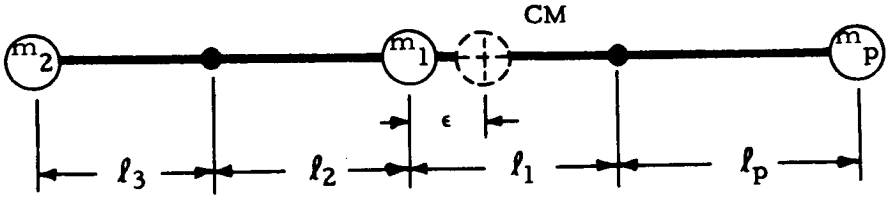

Figure D-2. Illustration of the Coefficients

Σ Mass Moments w. r. t. CM = 0

$$\epsilon = \frac{m_p (\ell_1 + \ell_p) - m_2 (\ell_2 + \ell_3)}{m_T} \qquad \text{(D-69)}$$

$$I_v = I_1 + I_2 + I_p + m_p (\ell_1 + \ell_p)^2 + m_2 (\ell_2 + \ell_3)^2 - \frac{1}{m_T} \left[m_p (\ell_1 + \ell_p) - m_2 (\ell_2 + \ell_3) \right]^2 \qquad \text{(D-70)}$$

I_v = moment of inertia about CM.

APPENDIX E. COMPUTER PROGRAM DESCRIPTION

Various computer programs were used to develop the parametric data contained in this report. A brief description of each, including their current status and available documentation, is listed below.

Performance Programs

1. Program Title: Three-Dimensional Trajectory Optimization Program

   Number: AP 188

   Description: This program computes the trajectory of a multistage rocket vehicle under the influence of a central force field (including gravitational harmonics through the 4th for the earth), over a rotating, oblate spheroid. The atmospheric portion of the trajectory (if any) employs predetermined steering histories (usually zero-lift), while the exoatmospheric trajectory is determined through the indirect method of the calculus-of-variations. A variety of two- and three-dimensional end conditions may be specified.

   Language: 7094 Fortran IV

   Status: Operational

   Documentation: Internal only

2. Program Title: Three-Dimensional Powered Trajectory Program

   Number: AP 113

   Description: The basic version of AP 113 is a general purpose, multistage powered trajectory program which computes a trajectory under the influence of a central force field (including gravitational harmonics through the fourth for the earth) over a rotating oblate

spheroid. The steering attitude angles are input (in a variety of coordinate systems), and can be modified by an iteration routine to effect convergence to a desired set of end conditions.

A modified version of the program allows input of steering rates and includes an expanded convergence technique.

Language: OS 360/Fortran G and H

Status: Basic - Operational

Modified - Not checked out

Documentation: Incomplete

3. Program Title: Two-Dimensional Trajectory Program

Number: TDTP

Description: Simplified trajectory program employing a simple numerical integration procedure for atmospheric flight and the closed form "linear tangent" solution for the upper stages. Sizing loops are employed to determine the optimum energy distribution among as many as five stages. Fixed liftoff weight and fixed payload weight options are available.

Language: Fortran IV Coded for NR RAX System; OS 360/Fortran H

Status: Operational

Documentation: None

4. Title: Lunar Flying Vehicle Program

Program Number: None

The trajectory performance program computes a time history of the trajectory for modified ballistic or constant altitude flight modes. The equations of motion were formulated assuming a flat moon and constant lunar gravity.

Language: Fortran IV Coded for the NR RAX System

Status: Operational

Documentation: Internal

Orbit Transfer and Rendezvous

1. Program Title: Program for Optimization of Two-Impulse Transfers by Contouring and Steepest Descent

   Number: None

   Description: This program surveys the energy requirements for two impulse transfer between any two closed orbits around a single attracting center. The program contours the entire range of departure and arrival conditions as a function of ΔV and produces detailed plots of the results indicating graphically the regions of optima. It converges to the minimum ΔV in each region, and gives these results numerically. One case requires about one minute of IBM 360 time. The minimum information required is name of central body, name of unit system, and elements of the two orbits.

   Language: OS 360/Fortran H, Double Precision

   Status: Operational

   Documentation: SD 69-3

2. Program Title: Rendezvous Data and Contouring Program

   Number: ST 025

   Description: This computer program makes use of two impulse transfer to effect rendezvous between an active and a passive spacecraft in any two closed orbits around a single attracting center. For an array of given initial conditions at the time of the first impulse, it generates the characteristics of the rendezvous at specified arrival points and the characteristics of the rendezvous optimized on arrival point. The contouring phase of the program is designed to yield a plot showing the optimum ΔV for rendezvous for the range of initial conditions. It also shows the way in which the initial condition propagates if the first impulse is delayed, and indicates the optimum ΔV to rendezvous from those conditions.

3. Program Title: Orbit-to-Orbit Line-of-Sight Viewing Conditions

Number: None

Description: Given the orbital elements of two vehicles orbiting a central attracting body, the program computes and plots automatically the line of sight between the vehicles and the viewing conditions with respect to the sun and the horizon. A simplified model is used with the sun being contained in the orbital plane of the primary vehicle.

Language: OS/360 Fortran H

Status: Operational

Documentation: None

Stability and Control

1. Program Title: CRAM

Program Number: None

Description: This program converts equations in matrix form to transfer functions with roots evaluated at specified input coefficient values. It also produces cathode ray tube outputs, in root locus format, of the closed loop roots at each point. The program is general in operation and, thus, requires a coded matrix coefficient (to second order) subroutine for each set of equations.

Language: Fortran IV, IBM 7094

Status: Operational

Documentation: Internal

APPENDIX F. RECOMMENDED LESS DEVELOPMENT ACTIONS

The material contained in the main body of this report constitutes a bank of parametric (Phase A type) escape system feasibility data, including the possible adaptation of LESS to surface flyer missions. Parallel studies conducted by North American Rockwell Corporation show that there are other potential mission applications basically compatible with the LESS vehicle which should be considered to assure that the investment in hardware development will be fully exploited.

The LESS could be conceived as following one of several optional development paths:

1. An earliest possible (crash) development and operational use of a minimum escape-only system (no other mission considerations).

2. A normal development cycle for an escape system, still with no other mission requirements.

3. A normal development cycle of a system having alternate mission capability by suitable incorporation of extra design features and equipment.

    a. An escape vehicle development which includes requirements for alternate use as a long-range surface-to-surface flyer for rescue and/or exploration missions.

    b. An escape vehicle development which includes alternate orbit-to-surface control elements and capabilities for use as a manned shuttle vehicle.

    c. An escape vehicle development which incorporates versatile multimission capabilities including unmanned landing missions such as an orbit-to-surface shuttle or logistic lander, rescue/resupply vehicle, or automated escape delivery system.

Considering the probable constraints of budget, lunar program evolution, and hardware growth capabilities, a preliminary development plan summary is offered, figure F-1. Manual control system studies should be initiated (and continued, as at Langley) to optimize control parameters for

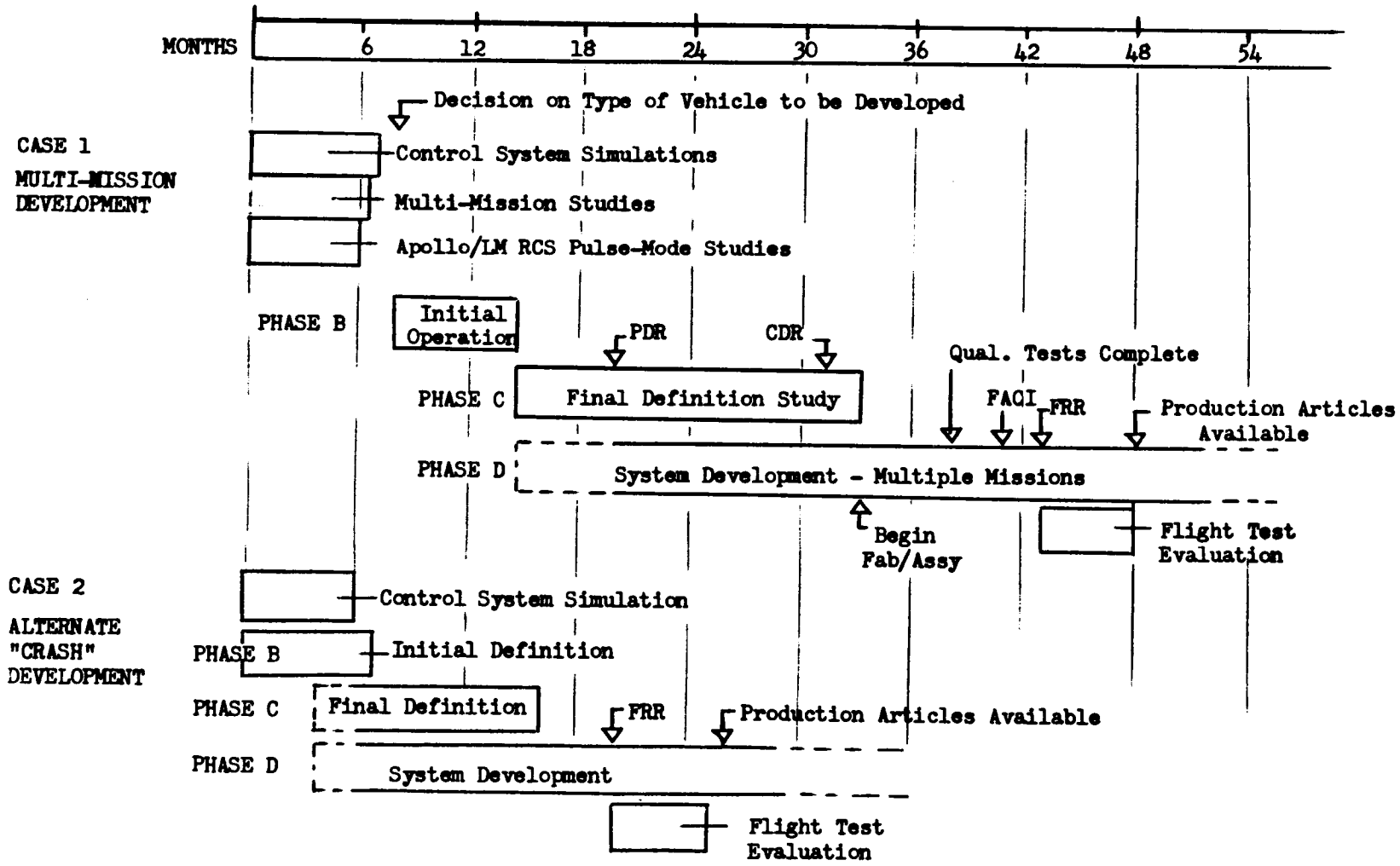

Figure F-1. - LESS Preliminary Development Plan Summary

best handling qualities and to determine the ultimate potential of these systems. Mechanical/electrical shaping networks with hardwire control mode should be evaluated to demonstrate their effectiveness and their design parameters. At the same time, multimission studies should be inaugurated to determine the other missions for which LESS vehicles could be adapted and to determine the design compromises in LESS necessary for alternate mission use. The very promising concept of utilizing existing Apollo/LM RCS engines in clusters with throttling and thrust vector control by differential pulsing should be studied to determine its applicability and advantages to LESS. With this information, it should then be possible for NASA to choose a design approach for initial definition study within 6 to 8 months.

Succeeding development phases could yield a first flight test article in the middle of the third year. A major problem will be to define an initial flight test program which is both feasible and meaningful. The NASA/LRC fixed-base visual simulator and FLEEP tethered flight vehicle constitute the best facilities for terrestrial evaluations and pilot training. A realistic mission simulation could be achieved by operating a prototype system in earth orbit in conjunction with AAP early space station facilities. The LESS could be "launched" from the station and could then boost to a higher orbit where a CSM could accomplish the rendezvous. The whole operation would simulate all elements of a lunar escape mission while in the comparative safety of the earth orbital environment. For multimission versions, lunar flight tests could be conducted if engine throttling and landing gear are provided. The first experimental checkout mission could be low altitude hovering flight in the vicinity of LM while stability and control characteristics are being evaluated. After confidence in the system has been developed through the earth orbital and/or lunar simulations, the system could be certified for operational use.

Should the need arise for the LESS to be developed on a compressed or crash schedule basis, the simulation testing would need to be accelerated to yield usable design information or confirmation within a few months. Initial system definition might begin concurrently to save time, using a conservative design approach until testing or additional studies show that less conservatism is justified. By conducting Phase D with considerable overlap on Phase C study, the system might be made available in prototype form for first flight test in 13 months from Phase C-D beginning. The highly accelerated nature of this development would involve risks not present in the normally paced program.

The specific and immediate actions considered advisable at this time to explore further promising options for system development are summarized as follows:

1. Perform simulation tests to further evaluate the potential of manual control modes which could be used with escape vehicles and other flying vehicles. Develop the criteria for predicting and maximizing the handling qualities of such vehicles.

2. Conduct mission studies of other flying vehicle applications to describe the range of requirements for such vehicles. Determine the possible commonality in these requirements such that the potentials and compromises necessary for multimission design of an escape vehicle would be apparent. Consider such missions as long-range flyer for surface exploration, future site reconnaissance, rescue, logistics support, etc.; shuttle vehicle to and from orbit; rescue or logistics delivery system from orbit; automated logistics lander or remote experiment lander from orbit; etc.

3. Conduct a feasibility study of the very promising pulse mode propulsion and control concept which employs existing Apollo/LM RCS engines rather than requiring development of a new throttled engine. Determine and confirm the apparent advantages of the concept in terms of such items as configuration arrangement, system dynamic characteristics, engine redundancy/reliability potential, control adaptability and flexibility, early engine availability, and low cost.

NASA-Langley, 1970 — 31 CR-1620